Modeling of Horns and Enclosures for Loudspeakers

Gavin Richard Putland

▶ **To cite this version:**

Gavin Richard Putland. Modeling of Horns and Enclosures for Loudspeakers. Acoustics [physics.class-ph]. University of Queensland, 1996. English. NNT : . tel-01546159

HAL Id: tel-01546159
https://hal.science/tel-01546159

Submitted on 8 Jul 2017

HAL is a multi-disciplinary open access archive for the deposit and dissemination of scientific research documents, whether they are published or not. The documents may come from teaching and research institutions in France or abroad, or from public or private research centers.

L'archive ouverte pluridisciplinaire **HAL**, est destinée au dépôt et à la diffusion de documents scientifiques de niveau recherche, publiés ou non, émanant des établissements d'enseignement et de recherche français ou étrangers, des laboratoires publics ou privés.

Modeling of Horns and Enclosures for Loudspeakers

by
Gavin Richard Putland, BE (Qld)
Department of Electrical and Computer Engineering
University of Queensland

Submitted for the degree of Doctor of Philosophy
December 23, 1994

Revised November 1995

Accepted February 6, 1996

Examiners:

Dr. John T. Post
Klipsch Professional,
Hope, Arkansas, USA;

Prof. H. Holmes
Dept. of Electrical Engineering
University of New South Wales, Australia;

Dr. N. Shuley
Dept. of Electrical & Computer Engineering
University of Queensland, Australia.

Supervisor: Dr. L. V. Skattebol.

To my parents,

Frank and Del Putland

Acknowledgments

My interest in horn theory was inspired by Dr E. R. Geddes, whose paper "Acoustic Waveguide Theory" [18] raised the questions addressed in Chapters 3 to 5 of this thesis, suggested some of the answers, and provided many of the related references. These debts are not diminished by my disagreement with Geddes' analysis of the oblate spheroidal waveguide, which he subsequently revised [19]. My paper on one-parameter waves and Webster's equation [43] was improved as a result of a personal communication from Dr Geddes (October 10, 1992), which alerted me to the existence of Fresnel diffraction fringes within the coverage angles of finite horns at high frequencies.

I wish to thank the Executive Editor and Review Board of the *Journal of the Audio Engineering Society* for their patient handling of the complex exchange of correspondence that followed my "Comments on 'Acoustic Waveguide Theory' " [42].

I am indebted to an anonymous reviewer of my article "Acoustical Properties of Air versus Temperature and Pressure" [44] for correcting my explanation of the effect of humidity on absorption, and for drawing my attention to ANSI S1.26-1978 [41], which is cited frequently in the final version of the article and in Chapter 9.

My supervisor, Dr Larry Skattebol, provided critical feedback on my three publications and on numerous partial drafts of this thesis. I thank him for his flexibility in accepting my research proposal, and for his subsequent prudence in curbing my tendency to pursue new lines of inquiry; without his guidance, this already protracted project would have taken considerably longer. I also thank Prof. Tom Downs and Dr Nick Shuley, colleagues of Dr Skattebol in the Dept. of Electrical and Computer Engineering, University of Queensland, for their comments on reference [42].

The Italian text of Somigliana's letter [51] (paraphrased in Appendix A) was translated by Br. Alan Moss, who was then a graduate student in the Department of Studies in Religion, University of Queensland.

The Japanese text of Sections 1 to 3 of Arai's paper [2] was translated by Adrian Treloar of the Department of Japanese and Chinese Studies, University of Queensland.

The titles and authors of the major public-domain software used in this project are as follows. Equivalent circuit simulations were performed using SPICE3 by Tom Quarles, with the `nutmeg` user interface by Wayne Christopher. Programs were compiled by the GNU project C compiler. Most diagrams were drawn using `xfig` by Supoj Sutanthavibul et al., converted to LaTeX `picture` commands using `fig2dev` by Micah Beck et al., and finally edited as text files. All source files were edited with `jove` by Jonathan Payne, and spell-checked with `ispell` by Pace Willisson et al. This document was typeset and printed within the Department of Electrical and Computer Engineering, University of Queensland, using LaTeX 2_ε by Leslie Lamport.

This project was supported by an Australian Postgraduate Research Award.

Statement of Originality

I declare that the content of this thesis is, to the best of my knowledge and belief, original except as acknowledged in the text and footnotes, and that no part of it has been previously submitted for a degree at this University or at any other institution.

In a thesis drawing on such diverse subjects as mechanics, thermodynamics, circuit theory, differential geometry, vector analysis and Sturm-Liouville theory, the author must make exaggerated efforts to maintain some theoretical coherence. This may involve deriving well-known results in a manner appropriate to the context; examples include the hierarchy of forms of the equations of motion and compression (Chapter 2), and the derivation of admittances and Green's functions from Webster's equation (Chapter 3). Furthermore, when a thesis contains results at variance with earlier results in the literature, the author will be expected to justify his findings with exceptional thoroughness. In particular, he may be obliged to conduct mathematical arguments at a more fundamental level than would normally be appropriate; an example is my detailed solution of the heat equation to determine the basic thermal time constant of the air-fiber system (Chapter 8). In such cases, the context will indicate that the result is included for the sake of clarity, cohesion or rigor, and not necessarily because of novelty.

To avoid excessive reliance on "the context", I offer the following summary of what I believe to be my principal original contributions and their dependence on the work of earlier researchers. This summary also serves as an extended abstract.

- In Chapter 2, I have shown how the numerous familiar equations related to the inertia and compliance of air can be understood as alternative forms of two basic equations, which I call the equations of motion and compression. The hierarchy of forms eliminates redundancy in the derivations and clearly shows what simplifying assumptions are involved in each form. The "one-parameter" or "1P" forms apply when the excess pressure p depends on a single spatial coordinate ξ, which measures arc length normal to the isobaric surfaces. These forms are expressed with unprecedented generality, and are critical to the mathematical argument of subsequent chapters. Other forms lead to the familiar electrical analogs for acoustic mass and compliance (both lumped and distributed).

- After a review of previous literature, I have shown that the "Webster" horn equation, which is usually presented as a plane-wave approximation, follows *exactly* from the 1P forms of the equations of motion and compression, without any explicit assumption concerning the wavefront shape. The ξ coordinate is the axial coordinate of the horn while $S(\xi)$ is the area of a constant-ξ surface segment bounded by a tube of orthogonal trajectories to all the constant-ξ surfaces; such tubes (and no others) are possible guiding surfaces.

- I have shown that the Helmholtz equation admits solutions depending on a single spatial coordinate u if and only if $|\nabla u|$ and $\nabla^2 u$ are functions of u alone. The $|\nabla u|$ condition allows u to be transformed to another coordinate ξ, which measures arc length along the orthogonal trajectories to the constant-ξ surfaces. Hence, in the definition of a "1P" pressure field, the normal-arc-length condition is redundant. Using an expression for the Laplacian of a 1P pressure field, I have shown that the wave equation reduces *exactly* to Webster's equation; this is a second geometry-independent derivation. I have also shown that the term "1P acoustic field" can be defined in terms of pressure, velocity potential or velocity, and that all three definitions are equivalent.

- I have expressed the 1P existence conditions in terms of coordinate scale factors and found that *in the eleven coordinate systems that are separable with respect to the Helmholtz equation*, the only coordinates admitting 1P solutions are those whose level surfaces are planes, circular cylinders and spheres (Chapter 5). Geddes [18] reported in 1989 that Webster's equation is exact in the same list of coordinates, but did not make the connection between Webster's equation and 1P waves.

- *Without using separable coordinates*, Somigliana [51] showed that there are only three 1P wavefront shapes allowing parallel wavefronts and rectilinear propagation; the permitted shapes are planar, circular-cylindrical and spherical. I have shown (Chapter 5) that the conditions of parallel wavefronts and rectilinear propagation are implicit in the 1P assumption, so that the three geometries obtained by Somigliana are the only possible geometries for 1P waves. This result has the practical implication that no new 1P horn geometries remain to be discovered.

- I have produced an annotated paraphrase, in modern notation, of Somigliana's proof (Appendix A), and adapted his proof so as to take advantage of the 1P existence conditions (Chapter 5). In the theorems of Chapter 5 and the footnotes to Appendix A, I have filled in several missing steps in Somigliana's argument. I found it most convenient to prove these results independently, although related results exist in the literature on differential geometry.

- Working from the permitted 1P wavefront shapes and the exact derivations of Webster's equation, I have given wide conditions under which that equation is *approximately* true, so that traditional approximate derivations of the equation can be replaced by the more general 1P theory.

- I have extended the finite-difference equivalent-circuit (FDEC) method proposed in 1960 by Arai [2]. In Chapter 6, I have shown that a finite-difference approximation to Webster's equation yields the nodal equations of an L-C latter network (confirming Arai's unproven assertion that his one-dimensional method can be adapted for horns), while a similar approximation to the wave equation in general curvilinear orthogonal coordinates yields the nodal equations of a three-dimensional L-C network. I have obtained the same circuits from the equations of motion and compression in order to show that "current" in the equivalent circuit is volume flux, as expected. I have shown how the network should be truncated at the boundaries of the model and terminated with additional components to represent a range of boundary conditions.

- Arai suggested that fibrous damping materials could be handled by using complex values of density and bulk modulus for the air. In Chapter 7, I have derived expressions for complex density and "complex gamma" (related to complex bulk modulus) and shown how these quantities can be represented by introducing additional components into the equivalent circuit.

- An equivalent circuit for a fiber-filled bass enclosure was given by Leach [30] in 1989. Leach's derivation does not use the finite-difference method, is less rigorous than mine (especially in its treatment of compliance), makes different assumptions in the determination of complex density, does not use any concept related to complex bulk modulus, does not use the most appropriate definition of the thermal time constant (as Leach himself acknowledges), and does not fully explore the relationships between the possible definitions (the value of the time constant depends on what conditions are held constant during the heat transfer). In Chapter 7, I have defined five different thermal time constants, of which one is useful for deriving the complex gamma and another (which I call "basic") is easier to calculate from the specifications of the damping material. I have shown that two of the five time constants can be read off the equivalent circuit, and hence expressed all the time constants in terms of the "basic" one, denoted by $\tau_{\mathrm{f}p}$, which is the time constant at constant fiber temperature and constant pressure.

- Values of $\tau_{\mathrm{f}p}$ found by Leach [30] and Chase [14] are extremely inaccurate, and neither author gives a convenient method of calculating the time constant for arbitrary fiber diameters and packing densities. In Chapter 8, I have rectified these deficiencies by reworking the solution of the heat equation (finding the error in Leach's analysis) and fitting an algebraic formula to the results. The formula is

$$\tau_{\mathrm{f}p} \approx \frac{\mathsf{d}^2}{8\alpha}\,(m^2 - m^{0.37})\,\ln\left(\tfrac{m+1}{2}\right)$$

  where d is the fiber diameter, α is the thermal diffusivity of air, f (not in the formula) is the fraction of the overall volume occupied by the fiber, and $m = f^{-1/2}$.

- Chapter 9 gives some simple algebraic formulae for calculating α and other relevant properties of air from the temperature and pressure. This chapter is mostly a compilation of results from the literature; my only original contributions are some simple curve-fitting and a discussion of errors.

- In Chapter 10, using the results of Chapters 6 to 9, I have constructed a two-dimensional finite-difference equivalent-circuit model to predict the frequency response of a moving-coil loudspeaker in a fiber-filled box. The model incorporates an equivalent circuit of a moving-coil driver, which I have modified so as to allow the diaphragm to span several volume elements in the interior of the box. Unlike conventional equivalent-circuit models of loudspeakers, this model allows for spatial variations of pressure inside the box and *shows the effects of internal resonances on the frequency response*. By observing the effects of omitting selected components from the model, I have found that viscosity is the dominant mechanism of damping and that, in the cases considered, the predicted response is not greatly altered by assuming thermal equilibrium. The

latter finding diminishes the significance of, but depends on, the calculation of the thermal time constant.

- In Chapter 11, I have illustrated and validated the FDEC representation of a free-air radiation condition in curvilinear coordinates, by applying it to the classical problem of the circular rigid-piston radiator.

This thesis contains three additional proofs or derivations which I have devised independently, but which were presumably first discovered by mathematicians of earlier centuries; in particular, Somigliana [51] seems to have been familiar with the first two results as early as 1919. The three passages are:

- the proof that if $|\nabla\xi| = 1$, the orthogonal trajectories to the level surfaces of ξ are straight lines (Theorem 5.1),
- the proof that the only surfaces having constant principal curvatures are planes, circular cylinders and spheres (Theorem 5.4), and
- the derivation of the so-called "modified Newton method" or "third-order Newton method" for estimating a zero of a non-linear function (Section B.1).

Gavin R. Putland
December 21, 1994

Abstract

It is shown that the "Webster" horn equation is an exact consequence of "one-parameter" or "1P" wave propagation. If a solution of the Helmholtz equation depends on a single spatial coordinate, that coordinate can be transformed to another coordinate, denoted by ξ, which measures arc length along the orthogonal trajectories to the constant-ξ surfaces. Webster's equation, with ξ as the axial coordinate, holds inside a tube of such orthogonal trajectories; the cross-sectional area in the equation is the area of a constant-ξ cross-section. This derivation of the horn equation makes no explicit assumption concerning the shape of the wavefronts. It is subsequently shown, however, that the wavefronts must be planar, circular-cylindrical or spherical, so that *no new geometries for exact 1P acoustic waveguides remain to be discovered.*

It is shown that if the linearized acoustic field equations are written in arbitrary curvilinear orthogonal coordinates and approximated by replacing all spatial derivatives by finite-difference quotients, the resulting equations can be interpreted as the nodal equations of a three-dimensional L-C network. This "finite-difference equivalent-circuit" or "FDEC" model can be truncated at the boundaries of the simulated region and terminated to represent a wide variety of boundary conditions. The presence of loosely-packed fibrous damping materials can be represented by using complex values for the density and ratio of specific heats of the medium. These complex quantities lead to additional components in the FDEC model.

Two examples of FDEC models are given. The first example predicts the frequency response of a moving-coil loudspeaker in a fiberglass-filled box, *showing the effects of internal resonances.* Variations of the model show how the properties of the fiberglass contribute to the damping of resonances and the shaping of the frequency response. It is found that viscosity, rather than heat conduction, is the dominant mechanism of damping. The second example addresses the classical problem of radiation from a circular rigid piston, and confirms that a free-air anechoic radiation condition with oblique incidence can be successfully represented in the FDEC model.

Related publications

- G. R. Putland: "Comments on 'Acoustic Waveguide Theory' " (letter), *J. Audio Engineering Soc.*, vol. 39, pp. 469–71 (1991 June). Reply by E. R. Geddes: pp. 471–2.
- G. R. Putland: "Every One-Parameter Acoustic Field Obeys Webster's Horn Equation", *J. Audio Engineering Soc.*, vol. 41, pp. 435–51 (1993 June).
- G. R. Putland: "Acoustical Properties of Air versus Temperature and Pressure", *J. Audio Engineering Soc.*, vol. 42, pp. 927–33 (1994 November).

The *Journal of the Audio Engineering Society* is published in New York. In anticipation of submitting further material to the same journal, the author has adopted U.S. spellings throughout this thesis.

Contents

Acknowledgments iii

Statement of Originality (with extended abstract) iv

Abstract viii

Related publications ix

Contents xiv

List of Figures xvi

List of Tables xvii

Symbols and Abbreviations xviii

1 Introduction 1
1.1 Scope . . . 4

2 Foundations 6
2.1 Forms of the equation of motion . . . 7
2.1.1 Integral form . . . 7
2.1.2 Differential or point form . . . 7
2.1.3 One-parameter or thin-shell form . . . 10
2.1.4 Lumped-inertance (one-parameter incompressible) form . . . 12
2.2 Forms of the equations of continuity & compression . . . 12
2.2.1 Continuity: integral form . . . 13
2.2.2 Continuity: differential or point form . . . 13
2.2.3 Compression: differential or point form . . . 13
2.2.4 Digression: Alternative expressions for c^2 . . . 14
2.2.5 Compression: integral form . . . 15
2.2.6 Compression: lumped-compliance (uniform-pressure) form . . . 16
2.2.7 Compression: one-parameter or thin-shell form . . . 16
2.3 Velocity potential . . . 17
2.3.1 Existence . . . 17
2.3.2 Relationship to excess pressure . . . 19
2.4 The wave equation . . . 19
2.4.1 Further discussion of approximations . . . 20
2.5 Acoustic circuits . . . 20
2.5.1 Ohm's law and Kirchhoff's laws . . . 20

2.5.2 Acoustic resistance and impedance . . . 21
2.5.3 Reasons for using the direct analogy . . . 22
2.5.4 Analogous, equivalent and pseudo-equivalent circuits . . . 23

3 The "Webster" horn equation 25
3.1 Classical derivations (1760–1948) . . . 26
3.2 Exact derivation from the 1P equations . . . 30
3.2.1 Alternative forms . . . 31
3.3 Application to spherical waves . . . 32
3.3.1 Radiation from a point source . . . 32
3.3.2 Green's functions . . . 33
3.3.3 Driving admittance and impedance . . . 35
3.3.4 Specific acoustic admittance and impedance . . . 35
3.3.5 Characteristic impedance . . . 37

4 Every one-parameter acoustic field is a solution of Webster's equation. 38
4.1 Introduction: a wider definition of "1P" . . . 38
4.2 Existence of 1P waves . . . 39
4.2.1 Seeking a 1P solution . . . 40
4.2.2 Sufficient conditions . . . 41
4.2.3 Necessary conditions . . . 41
4.2.4 Infinite bandwidth . . . 42
4.2.5 Transforming the parameter to an arc length . . . 42
4.2.6 Webster's equation (again) . . . 43
4.3 Deriving Webster's equation from the wave equation . . . 43
4.4 Alternative definitions of "1P" . . . 45

5 1P waves are planar, cylindrical or spherical. 47
5.1 Testing orthogonal coordinate systems . . . 47
5.2 Testing separable systems . . . 48
5.3 A wider search: the work of Webster and Somigliana . . . 49
5.4 Proof that there are only three cases . . . 52
5.4.1 Geometric interpretation . . . 57
5.5 Approximately-1P horns . . . 58
5.6 "Constant directivity" . . . 59
5.7 Note on the work of E. R. Geddes (1989, 1993) . . . 60
5.8 Discussion and summary . . . 61

6 The Finite-Difference Equivalent-Circuit model: a lumped equivalent circuit for a distributed acoustic field 63
6.1 Introduction: the work of M. Arai (1960) . . . 63
6.1.1 A note on computational efficiency . . . 65
6.2 The finite-difference method: theory and notation . . . 66
6.3 The 1P case . . . 67
6.3.1 Webster's equation . . . 67
6.3.2 The equations of motion and compression . . . 68
6.3.3 Truncated elements at ends . . . 71
6.4 The 3D case . . . 73

6.4.1 The wave equation . . . 73
6.4.2 The equations of motion and compression . . . 76
6.4.3 Truncated elements at boundary surfaces . . . 80
6.5 3D boundary conditions . . . 83
6.5.1 Pressure condition . . . 84
6.5.2 Normal velocity condition . . . 84
6.5.3 Normal admittance condition . . . 85
6.5.4 Anechoic or free-air radiation condition . . . 86
6.5.5 Non-equicoordinate boundaries . . . 88
6.6 Reduction to two dimensions . . . 89

7 The damped FDEC model (for fiber-filled regions) 91
7.1 Equation of motion: complex density . . . 91
7.1.1 Discussion of approximations; review of literature . . . 92
7.1.2 Derivation of complex density . . . 94
7.1.3 Equivalent circuit . . . 97
7.1.4 Computation of mass elements . . . 99
7.2 Equation of compression: complex gamma . . . 100
7.2.1 Thermal and mechanical definitions of γ . . . 101
7.2.2 Derivation of complex gamma . . . 103
7.2.3 High- and low-frequency limits of $\gamma^\star$ . . . 106
7.2.4 Equation of compression and equivalent circuit . . . 107
7.2.5 Thermal time constants from the acoustic circuit . . . 111
7.2.6 Thermal time constants from the heat circuit . . . 113
7.2.7 Acoustic circuit from thermal time constants? . . . 115
7.2.8 Computation of compliance elements . . . 116
7.3 Truncated elements at boundary surfaces . . . 117

8 The thermal time constant $\tau_{\mathrm{f}p}$ 118
8.1 Analytical approximation . . . 119
8.2 Solving the heat equation . . . 123
8.2.1 Separation of variables . . . 124
8.2.2 Solution in terms of Bessel functions . . . 127
8.2.3 Behavior of eigenfunctions; estimates of eigenvalues . . . 127
8.2.4 Numerical solution of the radial equation . . . 129
8.2.5 Results of Chase (1974) and Leach (1989) . . . 131
8.2.6 Why higher-order modes are neglected . . . 135
8.2.7 Refining the analytical approximation . . . 137
8.3 Some numerical results . . . 140

9 Acoustical properties of air vs. temperature and pressure 142
9.1 The dry-air formulae . . . 142
9.1.1 Constants . . . 142
9.1.2 Density . . . 143
9.1.3 Speed of sound; characteristic impedance; bulk modulus . . . 143
9.1.4 Viscosity . . . 143
9.1.5 Heat conduction . . . 144
9.2 Numerical results . . . 144
9.3 Errors due to humidity . . . 146

9.4 Absorption and humidity . . . 147
9.5 Refined formulae for η and κ . . . 149
9.6 Conclusion . . . 150

10 Simulation of a fiber-filled bass enclosure 151
10.1 The moving-coil driver . . . 152
10.1.1 Radiation impedance, radiated power, sound intensity level . . 153
10.1.2 Equation of motion . . . 154
10.1.3 Equivalent circuit . . . 156
10.1.4 Calculation of component values from data sheets . . . 158
10.1.5 Sharing the diaphragm area among several volume elements . 159
10.2 The interior of the box . . . 162
10.3 Description of modeling programs . . . 166
10.3.1 Command-line options . . . 167
10.3.2 Circuit modifications required by SPICE . . . 168
10.3.3 Program limitations . . . 168
10.4 10-inch woofer in 36-liter box . . . 169
10.4.1 Full simulation . . . 170
10.4.2 Undamped response and effect of fiber filling . . . 170
10.4.3 FDEC and lumped-box models . . . 173
10.4.4 Importance of viscous damping . . . 174
10.4.5 Unimportance of fiber stiffness . . . 176
10.4.6 Secondary importance of thermal relaxation . . . 177
10.4.7 Approximate model of thermal relaxation changes bass rolloff. 179
10.4.8 Effects of halving the element size . . . 181
10.4.9 Effects of ambient temperature and pressure . . . 185
10.5 6.5-inch woofer in 5-liter box . . . 185
10.6 Simulations vs. experiments . . . 188

11 Radiation from a circular rigid piston 189
11.1 Choosing the test problem . . . 189
11.1.1 Alternative coordinates—a digression . . . 191
11.2 The FDEC components . . . 192
11.2.1 Compliance and mass elements . . . 193
11.2.2 Anechoic-boundary elements . . . 193
11.2.3 Diaphragm interface . . . 195
11.3 The normalized FDEC model . . . 196
11.3.1 General principles; accuracy . . . 196
11.3.2 Components . . . 198
11.3.3 Pressure, flux, diaphragm interface . . . 199
11.4 AC analysis: radiation impedance . . . 203
11.5 Transient analysis: checking for echoes . . . 207
11.5.1 Normalized time . . . 208
11.5.2 The test signal . . . 208
11.5.3 Prediction of reflections by geometrical optics . . . 209
11.5.4 Simulation results and discussion . . . 212

12 Conclusions 214
12.1 Further work . . . 218

Appendices **221**

A Somigliana's letter to *Atti Torino* (1919) **222**

B Program listings and explanatory notes **228**
B.1 IVP solver and modified Newton method 228
B.2 Root-finder `root.c` 232
B.3 Eigenfunction plotter `efunc.c` 233
B.4 Program `chase.c`: Check results of Chase. 236
B.5 Program `f2.c`: Locate 2nd-mode heatshed. 238
B.6 Program `mu.c`: Check eigenvalue approximations. 240
B.7 Program `tafp.c`: Tabulate thermal time constant τ_{fp}. 243
B.8 Program `air.c`: Tabulate acoustical properties of air. 245
B.9 Model builder `box.c` (for loudspeaker) 247
B.10 Sample circuit file `cct` (for loudspeaker) 258
B.11 Graphing program `sp2tex.c` 264
B.12 Model builder `disk.c` (for circular piston) 267
B.13 Sample circuit file `d35u.cir` (for circular piston) 276
B.14 Table-formatting programs 281
B.15 Transient response plotter `tr2tex.c` 285

Bibliography **289**

List of Figures

6.1 *FDEC representation of Webster's equation.* 68
6.2 *FDEC representation of 3D wave equation.* 75
6.3 *FDEC representation of equation of motion in u direction, in free air.* 77
6.4 *FDEC representation of 3D equation of compression, in free air.* . . . 80

7.1 *FDEC model for equation of motion in u direction, with damping.* . . 98
7.2 *FDEC model for 3D equation of compression, with damping.* 110
7.3 *Air-fiber heat circuit at constant pressure.* 114

8.1 *Radial eigenfunctions for $m = 20$, and limiting function.* 132

10.1 *Loudspeaker box to be simulated* 152
10.2 *Equivalent circuit of moving-coil driver connected to time-dependent voltage source v_g.* 157
10.3 *Electroacoustic circuit of Fig. 10.2, with the gyrator remodeled as a bilateral transconductance. Node numbers are also shown.* 160
10.4 *Electroacoustic circuit of a moving-coil driver whose diaphragm area is shared between three volume elements* 163
10.5 *Two-dimensional finite-difference equivalent circuit of the interior of the box in Fig. 10.1* 165
10.6 *Half-space SIL vs. frequency for a 10-inch woofer in a 36-liter box; full simulation. The SIL (sound intensity level) is the IL at one meter, assuming isotropic radiation into half-space and constant parallel radiation resistance.* 171
10.7 *Undamped approximation and full simulation* 171
10.8 *Undamped and lumped approximations* 173
10.9 *"Free" approximation, for which viscosity is neglected, and full simulation* 174
10.10 *"Unison" approximation, for which the fiber is assumed to move with the air, and full simulation* 175
10.11 *"Stiff" approximation, for which the fiber is assumed stationary, and full simulation* 176
10.12 *Adiabatic approximation and full simulation* 177
10.13 *Thermal-equilibrium approximation and full simulation* 178
10.14 *"Free" approximation and undamped approximation* 179
10.15 *"Near-adiabatic" approximation, for which ΔC_{th} is shorted, and full simulation* 180
10.16 *Full simulation with 25 mm elements and with 50 mm elements* 181
10.17 *"Free" approximation with 25 mm elements and with 50 mm elements* 182

10.18 *Undamped approximation with 25 mm elements and with 50 mm elements* . . . 183
10.19 *Full simulation at 40° C and at 20° C* . . . 185
10.20 *Full simulation at an altitude of 1500 meters and at sea level* . . . 186
10.21 *6.5-inch driver in 5-liter box; adiabatic approximation and full simulation* . . . 187
10.22 *6.5-inch driver in 5-liter box; thermal-equilibrium approximation and full simulation* . . . 187

11.1 *Normalized FDEC model of a circular rigid-piston source, in cylindrical coordinates* . . . 201
11.2 *FDEC calculation of the transient response at two points in the field of a circular rigid piston in an infinite planar baffle* . . . 211

List of Tables

8.1 *Algorithm for finding the first three eigenvalues of the radial Sturm-Liouville problem.* 131
8.2 *Algorithm for checking the calculations of L. M. Chase (1974).* 134
8.3 *Check on eigenvalues used by Chase* 134
8.4 *Fraction of air volume involved in heat exchange for second mode (right column) vs. filling factor (left column).* 136
8.5 *Algorithm for checking a trial value of ζ in Eqs. (8.15) and (8.67).* . . 137
8.6 *Errors in analytical approximations to the eigenvalue* 138
8.7 *Thermal time constant $\tau_{\mathrm{f}p}$ vs. filling factor and fiber diameter* 141

9.1 *Computed acoustical properties of air vs. temperature and pressure* . 145

11.1 *Normalized radiation impedance of a circular rigid piston in an infinite planar baffle, calculated by the FDEC method* 204
11.2 *Normalized radiation impedance on one side of an unbaffled circular rigid piston, calculated by the FDEC method* 206

Symbols and Abbreviations

List of symbols

In a thesis containing elements of vector analysis, differential geometry, acoustics, mechanics and thermodynamics, one is likely to encounter different quantities having the same conventional symbol. Reuse of symbols could perhaps be avoided by choosing arbitrary symbols instead of familiar ones, but the reader (not to mention the author) would have trouble remembering the arbitrary meanings. For better or worse, the author has decided to use familiar symbols for familiar quantities, and let some symbols have different meanings in different contexts. Hence some symbols are repeated in the following list. In assigning symbols for related quantities, the following rules have been followed with reasonable consistency:

1. A bold upright character denotes a vector quantity. The same character in an unbold italic typeface, without a subscript, denotes the magnitude of the vector (in a 3D context) or its component in an understood direction (in a 1P context). With a coordinate subscript, it denotes the component in the direction of that coordinate.

2. An alternating time-dependent quantity is denoted by a lower-case italic letter; its phasor form or Fourier transform is denoted by the corresponding capital italic letter. When this is impractical, as when a Greek letter has an upper case that is indistinguishable from an English letter, an underscore is used for the phasor.

3. A subscript "0" indicates an equilibrium value (such as P_0 or $\gamma_o^\star$), a mean value (ρ_o) or a value pertaining to the reference surface Σ_0 (Chapter 5).

4. Classical (lumped) acoustic components have a subscript "a" for "acoustic". This subscript is not used for FDEC elements (which are distinguished by the leading "Δ") unless damping material is involved, in which case the subscript "a" distinguishes the components due to the air alone.

5. An overbar indicates a per-mole quantity.

6. In Chapter 11, normalized values are indicated by lower case (for circuit elements) or a hat (for time-dependent quantities or phasors).

The overall arrangement of the following list is alphabetical, ignoring case, with English letters before Greek letters. Logical groups, like the coordinates u, v and w, cause some local variations from this order.

a	radius of diaphragm or fiber
b	outer radius of region under study
c	speed of sound, or (with subscripts) normalized compliance element
C_{a}	acoustic compliance
C_{ab}	acoustic compliance of box
C_{ad}	distributed acoustic compliance (1P)
C_{as}	acoustic compliance of suspension
C_{f}	mass-specific heat of fiber
C_p	mass-specific heat at constant pressure
C_v	mass-specific heat at constant volume
d	fiber diameter
$\mathbf{e}_u, \mathbf{e}_v, \ldots$	unit vectors for coordinates u, v, etc.
f	filling factor (see also ν)
f_{ri}	relaxation frequency for i^{th} mode
f_{s}	free-air resonance frequency of driver
G_{th}	air-fiber thermal conductance per unit volume
G	gyrator transconductance (Chapter 10)
h	step size in numerical SLP solution (Chapter 8), or normalized angular frequency (Chapter 11)
H	gyrator transfer resistance (Chapter 10)
H, H_0	mean curvatures of Σ and Σ_0 (Chapter 5)
$h_u, h_v, \ldots$	scale factors for coordinates u, v, etc.
$\mathbf{i}, \mathbf{j}, \mathbf{k}$	Cartesian unit vectors
k	wave number ($= \omega/c$), or a counter in the z direction (Chapter 11)
K, K_0	total (Gaussian) curvatures of Σ and Σ_0
K_v, K_w	principal curvatures of surface Σ
K_{v0}, K_{w0}	principal curvatures of surface Σ_0
m	mass (various contexts), or $m = f^{-1/2} = b/a$ (Chapter 8), or (with subscripts) normalized mass element
$\bar{m}$	mean molar mass
M_{a}	acoustic mass
M_{ab}	back air load on driver (FDEC model)
M_{ad}	distributed acoustic mass (1P), or acoustic mass of driver (no air load)
M_{af}	front air load on disk
m_{af}	normalized M_{af}
M_{ar}	radiation mass
m_{ar}	normalized M_{ar}
M_{as}	acoustic mass of driver (free-air, with air load)
n	amount of gas (moles), or a general-purpose counter
$\mathbf{n}$	unit normal vector to surface
Np	neper (dimensionless unit)
p	excess pressure (= pressure rise above P_0)
P	phasor form of p
P_0	static (equilibrium) pressure

p_{b}	back pressure on diaphragm (average)
$p_{\mathrm{b}j}$	back pressure on j^{th} area element
p_{d}	developed pressure of driver (average)
$p_{\mathrm{d}j}$	developed pressure for j^{th} area element
p_{f}	front pressure
p_{r}	radiated pressure ($= p_{\mathrm{f}}$)
P_{r}	phasor form of p_{r}
$\hat{P}_{\mathrm{r}}$	normalized P_{r}
P_{r0}	reference P_{r}
p_{t}	total pressure ($= P_0 + p$)
q	heat energy density (Subsection 7.2.6)
$\mathbf{q}$	air velocity, or heat flux density (Chapter 8)
$\mathbf{Q}$	phasor form of $\mathbf{q}$
$\mathbf{q}_{\mathrm{f}}$	fiber velocity
$\mathbf{Q}_{\mathrm{f}}$	phasor form of $\mathbf{q}_{\mathrm{f}}$
$Q_{\mathrm{es}}, Q_{\mathrm{ms}}, Q_{\mathrm{ts}}$	free-air Q factors of driver (after Small)
r	radial coordinate (cylindrical or spherical)
R	spherical radial coordinate (Chapter 11), or gas constant (mass basis)
$\bar{R}$	universal (molar) gas constant
$\mathbf{r}$	position vector (general, or on Σ)
$\mathbf{r}_0$	position vector on Σ_0
R_{a}	acoustic resistance
R_{ar}	radiation resistance
r_{ar}	normalized R_{ar}
R_{as}	acoustic resistance of suspension
R_{e}	resistance of voice coil
s	arc length (more general than ξ)
S	diaphragm area
$S(\xi)$	cross-sectional area of ξ-tube
$\mathbf{t}$	unit tangent vector of space curve or of curve on Σ
$\mathbf{t}_0$	unit tangent of curve on Σ_0
T	instantaneous temperature (K) in Chapter 7; equilibrium temperature (K) elsewhere
T_0	equilibrium temperature in Chapter 7
T_{f}	temperature of fiber
u	flux (volume velocity)
U	phasor form of u
u, v, w	curvilinear orthogonal coordinates
v	specific volume
V	overall volume
V_{a}	volume of acoustic compliance
V_{as}	suspension equivalent volume
v_{g}	terminal voltage
V_{g}	phasor form of v_{g}
$\mathbf{y}$	specific acoustic admittance
y_{n}	normal specific acoustic admittance

$Z_{\mathrm{a}0}$	reference acoustic impedance (Chapter 11)
Z_{ar}	radiation impedance
z_{ar}	normalized Z_{ar}
α	thermal diffusivity
$\alpha_{\mathrm{r}i}$	absorption coefficient due to i^{th} thermal relaxation mode
α_{t}	total absorption coefficient
α_η	absorption coefficient due to viscosity
α_κ	absorption coefficient due to heat conduction
β	normalized volume-specific heat of fiber
γ	ratio of C_p to C_v
$\gamma^\star$	complex gamma
$\gamma_{\mathrm{o}}^\star$	low-frequency limit of $\gamma^\star$
ΔC	acoustic compliance element
ΔC_{a}	adiabatic compliance element
ΔC_{th}	thermal relaxation compliance element
$\Delta C_{\mathrm{th\,f}}$	ΔC_{th} for infinite-heatsink assumption
ΔM	acoustic mass element (1P)
ΔM_u	mass element in u direction (other subscripts for other coordinates)
$\Delta M_{u\mathrm{a}}$	air mass element in u direction
$\Delta M_{u\mathrm{f}}$	fiber mass element in u direction
ΔR_{th}	thermal relaxation resistance element
ΔR_u	viscous resistance element in u direction (other subscripts for other coordinates)
Δu	increment in coordinate u (similarly for other coordinates)
ΔU	phasor flux element (1P); note contrast with Δu.
ΔU_{in}	phasor flux into volume element
ΔU_u	phasor flux element in u direction (other subscripts for other coordinates)
ΔV	volume element
ζ	index in formula for $\tau_{\mathrm{f}p}$ (Chapter 8)
η	dynamic viscosity (of air)
θ	excess temperature of air, or spherical angular coordinate from polar axis
Θ	phasor form of θ (excess temperature)
θ_0	initial value of θ (Chapter 8)
θ_{f}	excess temperature of fiber
Θ_{f}	phasor form of θ_{f}
κ	thermal conductivity (Chapter 9)
$\boldsymbol{\kappa}$	vector curvature of space curve (Chapter 5)
λ	pneumatic resistivity
μ	Sturm-Liouville eigenvalue (Chapter 8)
μ_1	first eigenvalue
μ_a	"rough" analytical estimate of μ_1
μ_b	"refined" analytical estimate of μ_1

ν	kinematic viscosity (Chapter 9), or frequency (Chapter 10)
ξ	normal arc length coordinate
ρ	instantaneous density
ρ_{o}	mean density (spatial and temporal)
ρ_{e}	excess density (above equilibrium)
$\underline{\rho_{\mathrm{e}}}$	phasor form of ρ_{e}
ρ_{f}	fiber density (intrinsic glass density)
$\rho^\star$	complex density
σ	closed surface
Σ, Σ_0	general constant-ξ surfaces
τ_i	relaxation time for i^{th} mode
τ_{a}	thermal time constant, constant air temperature
$\tau_{\mathrm{f}p}$	thermal time constant, constant T_{f} and p
$\tau_{\mathrm{f}v}$	thermal time constant, constant T_{f} and v
τ_p	thermal time constant, constant p
τ_v	thermal time constant, constant v
ϕ	angular coordinate common to cylindrical and spherical systems
ψ	velocity potential
Ψ	phasor form of ψ
ω	angular frequency
ω_{s}	free-air-resonance angular frequency ($= 2\pi f_{\mathrm{s}}$)
Ω	solid angle

List of abbreviations

1P	one-parameter
2D	two-dimensional
3D	three-dimensional
c.d.	continuously differentiable
FDEC	finite-difference equivalent-circuit
FDM	finite-difference method
HF	high-frequency
IL	intensity level
LF	low-frequency
ODE	ordinary differential equation
OS	oblate spheroidal
PDE	partial differential equation
SIL	sound intensity level (Chapter 10)
SLP	Sturm-Liouville problem
w.r.t.	with respect to

Chapter 1

Introduction

> This problem of horns is a "house-on-fire" problem, in the sense that loud speakers are now being manufactured by the thousand, and while they are being manufactured and sold, we are trying to find out their fundamental theory.
>
> — Prof. V. Karapetoff [22, p. 405].

Karapetoff was speaking at a convention of the American Institute of Electrical Engineers in 1924. Seventy years later, "loud speakers" are being manufactured by the millions, do not necessarily have horns, and have followed the usual pattern of linguistic evolution by becoming "loudspeakers"—and we are still trying to find out their fundamental theory.

Of course there has been spectacular progress along this path. Fourteen months after Karapetoff's lament came the magisterial paper by Rice and Kellogg [46], showing that a mass-controlled direct-radiating moving-coil transducer could produce a uniform sound-pressure response over a wide frequency range. In later decades, the modeling of moving-coil transducers *with enclosures* was advanced by Thuras, Olson, Preston, Locanthi, Beranek, Villchur, van Leeuwen, Novak, Thiele, Small, Benson and others (see, for example, the historical notes and original references given by Augspurger [3], Hunt [25, pp. 79–91] and Small [49, 50]). These achievements, together with reasonable criteria for the design of crossover networks, have produced affordable loudspeakers giving tolerably realistic reproduction of sound.

In the course of these developments, however, certain issues that one might well regard as "fundamental" have been omitted. The impressive record of progress in other areas makes these omissions all the more conspicuous and surprising, and demands that they be rectified.

Karapetoff went on to mention two papers by A. G. Webster, one of which [62] contained a simple differential equation describing the propagation of sound in horns. Webster's equation, as it is now usually called, must surely be classified as part of the "fundamental theory" of loudspeakers; particular solutions of this equation have inspired a wide variety of horn designs [4], and the properties of its general solutions have been extensively studied [10, 16] with a view to predicting the throat impedance[1] of a given horn and hence the frequency response of the driver-horn system. If Webster's equation is fundamental, so are the assumptions on which it depends. Hence one might ask under what ideal theoretical conditions the equation

[1] Acoustic impedance is one of the basic quantities defined in Chapter 2.

is exactly true, and under what non-ideal practical conditions it is approximately true, in the expectation that these questions had been answered decades ago. It appears, however, that the first reasonably complete and rigorous answers were given in 1993 by the present author [43]. That study, with some subsequent additions and improvements, is presented in Chapters 3 to 5 of this thesis.

Another problem that has received surprisingly little attention is the effect of internal resonances in loudspeaker enclosures. The wave-like distribution of pressure inside an enclosure exhibits "modes" or "resonances" at certain frequencies, causing the load on the back of the diaphragm to vary strongly with frequency (calculations and measurements of the impedance presented by a rectangular box were given by Meeker et al. [35] in 1949). This represents a departure from the pure mass-loading prescribed by Rice and Kellogg [46], and consequently causes non-uniform frequency response. The phenomena of resonance and frequency-dependent impedance are unquestionably part of the "fundamental theory" of linear systems, and are usually thought to be theoretically and computationally tractable. But in the field of loudspeaker design, the problem of resonance has been attacked by lining or filling the enclosures with damping material, while the matter of *calculating* the adverse effects of resonance—with or without the damping—has been largely ignored in the published literature. (Meeker et al. [35] gave a graph of measured box impedance vs. frequency, with and without "sound absorbing lining", but did not show the effect on frequency response. Sakai et al. [47] gave a very approximate calculation of the effect on frequency response; their work is discussed later.)

As is well known, the most successful models of moving-coil loudspeakers in enclosures are based on equivalent circuits. These models have the convenient ability to represent the complete signal path, from electrical input to acoustic output, in a single circuit diagram which can be analyzed using standard computer software. However, all such models that the author has seen in the published literature are *low-frequency approximations* developed for the purpose of calculating and optimizing the bass rolloff of the driver. At higher frequencies, these models are misleading because they cannot predict the internal resonances in the enclosure—they allow for the compressibility of the air, and for the contribution of the air to the effective moving mass of the diaphragm at low frequencies, but *not* for a more complex pressure distribution such as would be capable of representing multiple standing-wave modes. An equivalent-circuit model can be modified to account (at least approximately) for the effects of damping materials added in an effort to suppress resonances [30, 49, 50]. However, when the original model is valid only at low frequencies, the version with added damping can do no more than predict the "side-effects" of damping on the low-frequency rolloff; it cannot predict the degree to which the damping material achieves its primary purpose of suppressing resonances in the midband.

These deficiencies can be overcome using the "finite-difference equivalent-circuit" or "FDEC" model, which is the subject of Chapters 6 to 11 of this thesis. If the differential equations describing an acoustic field are approximated by the *finite-difference method*, the resulting difference equations can be written as the nodal equations of a three-dimensional L-C network. This was shown, for Cartesian and cylindrical coordinates only, by Arai [2] in 1960. In Chapter 6 of this thesis, Arai's method is shown to be valid for general curvilinear orthogonal coordinates. Chapter 6 also shows how the network can be truncated at the boundaries of the simulated

region and terminated with additional components to represent a variety of boundary conditions. Chapter 7 shows how the equivalent circuit can be modified to include the mechanical and thermal effects of fibrous damping materials. Chapter 8 obtains an approximate algebraic formula for calculating the thermal time constant between the fiber and the air for constant pressure and constant fiber temperature; one component in each unit-cell of the FDEC model depends on that time constant. The FDEC components also depend on certain properties of air (density, viscosity, thermal diffusivity, etc.), which can be calculated from the temperature and pressure using a set of formulae collected in Chapter 9. In Chapter 10, the results of the preceding chapters are combined with an equivalent-circuit model of a moving-coil transducer to produce a two-dimensional FDEC model predicting the frequency response of a loudspeaker in a fiber-filled box, *including the influence of internal resonances*. The model can also handle an undamped box, or neglect selected properties of the damping material in order to evaluate the mechanisms of damping. The FDEC model is still a low-frequency approximation, but the highest usable frequency can be made arbitrarily high (given sufficient computational capacity) by making the step size sufficiently small, and is easily made high enough to show a useful number of resonant modes. To show that the FDEC model can accurately represent an anechoic free-air radiation condition at the model boundary, Chapter 11 applies the method to the well-known circular-rigid-piston radiation problem in cylindrical coordinates.

The model presented in Chapter 10 is not the world's first model showing the effect of enclosure resonances on the frequency response of a loudspeaker. Another such model was reported in 1984 by Sakai et al. [47], who used the finite-*element* method (not to be confused with the finite-*difference* method used in this thesis) to calculate the acoustic impedance presented by the enclosure to the back of the diaphragm. Sakai et al. went further than the present author in that their model was fully three-dimensional and allowed the shape of a conical diaphragm with a specified semi-apex angle to be accurately represented. They also gave an equivalent-circuit model of the driver and enclosure, incorporating the enclosure impedance. However, instead of solving the circuit with the computed impedance in place, the authors used a mass-limited approximation to the circuit and assumed that the radiated pressure is proportional to the diaphragm acceleration, obtaining a simple formula expressing the sound pressure level in terms of the impedance of the enclosure. The formula was valid only in the midband and discarded the information provided by the equivalent circuit concerning the low-frequency rolloff. Moreover, the assumption of rigid walls together with the neglect of damping in the suspension and pole gap of the driver produced a completely undamped model; hence, at those frequencies for which the reactance of the enclosure canceled the moving mass of the driver, the model predicted an infinite acoustic output.

Unlike the model of Sakai et al., the model presented in Chapter 10 always allows for damping in the suspension and consequently does not predict infinite output at any frequency, even for an undamped box. It also allows the modeling of damping due to fiber filling. Whereas Sakai et al. made only temporary use of an equivalent circuit, Chapter 10 of this thesis presents a purely electrical model which places all the capabilities of standard circuit-analysis software, such as SPICE, at the designer's disposal. (Chapters 10 and 11 assume that the reader has some familiarity with SPICE.) The use of controlled sources in the model allows acoustical quantities

to be represented without scaling or conversion of units. Electrical quantities are of course also represented literally, so that the model can be immediately extended to account for additional electrical components, such as crossover networks (although this option is not pursued in Chapter 10). Hence, while priority in solving the basic problem is conceded to Sakai et al., the approach adopted in this thesis offers significant advantages.

1.1 Scope

Any research project is liable to raise more questions than it answers, and consequently will never be "completed" unless some more or less arbitrary limits are imposed on its scope. This is especially the case if the project, like this one, begins on more than one front. But that is not to say that every decision to terminate a particular line of inquiry is arbitrary. Hence a few remarks on the scope of this thesis are in order.

In Chapters 6 and 7, the formulae for the FDEC components are expressed in general curvilinear orthogonal coordinates. This decision was motivated by a paper by Geddes [18], which included a discussion of separable coordinate systems and proposed a variety of acoustic waveguides whose walls could be represented as equicoordinate surfaces in suitably chosen coordinate systems; the use of equicoordinate boundaries makes the FDEC method slightly more accurate and much more convenient. Thus the FDEC method is just as applicable to waveguides or horns as to loudspeaker enclosures. Unfortunately it was not opportune to include an analysis of one of Geddes' waveguides in the long list of contents of the present thesis. It should be noted, however, that the free-air radiation condition modeled in Chapter 11 is a key component in the analysis of any waveguide, and that the FDEC method handles all orthogonal coordinate systems with equal ease provided that the scale factors are known as functions of the coordinates. In other words, this thesis contains sufficient information to enable any interested researcher to undertake a wide-ranging study of exotic waveguides.

Of course the limited range of computational examples in this thesis reflects the novelty of the methods, which requires an emphasis on their derivation rather than their application to realistic designs. The absence of a novel waveguide analysis is one illustration. Another is that the loudspeaker models are two-dimensional, with volume elements spanning the full width of the enclosure; one would expect production-quality software to generate fully 3D models, although the 2D treatment in this thesis is a justifiable approximation and yields useful information on the mechanisms of damping while using only modest computational resources.

This thesis does not consider all the resonances that might affect the performance of a loudspeaker; it considers aeroacoustic resonances in the cabinet, but neglects structural resonances in the cabinet walls and in the diaphragms and surrounds of the drivers. Structural resonances, like aeroacoustic resonances, can be analyzed by linear approximations, and might therefore be classified as "fundamental". It may even be possible to include structural deformations in an FDEC model, representing the non-local boundary impedances by means of elaborate patterns of coupled sources. The author has not had time to pursue these issues. However, there is some evidence that structural resonances are—or at least can be made—secondary influences on the performance of practical loudspeakers. The literature reviewed at

the beginning of Section 10.1 suggests that the resonance frequencies of a diaphragm can be kept above the operating frequency range by means of modern materials and structures; suitable structures include honeycomb sandwiches and foam sandwiches, which offer high ratios of flexural stiffness to mass. The same structures can be used in cabinet walls to keep their resonance frequencies high [57, p. 229]. Lipschitz et al. [32] have computed the radiation from the walls of several loudspeaker cabinets, using measurements of the wall vibrations. Their results indicate that, even with conventional wooden construction, variations in frequency response due to cabinet wall vibrations can be reduced below the level of audibility, provided that the cabinet includes adequate internal bracing.[2] The "ripples" in the frequency response of a typical high-quality loudspeaker may amount to several dB, which is more than can be accounted for by any of the results obtained by Lipschitz et al.

In summary, structural resonances have received more attention in the literature than aeroacoustic resonances, and the results suggest that structural resonances need not be a major influence on performance. The comparative shortage of literature on aeroacoustic resonances and the influence of damping materials, together with the comparative ease with which these questions can be tackled by equivalent-circuit methods, supports the decision to study only aeroacoustic resonances in this thesis. Other resonances may be considered in future work.

[2]Of course, careless design of the cabinet may produce objectionable resonances. Barlow [7] has investigated structural resonances in various loudspeaker components; he reports that in some cases, sound radiation from resonating cabinet walls can exceed the radiation from the driver. But the findings of Tappan and Lipschitz et al. convince the present author that such problems are readily preventable.

Chapter 2

Foundations

While this chapter contains material that can be found in undergraduate textbooks on acoustics, it also presents the one-parameter (1P) forms of the equations of motion and compression, a rigorous derivation of electrical-acoustical analogs (including the justification for connecting the analogous components to form circuits), and a unified discussion of linearizing approximations, including the neglect of gravity. Such issues cannot be discussed in isolation from the most elementary theory. Hence an introductory chapter presenting only the original material while quoting the rest from textbooks, if it were possible at all, would be incoherent.

Moreover, acoustics textbooks tend to derive the equation of motion and the equations of continuity and compression in an *ad hoc* manner, assuming a specific coordinate system and without exploiting the machinery of vector analysis. The textbook approach accommodates readers with modest mathematical background, but would not be appropriate here because its lack of generality would lead to needless repetition and loss of logical continuity, thus obscuring the close interdependence of the results. The approach adopted here is to begin with the most general form of each equation, then obtain the other forms by successive specialization. Among the advantages of this discipline are the following:

- Repetition of mathematical steps is avoided;
- Each approximation or assumption is made only once, not only saving time, but also showing clearly which results depend on which assumptions;
- The generality of the results is maximized (for example, the first formula for the acoustic mass of a port does not assume a uniform cross-section);
- The common theoretical foundation provides some intuitive rationale for the results of later chapters (for example, the expressions for the components of the finite-difference equivalent circuit in Chapter 6 will have familiar forms, and will seem plausible).

Finally, as this thesis is nominally in the discipline of electrical engineering, one measure of its merit is its potential to attract electrical engineers into the field of electroacoustics. That potential will be enhanced if the thesis serves as its own introduction to any necessary theory that is not part of the standard training of electrical engineers. Such is the theory presented in this chapter.

2.1 Forms of the equation of motion

The equation of motion expresses Newton's second law for a non-viscous fluid. It will be derived first in its most general integral form, then reduced to a point form valid for *irrotational flow*, *low gravity* and *small oscillations and compressions*. The point form is integrated to give a "one-parameter" or "1P" form, which applies to normal oscillations of a uniform thin shell of the fluid and is useful in the analysis of horns and ducts. This in turn is integrated to give a fourth form applicable to ports or vents (mass elements) in loudspeaker boxes. Note that each form of the equation will inherit all the assumptions contained in the previous form.

2.1.1 Integral form

In a non-viscous fluid, let σ be a simple closed surface *moving with the fluid*. Let $d\sigma$ denote the element of surface area and $\mathbf{n}$ the (outward) unit normal to σ. Let the three-dimensional region enclosed by σ be called $\mathcal{V}$, with every differential volume element $d\mathcal{V}$ also moving with the fluid. Each volume element will then contain a constant mass $dm = \rho\, d\mathcal{V}$, where ρ is the density. Let p_t be the total instantaneous pressure and $\mathbf{q}$ the instantaneous velocity ($\mathbf{q}$ is a vector; in this thesis, unless otherwise noted, symbols representing vector quantities will be in bold, upright type). In general ρ, p_t and $\mathbf{q}$ will depend on position and time. Let $\mathbf{g}$ be the local acceleration due to gravity, which is assumed to be the only *external* force ("body force") acting on the fluid. Newton's second law for the enclosed sample of fluid is

$$\frac{d}{dt}\,(\text{total momentum}) = \text{total force}, \tag{2.1}$$

i.e.

$$\frac{d}{dt}\iiint_{\mathcal{V}} \mathbf{q}\, dm \;=\; \iiint_{\mathcal{V}} \mathbf{g}\, dm \;-\; \oiint_{\sigma} p_\mathrm{t}\, \mathbf{n}\, d\sigma\,, \tag{2.2}$$

where the first integral on the right is the weight of the enclosed fluid, and the signed second integral is the force exerted by the pressure of the surrounding fluid (the sign is negative because each element of this force is in the direction of $-\mathbf{n}$).

2.1.2 Differential or point form

The right-hand term in Eq. (2.2) can be expressed as a volume integral using the gradient theorem [24, pp. 141–2] and rewritten in terms of mass elements, as follows:

$$\oiint_{\sigma} p_\mathrm{t}\, \mathbf{n}\, d\sigma \;=\; \iiint_{\mathcal{V}} \nabla p_\mathrm{t}\, d\mathcal{V} \;=\; \iiint_{\mathcal{V}} \frac{\nabla p_\mathrm{t}}{\rho}\, dm. \tag{2.3}$$

This may be substituted into Eq. (2.2) to obtain

$$\frac{d}{dt}\iiint_{\mathcal{V}} \mathbf{q}\, dm \;=\; \iiint_{\mathcal{V}} \left(\mathbf{g} - \frac{\nabla p_\mathrm{t}}{\rho}\right) dm. \tag{2.4}$$

Let us treat dm as a small mass contained in the small volume $d\mathcal{V}$, so that the volume integral represents a summation. Then, since the above equation holds for all volumes moving with the fluid, it applies to each volume element $d\mathcal{V}$. For each

element there is only one term in the "summation", so that the above result reduces to Euler's equation[1]:

$$\frac{d\mathbf{q}}{dt} = \mathbf{g} - \frac{1}{\rho}\nabla p_{\mathrm{t}}. \tag{2.5}$$

Euler's equation expresses Newton's second law at a point moving with the fluid, so that $d\mathbf{q}/dt$ is the acceleration of a single particle of the fluid. Hence the convention in fluid mechanics that the *total* derivative of a function with respect to (w.r.t.) time is evaluated at a point moving with the fluid, while the corresponding *partial* derivative is evaluated at a stationary point. Since the partial derivative will prove easier to work with, it is desirable to rewrite Euler's equation in terms of $\partial\mathbf{q}/\partial t$. In Cartesian coordinates, from the chain rule for partial derivatives, we have

$$\begin{aligned}\frac{d\mathbf{q}}{dt} &= \frac{\partial\mathbf{q}}{\partial t} + \frac{\partial\mathbf{q}}{\partial x}\frac{dx}{dt} + \frac{\partial\mathbf{q}}{\partial y}\frac{dy}{dt} + \frac{\partial\mathbf{q}}{\partial z}\frac{dz}{dt} \\ &= \frac{\partial\mathbf{q}}{\partial t} + \frac{\partial\mathbf{q}}{\partial x}q_x + \frac{\partial\mathbf{q}}{\partial y}q_y + \frac{\partial\mathbf{q}}{\partial z}q_z \\ &= \frac{\partial\mathbf{q}}{\partial t} + (\mathbf{q}.\nabla)\mathbf{q}\end{aligned} \tag{2.6}$$

where q_x, q_y and q_z are the components of $\mathbf{q}$ in the directions of $\mathbf{i}$, $\mathbf{j}$ and $\mathbf{k}$ (cf. Hsu [24], pp. 222–3). We now introduce the vector identity[2]

$$(\mathbf{q}.\nabla)\mathbf{q} = \tfrac{1}{2}\nabla(\mathbf{q}.\mathbf{q}) - \mathbf{q}\times(\operatorname{curl}\mathbf{q}) \tag{2.7}$$

and write $|\mathbf{q}| = q$, so that $\mathbf{q}.\mathbf{q} = q^2$. Substituting all this into Eq. (2.6) yields the *general* relationship between $d\mathbf{q}/dt$ and $\partial\mathbf{q}/\partial t$ in coordinate-independent form:

$$\frac{d\mathbf{q}}{dt} = \frac{\partial\mathbf{q}}{\partial t} + \tfrac{1}{2}\nabla(q^2) - \mathbf{q}\times(\operatorname{curl}\mathbf{q}). \tag{2.8}$$

Substituting this into Eq. (2.5), and adopting the convention—to be followed in the remainder of this thesis—that a dot denotes *partial* differentiation w.r.t. time, we obtain Euler's equation in terms of $\dot{\mathbf{q}} = \partial\mathbf{q}/\partial t$:

$$\dot{\mathbf{q}} + \tfrac{1}{2}\nabla(q^2) - \mathbf{q}\times(\operatorname{curl}\mathbf{q}) = \mathbf{g} - \frac{1}{\rho}\nabla p_{\mathrm{t}}. \tag{2.9}$$

Thus the general form of Euler's equation—which assumes only that the fluid is non-viscous—is nonlinear in $\mathbf{q}$ and ρ (note the q^2 and $1/\rho$ factors) and non-homogeneous (the terms contain unlike powers of the dependent variables). This rules out superposition and all solution methods that follow therefrom, including separation of variables and integration of Green's functions. To linearize and homogenize the equation, we make the following approximations:

- The flow is *irrotational*; that is, $\operatorname{curl}\mathbf{q} = 0$, so that one nonlinear term is eliminated from Eq. (2.9).

[1] Euler's equation may also be obtained by moving the d/dt operator inside the volume integral, as in Hsu [24], pp. 216–7.

[2] Hsu [24, pp. 111, 223] derives identity (2.7) by an unusual operational method. A more conventional approach is to use Cartesian coordinates and show that the $\mathbf{i}$ components of both sides are equal; the $\mathbf{j}$ and $\mathbf{k}$ components behave similarly.

- Oscillations are small; that is, $\mathbf{q}$ is small. The first term is Eq. (2.9) is linear in $\mathbf{q}$ while the next two terms are quadratic in $\mathbf{q}$. Hence, if $\mathbf{q}$ is sufficiently small, the second and third terms will be negligible compared with the first. We do not yet know how small is "sufficiently small", although this can always be checked by calculating the first and second terms after an approximate solution has been found (see e.g. Ballantine [4], pp. 88–9). The meaning of "small oscillations" will be clarified in Subsection 2.4.1.

  Also note that the irrotational-flow assumption seems to have been made redundant, since the small-oscillations assumption makes the term containing $\operatorname{curl}\mathbf{q}$ negligible. This issue will be taken up again in Subsection 2.3.1.

- The external force per unit mass is *conservative*—which is certainly the case for gravity. Hence $\mathbf{g}$ has a potential function: let

$$\mathbf{g} = -\nabla V. \tag{2.10}$$

- Compressions are small; that is, all spatial and temporal variations in ρ are small compared with its mean value. This applies not only to variations caused by excitation of the fluid, but also to those caused by the gravitational pressure gradient—this is the *low-gravity* assumption. Thus we can write

$$\rho \approx \rho_\mathrm{o}\ , \tag{2.11}$$

  where ρ_o is the mean density. The above substitution linearizes the last term in Eq. (2.9) and, when combined with Eq. (2.10), allows the right side of Eq. (2.9) to be written as a single gradient.

After the above approximations and substitutions, Eq. (2.9) becomes

$$\dot{\mathbf{q}} = -\frac{1}{\rho_\mathrm{o}}\nabla(p_\mathrm{t} + \rho_\mathrm{o}V) \tag{2.12}$$

which is much simpler than the exact form. But because of the $\rho_\mathrm{o}V$ term, this result is still inhomogeneous in p_t and $\mathbf{q}$. (That is, if we have a solution (p_t,$\mathbf{q}$), we do not obtain another solution by multiplying p_t and $\mathbf{q}$ by an arbitrary constant α, unless $\nabla V = 0$; for a proof, replace p_t and $\mathbf{q}$ in Eq. (2.12) by αp_t and $\alpha\mathbf{q}$, then subtract α times Eq. (2.12).)

We can homogenize Eq. (2.12) by rewriting it in terms of the *excess pressure*, denoted by p, which is the pressure rise above equilibrium. Let the equilibrium pressure be P_0 (note that P_0 is a function of position, although ρ_o is not). Then the excess pressure is

$$p = p_\mathrm{t} - P_0. \tag{2.13}$$

For the equilibrium condition, we put $\dot{\mathbf{q}} = \mathbf{0}$ and $p_\mathrm{t} = P_0$ in Eq. (2.12) and find[3]

$$\mathbf{0} = -\frac{1}{\rho_\mathrm{o}} \nabla(P_0 + \rho_\mathrm{o} V). \tag{2.14}$$

Subtracting this from Eq. (2.12), and using Eq. (2.13) to write the result in terms of p, we obtain the desired linear homogeneous form:

$$\dot{\mathbf{q}} = -\frac{1}{\rho_\mathrm{o}} \nabla p. \tag{2.15}$$

2.1.3 One-parameter or thin-shell form

A third form of the equation of motion assumes a one-parameter (1P) distribution of pressure; that is, it assumes that the excess pressure p is a function of time and of a single spatial coordinate ξ, whose level surfaces may in general be curved. To facilitate concise discussion, the following terminology will be used throughout this thesis:

ξ-surface: surface of constant ξ;

ξ-trajectory: orthogonal trajectory to the ξ-surfaces;

ξ-tube: tube of ξ-trajectories, i.e. the surface generated by all the ξ-trajectories intersecting a simple closed curve contained in a ξ-surface;

ξ-shell: three-dimensional region between two infinitesimally close ξ-surfaces;

ξ-shell segment: three-dimensional region bounded by two infinitesimally close ξ-surfaces and a ξ-tube.

The 1P form of the equation of motion also assumes that ξ is an *arc-length coordinate*, i.e. that the ξ coordinate of a point R is the directed arc length along the ξ-trajectory from the surface $\xi = 0$ to the point R.[4] Familiar examples of arc-length coordinates are the three Cartesian coordinates and the radial coordinates in the cylindrical and spherical coordinate systems. For some examples of the mathematical objects defined above, we may replace ξ with the radial coordinate r in the

[3] For interest's sake, and for a check on the preceding work, we can use Eq. (2.14) to find the equilibrium pressure P_0. Since a function of position with zero gradient is constant, we see that $P_0 + \rho_\mathrm{o} V$ is equal to a constant, say P_m. Then

$$P_0 = P_\mathrm{m} - \rho_\mathrm{o} V.$$

If $\mathbf{g}$ is the acceleration due to gravity, we can take a Cartesian coordinate system with the z axis pointing upward and write $\mathbf{g} = -g\mathbf{k}$, for which a potential function is $V = gz$. The equilibrium pressure then becomes

$$P_0 = P_\mathrm{m} - \rho_\mathrm{o} g z$$

which shows the familiar variation of hydrostatic pressure with height.

[4] It will be shown in Chapter 4 that if p depends on only one spatial coordinate, that coordinate can be transformed to an arc-length coordinate. Hence the second assumption is redundant. In Chapter 5, it is further shown that the orthogonal trajectories to the level surfaces of an arc-length coordinate are straight lines; this justifies the assumed existence of ξ-tubes. For the moment, however, the single-coordinate assumption and the arc-length assumption will be treated as independent hypotheses, and the existence of ξ-tubes will be regarded as self-evident.

spherical coordinate system (r, θ, ϕ). An r-surface is a sphere centered on the origin. An r-trajectory is a ray emanating from the origin. An r-tube is a cone with its apex at the origin. An r-shell is a spherical shell of uniform infinitesimal thickness centered on the origin, or the region between two infinitesimally close concentric spheres centered on the origin. An r-shell segment is the region inside an r-shell and inside an r-tube.

Since p depends on no spatial coordinate but ξ,

$$\nabla p = \frac{1}{h_\xi} \frac{\partial p}{\partial \xi} \mathbf{e}_\xi \tag{2.16}$$

where h_ξ is the scale factor of ξ in the direction of $\nabla\xi$, and $\mathbf{e}_\xi$ is a unit vector in that direction. But ξ is an arc length, so its scale factor is unity. Hence, if we substitute the above equation into Eq. (2.15) and use a prime ($'$) to denote partial differentiation w.r.t. ξ, we obtain

$$\dot{\mathbf{q}} = -\frac{1}{\rho_o} p'(\xi, t)\, \mathbf{e}_\xi \tag{2.17}$$

showing that $\dot{\mathbf{q}}$ is in the direction of $\mathbf{e}_\xi$. Assuming quiescent initial conditions, it follows that $\mathbf{q}$ is also in the direction of $\mathbf{e}_\xi$. Hence we may write $\mathbf{q} = q\, \mathbf{e}_\xi$, reducing the above equation to the scalar form

$$\dot{q}(\xi, t) = -\frac{1}{\rho_o} p'(\xi, t). \tag{2.18}$$

Now consider a ξ-tube (as defined above) and let $S(\xi)$ denote the "normal cross-sectional area" of the tube, i.e. the area of the segment of a general ξ-surface bounded by the tube. Since $\mathbf{q}$ is normal to the ξ-surface, the total *volume velocity* (volume per unit time) crossing the ξ-surface within the tube is

$$u(\xi, t) = q(\xi, t)\, S(\xi). \tag{2.19}$$

In this thesis, "volume velocity" is also referred to as *volume flux* or simply *flux*. Differentiating Eq. (2.19) w.r.t. time and substituting from Eq. (2.18), we find

$$\dot{u}(\xi, t) = -\frac{1}{\rho_o} p'(\xi, t)\, S(\xi). \tag{2.20}$$

This may be rearranged to yield

$$-\frac{\partial p}{\partial \xi} = M_{\text{ad}}\, \dot{u} \tag{2.21}$$

where

$$M_{\text{ad}}(\xi) = \frac{\rho_o}{S(\xi)}. \tag{2.22}$$

These two equations introduce a concept that will unite most of the following chapters: electrical-acoustical analogs. This thesis will adhere to the so-called "impedance analogy" or "direct analogy" [11, pp. 51–2, 64–5], in which excess pressure p is analogous to voltage and flux u is analogous to current. With this convention, we see from Eq. (2.21) that M_{ad} is analogous to distributed inductance and that the inertial properties of a ξ-tube can be modeled by those of a transmission line; in electrical terms, Eq. (2.21) says that the voltage drop per unit length is equal to the inductance per unit length multiplied by the time-derivative of the current.

If Eq. (2.21) is multiplied by $d\xi$, it expresses the pressure drop across a ξ-shell segment in terms of the rate of change of flux and the (infinitesimal) shell thickness. Hence Eq. (2.21) may be described as the *thin-shell* form of the equation of motion.

2.1.4 Lumped-inertance (one-parameter incompressible) form

Consider a region bounded by a ξ-tube and two ξ-surfaces which are *not* infinitesimally spaced (it is tempting to call this a "ξ-cylinder", except that the cross-section is not necessarily uniform nor the "ends" necessarily planar). Because $\mathbf{q}$ is normal to every ξ-surface, it has no component normal to the ξ-tube, so the only flux into or out of the region flows through the "ends", i.e. through the ξ-surfaces. If we further assume that the fluid is incompressible, i.e. that volume is conserved, it follows that the flux into one end equals the flux out of the other, i.e. that $u(\xi, t)$ is independent of ξ. Therefore if we integrate Eq. (2.21) w.r.t. ξ from ξ_1 to ξ_2, we may take $\dot{u}$ outside the integration and obtain

$$p(\xi_1, t) - p(\xi_2, t) = M_\mathrm{a}\, \dot{u}(t) \tag{2.23}$$

where M_a, known as the *acoustic inertance* or *acoustic mass*, is given by

$$M_\mathrm{a} = \int_{\xi_1}^{\xi_2} M_\mathrm{ad}(\xi)\, d\xi = \int_{\xi_1}^{\xi_2} \frac{\rho_\mathrm{o}\, d\xi}{S(\xi)}. \tag{2.24}$$

Using the analogies given in the previous subsection, Eq. (2.23) shows that M_a is analogous to inductance; Eq. (2.24) corresponds to finding the total inductance of a length of transmission line by integrating the distributed inductance, while the assumption of incompressibility corresponds to the neglect of distributed capacitance.

A useful special case of Eq. (2.24) is found by assuming a constant cross section S and letting $l = \xi_2 - \xi_1$, so that l is the length of the tube segment (which now *is* a cylinder, albeit not necessarily of circular cross-section). The result is

$$M_\mathrm{a} = \frac{\rho_\mathrm{o} l}{S} \tag{2.25}$$

which is easy to remember because it looks like the formula for the resistance of a cylindrical wire. This result can also be written

$$M_\mathrm{a} = \frac{m}{S^2} \tag{2.26}$$

where $m = \rho_\mathrm{o} l S$ is the total mass in the tube segment.

The preceding three formulae are useful for modeling ports or vents in loudspeaker enclosures. The last two apply to cylindrical ports, while Eq. (2.24) applies to other regular geometries in which the 1P assumptions hold. These assumptions break down near the ends of the ports, and the motion of the fluid in the regions surrounding the ends may contribute significantly to the total effective acoustic mass; these "end effects" can be accounted for, at least approximately, by adding correction terms to the above formulae [11, pp. 132–3].

Eqs. (2.23) to (2.26) have been derived by assuming conservation of volume. Hence they are approximately true for a compressible fluid provided that any variation in flux from one cross-section to another is negligible, i.e. provided that the overall motion of the fluid dominates any variation due to compressibility.

2.2 Forms of the equations of continuity & compression

The equation of continuity expresses conservation of mass and, when combined with a relationship between pressure and density, yields the equation of compression.

Beginning with the most general integral form of the equation of continuity, this section proceeds to derive the equation of compression in a point form valid for *barotropic conditions* and *small compressions*. A volume integration then yields the integral form of the equation of compression, which can be particularized to give a uniform-pressure or lumped-compliance form (suitable for modeling chambers in loudspeaker enclosures) or differentiated to give a one-parameter or thin-shell form (useful in the theory of horns and ducts). In this case we do not obtain a neat sequence in which each form of the equation inherits the assumptions of its predecessor, but the assumptions are fewer than those required for the equation of motion.

2.2.1 Continuity: integral form

In a moving non-viscous fluid, let σ be a simple closed surface *fixed in an inertial coordinate system* (not moving with the fluid as in the previous section). Let $d\sigma$ denote the element of surface area and $\mathbf{n}$ the (outward) unit normal to σ. Let $\mathcal{V}$ represent the three-dimensional region enclosed by σ and let the differential volume element be $d\mathcal{V}$. By conservation of mass, the rate of change of mass inside $\mathcal{V}$ must equal the total rate of inward mass flow through the surface σ; that is

$$\frac{d}{dt} \iiint_{\mathcal{V}} \rho \, d\mathcal{V} = - \oiint_{\sigma} \rho \mathbf{q} \,.\, \mathbf{n} \, d\sigma. \tag{2.27}$$

2.2.2 Continuity: differential or point form

Reversing the order of differentiation and integration on the left of Eq. (2.27) and using the divergence theorem of Gauss on the right, we obtain

$$\iiint_{\mathcal{V}} \dot{\rho} \, d\mathcal{V} = - \iiint_{\mathcal{V}} \operatorname{div} (\rho \mathbf{q}) \, d\mathcal{V}. \tag{2.28}$$

Since this applies to every $\mathcal{V}$, we must have

$$\dot{\rho} = - \operatorname{div} (\rho \mathbf{q}) \tag{2.29}$$

which is the exact differential form of the equation of continuity (cf. Hsu [24], pp. 214–5). Note that the convention of Subsection 2.1.2 is followed here: the dot denotes partial differentiation w.r.t. time, which is appropriate because the volume $\mathcal{V}$ and all its differential elements are fixed, not moving with the fluid.

2.2.3 Compression: differential or point form

Now we invoke the assumption of small compressions. If the fluid velocity varies about a mean of zero, and if the variations in density are small compared with the mean density, then for the purpose of evaluating surface integrals of $\rho\mathbf{q}$ and hence $\operatorname{div} (\rho\mathbf{q})$, we may neglect the variations in density and consider only the variations in velocity. Thus we may replace ρ in Eq. (2.29) with the mean density ρ_{o}, which is uniform, so that we obtain

$$\dot{\rho} = -\rho_{\mathrm{o}} \operatorname{div} \mathbf{q}. \tag{2.30}$$

Converting this result into an equation of compression requires a relation between pressure and density. For this purpose we assume *barotropic* conditions; that is, we

assume that all intensive properties of the fluid, including density, are determined by the pressure. (The most useful set of conditions under which the barotropic assumption holds is described in the next subsection. More general conditions are given in Subsection 2.3.1.) If density is a monotonic increasing function of pressure, this function is invertible and the quantity $dp/d\rho$ is well defined and positive; let

$$\frac{dp}{d\rho} = c^2 \tag{2.31}$$

(this notation anticipates the result that c is the speed of sound). Under the assumption of small compressions it suffices to evaluate the above derivative at $\rho = \rho_o$, so that c may be regarded as a constant. Multiplying Eq. (2.30) by Eq. (2.31) and applying the chain rule on the left yields the equation of compression in the point form:

$$\dot{p} = -\rho_o c^2 \operatorname{div} \mathbf{q}. \tag{2.32}$$

2.2.4 Digression: Alternative expressions for c^2

The argument so far assumes small barotropic compressions of a non-viscous fluid. But the practical purpose of studying sound propagation in air (or another gas) allows much more specific assumptions.

First we may assume that the medium is an ideal gas, in which case its behavior satisfies the familiar equation of state

$$p_t V = n\bar{R}T \tag{2.33}$$

where p_t is the total pressure (assumed uniform over the sample), V is the volume of the sample, n is the amount of gas (in moles), $\bar{R}$ is the universal gas constant ($\mathrm{J\,K^{-1}\,mol^{-1}}$) and T is the absolute temperature. To put this equation in a more usable form, let $\bar{m}$ be the average molar mass (in kg/mol, *not* g/mol), m the total mass of the sample, and R the gas constant in terms of mass ($\mathrm{J\,kg^{-1}\,K^{-1}}$). Then we may write

$$n = m/\bar{m}\,;\ \bar{R} = R\bar{m}. \tag{2.34}$$

Substituting these expressions into the equation of state and dividing through by V yields

$$p_t = \rho R T \tag{2.35}$$

which involves only intensive quantities. Note that R is not the universal gas constant but depends on the molecular or molar mass of the particular gas. At equilibrium with nearly uniform density, this result reduces to

$$P_0 = \rho_o R T. \tag{2.36}$$

Second, we may assume that compressions of the gas are adiabatic, i.e. that there is no conduction of heat and, in particular, no conduction of the heat of compression. This is reasonable at audible frequencies because the excess pressure alternates rapidly, leaving little time for heat conduction during a single pressure excursion, and because the pressure changes average out to zero, so that there is no long-term accumulation of energy of compression. If V denotes the volume of a

fixed mass of gas and $p_t = P_0 + p$ is the total pressure, the adiabatic compression of the sample is described by

$$(P_0 + p)V^\gamma = \text{constant} \tag{2.37}$$

[9, pp. 139–40], where γ, concisely called the "ratio of specific heats", is defined as C_p/C_v, where C_p and C_v are the specific heats at constant pressure and constant volume, respectively. For ideal gases, this ratio is insensitive to temperature and pressure, being approximately 5/3 for monoatomic gases, and 7/5 for diatomic gases including air [21, p. *3*-4, 71].

For a given mass, the volume V is inversely proportional to the density ρ, so that Eq. (2.37) may be rewritten

$$(P_0 + p)\rho^{-\gamma} = \text{constant}. \tag{2.38}$$

Differentiating both sides w.r.t. ρ, putting $\rho = \rho_o$ and $p = 0$ (for small compressions), writing c^2 for $dp/d\rho$ and solving for c^2, we obtain

$$c^2 = \frac{\gamma P_0}{\rho_o}. \tag{2.39}$$

Substituting from Eq. (2.36) gives the alternative formula

$$c^2 = \gamma RT. \tag{2.40}$$

For a given gas, R and γ may be assumed constant, so that c is a function of temperature alone.

It has not yet been shown that c is the speed of sound, but the above substitutions for c^2 are of interest in developing further forms of the equation of compression. It is especially useful to note, from Eq. (2.39), that

$$\rho_o c^2 = \gamma P_0. \tag{2.41}$$

Eq. (2.31) can also be written in the form

$$dp = c^2 d\rho = \rho_o c^2 \frac{d\rho}{\rho_o}. \tag{2.42}$$

Since $d\rho/\rho_o$ is the fractional condensation, it follows that $\rho_o c^2$ is the *adiabatic bulk modulus of elasticity* of the medium. Of course this fact may be used to calculate c in any inviscid fluid whose density and adiabatic bulk modulus are known. For an ideal gas, Eq. (2.41) indicates that the adiabatic bulk modulus is γP_0; for a given gas, this is a function of pressure alone.

2.2.5 Compression: integral form

Let $\mathcal{V}$ and σ be defined as in the derivation of the integral form. Taking volume integrals of both sides of Eq. (2.32) over the region $\mathcal{V}$ and using the divergence theorem on the right gives

$$\iiint_{\mathcal{V}} \dot{p}\, d\mathcal{V} = -\rho_o c^2 \oiint_{\sigma} \mathbf{q} \,.\, \mathbf{n}\, d\sigma. \tag{2.43}$$

2.2.6 Compression: lumped-compliance (uniform-pressure) form

Let us assume that the region under consideration is sufficiently small, or the variation with time sufficiently slow, that the excess pressure p may be considered uniform (but not necessarily constant in time). Then we can take $\dot{p}$ outside the volume integral in Eq. (2.43) and obtain the form

$$\dot{p} \iiint_{\mathcal{V}} d\mathcal{V} = -\rho_o c^2 \oiint_{\sigma} \mathbf{q} \,.\, \mathbf{n} \, d\sigma. \tag{2.44}$$

Now the volume integral on the left is just the volume of the region $\mathcal{V}$, which is constant; let this volume be V_a ("acoustic volume"). The surface integral on the right is the volume flux out of the region; with the minus sign it becomes the flux into the region, denoted by u, and is a function of time. (While the volume of the region is fixed, fluid volume is not necessarily conserved because p and hence ρ may vary with time; remember that ρ is only approximately equal to ρ_o. Hence we have the paradox of volume flowing into a fixed volume.) Thus we have

$$\dot{p} \, V_a = \rho_o c^2 u. \tag{2.45}$$

This may be written

$$u = C_a \, \dot{p} \tag{2.46}$$

where

$$C_a = \frac{V_a}{\rho_o c^2}. \tag{2.47}$$

C_a is called the *acoustic compliance* of the volume V_a. Substituting Eq. (2.41) into Eq. (2.47) gives the alternative form

$$C_a = \frac{V_a}{\gamma P_0} \tag{2.48}$$

which shows that the compliance of a given volume of air depends on the atmospheric pressure but not on the temperature.

When p is analogous to voltage and u to current, Eq. (2.47) shows that C_a is analogous to capacitance. The "potential" on one plate of the "capacitor" is p; the other plate is grounded, and the "current" to ground is u. Since p is the pressure rise above equilibrium, the equilibrium pressure is analogous to ground potential.

2.2.7 Compression: one-parameter or thin-shell form

Using the assumptions and notations of Subsection 2.1.3, we may take $\mathcal{V}$ in Eq. (2.43) as the region bounded by a ξ-tube and two ξ-surfaces, and divide $\mathcal{V}$ into ξ-shell segments by writing $d\mathcal{V} = S(\xi) \, d\xi$. Eq. (2.43) then becomes

$$\int_{\xi_1}^{\xi_2} \dot{p}(\xi, t) \, S(\xi) \, d\xi = -\rho_o c^2 \left(u(\xi_2, t) - u(\xi_1, t) \right). \tag{2.49}$$

Differentiating w.r.t. ξ_2 and writing ξ for ξ_2 yields

$$\dot{p}(\xi, t) \, S(\xi) = -\rho_o c^2 \, u'(\xi, t) \tag{2.50}$$

which may be rearranged to give

$$-\frac{\partial u}{\partial \xi} = C_{\text{ad}}\,\dot{p} \tag{2.51}$$

where

$$C_{\text{ad}}(\xi) = \frac{S(\xi)}{\rho_{\text{o}} c^2}. \tag{2.52}$$

C_{ad} is called the distributed acoustic compliance (acoustic compliance per unit length). Again, using Eq. (2.41), the denominator in the above result may be replaced by γP_0.

With the established electrical-acoustical analogies, Eq. (2.51) shows that the ξ-tube is analogous to a transmission line and C_{ad} is analogous to distributed capacitance; in electrical terms, the equation says that the capacitive current leakage per unit length is equal to the capacitance per unit length multiplied by the time-derivative of voltage.

If Eq. (2.51) is multiplied by $d\xi$, it expresses the net flux into a ξ-shell segment in terms of the rate of change of pressure and the (infinitesimal) shell thickness. Hence Eq. (2.51) may be described as the *thin-shell* form of the equation of compression.

2.3 Velocity potential

2.3.1 Existence[5]

If the fluid velocity is denoted by $\mathbf{q}$, a velocity potential is a scalar field ψ such that

$$\mathbf{q} = -\nabla\psi \tag{2.53}$$

(note that the minus sign is used for scalar potential functions in this thesis, in keeping with electrostatic conventions). To establish the existence of a velocity potential in a fluid, it is sufficient that

(a) the fluid is non-viscous (this is obviously an approximation);

(b) the fluid is *barotropic*; that is, the density depends only on the pressure;

(c) any external forces acting on the fluid (e.g. gravity) are conservative, and

(d) the *initial* fluid velocity is everywhere zero, or at least irrotational.

Given the first three conditions, we can apply Kelvin's theorem, also called the law of conservation of circulation, which states [24, pp. 219–20]

$$\oint_{\mathcal{C}} \mathbf{q}\,.\,d\mathbf{r} = \text{constant}\,, \tag{2.54}$$

where $\mathbf{q}$ is the fluid velocity and $\mathcal{C}$ is a closed contour *moving with the fluid*. The quiescent initial condition (d) implies that the constant in this equation is zero, so that the same equation applies to *every* closed curve $\mathcal{C}$ (and it no longer matters

[5] A discussion similar to the one in this subsection appeared in an appendix to the author's 1993 paper [43]. The author has produced this information independently, but presumes that it is not new.

whether the curve moves with the fluid). Hence, by Stokes' theorem, we have the irrotational flow condition

$$\operatorname{curl} \mathbf{q} = \mathbf{0} \tag{2.55}$$

which implies the existence of a scalar ψ satisfying Eq. (2.53).

One can also establish more elementary conditions under which the barotropic assumption (b) holds. Sufficient conditions are:

(i) The fluid contains only one phase, i.e. is a pure substance or a solution, and not a heterogeneous mixture;

(ii) Compression/expansion of the fluid is adiabatic;

(iii) The fractional composition of the fluid is invariant (so all chemical components are compressed and expanded in the same ratio);

(iv) Initial conditions are uniform.

A general proof of sufficiency may be constructed using the Gibbs phase rule

$$\Phi = C - P + 2 \tag{2.56}$$

where Φ is the number of degrees of freedom in the intensive properties, C is the number of chemical components and P is the number of phases (see Barrow [9], pp. 315–20). By condition (i), we have $P = 1$, so that the rule reduces to

$$\Phi = C + 1. \tag{2.57}$$

Now, condition (ii) takes away one degree of freedom, and condition (iii) takes away $C - 1$ degrees because the fractional composition is determined by specifying the mass fractions or molar fractions of all but one component. That leaves one degree of freedom, so that specifying one intensive property (e.g. pressure) determines all others (including density). The relationship between the properties will depend on the initial conditions (the adiabatic assumption forbids transfer of heat energy but does not specify the initial energy content), so if the initial conditions are uniform, density will be a function of pressure alone throughout the fluid. (Note: The notations in Eqs. (2.56) and (2.57) will not be used again.)

As an example, an ideal gas of fixed fractional composition is described by the ideal gas equation, which has two degrees of freedom. The adiabatic assumption takes away one degree, so that the barotropic assumption is satisfied if initial conditions are uniform.

In air, all four conditions tend to be good approximations. Condition (i) requires that the air be free of dust and mist. Condition (ii) requires that acoustic disturbances propagate much faster than thermal disturbances. Condition (iii) requires that if there is any diffusion of chemical components in response to nonuniform compression, the diffusion is very slow compared with the propagation of the acoustic disturbance. Condition (iv) requires, among other things, that the pressure variation due to gravity is negligible—the low-gravity assumption.

The most important point in the preceding discussion is that the existence of ψ is guaranteed by irrotational flow, which was one of the explicit assumptions made in deriving the linearized point form of the equation of motion. It was also suggested, however, that the irrotational assumption was made redundant by the

assumption of small oscillations. In that case, we may look at the sufficient conditions for the existence of ψ, and note that (a) and (c) were assumed in deriving the point form of the equation of motion, (b) was assumed in deriving all four forms of the equation of compression, and (d) is a *weakened* form of the ubiquitous quiescent-initial-conditions assumption without which some basic concepts in linear systems—such as the transfer function—become meaningless, and which was used without apology in deriving the 1P form of the equation of motion. If we accept the quiescent-initial-conditions assumption as universal, we may conclude that whenever we use the point forms of the equations of motion and compression, or any other forms derived therefrom, we can also use velocity potential without further loss of generality.

2.3.2 Relationship to excess pressure

To find an equation relating between ψ and p, we combine the definition of ψ with the point form of the equation of motion: substituting Eq. (2.53) into Eq. (2.15) gives

$$\nabla p = \nabla(\rho_o \dot{\psi}) \tag{2.58}$$

which implies that

$$p = \rho_o \dot{\psi} + A(t) \tag{2.59}$$

where A is an arbitrary function of time (independent of location). This is the equation of motion expressed in terms of ψ. As we are defining ψ, we might as well take $A = 0$, so that

$$p = \rho_o \dot{\psi}. \tag{2.60}$$

We shall see, however, that there are some theoretical purposes for which the more general Eq. (2.59) can be used.

2.4 The wave equation

The wave equation is obtained by combining the point forms of the equations of motion and compression: differentiating Eq. (2.32) w.r.t. time and substituting from Eq. (2.15) gives the d'Alembert equation

$$\ddot{p} = c^2 \nabla^2 p \tag{2.61}$$

and confirms that c, as defined by Eq. (2.31) and calculated by Eqs. (2.39) and (2.40), is the speed of sound. We can then use the wave equation and the equation of motion as the basic equations describing the acoustic field.

Eq. (2.61) has p as the wave function. We can also obtain a wave equation in ψ by combining the point forms of the equations of motion and compression, provided that both equations are first expressed in terms of ψ. For the equation of motion we use Eq. (2.60) (although we can also a form of Eq. (2.59) in which A is a constant, not necessarily zero). For the equation of compression we substitute Eq. (2.53) into Eq. (2.32) and obtain

$$\dot{p} = \rho_o c^2 \nabla^2 \psi. \tag{2.62}$$

Differentiating Eq. (2.60) w.r.t. time and substituting the result into Eq. (2.62) gives

$$\ddot{\psi} = c^2 \nabla^2 \psi. \tag{2.63}$$

We can then use Eqs. (2.63), (2.53) and (2.60) as the basic acoustic field equations.

2.4.1 Further discussion of approximations

Having established the wave-like nature of the acoustic field, we can refine the meaning of "small oscillations" and "small compressions". The derivation of Eq. (2.6) makes it clear that the term $\partial\mathbf{q}/\partial t$ is due to the changing velocity field, which may be understood as the motion of waves over the equilibrium position of the particle, while the term $(\mathbf{q}.\nabla)\mathbf{q}$ is due to the motion of the particle within the field. So the second term will be negligible if the fluid motion is slow compared with the wave motion, i.e. if

$$|\mathbf{q}| \ll c. \tag{2.64}$$

The term $(\mathbf{q}.\nabla)\mathbf{q}$ gives rise to the two nonlinear terms on the left of Eq. (2.9), which are said to be negligible if $\mathbf{q}$ is "sufficiently small". We now see that a "sufficiently small" velocity is one whose magnitude is small compared with the speed of sound. Multiplying both sides of the inequality (2.64) by a time constant comparable with a period of oscillation, we see that the displacement of each particle from equilibrium must be much smaller than a wavelength. This in turn means that the fractional changes in density are very small, which is the "small compressions" assumption. So the assumptions of small oscillations and small compressions are in fact equivalent.

2.5 Acoustic circuits

2.5.1 Ohm's law and Kirchhoff's laws

The analysis of electrical circuits involves two kinds of equations. An equation of the first kind relates the voltage(s) and current(s) in a single component. Ohm's law for a resistor is the most familiar example. For an inductor or capacitor, the differential relationship between voltage and current can be converted to an equation resembling Ohm's law using phasors or transforms. In a component having three or more terminals, "mutual" or "transfer" quantities may appear. Equations of the *second* kind apply not to the components themselves, but to their interconnections. They arise from Kirchhoff's laws, which relate the currents into each node and the voltage drops around each loop; the properties of *circuits* and their *topologies*, as distinct from the components therein, are contained in these laws.

Equations expressing the properties of some acoustic components have been derived in this chapter. We have seen that acoustic mass is analogous to inductance, and acoustic compliance to capacitance. Subsection 2.5.2 will define an acoustic resistance analogous to electrical resistance. The concepts of acoustic transfer resistance and transconductance (with obvious electrical analogs) will be used in Chapter 10. If these electrical analogs are to be of any use in the analysis of acoustic systems, acoustic components must be connected into circuits. To see how this should be done—or whether it can be done at all—we require acoustical equivalents of Kirchhoff's laws.

Kirchhoff's voltage law follows immediately from the fact that electrostatic potential is a point function, i.e. a function of position. The acoustic analog of voltage is pressure, which is also a point function. Thus we have "Kirchhoff's pressure law": the sum of the pressure drops around a loop is zero. If two or more acoustic components are connected end-to-end (perhaps via regions of constant pressure, analogous to conductors which are regions of constant potential), the pressure drops across

the components are additive; hence the voltage drops across the analogous electrical components must also be additive, so that the electrical components may be connected in series—i.e. end-to-end. Thus there is a topological similarity between acoustic and electrical series connections.

Kirchhoff's current law expresses conservation of charge, which is the time integral of current. The acoustic analog of current is volume flux, whose time integral is volume. Because air is compressible, volume is *not* conserved. It has been shown, however, that the compressibility of air can be modeled by acoustic compliances. These may be understood as places where volume is stored and reclaimed, rather than destroyed and created. Thus we can assume conservation of volume provided that all significant compression or expansion in the system is explicitly represented using compliance elements. For example, if air is flowing into a chamber in which the pressure is assumed uniform (but time-dependent), the pressure in the chamber is the pressure (analogous to voltage) at a circuit node, and the compressibility of the air is indicated by a compliance connected between that node and ground, in accordance with Eqs. (2.46) and (2.47). Having added compliances where necessary so as to obtain conservation of volume, we may exploit "Kirchhoff's flux law": the sum of the fluxes into a node is zero. If several acoustic components, including any necessary compliances, have a common junction, the sum of fluxes from the components into that junction is zero; hence the sum of the currents in the analogous electrical components is zero, so that these currents may be directed into a single node. Thus there is also a topological similarity between acoustic junctions and electrical nodes.

In summary, as long as the significant changes in volume in an acoustic system are represented by compliances, Kirchhoff's laws hold and the system can be represented as an equivalent circuit. The form of the circuit is made obvious by the topological similarity between the acoustic and electrical systems. Of course, certain conditions were assumed in the definitions of lumped and distributed acoustic components, and these conditions limit the applicability of the conventional equivalent-circuit approach. For example, the common practice of modeling a loudspeaker enclosure as a lumped compliance is valid only at low frequencies, because the lumped-compliance form of the equation of compression assumes uniform excess pressure throughout the volume. The theory presented in Chapter 6 will extend the applicability of equivalent-circuit methods.

2.5.2 Acoustic resistance and impedance

A vented box is a resonant circuit comprising the acoustic compliance of the box and the acoustic mass of the vent. If such a box is constructed with dimensions typical of a bass-reflex loudspeaker enclosure, but without any internal lining or apertures for the insertion of drivers, its resonance may have a Q of 50 to 100 [50, p. 320], indicating that the damping effect of the viscosity of air is slight, even in the constricted flow through the vent. Thus the neglect of viscosity in macroscopic regions of unobstructed air is well justified.

Because of the viscosity of air, the cylindrical wall of the vent imposes not only zero normal velocity, but also zero *tangential* velocity. If a grille—or some other fine, rigid, permeable structure—is inserted in the vent, that boundary condition is imposed at frequent intervals across the aperture of the vent, so that viscosity may

become the dominant influence on the airflow. By deliberately exploiting viscosity in this way, one can construct an acoustic component with the property that the flux through the component is proportional to the pressure drop across it. The ratio of pressure to flux is *acoustic resistance* (or pneumatic resistance), and is analogous to electrical resistance. In this thesis, acoustic resistance has the symbol R_{a} (perhaps with additional subscripts).

Acoustic impedance, denoted by Z_{a}, is obviously a generalization of acoustic resistance in which the pressure and flux are represented by phasors or transforms. This thesis, wherever possible, uses lower-case characters for time-dependent quantities and the corresponding upper-case characters for their phasor representations. Thus the phasor forms of p, $\mathbf{q}$ and ψ are P, $\mathbf{Q}$ and Ψ, respectively. In most cases, the word "phasor" may be read as "phasor or Fourier transform" because both transformations result in the operational substitution

$$\frac{\partial}{\partial t} \rightarrow j\omega \tag{2.65}$$

(the phasor form assumes a time-dependent factor $e^{j\omega t}$). Like electrical impedance, acoustic impedance is in general a complex, frequency-dependent quantity.

The acoustic impedance of an aperture is the ratio of the *average* excess pressure over the aperture to the flux through the aperture; the "average" pressure is area-weighted and both pressure and flux are expressed as phasors or transforms. Because pressure is measured w.r.t. the equilibrium atmospheric pressure, the impedance appears between the aperture and "ground". If the aperture contains a (driven or passive) diaphragm, the pressures on the two sides of the diaphragm will differ; hence we may speak of the acoustic impedance "seen" by each side of the diaphragm, defining each in terms of the pressure on one side and the flux away from the diaphragm. If the aperture opens into an infinite expanse of free air—or a sufficiently large expanse to show traveling waves diverging from the aperture—the impedance of the aperture is called a *radiation impedance* (denoted by Z_{ar}). So a radiation impedance appears between the aperture and ground. It may also be understood as appearing between the aperture and a "surface at infinity" because the excess pressure approaches zero at large distances.

Acoustic admittance is obviously the reciprocal of acoustic impedance. Other impedances and admittances can be defined on a differential or "per unit area" basis. These will be introduced in Subsections 3.3.4, 3.3.5 and 6.5.3.

2.5.3 Reasons for using the direct analogy

As seen in Subsection 2.5.1, the use of the direct analogy—voltage for pressure and current for flux—produces some topological similarity between the acoustic system and its equivalent circuit. The similarity arises because the pressure drop, like a voltage drop, is an "across" variable, while a flux, like a current, is a "through" variable. The dual analogy—current for pressure and voltage for flux—may still permit the construction of an electrical circuit satisfying the same differential equations as the acoustic system, but the topological analogies will be switched—loops will become nodes and vice versa. Hence, whereas the direct equivalent circuit can often be drawn by inspection of the acoustic system, the dual circuit is more difficult to construct.

One argument in favor of the dual analogy is that it allows the transduction equations of a moving-coil driver to be represented by a transformer [25, pp. 109–10], which can then be eliminated by "referring" the secondary circuit to the primary. It may even be possible to obtain a transformerless circuit (with "referred" acoustic components) directly from the system equations; this was demonstrated by Locanthi [33] for a moving-coil driver in a sealed or vented enclosure. Before fast digital computers became widely available, these techniques were useful because they gave physically realizable circuits that could be built on breadboards and tested in the laboratory—*before* incurring the expense of building an acoustic prototype. But with the availability of circuit-analysis software such as SPICE, the realizability of the equivalent circuit has become irrelevant and the case for the dual analogy has been consequently weakened.

The greater part of this thesis concerns itself with the analysis of two- and three-dimensional acoustic fields by equivalent-circuit methods. For this purpose, it is absolutely necessary that the adopted electrical-acoustical analogy should be meaningful in three dimensions. First consider the direct analogy. Pressure and electrostatic potential are scalar quantities and are well-defined in one, two or three dimensions. Flux and current are also scalars, but in three dimensions they are defined in terms of components of vectors: flux is the dot product of velocity and vector area, while current is the dot product of current density and vector area. As these relationships hold for all orientations of the vector area (whose direction is that of the normal to the surface element), we see that velocity is analogous to current density. As velocity and current density are both vectors, the direct analogy is acceptable. But in the dual analogy, in which pressure corresponds to current and flux to voltage, only one quantity of each analogous pair is defined as a dot product with area, so we cannot find a meaningful acoustic analog for current density, nor a meaningful electrical analog for velocity. Hence, in this thesis, the need for extensibility to three dimensions requires the use of the direct analogy.

2.5.4 Analogous, equivalent and pseudo-equivalent circuits

According to Hunt [25, pp. 108–9], the term *analogous circuit* applies to a true electrical circuit whose behavior models that of a non-electrical system. The voltages and currents in the circuit represent "effort" and "flow" variables in the non-electrical system, using scale factors which are not just dimensionless numbers. Time may also be scaled. Before digital computers were widely available, such a circuit would be built and studied in the laboratory; hence the requirement of physical realizability became attached to the meaning of "analogous".

This chapter has made free use of the words "analog" and "analogous" in describing "electrical" models of acoustic systems. But the circuits are not electrical; they are acoustic. The quantities in the circuits are not analogous to acoustic quantities, but identical with them—the "voltages" and "currents" are not voltages and currents, but pressures and fluxes, and so on. The circuits use no scale factors and do not need to be physically realizable. Such circuits, according to Hunt, should be called *equivalent circuits* rather than analogous circuits.

Hence some of the terminology used in this chapter has been imprecise. In the following chapters, the term "equivalent circuit" will be adopted, and the word "electrical" will become rare. But the words "analog" and "analogous", together with

electrical quantities such as voltage, current, inductance and capacitance, will not disappear from acoustical contexts, because the conceptual advantages of equivalent circuits obviously depend on the use of electrical terms. These terms are rendered inaccurate by the lack of scaling and unit-conversions in the equivalent circuits; thus, paradoxically, the price of direct modeling is loose terminology.

The product of pressure and flux, like that of voltage and current, is power.[6] Hence, in a system involving electrical and acoustic components, we often find that the electric-acoustic interface can be modeled using power-conserving two-port devices; an example of this will be seen in Chapter 10. There are other "circuit" models which are "equivalent" in the sense that the effort and flow variables are literally represented (without scaling or unit-conversion), but in which the product of the two variables is not power. We may describe such a model as a *pseudo-equivalent circuit*, following the example of Karnopp and Rosenberg [28, p. 65].

The most familiar example of a pseudo-equivalent circuit is the "heat circuit" in which voltage and current are analogous (in the loose sense) to temperature and heat flow, respectively. The product of these variables is not power; rather, heat flow itself is a power. A heat circuit will be used in Chapter 8 to estimate a thermal time constant pertaining to a fiber-filled loudspeaker enclosure. Another heat circuit (in which the variables are defined "per unit volume") will be used in Chapter 7 to determine the relationships between the various thermal time constants of the air-fiber system. Because these heat circuits are pseudo-equivalent circuits, the interface between the acoustic and thermal domains will not be visible in the *acoustic* circuit derived in Chapter 7; rather, the equations derived from the heat circuit will be used in an analytical derivation of the acoustic circuit. Hence the values of the acoustic components called ΔR_{th} and ΔC_{th}, representing the influence of the thermal properties of the fiber, will be less intuitive than those of other components in the acoustic circuit.

[6] If pressure is expressed as the sum of the equilibrium pressure P_0 and the excess pressure p, the product of P_0 and flux averages to zero (in a system with sinusoidal or alternating velocity), so that only the excess pressure p needs to be considered when calculating *average* power.

Chapter 3

The "Webster" horn equation

> . . . it is well known that very little sound is emitted by the phonograph or the telephone with the horn taken off, although in the former case the motion of the diaphragm is exactly the same. . .
>
> — A. G. Webster [62, p. 277], May 1919.

> Contrary to the prevalent conception, the horn does not merely gather up the sound energy from the receiver and concentrate it in certain directions. Its relation to the diaphragm is much more intimate. It causes an actual increase in the load on the diaphragm, making it advance against a greater air pressure, and withdraw from a greater opposing rarefaction. Anyone can assure himself that the average sound energy in a room is greatly reduced on removing the horn from a good loud speaker. And frequently when the horn is removed the amplitude of vibration of the diaphragm becomes so great that it strikes against the pole pieces.
>
> — C. R. Hanna & J. Slepian [22, p. 393], February 1924.

Similarly, anyone who plays a trumpet can assure himself that the average sound energy in a room is greatly reduced on removing the trumpet from his vibrating lips. The diaphragm of an acoustic phonograph is an almost ideal flux source (if it is not so heavily loaded that it mistracks), so that its power output is proportional to the equivalent series acoustic resistance of the load. That resistance is very low in free air, but is increased by attaching a horn. The diaphragm of a moving-magnet receiver is not a pure flux source (wherefore it may strike the pole pieces if the horn is removed), but it is still a high-impedance source. In free air, the load impedance is too low for efficient power transfer, but a horn improves the impedance match. The same principle applies to the trumpeter's lips or the reed of a clarinet.

Thus a horn is an impedance-matching device. In a phonograph or loudspeaker, the impedance at the "throat" of the horn must present an appropriate load over a wide frequency range. In a trumpet or clarinet, the horn gives the best loading at certain harmonically-related resonance frequencies.

Accordingly, Webster (quoted above) was interested in calculating the impedance at one end of a horn, given the profile of the horn and the impedance at the other end. He began his historic paper [62] by defining "acoustical impedance" as the ratio of pressure to volume *displacement*. But he also considered current to be analogous to volume *velocity* or flux, and consequently remarked that "the definition as given above makes our impedance lead by a right angle the usual definition." After giving

a few applications of the impedance, he introduced the heading "Tubes and Horns" and proceeded to derive the famous differential equation

$$\frac{\partial^2 p}{\partial t^2} = c^2 \left[\frac{1}{S} \frac{\partial}{\partial x} \left(S \frac{\partial p}{\partial x} \right) \right] \tag{3.1}$$

where p is the instantaneous excess pressure, t the time, c the speed of sound, x the distance along the axis of the horn, and $S(x)$ the cross-sectional area (Webster's notation was different; the notation of the present thesis will usually be used when quoting him). Webster obtained the bilinear impedance-transformation functions in terms of the solutions to this equation. He then found the solutions and transformations for a cylindrical tube and a conical horn, and the solutions for an exponential horn.[1] His impedance transformations look unfamiliar to modern readers because of his idiosyncratic (but pioneering) definition of impedance.

In Webster's time, it was not possible to obtain sufficient acoustic output from a phonograph or loudspeaker without an impedance-matching horn. In modern times, high-powered amplifiers have reduced the importance of efficiency in loudspeakers, so that the motivation for using horns may have more to do with control of directivity than with matching of impedances [18, pp. 554–6]. But even if the impedance-transforming property of a horn is not the reason for its use, that property still exists and must be taken into account in the audio system design. As Webster's equation offers the simplest available approach to this problem, it is necessary to determine the conditions under which the equation is applicable.

3.1 Classical derivations (1760–1948)

Webster was not the first author to publish a differential equation describing the oscillations of a compressible fluid in a tube of varying cross-section. According to Eisner [16], that distinction belongs to Lagrange, who published his work in 1760 or 1761. Lagrange derived the equation for "a pipe whose shape is a general conoid", solved it explicitly for a cone and a wedge (cylindrical sector), and gave a solution procedure for the case $S \propto x^m$. Daniel Bernoulli derived the equation for a tube of arbitrarily variable cross-section and solved it for a cone; he apparently did this before Lagrange, but did not publish the work until 1764. Euler studied propagation in two and three dimensions (inventing the method of separation of variables), and in a tube of arbitrarily varying *small* cross-section with finite amplitude and non-uniform fluid density.

Eisner [16] could find only one 19th-century publication on sound in tubes of arbitrarily variable cross-section. That work, by H. L. F. von Helmholtz, concerned short non-cylindrical sections joined to cylindrical tubes, and did not contain Eq. (3.1) explicitly. Helmholtz was the teacher of Webster [63]. (The discussion from this point onwards uses primary sources and no longer relies on Eisner.)

An equation equivalent to Eq. (3.1), but applicable only to axisymmetric tubes, was published in 1916 by Lord Rayleigh [45]. The main steps in the derivation were

[1] Note that Webster subsequently published a list of errata in his paper, which critically affected the solutions for the exponential horn (see the Bibliography under reference [62]). The 1977 reprint of the paper in the *Journal of the Audio Engineering Society* (see under [62]) does not include Webster's corrections. One typographical error that escaped Webster's notice is in his Eq. (21), where "d^2/dt^2" should read "d^2/dx^2".

as follows:

1. Write the Helmholtz equation (the phasor form of the wave equation, with $k = \omega/c$) in the cylindrical coordinates x (axial) and r (radial);

2. Solve the equation as an ordinary differential equation in the independent variable r, treating the differential operator $\partial^2/\partial x^2$ as a coefficient, and expressing the solution as the product of the axial wave function $F(x)$ and a Bessel function in which the operator $\partial^2/\partial x^2$ appears as a term inside the argument;

3. Using a series expansion of the Bessel function, find the derivatives of the solution w.r.t. r and x;

4. Set the ratio of these derivatives so as to satisfy the boundary condition at the wall; this requires expanding the product of two infinite series in increasing powers of the second-order operator $(k^2 + \partial^2/\partial x^2)$.

Rayleigh's Eq. (8), which is equivalent to the above Eq. (3.1) with the axial wave function $F(x)$ as the dependent variable, can then be obtained by neglecting all terms of order higher than 2, i.e. all but the first term on the right of his Eq. (6). Rayleigh's explanation of this step is unclear. His Eq. (8) is then used to find substitutions for higher-order terms in his Eq. (6), leading to an improved axial wave equation, for which an approximate solution is given in terms of indefinite integrals.

Rayleigh's derivation is of interest here because, like the present author's derivation in Chapter 4, it obtains the horn equation *from the wave equation*. However, whereas Rayleigh's derivation is approximate, the derivation to be given in Chapter 4 is exact when its assumptions are satisfied.

Webster's paper [62], which was read at a meeting in 1914 but not published until 1919, is primarily concerned not with the derivation of Eq. (3.1), but with the uses of impedance and the calculation of impedance transformations in horns. Hence its status is not greatly diminished by the prior discoveries and rediscoveries of the horn equation. Moreover, Webster's rediscovery of the equation led to solutions of engineering problems raised by the invention of the telephone and the phonograph. The practical and economic importance of these devices made it inevitable that Webster's name would become attached to the basic equation.

Webster also obtained the horn equation from the wave equation; but instead of assuming a tube of revolution, he assumed an *infinitesimal cross-section* (like Euler). His Eq. (18) is an equation of compression in terms of pressure and displacement, and may be written

$$p = -\rho_o c^2 \operatorname{div} \mathbf{q} = -\rho_o c^2 \frac{1}{S} \frac{\partial}{\partial x} (Sq) \tag{3.2}$$

where $\mathbf{q}$ in this case represents the displacement instead of the velocity, and q is its axial component.[2] The substitution for $\operatorname{div} \mathbf{q}$ is unexplained. Webster's "deriva-

[2]This q is Webster's symbol. An usual feature of the mathematical arguments in this thesis is that the fluid displacement does not appear in any equations. Hence no symbol for displacement is needed, except when quoting other authors. Neither does this thesis require a symbol for the "condensation" (fractional change in density).

tion" of the horn equation is entirely contained in his Eq. (19), which may be expressed in modern notation as

$$\frac{\partial^2 p}{\partial t^2} = c^2 \nabla^2 p = c^2 \left[\frac{1}{S} \frac{\partial}{\partial x} \left(S \frac{\partial p}{\partial x} \right) \right]. \tag{3.3}$$

The left-hand equality is obviously the wave equation, while the expression in square brackets on the right is an unexplained substitution for $\nabla^2 p$. (Webster used the notations "div" and "grad", together with "Δ" for the Laplacian operator.) The substitution for the Laplacian may have been inspired by the substitution for the divergence in the previous equation, but the two equations are otherwise unrelated. Webster's Eq. (20) can be written

$$\frac{\partial^2 q}{\partial t^2} = -\frac{1}{\rho_o} \frac{\partial p}{\partial x} = c^2 \frac{\partial}{\partial x} \left[\frac{1}{S} \frac{\partial}{\partial x} (Sq) \right] \tag{3.4}$$

where q again is the axial displacement. The left-hand equality is the equation of motion, while the right-hand equality follows from a substitution for pressure taken from the earlier Eq. (18). The result is a second "horn equation" involving displacement instead of pressure. Thus Webster's Eq. (18) leads to his Eq. (20), but this train of reasoning is interrupted by the famous Eq. (19), making the whole argument difficult to follow.

Derivations based on the wave equation, like those of Rayleigh and Webster, have the advantage that they are valid for both the excess pressure and the velocity potential, both of which are modeled by the wave equation to the same approximation (Section 2.4).

Hanna and Slepian (quoted at the beginning of this chapter) derived the horn equation in an appendix to their 1924 paper [22]. Their Eq. (49) is equivalent to Eq. (3.1) when the adiabatic bulk modulus (k in their notation) is replaced by $\rho_o c^2$, but this substitution is not made until the equation has been solved for an exponential horn. The derivation of their Eq. (49) does *not* require an infinitesimal cross-section, but assumes the existence of a family of wavefront surfaces having the following properties:

- Pressure is uniform over each wavefront;
- Velocity is uniform over each wavefront;
- Velocity is normal to the wavefronts;
- The perpendicular distance between nearby wavefronts is uniform.

The first two assumptions are stated at the beginning of the derivation, but the third is an afterthought and the fourth is only tacitly assumed when setting up the equation of motion. The wavefronts are allowed to be curved, and $S(x)$ is the cross-sectional area of the actual wavefront. Together, these assumptions are equivalent to the "1P" assumptions used in Chapter 2 of this thesis.

The derivation by Hanna and Slepian begins with the equations of motion and compression, with the latter expressed in terms of the bulk modulus. The existence of a velocity potential having prescribed relationships with pressure and velocity is assumed. These relationships satisfy the equation of motion, and are substituted into

the equation of compression to obtain the horn equation in the velocity potential. The derivation is quick and painless, but objectionable on several grounds. It does not acknowledge that the direction of velocity varies throughout the mass element, so that the equation of motion is not a straightforward application of Newton's second law. The variation in area is taken into account when evaluating the flux imbalance between the two sides of the volume element, but not when evaluating the force imbalance; this seems inconsistent. It is also unclear whether the linearizing approximations in the equations of motion and compression are equivalent to those which would be used in other contexts, and hence whether the horn problem is a generalization or specialization of another problem. In summary, the derivation does not show that Eq. (3.1) follows exactly from a particular set of assumptions.

Webster's earlier paper was apparently unknown to Hanna and Slepian, but was known to V. Karapetoff and J. Minton, both of whom drew attention to Webster's work in their discussion of the paper of Hanna and Slepian [22, pp. 405, 408, 409]. Minton's contribution was of particular interest—he considered the implications of a 90° phase difference between pressure and velocity, and referred to the frequency at which this occurs as the "cut-off frequency, so to speak". His references to Prof. Webster undoubtedly helped to associate Webster's name with Eq. (3.1).

Hanna and Slepian stated that their assumptions do not hold strictly for any but conical horns, although in fact they can also hold for cylindrical-sectorial horns (carrying cylindrical waves) and cylindrical pipes (carrying plane waves). This idea was taken further in 1927 by Ballantine [4, p. 91], who studied horns with the profile $S \propto x^m$, and noted that the horn equation (which he attributed to Webster, although he used velocity potential instead of pressure) becomes the equation for a spherical wave when $m = 2$ "and into such a wave a conical surface with apex at the source may be inserted without disturbing the symmetry of motion." Again he erred by asserting that the conical horn is the only such case. But his remarks were significant for establishing the horn equation as an exact special case of the wave equation in a specific geometry.

One of the co-workers mentioned by Webster was Prof. G. W. Stewart [62, p. 280]. In 1931 there appeared an acoustics textbook by G. W. Stewart and R. B. Lindsay, containing a derivation of an equation equivalent to Webster's, with pressure as the dependent variable [54, pp. 132–3]. Like Webster's, this derivation assumes a small cross-section, albeit one that is merely "small compared with the wave length" rather than infinitesimal. But the wave equation is not used. Instead, it is noted that the small cross section makes the phase approximately constant over every *plane* perpendicular to the axis. The equations of motion, continuity and compression are established with reference to a planar slice of air of uniform thickness dx, and these equations are combined to produce the horn equation, albeit with an awkward justification for what amounts to writing ρ_o for ρ in the equation of compression (compare Eqs. (6.4) and (6.6) in [54]).

The plane-wave assumption retains the disadvantages of the Hanna-Slepian approach, except that the varying direction of velocity is replaced by an assumed direction that is inconsistent with the boundary condition at the wall. Furthermore, plane waves do not vary in intensity has they propagate, whereas solutions to Webster's equation may grow or decay under the influence of a varying cross-section. The plane-wave assumption is also clearly unnecessary in view of Ballantine's observation that Webster's equation is correct for spherical waves in a conical horn.

P. M. Morse, in his still-popular 1948 textbook *Vibration and Sound* [36], used an equivalent set of assumptions to those of Hanna and Slepian, and similarly refrained from listing all his assumptions in one place. His derivation is open to the same objections as the Hanna-Slepian treatment, and also relies on an unproven generalization of the equation of continuity for a *uniform* cross-section. But his discussion is notable for introducing the term "one-parameter wave" to refer to an acoustic field that can be described in terms of a single spatial coordinate. In that sense, his treatment of the problem is a step closer to that of the present author.

Morse's one-parameter assumption can be related to Webster's assumption of an infinitesimal cross section: if the cross-section is small compared with the wavelength, the excess pressure is nearly uniform over the cross section and may therefore be approximated as a function of the axial coordinate only. The plane-wave assumption also says that the wave function (pressure or velocity potential) depends on a single coordinate—in this case a Cartesian coordinate.

It seems to have become a truism that Webster's equation is based on a plane-wave assumption; see, for example, the historical discussion by Geddes [18, p. 555]. But the above literature review—which is by no means exhausive—makes it clear that there are numerous other approaches.

3.2 Exact derivation from the 1P equations

The following derivation differs from those discussed above in that it shows that Webster's equation follows *exactly* from a particular set of assumptions, namely the linearizing assumptions and 1P assumptions in Chapter 2. But it is similar to some of the above in that it uses the equations of motion and compression (1P forms).

The required form of the equation of motion is obtained by combining Eqs. (2.21) and (2.22) and solving for $\dot{u}$:

$$\dot{u}(\xi, t) = -\frac{S(\xi)}{\rho_o} \frac{\partial p}{\partial \xi}. \tag{3.5}$$

Similarly, the required form of the equation of compression is obtained by combining Eqs. (2.51) and (2.52) and solving for $\dot{p}$:

$$\dot{p}(\xi, t) = -\frac{\rho_o c^2}{S(\xi)} \frac{\partial u}{\partial \xi}. \tag{3.6}$$

Differentiating Eq. (3.5) w.r.t. ξ and Eq. (3.6) w.r.t. t, and substituting the first result into the second, we obtain

$$\frac{\partial^2 p}{\partial t^2} = c^2 \left[\frac{1}{S} \frac{\partial}{\partial \xi} \left(S \frac{\partial p}{\partial \xi} \right) \right] \tag{3.7}$$

which is Eq. (3.1), with ξ in place of x.

To obtain Webster's equation in terms of the velocity potential ψ, we take components of Eq. (2.53) in the ξ direction to obtain

$$q = -\frac{\partial \psi}{\partial \xi}. \tag{3.8}$$

Multiplying through by $S(\xi)$ yields

$$u = -S(\xi)\,\frac{\partial \psi}{\partial \xi}. \tag{3.9}$$

The relationship between p and ψ is given by Eq. (2.60), which is repeated here for convenience:

$$p = \rho_o \dot{\psi}. \tag{3.10}$$

It is easily verified that Eqs. (3.9) and (3.10) satisfy Eq. (3.5). Substituting the same two equations into Eq. (3.6) yields a result identical to Eq. (3.7), but with ψ in place of p.

In a horn carrying a 1P wave, Webster's equation applies to any tube of orthogonal trajectories to the ξ-surfaces. To prove that it applies to the whole horn, we show that the horn boundary must be one such tube. If the boundary of the horn is rigid, it must be tangential to $\mathbf{q}$, which is parallel to $\mathbf{e}_\xi$ (a consequence of the 1P assumption; see Subsection 2.1.3) and hence orthogonal to the ξ-surfaces. So the boundary, at every point, has a tangent orthogonal to the ξ-surfaces, so that the points on the boundary may be joined to form ξ-trajectories.

Conversely, if the wall of the horn is a ξ-tube, the rigid-wall boundary condition permits fluid motion in the ξ direction and hence does not interfere with 1P propagation in the horn. This does *not* mean that 1P propagation is guaranteed. A horn of appropriate geometry *admits* 1P waves in ξ, but also admits other kinds of waves. If the horn is driven in such a way that the pressure over one cross-section is not uniform, then obviously these non-1P waves will be excited.

Moreover, if ξ is a coordinate measuring arc length normal to its level surfaces, nothing that has been said to date implies the existence of 1P acoustic fields in the parameter ξ. The question of which coordinates admit 1P fields will be fully examined in Chapters 4 and 5. In the mean time, we can exploit particular cases in which the existence of 1P waves is made obvious by symmetry (as in Section 3.3, below).

3.2.1 Alternative forms

The "expanded" form of Webster's equation is obtained by using the chain rule on the right-hand side of Eq. (3.7). The result may be written

$$p'' + \frac{S'}{S}\,p' - \frac{1}{c^2}\frac{\partial^2 p}{\partial t^2} = 0 \tag{3.11}$$

where the prime ($'$) denotes differentiation w.r.t. ξ (partial for p, total for S).

For *sinusoidal* time-dependence, we take a phasor transformation of Eq. (3.11), obtaining

$$P'' + \frac{S'}{S}\,P' + k^2 P = 0 \tag{3.12}$$

where $k = \omega/c$; this is the "time-independent" form of Webster's equation. Similarly, a phasor transformation of Eq. (3.5) gives the time-independent form of the equation of motion:

$$U = -\frac{S}{jk\rho_o c}\,P'. \tag{3.13}$$

Eqs. (3.12) and (3.13) are both *ordinary* differential equations (ODE's).

3.3 Application to spherical waves

This section illustrates the power of methods based on Webster's equation for analysing 1P acoustic fields, even in situations which would not usually be regarded as "horn" problems. Subsection 3.3.2 uses these methods to obtain Green's functions for harmonic point sources in free air, in planar baffles and in dihedral angles; these three geometries are all degenerate cases of conical horns. Later subsections determine the driving impedance of a conical horn, the radiation impedance of a pulsating sphere, and the specific acoustic admittances and impedances for spherical and planar wavefronts. Most of the results will be familiar to readers trained in acoustics, although the derivations will be novel. Some results will also be useful in later chapters.

3.3.1 Radiation from a point source

Suppose a point-source of flux, with *sinusoidal* time dependence, is located in free air at the origin of a spherical coordinate system (r, θ, ϕ). The excess pressure p depends on r and t only (by symmetry) and r measures arc length normal to the isobaric surfaces. Therefore Webster's equation and the other 1P equations, with r as the spatial coordinate, hold inside any r-tube. The most general r-tube is a cone of arbitrary cross section with its apex at the origin. If the cone subtends a solid angle Ω at the apex, the cross sectional area at a general r-surface is

$$S(r) = \Omega r^2. \tag{3.14}$$

Substituting Eq. (3.14) into Eq. (3.12), with r in place of ξ, gives the familiar ODE

$$P''(r) + \frac{2}{r} P'(r) + k^2 P(r) = 0 \tag{3.15}$$

which may be recognized as the time-independent Webster equation for a conical horn, or as the time-independent wave equation for spherical waves. Its general solution is

$$P = \frac{A}{r} e^{-jkr} + \frac{B}{r} e^{jkr} \tag{3.16}$$

where A and B are arbitrary complex constants. As the phasor notation used in this thesis assumes a time-dependent factor $e^{j\omega t}$, the term in e^{-jkr} is an outward-traveling wave while the term in e^{jkr} is an inward-traveling wave. For a single point-source, the latter term violates causality, so we must have $B = 0$. The solution then reduces to

$$P(r) = \frac{A}{r} e^{-jkr}. \tag{3.17}$$

For the equation of motion, we substitute Eq. (3.14) into Eq. (3.13), with r in place of ξ, obtaining

$$U = -\frac{\Omega r^2}{jk\rho_o c} P'. \tag{3.18}$$

P' may be found from Eq. (3.17) and substituted, yielding the result

$$U(r) = \frac{A\Omega}{\rho_o c} \left(r + \frac{1}{jk} \right) e^{-jkr}. \tag{3.19}$$

$U(r)$ is the flux passing through a spherical segment of radius r, centered on the origin and subtending a solid angle Ω at the origin.

3.3.2 Green's functions

Let U_0 be the flux "pumped" by the source into the solid angle Ω. To express U_0 in terms of A, we let $r \to 0$ in Eq. (3.19):

$$U_0 = \frac{A\Omega}{jk\rho_o c} = \frac{A\Omega}{j\omega\rho_o}. \tag{3.20}$$

Now the *transfer impedance* from the source to radius r is defined as

$$H(r) = \frac{P(r)}{U_0}. \tag{3.21}$$

This is the pressure at radius r for unit source flux, as can be seen by putting $U_0 = 1$ in the definition. Substituting Eqs. (3.17) and (3.20) into Eq. (3.21) gives the explicit form

$$H(r) = \frac{j\omega\rho_o}{\Omega}\,\frac{e^{-jkr}}{r} \tag{3.22}$$

which may be remembered as the product of a constant $j\omega\rho_o/\Omega$, a *delay factor* e^{-jkr} and a *geometric spreading factor* $1/r$.

Eq. (3.22) has been derived for an arbitrary Ω. Now let us suppose that the total flux from the source is confined by a rigid conical horn with its apex at the source (origin), and that Ω is the solid angle enclosed by the confining cone. Then U_0 becomes simply the total flux pumped out by the source, which we shall call the *strength* of the source.

The wall of the conical horn is of course an r-tube, which permits 1P waves in r. So the equations of Subsection 3.3.1 remain valid in the presence or absence of the horn. The introduction to that subsection assumed a point-source radiating omnidirectionally into free air. Hence the first confining "cone" to be considered is the whole of 3D space, for which we take $\Omega = 4\pi$ in Eq. (3.22). Also, since r is just the distance from the source, we can obtain the pressure at position $\mathbf{r}$ due to a unit source at position $\mathbf{r}'$ by writing $|\mathbf{r} - \mathbf{r}'|$ for r. Thus we obtain

$$H_{\mathrm{FA}}(\mathbf{r}|\mathbf{r}') = \frac{j\omega\rho_o}{4\pi}\,\frac{e^{-jk|\mathbf{r}-\mathbf{r}'|}}{|\mathbf{r}-\mathbf{r}'|} \tag{3.23}$$

where the subscript "FA" means "free air" and the first vertical bar means "due to a unit source at". Using the generalized transfer impedance H_{FA}, we can find the pressure at $\mathbf{r}$ due to several point-sources by superposition. Of course we cannot have a *point*-source of *finite* (non-zero) flux in free air; in practice, a small source would be generated by a comparatively large piece of apparatus whose presence would violate the free-air assumption. But every differential volume element $d\mathcal{V}$ is a source of flux $\operatorname{div}\mathbf{Q}\, d\mathcal{V}$. So if the velocity is known at every point $\mathbf{r}'$ in free air, the pressure at $\mathbf{r}$ is

$$P(\mathbf{r}) = \iiint_{\mathbf{r}'} H_{\mathrm{FA}}(\mathbf{r}|\mathbf{r}')\operatorname{div}\mathbf{Q}(\mathbf{r}')\, d\mathcal{V} \tag{3.24}$$

where the integral is taken over all $\mathbf{r}'$ in 3D space. Thus $H_{\mathrm{FA}}(\mathbf{r}|\mathbf{r}')$ is the *Green's function* for free air. (An expression for the pressure field in a restricted region of air can be found by converting the above volume integral to a boundary surface integral. The latter integral leads to the widely-used Boundary Element Method [23].)

Another confining cone is an infinite planar baffle; a plane is a degenerate cone, and every point on the plane is an apex. At any apex, the baffle subtends a solid

angle 2π, so we take $\Omega = 2\pi$ in Eq. (3.22). Again we can write $|\mathbf{r} - \mathbf{r}'|$ in place of r to obtain the pressure at the observing position $\mathbf{r}$ due to a unit source *against the baffle* at position $\mathbf{r}'$. The result is

$$H_{\mathrm{PB}}(\mathbf{r}|\mathbf{r}') = \frac{j\omega\rho_{\mathrm{o}}}{2\pi} \frac{e^{-jk|\mathbf{r}-\mathbf{r}'|}}{|\mathbf{r} - \mathbf{r}'|} \tag{3.25}$$

where the subscript "PB" means "planar baffle". Again we can use superposition to find the pressure due to several point-sources, provided that all sources are on the baffle.[3] Moreover, if part of the baffle moves with (phasor) normal velocity $V(\mathbf{r}')$, each area element dS contributes a flux $V\,dS$, so that the pressure at $\mathbf{r}$ is

$$P(\mathbf{r}) = \iint_{\mathbf{r}'} H_{\mathrm{PB}}(\mathbf{r}|\mathbf{r}')\, V(\mathbf{r}')\, dS \tag{3.26}$$

where the integral is taken over all $\mathbf{r}'$ on moving parts of the baffle. So $H_{\mathrm{PB}}(\mathbf{r}|\mathbf{r}')$ is the "half-space" Green's function. (It is assumed that the maximum displacement of the vibrating portion of the baffle is small compared with the wavelength, so that we can neglect the variation in $|\mathbf{r} - \mathbf{r}'|$ due to the vibration.)

A third example of a confining cone is the dihedral angle between two semi-infinite planar baffles; any point on the line of intersection between the half-planes is an apex of the cone. If the enclosed dihedral angle is α, the cone subtends a solid angle 2α at any apex. Putting $\Omega = 2\alpha$ and $r = |\mathbf{r} - \mathbf{r}'|$ in Eq. (3.22), we obtain the pressure at position $\mathbf{r}$ in the field radiated by a unit source at position $\mathbf{r}'$ *on the line of intersection*. The result is

$$H_{\mathrm{DA}}(\mathbf{r}|\mathbf{r}') = \frac{j\omega\rho_{\mathrm{o}}}{2\alpha} \frac{e^{-jk|\mathbf{r}-\mathbf{r}'|}}{|\mathbf{r} - \mathbf{r}'|}. \tag{3.27}$$

where the subscript "DA" means "dihedral angle". We can use superposition to find the pressure due to several point-sources provided that each source is "in the corner", i.e. on the line of intersection. If the dihedral corner contains a line source producing a (phasor) flux per unit length of $W(s)$, where s is a coordinate measuring distance along the line of intersection, then each length element ds contributes a flux $W\,ds$, so that the pressure at $\mathbf{r}$ is

$$P(\mathbf{r}) = \int_{-\infty}^{\infty} H_{\mathrm{DA}}(\mathbf{r}|\mathbf{r}'(s))\, W(s)\, ds. \tag{3.28}$$

Note that $\mathbf{r}'$ has become a function of s. So $H_{\mathrm{DA}}(\mathbf{r}|\mathbf{r}')$ is the Green's function for a dihedral angle α.

In each of the above three cases, the Green's-function method is possible because there exists a continuum of points all of which are apexes of the cone and "see" the same solid angle; the continuum is three-dimensional for free air, two-dimensional for the planar baffle, and one-dimensional for the dihedral angle. In each case, the Green's function has been found using Webster's equation for a general conical horn. But in most cones there is only one apex at which a source sees a simple solid angle; other points see more complex geometries, and there is not necessarily a continuum of points that see the same geometry.

[3] Of course, sources on and off the baffle can be handled by using the free-air Green's function and superposing the pressures due to the sources and to their "images" on the other side of the baffle. Sources on the baffle are coincident with their images; this doubling of the sources is consistent with the observation that H_{PB} is twice H_{FA}.

3.3.3 Driving admittance and impedance

Consider a conical horn subtending a solid angle Ω at the origin, in spherical coordinates. Let us define the *driving admittance* $Y(r)$ as the acoustic admittance of the cross-section at radius r; that is

$$Y(r) = \frac{U(r)}{P(r)}. \tag{3.29}$$

This is the admittance seen by a radially-pulsating spherical diaphragm "driving" the conical horn. Because of the spherical symmetry, the equations of Subsection 3.3.1 are applicable; the numerator and denominator of Eq. (3.29) are given by Eqs. (3.19) and (3.17), respectively. After making these substitutions, we can express $Y(r)$ in the form

$$Y(r) = \frac{1}{R_\mathrm{a}(r)} + \frac{1}{j\omega M_\mathrm{a}(r)} \tag{3.30}$$

where

$$R_\mathrm{a}(r) = \frac{\rho_\mathrm{o} c}{\Omega r^2} \tag{3.31}$$

and

$$M_\mathrm{a}(r) = \frac{\rho_\mathrm{o}}{\Omega r}. \tag{3.32}$$

So the driving admittance is an acoustic resistance $R_\mathrm{a}(r)$ in parallel with an acoustic mass $M_\mathrm{a}(r)$, and is resistive for $\omega \gg R_\mathrm{a}/M_\mathrm{a}$ and inductive[4] for $\omega \ll R_\mathrm{a}/M_\mathrm{a}$. The formula for $R_\mathrm{a}(r)$ is easy to remember because it is just the characteristic impedance (see Subsection 3.3.5) divided by the area. The formula for $M_\mathrm{a}(r)$ can be put into the form "density times length over area" (as in Eq. (2.25)) by multiplying the numerator and denominator by r, or in the form "mass over area squared" (as in Eq. (2.26)) by multiplying the numerator and denominator by Ωr^3.

In the case of a point-source radiating into *free air*, the largest cross-section over which $Y(r)$ can be evaluated (for given r) is a complete sphere, subtending an angle $\Omega = 4\pi$ at the source. Hence, to find the driving admittance of a spherical surface at radius a from the point-source, or the *radiation admittance* of a radially pulsating sphere of radius a in free air, we simply put $r = a$ and $\Omega = 4\pi$ in Eqs. (3.31) and (3.32). If the result for M_a is written in the "mass over area squared" form, the numerator becomes $\rho_\mathrm{o}\, 4\pi a^3$, which is three times the mass of the air enclosed by the spherical surface (cf. Keele [29], p. 459).

The *driving impedance* at radius r is of course defined as

$$Z(r) = \frac{P(r)}{U(r)} = 1/Y(r). \tag{3.33}$$

3.3.4 Specific acoustic admittance and impedance

If the r component of velocity is $Q_r(r)$, the flux at radius r is

$$U(r) = Q_r(r)\, S(r). \tag{3.34}$$

[4]The implication of the inductive low-frequency behavior for the design of anechoic chambers has only recently been pointed out in the literature [29].

Solving for Q_r and substituting from Eqs. (3.14) and (3.19) gives

$$Q_r = \frac{A}{r}\left(\frac{1}{\rho_o c} + \frac{1}{j\omega\rho_o r}\right) e^{-jkr}. \tag{3.35}$$

Because we have 1P waves in r, the vector velocity is simply

$$\mathbf{Q} = Q_r\,\mathbf{e}_r. \tag{3.36}$$

Now let us define the *specific acoustic admittance* at a point in the acoustic field as the complex vector

$$\mathbf{y} = \frac{\mathbf{Q}}{P}. \tag{3.37}$$

The radial component of $\mathbf{y}$ is the complex scalar

$$y_r = \frac{\mathbf{Q}.\mathbf{e}_r}{P} = \frac{Q_r}{P}. \tag{3.38}$$

Substituting from Eqs. (3.17) and (3.35) yields

$$y_r = \frac{1}{\rho_o c} + \frac{1}{j\omega\rho_o r}. \tag{3.39}$$

The *specific acoustic impedance* in the radial direction is

$$z_r = \frac{P}{Q_r} = 1/y_r \tag{3.40}$$

(cf. Beranek [11], p. 11). Substituting from Eq. (3.39) and noting that $k = \omega/c$, we can write z_r in the form

$$z_r = \rho_o c\,\frac{jkr}{1+jkr}. \tag{3.41}$$

(Although $\mathbf{y}$, y_r and z_r are complex, they are written in lower case to distinguish them from the driving admittance Y and its reciprocal Z. They do not need to be distinguished from time-dependent quantities—which are usually also written in lower case—because they are not phasors but ratios of phasors.)

Another interpretation of $y(r)$ can be obtained by dividing Eq. (3.34) through by $P(r)$ and substituting from Eqs. (3.29) and (3.38):

$$Y(r) = y_r(r)\,S(r). \tag{3.42}$$

Substituting from Eqs. (3.14) and (3.39) again gives Eq. (3.30). Eq. (3.42) indicates that the acoustic admittance of the cross-section is the radial component of the specific acoustic admittance multiplied by the area; for an acoustic admittance, "specific" means "per unit area".

Substituting $1/Z$ for Y and $1/z_r$ for y_r in Eq. (3.42), and cross-multiplying, we find

$$z_r(r) = S(r)\,Z(r). \tag{3.43}$$

Note that the specific acoustic impedance is *not* the acoustic impedance per unit area, but rather the impedance-area product.

3.3.5 Characteristic impedance

To find the specific acoustic impedance for plane waves, known as the *characteristic impedance* of the medium [11, p. 11], we let $r \to \infty$ in Eq. (3.41). The limit is

$$z_0 = \rho_o c \tag{3.44}$$

which is real and frequency-independent. This result assumes *unidirectional propagation* (because Eq. (3.17) is obtained by rejecting the incoming wave). If we write $\rho_o c$ for z_r in Eq. (3.40) and change the subscript r to x (a Cartesian coordinate, emphasizing the new plane-wave assumption), we obtain

$$P = \rho_o c\, Q_x. \tag{3.45}$$

If P and Q_x are single-frequency phasors, we can convert this equation to the time domain for each frequency and superpose the results. Alternatively, we can consider P and Q_r to be Fourier transforms and take the inverse transforms. In either case, we obtain

$$p = \rho_o c\, q_x \tag{3.46}$$

for a very general class of functions $p(x,t)$ and $q_x(x,t)$. So for progressive plane-wave propagation, the pressure and velocity waves are geometrically similar and coincident in time and space; they differ only by a scale factor, which is the characteristic impedance.

Chapter 4

Every one-parameter acoustic field is a solution of Webster's equation.[1]

4.1 Introduction: a wider definition of "1P"

The notion of 1P acoustic fields has been used in Chapter 2 to derive the 1P or "thin-shell" forms of the equations of motion and compression, and in Chapter 3 to derive Webster's equation from the thin-shell equations. In Chapter 2, a 1P acoustic field was defined as one in which the excess pressure depends on a single spatial coordinate ξ, which measures arc length normal to the isobaric surfaces. In this chapter it will be shown that the normal arc-length assumption is redundant in the sense that if pressure is a function of a single coordinate, that coordinate (and hence the pressure) can be expressed in terms of a normal-arc-length coordinate.

So, for the purposes of this and subsequent chapters, let us begin with a weakened definition of "1P": a 1P acoustic field is one in which the pressure depends on only one spatial coordinate. Noting that the excess pressure satisfies the wave equation, let us further define a *1P wave* as a solution to the wave equation depending on only one spatial coordinate; if that coordinate is called u, the solution is called a *1P wave in the parameter* u. This chapter establishes conditions for the existence of such waves. One of the conditions implies that u can be transformed to an arc-length coordinate. Webster's substitution for $\nabla^2 p$ (see Eq. (3.3)) is then explained, enabling Webster's equation to be obtained directly from the wave equation. This derivation is valid for both the pressure and the velocity potential.

Before the rigorous argument begins, it is worth remarking that the results should not be surprising, for three reasons. First, and most obviously, the acoustic field in a horn satisfies the wave equation, which involves three spatial coordinates. But Webster's equation describes the field in terms of only one spatial coordinate. So if Webster's equation is exact in the sense that its solution satisfies the wave equation, its solution is a 1P wave. Hence it is natural to ask whether the converse also holds—that is, whether *every* one-parameter wave confined to a horn is a solution of Webster's equation. Second, if the acoustic pressure depends only on the coordinate

[1] The content of this chapter is similar to that of Sections 1, 2 and 5 of the author's 1993 paper [43]. The discussion of alternative definitions of "1P", corresponding to Section 5 of the paper, has been improved.

u, the acceleration and hence the velocity of the air will be in the direction of ∇u, i.e. normal to the level surfaces of u. This is consistent with the boundary condition imposed by the side wall of a horn if the side wall is a locus of orthogonal trajectories to the level surfaces of u. Third, it is a straightforward exercise to write down Webster's equation for a straight tube of constant cross-section, for a cylindrical sectorial horn and for a conical horn (taking an arbitrary cross-section in each case), and verify that the results are identical with the one-dimensional wave equation in Cartesian, cylindrical and spherical coordinates respectively (as Ballantine [4] noted in the case of the spherical wave). As these three coordinate systems admit 1P waves in their linear or radial coordinates, one might ask whether Webster's equation holds for *all* coordinates admitting 1P waves. The present chapter answers "yes", using an argument that makes no *a priori* assumption about the shapes of the equicoordinate surfaces or wavefronts.

One might also ask whether there are any "1P coordinates" other than those already mentioned, i.e. those whose level surfaces are parallel planes, coaxial cylinders or concentric spheres. The answer to this question requires further development of the existence conditions for 1P waves and will be addressed in Chapter 5. There it is shown that *there are only three 1P wave geometries*, and hence only three basic shapes for exact 1P horns.

4.2 Existence of 1P waves

The wave equation in terms of excess pressure (Eq. (2.61)) may be written

$$\nabla^2 p - \frac{1}{c^2}\frac{\partial^2 p}{\partial t^2} = 0. \tag{4.1}$$

The linearized point form of the equation of motion (Eq. (2.15)) may be written

$$\rho_\mathrm{o}\frac{\partial \mathbf{q}}{\partial t} = -\nabla p. \tag{4.2}$$

Let us agree that a 1P waveguide, to be worthy of the name, must support a 1P wave with sinusoidal time-dependence for at least one angular frequency ω. (We shall find that any waveguide that admits 1P waves at one frequency does so at *all* frequencies, but only one frequency need be assumed *a priori*.) Then we may let

$$p = \sqrt{2}\,P e^{j\omega t};\quad \mathbf{q} = \sqrt{2}\,\mathbf{Q} e^{j\omega t} \tag{4.3}$$

so that Eq. (4.1) reduces to the Helmholtz equation

$$\nabla^2 P + k^2 P = 0 \tag{4.4}$$

and Eq. (4.2) becomes

$$\mathbf{Q} = \frac{-1}{j\omega\rho_\mathrm{o}}\nabla P. \tag{4.5}$$

In most mathematical arguments in this thesis, the "phasor forms" of time dependent variables can be taken either as phasors or as Fourier transforms. In this chapter, however, the assumption of sinusoidal time-dependence is confined to *one* frequency, so that the ability of the Fourier transform to handle signals containing a

range of frequencies is not an advantage. Moreover, the determination of necessary conditions for the existence of 1P solutions (Subsection 4.2.3) will use properties of the Wronskian of two solutions. The rigor of this argument would be compromised if the "solutions" were in the form of Fourier transforms, because the transforms of pure sinusoids are impulse functions. So in this chapter, "phasors" must be interpreted strictly as phasors.

4.2.1 Seeking a 1P solution

For a 1P wave, we want P to be a function of a single spatial coordinate u, which in turn may be regarded as a function of the three Cartesian coordinates x, y, z; that is

$$P = P\left(u(x, y, z)\right). \tag{4.6}$$

We assume that $\nabla u \neq \mathbf{0}$ (i.e. that the scale factor for u is finite), and that all second partial derivatives of u w.r.t. the Cartesian coordinates are continuous. Indicating total differentiation w.r.t. u by a prime ($'$) and partial differentiation w.r.t. x, y and z by subscripts, we may use the chain rule on Eq. (4.6) to obtain

$$P_x = P'(u)\, u_x \tag{4.7}$$
$$P_y = P'(u)\, u_y \tag{4.8}$$
$$P_z = P'(u)\, u_z. \tag{4.9}$$

Multiplying these three equations by $\mathbf{i}$, $\mathbf{j}$ and $\mathbf{k}$ respectively and adding the results yields

$$\nabla P = P'(u)\, \nabla u. \tag{4.10}$$

This is a vector identity, applicable to a scalar field that is a function of another scalar field.

Using the product and chain rules, we may differentiate Eqs. (4.7), (4.8) and (4.9) w.r.t. x, y and z, respectively, and obtain

$$P_{xx} = P''(u)\, u_x^2 + P'(u)\, u_{xx} \tag{4.11}$$
$$P_{yy} = P''(u)\, u_y^2 + P'(u)\, u_{yy} \tag{4.12}$$
$$P_{zz} = P''(u)\, u_z^2 + P'(u)\, u_{zz}. \tag{4.13}$$

Adding these three equations gives

$$\nabla^2 P = P''(u)\, |\nabla u|^2 + P'(u)\, \nabla^2 u \tag{4.14}$$

which is also a vector identity.

We can now rewrite the Helmholtz equation in terms of the desired single parameter. Substituting Eq. (4.14) into Eq. (4.4) and dividing through by $|\nabla u|^2$ yields

$$P'' + fP' + gP = 0 \tag{4.15}$$

where

$$f = \frac{\nabla^2 u}{|\nabla u|^2} \tag{4.16}$$

$$g = \frac{k^2}{|\nabla u|^2}. \tag{4.17}$$

Eq. (4.15) is an *ordinary* differential equation (ODE). The assumed smoothness of $u(x, y, z)$ means that f and g are continuous w.r.t. u, so solutions to Eq. (4.15) must exist. The question is whether there are any solutions that are functions of u alone. If there are not, our initial assumption (Eq. (4.6)) is contradicted. If there are, these solutions satisfy Eqs. (4.6) to (4.14) and hence reduce the Helmholtz equation to Eq. (4.15), so that we have indeed found 1P solutions to the Helmholtz equation. So the Helmholtz equation has 1P solutions in u if and only if Eq. (4.15) has solutions depending only on u.

4.2.2 Sufficient conditions

For Eq. (4.15) to have 1P solutions, it is sufficient that $|\nabla u|$ and $\nabla^2 u$ be functions of u alone; that is, it is sufficient that

$$\nabla u = M(u)\,\mathbf{e}_u \tag{4.18}$$

$$\nabla^2 u = N(u) \tag{4.19}$$

where M and N are real functions and $\mathbf{e}_u$ is a unit vector in the direction of ∇u. (Note that $M(u)$, being the magnitude of a nonzero vector, is positive.) These conditions are sufficient because, when substituted into Eqs. (4.16) and (4.17), they make f and g functions of u alone, so that the coefficients of Eq. (4.15), and hence some of its solutions, depend only on u. (The general solution of Eq. (4.15) will depend on u and contain two arbitrary constants, but will have no essential dependence on any variable but u.)

4.2.3 Necessary conditions

Conditions (4.18) and (4.19) can also be shown to be necessary. Let

$$P(u) = y_1(u) + jy_2(u) \tag{4.20}$$

where y_1 and y_2 are real. Substituting Eq. (4.20) into Eq. (4.15) and taking real and imaginary parts (noting that f and g are also real), we obtain the two real equations

$$y_1'' + fy_1' + gy_1 = 0 \tag{4.21}$$

$$y_2'' + fy_2' + gy_2 = 0\,; \tag{4.22}$$

that is, y_1 and y_2 are solutions of Eq. (4.15). We can also reconstruct Eq. (4.15) from Eqs. (4.21) and (4.22) using Eq. (4.20), so Eqs. (4.21) and (4.22) together are equivalent to Eq. (4.15). If we treat Eqs. (4.21) and (4.22) as simultaneous equations in f and g, the solutions are

$$f = \frac{y_1'' y_2 - y_2'' y_1}{y_1 y_2' - y_2 y_1'} \tag{4.23}$$

$$g = \frac{y_1' y_2'' - y_2' y_1''}{y_1 y_2' - y_2 y_1'}. \tag{4.24}$$

Thus f and g are expressed in terms of y_1 and y_2 and their derivatives, i.e. as functions of u. Returning to Eq. (4.17), we see that since g depends only on u, so does $|\nabla u|$. Then we see from Eq. (4.16) that because f and $|\nabla u|$ depend only on u,

so does $\nabla^2 u$. So for existence of a 1P wave $P(u)$, it is necessary that $|\nabla u|$ and $\nabla^2 u$ be functions of u alone.

Note however that if the above proof is to be valid, we must check that the denominator in Eqs. (4.23) and (4.24) is nonzero. We can make the denominator nonzero for just *one* value of u by imposing appropriate initial conditions on Eqs. (4.21) and (4.22). But that denominator is of course the Wronskian of y_1 and y_2, which are solutions of a 2nd-order homogeneous linear ODE, so that if their Wronskian is nonzero for one value of u, it is nonzero everywhere (this follows from Abel's Identity; see Wylie [64], p. 74). So there exists a solution to Eq. (4.15) for which the denominator in Eqs. (4.23) and (4.24) is everywhere nonzero, and for which f and g therefore depend on u alone. Now although the right-hand sides of Eqs. (4.23) and (4.24) involve the real and imaginary parts of P, the left-hand sides, according to Eqs. (4.16) and (4.17), depend only on position and are the same for all P. So, for all $P(u)$ satisfying Eq. (4.15), we have shown that f and g depend on u alone, as asserted in the above proof that conditions (4.18) and (4.19) are necessary.

4.2.4 Infinite bandwidth

Conditions (4.18) and (4.19) have been proven sufficient and necessary to allow 1P propagation at one frequency. But, in proving sufficiency, nothing was assumed concerning ω or k. Hence the conditions necessary for one frequency are sufficient for *all* frequencies; that is, a coordinate system that admits 1P waves at one frequency does so at all frequencies.

4.2.5 Transforming the parameter to an arc length

Suppose u is transformed to another coordinate $\xi(u)$. Since ξ, like P, is a function of u alone, we may write ξ instead of P in Eq. (4.10). Then if we substitute from Eq. (4.18), we obtain

$$\nabla\xi = \xi'(u)\, M(u)\, \mathbf{e}_u. \tag{4.25}$$

If we choose ξ to be

$$\xi(u) = \int \frac{du}{M(u)}\,, \tag{4.26}$$

we have $\xi'(u) = 1/M(u)$, so that Eq. (4.25) reduces to

$$\nabla\xi = \mathbf{e}_u \tag{4.27}$$

whence

$$|\nabla\xi| = 1. \tag{4.28}$$

Since $M(u)$ is positive, Eq. (4.26) implies that ξ is an increasing function of u; hence $\mathbf{e}_\xi = \mathbf{e}_u$ (with no reversal of direction). So Eq. (4.27) becomes

$$\nabla\xi = \mathbf{e}_\xi\,, \tag{4.29}$$

which also follows from Eq. (4.28) since $\mathbf{e}_\xi$ is defined as a unit vector in the direction of $\nabla\xi$. Also, since ξ is a special case of u, Eq. (4.19) may be rewritten

$$\nabla^2\xi = L(\xi) \tag{4.30}$$

where L depends on ξ alone. Eqs. (4.29) and (4.30) are the 1P existence conditions expressed in terms of ξ.

We can now show that ξ measures arc length along any ξ-trajectory.[2] If s is the arc length along one such trajectory in the direction of increasing ξ, then the directed unit tangent vector to this trajectory is just $\mathbf{e}_\xi$. So, using the fundamental relation between gradient and directional derivative, then taking the gradient from Eq. (4.29), we have

$$\frac{d\xi}{ds} = \nabla\xi.\,\mathbf{e}_\xi = \mathbf{e}_\xi.\mathbf{e}_\xi = 1\,, \tag{4.31}$$

indicating that ξ and s differ by at most a constant along the trajectory. By suitably choosing the origin for s on each trajectory, we can have $\xi = s$ everywhere; thus ξ measures arc length along every ξ-trajectory from the reference surface $\xi = 0$.

N.B.: We cannot sum up the normal-arc-length property of ξ by saying that ξ has a scale factor of unity, unless we also specify the direction in which the scale factor is measured. (Even so, the reader may care to rewrite Eq. (2.16) more rigorously using Eq. (4.10).) The notion of scale factor assumes the presence of two more coordinates which are held constant when measuring the scale factor. If the coordinate system is not orthogonal, a coordinate that measures arc length does not necessarily do so in a direction normal to its level surfaces. At this point in the argument we do not know whether u or ξ can be embedded in an orthogonal coordinate system. Hence this chapter does not proceed by setting up the wave equation in general orthogonal coordinates and assuming that the wave function depends on only one of them.

4.2.6 Webster's equation (again)

In summary, it has been shown that if an acoustic field is 1P in the sense that the pressure depends on only one spatial coordinate, that coordinate in turn is a function of a coordinate ξ which measures arc length normal to its level surfaces. Hence the acoustic field is also "1P" in the sense of Chapter 2 and satisfies the "1P" or "thin-shell" forms of the equations of motion and compression (Subsections 2.1.3 and 2.2.7), which in turn imply that Webster's equation (in terms of pressure or velocity potential) is true for every ξ-tube (Section 3.2).

4.3 Deriving Webster's equation from the wave equation

To show that Webster's equation is a special case of the wave equation in a 1P acoustic field, we shall revert to the time-dependent 1P wave problem (i.e. consider p instead of P), but the time-dependence will not have to be indicated explicitly because all the derivatives and integrals in the following derivation are w.r.t. spatial variables. Let us also consider p to be a function of ξ instead of u, so that a prime ($'$) now denotes differentiation w.r.t. ξ. Because p depends on no spatial coordinate but ξ, we may write p for P and ξ for u in identity (4.10), then use condition (4.29) to obtain

$$\nabla p = p'(\xi)\,\mathbf{e}_\xi. \tag{4.32}$$

[2]See Subsection 2.1.3 for definitions of the terms "ξ-surface", "ξ-trajectory" and "ξ-tube".

Notice that this result follows from Eq. (4.29), which in turn depends on Eq. (4.18) but *not* on Eq. (4.19); the condition on $\nabla^2 u$ will not be used in deriving Webster's equation. This point will become significant in Section 5.8.

Now consider a ξ-tube (as defined in Subsection 2.1.3). A general ξ-surface will intersect the tube and produce a surface segment bounded by the tube; let the area of that segment (the "cross-sectional area") be $S(\xi)$. Let $\mathcal{V}$ denote the volume bounded by the ξ-tube and the two surfaces $\xi = \xi_1$ and $\xi = \xi_2$, with $\xi_1 < \xi_2$; in the terminology of Subsection 2.1.3, $\mathcal{V}$ is a ξ-shell segment. Let σ denote the enclosing surface of $\mathcal{V}$, and $\mathbf{n}$ the outward unit normal from σ. By the divergence theorem,

$$\iiint_{\mathcal{V}} \nabla^2 p \, d\mathcal{V} = \oiint_{\sigma} \nabla p \,.\, \mathbf{n} \, d\sigma. \tag{4.33}$$

Substituting Eq. (4.32) into Eq. (4.33) gives

$$\iiint_{\mathcal{V}} \nabla^2 p \, d\mathcal{V} = \oiint_{\sigma} p'(\xi) \, \mathbf{e}_\xi \,.\, \mathbf{n} \, d\sigma. \tag{4.34}$$

From Eq. (4.1), we see that if p is a function of u and t only, so is $\nabla^2 p$. Because a u-dependence is equivalent to a ξ-dependence, and because the time-dependence is not under study here, we may treat $\nabla^2 p$ as a function of ξ. Since ξ measures arc length normal to the ξ-surfaces, we may write $d\mathcal{V} = S(\xi)\, d\xi$, so that the left-hand integral in Eq. (4.34) simplifies to

$$\int_{\xi_1}^{\xi_2} S(\xi) \; \nabla^2 p\Big|_\xi \, d\xi. \tag{4.35}$$

Next, consider the right-hand side of Eq. (4.34). On the face of σ for which $\xi = \xi_2$, we have $\mathbf{n} = \mathbf{e}_\xi$, so $\mathbf{e}_\xi.\mathbf{n} = 1$ and the integral over that face is $p'(\xi_2)\, S(\xi_2)$. On the face for which $\xi = \xi_1$, we have $\mathbf{n} = -\mathbf{e}_\xi$, so $\mathbf{e}_\xi.\mathbf{n} = -1$ and the integral over that face is $-p'(\xi_1)\, S(\xi_1)$. On the face of σ which forms part of the ξ-tube, we have $\mathbf{e}_\xi.\mathbf{n} = 0$, so that there is no contribution to the integral. Thus the integral reduces to

$$p'(\xi_2)\, S(\xi_2) - p'(\xi_1)\, S(\xi_1). \tag{4.36}$$

Substituting expressions (4.35) and (4.36) for the two sides of Eq. (4.34) and differentiating both sides w.r.t. ξ_2 gives

$$S(\xi_2) \; \nabla^2 p\Big|_{\xi_2} = (Sp')'\Big|_{\xi=\xi_2}. \tag{4.37}$$

Since ξ_2 is general, we can write ξ for ξ_2. Then we can divide through by $S(\xi)$ and obtain

$$\nabla^2 p\Big|_\xi = \frac{1}{S} \; (Sp')' \tag{4.38}$$

which is just Webster's substitution in Eq. (3.3), with ξ instead of x.

Of course the above derivation is valid for both the excess pressure and the velocity potential, because both satisfy the wave equation (to the same approximation).

In summary, Section 4.2 has shown that if the Helmholtz equation has a 1P solution in the parameter u, then u can be transformed to another coordinate ξ which measures arc length normal to the ξ-surfaces (u-surfaces). Under these conditions, the present section has shown that in any ξ-tube (u-tube), the wave equation reduces to Webster's equation, in which ξ is the axial coordinate and $S(\xi)$ is the area of the general constant-ξ (constant-u) cross-section.

4.4 Alternative definitions of "1P"

The discussion to this point has concentrated on the wave functions (pressure and velocity potential), saying little about the particle velocity and nothing about the radiated intensity. Properties of the velocity and intensity may be found by introducing the equation of motion: substituting Eq. (4.32) into Eq. (4.2) gives

$$\frac{\partial \mathbf{q}(\mathbf{r},t)}{\partial t} = \frac{-p'(\xi,t)}{\rho_o}\,\mathbf{e}_\xi \tag{4.39}$$

where $\mathbf{r}$ is the position vector and the prime denotes partial differentiation w.r.t. ξ; the position- and time-dependence of p and $\mathbf{q}$ are here made explicit. Assuming quiescent initial conditions, i.e. $\mathbf{q} = \mathbf{0}$ at $t = 0$, we may integrate w.r.t. time and obtain

$$\mathbf{q}(\mathbf{r},t) = -\int_0^t \frac{p'(\xi,\bar{t})}{\rho_o}\,d\bar{t}\;\mathbf{e}_\xi \tag{4.40}$$

showing that the fluid velocity $\mathbf{q}$ has magnitude depending on ξ and t only and has the direction of $\mathbf{e}_\xi$. These properties of $\mathbf{q}$ are shared by the instantaneous intensity vector $p\mathbf{q}$, since p is a function of ξ and t. The time-average of $p\mathbf{q}$ is the radiated or transmitted power per unit area (in magnitude and direction).

Recall from Subsection 4.2.5 that the level surfaces of ξ are also those of u, the parameter of the assumed 1P wave. Thus we have now shown that *a 1P acoustic field in the parameter u has velocity and intensity fields which are normal to the u-surfaces and are uniform in magnitude over any u-surface.* Speaking loosely, we say that a 1P wavefront possesses *normal uniform velocity* and *uniform intensity.*

Since a 1P pressure distribution implies normal uniform velocity, it is natural to ask whether the converse holds. If it does not, the range of wavefront shapes possessing normal uniform velocity might be wider than that possessing a 1P wave function, and some of these shapes might lead to new exact horn designs based on a "1P" velocity equation. That the converse *does* hold is guaranteed by the following theorem.

Theorem 4.1 *In a linear acoustic field, let p be the excess pressure, ψ the velocity potential, and $\mathbf{q}$ the fluid velocity. Let u be a spatial coordinate.*[3] *Then the following three statements are equivalent:*

(a) *p is a function of u and t only;*

(b) *ψ is a function of u and t only;*

(c) *$\mathbf{q}$ is parallel to ∇u, and $|\mathbf{q}|$ is a function of u and t only.*

[3]Note that the theorem does *not* assume *a priori* that u admits 1P solutions to the wave equation. The corresponding theorem in the author's paper [43, p. 446] *does* include this assumption in the hypothesis. Hence the present theorem is stronger than that in [43]. Concerning the implications of (c), for example, the present theorem says that any coordinate admitting "1P velocity" also admits 1P pressure and velocity potential, while the result in [43] says that if a *given* coordinate admits 1P p and ψ, then p and ψ are 1P whenever velocity is 1P. In other words, the present theorem concerns existence conditions on u, while the result in [43] concerns the mode of operation of a waveguide with given u. That the result in [43] was not as strong as it might have been is of course a matter of some annoyance.

Proof: To establish the equivalence, it suffices to show that (a) implies (c), that (c) implies (b), and that (b) implies (a). To show that (a) implies (c), we can use a transformation to an arc-length coordinate ξ, because p is a solution to the wave equation and is 1P by hypothesis. But we cannot use such a transformation to show that (c) implies (b).

That (a) implies (c) was shown above (Eq. (4.40)), using a transformation to ξ.

To show that (c) implies (b), we only need to use the first part of (c), i.e. that $\mathbf{q}$ is parallel to ∇u. By Eq. (2.53), this means $\nabla\psi$ is parallel to ∇u. Hence the level surfaces of ψ and u have common normals; i.e. they are everywhere tangential; i.e. they coincide, so that at any time, ψ is determined by u.

Finally, to show that (b) implies (a), we recall Eq. (2.59), which shows the most general possible relationship between ψ and p:

$$p = \rho_o\dot{\psi} + A(t).$$

If ψ is a function of u and t only, so is $\dot{\psi}$, and hence, by the above equation, so is p (end of proof). •

If conditions (a), (b) and (c) are regarded as alternative definitions of a 1P acoustic field, the above theorem shows that

- the coordinates admitting 1P acoustic fields are the same for all three definitions of "1P", and
- if a particular acoustic field is 1P according to one definition, it is 1P according to all three.

Chapter 5

1P waves are planar, cylindrical or spherical.[1]

The purpose of this chapter is to find all possible coordinates admitting 1P solutions to the Helmholtz equation. An initial search is made among the coordinate systems that are separable w.r.t. the Helmholtz equation or Laplace's equation. This search produces only three wavefront geometries: planar, cylindrical and spherical. It is then proven by a more rigorous method that *no other geometries exist*. Thus the only possible 1P waveguides are those whose 1P property is obvious from symmetry. No subtle cases remain to be discovered. There is no scope for advancing the art of horn design by discovering a fundamentally new 1P geometry.

This disappointing conclusion is balanced by a discussion of the conditions under which a waveguide admits *approximately* 1P waves and is approximately described by Webster's equation. The notion of "constant directivity" is then examined in relation to the three 1P geometries.

5.1 Testing orthogonal coordinate systems

Testing a given orthogonal coordinate system to see if admits 1P waves is most convenient if conditions (4.18) and (4.19) are expressed in terms of coordinate scale factors. Let u, v, w be a set of orthogonal curvilinear coordinates, with scale factors h_u, h_v, h_w.[2] In these coordinates, the gradient and Laplacian are given by

$$\nabla\phi = \frac{1}{h_u}\frac{\partial\phi}{\partial u}\,\mathbf{e}_u + \frac{1}{h_v}\frac{\partial\phi}{\partial v}\,\mathbf{e}_v + \frac{1}{h_w}\frac{\partial\phi}{\partial w}\,\mathbf{e}_w \tag{5.1}$$

$$\nabla^2\phi = \frac{1}{h_u h_v h_w}\left[\frac{\partial}{\partial u}\left(\frac{h_v h_w}{h_u}\frac{\partial\phi}{\partial u}\right) + \frac{\partial}{\partial v}\left(\frac{h_w h_u}{h_v}\frac{\partial\phi}{\partial v}\right) + \frac{\partial}{\partial w}\left(\frac{h_u h_v}{h_w}\frac{\partial\phi}{\partial w}\right)\right] \tag{5.2}$$

[24, p. 174]. Putting $\phi = u$, we obtain

$$\nabla u = \frac{1}{h_u}\,\mathbf{e}_u \tag{5.3}$$

[1] The content of this chapter is similar to that of Sections 3, 4 and 6 of the author's 1993 paper [43].

[2] As we will not be expressing any cross-products or curls in these coordinates, the right-handedness or left-handedness of the coordinate system is immaterial.

$$\nabla^2 u = \frac{1}{h_u h_v h_w} \frac{\partial}{\partial u} \left(\frac{h_v h_w}{h_u} \right). \tag{5.4}$$

We can now apply the existence conditions. Comparing Eqs. (5.3) and (4.18), we see that

$$h_u = 1/M(u)\,,$$

i.e. that h_u depends only on u. So let us simply remember

$$h_u = h_u(u). \tag{5.5}$$

Substituting Eq. (4.19) into Eq. (5.4) and rearranging, we find

$$\frac{\partial}{\partial u} \left(\frac{h_v h_w}{h_u} \right) - h_u^2 N(u) \left(\frac{h_v h_w}{h_u} \right) = 0 \tag{5.6}$$

for which an integrating factor is

$$I(u) = \exp\left(-\int h_u^2 N(u)\, du \right).$$

Multiplying Eq. (5.6) by $I(u)$ yields

$$\frac{\partial}{\partial u} \left[I(u) \frac{h_v h_w}{h_u} \right] = 0.$$

Finally, integrating w.r.t. u and solving for $h_v h_w$ gives

$$h_v h_w = A(u)\, B(v, w)\,, \tag{5.7}$$

where

$$A(u) = h_u(u)/I(u)$$

and B (the "constant of integration") is an arbitrary function of v and w.

So conditions (5.5) and (5.7) are necessary if the orthogonal coordinate system is to admit 1P waves in the parameter u. By substituting Eqs. (5.5) and (5.7) into Eqs. (5.3) and (5.4), one may easily verify that the necessary conditions are also sufficient, i.e. that they satisfy conditions (4.18) and (4.19), for arbitrary A and B.

In words, the orthogonal coordinates u, v, w admit 1P waves in the parameter u if and only if h_u is a function of u alone and $h_v h_w$ is a function of u times a function of v and w.

5.2 Testing separable systems

We are now in a position to test some known coordinate systems. Morse and Feshbach [37, pp. 655–66] indicate that there are eleven coordinate systems in which the Helmholtz equation separates, and a further two in which Laplace's equation separates but the general Helmholtz equation does not. They give expressions for the scale factors in terms of the coordinates, from which we can see by inspection whether conditions (5.5) and (5.7) are satisfied.

For all thirteen coordinate systems, it turns out that if one coordinate satisfies condition (5.5), the other two coordinates in the same system satisfy condition (5.7), so that the system admits 1P waves in the first coordinate. The coordinates

satisfying condition (5.5) are the three Cartesian coordinates, the z coordinate in the three cylindrical systems (circular, parabolic and elliptic), the radial coordinate in the circular cylindrical system, and the r coordinate in the spherical and conical systems. That is, the only coordinates that can serve as parameters for 1P waves are those whose level surfaces are

- parallel planes,
- coaxial cylinders, or
- concentric spheres.

Because the search for suitable coordinates has been confined to separable systems, it does not constitute a proof that there are no other possible 1P wave shapes. This point should be explained further by dispelling a fallacious argument to the contrary. A separable solution to the Helmholtz equation has the product form

$$P = U(u)V(v)W(w) \tag{5.8}$$

while a one-parameter solution in u has the form

$$P = U(u) \tag{5.9}$$

which is a product solution in which $V = W = 1$. So one may be tempted to conclude that 1P solutions are special cases of separable solutions, and that therefore the search for 1P coordinates may be confined to separable coordinate systems. This argument is invalid because it does not acknowledge the full implications of separability: when we describe a coordinate system as separable with respect to a particular partial differential equation (PDE), we mean not only that the solution is of a particular form, but also that we can resolve the PDE into three ODE's by following a fixed formal procedure. So the class of separable solutions is narrower than suggested by Eq. (5.8) alone. Moreover, for the Helmholtz equation, the success of the separation procedure depends on certain conditions (given by Morse and Feshbach [37], pp. 509–10, 655), not all of which follow from conditions (5.5) and (5.7). So we do not yet have a proof that a coordinate admitting 1P solutions to the Helmholtz equation is part of a separable system.

(Among the requirements for separability given in reference [37] are

$$h_v h_w / h_u = f_1(u)\, g_1(v, w) \tag{5.10}$$
$$h_w h_u / h_v = f_2(v)\, g_2(w, u) \tag{5.11}$$
$$h_u h_v / h_w = f_3(w)\, g_3(u, v). \tag{5.12}$$

If we substitute Eq. (5.5) into Eq. (5.10), the result meets condition (5.7), accounting for the observation that among coordinate systems which are separable w.r.t the Helmholtz equation, compliance with the h_u condition implies compliance with the $h_v h_w$ condition.)

5.3 A wider search: the work of Webster and Somigliana

An investigation of permissible 1P wave shapes was made in 1908, and published in 1920, by A. G. Webster [63]—the same Webster whose name recurs in Chapters 3

and 4. Starting from the assumed existence of a 1P solution to the Helmholtz equation, Webster derived the single necessary condition

$$\nabla^2 u = Q(u)\,|\nabla u|^2 \;-\; k^2\, e^{\int Q(u)\,du} \left(B + \int e^{-\int Q(u)\,du}\, du \right) \tag{5.13}$$

where B is an arbitrary constant and $Q(u)$ an arbitrary function of u alone (Webster's notation is again different from that given here).

Webster reported that his condition was satisfied by parameters whose level surfaces were parallel planes, coaxial cylinders or concentric spheres, but not "confocal ellipsoids" (presumably including oblate and prolate spheroids). Thus he was able to test most of the separable coordinate systems using a much less convenient criterion than Eq. (4.18) above. But he was aware of the limited scope of his search and therefore hesitated to publish his findings.

(Webster indicated that his 1908 investigation was made "in the attempt to advance the theory of the megaphone" [63, p. 605]. This shows that he suspected a link between 1P waves and horns, of which the megaphone is an example. There is nothing in the cited references to imply that the suspected link involved the horn *equation*; Webster seems not to have mentioned the equation in any public forum until 1914 [62, p. 275n], and his 1919 paper retains the infinitesimal-cross-section approximation. But as there is indeed a connection between 1P waves and the horn equation, it is intriguing that Webster was working on both.)

What eventually prompted Webster to publish his 1P condition was a letter by Somigliana [51] showing that the three wavefront shapes mentioned above are the only ones allowing propagation "according to Huygens' principle". Somigliana's assumptions (which he did not list in one place) were

- one-parameter waves,
- parallel wavefronts, and
- rectilinear propagation.

Because Webster assumed only 1P waves, he apparently thought his result was more general than Somigliana's. However, it can be shown from Eq. (4.28) that the existence of 1P waves *implies* parallel wavefronts and rectilinear propagation, thereby satisfying the assumptions of Somigliana, and completing the proof that there are only three 1P wavefront shapes. Because the parameters of these waves are coordinates in separable systems, it now follows that 1P solutions to the Helmholtz equation are separable solutions (recall the discussion of Eqs. (5.8) and (5.9), above).

Concerning Somigliana's assumption of parallel wavefronts, we have established that for any 1P solution to the Helmholtz equation, the level surfaces of the wave function (the "wavefronts") are also level surfaces of a coordinate ξ measuring arc length normal to the surfaces. So if the wavefronts $\xi = \xi_1$ and $\xi = \xi_2$ are infinitesimally close together, the normal distance between them is just $\xi_2 - \xi_1$, which is uniform over the surfaces. Speaking loosely, we say that the ξ-surfaces are uniformly spaced, so that we have "parallel wavefronts"—as Somigliana assumed.

Concerning Somigliana's assumption of rectilinear propagation, it is intuitively clear that if a curve is not a straight line, its normal surfaces are not parallel. So if the ξ-surfaces (i.e. the 1P wavefronts) are parallel, their orthogonal trajectories (i.e. the rays) must be rectilinear.

That 1P waves propagate rectilinearly can be proven more rigorously using only Eq. (4.28). But first it is necessary to introduce some elementary differential geometry of curves. Let a smooth curve be represented by $\mathbf{r} = \mathbf{r}(s)$, where s is the arc length along the curve. Then the *unit tangent vector* is given by $\mathbf{t}(s) = \mathbf{r}'(s)$ and the *curvature vector* is defined as $\boldsymbol{\kappa}(s) = \mathbf{t}'(s)$.

Lemma 5.1 *A segment of a curve is rectilinear if and only if* $\boldsymbol{\kappa} = \mathbf{0}$ *on that segment.*

Proof: A straight line has the form

$$\mathbf{r} = \mathbf{r}_0 + s\mathbf{t}_0 \tag{5.14}$$

where $\mathbf{t}_0$ is the (constant) unit tangent vector. Differentiating twice w.r.t. s gives $\mathbf{r}'' = \mathbf{0}$, i.e. $\boldsymbol{\kappa} = \mathbf{0}$.

Conversely, if $\boldsymbol{\kappa} = \mathbf{0}$, two integrations w.r.t. s give Eq. (5.14), in which $\mathbf{t}_0$ and $\mathbf{r}_0$ are the constants of integration. •

(A theorem-proof format will be used frequently in the remainder of this chapter. The end of a proof will be indicated by a bullet (•) against the right margin.)

From the assumed existence of a 1P wave $P(u)$, we have shown that u can be transformed to a coordinate ξ with the property $|\nabla\xi| = 1$ (Eq. (4.28)). Since ξ is chosen to be an increasing function of u, it follows that

$$\nabla\xi = \frac{\nabla u}{|\nabla u|}. \tag{5.15}$$

We have also assumed (in Subsection 4.2.1) that ∇u is nonzero and that u is twice continuously differentiable (twice c.d.), i.e. that ∇u is c.d. Hence, if we differentiate Eq. (5.15) by the quotient rule, we will find that $\nabla\xi$ is also c.d., i.e. that ξ is twice c.d. So ξ meets the conditions of the following theorem.

Theorem 5.1 *If* ξ *is a twice-continuously-differentiable scalar field with the property* $|\nabla\xi| = 1$*, and if* Γ *is a* ξ*-trajectory, then* Γ *is a straight line.*

Proof: Let s be the arc length along Γ in the direction of increasing ξ, so that the unit tangent vector of Γ is just $\nabla\xi$. The the vector curvature of Γ is

$$\boldsymbol{\kappa} = \frac{d}{ds}\left(\nabla\xi\right). \tag{5.16}$$

The **i** component of this is

$$\kappa_x = \frac{d}{ds}\left(\frac{\partial\xi}{\partial x}\right) \tag{5.17}$$

Using the fundamental relation between gradient and directional derivative, this becomes

$$\kappa_x = \nabla\left(\frac{\partial\xi}{\partial x}\right).\nabla\xi. \tag{5.18}$$

Now we can interchange the ∇ and $\partial/\partial x$ operators, since this only involves changing the order of partial differentiation w.r.t. the Cartesian coordinates, which is permissible for second-order partial derivatives of a twice c.d. scalar field. So

$$\kappa_x = \nabla\xi\,.\frac{\partial}{\partial x}\left(\nabla\xi\right) = \frac{1}{2}\frac{\partial}{\partial x}\left(\nabla\xi.\nabla\xi\right) = \frac{1}{2}\frac{\partial}{\partial x}\left(1\right) = 0. \tag{5.19}$$

Similarly, $\kappa_y = \kappa_z = 0$, so $\boldsymbol{\kappa} = \mathbf{0}$. Hence, by Lemma 5.1, Γ is rectilinear. •

Thus the orthogonal trajectories of 1P wavefronts are straight lines; that is, 1P waves exhibit rectilinear propagation.

Having shown that Somigliana's assumptions are true for all 1P waves, we may appropriate his conclusion: the only possible 1P wavefront shapes are parallel planes, coaxial cylinders and concentric spheres.

5.4 Proof that there are only three cases

Somigliana's letter is not widely accessible to modern engineers, and not only because it is written in Italian. It predates the popularization of the Gibbs vector notation, so that its meaning is often hidden in a proliferation of scalar symbols arranged in triplets. It assumes considerable knowledge of the differential geometry of surfaces, using theorems without naming or stating them, and making only one supporting reference to a rare textbook[3]. The reader who wishes to understand Somigliana's entire argument is referred to Appendix A, which is an English paraphrase of his letter, in modern notation, with added explanatory notes.

Some of the missing links in Somigliana's proof are too long to be be included as footnotes in Appendix A. Moreover, much of Somigliana's argument can be bypassed by exploiting the 1P existence conditions (4.18) and (4.19). For these reasons, a substantially complete proof of Somigliana's result is given below. Some of the preliminary results are quoted from textbooks; others are proven from first principles because this seems easier than adapting related results found in books. The proof of the pivotal Theorem 5.3 is a shortened version of Somigliana's and may be compared with Appendix A. The proof of the concluding Theorem 5.4 was devised by the present author, although it is likely that the same theorem was proven in the works of Bianchi [12] or of his contemporary, Darboux [15]. (The author has not seen references [12] and [15]; they are listed by Struik [55] in his bibliography.)

Condition (4.18) implies that the wave can be expressed in terms of a coordinate ξ which measures arc length normal to its level surfaces. Its scale factor is unity, its level surfaces are parallel and their orthogonal trajectories are straight lines. Let Σ_0 denote a general constant-ξ surface, and let the parametric form of Σ_0 be

$$\mathbf{r} = \mathbf{r}_0(v, w).$$

Let us choose the origin of ξ so that $\xi = 0$ on Σ_0. Then another general constant-ξ surface, which we will call Σ, is given by

$$\mathbf{r} = \mathbf{r}_0(v, w) + \xi \mathbf{n}(v, w) \tag{5.20}$$

where $\mathbf{n}$ is the unit normal to Σ_0 in the direction of increasing ξ; that is, $\mathbf{n} = \mathbf{e}_\xi$.

If ξ is fixed, Eq. (5.20) represents a general point on Σ; but if ξ is allowed to vary, Eq. (5.20) can represent any point in space, so that, at least in some region containing Σ, we can use (ξ, v, w) as spatial coordinates. To formulate the 1P existence conditions in terms of this coordinate system, it is convenient to use Eq. (5.4), which assumes that the coordinates are orthogonal, i.e. that the equicoordinate surfaces are triply orthogonal. Not every singly infinite family of surfaces can be embedded

[3]Bianchi, *Lezioni di Geometria differenziale* (Pisa, 1902), vol. 1, p. 131. This is apparently the second edition, in two volumes; see reference [12].

in a triply orthogonal system of surfaces [55, p. 103]. But it is shown below that the ξ-surfaces, being parallel and having rectilinear orthogonal trajectories, can be so embedded.

Again we will need some results from classical differential geometry. Let the surface Σ contain a curve $\mathbf{r} = \mathbf{r}(s)$ with unit tangent vector $\mathbf{t}(s)$ and vector curvature $\boldsymbol{\kappa}(s)$. Then the component of $\boldsymbol{\kappa}$ normal to Σ is

$$K_{\mathrm{N}} = \boldsymbol{\kappa}.\mathbf{n} \tag{5.21}$$

where $\mathbf{n}$ is the unit normal to the surface Σ. At a given point on Σ, the value of K_{N} depends only on $\mathbf{t}$; that is, K_{N} is the same for all curves on Σ having the same tangent at the given point [60, pp. 73–5]. Thus K_{N} is a property of the surface (depending on location and direction) and is called the *normal curvature* of the surface in the direction $\mathbf{t}$. One of the curves with the tangent $\mathbf{t}$ is the *normal section*, which is the intersection of Σ with the plane of $\mathbf{n}$ and $\mathbf{t}$. It is easily shown that the vector curvature of the normal section is either parallel or antiparallel to $\mathbf{n}$. (By parameterizing the normal section in terms of arc length s, using $\mathbf{n}$ and $\mathbf{t}$ as basis vectors in the normal plane, we see that $\boldsymbol{\kappa} = \mathbf{r}''(s)$ is in the normal plane. Then, by differentiating the equation $\mathbf{t}.\mathbf{t} = 1$, we see that $\boldsymbol{\kappa} = \mathbf{t}'(s)$ is normal to $\mathbf{t}$.) So the normal curvature K_{N} may be alternatively defined as the magnitude of the vector curvature of the normal section, with a minus sign if the section is convex in the agreed direction of $\mathbf{n}$. (Both definitions of K_{N} are needed in the proofs below.)

The directions of $\mathbf{t}$ in which K_{N} reaches its extreme values are called the *principal directions*, and are orthogonal [60, p. 80] (unless K_{N} is the same in all directions at the point in question, in which case we can still choose two orthogonal directions with extreme, but equal, normal curvatures). A curve which lies on Σ and whose tangent is always in a principal direction is called a *line of curvature*; two families of lines of curvature form an orthogonal grid over Σ. At any point on Σ, the normal curvatures in the principal directions (i.e. in the directions of the lines of curvature) are called the *principal curvatures*. Letting K_v and K_w denote the principal curvatures, we define the *mean curvature* as

$$H = \tfrac{1}{2}(K_v + K_w) \tag{5.22}$$

and the *Gaussian curvature* or *total curvature* as

$$K = K_v K_w. \tag{5.23}$$

Now, Dupin's theorem [60, pp. 58–9] states that in a triply orthogonal system of surfaces, all the surfaces intersect in lines of curvature. So if we want (ξ, v, w) to be orthogonal, we must choose the lines of curvature over Σ_0 as the parametric curves for v and w. Assuming that the coordinates have been so chosen, let the lines of curvature over which v varies be known as the v-curves, and likewise for w. The principal curvatures will then be the normal curvatures of the v- and w-curves, which is why they have been called K_v and K_w above. We can now prove the desired result:

Theorem 5.2 *The ξ-surfaces can be embedded in a triply orthogonal system of surfaces.*

Proof: Σ_0 and Σ are general ξ-surfaces. Let s_0 denote the arc length along a v-curve on Σ_0, and s the arc length of the corresponding curve (i.e. the curve with

the same values of v and w) on Σ. Differentiating Eq. (5.20) w.r.t. s_0 (and using a prime to denote d/ds_0), we obtain

$$s' \frac{dr}{ds} = \mathbf{r}_0' + \xi \mathbf{n}'.$$

This may be written

$$s'\mathbf{t} = \mathbf{t}_0 + \xi \mathbf{n}' \tag{5.24}$$

where $\mathbf{t}_0$ is the unit tangent to the curve on Σ_0, and $\mathbf{t}$ the corresponding unit tangent to the curve on Σ. (The zero subscript will be used consistently in symbols referring to Σ_0, except for the normal vector $\mathbf{n}$, which is common to both Σ and Σ_0 for given v and w.) On Σ_0, we have by Rodrigues' theorem [60, pp. 59–60]

$$\mathbf{n}' = -K_{v0}\, \mathbf{r}_0' = -K_{v0}\, \mathbf{t}_0 \tag{5.25}$$

where K_{v0} is the normal curvature of the v-curve. Substituting Eq. (5.25) into Eq. (5.24) yields

$$s'\mathbf{t} = (1 - \xi K_{v0})\, \mathbf{t}_0.$$

Since $\mathbf{t}$ and $\mathbf{t}_0$ are unit vectors, this result implies

$$\mathbf{t} = \mathbf{t}_0 \tag{5.26}$$

and

$$s' = 1 - \xi K_{v0} \tag{5.27}$$

(where we agree to let s' change sign if necessary, rather than let $\mathbf{t}$ reverse its direction). Eq. (5.26) means that, for given values of v and w, the v-curves on Σ are parallel to those on Σ_0. Similarly, the w-curves on Σ are parallel to those on Σ_0. Therefore, since the v- and w-curves are orthogonal on Σ_0, they are also orthogonal on Σ.

Thus the two families of surfaces generated by the normal to any ξ-surface as it moves along the lines of curvature intersect any other ξ-surface in two orthogonal families of curves; that is, these two families of surfaces together with the ξ-surfaces form a triply orthogonal system. •

The proof of this theorem establishes that (ξ, v, w) form a triply orthogonal coordinate system. Moreover, by Dupin's theorem, the three families of coordinate surfaces intersect each other in lines of curvature, so the coordinate curves on *any* ξ-surface (not just Σ_0) are lines of curvature. (These facts are implicitly stated by Somigliana in his opening sentence, but not proven or justified by any references.)

The preceding proof uses only the first 1P existence condition, i.e. that the ξ-surfaces are parallel. But given the existence of an orthogonal coordinate system including ξ, we may proceed to express the second 1P existence condition (4.30) in terms of the scale factors. Putting $u = \xi$ and $h_u = 1$ in Eq. (5.4) and using condition (4.30), we obtain

$$\frac{1}{h_v h_w} \frac{\partial}{\partial \xi} (h_v h_w) = L(\xi). \tag{5.28}$$

This condition lets us shorten the proof of the pivotal result in Somigliana's argument:

Theorem 5.3 *Every ξ-surface has constant mean and total curvatures.*

Proof: First we express the scale factors for v and w on the ξ-surface Σ in terms of the corresponding values on Σ_0. Multiplying both sides of Eq. (5.27) by ds_0/dv and using the chain rule on the left yields

$$\frac{ds}{dv} = (1 - \xi K_{v0}) \frac{ds_0}{dv}$$

or, in terms of the scale factors on Σ and Σ_0,

$$h_v = (1 - \xi K_{v0})\, h_{v0}. \tag{5.29}$$

Similarly,

$$h_w = (1 - \xi K_{w0})\, h_{w0}. \tag{5.30}$$

Now we substitute Eqs. (5.29) and (5.30) into Eq. (5.28) and perform the indicated differentiation w.r.t. ξ, noting that h_{v0}, h_{w0}, K_{v0} and K_{w0} depend on ξ_0 and not on ξ. The result is

$$-L(\xi) = \frac{(1 - \xi K_{v0})K_{w0} + (1 - \xi K_{w0})K_{v0}}{(1 - \xi K_{v0})(1 - \xi K_{w0})}. \tag{5.31}$$

Putting $\xi = 0$ reduces this to

$$-L(0) = K_{v0} + K_{w0} = 2H_0 \tag{5.32}$$

where H_0 is the mean curvature of Σ_0 (cf. Eq. (5.22)). Since L is a function of ξ alone, Eq. (5.32) implies that H_0 is constant over the surface, as claimed.

Expanding the numerator and denominator on the right of Eq. (5.31), and writing $K_{v0} + K_{w0} = 2H_0$ and $K_{v0}K_{w0} = K_0$ (after Eqs. (5.22) and (5.23)), we find

$$-L(\xi) = \frac{2H_0 - 2K_0\xi}{1 - 2H_0\xi + K_0\xi^2}\,, \tag{5.33}$$

which may be solved for K_0 to obtain

$$K_0 = \frac{(1 - 2H_0\xi)L(\xi) + 2H_0}{2\xi - \xi^2 L(\xi)}. \tag{5.34}$$

Since H_0 is independent of v and w, so is K_0; that is, the total curvature of Σ_0 is also constant. Because Σ_0 is a general ξ-surface, it follows that *every* ξ-surface has constant mean and total curvatures. •

Given that H and K are constant, we may invert Eqs. (5.22) and (5.23) and conclude that *every ξ-surface has constant principal curvatures.*

At this point, Somigliana immediately concludes that every ξ-surface is planar or circular-cylindrical or spherical—as if it were widely known that these are the only shapes of surfaces having constant principal curvatures. A proof of that unstated premise is given below; it requires an preliminary lemma.

Lemma 5.2 *A surface segment is planar if and only if both principal curvatures are identically zero on that segment.*

Proof: If the surface is planar, all the normal sections through a given point are

straight lines. Hence, by Lemma 5.1, all the normal sections have zero vector curvature. Hence the normal curvature K_{N} (which, according to the second definition given above, is the magnitude of the vector curvature of the normal section, with a sign) is zero in every direction. Therefore the principal curvatures (extrema of K_{N}) are also zero.

For the converse, simply note that every step in the argument is an equivalence.•

Theorem 5.4 *If Σ_0 is a surface having constant principal curvatures, Σ_0 must be a plane or a circular cylinder or a sphere.*

Proof: Let v and w be the parameters of Σ_0, with the lines of curvature as parametric curves, and let Σ be a parallel surface at a distance ξ from Σ. Then Eq. (5.20) and all steps in the proof of Theorem 5.2 are applicable. Recalling that s_0 measures arc length along a v-curve, we may differentiate Eq. (5.26) w.r.t. s_0 and obtain

$$\boldsymbol{\kappa} s' = \boldsymbol{\kappa}_0. \tag{5.35}$$

If we dot-multiply both sides with $\mathbf{n}$, write $\boldsymbol{\kappa}.\mathbf{n} = K_v$ and $\boldsymbol{\kappa}_0.\mathbf{n} = K_{v0}$ (by the first definition of the normal curvature), substitute from Eq. (5.27) and solve for K_v, we find

$$K_v = \frac{K_{v0}}{1 - \xi K_{v0}}. \tag{5.36}$$

Similarly,

$$K_w = \frac{K_{w0}}{1 - \xi K_{w0}}. \tag{5.37}$$

These equations confirm that K_v and K_w are uniform over *every* parallel surface Σ (since, by hypothesis, K_{v0} and K_{w0} are constant over Σ_0). They also allow us to deduce the possible shapes of Σ_0:

Case 1: If K_{v0} and K_{w0} are both zero, so are K_v and K_w. By Lemma 5.2, this means that if Σ_0 is a plane, so is any parallel surface Σ.

Case 2: Now suppose one of the principal curvatures of Σ_0 is nonzero, and assume without loss of generality that it is K_{v0}. Then, from Eq. (5.36), there exists a value of ξ for which K_v is infinite. Since K_v is uniform over every surface Σ, a singularity in K_v implies that Σ is a degenerate surface, i.e. a point or a curve. Thus case 2 resolves into two sub-cases:

Case 2(a): If Σ is a point, the parallel surface Σ_0 is a sphere (and all the other parallel surfaces are concentric spheres).

Case 2(b): If Σ is a curve, consider a parallel surface Σ' which is infinitesimally close to Σ. We may visualize Σ' as a thin tube of circular cross-section with Σ as its axis. If the curve Σ has nonzero curvature, then the total curvature of the surface Σ' varies continuously, being positive (like an ellipsoid) on the convex side of Σ and negative (like a saddle) on the concave side, which contradicts the above conclusion that the principal curvatures (hence the total curvature) of every parallel surface are constant. Hence Σ must be a straight line, so that the parallel surface Σ_0 is a circular cylinder (and all the other parallel surfaces must be coaxial cylinders). •

Before applying this result to the 1P wavefronts, there is one loose end to be tied. It is stated above that if H and K are constant, then "we may invert Eqs. (5.22)

and (5.23)" to find that K_v and K_w are constant. In fact K_v and K_w are found to be roots of the quadratic equation

$$x^2 - 2Hx + K = 0. \tag{5.38}$$

Since the coefficients of this equation are constant, so are the roots. But of course the roots may be interchanged, raising the possibility that K_v and K_w are only piecewise constant, i.e. that the surface is made of segments with constant principal curvatures, but that the principal curvatures are swapped as we cross a segment boundary. However, swapping the principal curvatures is significant only if the curvatures are unequal, which happens only in the cylindrical case, and it is clear that two cylindrical segments of equal radius can be joined into a smooth surface *only if they are segments of the same cylinder*, in which case the normal curvature in a particular direction does not change at the segment boundary. This rules out any interchange of principal curvatures in the 1P wavefronts, so that Theorem 5.4 is applicable to the wavefronts.

5.4.1 Geometric interpretation

Credence may be added to the above argument by developing geometric interpretations of some of its intermediate results. Let the normal radii of curvature of Σ in the directions of the v-curves and w-curves, i.e. the principal radii of curvature, be defined by

$$R = -1/K_v\,; \quad S = -1/K_w \tag{5.39}$$

where the minus signs give positive radii for a surface which is *convex* in the $\mathbf{n}$ direction, i.e. the direction of increasing ξ. Similarly, let

$$R_0 = -1/K_{v0}\,; \quad S_0 = -1/K_{w0}. \tag{5.40}$$

Solving these equations for K_v, K_w, K_{v0} and K_{w0} and substituting into Eqs. (5.36) and (5.37) yields

$$R = R_0 + \xi\,; \quad S = S_0 + \xi. \tag{5.41}$$

These results indicate that the change in each principal radius of curvature is just the change in ξ. Somigliana thought this fact so obvious that he used it without proof in his argument, but we see here that it is a redundant premise.

Using Eqs. (5.39) to (5.41), we can rewrite Eqs. (5.29) and (5.30) as

$$\frac{h_v}{h_{v0}} = \frac{R_0 + \xi}{R_0} = \frac{R}{R_0}$$

and

$$\frac{h_w}{h_{w0}} = \frac{S_0 + \xi}{S_0} = \frac{S}{S_0}\,,$$

indicating that the scale factors on the ξ-surface are proportional to the principal radii of curvature. This is a familiar property of cylindrical and spherical coordinates; in both systems, the scale factor of an angular coordinate is proportional to the radial coordinate.

5.5 Approximately-1P horns

Webster's equation by its nature requires a 1P field (the effort in Chapter 4 was directed at proving the sufficiency, rather than the necessity, of a 1P field). The implication of Section 5.4 is that there are only three permissible geometries for 1P waves, and hence only three profiles for horns that can be modeled by Webster's equation (cylindrical, cylindrical-sectorial, and conical). In view of this extremely restrictive finding, it is of interest to salvage the equation by finding conditions under which it is approximately true, but not an exact consequence of the wave equation or the linearized acoustic equations.

The derivations of Webster's equation in Sections 3.2 and 4.3 assume that p depends on only one spatial coordinate, whose level surfaces are parallel, and which may therefore be transformed to another coordinate measuring arc length along the orthogonal trajectories to its level surfaces. So if p is *nearly* a function of only one coordinate (i.e. nearly independent of the other two), and if that coordinate has *nearly* parallel level surfaces (so that the arc lengths between any two level surfaces, along the orthogonal trajectories, are all nearly equal, allowing an approximate transformation to an arc-length coordinate), then Webster's equation is still approximately true.

These assumptions hold inside a rigid-walled tube whose cross-section varies only gradually (in the sense that the wall makes a small angle with the axis) and remains *small compared with the wavelength*; this is a slight generalization of Webster's "infinitesimal cross section" assumption. The coordinate surfaces *need not* be assumed planar, but they must cut the tube approximately at right angles and their radii of curvature must be large compared with the cross-sectional dimensions. The pressure variation over each small cross-section is then negligible, so that pressure may be considered a function of single coordinate whose level surfaces are the cross-sections. The assumptions still hold if such a tube is bent with a radius of curvature much larger than the cross-sectional dimensions. (For example, if the tube is bent into a circular arc, we can use planes through the axis of the arc as coordinate surfaces, because the spacing of the planes, although non-uniform in the large, is nearly uniform within the thin tube.)

The assumptions can also be made to hold in a tube of *large* cross-section whose shape does not depart greatly from that of an exact 1P waveguide; if such a tube is driven uniformly over one cross-section, the wave function will remain nearly 1P as it propagates. In the case of an approximately conical horn, it is possible that the throat cross-sectional dimensions are small compared with the wavelength while the corresponding mouth dimensions are large enough to suppress reflections (see Section 5.6, below), in which case the wave function will be nearly 1P if the horn is driven at the throat, because the narrowness of the throat will guarantee nearly uniform conditions over the throat cross-section. Of course, when we apply Webster's equation to a nearly conical horn, the cross-sectional area $S(\xi)$ must be calculated on the assumption that the wavefronts are nearly spherical, not planar.

One can also combine the two cases mentioned above: if a thin tube (not necessarily of uniform cross-section) is tangentially joined to a sufficiently long, nearly conical horn, and if this assembly is driven at the thin end, then the resulting wave function will be nearly 1P throughout, so that Webster's equation may be used for the whole assembly.

5.6 "Constant directivity"

It was shown in Subsection 4.2.4 that a coordinate admitting 1P waves at one frequency does so at all frequencies. Hence a 1P waveguide can be driven so as to exhibit the uniform-intensity property (Section 4.4) at all frequencies. Moreover, because the orthogonal trajectories to the wavefronts are rectilinear, the waveguide boundary must be a *ruled surface* (a tube of straight lines), so that an infinitely long 1P waveguide has an unambiguous angle of coverage at infinity. (The coverage angle is also fully determined by the curvature of any single wavefront.) Thus a properly driven *infinite* 1P waveguide possesses *constant directivity* over an infinite bandwidth, in the sense that the intensity is uniform over a fixed coverage angle at all frequencies.

If this infinite waveguide is now truncated, the wavefront will diffract and reflect at the open mouth of the waveguide, so that the wave function inside and outside the waveguide will no longer be 1P. If the wavelength is small compared with the dimensions of the mouth, however, the effect of diffraction and reflection will be slight, so that the wave function will still be *approximately* 1P inside the waveguide, and the wavefront will continue to propagate beyond the mouth in a roughly rectilinear pattern, maintaining the coverage angle. So at sufficiently high frequencies, a properly driven "finite 1P" waveguide has *approximately* constant directivity in the sense that it produces a roughly uniform intensity over a nearly constant coverage angle; as frequency increases, the intensity becomes more uniform, and the coverage angle becomes more sharply defined as it approaches the coverage angle of the equivalent infinite waveguide.

This statement can be refined by considering the three 1P waveshapes. Plane waves are guided by a cylindrical tube, whose boundary surface is defined by a relation between y and z (independent of x) in a suitably oriented Cartesian coordinate system. The coverage angle of this tube, in any plane, is zero. When truncated, the tube will give approximately constant directivity only in the near field; in the far field, the effects of diffraction will dominate the radiation pattern, because the angular dimensions of the diffraction pattern, however small, will be greater than the zero coverage angle. Cylindrical waves are guided by a cylindrical sectorial horn, whose boundary surface is defined in circular-cylindrical coordinates by specifying a relation between ϕ and z. This horn has zero coverage angle in any plane through the z axis and a nonzero coverage angle in all planes that are normal to the z axis and cut the boundary surface. When truncated, this horn will also give approximately constant directivity only in the near field; the far-field radiation pattern in any plane through the z axis will be dominated by diffraction. Spherical waves are guided by a conical horn, whose boundary surface is defined in spherical coordinates by a relation between θ and ϕ. This horn has a nonzero coverage angle in any plane through its centroidal axis; at sufficiently high frequencies, this coverage angle will dominate the effects of diffraction, giving approximately constant directivity in both the near and far fields. If we assume that all loudspeaker horns are to be used in the far field, the conical horn is the only 1P waveguide whose constant directivity can be exploited. The angular dimension(s) of the cone, measured at the apex, determine the coverage angle(s) of the horn.

Of course, the cross-sections of the three waveguides referred to in the preceding paragraph may have arbitrarily-shaped boundary curves; that is, the cylindrical tube and the conical horn are not restricted to circular cross-sections, nor the cylin-

drical sectorial horn to a rectangular cross-section. The only restriction is that the waveguide boundary should be a tube of perpendiculars to the wavefronts. For this reason, it is sometimes useful to describe the shape of a "waveguide" with reference to the guided wavefront rather than the guiding surface. Geddes [18] seems to favor the convention that the shape of a "waveguide" refers to the wavefront while the shape of a "horn" refers to the boundary surface; thus a conical horn is a spherical waveguide, a cylindrical sectorial horn is a cylindrical waveguide, and a cylindrical horn or tube is a planar waveguide.

One qualification should be made concerning the conical horn. While it is reasonable to describe the intensity as "roughly uniform" at high frequencies, only in the near field does the intensity asymptotically approach perfect uniformity as frequency increases. In the far field, the radiation pattern will exhibit diffraction fringes *within the coverage area*; the fringes become narrower as frequency increases, but the fractional variation in intensity does not necessarily approach zero.[4] This phenomenon, which affects any non-planar source whose dimensions are large compared with the wavelength, is known as *Fresnel diffraction* and is discussed in almost any textbook on general or physical optics; it is more familiar in optics than in acoustics.

5.7 Note on the work of E. R. Geddes (1989, 1993)

Geddes' paper [18] begins with a short history of horn theory, followed by an inspiring discussion of acoustic waveguide geometries derivable from separable curvilinear orthogonal coordinate systems; several of these geometries are yet to be studied. In the eleven coordinate systems that are separable w.r.t. the wave equation, Geddes correctly identified the coordinates in which Webster's equation is exact, noting that they have unit scale factors, that the wavefront does not change shape as it propagates, and that in two cases the wavefronts are non-planar. He also recognized the connection between 1P waves and constant directivity, underscoring the practical importance of 1P waveguides.

The core of the paper uses separation of variables to analyze an oblate spheroidal (OS) waveguide, and makes the unfortunate claim that the waveguide admits 1P waves in the "radial" coordinate μ. Geddes' expectation of 1P behavior seems to have effected his treatment of the boundary conditions in the problem [42]; compare the analysis by Freehafer [17]. Chapters 4 and 5 of this thesis offer three reasons why the 1P claim cannot be true. First, the constant-μ surfaces are confocal oblate spheroids, which do not conform to any of the three permitted geometries for 1P wavefronts. Second, the μ coordinate fails to satisfy the gradient condition (Section 5.1), and Webster apparently found that it failed his more unwieldy test [63, p. 607]. Third, Chapter 4 has shown that if the OS waveguide admitted 1P waves, it could be analyzed exactly using Webster's equation and would not require the elaborate separation of variables used by Geddes. These reasons are based on general theory. However, because Geddes' claim relates to a specific waveguide, it can also be tested using more *ad hoc* methods: working directly from the scale factors of the OS coordinate system, the present author has proven that there are no non-trivial

[4] This "qualification", which also appears in the author's 1993 paper [43, p. 445], was prompted by a personal communication from Dr Geddes (October 10, 1992), to which was attached a copy of Geddes' conference paper on diffraction from acoustic apertures. A modified version of that paper was subsequently published as a journal article [20].

1P solutions to the wave equation in the coordinate μ [42]. Although Geddes was not initially persuaded by this proof (see his reply in [42]), he eventually published a corrected analysis of the OS waveguide and withdrew the claim that it admits 1P waves [19]. The OS waveguide is in fact one of the "approximately-1P horns" described in Section 5.5.

5.8 Discussion and summary

As stated in the introduction to Chapter 4, it is easy to show that Webster's equation is equivalent to the one-dimensional wave equation in the following coordinate systems:

- Cartesian (plane waves),
- circular-cylindrical (cylindrical and plane waves), and
- spherical (spherical waves).

So if the linear and radial coordinates in these three systems are the only coordinates admitting 1P waves—as has been shown in this chapter—then it follows that every 1P wave field satisfies Webster's equation. One might therefore ask why we need a derivation of Webster's equation like that given in Section 4.3, which proceeds directly from the 1P existence conditions without first listing the coordinates that satisfy these conditions. In the author's opinion, there are three reasons.

First, the direct derivation is more instructive because it identifies the general properties of 1P waves which make Webster's equation applicable; in particular, it shows that the $|\nabla u|$ condition (Eq. (4.18)) is significant while the $\nabla^2 u$ condition (Eq. (4.19)) is not. Deriving Webster's equation from the wave equation in each of the 1P coordinate systems is just a proof by exhaustive testing—it is a proof, but not an explanation. Furthermore, identifying the permissible coordinate systems uses the $\nabla^2 u$ condition, which is not relevant to Webster's equation.

Second, the general derivation in Section 4.3, unlike a derivation tied to a finite list of specific coordinate systems, yields conditions under which Webster's equation is *approximately* correct (Section 5.5).

Third, the general derivation is much shorter than the case-by-case derivation; although the latter needs to consider only three cases, the proof that there are only three cases is long and complex. Let us compare the outlines of the two derivations and, in so doing, summarize the main lines of argument in Chapters 4 and 5. The general derivation proceeds as follows:

1. Assuming that P depends only on the coordinate u, find conditions on $|\nabla u|$ and $\nabla^2 u$ (Subsections 4.2.1 to 4.2.4);
2. Using the $|\nabla u|$ condition, transform u to ξ (Subsection 4.2.5);
3. Find $\nabla^2 p$ by applying the divergence theorem to a segment of a ξ-tube, and substitute the result into the wave equation (Section 4.3).

The main steps in the exhaustive derivation are:

1. As above;

2. As above;

3. Using the condition on $|\nabla\xi|$ (which follows from that on $|\nabla u|$), show that the ξ-trajectories are rectilinear (Lemma 5.1 and Theorem 5.1);

4. Hence prove the existence of a triply orthogonal coordinate system including ξ (Theorem 5.2);

5. Express the $\nabla^2\xi$ condition in terms of the coordinate scale factors (referring to Section 5.1);

6. Relate the scale factors on one ξ-surface to the principal curvatures of another ξ-surface, then apply the $\nabla^2\xi$ condition to deduce that the latter surface, hence every ξ-surface, has constant principal curvatures (Theorem 5.3);

7. Obtain expressions relating the principal curvatures of parallel surfaces, require these curvatures to be constant, and deduce that the surfaces are planes, circular cylinders or spheres (Theorem 5.4);

8. For the linear or radial coordinate in each of the three geometries, write Webster's equation and the one-dimensional wave equation and note that they are the same.

Thus the exhaustive derivation is much longer. Moreover, the exhaustive derivation includes the first two steps of the general derivation, which requires only one more step for its completion.

For these reasons it has been both instructive and convenient to derive Webster's equation directly from the 1P existence conditions.

Chapter 6

The Finite-Difference Equivalent-Circuit model: a lumped equivalent circuit for a distributed acoustic field

6.1 Introduction: the work of M. Arai (1960)

The analogies between acoustic and electrical quantities suggest that some large and expensive acoustic devices can be simulated by cheap electrical circuits, thereby reducing the cost of building and testing prototypes. This possibility was noted in the late 1950's by Masaaki Arai of the Japanese Railway Technical Research Institute, who was apparently interested in the analysis and design of mufflers. Arai's theoretical work provides much of the inspiration for Chapters 6 to 11 of this thesis.

For the modern audio engineer, the existence of electrical-acoustical analogs implies that some acoustic systems can be simulated using computer software designed for electrical circuit analysis. Such software is highly developed, readily available, and familiar. Moreover, if an acoustic field is being generated or processed by electroacoustic transducers having some electrical elements, as is usually the case in audio engineering, then electrical analogs offer a unified method for the analysis of both the electrical and acoustic components of the mixed-domain system. Such a unified approach is convenient even if off-the-shelf software is not used. The difficulty is that the electrical-acoustical analogs presented in the preceding chapters are restricted to certain classes of acoustic fields, e.g. one-parameter fields or regions of uniform density. What is needed is an electrical model that is valid for more general acoustic fields.

The first step in the development of such a model was made by Arai [2], who applied the *finite-difference method* (FDM) to the acoustic wave equation and found that the resulting difference equations had the same form as the nodal equations of a network of inductors and capacitors. Thus he modeled a *distributed* acoustic field using a network of *lumped* electrical components.

To introduce his method, Arai first considered the simplest one-dimensional case: plane waves propagating in a straight tube of constant cross-section. Beginning with the one-dimensional time-dependent equations of motion and compression in

Cartesian coordinates, then assuming sinusoidal time-dependence, he obtained a result equivalent to the one-dimensional Helmholtz equation (or the time-independent Webster equation for a uniform cross-section) with pressure as the wave function. Then, using the finite-difference approximation and making convenient notational substitutions, he produced the nodal equations[1] of an L-C ladder network (Eqs. (4) and (5) and Fig. 1 in reference [2]). End conditions were handled by partitioning the terminal circuit elements (Figs. 1(c) and 2(c), ibid.) and adding end equivalent circuits (Fig. 3, ibid.). *N.B.: In the remainder of this section, all equation numbers and diagram numbers refer to Arai's paper [2].*

Arai discussed the error of approximation in the one-dimensional case and concluded that the phase error would be less than 5% provided that $k\Delta x < 1$, where k is the wave number and Δx is the step size. This condition holds for frequencies up to $c/(2\pi\Delta x)$. So the FDM is a low-frequency approximation, and the maximum frequency at which the model is valid is determined by the step size.

Turning to the three-dimensional case, Arai began with the time-dependent 3D equations of motion and compression, converted them to phasor form, and combined them to give a result equivalent to the 3D Helmholtz equation in Cartesian coordinates. Then, following the example of the one-dimensional case, he made finite-difference substitutions for the derivatives of pressure, and defined symbols for subexpressions with the dimensions of acoustic mass and acoustic compliance. The result was a set of nodal equations for a 3D rectangular network of inductors and capacitors (Eqs. (25) and (26)), in which each grid point was connected to its six neighbors via inductors and to ground via a capacitor (Fig. 5).

He also rewrote the 3D Helmholtz equation in *cylindrical* coordinates and repeated the finite-difference substitution to derive another set of network equations (Eqs. (29) and (30) and Fig. 6). The cylindrical network had components whose values varied with the radial coordinate, whereas the Cartesian network had equal capacitors and only three values of inductance (one for each coordinate direction).

Finally, Arai showed how the 3D networks reduce to 1D ladder networks when propagation is restricted to one coordinate direction. The simplification was carried out by grouping components in parallel. In the case of radial propagation in cylindrical coordinates—which was not considered in the introductory one-dimensional analysis—the reduction gave an L-C ladder network with unequal components. Arai then asserted that such a network can be used to model a horn whose cross-section varies arbitrarily, provided that the cross section remains small compared with the wavelength. With this intuitive leap, he concluded the theoretical part of his paper.

This chapter is a generalization and extension of Arai's work. It covers a wider range of coordinate systems, yields information concerning flux as well as pressure, and extends the treatment of boundary conditions to three dimensions.[2]

[1] In the one-dimensional case, Arai also obtained a Helmholtz-like equation in terms of volume velocity. Substituting a finite-difference approximation into this equation gave the *mesh* equations of an L-C ladder network (Eq. (7) and Fig. 2 in reference [2]).

[2] Before discovering Arai's paper, the present author derived a 3D L-C network from the integral forms of the equations of motion and compression, using hexahedral volume elements bounded by equicoordinate surfaces in arbitrary curvilinear orthogonal coordinates. The derivation involved some *ad hoc* approximations and had no visible connection with the FDM. Arai's work suggested that an equally general result could be obtained more rigorously by applying the FDM in arbitrary orthogonal coordinates. Hence the theory in this chapter is presented using Arai's finite-difference approach, and the integral-form approach has been abandoned. The development of the damped

In the one-dimensional case, Arai derived his ladder network from the Helmholtz equation for Cartesian and (eventually) cylindrical coordinates. Here it will be shown that such a network emerges when the finite-difference approximation is applied to the time-dependent Webster equation, or to the general 1P forms of the equations of motion and compression. The use of Webster's equation justifies Arai's claim that his network is applicable to general horn profiles (if propagation is nearly 1P so that Webster's equation can be used). Similar treatment of the equations of motion and compression proves that the ladder network correctly models flux, and shows how to represent boundary conditions using circuit elements.

In the three-dimensional case, Arai derived his L-C network from the Helmholtz equation in Cartesian and cylindrical coordinates only. In this chapter a more general network will be derived in arbitrary curvilinear orthogonal coordinates. Two derivations will be given, the first based on the wave equation and the second on the equations of motion and compression; the former derivation will adhere strictly to the FDM, while the latter will yield information on flux and allow a variety of boundary conditions to be included in the electrical model.

Finally, this chapter will not only consider the reduction from three dimensions to one (as did Arai's paper) but will also show how a two-dimensional network can sometimes be used to advantage, e.g. in the case of axial symmetry.

In this thesis, an electrical network derived from the finite-difference approximation will be called a *finite-difference equivalent circuit* or FDEC. The abbreviation "FDEC" will also be used as an adjective to describe the resulting model or a simulation based thereon.

6.1.1 A note on computational efficiency

The advantages of the FDEC method are:

- It produces a unified model of the electrical and acoustic components of a mixed-domain system, and
- The model can be analyzed using off-the-shelf software.

Note that computational efficiency is *not* among the claimed advantages. The author does not suggest that the FDEC model is computationally competitive with other methods of analysing acoustic fields, such as finite-element or boundary-element methods. Neither does he suggest that the off-the-shelf software, such as SPICE, gives optimal efficiency in the analysis of the resulting FDEC networks; the topological restrictions applicable to these networks are not exploited by general-purpose software.

However, in the overall time-scale of a research or design project, the convenience of the FDEC method may be more important than computational efficiency.

---

finite-difference equivalent-circuit model for fiber-filled regions (see Chapter 7) was commenced after Arai's work was discovered; no attempt was made to derive the same damped equivalent circuit using the integral-form approach.

6.2 The finite-difference method: theory and notation

The finite-difference method used in this chapter is based on the second-order approximation

$$f'(x) \approx \frac{f(x+\frac{\Delta x}{2}) - f(x-\frac{\Delta x}{2})}{\Delta x}. \tag{6.1}$$

It can be shown by direct substitution that the approximation is exact if $f(x)$ is a polynomial of degree two or less. Otherwise, if $f(x+\frac{\Delta x}{2})$ and $f(x-\frac{\Delta x}{2})$ are expanded in Taylor series about x, the principal error term is found to be

$$\frac{f'''(x)}{24}(\Delta x)^2.$$

Because f''' is not likely to be known, the important point is that the error is proportional to $(\Delta x)^2$.

For a 1P wave, the excess pressure p and flux u are functions of ξ and t, where ξ is a spatial coordinate measuring arc length normal to its level surfaces, and t is time. Now let ξ take a series of discrete values ξ_n, defined by

$$\xi_n = \xi_0 + n\Delta\xi \tag{6.2}$$

where n is a multiple of *one half*, and define the notations

$$p_n(t) = p(\xi_n, t) \tag{6.3}$$
$$u_n(t) = u(\xi_n, t). \tag{6.4}$$

Then the basic rule expressed in Eq. (6.1) gives the approximations

$$\left.\frac{\partial p}{\partial \xi}\right|_{\xi_{n+\frac{1}{2}},t} \approx \frac{p_{n+1}(t) - p_n(t)}{\Delta\xi} \tag{6.5}$$

and

$$\left.\frac{\partial u}{\partial \xi}\right|_{\xi_n,t} \approx \frac{u_{n+\frac{1}{2}}(t) - u_{n-\frac{1}{2}}(t)}{\Delta\xi}. \tag{6.6}$$

For a three-dimensional acoustic field we use curvilinear orthogonal coordinates u, v, w, which take the discrete values

$$u_i = u_0 + i\Delta u \tag{6.7}$$
$$v_j = v_0 + j\Delta v \tag{6.8}$$
$$w_k = w_0 + k\Delta w \tag{6.9}$$

where i, j, k are multiples of $\frac{1}{2}$. When the subscripts "i, j, k" are written together (often after a vertical bar or closing square bracket), they mean "evaluated at u_i, v_j, w_k", so that (for example)

$$p_{i+\frac{1}{2},j,k}(t) = p(u_{i+\frac{1}{2}}, v_j, w_k, t). \tag{6.10}$$

With these notations, one example of the application of Eq. (6.1) is

$$\left.\frac{\partial p}{\partial u}\right|_{i,j,k} \approx \frac{p_{i+\frac{1}{2},j,k}(t) - p_{i-\frac{1}{2},j,k}(t)}{\Delta u}. \tag{6.11}$$

Further notations will need to be defined as the chapter progresses, but will follow the pattern established above.

In this chapter and in Chapter 7, the approximation symbol "≈" will be used only for finite-difference approximations and results derived therefrom. When other approximations, e.g. linearizing approximations, are of interest, they will be noted in the text.

6.3 The 1P case

This section relates the present chapter to earlier chapters on 1P horn theory by linking Webster's equation, the 1P equations of motion and compression, the finite-difference method, and *L-C* latter networks. It is a useful introduction to the methods of this chapter because it illustrates the use of the FDM to derive equivalent circuits from acoustic equations, but avoids the more cumbersome notation and algebra that will be encountered in the 3D case.

6.3.1 Webster's equation

Arai developed his ladder network from the one-dimensional Helmholtz equation in Cartesian coordinates. Eight years earlier, Locanthi [33] had shown that a more general ladder network can be obtained from a finite-difference approximation to the time-dependent Webster equation. So it is not necessary to assume a uniform cross-section or sinusoidal time-dependence. However, whereas Arai used the "direct" or "impedance" analogy (voltage for pressure and current for flux), Locanthi used the "dual" or "mobility" analogy (vice versa). So Locanthi's work is not a generalization of Arai's and is not suitable for extension to three dimensions, although it remains a noteworthy precedent for the FDEC concept. The following derivation, in keeping with the conventions of this thesis, uses the direct analogy.

The time-dependent Webster equation (3.1) may be written

$$\left.\frac{\partial}{\partial \xi}\left(S\,\frac{\partial p}{\partial \xi}\right)\right|_{\xi,t} = \frac{S(\xi)}{c^2}\,\ddot{p}(\xi,t). \tag{6.12}$$

Putting $\xi = \xi_n$, replacing the outer derivative w.r.t. ξ by its finite-difference approximation (see Section 6.2) and multiplying through by $\Delta\xi$, we obtain

$$S_{n+\frac{1}{2}}\left.\frac{\partial p}{\partial \xi}\right|_{\xi+\frac{\Delta\xi}{2},t} - S_{n-\frac{1}{2}}\left.\frac{\partial p}{\partial \xi}\right|_{\xi-\frac{\Delta\xi}{2},t} \approx \frac{S_n\Delta\xi}{c^2}\,\ddot{p}_n(t). \tag{6.13}$$

Making the same approximation to the inner derivative then yields

$$S_{n+\frac{1}{2}}\,\frac{p_{n+1}(t) - p_n(t)}{\Delta\xi} - S_{n-\frac{1}{2}}\,\frac{p_n(t) - p_{n-1}(t)}{\Delta\xi} \approx \frac{S_n\Delta\xi}{c^2}\,\ddot{p}_n(t). \tag{6.14}$$

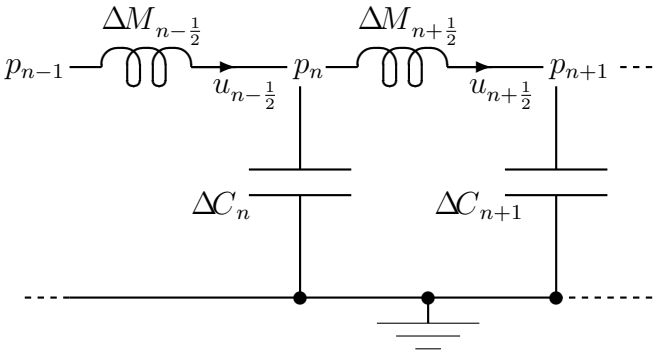

Figure 6.1: *FDEC representation of Webster's equation.*

Dividing through by ρ_o gives

$$\frac{p_{n+1}(t) - p_n(t)}{\Delta M_{n+\frac{1}{2}}} + \frac{p_{n-1}(t) - p_n(t)}{\Delta M_{n-\frac{1}{2}}} \approx \Delta C_n \, \ddot{p}_n(t) \tag{6.15}$$

where

$$\Delta M_{n+\frac{1}{2}} = \frac{\rho_o \, \Delta\xi}{S_{n+\frac{1}{2}}} \tag{6.16}$$

$$\Delta M_{n-\frac{1}{2}} = \frac{\rho_o \, \Delta\xi}{S_{n-\frac{1}{2}}} \tag{6.17}$$

$$\Delta C_n = \frac{S_n \Delta\xi}{\rho_o c^2}. \tag{6.18}$$

Eq. (6.15) is the differentiated nodal equation for the central node of the ladder network shown in Fig. 6.1; the two terms on the left are the time-derivatives of the currents flowing into the n^{th} node from the two neighboring nodes (voltage drop equals inductance times derivative of current), and the right-hand side is the time-derivative of the current from the n^{th} node to ground (current equals capacitance times *first* derivative of voltage). To avoid cluttering the diagram, nodal pressures are written "in the nodes".

While Eq. (6.15) models the excess pressure and gives an analogy between pressure and voltage, it does not of itself show that the associated current in Fig. 6.1 is analogous to volume flux (this shortcoming was not addressed by Arai). To show that the equivalent circuit also models flux, it is necessary to establish a relationship between pressure and flux using either the equation of motion or the equation of compression.

6.3.2 The equations of motion and compression

The inertial properties of a 1P horn may be described by combining Eqs. (2.21) and (2.22):

$$-\left.\frac{\partial p}{\partial \xi}\right|_{\xi,t} = \frac{\rho_o}{S(\xi)} \, \dot{u}(\xi, t). \tag{6.19}$$

Now if we let $\xi = \xi_{n+\frac{1}{2}}$, replace the derivative on the left with its finite-difference approximation (see Section 6.2) and let

$$S_n = S(\xi_n) \, , \tag{6.20}$$

we have

$$\frac{p_n(t) - p_{n+1}(t)}{\Delta\xi} \approx \frac{\rho_o}{S_{n+\frac{1}{2}}}\, \dot{u}_{n+\frac{1}{2}}(t). \tag{6.21}$$

This may be written

$$p_n(t) - p_{n+1}(t) \approx \Delta M_{n+\frac{1}{2}}\, \dot{u}_{n+\frac{1}{2}}(t) \tag{6.22}$$

where $\Delta M_{n+\frac{1}{2}}$ is as defined in Eq. (6.16). This result is the branch equation for a general series branch in the ladder network of Fig. 6.1, and indicates that $\Delta M_{n+\frac{1}{2}}$ is the estimated acoustic mass of the horn segment between ξ_n and ξ_{n+1}. Eq. (6.16) has the form of Eq. (2.25) and says that $\Delta M_{n+\frac{1}{2}}$ is the acoustic mass of a *cylindrical* segment whose length is that of the actual horn segment and whose cross-sectional area is that of the actual horn at the midpoint of the segment. The appearance of a cylindrical-segment formula in the analysis of a non-cylindrical segment is an artifact of the finite-difference approximation.

Similarly, the compliance properties of a 1P horn may be described by combining Eqs. (2.51) and (2.52):

$$-\left.\frac{\partial u}{\partial \xi}\right|_{\xi,t} = \frac{S(\xi)}{\rho_o c^2}\, \dot{p}(\xi, t). \tag{6.23}$$

Letting ξ take a series of discrete values (as before), setting $\xi = \xi_n$ in the above equation, and replacing the derivative w.r.t. ξ by the finite-difference quotient, we obtain

$$\frac{u_{n-\frac{1}{2}}(t) - u_{n+\frac{1}{2}}(t)}{\Delta\xi} \approx \frac{S_n}{\rho_o c^2}\, \dot{p}_n(t). \tag{6.24}$$

This may be written

$$u_{n-\frac{1}{2}}(t) - u_{n+\frac{1}{2}}(t) \approx \Delta C_n\, \dot{p}_n(t) \tag{6.25}$$

where ΔC_n is as defined in Eq. (6.18). This result is the branch equation for a general parallel branch in Fig. 6.1, and indicates that ΔC_n is the estimated acoustic compliance of the volume between $\xi_{n-\frac{1}{2}}$ and $\xi_{n+\frac{1}{2}}$. Eq. (6.18) has the form of Eq. (2.47) and says that ΔC_n is the compliance of the volume contained in a cylinder whose length is that of the actual horn segment and whose cross-sectional area is that of the actual horn at the midpoint of the segment. Again, the substitution of a cylindrical volume for a non-cylindrical volume is an artifact of the FDM.

Eqs. (6.22) and (6.25), taken together, are equivalent to Fig. 6.1 and may be used instead of Eq. (6.15) to derive the equivalent circuit. This derivation, unlike that of Arai, gives the acoustic analog of current as well as voltage. Alternatively, because Eq. (6.22) shows that the current in the series branches of the equivalent circuit represents flux in the horn, it can be combined with Eq. (6.15) to complete the interpretation of the equivalent circuit. Eq. (6.25) can also be used to interpret the current in the equivalent circuit, but it gives differences between fluxes rather than the fluxes themselves, and is therefore less convenient than Eq. (6.22).

Comparing the two derivations of the equivalent circuit raises a point which will become important when the above methods are extended to the three-dimensional case. If the equivalent circuit is constructed from Eqs. (6.22) and (6.25), it seems that the circuit incorporates information on both pressure and flux. However, the same circuit can be derived from Eq. (6.15), which refers to pressure only. Hence

the accuracy with which the equivalent circuit models pressure does not depend on the accuracy with which it models flux. In particular, the equivalent circuit would remain a "pure" finite-difference representation of the pressure equation (Webster's equation) even if it had been necessary to depart from the FDM approach in the treatment of flux. No such departure was necessary in the 1P case. In the 3D case we shall need to estimate the fluxes using *ad hoc*, non-FDM approximations, but the modeling of pressure will still be a pure finite-difference representation of the wave equation (the 3D equivalent of Webster's equation).

There remains one obscure point on which the present author disagrees with Arai [2]. Eqs. (6.22) and (6.15) remain applicable to the circuit in Fig. 6.1 if each ΔM is split into a number of series components having the same total value, or even if it is distributed along the entire segment between the two adjacent nodes. Similarly, Eqs. (6.25) and (6.15) remain consistent with Fig. 6.1 if each ΔC is split into parallel components or distributed along the segment between two adjacent lumped ΔM's. One can even distribute $\Delta M_{n-\frac{1}{2}}$ along part of the unit cell and ΔC_n along the remainder; as long as the distributed components do not overlap, the branch and node equations remain unchanged.

In contrast to this, Arai concluded that when the FDM is applied to the pressure equation (that is, to his special case of the time-independent Webster equation), the resulting equations describe a distributed-mass, lumped-compliance network [2, pp. 17–8]. Pressure, said Arai, is a piecewise-linear, continuous function of position; therefore the flux (whose phasor representation is proportional to the gradient of pressure) is piecewise-constant with step-discontinuities. Linear pressure implies uniform distributed acoustic mass, and a step discontinuity in flux implies a lumped compliance.

The fault in Arai's argument is in his first premise. If the pressure were piecewise-linear, its second derivative would be undefined at discrete points and zero everywhere else, so that one could not meaningfully substitute for the second derivative as required by the second-order pressure equation. Furthermore, Arai's finite-difference substitution is based on the approximation

$$p''(x) \approx \frac{p(x-\Delta x) - 2p(x) + p(x+\Delta x)}{(\Delta x)^2} \tag{6.26}$$

which is exact when $p(x)$ is a polynomial of degree three or less, as may be proven by performing the indicated operations on a general cubic. Even if Arai's method is interpreted as a double application of Eq. (6.1), it is exact for quadratic functions. Hence the pressure does not have to vary linearly.

Although it is permissible to distribute the equivalent circuit elements over non-overlapping intervals, the remainder of this thesis will use only lumped components, with the compliance elements located at the pressure sampling points and the mass elements at the flux sampling points. Thus, in the equivalent circuit, both pressure and flux will be piecewise-constant with step-discontinuities. In contrast, the initial finite-difference approximation assumes that $p(\xi)$ and $u(\xi)$ are smooth functions. This contradiction arises simply because the FDM involves sampling of the pressure and flux waveforms, and only the sampled values are represented in the lumped equivalent circuit. To distribute the components may not change the equations describing the circuit, but it introduces pressures or fluxes other than the sampled values and in that sense is a departure from the FDM.

6.3.3 Truncated elements at ends

When voltage represents excess pressure and current represents volume flux, it is a trivial matter to draw a circuit representing a pressure source, a volume source, or an acoustic impedance (ratio of pressure to flux when both are expressed as phasors). A problem can arise, however, when such components are used to terminate a 1P FDEC model: if the equivalent circuit models the pressure at $\xi = \xi_n$ for integral values of n, it models the flux for values of n which are odd multiples of one half, and *vice versa*; that is, pressure and flux are sampled at different points.

This problem can be side-stepped if the only boundary conditions involved are sources. If a horn has a pressure source at each end, suitable choices of ξ_0 and $\Delta\xi$ will place both ends of the horn at pressure-sampling points. The value of the terminating compliance at each end does not matter, because loading an ideal pressure source does not affect its pressure. If the horn is terminated in a flux source, it does not matter how much series inertance is included in the branch containing the source, because such inertance has no effect on the flux in the branch. Hence the flux source may be assumed to be connected to the nearest pressure-sampling point. A rigid wall or obstruction is a special case of a flux source: an open circuit. But an impedance boundary condition requires special treatment because it gives a relationship between pressure and flux at the *same* point, while the equivalent circuit shows pressure and flux at *different* points.

Arai's solution was to synthesize an extra sample by linear interpolation. From Eqs. (2.21) and (2.51) it can be seen that a uniformly distributed inertance with no distributed compliance gives uniform $\partial p/\partial\xi$, hence a linear pressure interpolation. In the equivalent circuit, the interpolation is performed by distributing the inductance uniformly between two adjacent lumped capacitances. If the circuit is then truncated at the midpoint (the original flux-sampling point), the original lumped inductance is halved, as shown in Arai's Fig. 1. Similarly, a uniformly distributed compliance with no distributed inertance gives uniform $\partial u/\partial\xi$, hence a linear flux interpolation. In the equivalent circuit, the interpolation is performed by distributing the capacitance uniformly between two adjacent lumped inductances. If the circuit is then truncated at the midpoint (the original pressure-sampling point), the original lumped capacitance is halved, as shown in Arai's Fig. 2.

While a linear interpolation seems reasonable in itself, it is not prescribed by the FDM approximation (which is exact for quadratic functions) and is not related to the original acoustic system (for which the appropriate interpolating function is wave-like and time-dependent). The approach taken in this chapter is to apply the finite-difference approximation once with a reduced step size, thereby taking an an additional sample from the acoustic waveform. This approach avoids non-FDM approximations. It requires only that the notations defined in Section 6.2 be extended to allow n to be a multiple of *one quarter*, and that the finite-difference approximations in Subsection 6.3.2 be reworked with a step size of $\Delta\xi/2$ instead of $\Delta\xi$.

In Eq. (6.19), if we let $\xi = \xi_{n+\frac{1}{4}}$ and replace the derivative on the left with its finite-difference approximation using the new step size, we obtain

$$\frac{p_n(t) - p_{n+\frac{1}{2}}(t)}{\frac{1}{2}\Delta\xi} \approx \frac{\rho_0}{S_{n+\frac{1}{4}}}\, \dot{u}_{n+\frac{1}{4}}(t). \tag{6.27}$$

This may be written

$$p_n(t) - p_{n+\frac{1}{2}}(t) \approx \tfrac{1}{2}\Delta M_{n+\frac{1}{4}}\, \dot{u}_{n+\frac{1}{4}}(t) \tag{6.28}$$

where the subscripts on ΔM and S are defined according to Eqs. (6.16) and (6.20); in particular,

$$\tfrac{1}{2}\Delta M_{n+\frac{1}{4}} = \frac{1}{2}\,\frac{\rho_o \Delta\xi}{S_{n+\frac{1}{4}}} = \frac{\rho_o\, \frac{1}{2}\Delta\xi}{S_{n+\frac{1}{4}}}. \tag{6.29}$$

This result is not surprising; it says that between the "original" pressure sample p_n and the "extra" sample $p_{n+\frac{1}{2}}$, there is an acoustic mass of length $\frac{1}{2}\Delta\xi$ (instead of the usual $\Delta\xi$), whose inertance is computed from the cross-sectional area at the midpoint of its length. The symbol for the truncated acoustic mass contains the factor $\frac{1}{2}$ in order to be consistent with Eq. (6.16), which seems to define $\Delta M_{n+\frac{1}{2}}$ as a function of the subscript.

If the desired extra sample is $p_{n-\frac{1}{2}}$ instead of $p_{n+\frac{1}{2}}$, the required acoustic mass is $\frac{1}{2}\Delta M_{n-\frac{1}{4}}$. The relevant equations are easily obtained by substituting $n - \frac{1}{2}$ for n in Eqs. (6.28) and (6.29).

In Eq. (6.23), if we set $\xi = \xi_{n-\frac{1}{4}}$ and replace the derivative w.r.t. ξ with the finite-difference quotient using the new step size, we obtain

$$\frac{u_{n-\frac{1}{2}}(t) - u_n(t)}{\frac{1}{2}\Delta\xi} \approx \frac{S_{n-\frac{1}{4}}}{\rho_o c^2}\, \dot{p}_{n-\frac{1}{4}}(t). \tag{6.30}$$

This may be written

$$u_{n-\frac{1}{2}}(t) - u_n(t) \approx \tfrac{1}{2}\Delta C_{n-\frac{1}{4}}\, \dot{p}_{n-\frac{1}{4}}(t) \tag{6.31}$$

where the subscripts on ΔC and S are defined according to Eqs. (6.18) and (6.20); in particular,

$$\tfrac{1}{2}\Delta C_{n-\frac{1}{4}} = \frac{1}{2}\,\frac{S_{n-\frac{1}{4}}\,\Delta\xi}{\rho_o c^2} = \frac{S_{n-\frac{1}{4}}\,\frac{1}{2}\Delta\xi}{\rho_o c^2}. \tag{6.32}$$

Neither is this result surprising; it says that between the "original" flux sample $u_{n-\frac{1}{2}}$ and the "extra" sample u_n, there is an acoustic compliance of length $\frac{1}{2}\Delta\xi$ (instead of the usual $\Delta\xi$), whose volume is computed from the cross-sectional area at the midpoint of its length. The symbol for the truncated acoustic compliance contains the factor $\frac{1}{2}$ for consistency with Eq. (6.18).

If the "original" sample is $u_{n+\frac{1}{2}}$ instead of $u_{n-\frac{1}{2}}$, the required acoustic compliance is $\frac{1}{2}\Delta C_{n+\frac{1}{4}}$. The relevant equations are easily obtained by substituting $n + \frac{1}{2}$ for n in Eqs. (6.31) and (6.32).

The above results concerning a truncated element and the associated extra sample may be summarized as follows:

- subscripts are generalized (to allow multiples of $\frac{1}{4}$);
- cross-sectional area is evaluated at the center of the element;
- pressure is sampled at the center of a compliance element and at the ends of an inertance element;

- flux is sampled at the center of an inertance element and at the ends of a compliance element;
- the value of the element is calculated from its actual length, and
- when the length of an element is a fraction of the normal step size, the same fraction appears in the symbol for the value of the element.

In other words, apart from the generalization of the subscripts, the rules applying to truncated elements are precisely the same as those applying to the normal (interior, non-truncated) elements. This is no accident. Eqs. (6.22) and (6.16) involve the coordinates of the endpoints and midpoint, and the length, of one inertance element. Similarly, Eqs. (6.25) and (6.18) involve the endpoints, midpoint and length of one compliance element. In each case, the endpoints are quite general, as can be seen from Eq. (6.2); given two different values of n (as subscripts for the coordinates of the endpoints), we can match these to any two values of ξ_n by choosing ξ_0 and $\Delta\xi$. The subscript notation has the advantage of economy of expression, and the disadvantage of obscuring the generality of the endpoints (which determine the midpoint and length) of each element. But the generality of the endpoints implies that they can be varied, and the variation is expressed by changing the subscripts.

In the three-dimensional problem, the coordinates of the bounding surfaces of each element, which are indicated by subscripts according to Eqs. (6.7) to (6.9), are also quite general. This fact will be used to obtain expressions for truncated 3D elements without reworking the entire FDEC derivation.

6.4 The 3D case

Now the techniques used in developing the 1P finite-difference equivalent-circuit model will be extended to the 3D case. An equivalent circuit will be derived from the wave equation (the 3D equivalent of Webster's equation) and from the equations of motion and compression, with the latter two equations yielding information about flux.

In the 1P case, all equations were treated in their time-dependent forms. In this section, however, only the wave equation will be treated in time-dependent form; the equations of motion and compression will be written in terms of phasors or Fourier transforms in preparation for Chapter 7, in which the results of the present section will be extended to the case of damped (fiber-filled) loudspeaker enclosures.

6.4.1 The wave equation

In a 3D acoustic field, the excess pressure is modeled by the wave equation

$$\ddot{p} = c^2 \nabla^2 p. \tag{6.33}$$

In curvilinear orthogonal coordinates u, v, w, with scale factors h_u, h_v, h_w, the Laplacian is given by [24, p. 174]

$$\nabla^2 p = \frac{1}{h_u h_v h_w} \left[\frac{\partial}{\partial u} \left(\frac{h_v h_w}{h_u} \frac{\partial p}{\partial u} \right) + \frac{\partial}{\partial v} \left(\frac{h_w h_u}{h_v} \frac{\partial p}{\partial v} \right) + \frac{\partial}{\partial w} \left(\frac{h_u h_v}{h_w} \frac{\partial p}{\partial w} \right) \right]. \tag{6.34}$$

Substituting this into the wave equation and rearranging, we obtain

$$h_u h_v h_w \, \ddot{p}/c^2 = \frac{\partial}{\partial u}\left(\frac{h_v h_w}{h_u}\frac{\partial p}{\partial u}\right) + \frac{\partial}{\partial v}\left(\frac{h_w h_u}{h_v}\frac{\partial p}{\partial v}\right) + \frac{\partial}{\partial w}\left(\frac{h_u h_v}{h_w}\frac{\partial p}{\partial w}\right). \tag{6.35}$$

Notice that each term on the left side can be obtained from its predecessor by a forward rotation of the subscripts, i.e. by changing u to v, v to w, and w to u. However, if arguments were used to indicate functional dependence—e.g. by writing $p = p(u, v, w)$, $h_v = h_v(u, v, w)$, etc.—the order of arguments would of course remain fixed. These observations will enable us to process Eq. (6.35) by working on the first term in detail, then comparing the other terms with the first.

Suppose p is sampled at a three-dimensional array of discrete points. Let the general (i, j, k^{th}) point in the array have the coordinates (u_i, v_j, w_k), defined by equations (6.7) to (6.9). In the following derivation, the discrete point at which a variable or expression is evaluated is indicated by subscripts, as explained in Section 6.2.

In Eq. (6.35), let $(u, v, w) = (u_i, v_j, w_k)$. Working on the first term, we replace the outer derivative with the finite-difference quotient, then do likewise for the inner derivative:

$$\begin{aligned}
\left.\frac{\partial}{\partial u}\left(\frac{h_v h_w}{h_u}\frac{\partial p}{\partial u}\right)\right|_{i,j,k} &\approx \frac{1}{\Delta u}\left(\left[\frac{h_v h_w}{h_u}\frac{\partial p}{\partial u}\right]_{i+\frac{1}{2},j,k} - \left[\frac{h_v h_w}{h_u}\frac{\partial p}{\partial u}\right]_{i-\frac{1}{2},j,k}\right) \\
&\approx \left.\frac{h_v h_w}{h_u \Delta u}\right|_{i+\frac{1}{2},j,k} \frac{p_{i+1,j,k}(t) - p_{i,j,k}(t)}{\Delta u} \\
&\quad - \left.\frac{h_v h_w}{h_u \Delta u}\right|_{i-\frac{1}{2},j,k} \frac{p_{i,j,k}(t) - p_{i-1,j,k}(t)}{\Delta u}.
\end{aligned} \tag{6.36}$$

(Excess pressure p depends on time as well as position, but the time-dependence is made explicit only in the final expression.) Substituting this into Eq. (6.35), filling in the corresponding results for the second and third terms of Eq. (6.35), and multiplying throughout by $\Delta u \Delta v \Delta w/\rho_{\text{o}}$, we obtain

$$\begin{aligned}
\Delta C_{i,j,k}\, \ddot{p}_{i,j,k}(t) &\approx \frac{p_{i+1,j,k}(t) - p_{i,j,k}(t)}{\Delta M_u|_{i+\frac{1}{2},j,k}} + \frac{p_{i-1,j,k}(t) - p_{i,j,k}(t)}{\Delta M_u|_{i-\frac{1}{2},j,k}} \\
&\quad + \frac{p_{i,j+1,k}(t) - p_{i,j,k}(t)}{\Delta M_v|_{i,j+\frac{1}{2},k}} + \frac{p_{i,j-1,k}(t) - p_{i,j,k}(t)}{\Delta M_v|_{i,j-\frac{1}{2},k}} \\
&\quad + \frac{p_{i,j,k+1}(t) - p_{i,j,k}(t)}{\Delta M_u|_{i,j,k+\frac{1}{2}}} + \frac{p_{i,j,k-1}(t) - p_{i,j,k}(t)}{\Delta M_u|_{i,j,k-\frac{1}{2}}}
\end{aligned} \tag{6.37}$$

where

$$\Delta C_{i,j,k} = \left.\frac{h_u \Delta u \, h_v \Delta v \, h_w \Delta w}{\rho_{\text{o}} c^2}\right|_{i,j,k} \tag{6.38}$$

$$\Delta M_u|_{i+\frac{1}{2},j,k} = \left.\frac{\rho_{\text{o}} h_u \Delta u}{h_v \Delta v \, h_w \Delta w}\right|_{i+\frac{1}{2},j,k} \tag{6.39}$$

$$\Delta M_u|_{i-\frac{1}{2},j,k} = \left.\frac{\rho_{\text{o}} h_u \Delta u}{h_v \Delta v \, h_w \Delta w}\right|_{i-\frac{1}{2},j,k} \tag{6.40}$$

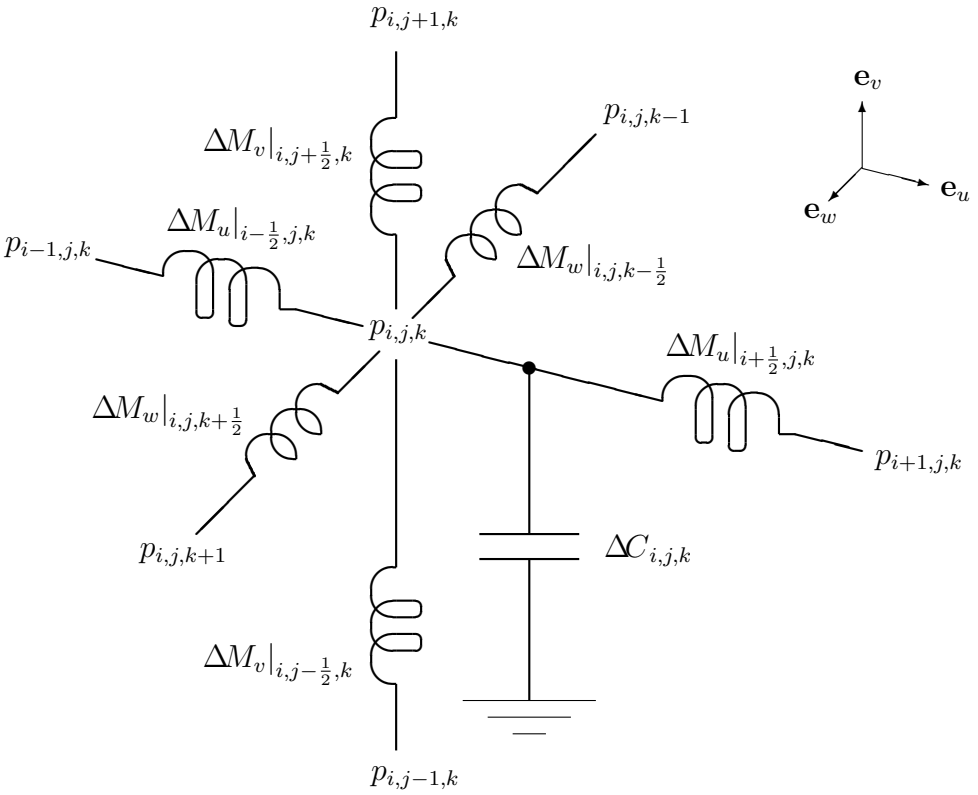

Figure 6.2: *FDEC representation of 3D wave equation.*

$$\Delta M_v|_{i,j+\frac{1}{2},k} = \left.\frac{\rho_o h_v \Delta v}{h_w \Delta w \, h_u \Delta u}\right|_{i,j+\frac{1}{2},k} \tag{6.41}$$

$$\Delta M_v|_{i,j-\frac{1}{2},k} = \left.\frac{\rho_o h_v \Delta v}{h_w \Delta w \, h_u \Delta u}\right|_{i,j-\frac{1}{2},k} \tag{6.42}$$

$$\Delta M_w|_{i,j,k+\frac{1}{2}} = \left.\frac{\rho_o h_w \Delta w}{h_u \Delta u \, h_v \Delta v}\right|_{i,j,k+\frac{1}{2}} \tag{6.43}$$

$$\Delta M_w|_{i,j,k-\frac{1}{2}} = \left.\frac{\rho_o h_w \Delta w}{h_u \Delta u \, h_v \Delta v}\right|_{i,j,k-\frac{1}{2}} \tag{6.44}$$

Eq. (6.37) is the differentiated nodal equation for the central node of the 3D rectangular network shown in Fig. 6.2; the left-hand side is the time-derivative of the current from the i, j, k^{th} node to ground (current equals capacitance times *first* derivative of voltage) and the six terms on the right are the time-derivatives of the currents flowing into the i, j, k^{th} node from the six neighboring nodes (voltage drop equals inductance times derivative of current). To save space in the diagram, the nodal pressures are written "in the nodes". The unit vectors in the three coordinate directions are shown at the top right; Fig. 6.2 is both a circuit diagram and a pictorial projection.

While the preceding analysis shows that excess pressure in the acoustic field is analogous to voltage in the equivalent circuit, it does not show any analogy between flux and current. For the latter purpose, as in the one-parameter case, we must work from the more fundamental equations of motion and compression.

6.4.2 The equations of motion and compression

Recall that the linearized equation of motion in point form is

$$\nabla p = -\rho_o \dot{\mathbf{q}} \tag{6.45}$$

(see Eq. (2.15)). For reasons which will become clear in Section 7.1, it is convenient to rewrite this equation in terms of phasors or Fourier transforms, obtaining

$$\nabla P = -j\omega\rho_o \mathbf{Q}. \tag{6.46}$$

(Because the Fourier transform is defined for a wide range of functions, including any function having a magnitude whose integral over the real line is finite, the loss of generality is not serious.)

If we introduce curvilinear orthogonal coordinates u, v, w, and take components in the u direction, Eq. (6.46) becomes

$$\frac{1}{h_u}\frac{\partial P}{\partial u} = -j\omega\rho_o Q_u \tag{6.47}$$

which is the starting point for the finite-difference analysis.

Let u, v, w take discrete values as defined in Section 6.2, and let the derivative and other quantities in Eq. (6.47) be evaluated at $(u_{i+\frac{1}{2}}, v_j, w_k)$. Then the finite-difference form of the equation is

$$\frac{1}{h_u}\Big|_{i+\frac{1}{2},j,k} \frac{P_{i+1,j,k} - P_{i,j,k}}{\Delta u} \approx -j\omega\rho_o \, Q_u|_{i+\frac{1}{2},j,k} \ , \tag{6.48}$$

which may be written

$$P_{i,j,k} - P_{i+1,j,k} \approx [j\omega\rho_o h_u \Delta u \, Q_u]_{i+\frac{1}{2},j,k} \, . \tag{6.49}$$

Now let us define "the unit cell centered on $(u_{i+\frac{1}{2}}, v_j, w_k)$" as the quasi-cubic region

$$u_i < u < u_{i+1} \ ; \ \ v_{j-\frac{1}{2}} < v < v_{j+\frac{1}{2}} \ ; \ \ w_{k-\frac{1}{2}} < w < w_{k+\frac{1}{2}} \, . \tag{6.50}$$

The cross-sectional area of this unit cell at the surface $u = u_{i+\frac{1}{2}}$ may be estimated as

$$[h_v \Delta v \, h_w \Delta w]_{i+\frac{1}{2},j,k} \, .$$

To estimate the flux flowing through this cross-section in the direction of increasing u, we multiply the "area" by $Q_u|_{i+\frac{1}{2},j,k}$. Hence the estimated flux is

$$\Delta U_u|_{i+\frac{1}{2},j,k} = [h_v \Delta v \, h_w \Delta w \, Q_u]_{i+\frac{1}{2},j,k} \, . \tag{6.51}$$

So, if we multiply and divide the right side of Eq. (6.49) by the estimated cross-sectional area and arrange the factors into appropriate groups, we obtain

$$P_{i,j,k} - P_{i+1,j,k} \approx j\omega \ \Delta M_u|_{i+\frac{1}{2},j,k} \ \Delta U_u|_{i+\frac{1}{2},j,k} \, . \tag{6.52}$$

where $\Delta M_u|_{i+\frac{1}{2},j,k}$ is defined in Eq. (6.39), above.

From the right-hand side of Eq. (6.39), we see that $\Delta M_u|_{i+\frac{1}{2},j,k}$ has the dimensions of acoustic mass—the numerator is ρ_o times the estimated length of the unit cell

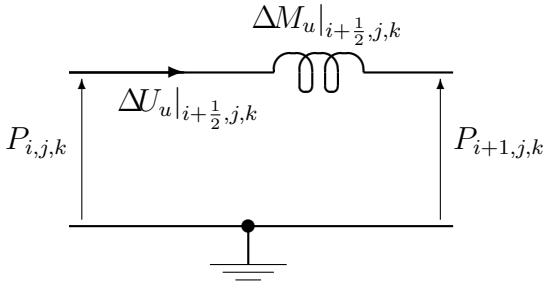

Figure 6.3: *FDEC representation of equation of motion in u direction, in free air.*

centered on $(u_{i+\frac{1}{2}}, v_j, w_k)$, and the denominator is the estimated cross-sectional area of the same unit cell. (Indeed, the definitions of the ΔC's and ΔM's in equations (6.38) to (6.44) were guided by the desire to find subexpressions with the dimensions of familiar quantities, and these dimensions were tacitly used in Fig. 6.2.) Hence one may be tempted to conclude from Eq. (6.37) and Fig. 6.2 that the time-derivative of the flux through the unit cell may be found by dividing the pressure difference by the acoustic mass. Caution is required, however, because the velocity is not constrained to lie in the direction of any one of the three coordinate unit vectors—the unit cell is not a horn or pipe. Moreover, the definition of acoustic mass makes a 1P assumption (see the derivation of Eqs. (2.23) and (2.24)), whereas the derivation of Eq. (6.37) makes no such assumption. Eq. (6.52) has now settled the issue: if the pressures are evaluated at the midpoints of opposite faces of the unit cell, and if the flux is measured through the mid cross-section, then we have the usual relationship between pressure, flux and acoustic mass.

Eq. (6.52) relates the pressure at the i, j, k^{th} point to the pressure at one of the six neighboring points in the 3D lattice. The pressure at the opposite neighboring point is modeled by substituting $i - 1$ for i, yielding another equation similar to Eq. (6.52). Four more equations, incorporating the pressures at the other four neighboring points, may be obtained by incrementing and decrementing j and k instead of i. Note that in the three equations in which the pressure at the neighboring point is indicated by decrementing a counter instead of incrementing it, the assumed direction of the flux is towards the i, j, k^{th} point instead of away from it.

Eq. (6.52) has the equivalent circuit shown in Fig. 6.3. Similar diagrams can be drawn for the other five equations in the family; the positive direction of the flux will be towards the i, j, k^{th} node in three cases, and away from it in the other three cases. When the six diagrams are combined, they give the six-way star connection of acoustic masses shown in Fig. 6.2, with the same pressures (albeit in phasor form) and the same acoustic masses. Hence the fluxes must also be the same. It can be seen from the derivation of Eq. (6.51) that the flux in Fig. 6.3 is an estimate of the flux through one face of the init cell centered on (u_i, v_j, w_k); hence all the fluxes in Fig. 6.2 have that physical significance.

Further physical insights can be gained by finding an equivalent circuit for the equation of compression. Instead of using one of the existing forms of the equation, we shall revert to the equation of continuity, convert it to phasor form, then use a pressure-density relation involving γ. This is not the most direct approach for the immediate purpose of deriving an equivalent circuit, but will be useful for future

reference (Section 7.2).

Recall that for small compressions, the point form of the equation of continuity is

$$\dot{\rho} = -\rho_o \operatorname{div} \mathbf{q}$$

(Eq. (2.30)). Let ρ_e be the *excess density*, i.e. the difference between the instantaneous density ρ and the equilibrium or time-averaged density (not to be confused with ρ_o, which is a temporal *and spatial* average). As the equilibrium density is time-invariant, we have

$$\dot{\rho} = \dot{\rho}_e. \tag{6.53}$$

Let the phasor representations of p and ρ_e be P and $\underline{\rho_e}$, respectively. Writing $\dot{\rho}_e$ for $\dot{\rho}$ in the equation of continuity and converting immediately to phasor form, we obtain

$$j\omega\underline{\rho_e} = -\rho_o \operatorname{div} \mathbf{Q}. \tag{6.54}$$

Next we combine Eqs. (2.31) and (2.39) to obtain the pressure-density relation

$$\frac{dp}{d\rho} = \frac{\gamma P_0}{\rho_o}. \tag{6.55}$$

Multiplying both sides by $\dot{\rho}$ and using the chain rule on the left gives

$$\dot{p} = \frac{\gamma P_0}{\rho_o}\,\dot{\rho} = \frac{\gamma P_0}{\rho_o}\,\dot{\rho}_e \tag{6.56}$$

which may be written in phasor form and divided through by $j\omega$ to obtain

$$P = \frac{\gamma P_0}{\rho_o}\,\underline{\rho_e}. \tag{6.57}$$

This is an alternative definition of γ (and will be used again in Section 7.2). Multiplying both sides of Eq. (6.54) by $\gamma P_0/\rho_o$, then using Eq. (6.57) to rewrite the left-hand side in terms of P, we obtain the equation of compression in phasor form:

$$j\omega P = -\gamma P_0 \operatorname{div} \mathbf{Q}. \tag{6.58}$$

This is the starting point for the finite-difference treatment.

In curvilinear orthogonal coordinates u, v, w, the divergence is given by [24, p. 174]

$$\operatorname{div} \mathbf{Q} = \frac{1}{h_u h_v h_w}\left[\frac{\partial}{\partial u}\left(h_v h_w Q_u\right) + \frac{\partial}{\partial v}\left(h_w h_u Q_v\right) + \frac{\partial}{\partial w}\left(h_u h_v Q_w\right)\right]. \tag{6.59}$$

Now let us take discrete values of u, v, w as in the previous section. Then the i, j, k^{th} unit cell—that is, the unit cell centered on (u_i, v_j, w_k)—has an estimated volume

$$\Delta V_{i,j,k} = \left[h_u \Delta u\, h_v \Delta v\, h_w \Delta w\right]_{i,j,k} \tag{6.60}$$

and hence the estimated compliance

$$\Delta C_{i,j,k} = \frac{\Delta V_{i,j,k}}{\rho_o c^2} = \frac{\Delta V_{i,j,k}}{\gamma P_0} = \left[\frac{h_u \Delta u\, h_v \Delta v\, h_w \Delta w}{\gamma P_0}\right]_{i,j,k} \tag{6.61}$$

(the second equality follows from Eq. (2.41)). So let us multiply the numerator and denominator in Eq. (6.59) by $\Delta u \Delta v \Delta w$, substitute for $\operatorname{div} \mathbf{Q}$ in Eq. (6.58) and use Eq. (6.61). This yields

$$j\omega P_{i,j,k} = -\frac{1}{\Delta C_{i,j,k}} \Delta u \Delta v \Delta w \left[\frac{\partial}{\partial u}(h_v h_w Q_u) + \frac{\partial}{\partial v}(h_w h_u Q_v) + \frac{\partial}{\partial w}(h_u h_v Q_w) \right]_{i,j,k} . \tag{6.62}$$

Multiplying through by $\Delta C_{i,j,k}$ and replacing the partial derivatives by their finite-difference approximations, we obtain

$$\begin{aligned} j\omega \Delta C_{i,j,k}\, P_{i,j,k} \approx\ -\Delta u \Delta v \Delta w \Bigg[& \frac{[h_v h_w Q_u]_{i+\frac{1}{2},j,k} - [h_v h_w Q_u]_{i-\frac{1}{2},j,k}}{\Delta u} \\ & + \frac{[h_w h_u Q_v]_{i,j+\frac{1}{2},k} - [h_w h_u Q_v]_{i,j-\frac{1}{2},k}}{\Delta v} \\ & + \frac{[h_u h_v Q_w]_{i,j,k+\frac{1}{2}} - [h_u h_v Q_w]_{i,j,k-\frac{1}{2}}}{\Delta w} \Bigg] . \end{aligned} \tag{6.63}$$

Now in the i,j,k^{th} unit cell, the flux in the positive u direction through the face $u = u_{i+\frac{1}{2}}$ is

$$\Delta U_u|_{i+\frac{1}{2},j,k} = [h_v \Delta v\, h_w \Delta w\, Q_u]_{i+\frac{1}{2},j,k} \tag{6.64}$$

(which agrees with Eq. (6.51)), and the flux in the same direction through the face $u = u_{i-\frac{1}{2}}$ is

$$\Delta U_u|_{i-\frac{1}{2},j,k} = [h_v \Delta v\, h_w \Delta w\, Q_u]_{i-\frac{1}{2},j,k} . \tag{6.65}$$

In an analogous manner we may define $\Delta U_v|_{i,j+\frac{1}{2},k}$, $\Delta U_v|_{i,j-\frac{1}{2},k}$, $\Delta U_w|_{i,j,k+\frac{1}{2}}$ and $\Delta U_w|_{i,j,k-\frac{1}{2}}$. Expanding the right-hand side of Eq. (6.63) and renaming the subexpressions just defined, we obtain the desired result

$$\begin{aligned} j\omega \Delta C_{i,j,k}\, P_{i,j,k} \ \approx\ & \Delta U_u|_{i-\frac{1}{2},j,k} - \Delta U_u|_{i+\frac{1}{2},j,k} \\ & + \Delta U_v|_{i,j-\frac{1}{2},k} - \Delta U_v|_{i,j+\frac{1}{2},k} \\ & + \Delta U_w|_{i,j,k-\frac{1}{2}} - \Delta U_w|_{i,j,k+\frac{1}{2}} . \end{aligned} \tag{6.66}$$

This equation describes the circuit shown in Fig. 6.4. To save space in the diagram, the pressure at the i,j,k^{th} node is written "in the node", while the branch fluxes are written in line with the branches. The unit vectors in the three coordinate directions are shown at the top right. Eq. (6.66) states that the compliant admittance times the pressure is equal to the sum of fluxes into the compliant element—or, in analogous electrical terms, that the capacitive admittance times the voltage is equal to the sum of currents into the capacitive element.

The fluxes in Fig. 6.4 are the same as those in Fig. 6.3 and the other five equivalent circuits from the equation of motion. The six circuits for the equation of motion also include $P_{i,j,k}$. So Fig. 6.4 may be combined with the six inertance circuits to produce the complete circuit of Fig. 6.2, with the flux information added.

Fig. 6.2 is the result of a "pure" finite-difference approximation to the wave equation. The derivations of Figs. 6.3 and 6.4 used "estimated" values of area, flux, volume and compliance, but these estimates were not used in deriving Fig. 6.2, which

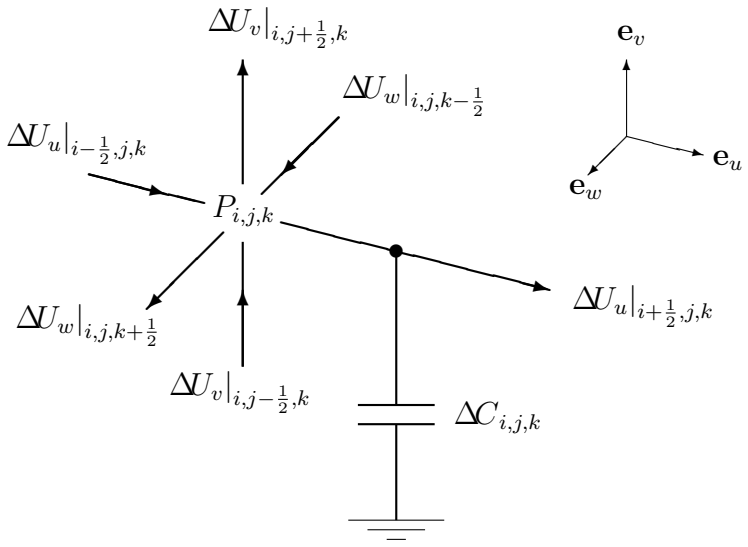

Figure 6.4: *FDEC representation of 3D equation of compression, in free air.*

includes all the information in Figs. 6.3 and 6.4 except the fluxes. Thus the fluxes are the only quantities in the equivalent circuits which involve approximations other than the basic finite-difference approximation. The flux approximation becomes significant when the velocity at the boundary of a unit cell must be modeled as a flux through one face of the unit cell.

6.4.3 Truncated elements at boundary surfaces

Arai [2] did not consider boundary conditions in the 3D case; he did not need to, because all his computational examples were one-dimensional. In this thesis, 3D boundary conditions will be considered only at equicoordinate boundaries. The use of curvilinear orthogonal coordinates allows a limited but useful variety of boundary surfaces to be modeled as equicoordinate surfaces. More complex surface shapes may be approximated by piecewise-equicoordinate surfaces.

As in the 1P case, the difficulty with boundary conditions is that the pressure and the velocity are sampled at different points; the velocity sampling points for ΔU_u, ΔU_v and ΔU_w are displaced from the pressure sampling points by $\pm\Delta u/2$, $\pm\Delta v/2$ and $\pm\Delta w/2$ in the u, v and w directions, respectively. The solution, modeled on Subsection 6.3.3, is to extend the definitions in Section 6.2 so as to allow i, j, k to be multiples of one quarter, and take extra samples at the boundary. As far as the equations describing a *single* element are concerned, there is nothing special about the "standard" increments $\Delta u, \Delta v, \Delta w$; the increments are arbitrary and can be changed at our convenience. The purpose of using uniformly spaced sampling points, referred to by subscripts, is to ensure that each sample of pressure or velocity is involved in the difference equations of several elements, so that the elements can be connected into circuits. At the boundaries of the region under study, however, it is convenient to vary the spacing of sample points. The necessary variations are easily expressed by modifying the subscripts.

The rules for evaluating the normal (interior, non-truncated) FDEC elements are as follows:

- In the formula for a component value, scale factors are evaluated at the body-center of the element (mass or compliance);
- In a circuit equation involving a mass element, pressure is sampled at the centers of two opposite faces of the element, chosen so that the normals to the two faces are in the direction of the velocity component governed by that element;
- In a circuit equation involving a compliance element, the areas of the six faces and the fluxes passing through them are calculated using the scale factors and velocities sampled at the centers of the six faces of the element.

For the truncated elements, we simply apply the same rules using the new element dimensions, using subscripts to indicate the coordinates of the new element surfaces. In the above list, the word "center" refers to the midranges of the variable coordinates—two coordinates for a face-center and three for a body-center. As in Subsection 6.3.3, if we wish to interpret the names of the elements as functions of the subscripts, the name of a truncated element will include a multiplier.

Suppose we wish to impose a boundary condition at the surface $u = u_{i+\frac{1}{2}}$ when the pressure is sampled at an array of points on the surface $u = u_i$. By rotating coordinates in Eq. (6.50)), it can be seen that the boundary surface passes between two layers of inertia elements in the v direction, and between two layers of inertia elements in the w direction, so that the inertia elements in those directions are unaffected. But Eq. (6.50), as written, indicates that the boundary surface cuts *through* a layer of inertia elements in the u direction. Accordingly, given an original pressure sample $P_{i,j,k}$, we need to take an extra sample $P_{i+\frac{1}{2},j,k}$. If the pressure is evaluated at $(u_{i+\frac{1}{2}}, v_j, w_k)$ instead of (u_{i+1}, v_j, w_k), Eqs. (6.52) and (6.39) are replaced by

$$P_{i,j,k} - P_{i+\frac{1}{2},j,k} \approx j\omega \, \tfrac{1}{2} \, \Delta M_u|_{i+\frac{1}{4},j,k} \, \Delta U_u|_{i+\frac{1}{4},j,k} \tag{6.67}$$

where $\Delta U_u|_{i+\frac{1}{4},j,k}$ and $\Delta M_u|_{i+\frac{1}{4},j,k}$ are defined as in Eqs. (6.51) and (6.39), with $i + \frac{1}{4}$ in place of $i + \frac{1}{2}$; that is,

$$\Delta U_u|_{i+\frac{1}{4},j,k} = [h_v \Delta v \, h_w \Delta w \, Q_u]_{i+\frac{1}{4},j,k} \tag{6.68}$$

and

$$\tfrac{1}{2} \, \Delta M_u|_{i+\frac{1}{4},j,k} = \frac{1}{2} \left. \frac{\rho_o h_u \Delta u}{h_v \Delta v \, h_w \Delta w} \right|_{i+\frac{1}{4},j,k} = \left. \frac{\rho_o h_u \, \frac{1}{2} \Delta u}{h_v \Delta v \, h_w \Delta w} \right|_{i+\frac{1}{4},j,k} . \tag{6.69}$$

Thus, between the original sample $P_{i,j,k}$ and the extra sample $P_{i+\frac{1}{2},j,k}$, there is an acoustic mass with the usual cross sectional area and half the usual length, with the "area" and "length" estimated from the scale factors at the mean values of u, v, w. A similar conclusion follows if the desired extra sample is $P_{i-\frac{1}{2},j,k}$ instead of $P_{i+\frac{1}{2},j,k}$; the relevant equations may be found by writing $i - \frac{1}{2}$ for i in Eqs. (6.67) and (6.69). Four more equations, expressing similar conclusions, may be written for the other two coordinate directions. In total, we have six ways to construct an equivalent circuit incorporating an extra pressure sample. One of the six variations will be used in Chapter 11 to impose a far-field radiation condition in a simulation of a piston-radiator in an infinite planar baffle.

Recall that $\Delta U_u|_{i+\frac{1}{4},j,k}$ is a non-FDM estimate of the flux through the mean surface ($u = u_{i+\frac{1}{4}}$) of the shortened inertia element $\Delta M_u|_{i+\frac{1}{4},j,k}$. Because this inertial element is lumped and is a terminal element in the network, $\Delta U_u|_{i+\frac{1}{4},j,k}$ also estimates the flux through the boundary surface element

$$u = u_i \; ; \;\; v_{j-\frac{1}{2}} < v < v_{j+\frac{1}{2}} \; ; \;\; w_{k-\frac{1}{2}} < w < w_{k+\frac{1}{2}}. \tag{6.70}$$

A second method of truncating a 3D equivalent circuit, which will be derived but not used in this thesis, is required if we wish to impose a boundary condition at the surface $u = u_i$ when the velocity is sampled at an array of points on the surface $u = u_{i-\frac{1}{2}}$. Given an original velocity sample $Q_u|_{i-\frac{1}{2},j,k}$, we must take an extra sample $Q_u|_{i,j,k}$. The boundary surface passes between two layers of inertia elements in the u direction, so these elements are unaffected. But the boundary cuts through a layer of compliance elements, a layer of inertia elements in the v direction, and a layer of inertia elements in the w direction, so these elements must be redefined as truncated elements. Thus the second method of truncation affects three sets of elements while the first method affects only one; that is why the first method is preferred in Chapters 10 and 11.

The "half unit cell" defined by

$$u_{i-\frac{1}{2}} < u < u_i \; ; \;\; v_{j-\frac{1}{2}} < v < v_{j+\frac{1}{2}} \; ; \;\; w_{k-\frac{1}{2}} < w < w_{k+\frac{1}{2}}. \tag{6.71}$$

has an estimated compliance of $\frac{1}{2}\Delta C_{i-\frac{1}{4},j,k}$. The estimated flux in the positive u direction through the face $u = u_i$ is

$$\Delta U_u|_{i,j,k} = [h_v \Delta v \, h_w \Delta w \, Q_u]_{i,j,k} \tag{6.72}$$

and the estimated flux in the same direction through the face $u = u_{i-\frac{1}{2}}$ is

$$\Delta U_u|_{i-\frac{1}{2},j,k} = [h_v \Delta v \, h_w \Delta w \, Q_u]_{i-\frac{1}{2},j,k} \, . \tag{6.73}$$

In the above two equations, the quantity ΔU_u is defined, with its subscripts, as in Eq. (6.51). In the next four equations, corresponding definitions will be used for ΔU_v and ΔU_w. In the half unit cell defined by Eq. (6.71), the estimated flux in the positive v direction through the face $v = v_{j+\frac{1}{2}}$ is

$$\tfrac{1}{2} \, \Delta U_v|_{i-\frac{1}{4},j+\frac{1}{2},k} = \left[h_u \, \tfrac{1}{2}\Delta u \, h_w \Delta w\right]_{i-\frac{1}{4},j+\frac{1}{2},k} \tag{6.74}$$

and the estimated flux in the same direction through the face $v = v_{j-\frac{1}{2}}$ is

$$\tfrac{1}{2} \, \Delta U_v|_{i-\frac{1}{4},j-\frac{1}{2},k} = \left[h_u \, \tfrac{1}{2}\Delta u \, h_w \Delta w\right]_{i-\frac{1}{4},j-\frac{1}{2},k} \, . \tag{6.75}$$

The estimated flux in the positive w direction through the face $w = w_{k+\frac{1}{2}}$ is

$$\tfrac{1}{2} \, \Delta U_w|_{i-\frac{1}{4},j,k+\frac{1}{2}} = \left[h_u \, \tfrac{1}{2}\Delta u \, h_v \Delta v\right]_{i-\frac{1}{4},j,k+\frac{1}{2}} \tag{6.76}$$

and the estimated flux in the positive w direction through the face $w = w_{k-\frac{1}{2}}$ is

$$\tfrac{1}{2} \, \Delta U_w|_{i-\frac{1}{4},j,k-\frac{1}{2}} = \left[h_u \, \tfrac{1}{2}\Delta u \, h_v \Delta v\right]_{i-\frac{1}{4},j,k-\frac{1}{2}} \, . \tag{6.77}$$

With the new compliance and fluxes thus defined, Eq. (6.66) is replaced by

$$\begin{aligned} j\omega\,\tfrac{1}{2}\Delta C_{i-\frac{1}{4},j,k}\,P_{i-\frac{1}{4},j,k} \;&\approx\; \Delta U_u|_{i-\frac{1}{2},j,k} \;-\; \Delta U_u|_{i,j,k} \\ &+\; \tfrac{1}{2}\,\Delta U_v|_{i-\frac{1}{4},j-\frac{1}{2},k} \;-\; \tfrac{1}{2}\,\Delta U_v|_{i-\frac{1}{4},j+\frac{1}{2},k} \\ &+\; \tfrac{1}{2}\,\Delta U_w|_{i-\frac{1}{4},j,k-\frac{1}{2}} \;-\; \tfrac{1}{2}\,\Delta U_w|_{i-\frac{1}{4},j,k+\frac{1}{2}}\,. \end{aligned} \tag{6.78}$$

This equation has the same form as Eq. (6.66) and describes a circuit of the form shown in Fig. 6.4, but with different component values and fluxes to reflect the different location and dimensions of the volume element.

Considering the fluxes in Eq. (6.78), we may observe that $\Delta U_u|_{i-\frac{1}{2},j,k}$ is just the estimated flux in the internal mass element $\Delta M_u|_{i-\frac{1}{2},j,k}$ (cf. Eq. (6.52)), and is therefore already represented in the equivalent circuit. $\Delta U_u|_{i,j,k}$ is the estimated flux through the boundary surface element given by Eq. (6.70). The remaining four fluxes flow in the truncated mass elements which are left after the boundary surface has cut through a layer of original mass elements in the v and w directions. For example, an equation of motion involving $\frac{1}{2}\,\Delta U_v|_{i-\frac{1}{4},j-\frac{1}{2},k}$ may be constructed by modifying the subscripts in Eqs. (6.52) and (6.39):

$$P_{i-\frac{1}{4},j-1,k} - P_{i-\frac{1}{4},j,k} \approx j\omega\,2\,\Delta M_v|_{i-\frac{1}{4},j-\frac{1}{2},k}\;\tfrac{1}{2}\,\Delta U_v|_{i-\frac{1}{4},j-\frac{1}{2},k} \tag{6.79}$$

where

$$2\,\Delta M_v|_{i-\frac{1}{4},j-\frac{1}{2},k} = \left.\frac{\rho_o h_v \Delta v}{h_u\,\frac{1}{2}\Delta u\,h_w \Delta w}\right|_{i-\frac{1}{4},j-\frac{1}{2},k}. \tag{6.80}$$

The reason for the factors 2 and $\frac{1}{2}$ in the above two equations is that the symbols ΔM_v and ΔU_v are defined for unit cells of standard dimensions; see Eqs. (6.39) to (6.44) and Eq. (6.51). The multiplying factor in front of the inertance not only preserves notational consistency, but also indicate how the changes in cell dimensions affect the boundary inertances, and hence how the boundary inertances compare with adjacent interior inertances.

Another three pairs of equations may be written for the other fluxes in Eq. (6.78), and another five equations similar to Eq. (6.78) may be written for the other five ways in which one might impose a boundary at an array of pressure sampling points, requiring additional velocity samples.

6.5 3D boundary conditions

The discussion of 1P boundary conditions in Subsection 6.3.3 concerned the problem of truncating the *L-C* ladder network at a single point when pressure and flux were sampled at different points. The solution was to use the finite-difference approximation with a reduced step size to take an additional sample. Once the network was successfully truncated at the boundary, the problem of applying the actual boundary condition—source or impedance—was trivial, and did not need to be discussed at length.

Subsection 6.4.3 is modeled on Subsection 6.3.3 and therefore also concerns itself with truncating the network at the given boundary, and not with applying the actual boundary condition. But in the 3D case, the application of the boundary condition involving velocity or admittance is no longer trivial, for two reasons. First,

the boundary condition applies to a *distributed* quantity, whereas the equivalent circuit comprises lumped components. Second, a velocity or admittance has a direction, which is not necessarily normal to the boundary. The procedure for modeling a 3D boundary condition will usually involve replacing a velocity with a lumped flux, and this step (as noted at the end of Subsection 6.4.2) requires a non-FDM approximation.

6.5.1 Pressure condition

The imposition of a pressure at a boundary is easily modeled. Because p is a scalar, the orientation of the boundary is not involved in the specification of the boundary condition. Moreover, p is directly represented in the equivalent circuit; the finite step size requires that p be sampled, but does not require conversion to a lumped quantity, e.g. a force. Thus it suffices to terminate the equivalent circuit with pressure sources at the appropriate nodes.

The pressure condition is the only 3D boundary condition that does not require a non-FDM approximation.

6.5.2 Normal velocity condition

A smooth vibrating surface in contact with a fluid determines the fluid velocity normal to the surface. Because the surface is moving, it imposes its normal velocity at a point moving with the fluid, whereas the linearized equations of motion and compression, on which the FDEC model is based, involve the fluid velocity at stationary points. Thus it is necessary to distinguish between the *physical boundary*, which moves, and the *model boundary*, which is stationary at the mean position of the physical boundary. For small oscillations, the fluid velocity at any point on the physical boundary will be nearly equal to the fluid velocity at the mean position of that point, so that we may consider the boundary condition to be imposed at the model boundary rather than the physical boundary. This approximation is the time integral of the corresponding approximation in Subsection 2.1.2, on which the linearization of the equation of motion is based; if we neglect the quadratic terms in Eq. (2.8), we see that the acceleration of a point moving with the fluid (the total derivative of velocity) can be approximated by the derivative of the velocity at a fixed point (the partial derivative of velocity).

Let q_n be the imposed normal velocity, $\mathbf{n}$ the unit normal vector to the model boundary (in the agreed positive direction of q_n), and $\mathbf{q}$ the fluid velocity. Then the boundary condition is simply

$$\mathbf{q}.\mathbf{n} = q_\mathrm{n} \tag{6.81}$$

or, in phasor form,

$$\mathbf{Q}.\mathbf{n} = Q_\mathrm{n}. \tag{6.82}$$

Now suppose the model boundary is a constant-u surface, so that the area element of the surface is approximately $h_v \Delta v \, h_w \Delta w$. If we multiply both sides of Eq. (6.82) by this area, the left-hand side becomes an estimate of the (phasor) flux through the area element. Denoting this flux by ΔU, we may rewrite the boundary condition as

$$\Delta U = h_v \Delta v \, h_w \Delta w \, Q_\mathrm{n}. \tag{6.83}$$

As usual, the scale factors and Q_n should be evaluated at the middle values of v and w for each surface element. Surfaces of constant v or w are treated similarly. Thus a normal velocity condition is modeled by terminating the network with an array of flux sources.

6.5.3 Normal admittance condition

Let P denote the phasor pressure. As in Subsection 3.3.4, let us define the *specific acoustic admittance* at a point in the acoustic field as the complex vector

$$\mathbf{y} = \frac{\mathbf{Q}}{P}. \tag{6.84}$$

Let us also define the *normal specific acoustic admittance* at a point on the boundary as the complex scalar

$$y_\mathrm{n} = \frac{Q_\mathrm{n}}{P}. \tag{6.85}$$

Using these two notations, we may divide Eq. (6.82) through by P and obtain

$$\mathbf{y}.\mathbf{n} = y_\mathrm{n} \tag{6.86}$$

which shows that y_n is the normal component of $\mathbf{y}$.[3]

Now let us define the *acoustic admittance* of the boundary element as the complex scalar

$$\Delta Y = \frac{\Delta U}{P}. \tag{6.90}$$

Dividing Eq. (6.83) by P and using the notations of Eqs. (6.85) and (6.90) gives

$$\Delta Y = h_v \Delta v \, h_w \Delta w \, y_\mathrm{n}. \tag{6.91}$$

In words, this result says that the acoustic admittance is approximately equal to the normal specific acoustic admittance multiplied by the area element; "specific" means "per unit area" (the same conclusion was made concerning the *radial* specific acoustic admittance in Subsection 3.3.4). Thus a normal admittance condition is modeled by terminating the network with an array of lumped admittances.

[3]There is no corresponding result concerning impedances. The reciprocal of the vector $\mathbf{y}$ is not defined, so there is no obvious way to define a vector impedance. We can obtain a *scalar* impedance by defining the *normal specific acoustic impedance* as

$$z_\mathrm{n} = 1/y_\mathrm{n}. \tag{6.87}$$

But, if the angle between $\mathbf{y}$ and $\mathbf{n}$ is α, Eq. (6.86) can be written

$$y_\mathrm{n} = |\mathbf{y}| \cos\alpha. \tag{6.88}$$

Taking reciprocals gives the normal specific acoustic impedance

$$z_\mathrm{n} = \frac{1}{|\mathbf{y}|} \sec\alpha \tag{6.89}$$

which is clearly not the normal component of a vector.

6.5.4 Anechoic or free-air radiation condition

For engineering purposes it is convenient to describe an acoustic radiator in terms of its *free-air radiation pattern*, i.e. its radiation into an infinite three-dimensional expanse of air (cf. the free-space radiation pattern of a radio antenna). Because no infinite expanse of air exists, practical measurements of free-air radiation characteristics are often performed in an *anechoic chamber*, whose walls are designed to absorb sound waves just as they would be "absorbed" by an imaginary surface in free air. Calculation of free-air radiation by the FDEC method presents a similar problem with a similar solution: because the modeling of an infinite volume of air with a finite step size would require an infinite amount of computation, one must model a finite volume and simulate the interface between the finite and infinite volumes by imposing an appropriate boundary condition.

A thin, impermeable membrane suspended in a fluid will not interfere with the propagation of sound through the fluid if the membrane moves exactly as the fluid would move in the absence of the membrane. If the fluid is inviscid, it is sufficient that the *normal* velocity of the membrane match the normal velocity of the fluid in the absence of the membrane (here "normal" means "normal to the membrane"). Hence, if the pressure distribution on one side of the membrane is given, it is sufficient that the *ratio* of the normal velocity phasor to the pressure phasor be the same as if the membrane were absent; this ratio is the above-mentioned normal specific acoustic admittance, denoted by y_n. So, as far as the acoustic field on one side of the membrane is concerned, the membrane will be indistinguishable from a continuation of the fluid if it imposes the same y_n.

Therefore, to model the acoustic field radiated by a distributed source in free air using the FDEC method, we choose an equicoordinate (or piecewise-equicoordinate) surface enclosing the source, construct the FDEC model of the enclosed volume, and terminate the network so as to represent the normal admittance condition as described above (Subsection 6.5.3).

The difficulty with this procedure is that the representation of the normal admittance condition depends on the specific acoustic admittance $\mathbf{y}$, which in turn depends on the radiated acoustic field—i.e. on the unknown quantity that we are trying to determine. However, if the dimensions of a distributed acoustic source are much smaller than the shortest distance from the source to the boundary of the simulated region, we might expect to be able to estimate $\mathbf{y}$ at every point on the boundary by replacing the distributed source with a point-source. The apparent strength of the point source may vary with angular position (due to diffraction and interference), but the admittance should not be affected. This intuitive expectation is supported by the following argument.

Suppose a distributed acoustic source, of finite size and with sinusoidal time dependence, is placed near the center of a spherical coordinate system (R, θ, ϕ) in free air. Let U_0 be the total flux produced by the source (integrated over the radiating surface). If U_0 is non-zero, the pressure phasor at a general point may be written in the form

$$P = D(\omega, r, \theta, \phi)\, U_0\, \frac{j\omega\rho_\mathrm{o}}{4\pi}\, \frac{e^{-jkr}}{r} \tag{6.92}$$

where $k = \omega/c$, as usual. Because $D(\omega, r, \theta, \phi)$ is a perfectly general function, and because the other factors on the right are non-zero, we can always find D to satisfy

Eq. (6.92). The form of this equation has been chosen because it is equivalent to

$$P = D(\omega, r, \theta, \phi)\, P_{\rm PS}(\omega, r) \tag{6.93}$$

where $P_{\rm PS}(\omega, r)$ is the pressure due to a point-source at the origin producing the same total flux as the distributed source (cf. Eq. (3.22)). Thus D is introduced by the spatial distribution of the source and may be called a *distribution factor*.

Let us define a "wavefront" as a surface over which the phase of P is constant. For large r, the source subtends a small angle, so that we can speak of a "line of sight to the source", to which the wavefronts are perpendicular; hence the wavefronts can be approximated by r-surfaces, i.e. by spheres centered on the origin. Now consider a narrow cone with its apex at the origin. Because the cone is narrow, there is negligible variation of $|P|$ with θ and ϕ within the cone, so that the r-surfaces within the cone are surfaces of nearly constant P. Moreover, the cone is a tube of orthogonal trajectories to the r-surfaces, and r has a scale factor of unity. Therefore Webster's equation in the coordinate r is an approximate model of the field within the cone. The most general solution to the time-independent Webster equation in r, subject to the restriction that there is only an *outward-traveling wave*, can be written in the form

$$P = D(\omega)\, P_{\rm PS}(\omega, r) \tag{6.94}$$

(cf. Eqs. (3.17) and (3.22)). Note that $D(\omega)$ has no r-dependence. Widening the cone to include all of 3D space may cause D to depend on θ and ϕ, but it cannot make D depend on r as in Eq. (6.93), because the r-dependence is in the factor $P_{\rm PS}$. So for sufficiently large r, we can neglect the r-dependence of D in Eq. (6.93) and obtain

$$P \asymp D(\omega, \theta, \phi)\, P_{\rm PS}(\omega, r). \tag{6.95}$$

If we think of D as modifying the U_0 factor in $P_{\rm PS}$, the above expression looks like the pressure due to a point-source whose apparent strength varies with angular position.

To find an expression for the velocity, we first use Eq. (6.93) in the equation of motion:

$$\begin{aligned} \mathbf{Q} = -\frac{1}{j\omega\rho_{\rm o}}\nabla P &= -\frac{1}{j\omega\rho_{\rm o}}\nabla(DP_{\rm PS}) \\ &= -\frac{1}{j\omega\rho_{\rm o}}\left(D\,\nabla P_{\rm PS} + P_{\rm PS}\nabla D\right) \\ &= D\left(-\frac{1}{j\omega\rho_{\rm o}}\nabla P_{\rm PS}\right) - \frac{P_{\rm PS}}{j\omega\rho_{\rm o}}\nabla D. \end{aligned} \tag{6.96}$$

The expression in parentheses may be recognized as $\mathbf{Q}_{\rm PS}$, the velocity accompanying the point-source pressure field $P_{\rm PS}$. Hence, if we divide Eq. (6.96) by Eq. (6.95), we obtain

$$\frac{\mathbf{Q}}{P} = \frac{\mathbf{Q}_{\rm PS}}{P_{\rm PS}} - \frac{1}{j\omega\rho_{\rm o}}\frac{\nabla D}{D}. \tag{6.97}$$

The left-hand side is the specific acoustic admittance $\mathbf{y}$. The first term on the right is the point-source specific acoustic admittance, which we may call $\mathbf{y}_{\rm PS}$. The gradient of D, in spherical coordinates with negligible r-dependence, is

$$\nabla D \asymp \frac{1}{r}\frac{\partial D}{\partial \theta}\,\mathbf{e}_\theta + \frac{1}{r\sin\theta}\frac{\partial D}{\partial \phi}\,\mathbf{e}_\phi \tag{6.98}$$

(it is here that we first exploit the form of D in Eq. (6.95)). Making these substitutions in Eq. (6.97), we obtain

$$\mathbf{y} \asymp \mathbf{y}_{\mathrm{PS}} - \frac{1}{j\omega\rho_{\mathrm{o}}D}\left(\frac{1}{r}\frac{\partial D}{\partial\theta}\,\mathbf{e}_\theta + \frac{1}{r\sin\theta}\frac{\partial D}{\partial\phi}\,\mathbf{e}_\phi\right). \tag{6.99}$$

If D is nearly independent of r, so are its derivatives w.r.t. θ and ϕ. So as r increases, both terms in parentheses approach zero and the entire right-hand side approaches $\mathbf{y}_{\mathrm{PS}}$. That is, the specific acoustic admittance in the far field can be estimated by assuming a point-source.

The derivation of this result assumes the existence of a function D to satisfy Eq. (6.92), which in turn requires that U_0, the total flux radiated by the source, is non-zero. Thus the far-field point-source approximation is not valid for a dipole source or for an oscillating rigid body whose volume remains constant. In particular, it is not valid for an unbaffled rigid disk oscillating along its axis; an example of the error caused by the point-source assumption in this case is given in Chapter 11.

While the assumption that $U_0 \neq 0$ is essential to the above argument, the free-air assumption can be widened in the manner of Subsection 3.3.2. A source near a rigid planar baffle can be handled by the image method: the source and its image are treated as a single source in free space, so the conclusion that $\mathbf{y} \asymp \mathbf{y}_{\mathrm{PS}}$ holds in the far field of the composite source. This result is used in Chapter 11 in the modeling of a circular rigid piston in an infinite planar baffle.

The same result can be extended, albeit with some loss of rigor, to the case of a source in the throat of an infinite "asymptotically conical horn", i.e. a horn which is approximately (or exactly) conical at large distances from the throat. $\mathbf{Q}$ and $\mathbf{y}$ are almost purely radial in the far field of a source in free air. Hence, if we introduce an asymptotically conical horn with the apex of its "asymptotic cone" at the origin, the far field will not be greatly disturbed, while the part of the horn in the near field can be considered part of the source. In free air, the specific acoustic impedance in the far field of this composite source is approximately the same as that due to a point-source, and is not greatly altered by adding the far-field portion of the horn.

6.5.5 Non-equicoordinate boundaries

Any boundary surface can be approximated by a piecewise-equicoordinate surface, and the approximation can be made arbitrarily accurate by taking a sufficiently small step size. However, unless the given surface is exactly equicoordinate, the piecewise-equicoordinate approximation cannot be made smooth but must be assembled from quasi-cubic "blocks". This non-smoothness does not prevent the approximation from being arbitrarily accurate in the sense that every point on the piece-wise equicoordinate surface can be made arbitrarily close to the desired surface. But it complicates the application of some boundary conditions.

For the pressure condition, the error in approximating the boundary surface becomes an error in the location of each imposed pressure. The well-known Rayleigh criterion indicates that the resulting error in the simulation will not be objectionable provided that the boundary is approximated to within a small fraction of a wavelength.

A normal-velocity (or normal-admittance) condition can be applied to each equicoordinate segment by multiplying the original normal velocity (or normal admittance) by the cosine of the angle between the equicoordinate segment and the

original surface. This cosine is of course a direction cosine of the normal to the original surface. The procedure works because the normal velocity then makes the same flux in the equicoordinate segment as it makes in the normal projection of the segment on the original surface, and because these projections are contiguous on the original surface.

A radiation condition is not affected at all, because there is no "given" surface to be approximated. The boundary of the model is arbitrarily chosen, and the radiation condition is expressed as a normal admittance condition by taking the normal component of the vector specific acoustic admittance $\mathbf{y}$. This procedure is convenient in the case of a piecewise-equicoordinate boundary because the component of $\mathbf{y}$ normal to each boundary segment is the component in the direction of one of the three coordinates. But in principle a piecewise-equicoordinate boundary is treated like any other.

In summary, only the normal-velocity and normal-admittance conditions require special treatment when a given boundary is replaced by a piecewise-equicoordinate approximation.

6.6 Reduction to two dimensions

We have seen in Section 6.3 that if P is a function of a single spatial coordinate, the FDEC model reduces to a ladder network. The present section shows that if P is a function of *two* coordinates, say u and v, then the FDEC model can be reduced to a two-dimensional network.

If P is independent of the coordinate w, any finite-difference estimate of $\frac{\partial P}{\partial w}$ will produce the correct result, namely zero, regardless of the step size. In Eq. (6.35), the inner derivative w.r.t. w will be correctly estimated as zero; hence the parenthesized expression containing $\frac{\partial p}{\partial w}$ will evaluate to zero, and its derivative w.r.t. w will also be correctly estimated as zero. So, when deriving the FDEC model from the wave equation, we can use any step size Δw without incurring any error. In the equation of motion in the w direction, which can be obtained by writing w for u in Eq. (6.47), the derivative w.r.t. w will be estimated as zero for all Δw. The same equation of motion gives $Q_w = 0$. Hence the derivative w.r.t. w in Eq. (6.62), which is an intermediate form of the equation of compression, will also be estimated as zero for all Δw. In summary, in all the equations from which we can derive the FDEC model, the finite-difference approximations to the derivatives w.r.t. w are exact for all Δw if P is independent of w.

The problem of finding necessary and sufficient conditions under which a coordinate system admits *two*-parameter waves, unlike the corresponding problem for one-parameter waves, is not considered in this thesis. In practice, however, we do not argue that "by symmetry, P is independent of w," unless all three scale factors and all three components of $\mathbf{Q}$ are also independent of w; if these conditions are not met, there will be no *prima facie* appearance of "symmetry".[4] If the scale factors and velocity components are independent of w, then the accuracy of the estimates

[4]Of course the w-independence of the components of $\mathbf{Q}$ can be deduced from the w independence of P and the scale factors, using the equation of motion. But if we assert "By symmetry…", we will consider all these facts to be self-evident. This argument applies when the wave function depends on *exactly* two coordinates; if it depends on only one coordinate, the scale factors for the other two coordinates must behave according to Eq. (5.7).

of areas and fluxes is not affected by the range of w (see e.g. Eq. (6.51)), so that no loss of accuracy is incurred by using a large Δw.

Similarly, the "by symmetry" argument will not be possible unless the range of (u, v) for the simulated region is independent of w or—which is the same thing—the range of w is independent of u and v.

So, if the range of w for the whole system is $a < w < b$, we might as well choose $\Delta w = b - a$ and let the compliance elements extend over the entire range of w. As there is no component of $\mathbf{Q}$ in the w direction, the truncated inertance elements in the w direction will carry no flux and can be ignored. Thus the FDEC network is only one element thick in the w direction; that is, it is two-dimensional. This technique will be used to advantage in Chapters (10) and (11). The two-parameter assumption will approximate in Chapter 10, but exact in Chapter 11.

Chapter 7

The damped FDEC model (for fiber-filled regions)

For the purpose of damping unwanted internal resonances, loudspeaker boxes are often filled with loose fiberglass or other low-density fibrous materials. Arai notes in passing that the viscous losses and thermal absorption losses of such materials may be modeled by using complex values of density and bulk modulus [2, p. 17]. But he gives no formulae, cites no references, and does not indicate how the results may be expressed as modified circuits.

This chapter shows that the presence of fiber gives two main mechanisms of damping: direct viscous damping of the air motion, and conduction of the heat of compression between the air and the fiber. The viscous effect can be represented by introducing a complex value of density into the phasor form of the differential equation of motion. In the equivalent circuit, this causes a parallel R-L circuit to appear in series with each ΔM. The thermal effect can be accounted for by using a complex value of γ in the phasor form of the differential equation of compression. In the equivalent circuit, this causes a series R-C circuit to appear in parallel with each ΔC. The complex bulk modulus (referred to by Arai) can be written in terms of the complex gamma.

In the terminology of this Chapter and Chapter 10, the word "fiber" (in the singular) usually denotes the loosely-packed damping material as a whole, or a small volume element thereof; a single strand is referred to as a "filament". In contrast, "fibers" (plural) always means a plurality of filaments, not a plurality of volume elements or materials. Although contradictory, this usage is convenient and the context prevents any confusion. (In Chapter 8, which contains a long mathematical analysis of the conduction of heat to and from "one fiber", it is more convenient to use the singular "fiber" in the discrete sense, consistent with the plural.)

7.1 Equation of motion: complex density

In free air, i.e. *without* damping material, Eq. (6.46) gives a relation between pressure and velocity in phasor form. We might expect the presence of the damping material to alter this relation in a frequency-dependent manner, so that the new relation could be described simply by replacing the density ρ_o with a frequency-dependent complex quantity $\rho^\star$; that is

$$\nabla P = -j\omega\rho^\star \mathbf{Q}. \tag{7.1}$$

We shall see that the equation of motion of air in the presence of fiber can indeed be written in this form, and leads to an intuitively plausible modification to the inertia elements of the finite-difference equivalent circuit.

7.1.1 Discussion of approximations; review of literature

A quantity called complex density was derived and used by Leach in his 1989 paper on fiber-filled enclosures [30]. Leach's application is simpler than the present one in that it does not involve the finite-difference method; the complex density expression is substituted into a conventional low-frequency model of an undamped enclosure. But Leach's expression for complex density is more complicated than the one to be derived here. His equation (21), which describes the motion of the fiber, includes three force terms, namely

> (a) a damping force proportional to the relative velocity between the fiber and the air,
>
> (b) a second damping force proportional to the "absolute" velocity of the fiber, and
>
> (c) an elastic restoring force proportional to the displacement of the fiber from the equilibrium position.

Leach's analysis assumes that forces (b) and (c) are *uncoupled*, i.e. independent of the motion of adjacent fibers or even adjacent parts of the same filament. This is unrealistic given that both forces are internal to the fiber and arise from non-uniformity in the motion of the fiber (which causes deformation) rather than the motion itself. In Leach's defense, it should be noted that the distinction between motion and deformation is not critical in his analysis because the two quantities may be assumed to be proportional; the entire volume of the fiber-filled box is modeled as a single volume element, with the fiber constrained to be stationary at the boundary. But in the general finite-difference volume element, no such constraint applies, so that deformation and displacement must not be confused.

If deformation and displacement are proportional, as Leach may have assumed, then velocity is proportional to strain rate, which in turn may be proportional to internal viscous forces. But one would not expect such forces to be significant when compared with elastic forces, especially in a brittle material such as glass. Moreover, frictional forces caused by fibers sliding over adjacent fibers are not proportional to velocity—absolute or relative. Hence one must question Leach's treatment of force (b) even for his own purposes.

One may be tempted to neglect forces (b) and (c) solely because of lack of realism. But it is preferable to show that these forces are negligible compared with (a), the air drag. The following argument proceeds in two steps, suggesting that (b) is less significant than (c), which in turn is negligible compared with (a).

Force (b) comprises viscous forces within each filament, plus friction due to fibers sliding over fibers. The internal viscous forces are expected to be smaller than elastic forces, as already stated. Concerning friction, the fibers are excited by a common airflow and therefore tend to move together with minimal sliding. If sliding is neglected, the only kind of frictional force is *static* friction, which is non-dissipative and serves only to transmit the elastic force (c) through the fiber network.

To show that elastic forces (c) are negligible compared with air drag (a), one may begin with a crude appeal to experience: anyone who has slept on an air mattress knows that the pillow section should not be fully inflated, or it will make an exceptionally hard "pillow". But even a conventional soft pillow contains stuffing which is denser and harder than typical loudspeaker filling. This means that the bulk modulus of elasticity of the loosely packed fiber is much less than that of air, i.e. much less than $\rho_o c^2$ (see Subsection 2.2.4). Assuming that the deformation of the fiber network is comparable with that of the air, the restoring forces within the fiber are small compared with those within the air, which in turn are comparable with the air drag (a) if damping is significant. Hence the restoring forces (c) in the fiber are small compared with the air drag (a).

In a loudspeaker box, only the air motion contributes to radiation from a diaphragm or vent. The fiber motion is of interest only insofar as it affects the air motion. Now the internal forces in the fiber do not act directly on the air; they must first accelerate the fiber, whose average density (mass per unit overall volume) is typically several times that of the air [30, p. 592]. We have established that the restoring forces in the fiber are small compared with the air drag provided that the bulk modulus of elasticity of the fiber network is much less than $\rho_o c^2$. But because internal forces in the fiber act on the fiber rather than the air, we can now weaken this condition by replacing ρ_o with the average density of the fiber network, and still be able to neglect the stiffness of the fiber for the purpose of calculating the air motion. Let f be the filling factor, i.e. the fraction of the volume taken up by the fiber.[1] Let the density of the glass (or other material of which the fiber is made) be ρ_f; this is the *intrinsic* density, or the mass per unit volume of glass. Then the *average* density of the fiber network is $f\rho_f$. Writing this density in place of ρ_o, we find that we can neglect restoring forces in the fiber if the bulk modulus of the fiber network is much less than $f\rho_f c^2$. This conclusion is expressed in different notation by Bradbury, in a footnote to his 1976 paper [13]. Bradbury does not explain why this condition is sufficient for the neglect of fiber stiffness, but indicates that the condition always holds in practice "even for densely packed fibers". The inflatable-pillow analogy, which leads to a stronger condition, makes his assurance easy to believe.

So Bradbury's analysis deliberately neglects the elastic restoring forces in the fiber. It also neglects internal damping forces (not even mentioning them), leaving air drag as the only force in the equation of motion for the fiber. Hence Bradbury's assumptions agree with those to be used here. His purpose, however, was quite different; he did not use equivalent circuits or define a complex density, but was interested in the propagation velocities, attenuation rates and impedances of fiber-filled pipes.

One force not mentioned by Bradbury or Leach is gravity. Here it will be assumed that the weight of the fibers is balanced by the *quiescent* internal forces in the fibers. But because of the low bulk modulus of the fiber network, the *variations* in the internal forces will be assumed negligible compared with the air drag, as explained above. So gravity and the internal forces will be assumed to cancel out, and neither will appear in the equation of motion for the fiber.

[1] In Chapters 7, 8 and 10, the symbol "f" denotes the filling factor; frequency is specified in terms of the angular frequency ω.

7.1.2 Derivation of complex density

To find an expression for complex density, we derive the equations of motion for the air and the fiber, then eliminate the fiber velocity between the two equations, expressing the result in the form of Eq. (7.1). The elimination step is facilitated by writing the equations of motion in terms of phasors or Fourier transforms, thereby converting the original differential equations into algebraic equations; it is a straightforward example of solving simultaneous differential equations by a transform method. (Leach [30, p. 590] uses Laplace transforms instead of phasors.)

The difficult part is obtaining the two equations of motion. In keeping with the standard established in Chapter 2, these equations will be derived more rigorously than in the papers of Leach and Bradbury. In particular, ρ and f will not be assumed constant from the beginning, and when it does become necessary to assume them constant, the approximation will be justified.

Let us suppose that the equilibrium values of all parameters of the fiber, including the filling factor f, are uniform throughout the filled region.[2] The volume fraction occupied by air is obviously $1 - f$. This is also the area fraction occupied by air in any cross-section through the filled region. Let $\mathbf{q}$ be the velocity of the air and $\mathbf{q}_\mathrm{f}$ the velocity of the fibers. Let λ be the acoustic (or pneumatic) resistivity of the fiber fill; for present purposes this will be defined as the viscous force per unit velocity per unit volume *of air*,[3] so that the viscous force per unit overall volume will be

$$(1 - f)\lambda(\mathbf{q} - \mathbf{q}_\mathrm{f})$$

on the fiber, with an equal and opposite force on the air. Note that λ is assumed to be isotropic. This will be true if the orientation of fibers is completely random, but will not if the fibers tend to run in a preferred direction or parallel to a preferred plane.

Now consider a three-dimensional region $\mathcal{V}$ enclosed by a surface σ *moving with the air*. Newton's second law for the air in this region is

$$\frac{d}{dt} \iiint_{\mathcal{V}} (1 - f)\, \rho \mathbf{q}\, d\mathcal{V} = - \iint_{\sigma} (1 - f)\, p\, .\, \mathbf{n}\, d\sigma - \iiint_{\mathcal{V}} (1 - f)\lambda(\mathbf{q} - \mathbf{q}_\mathrm{f})\, d\mathcal{V} \qquad (7.2)$$

where the integral on the left is the total momentum, and the integrals on the right (with the minus signs) are the hydrostatic and viscous forces.[4] Using the gradient

[2] Here we apply the differential form of the equation of motion to a discontinuous medium—such liberties are common in applied mathematics, as all media other than the perfect vacuum are made of subatomic particles and are therefore discontinuous. In general, the use of a differential equation in a discontinuous medium requires that the particle spacing is small compared with the step size of a good finite-difference approximation to the differential equation. In the present case, the fiber radii and spacings must be small compared with the step size. The filling factor f is a statistic which depends on the volume sample chosen, but which is assumed to approach some limit as the sample size increases; the assumption that f is uniform means that the limit is independent of the sample location. We assume that the value of f is close to its limit for volume samples of a size comparable to that of a unit cell in the finite-difference network. In the text, the symbol f refers to this limiting value.

[3] Bradbury [13, p. 163] apparently defines λ with respect to overall volume, so that the factor $(1 - f)$ does not appear in his equation (1).

[4] In the original derivation of the point form of the equation of motion (Subsection 2.1.2), it was shown that gravity and the gravitational pressure gradient may be neglected provided that we use the pressure rise above equilibrium instead of the total pressure. This result is now assumed to hold in the presence of damping material. (A more rigorous approach would be to rework Subsection 2.1.2 with the extra viscous force term.)

theorem to replace the surface integral with a volume integral, we obtain

$$\frac{d}{dt}\iiint_{\mathcal{V}}(1-f)\,\rho\mathbf{q}\,d\mathcal{V} = -\iiint_{\mathcal{V}}\nabla[(1-f)p]\,d\mathcal{V} - \iiint_{\mathcal{V}}(1-f)\lambda(\mathbf{q}-\mathbf{q}_\mathrm{f})\,d\mathcal{V}. \tag{7.3}$$

For small compressions, the fractional changes in f are small compared with those in p; remember that p is the alternating excess pressure, not the total pressure. Moreover, because f is less than 0.01 for typical filling material[5], the fractional variations in $(1-f)$ are small compared with those in f. Thus the variations in $(1-f)$ make negligible contribution to $\nabla[(1-f)p]$, so that $(1-f)$ may be treated as a constant and taken outside the ∇ operator. When this is done, the volume integrals can be rewritten in terms of the air mass element

$$dm = (1-f)\rho d\mathcal{V} \tag{7.4}$$

so that the equation of motion becomes

$$\frac{d}{dt}\iiint_{\mathcal{V}}\mathbf{q}\,dm = -\iiint_{\mathcal{V}}\frac{\nabla p}{\rho}\,dm - \iiint_{\mathcal{V}}\frac{\lambda(\mathbf{q}-\mathbf{q}_\mathrm{f})}{\rho}\,dm. \tag{7.5}$$

Note how the factor $(1-f)$ has canceled out; this is one advantage of defining the acoustic resistivity λ in terms of air volume rather than overall volume. Let us take the integrals over a single volume element, divide through by dm (as in Subsection 2.1.2), and make the small-amplitude approximation

$$\frac{d\mathbf{q}}{dt} = \dot{\mathbf{q}} \tag{7.6}$$

where the dot denotes partial differentiation (cf. Subsection 2.1.2 and especially Eq. (2.8)). This gives

$$\dot{\mathbf{q}} = -\frac{1}{\rho}\left[\nabla p + \lambda(\mathbf{q}-\mathbf{q}_\mathrm{f})\right]. \tag{7.7}$$

For small compressions we may replace ρ with ρ_o. Then we may convert to phasor form (assuming that λ is constant) and solve for ∇P, obtaining

$$\nabla P = \lambda(\mathbf{Q}_\mathrm{f} - \mathbf{Q}) - j\omega\rho_\mathrm{o}\mathbf{Q} \tag{7.8}$$

which is the desired form of the equation of motion for the air.[6]

Before shifting attention to the fiber, it is of interest to find another definition of λ. If the motion of the air is steady and the fiber is stationary, we may put $\dot{\mathbf{q}} = \mathbf{0}$ and $\mathbf{q}_\mathrm{f} = \mathbf{0}$ in Eq. (7.7), and obtain

$$\lambda\mathbf{q} = -\nabla p. \tag{7.9}$$

If electrical resistivity is represented (for the moment) by ρ, current density by $\mathbf{J}$ and potential by V, the definition of resistivity is

$$\rho\mathbf{J} = -\nabla V. \tag{7.10}$$

[5]The "typical" figures given by Leach [30, p. 592] imply a filling factor of about 0.0025.

[6]Eq. (7.8) agrees with Bradbury's equation (11) in spite of his different definition of λ. However, Bradbury also made it clear that he was not concerned about the small volume fraction occupied by the fibers [13, pp. 163, 169].

Thus the chosen definition of pneumatic resistivity makes it analogous to electrical resistivity if we take $\mathbf{q}$, rather than $(1-f)\mathbf{q}$, as the analog of $\mathbf{J}$.

Eq. (7.8) describes the motion of the air but involves the fiber velocity $\mathbf{Q}_\mathrm{f}$, which is usually not of interest except as regards its effect on the air motion. Another phasor equation will now be obtained from the equation of motion of the fiber, and will be used to eliminate $\mathbf{Q}_\mathrm{f}$. Consider a new control volume $\mathcal{V}$ enclosed by a new surface σ, this time *moving with the fiber*. Remembering that the average density of the fiber matrix (w.r.t. overall volume) is $f\rho_\mathrm{f}$, Newton's second law for the fiber in this control volume may be written

$$\frac{d}{dt}\iiint_{\mathcal{V}} f\rho_\mathrm{f}\mathbf{q}_\mathrm{f}\,d\mathcal{V} = \iiint_{\mathcal{V}} (1-f)\lambda(\mathbf{q}-\mathbf{q}_\mathrm{f})\,d\mathcal{V} \tag{7.11}$$

where the integral on the left is the total momentum of the fiber in the region, and the integral on the right is the viscous force on the fiber. Both integrals can be rewritten in terms of the fiber mass element

$$dm_\mathrm{f} = f\rho_\mathrm{f} d\mathcal{V}. \tag{7.12}$$

Then if we take the integrals over a single mass element, cancel dm_f and use Eq. (7.6) for small oscillations, we obtain

$$f\rho_\mathrm{f}\dot{\mathbf{q}}_\mathrm{f} = (1-f)\lambda(\mathbf{q}-\mathbf{q}_\mathrm{f}) \tag{7.13}$$

or, transposing all terms in $\mathbf{q}_\mathrm{f}$ to the left,

$$(1-f)\lambda\mathbf{q}_\mathrm{f} + f\rho_\mathrm{f}\dot{\mathbf{q}}_\mathrm{f} = (1-f)\lambda\mathbf{q}. \tag{7.14}$$

Because the velocities are alternating while f and λ are mostly "DC", we can treat f and λ as constants to obtain the phasor form

$$\left[(1-f)\lambda + j\omega f\rho_\mathrm{f}\right]\,\mathbf{Q}_\mathrm{f} = (1-f)\lambda\mathbf{Q}. \tag{7.15}$$

Solving this for $\mathbf{Q}_\mathrm{f}$ and subtracting $\mathbf{Q}$ from both sides, using a common denominator on the right, yields

$$\mathbf{Q}_\mathrm{f} - \mathbf{Q} = -\,\frac{j\omega f\rho_\mathrm{f}}{(1-f)\lambda + j\omega f\rho_\mathrm{f}}\,\mathbf{Q}. \tag{7.16}$$

To eliminate $\mathbf{Q}_\mathrm{f}$, we substitute Eq. (7.16) into Eq. (7.8), obtaining the desired form

$$\nabla P = -j\omega\rho^\star\mathbf{Q} \tag{7.17}$$

where

$$j\omega\rho^\star = \frac{\lambda\, j\omega f\rho_\mathrm{f}}{(1-f)\lambda + j\omega f\rho_\mathrm{f}} + j\omega\rho_\mathrm{o}. \tag{7.18}$$

For the purpose of simplifying this expression and deriving an equivalent circuit, it is convenient to define the *harmonic sum operator* "$\|$" as follows:

$$a\|b \triangleq \frac{1}{\frac{1}{a}+\frac{1}{b}} \equiv \frac{ab}{a+b}. \tag{7.19}$$

This is the operator by which two parallel impedances may be combined to give a single impedance; hence it is given the "parallel" symbol. In expressions, harmonic addition will have a priority below multiplication and division, but above

addition and subtraction. From the definition it is easily shown that multiplication is distributive over harmonic addition; that is,

$$\text{For all } a, b, \mu, \quad \mu(a \| b) = \mu a \| \mu b. \tag{7.20}$$

This rule will simplify algebraic manipulation.

Returning to our problem, we have

$$\begin{aligned} j\omega\rho^\star &= j\omega\rho_\mathrm{o} + \frac{\lambda\, j\omega f\rho_\mathrm{f}/(1-f)}{\lambda + j\omega f\rho_\mathrm{f}/(1-f)} \\ &= j\omega\rho_\mathrm{o} + \lambda \left\| \frac{j\omega f\rho_\mathrm{f}}{1-f} \right. \end{aligned} \tag{7.21}$$

or, if an explicit expression for $\rho^\star$ is preferred,

$$\rho^\star = \rho_\mathrm{o} + \frac{\lambda}{j\omega} \left\| \frac{f\rho_\mathrm{f}}{1-f}. \right. \tag{7.22}$$

To compare this result with that given by Leach [30] in his Eq. (25), we use the following notational conversions (which Leach's expressions are shown on the left):

$$\begin{aligned} s &\rightarrow j\omega \\ V_\mathrm{f}/V_\mathrm{B} &\rightarrow f \\ c_\mathrm{f} &\rightarrow \infty \\ r_\mathrm{f} &\rightarrow 0 \\ n\delta &\rightarrow (1-f)\lambda \\ nm_\mathrm{f} &\rightarrow f\rho_\mathrm{f} \\ \rho_\mathrm{c} &\rightarrow \rho^\star. \end{aligned}$$

The numerical replacements for c_f and r_f indicate that we neglect the stiffness and internal damping of the fiber. With these seven substitutions, Leach's Eq. (25) reduces to the above Eq. (7.22) except that his result has an extra overall factor $(1-f)$. This arises because his derivation of the equation of motion for the air does not allow for the reduced cross-sectional area; on the right-hand side of his Eq. (23), the area of air over which the pressure difference operates should be $(1-f)A$, not simply A. The difference is of minor importance because, in practice, f is small.

7.1.3 Equivalent circuit

To find an equivalent circuit from complex density, we follow the method by which Eq. (6.49) was obtained from Eq. (6.46), except that we use $\rho^\star$ instead of ρ_o. So instead of Eq. (6.46) we use Eq. (7.17), and instead of Eq. (6.49) we obtain

$$P_{i,j,k} - P_{i+1,j,k} \approx \left[j\omega\rho^\star h_u \Delta u\, Q_u \right]_{i+\frac{1}{2},j,k}. \tag{7.23}$$

Now consider a unit cell centered on $(u_{i+\frac{1}{2}}, v_j, w_k)$, with a cross-section at $u = u_{i+\frac{1}{2}}$. The estimated flux through this cross-section (with the u direction having the positive sense) is

$$\Delta U_u\big|_{i+\frac{1}{2},j,k} = \left[(1-f)\, h_v \Delta v\, h_w \Delta w\, Q_u \right]_{i+\frac{1}{2},j,k}. \tag{7.24}$$

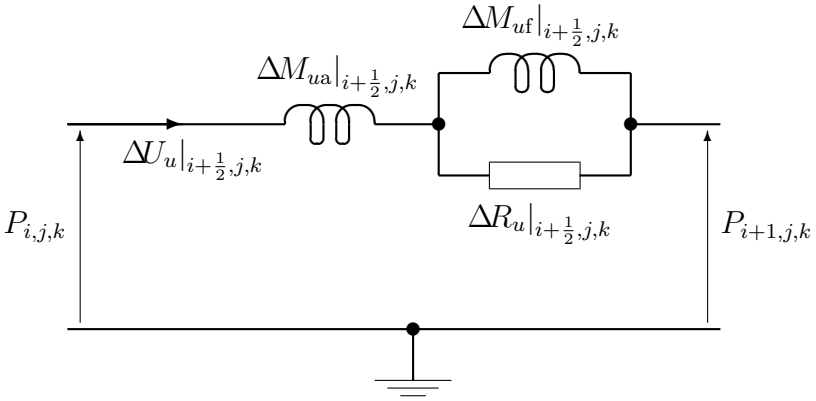

Figure 7.1: *FDEC model for equation of motion in u direction, with damping.*

Solving for $Q_u|_{i+\frac{1}{2},j,k}$ and substituting the result into Eq. (7.23) gives

$$P_{i,j,k} - P_{i+1,j,k} \approx \Delta Z_u|_{i+\frac{1}{2},j,k}\, \Delta U_u|_{i+\frac{1}{2},j,k} \tag{7.25}$$

where

$$\Delta Z_u|_{i+\frac{1}{2},j,k} = \left.\frac{j\omega\rho^\star h_u \Delta u}{(1-f)\, h_v \Delta v\, h_w \Delta w}\right|_{i+\frac{1}{2},j,k}. \tag{7.26}$$

Eq. (7.25) has the same form as Eq. (6.52), which describes the equivalent circuit of Fig. 6.3, except that the impedance $j\omega\Delta M_u|_{i+\frac{1}{2},j,k}$ is replaced by $\Delta Z_u|_{i+\frac{1}{2},j,k}$. Substituting Eq. (7.21) into Eq. (7.26) yields

$$\Delta Z_u|_{i+\frac{1}{2},j,k} = [j\omega\Delta M_{u\mathrm{a}} + \Delta R_u \| j\omega\Delta M_{u\mathrm{f}}]_{i+\frac{1}{2},j,k} \tag{7.27}$$

where

$$\Delta M_{u\mathrm{a}}|_{i+\frac{1}{2},j,k} = \left.\frac{\rho_\mathrm{o} h_u \Delta u}{(1-f)\, h_v \Delta v\, h_w \Delta w}\right|_{i+\frac{1}{2},j,k} \tag{7.28}$$

$$\Delta R_u|_{i+\frac{1}{2},j,k} = \left.\frac{\lambda h_u \Delta u}{(1-f)\, h_v \Delta v\, h_w \Delta w}\right|_{i+\frac{1}{2},j,k} \tag{7.29}$$

$$\Delta M_{u\mathrm{f}}|_{i+\frac{1}{2},j,k} = \left.\frac{f\rho_\mathrm{f} h_u \Delta u}{(1-f)^2 h_v \Delta v\, h_w \Delta w}\right|_{i+\frac{1}{2},j,k}. \tag{7.30}$$

So ΔZ_u is the impedance of $\Delta M_{u\mathrm{a}}$ in series with the parallel combination of ΔR_u and $\Delta M_{u\mathrm{f}}$, as shown in Fig. 7.1.

The component values in the equivalent circuit can be understood intuitively. The cross-sectional area of the air in the unit cell is $(1-f)\, h_v \Delta v\, h_w \Delta w$. This is the effective cross-sectional area for calculating both inertance and resistance (recall that the acoustic/pneumatic resistivity λ is defined w.r.t. the volume of air, not the total volume). $\Delta M_{u\mathrm{a}}$ (with subscript "a" for "air") is the acoustic mass, in the u direction, of the air in the unit cell; Eq. (7.28) gives its value as "ρ_o times length over area". $\Delta R_u$is the acoustic resistance of the unit cell in the u direction. Eq. (7.29) gives the resistance as "λ times length over area", confirming that λ is analogous to electrical resistivity provided that the reduced area is used. $\Delta M_{u\mathrm{f}}$ (with subscript "f" for "fiber") is the acoustic mass, in the u direction, of the fiber in the unit cell.

If the effective density of the fiber is taken as the mass per unit volume of air, i.e. $f\rho_\mathrm{f}/(1-f)$, then multiplying this by the length and dividing by the effective cross-sectional area gives a result agreeing with Eq. (7.30). The use of "effective density" thus explains the square in the denominator of ΔM_{uf}. For an alternative explanation, we can evaluate ΔM_{ua} and ΔM_{uf} using Eq. (2.26), which gives the inertance as the total enclosed mass divided by the *square* of the cross-sectional area. It is also worth noting that ΔM_{ua} and ΔM_{uf} are in the ratio of $(1-f)\rho_\mathrm{o}$ to $f\rho_\mathrm{f}$, i.e. the ratio of the density of the air to the density of the fiber when both densities are w.r.t. overall volume.

The topology of the equivalent circuit is also quite intuitive. To move the air in the unit cell, the pressure difference must overcome the inertia of the air plus the impedance of the fiber; hence ΔM_{ua} appears in series with the elements representing the fiber. To overcome the impedance of the fiber, the air can either flow through the fiber (which has resistance ΔR_u) or move the fiber (which has inertance ΔM_{uf}) and the fluxes due to these two effects are additive; hence ΔR_u and ΔM_{uf} are in parallel.

The equivalent circuit also yields a physical description of the high- and low- frequency behavior of the air and fiber. At low frequencies, most of the total flux flows through ΔM_{uf} (moving *with* the fiber) rather than through ΔR_u (moving *through* the fiber), indicating that the motion of the fiber almost keeps up with that of the air (remember that the term "flux" refers to the motion of the air only). At high frequencies, most of the total flux is carried by ΔR_u, indicating that the fiber remains almost stationary while the air moves through it. This conclusion agrees with that of Bradbury [13, p. 163], who uses a physical argument based on the "time taken for the fibrous material to be set in motion" by the air passing through it.

7.1.4 Computation of mass elements

The component values of the equivalent circuit in Fig. 7.1 may be found in practice using equations (7.28) to (7.30), provided that ρ_o, ρ_f, f and λ are known.

The density ρ_o, in common with all the other acoustical properties of air, can be calculated with acceptable accuracy from T and P_0. Algebraic formulae for a number of such properties are developed, in an appropriate computational order, in Chapter 9. Using these formulae, one can produce acoustic simulation software which requires the user to specify the ambient temperature and pressure and computes all the required properties of air therefrom; this is convenient for the user and minimizes the risk of erroneous or inconsistent data.

The intrinsic glass density ρ_f and the average glass density $f\rho_\mathrm{f}$ are specifications of the fibrous filling material; dividing the second by the first gives f. In a bale of low-density fiberglass, the mass of the air is not a negligible part of the total mass. Therefore, if $f\rho_\mathrm{f}$ is measured by weighing a known volume of the material, it is important to weigh only the glass and not also the air between the fibers. Fortunately the correct weight is measured almost by default, because the air between the fibers is buoyed up by the surrounding air. Of course the glass is also buoyed up—as is anything else weighed in air, including the known masses on the other side of the balance—but for materials of typical density, such as glass, the effect of buoyancy is negligible.

The interesting quantity in equations (7.28) to (7.30) is the pneumatic resistivity

λ. The pneumatic resistance of a cylindrical sample of fiber with length L and (total) cross-sectional area A is given by

$$R = \frac{\lambda L}{(1-f)\,A} \tag{7.31}$$

(cf. Eq. (7.29)). Solving for λ gives

$$\lambda = \frac{(1-f)\,AR}{L}. \tag{7.32}$$

By passing air through a sample of fiber and measuring the pressure drop and flux, one can find R and hence λ. Bradbury [13, pp. 164–5] has compared a number of such measurements with a theoretical model to produce the semi-empirical formula

$$\lambda \approx 27\,\eta\,\frac{f^{1.4}}{\mathsf{d}^2} \tag{7.33}$$

where η is the dynamic viscosity of air and d is the fiber diameter. Unfortunately there is considerable uncertainty in the proportionality factor 27. It is clear, however, that λ is proportional to η and depends on ambient temperature and pressure just as η does. Therefore even a *measurement* of λ under particular ambient conditions will not be valid under other conditions unless it is corrected for the change in η. Hence, whether one determines λ using Eq. (7.33) or by experiment, it is necessary to know η as a function of temperature and pressure. In fact η is remarkably insensitive to pressure and may be regarded as a function of temperature alone. For a wide range of temperatures, including any likely to be encountered in a listening room, η may be calculated from Eq. (9.10), given in Chapter 9.

In Chapter 10, Eqs. (7.33) and (9.10) will be used to obtain reasonable values of λ for the purpose of illustration. But it should be remembered that, because of the uncertainty in the proportionality factor and the possibility that λ may be anisotropic, Eq. (7.33) is the least accurate formula used in this thesis.

7.2 Equation of compression: complex gamma

In free air, i.e. *without* fibrous filling, Eq. (6.57) gives a relation between pressure and density in phasor form. Because pressure and density are related to temperature, and because temperature differences tend to decay due to heat conduction, we would expect the presence of heat-absorbent fiber to alter the pressure-density relation in a frequency-dependent manner, so that the new relation could be described simply by replacing γ with a frequency-dependent complex quantity $\gamma^\star$; that is

$$P = \frac{\gamma^\star P_0}{\rho_\mathrm{o}}\,\underline{\rho_\mathrm{e}}. \tag{7.34}$$

We shall see that the equation of compression in the presence of fiber can indeed be written in this form, and leads to a simple modification to the compliance elements of the finite-difference equivalent circuit. The form of the modified circuit is as intuitive as for the equation of motion, although the component values are not. Nevertheless, the components have physical significance; for example, two RC time constants in the equivalent circuit correspond to thermal time constants in the air-fiber system.

At this point it can be seen how $\gamma^\star$ is related to Arai's complex bulk modulus [2, p. 17]. In Eq. (7.34), the phasor representation of fractional compression is $\underline{\rho_\mathrm{e}}/\rho_\mathrm{o}$. So the complex bulk modulus, defined as the ratio of the pressure phasor to the fractional compression phasor, is $\gamma^\star P_0$. This is the same as the adiabatic bulk modulus for undamped air except that $\gamma^\star$ replaces γ.

7.2.1 Thermal and mechanical definitions of γ

The finite-difference model of compression in fiber-filled enclosures draws heavily on the thermodynamics of ideal gases. The present subsection prepares for this by applying conservation of energy to the adiabatic compression of air, without fiber, to verify that γ as defined by Eq. (6.57) is indeed the "ratio of specific heats" referred to in Subsection 2.2.4. Then Subsection 7.2.2 finds an expression in terms of specific heats for the $\gamma^\star$ of a fiber-filled region. Whereas the present subsection begins with a thermal definition of γ and derives a mechanical definition (namely Eq. (6.57)), Subsection 7.2.2 proceeds in the opposite direction. In both cases, the thermal definition is needed for calculating γ or $\gamma^\star$, while the mechanical definition is needed for deriving the acoustic equation of compression.

In a sample of an ideal gas, let p_t be the pressure, v the specific volume and u the specific internal energy, where "specific" means "per unit mass". Then the specific enthalpy h is defined as

$$h = u + p_\mathrm{t} v. \tag{7.35}$$

If T is the absolute temperature, the specific heats are defined as [9, p. 138]

$$C_p = \left.\frac{\partial h}{\partial t}\right|_{\text{constant } p_\mathrm{t}} \tag{7.36}$$

and

$$C_v = \left.\frac{\partial u}{\partial t}\right|_{\text{constant } v}. \tag{7.37}$$

Now an ideal gas is modeled by the familiar equation of state

$$p_\mathrm{t} v = RT \tag{7.38}$$

where R is the gas constant on a mass basis (see Subsection 2.2.4), so Eq. (7.35) may be rewritten

$$h = u + RT. \tag{7.39}$$

Another property of an ideal gas, less familiar but more fundamental than the equation of state, is that the specific internal energy u of a given gas is a function of temperature alone [9, pp. 135–7]. Therefore the "constant v" condition in the definition of C_v may be replaced by any other condition, including constant p_t. Using this fact, we can differentiate Eq. (7.39) w.r.t. T at constant p_t, obtaining the useful result

$$C_p = C_v + R \tag{7.40}$$

which relates the specific heats of an ideal gas.

Now γ is initially defined as

$$\gamma = C_p/C_v \tag{7.41}$$

wherefore it is called the ratio of specific heats. Substituting from Eq. (7.40) leads to the alternative definition

$$\gamma = \frac{C_v + R}{C_v} \tag{7.42}$$

which is valid for ideal gases only.

Eq. (7.42) is a *thermal* definition of γ. But for acoustical purposes we also require a *mechanical* definition of γ in terms of the behavior of the medium in compression.

Now consider a sample of ideal gas subject to *adiabatic* compression. Since there is no heat transfer, the change in internal energy of the gas is equal to the work done on the gas, which is minus the work done *by* the gas. That is, in terms of differential increments of work and energy per unit mass,

$$C_v\, dT = -p_\mathrm{t}\, dv. \tag{7.43}$$

From the ideal gas equation,

$$T = \frac{p_\mathrm{t}}{\rho R}. \tag{7.44}$$

Differentiating this using either the quotient rule or the chain rule for partial derivatives, we obtain

$$dT = \frac{1}{\rho R}\, dp_\mathrm{t} - \frac{p_\mathrm{t}}{R}\frac{d\rho}{\rho^2}. \tag{7.45}$$

Furthermore,

$$v = 1/\rho \tag{7.46}$$

so that

$$dv = -d\rho/\rho^2. \tag{7.47}$$

Also recall that $p_\mathrm{t} = P_0 + p$, where P_0 is the equilibrium pressure, so that $dp = dp_\mathrm{t}$. So we can substitute for dT and dv in Eq. (7.43), let $p_\mathrm{t} \to P_0$ and $\rho \to \rho_\mathrm{o}$ (for small compressions), write dp for dp_t, and solve for dp. The result is

$$dp = \frac{C_v + R}{C_v}\,\frac{P_0}{\rho_\mathrm{o}}\, d\rho \tag{7.48}$$

or, using Eq. (7.42),

$$dp = \gamma\,\frac{P_0}{\rho_\mathrm{o}}\, d\rho. \tag{7.49}$$

Two interesting points follow from this result. First, we can rewrite it in the form

$$\frac{dp}{P_0} = \gamma\,\frac{d\rho}{\rho_\mathrm{o}}$$

which shows that γ is the *sensitivity of pressure to density*. Thus γ has a mechanical definition that can be concisely expressed in words. Second, if we divide both sides of Eq. (7.49) by $d\rho$ and recall that

$$\frac{dp}{d\rho} = c^2$$

(Eq. (2.31)), we find an expression for c^2 agreeing with Eq. (2.39). Thus we have an alternative derivation of Eq. (2.39) which is independent of Eq. (2.37) and its supporting reference to Barrow [9, pp. 139–40].

Returning to the main problem, if we consider p and ρ to be functions of time t and divide Eq. (7.49) by dt, we obtain[7]

$$\dot{p} = \frac{\gamma P_0}{\rho_o}\,\dot{\rho} = \frac{\gamma P_0}{\rho_o}\,\dot{\rho}_e. \tag{7.50}$$

This is the same as Eq. (6.56), which leads to Eq. (6.57), which is the desired form of the mechanical definition of γ for an ideal gas. Substituting $\gamma^\star$ for γ in Eq. (6.57) gives Eq. (7.34), which will be adopted as the definition of $\gamma^\star$ in a fiber-filled region. It remains to convert this mechanical definition into a thermal definition in terms of specific heats; the thermal definition will serve as a computational formula for $\gamma^\star$.

7.2.2 Derivation of complex gamma

In Subsection 7.1.2, the complex density $\rho^\star$ was found by eliminating the fiber velocity between two equations of motion, one for the air and the other for the fiber. The complex gamma, however, is not found by eliminating the "fiber density" between two equations of compression. The fibers are assumed to be *intrinsically incompressible* in the sense that they occupy a constant (small) volume, but infinitely compressible in the sense that they make negligible contribution to the bulk modulus of the air-glass mixture (wherefore the rigidity of the fibers was neglected in deriving the complex density). Thus there is only one equation of compression—that of the air in the presence of fiber. It will be derived after the complex gamma has been determined.

In principle, $\gamma^\star$ is found by eliminating the air temperature and fiber temperature between three equations, one expressing the first law of thermodynamics for the air, one based on the ideal gas equation, and one describing the conduction of heat between the air and the fiber. It is convenient at the beginning to introduce specific volume as an additional variable, which is eliminated by an additional equation relating specific volume and density. As in Subsection 7.1.2, the elimination of variables is facilitated by using phasor forms of the equations.

Consider the compression of a sample of air which is permeated by a mass of low-density fiberglass. Rapid compression, such as occurs in loudspeaker enclosures, may be considered *adiabatic from the viewpoint of an external observer*, in the sense that if the air and fiber together are considered as a system, negligible heat is conducted across the boundary between the system and surroundings. But the compression is *not* adiabatic when we consider the air alone; the fine fiber matrix has a very large surface area per unit volume, allowing rapid conduction of heat between the fiber and the air, so that substantial heat conduction can occur during one cycle of an audio-frequency oscillation.

When the air-fiber mixture is compressed, the work done imparts energy to the mixture. Some of this energy appears as an increase in the internal energy of the air. Because the air is modeled as an ideal gas, the increase in internal energy is entirely manifested as an increase in air temperature. The rest of the energy heats the fiber. It is assumed that the glass (or other material of which the fiber is composed) is incompressible, so that no energy is consumed in compressing the glass. It is also assumed, as hinted above, that there is no leakage of energy due to heat conduction

[7]The reader who prefers rigor to clarity may rework the derivation from Eq. (7.43) using time derivatives instead of differentials and thereby avoid "dividing by dt".

between the air-fiber system and its surroundings. The work and energy terms will first be constructed on a per-unit-mass basis, as is most familiar. This will cause some quantities to be defined per unit mass of air and others per unit mass of fiber, whereas the energy balance requires all terms to have a common basis. Therefore all terms will be converted to "per unit overall volume" before they are inserted in the energy equation.

When the air is compressed so that its specific volume v is reduced by dv, the work done per unit mass of air is

$$dw = -p_{\mathrm{t}}\, dv. \tag{7.51}$$

The increase in the internal energy of the air, per unit mass of air, is

$$du = C_v\, dT \tag{7.52}$$

where T is the absolute temperature. To convert these two terms from a mass basis to an overall volume basis, we multiply by the average density of the air, which is

$$(1-f)\rho$$

where f is the filling factor as before. Let C_{f} be the specific heat of the fiber and T_{f} the average temperature of the fiber. Then the heat transferred to the fiber, per unit mass of fiber, is

$$dq = C_{\mathrm{f}}\, dT_{\mathrm{f}}. \tag{7.53}$$

To convert this to energy per unit overall volume, we must multiply by the average density of the fiber, which is

$$f\rho_{\mathrm{f}}.$$

Assembling all the terms, we find that the energy equation is

$$-(1-f)\rho p_{\mathrm{t}}\, dv = (1-f)\rho C_v\, dT + f\rho_{\mathrm{f}} C_{\mathrm{f}}\, dT_{\mathrm{f}}. \tag{7.54}$$

At this point it is convenient to consider all the thermodynamic variables as functions of time and divide through by dt, thus expressing the energy balance in terms of time derivatives, i.e. as a power balance.[8] Further, let T_0 be the system equilibrium temperature, i.e. the temperature of the air and fiber when the pressure is P_0 and the air-fiber system is in thermal and mechanical equilibrium. Then let θ and θ_{f} be the temperature rises (or excess temperatures) of the air and the fiber, so that

$$T = T_0 + \theta \tag{7.55}$$

and

$$T_{\mathrm{f}} = T_0 + \theta_{\mathrm{f}}. \tag{7.56}$$

Then we may write $\dot{\theta}$ for $\dot{T}$ and $\dot{\theta}_{\mathrm{f}}$ for $\dot{T}_{\mathrm{f}}$, so that the power balance equation becomes

$$-(1-f)\rho p_{\mathrm{t}}\dot{v} = (1-f)\rho C_v\dot{\theta} + f\rho_{\mathrm{f}} C_{\mathrm{f}}\dot{\theta}_{\mathrm{f}}. \tag{7.57}$$

[8]The reader who prefers not to "divide by dt" may rework the derivation from Eq. (7.51) using time derivatives instead of differentials and proceeding directly to a power balance, without using an energy balance as an intermediate step.

As we require a relationship between $\dot{p}$ and $\dot{\rho}$, we must eliminate all references to v, θ and θ_f. To this end, first note that Eqs. (7.44) and (7.46) from Subsection 7.2.1 remain valid. Differentiating Eq. (7.46) w.r.t. time yields

$$\dot{v} = -\dot{\rho}/\rho^2 = -\dot{\rho}_\mathrm{e}/\rho^2. \tag{7.58}$$

Substituting this into Eq. (7.57) gives

$$(1-f)p_\mathrm{t}\dot{\rho}_\mathrm{e}/\rho = (1-f)\rho C_v\dot{\theta} + f\rho_\mathrm{f}C_\mathrm{f}\dot{\theta}_\mathrm{f}. \tag{7.59}$$

and thus eliminates v. Differentiating Eq. (7.44) w.r.t. time gives

$$\dot{\theta} = \dot{T} = \frac{\rho\dot{p}_\mathrm{t} - p_\mathrm{t}\dot{\rho}}{\rho^2 R} = \frac{\rho\dot{p} - p_\mathrm{t}\dot{\rho}_\mathrm{e}}{\rho^2 R} \tag{7.60}$$

which can be used to eliminate θ. Then, to eliminate θ_f, we need an equation describing the heat conduction between the air and the fiber. Of course the conduction of heat requires a temperature gradient *within* both the air and the glass, so the temperature variables mentioned so far $(T, T_\mathrm{f}, \theta, \theta_\mathrm{f})$ must be understood as spatial averages. If we assume, as a linear approximation, that the rate of heat transfer is proportional to the difference between the average temperatures of the air and the fiber, we may write

$$\dot{\theta}_\mathrm{f} = \frac{\theta - \theta_\mathrm{f}}{\tau_\mathrm{a}} \tag{7.61}$$

where τ_a is a constant with the dimensions of time.[9]

The physical meaning of τ_a may be found by assuming that θ in the above equation is constant. Then we have a simple differential equation in θ_f whose solutions have the form

$$\theta_\mathrm{f} = \theta + Ae^{-t/\tau_\mathrm{a}} \tag{7.62}$$

where A is a constant. Thus τ_a is the thermal time constant between the air and the fiber *when the average air temperature is held constant* by an external energy source; the subscript "a" is for "air". While the definition of τ_a seems clumsy, it is responsible for the simplicity and generality of Eq. (7.61). Because the fiber is incompressible, no work can be done on it, so that no work term complicates the equation. If Eq. (7.61) were written for $\dot{\theta}$ instead of $\dot{\theta}_\mathrm{f}$, it would need to include a work term or assume a specific condition such as constant volume (which involves no work) or constant pressure (for which the specific heat C_p takes work into account). But Eq. (7.61) does not require constant pressure or constant volume or even constant θ; the constant-θ assumption is used only to find a physical interpretation of τ_a.

Now let $p_\mathrm{t} \to P_0$ and $\rho \to \rho_\mathrm{o}$ (for small compressions), and let the phasor representations of θ and θ_f be Θ and Θ_f, respectively. Then the phasor forms of equations (7.59) to (7.61) may be written

$$(1-f)P_0\underline{\rho_\mathrm{e}}/\rho_\mathrm{o} = (1-f)\rho_\mathrm{o}C_v\Theta + f\rho_\mathrm{f}C_\mathrm{f}\Theta_\mathrm{f} \tag{7.63}$$

$$\Theta = \frac{\rho_\mathrm{o}P - P_0\underline{\rho_\mathrm{e}}}{\rho_\mathrm{o}^2 R} \tag{7.64}$$

[9]The justification for modeling the heat exchange in terms of a *single* time constant is given in Chapter 8 (especially Subsection 8.2.6).

$$\Theta_\mathrm{f} = \frac{\Theta}{1 + j\omega\tau_\mathrm{a}} \tag{7.65}$$

(the first two equations have been divided through by $j\omega$ and the third has been solved for Θ_f).

It remains to eliminate Θ and Θ_f between the above three equations, solve for P, write the result in the form of Eq. (7.34) and extract the expression for $\gamma^\star$. But obtaining $\gamma^\star$ in a form amenable to physical interpretation requires some care. First, substituting Eq. (7.65) into Eq. (7.63) gives

$$(1-f)P_0\underline{\rho_\mathrm{e}}/\rho_\mathrm{o} = \left[(1-f)\rho_\mathrm{o}C_v + \frac{f\rho_\mathrm{f}C_\mathrm{f}}{1 + j\omega\tau_\mathrm{a}}\right]\Theta. \tag{7.66}$$

Next, substituting for Θ from Eq. (7.64), multiplying through by $\rho_\mathrm{o}^2 R$, and grouping the terms in $\rho_\mathrm{o}P$ on the left and the terms in $P_0\underline{\rho_\mathrm{e}}$ on the right, we obtain

$$\rho_\mathrm{o}P\left[(1-f)\rho_\mathrm{o}C_v + \frac{f\rho_\mathrm{f}C_\mathrm{f}}{1 + j\omega\tau_\mathrm{a}}\right] = P_0\underline{\rho_\mathrm{e}}\left[(1-f)\rho_\mathrm{o}(C_v + R) + \frac{f\rho_\mathrm{f}C_\mathrm{f}}{1 + j\omega\tau_\mathrm{a}}\right]. \tag{7.67}$$

Finally, writing C_p for $C_v + R$ (Eq. (7.40)) and solving for P gives

$$P = \frac{\gamma^\star P_0}{\rho_\mathrm{o}}\,\underline{\rho_\mathrm{e}} \tag{7.68}$$

(the form of Eq. (7.34)), where

$$\gamma^\star = \frac{(1-f)\rho_\mathrm{o}C_p + f\rho_\mathrm{f}C_\mathrm{f}/(1 + j\omega\tau_\mathrm{a})}{(1-f)\rho_\mathrm{o}C_v + f\rho_\mathrm{f}C_\mathrm{f}/(1 + j\omega\tau_\mathrm{a})}. \tag{7.69}$$

7.2.3 High- and low-frequency limits of $\gamma^\star$

As frequency increases, the term common to the numerator and denominator of Eq. (7.69) approaches zero, so that

$$\lim_{\omega\to\infty}\gamma^\star = \frac{C_p}{C_v} = \gamma. \tag{7.70}$$

Recall that $\gamma^\star$ was defined so that it would reduce to γ, the ratio of specific heats, in the case of adiabatic compression (Subsection 7.2.1). At sufficiently high frequencies the compression may indeed be regarded as adiabatic because there is little time for heat to conduct during one cycle. Thus the high-frequency limit of $\gamma^\star$ agrees with physical requirements.

The low-frequency behavior of $\gamma^\star$ has a more complex physical explanation. At sufficiently low frequencies, $\gamma^\star$ may be approximated by[10]

$$\gamma_\mathrm{o}^\star \triangleq \lim_{\omega\to 0}\gamma^\star = \frac{(1-f)\rho_\mathrm{o}C_p + f\rho_\mathrm{f}C_\mathrm{f}}{(1-f)\rho_\mathrm{o}C_v + f\rho_\mathrm{f}C_\mathrm{f}}. \tag{7.71}$$

To make sense of this expression it is necessary to define a few variants of the term "specific heat". The *heat capacity* of a sample of material is the ratio of the change

[10]Because the system approaches thermal equilibrium as $\omega \to 0$, the definition of $\gamma_\mathrm{o}^\star$ is consistent with the convention that a zero subscript denotes an equilibrium value.

in thermal energy to the change in temperature; it is an "extensive" property, being proportional to the sample size. What has hitherto been called the *specific heat* of the sample is the *mass-specific heat*, i.e. the heat capacity per unit mass; it is an "intensive" property, not being dependent on the sample size. The *volume-specific heat* will be defined for present purposes as the heat capacity per unit *overall* volume; the use of overall volume, rather than the volume occupied by the air or the glass, allows the volume-specific heat of the air-glass mixture to be found by adding the volume-specific heats of its components. Now the average densities (masses per unit overall volume) of the air and the fiber are $(1-f)\rho_\mathrm{o}$ and $f\rho_\mathrm{f}$, respectively. Hence the volume-specific heats are $(1-f)\rho_\mathrm{o}C_p$ for the air at constant pressure, $(1-f)\rho_\mathrm{o}C_v$ for the air at constant volume, and $f\rho_\mathrm{f}C_\mathrm{f}$ for the fiber (whether the air is at constant pressure or constant volume). So in the low-frequency limit of $\gamma^\star$, the numerator is the total *volume*-specific heat at constant pressure and the denominator is the total *volume*-specific heat at constant volume. This ratio is unchanged if both specific heats are made specific to the mass of air (by dividing by $(1-f)\rho_\mathrm{o}$). So at sufficiently low frequencies, $\gamma^\star$ is a ratio of heat capacities per unit mass of air, in agreement with the original definition of γ (Eq. (7.41)). This is to be expected because if the air and fiber are in thermal equilibrium, they behave as a single reservoir of heat; from the viewpoint of an external observer compressing the air, the heat capacity of the fiber simply adds to that of the air, so that the air itself appears to have increased specific heats. Moreover, because the added heat capacity of the fiber is the same for constant volume and constant pressure, the apparent C_p and C_v of the air still differ by R. So the air still behaves as an ideal gas—and the derivation of Eq. (6.57) from the specific heats (Subsection 7.2.1) remains valid—except that $\gamma_\mathrm{o}^\star$ replaces γ.

Thus in both the high-frequency limit and the low-frequency limit, $\gamma^\star$ is the ratio of the apparent specific heats of the air, satisfying the assumptions made in the derivation of Eq. (6.57). Both limiting values, of course, are real.

From Eq. (7.71) it is easily seen that $1 < \gamma_\mathrm{o}^\star < \gamma$. Thus it is often said that fiber filling reduces the effective γ at low frequencies and increases the compliance (or "apparent volume") of a bass enclosure (see e.g. Chase [14, p. 298]). Eq. (7.71) also indicates that $\gamma_\mathrm{o}^\star \approx 1$ if $f\rho_\mathrm{f}C_\mathrm{f} \gg \rho_\mathrm{o}C_p$, i.e. if the fiber can be approximated as an infinite heatsink. In this case, low-frequency compressions are nearly isothermal. Indeed, when $\gamma = 1$, Eq. (2.37) reduces to Boyle's law, which holds for isothermal compression.

7.2.4 Equation of compression and equivalent circuit

To simplify the derivation of an equivalent circuit from the expression for $\gamma^\star$, let us simplify the expression itself by defining

$$\beta = \frac{f\rho_\mathrm{f}C_\mathrm{f}}{(1-f)\rho_\mathrm{o}C_v}. \tag{7.72}$$

Then dividing the numerator and denominator of Eq. (7.69) by $(1-f)\rho_\mathrm{o}C_v$ gives

$$\gamma^\star = \frac{\gamma + \beta/(1+j\omega\tau_\mathrm{a})}{1 + \beta/(1+j\omega\tau_\mathrm{a})} \tag{7.73}$$

and taking low-frequency limits gives

$$\gamma_{\mathrm{o}}^{\star} = \frac{\gamma + \beta}{1 + \beta}. \tag{7.74}$$

This form of $\gamma_{\mathrm{o}}^{\star}$ can still be understood as a ratio of specific heats. In Eq. (7.72), the numerator is the volume-specific heat of the fiber and the denominator is the volume-specific heat of the air at constant volume. Thus β is the *normalized* volume-specific heat of the fiber, when the volume-specific heat of the air at constant volume is assigned a value of unity. Similarly, γ is the normalized volume-specific heat of the air at constant pressure. So in Eq. (7.74), the numerator is the total normalized volume-specific heat at constant pressure and the denominator is the total normalized volume-specific heat at constant volume.

From Eq. (6.61), note that the compliance element $\Delta C_{i,j,k}$ is proportional to $1/\gamma$, so that the associated acoustic admittance is proportional to $j\omega/\gamma$. This suggests that we should find an expression for $j\omega/\gamma^{\star}$ involving the harmonic sum operator "$\|$", which in this case will apply to admittances in series rather than impedances in parallel. Taking reciprocals of both sides of Eq. (7.73) and multiplying by $j\omega$, then multiplying the numerator and denominator by the factor $(1 + j\omega\tau_{\mathrm{a}})$, we obtain

$$\frac{j\omega}{\gamma^{\star}} = j\omega\,\frac{1 + j\omega\tau_{\mathrm{a}} + \beta}{\gamma(1 + j\omega\tau_{\mathrm{a}}) + \beta}. \tag{7.75}$$

Expressing the right-hand side in series-parallel form is straightforward if we notice that the third term of the numerator may be partitioned into two terms so that the first three terms of the new numerator are together a multiple of the denominator:

$$\begin{aligned}
\frac{j\omega}{\gamma^{\star}} &= j\omega\,\frac{1 + j\omega\tau_{\mathrm{a}} + \frac{\beta}{\gamma} + \frac{\gamma-1}{\gamma}\,\beta}{\gamma(1 + j\omega\tau_{\mathrm{a}}) + \beta} \\
&= j\omega\left[\frac{1}{\gamma} + \frac{\gamma - 1}{\gamma}\,\frac{\beta}{\gamma(1 + j\omega\tau_{\mathrm{a}}) + \beta}\right] \\
&= \frac{j\omega}{\gamma} + \frac{\beta(\gamma - 1)}{\gamma}\,\frac{j\omega}{\gamma + \beta + j\omega\tau_{\mathrm{a}}\gamma}.
\end{aligned} \tag{7.76}$$

Now we can multiply and divide the right-hand term by $(\gamma + \beta)\tau_{\mathrm{a}}\gamma$, obtaining a harmonic sum for the second factor, and apply the distributive law:

$$\begin{aligned}
\frac{j\omega}{\gamma^{\star}} &= \frac{j\omega}{\gamma} + \frac{\beta(\gamma - 1)}{\gamma(\gamma + \beta)\tau_{\mathrm{a}}\gamma}\,\frac{(\gamma + \beta)\,j\omega\tau_{\mathrm{a}}\gamma}{(\gamma + \beta) + j\omega\tau_{\mathrm{a}}\gamma} \\
&= \frac{j\omega}{\gamma} + \frac{\beta(\gamma - 1)}{\gamma^2\tau_{\mathrm{a}}(\gamma + \beta)}\,[(\gamma + \beta) \,\|\, j\omega\tau_{\mathrm{a}}\gamma] \\
&= \frac{j\omega}{\gamma} + \frac{\beta(\gamma - 1)}{\gamma^2\tau_{\mathrm{a}}} \,\Big\|\, \frac{j\omega\beta(\gamma - 1)}{\gamma(\gamma + \beta)}\,.
\end{aligned} \tag{7.77}$$

Derivation of an equivalent circuit requires a finite-difference approximation to the equation of compression in a fiber-filled region. Whereas the definition of $\rho^{\star}$ is the phasor form of the equation of motion (Eq. (7.1)), the present definition of $\gamma^{\star}$ (Eq. (7.34)) is not a form of the equation of compression (Eq. (6.58)). The phasor form of the equation of compression in a fiber-filled region must be derived from

the equation of continuity in its most general integral form. In other words we must return to first principles—and again acknowledge and justify the linearizing approximations. But the task can be expedited by exploiting previous results.

Consider a control volume $\mathcal{V}$ enclosed by a stationary surface σ with outward unit normal vector $\mathbf{n}$. Conservation of air requires that the time rate of change of mass inside $\mathcal{V}$ be minus the total mass flux outward through σ. For the purpose of calculating the mass of air in $\mathcal{V}$ and the mass flux of air out of $\mathcal{V}$ in the presence of fiber filling, the effective density of air is $(1-f)\rho$. Alternatively, we may consider the effective volume of $\mathcal{V}$ and surface area of σ to be modified by the factor $(1-f)$, and take the effective density as ρ. In either case, the equation of continuity is

$$\frac{d}{dt}\iiint_{\mathcal{V}}(1-f)\rho\,d\mathcal{V} = -\oiint_{\sigma}(1-f)\rho\mathbf{q}\,.\,\mathbf{n}\,d\sigma. \tag{7.78}$$

When both the air and the fiber are in motion, the fractional variations in f may be of similar magnitude to those in ρ. Variations in ρ are are not negligible in the equation of continuity, because ρ is the only time-varying quantity under the volume integral in the free-air form of the equation (Eq. (2.27)). But because f is small, the fractional variations in $(1-f)$ are small compared with those in f and hence in ρ. Fractional variations in $\mathbf{q}$ are of course much larger again. Hence, in Eq. (7.78), it is reasonable to treat $(1-f)$ as a constant and take it outside the integral and differential operators, where it cancels. Thus Eq. (7.78) reduces to Eq. (2.27), the equation of continuity in the absence of fiber.

As the familiar equation of continuity still holds (to an acceptable approximation), so too do Eqs. (2.30) and (6.54) which are derived therefrom. Multiplying both sides of Eq. (6.54) by $\gamma^\star P_0/\rho_\mathrm{o}$ and using Eq. (7.34) to rewrite the left-hand side in terms of P, we obtain

$$j\omega P = -\gamma^\star P_0 \operatorname{div}\mathbf{Q}. \tag{7.79}$$

This result is the phasor form of the equation of compression, identical to Eq. (6.58) except that $\gamma^\star$ replaces γ. Thus $\gamma^\star$ can be defined by a modified equation of compression just as $\rho^\star$ is defined by a modified equation of motion.

Eq. (7.79) is the starting point for the finite-difference approximation. Hence the equivalent circuit derivation will be almost identical to the argument from Eq. (6.58) to Eq. (6.66), and need not be repeated in full. The presence of fiber means that the volume element $\Delta V_{i,j,k}$ will contain an extra factor $(1-f)$. The same factor will appear in the complex admittance element $\Delta Y_{i,j,k}$, which corresponds to $j\omega\Delta C_{i,j,k}$ in Eq. (6.66). Hence, in deriving Eq. (6.63), we will multiply the numerator and denominator of Eq. (6.59) by $(1-f)\Delta u\Delta v\Delta w$. The factor $(1-f)$ will appear on the right of Eq. (6.63), but will be included in ΔY on the left. Now because the effective areas of the faces of the volume element are modified by the factor $(1-f)$, this factor must be included in the definitions of the fluxes $\Delta U_u|_{i+\frac{1}{2},j,k}$, etc. So the extra $(1-f)$ on the right of Eq. (6.63) is absorbed into the flux terms, leaving Eq. (6.66) *unchanged*, although the terms in it have been redefined. The new estimated fluxes are

$$\Delta U_u|_{i+\frac{1}{2},j,k} = \left[(1-f)\,h_v\Delta v\,h_w\Delta w\,Q_u\right]_{i+\frac{1}{2},j,k} \tag{7.80}$$

$$\Delta U_u|_{i-\frac{1}{2},j,k} = \left[(1-f)\,h_v\Delta v\,h_w\Delta w\,Q_u\right]_{i-\frac{1}{2},j,k} \tag{7.81}$$

and similarly for the ΔU_v and ΔU_w terms. The new estimated volume element is

$$\Delta V_{i,j,k} = \left[(1-f)\,h_u\Delta u\,h_v\Delta v\,h_w\Delta w\right]_{i,j,k} \tag{7.82}$$

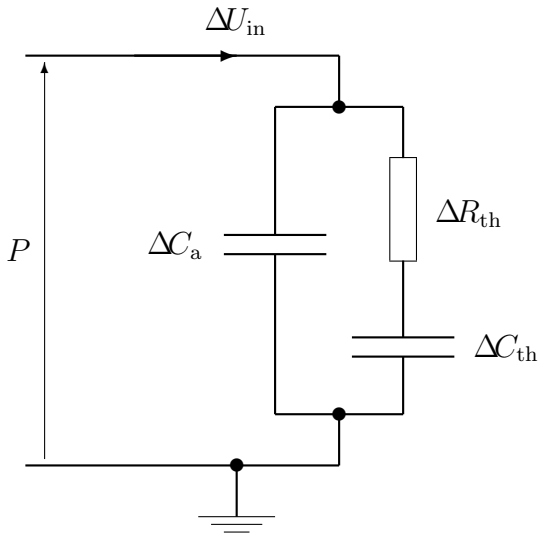

Figure 7.2: *FDEC model for 3D equation of compression, with damping.*

and its acoustic admittance (corresponding to $j\omega\Delta C_{i,j,k}$) is

$$\Delta Y_{i,j,k} = j\omega \frac{\Delta V_{i,j,k}}{\gamma^\star P_0}. \tag{7.83}$$

Substituting for $j\omega/\gamma^\star$ from Eq. (7.77), we can write the admittance in the form

$$\Delta Y_{i,j,k} = j\omega\Delta C_{\text{a}}|_{i,j,k} + \frac{1}{\Delta R_{\text{th}}|_{i,j,k}} \Big\| j\omega\Delta C_{\text{th}}|_{i,j,k} \tag{7.84}$$

where

$$\Delta C_{\text{a}}|_{i,j,k} = \frac{\Delta V_{i,j,k}}{\gamma P_0} \tag{7.85}$$

$$\Delta R_{\text{th}}|_{i,j,k} = \frac{\gamma^2\tau_{\text{a}}}{\beta(\gamma-1)} \frac{P_0}{\Delta V_{i,j,k}} \tag{7.86}$$

$$\Delta C_{\text{th}}|_{i,j,k} = \frac{\beta(\gamma-1)}{\gamma(\gamma+\beta)} \frac{\Delta V_{i,j,k}}{P_0} \tag{7.87}$$

and the "$\|$" operator is defined by Eq. (7.19).

According to Eq. (7.84), the acoustic admittance replacing $j\omega\Delta C_{i,j,k}$ in Eq. (6.66) is that of a compliance $\Delta C_{\text{a}}|_{i,j,k}$ in parallel with the series combination of a resistance $\Delta R_{\text{th}}|_{i,j,k}$ and a compliance $\Delta C_{\text{th}}|_{i,j,k}$, as shown in Fig. 7.2; this three-element subcircuit replaces $\Delta C_{i,j,k}$ in Fig. 6.4. $\Delta U_{\text{in}}|_{i,j,k}$ is the right-hand side of Eq. (6.66), i.e. the sum of the fluxes into the six faces of the i,j,k^{th} unit cell. The subscripts i,j,k are omitted from Fig. 7.2 because they do not vary within the scope of the diagram.

The validity of the equivalent circuit can be partially confirmed by examining its high- and low-frequency behavior. In the high-frequency limit, the overall admittance reduces to that of ΔC_{a}, which is the adiabatic compliance of the air in the volume element. This is as expected because compression is nearly adiabatic at high

frequencies. In the low-frequency limit, the overall admittance is that of ΔC_a and ΔC_th in parallel. Adding the two compliances using a common denominator gives

$$\Delta C_\mathrm{a}|_{i,j,k} + \Delta C_\mathrm{th}|_{i,j,k} = \frac{\Delta V_{i,j,k}}{P_0}\,\frac{1+\beta}{\gamma+\beta} = \frac{\Delta V_{i,j,k}}{\gamma_\mathrm{o}^\star P_0} \tag{7.88}$$

where $\gamma_\mathrm{o}^\star$ is the ratio of total specific heats at thermal equilibrium, as given by Eq. (7.74). Thus $\gamma_\mathrm{o}^\star$ replaces γ in the expression for the compliance of each element. And because $\gamma_\mathrm{o}^\star < \gamma$, while ΔV is almost the same as for an undamped region, the presence of fiber filling increases the compliance of each element at low frequencies, as stated in Subsection 7.2.3.

7.2.5 Thermal time constants from the acoustic circuit

The only thermal time constant considered so far is τ_a, which according to Eq. (7.62) is the thermal time constant when the average air temperature is held constant. This defining condition is not realistic. Moreover it cannot be expressed as a boundary condition for the heat equation, so the resulting time constant cannot be determined by the usual methods for solving partial differential equations. In Chapter 8 it will be seen that the easiest time constant to calculate is $\tau_{\mathrm{f}p}$, which applies to constant fiber temperature and constant air *p*ressure. A related constant is $\tau_{\mathrm{f}v}$, which applies to constant fiber temperature and constant air *v*olume. To relate $\tau_{\mathrm{f}p}$ and $\tau_{\mathrm{f}v}$ to τ_a, we must first find expressions in terms of τ_a for τ_p and τ_v, where τ_p and τ_v are the thermal time constants between the air and the fiber, at constant *p*ressure and constant *v*olume respectively, in the absence of external heat flow. (In the definitions of τ_p and τ_v, neither the air temperature nor the fiber temperature is constant, so there is no subscript "a" or "f".)

In this subsection, the acoustic circuit of Fig. 7.2 will be used to express $\tau_{\mathrm{f}p}$, $\tau_{\mathrm{f}v}$, τ_p and τ_v in terms of τ_a. Inverting the first of these results will enable all time constants to be expressed in terms of $\tau_{\mathrm{f}p}$, which in turn can be expressed in terms of the filament diameter and filling factor using a formula to be derived in Chapter 8.

First we find τ_p, which applies to constant pressure.[11] In Fig. 7.2, the excess pressure p appears in (or "across") ΔC_a. If this pressure is constant, no flux flows in ΔC_a, so that all of the external flux ΔU_in flows in ΔR_th and ΔC_th; that is, when the air expands, the volume of air flowing out of the volume element is supplied by "discharging" ΔC_th, so that the pressure in ΔC_th is proportional to minus the excess volume. But at constant pressure, specific volume is proportional to temperature, so that the excess volume is proportional to the excess temperature θ. Therefore the pressure in ΔC_th is proportional to $-\theta$, so that the thermal time constant is just the time constant of ΔR_th and ΔC_th; that is

$$\tau_p = \Delta R_\mathrm{th}\,\Delta C_\mathrm{th}. \tag{7.89}$$

Substituting from Eqs. (7.86) and (7.87) gives

$$\tau_p = \frac{\gamma\tau_\mathrm{a}}{\gamma+\beta}. \tag{7.90}$$

[11] Leach explicitly assumes that the heat exchange takes place at constant pressure [30, p. 588 and Fig. 3(b)], so his time constant "τ_f" is identical with the above "τ_p". His subscript "f" (in Roman type) apparently stands for constant force, which implies constant pressure. Here the subscript "f" (in Roman type) stands for constant fiber temperature, while the unsubscripted "f" (in italic type) is the filling factor.

Next we find τ_v. At constant volume (or constant density), the pressure and temperature of the air are proportional, so that the excess pressure appearing across ΔC_a (in Fig. 7.2) is proportional to the excess air temperature θ. Therefore the thermal time constant is the time constant applicable to the pressure across ΔC_a. Now at constant volume there is no external flux into the admittance element (that is, $\Delta U_\mathrm{in} = 0$), so that the equivalent circuit is isolated and its time constant is simply that of the series C-R-C circuit; that is

$$\tau_v = \Delta R_\mathrm{th}(\Delta C_\mathrm{a} \| \Delta C_\mathrm{th}). \tag{7.91}$$

Substituting from the above formulae for ΔR_th, ΔC_a and ΔC_th, then taking all factors of ΔR_th except $\gamma\tau_\mathrm{a}$ inside the harmonic sum and canceling where possible, we obtain[12]

$$\tau_v = \gamma\tau_\mathrm{a}\left(\frac{1}{\beta(\gamma-1)} \,\middle\|\, \frac{1}{\gamma+\beta}\right) = \frac{\tau_\mathrm{a}}{1+\beta}. \tag{7.92}$$

Now the time constants $\tau_{\mathrm{f}p}$ and $\tau_{\mathrm{f}v}$ are special cases of τ_p and τ_v, respectively, for which the fiber temperature is held constant. One way to achieve this condition is to assume that the fiber is an infinite heatsink, i.e. that β, the normalized volume-specific heat of the fiber, is infinite. But we cannot simply let $\beta \to \infty$ in Eqs. (7.90) and (7.92), because τ_a depends on β—the time taken to cause a given change in the temperature of the fiber depends on its specific heat, and indeed becomes infinite as $\beta \to \infty$. So let us define

$$\Delta C_{\mathrm{th\,f}} = \lim_{\beta\to\infty} \Delta C_\mathrm{th}. \tag{7.93}$$

From Eq. (7.87) the limit is found to be

$$\Delta C_{\mathrm{th\,f}} = \frac{\gamma-1}{\gamma}\,\frac{\Delta V_{i,j,k}}{P_0}. \tag{7.94}$$

Comparing this with Eq. (7.85), we see that $\Delta C_{\mathrm{th\,f}} = (\gamma-1)\,\Delta C_\mathrm{a} \approx 0.4\,\Delta C_\mathrm{a}$. So if the fiber is an infinite heatsink as assumed by Chase [14], and if the frequency is low so that $\Delta C_{\mathrm{th\,f}}$ is effectively in parallel with ΔC_a, and if the filling factor is small so that the reduction in air volume is negligible, then the presence of fiber filling increases the compliance by 40%, as implied by Chase's Figs. 2 and 3.

Using Eqs. (7.89) and (7.91) with $\Delta C_{\mathrm{th\,f}}$ in place of ΔC_th, we obtain

$$\tau_{\mathrm{f}p} = \frac{\gamma\tau_\mathrm{a}}{\beta} \tag{7.95}$$

and

$$\tau_{\mathrm{f}v} = \gamma\tau_\mathrm{a}\left(\frac{1}{\beta(\gamma-1)} \,\middle\|\, \frac{1}{\beta}\right) = \frac{\tau_\mathrm{a}}{\beta}. \tag{7.96}$$

Now, to express all the time constants in terms of $\tau_{\mathrm{f}p}$, we solve Eq. (7.95) for τ_a, obtaining

$$\tau_\mathrm{a} = \frac{\beta\tau_{\mathrm{f}p}}{\gamma}\,, \tag{7.97}$$

[12]The middle expression in Eq. (7.92) is simplified by noting that the harmonic sum of two fractions with the same numerator is the common numerator over the sum of the denominators; this is easily proven from the definition.

and substitute for τ_a in Eqs. (7.96), (7.90) and (7.92). The results are

$$\tau_{\mathrm{f}v} = \frac{\tau_{\mathrm{f}p}}{\gamma} \tag{7.98}$$

$$\tau_p = \frac{\beta\tau_{\mathrm{f}p}}{\gamma+\beta} \tag{7.99}$$

$$\tau_v = \frac{\beta\tau_{\mathrm{f}p}}{\gamma(1+\beta)}. \tag{7.100}$$

(In Eq. (7.99), notice that $\tau_p < \tau_{\mathrm{f}p}$. Leach [30, p. 592] uses $\tau_{\mathrm{f}p}$ (which he calls τ_1) as an estimate of τ_p (which he calls τ_f) and notes that it is an overestimate, resulting in a conservative estimate of the bandwidth over which the compression can be assumed "isothermal".)

Of the formulae for the component values in Fig. 7.2, the only one containing a time constant is Eq. (7.86); substituting Eq. (7.97) into Eq. (7.86) gives

$$\Delta R_\mathrm{th}|_{i,j,k} = \frac{\gamma\tau_{\mathrm{f}p}}{\gamma-1}\,\frac{P_0}{\Delta V_{i,j,k}} \tag{7.101}$$

which is simpler than the original expression in terms of τ_a.

7.2.6 Thermal time constants from the heat circuit

The relations between the five thermal time constants will now be verified using a conventional heat circuit. Although this exercise does not yield any new results, it confirms the derivation of the four equations (7.97) to (7.100) from the acoustic circuit (Fig. 7.2), providing further evidence that the acoustic circuit is correct.

At constant pressure, the heat capacities per unit overall volume are $(1-f)\rho_\mathrm{o}C_p$ for the air and $f\rho_\mathrm{f}C_\mathrm{f}$ for the fiber. Suppose that, starting from thermal equilibrium, we somehow transfer heat from the fiber to the air. Let q denote the transferred energy per unit overall volume. Then for the air,

$$q = (1-f)\rho_\mathrm{o}C_p\,\theta\,, \tag{7.102}$$

and for the fiber,

$$-q = f\rho_\mathrm{f}C_\mathrm{f}\,\theta_\mathrm{f}\,, \tag{7.103}$$

where the excess temperatures θ and θ_f are spatial averages. So if heat energy per unit volume is represented by charge and excess temperature by voltage, the above two equations show that the volume-specific heats are analogous to capacitances. Now let G_th denote the thermal conductance per unit overall volume between the air and the fiber (assuming that the rate of heat transfer is proportional to the temperature difference and to the air-glass surface area, the latter being proportional to overall volume). Then

$$\dot{q} = G_\mathrm{th}(\theta_\mathrm{f} - \theta) \tag{7.104}$$

so that G_th is analogous to electrical conductance.

Eqs. (7.102) to (7.104) are modeled by the heat circuit shown in Fig. 7.3. Ground potential represents the equilibrium temperature T_0. Nodal temperatures are relative to T_0 and are written "in the nodes". The conductance G_th is shown as a resistance $1/G_\mathrm{th}$.

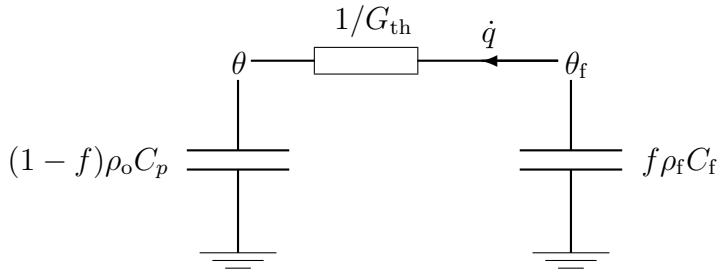

Figure 7.3: *Air-fiber heat circuit at constant pressure.*

From the figure, the constant-pressure thermal time constant between the air and the fiber is

$$\tau_p = \frac{1}{G_{\rm th}}\left[(1-f)\rho_{\rm o}C_p \| f\rho_{\rm f}C_{\rm f}\right]. \tag{7.105}$$

Now $\tau_{{\rm f}p}$ is the value of τ_p when $\theta_{\rm f}$ is constant. To impose constant $\theta_{\rm f}$, we can either "short out" $f\rho_{\rm f}C_{\rm f}$ in Fig. 7.3 or let $C_{\rm f} \to \infty$ in Eq. (7.105). In either case, the result is

$$\tau_{{\rm f}p} = \frac{1}{G_{\rm th}}(1-f)\rho_{\rm o}C_p. \tag{7.106}$$

At constant volume, the heat circuit is the same as Fig. 7.3 except that C_v replaces C_p. Making the same replacement in Eqs. (7.105) and (7.106) gives

$$\tau_v = \frac{1}{G_{\rm th}}\left[(1-f)\rho_{\rm o}C_v \| f\rho_{\rm f}C_{\rm f}\right]. \tag{7.107}$$

$$\tau_{{\rm f}v} = \frac{1}{G_{\rm th}}(1-f)\rho_{\rm o}C_v. \tag{7.108}$$

Recall that $\tau_{\rm a}$ was defined as the thermal time constant at constant air temperature, i.e. at constant θ. So $\tau_{\rm a}$ can be found from the heat circuit by shorting out the heat capacity of the air, or from Eq. (7.105) or Eq. (7.107) by letting C_p or C_v approach infinity. The result is

$$\tau_{\rm a} = \frac{1}{G_{\rm th}} f\rho_{\rm f}C_{\rm f}. \tag{7.109}$$

Checking the ratios between the time constants given by Eqs. (7.105) to (7.109) is straightforward if one remembers that $C_p = \gamma C_v$, that β is defined by Eq. (7.72), and that multiplication and division are distributive over harmonic addition. From Eqs. (7.109) and (7.106),

$$\frac{\tau_{\rm a}}{\tau_{{\rm f}p}} = \frac{f\rho_{\rm f}C_{\rm f}}{(1-f)\rho_{\rm o}C_p} = \frac{f\rho_{\rm f}C_{\rm f}}{\gamma\,(1-f)\rho_{\rm o}C_v} = \frac{\beta}{\gamma} \tag{7.110}$$

which agrees with Eq. (7.97). From Eqs. (7.108) and (7.106),

$$\frac{\tau_{{\rm f}v}}{\tau_{{\rm f}p}} = \frac{C_v}{C_p} = \frac{1}{\gamma} \tag{7.111}$$

which agrees with Eq. (7.98). From Eqs. (7.105) and (7.106),

$$\frac{\tau_p}{\tau_{{\rm f}p}} = 1 \left\| \frac{f\rho_{\rm f}C_{\rm f}}{(1-f)\rho_{\rm o}C_p} \right. = 1 \left\| \frac{f\rho_{\rm f}C_{\rm f}}{\gamma\,(1-f)\rho_{\rm o}C_v} \right. = 1 \left\| \frac{\beta}{\gamma} \right. = \frac{1}{\gamma}(\gamma \| \beta) = \frac{\beta}{\gamma+\beta} \tag{7.112}$$

which agrees with Eq. (7.99). From Eqs. (7.107) and (7.106),

$$\frac{\tau_v}{\tau_{\mathrm{f}p}} = \frac{1}{\gamma}\left\| \frac{f\rho_{\mathrm{f}}C_{\mathrm{f}}}{(1-f)\rho_{\mathrm{o}}C_p} = \frac{1}{\gamma}\right\| \frac{f\rho_{\mathrm{f}}C_{\mathrm{f}}}{\gamma\,(1-f)\rho_{\mathrm{o}}C_v} = \frac{1}{\gamma}\left\| \frac{\beta}{\gamma} = \frac{1}{\gamma}\,(1\|\beta) = \frac{\beta}{\gamma(1+\beta)}\right. \tag{7.113}$$

which agrees with Eq. (7.100).

7.2.7 Acoustic circuit from thermal time constants?

The reader has probably found that Subsection 7.2.6 is easier to understand than Subsection 7.2.5, i.e. that the relations between the thermal time constants are easier to derive from the heat circuit than from the acoustic circuit. Moreover, the derivation from the acoustic circuit depends on the the component values, whose determination has taken most of Section 7.2. But in Subsection 7.2.5, the argument showing that τ_p and τ_v can be read from the acoustic circuit (Fig. 7.2) depends only on the *form* of the circuit, and not on the component values.

The form of the acoustic circuit is readily established from the following intuitive argument. At high frequencies the circuit must reduce to the adiabatic compliance ΔC_{a} (whose value, as is well known, is given by Eq. (7.85)). If the air is subject to a step-reduction in volume, the initial compression is adiabatic; but then the heat of compression is conducted from the air to the fiber, causing the pressure to decrease and approach a limit as the system approaches thermal equilibrium. Thus the compliance increases as frequency decreases, approaching a limit as frequency approaches DC. Therefore the form of the acoustic circuit must be such that an additional compliance appears in parallel with ΔC_{a} at low frequencies; this *thermal relaxation compliance* may be given the symbol ΔC_{th}. Now the obvious way to make ΔC_{th} operative only at low frequencies is to put a resistance in series with it. If this *thermal relaxation resistance* is given the symbol ΔR_{th}, we have the complete form of Fig. 7.2 (together with the value of ΔC_{a}).

From the form of the acoustic circuit, we know that the time constant of ΔR_{th} and ΔC_{th} is τ_p. So, expressing τ_p in terms of $\tau_{\mathrm{f}p}$ using Eq. (7.99) (which can also be derived from the heat circuit), we have

$$\Delta R_{\mathrm{th}}\,\Delta C_{\mathrm{th}} = \frac{\beta\tau_{\mathrm{f}p}}{\gamma+\beta}. \tag{7.114}$$

Also from the form of the acoustic circuit, we know that the time constant of the complete series *C*-*R*-*C* circuit is τ_v. So, expression τ_v in terms of $\tau_{\mathrm{f}p}$ using Eq. (7.100) (which can also be derived from the heat circuit), we have

$$\Delta R_{\mathrm{th}}(\Delta C_{\mathrm{a}}\|\Delta C_{\mathrm{th}}) = \frac{\beta\tau_{\mathrm{f}p}}{\gamma(1+\beta)}. \tag{7.115}$$

Thus we have two equations in the two unknowns ΔR_{th} and ΔC_{th}. The solutions are

$$\Delta R_{\mathrm{th}} = \frac{\tau_{\mathrm{f}p}}{(\gamma-1)\Delta C_{\mathrm{a}}} \tag{7.116}$$

and

$$\Delta C_{\mathrm{th}} = \frac{(\gamma-1)\beta\Delta C_{\mathrm{a}}}{\gamma+\beta}. \tag{7.117}$$

These results are easily confirmed using Eqs. (7.85), (7.87) and (7.101).

At this point it is convenient to compare the results of the present section with the damped compliance circuit given by Leach [30]. Whereas Eqs. (7.85), (7.116) and (7.117) are derived in the context of the finite-difference method, Leach merely gives an equivalent circuit for a lumped total volume V_B, in which the fibers displace a volume V_f. Although Leach defines a complex density to describe the inertial properties of the fiber-damped air, he does not define a complex gamma or complex bulk modulus to describe the compressibility. While he derives his complex density from the equations of motion for the air and the fiber, he does not derive his damped compliance circuit from the differential equations describing the compression and heat conduction. Instead, he determines the thermal-equilibrium compliance by assuming an adiabatic initial compression followed by an isobaric transfer of heat, then assumes that in response to a step-change in pressure, the "apparent volume" of the box begins at the adiabatic value and exponentially approaches the thermal-equilibrium value. This "step response of the volume" is Laplace-transformed, converted to an impulse response, and finally converted from a volume to an admittance. So Leach's approach is less rigorous than the one used in the present section. Nevertheless, the results obtained above can be reconciled with Leach's work using the following identities or notational conversions:

$$\begin{aligned}
V_\mathrm{B}(1 - V_\mathrm{f}/V_\mathrm{B}) &\rightarrow \Delta V_{i,j,k} \\
\rho_\mathrm{o} c^2 &= \gamma P_0 \\
C_\mathrm{AB1} &\rightarrow \Delta C_\mathrm{a}|_{i,j,k} \\
C_\mathrm{AB2} &\rightarrow \Delta C_\mathrm{th}|_{i,j,k} \\
\frac{V_\mathrm{B}}{V_\mathrm{f}} &\rightarrow \frac{1}{f} \\
R_\mathrm{AB1} &\rightarrow \Delta R_\mathrm{th}|_{i,j,k} \\
\tau_\mathrm{f} &\rightarrow \tau_p = \frac{\beta \tau_{\mathrm{f}p}}{\gamma + \beta}.
\end{aligned}$$

With the above seven substitutions, Leach's Eq. (17) directly yields Eq. (7.85), while his Eq. (18) yields Eq. (7.117) with the aid of Eq. (7.72) and his Eq. (19) yields Eq. (7.116) with the aid of Eq. (7.117). The only inaccuracy in Leach's results (which he acknowledges) is his use of $\tau_{\mathrm{f}p}$ as an estimate of τ_p; this is corrected in the last of the above substitutions, which quotes Eq. (7.99).

7.2.8 Computation of compliance elements

If we wish to calculate ΔC_a, ΔR_th and ΔC_th using Eqs. (7.82), (7.85), (7.116) and (7.117), the quantities which must be known (other than those already discussed in Subsection 7.1.4) are γ, β and $\tau_{\mathrm{f}p}$.

Chapter 9 includes an expression for γ in terms of C_p, which is taken as a constant for air (see Eqs. (9.3) and (9.4)). It is therefore convenient to express β in terms of C_p also; substituting C_p/γ for C_v in Eq. (7.72), we obtain

$$\beta = \frac{\gamma f \rho_\mathrm{f} C_\mathrm{f}}{(1 - f)\rho_\mathrm{o} C_p}. \tag{7.118}$$

All parameters in this formula have been discussed already except C_f, which is a property of the glass. Leach [30, p. 588] gives the value $C_\mathrm{f} = 670\,\mathrm{J\,kg^{-1}\,K^{-1}}$.

The non-trivial part of the problem is to find $\tau_{\mathrm{f}p}$. Ideally we would like to compute the thermal time constant using a simple algebraic formula which is acceptably accurate for all filling factors, filament diameters, temperatures and pressures. Results given in the literature are neither as simple nor as general as desired, and are inconsistent with the present author's findings. Accordingly, the theory behind the calculation of $\tau_{\mathrm{f}p}$ is relegated to Chapter 8. For the moment it suffices to quote the result, which is

$$\tau_{\mathrm{f}p} \approx \frac{\mathsf{d}^2}{8\alpha}\,(m^2 - m^{0.37})\,\ln\left(\tfrac{m+1}{2}\right) \tag{7.119}$$

where d is the filament diameter, α is the thermal diffusivity of air, and $m = f^{-1/2}$; the estimated accuracy of the formula is 2%. Chapter 9 shows how α, like the other properties of air, can be computed from the temperature and pressure (see Eqs. (9.13) and (9.14)).

7.3 Truncated elements at boundary surfaces

In this chapter, as in Chapter 6, the use of discrete subscripts conceals the generality of the equicoordinate surfaces bounding each volume or mass element. In Eqs. (7.28), (7.29), (7.30), (7.85), (7.86), (7.87) and the associated circuit equations, there is nothing to prevent variation of the increments Δu, Δv and Δw and of the associated coordinates, provided that

- In the formula for a component value, scale factors are evaluated at the body-center of the element (mass or compliance);
- In a circuit equation involving a damped inertance, pressure is sampled at the centers of two opposite faces of the element, chosen so that the normals to the two faces are in the direction of the velocity component governed by that element;
- In a circuit equation involving a damped compliance, the areas of the six faces and the fluxes passing through them are calculated using the scale factors and velocities sampled at the centers of the six faces of the element.

In the above list, word "center" refers to the midranges of the variable coordinates—two coordinates for a face-center and three for a body-center. As in Subsection 6.4.3, if we wish to interpret the names of the elements as functions of the subscripts, the name of a truncated element will contain a multiplier (usually $\frac{1}{2}$).

In Chapter 10, which considers the FDEC model of a loudspeaker enclosure partially filled with fiber, a layer of truncated mass elements will appear against the diaphragm and against the walls of the enclosure; the former elements must be included in the model, while the latter can be ignored because they carry no flux. The boundary surface between the filled and unfilled regions will pass through a layer of inertance elements, producing two layers of truncated elements, one damped and the other undamped.

Chapter 8

The thermal time constant $\tau_{\mathrm{f}p}$

In Subsection 7.2.5, the isometric and isobaric thermal time constants between the air and the fiber network are expressed in terms of a basic time constant $\tau_{\mathrm{f}p}$, defined as the thermal time constant for constant fiber temperature and constant pressure. In this definition, the "temperature" of the fiber means the spatial average temperature. For the theoretical purposes of Subsection 7.2.5, nothing is assumed concerning the temperature distributions within the air and the fiber. But the calculation of $\tau_{\mathrm{f}p}$ obviously must take these distributions into account.

First it will be shown that, at least in the case of glass fibers, the temperature within each fiber[1] may be assumed uniform. According to the well-known Fourier law of heat conduction [21, p. *4*-143],

$$\mathbf{q} = -\kappa \nabla T \tag{8.1}$$

where $\mathbf{q}$ is the heat flux density (power per unit area), κ is the thermal conductivity and T is the temperature (absolute, or relative to an arbitrary reference).[2] At the air-glass surface, heat is transferred between the air and the glass by the normal component of $\mathbf{q}$. The parallel components of $\mathbf{q}$ are of lesser interest; moreover, in a loudspeaker box there is no mechanism by which a substantial parallel temperature gradient could be generated. By conservation of energy, the normal component of $\mathbf{q}$ is continuous across the surface. Hence a step-change in κ must be accompanied by a reciprocal step-change in the normal component of ∇T; that is, the ∇T ratio is the reciprocal of the κ ratio. The thermal conductivity of air at room temperature is about $0.026\,\mathrm{W\,m^{-1}\,K^{-1}}$ [27, p. 962]. Common soda-lime glasses have thermal conductivities around $1\,\mathrm{W\,m^{-1}\,K^{-1}}$ [31, pp. *12*-143 to 146]; conductivities of other common glasses are of the same order of magnitude. From the figures cited, the thermal conductivity of the glass is roughly forty times that of the air, so that the temperature gradient on the glass side of the surface is roughly one fortieth of that on the air side. Thus it is reasonable to neglect the spatial variation of temperature within the glass and assume that a "constant" glass temperature is constant *and uniform*.

[1] In this chapter it is convenient to use "fiber" to denote a single filament.

[2] The presence of spatial derivatives in the Fourier law (Eq. (8.1)) and in the heat equation (Eq. (8.22)) indicates that the conducting medium—air in this case—is assumed to be a continuum. Chase [14] reports a typical fiber diameter of $10\,\mu$m. According to the U.S. Standard Atmosphere tables [31, p. *14*-14], the molecular mean free path in air at altitudes up to 4000 m is less than 10^{-7} m, i.e. less than one percent of the typical fiber diameter. Thus the assumption of continuity is reasonable even for the microscopic dimensions of the fibers.

Next we must consider the pattern of heat conduction around each fiber. Suppose the air in some local region is compressed so that the air temperature rises above the fiber temperature and heat begins to flow from the air to the fibers. Over the surface of each fiber, the heat flux is inward. Hence, between any two fibers, there must exist a surface across which the normal component of the heat flux density is zero; heat flows away from this surface on both sides. Let us call this surface the *heatshed* (by analogy with "watershed"). In the presence of many fibers, the heatshed is a honeycomb-like surface which divides the space into a myriad of contiguous tubes, which we will naturally refer to as *heat tubes*. Each tube is threaded by one fiber.

In any heat tube, the maximum heat flux density, hence the maximum temperature gradient, occurs at the surface of the fiber. The temperature gradient is small in the outer regions of the heat tube, reaching zero at the outer surface. Hence the position and shape of the outer surface have little effect on the effective thermal resistance between the fiber and the air in the heat tube. Moreover, the position and shape of the heatshed do not affect the average heat capacity of the air in a heat tube; a shift in the heatshed causes an increase in the heat capacity of one heat tube and a compensating decrease in that of another. Therefore, for the purpose of calculating the thermal time constant, we may approximate the heatshed surrounding each heat tube using a surface of "average shape" containing the correct average volume; it does not greatly matter that individual heat tubes have different shapes or volumes, or even that the heatshed may move with time.

In a sufficiently small region, each fiber may be assumed cylindrical; that is, the curvature of the axis of each fiber may be neglected. Hence it is most convenient to assume that the surrounding heatshed is a cylindrical surface coaxial with the fiber. Let the radii of the fiber and heatshed be a and ma, respectively, where $m > 1$. Then the filling factor is

$$f = \frac{\pi a^2}{\pi (ma)^2} = m^{-2} \tag{8.2}$$

whence

$$m = f^{-1/2}. \tag{8.3}$$

Subsequent analysis will use a cylindrical coordinate system coaxial with the fiber and heatshed. If r is the radial coordinate, the region of interest is $a \leq r \leq ma$.

8.1 Analytical approximation

For the typical case of $a = 5\,\mu$m and $f = 1/400$, Leach [30] calculates a transition frequency ($f_c = 1/2\pi\tau_{fp}$) of 6400 Hz. For the same case, Chase [14] obtains about 3.5 Hz. The present author, using methods to be presented in this chapter, calculates a transition frequency of about 289 Hz. These diverse results require investigation because of their conflicting implications for the analysis and design of loudspeakers. In a typical bass enclosure, Chase's result implies that the compression of the air is almost adiabatic at all audio frequencies; in his conclusion, Chase explicitly states that the fiber network must be compacted if we wish to obtain nearly isothermal compression of the air even at the lowest operating frequencies, and that uncompacted fibers "would have no effect in the audio range." Leach disagrees with Chase and concludes that the air may be assumed to be in thermal equilibrium with the

fibers at all operating frequencies of the bass driver. The present author's result implies that neither the adiabatic assumption nor the equilibrium assumption is valid at all operating frequencies, and that the thermal time constant must be taken into account in any realistic model of the enclosure.

Both Leach and Chase have used separation of variables to solve the heat equation in cylindrical coordinates.[3] The same procedure will eventually be followed here. But first an approximate analytical formula for τ_{fp} will be found by a simpler and less error-prone method. The formula assumes that τ_{fp} is just an "RC" time constant, where R is the thermal resistance between the fiber and the air in the heat tube, and C is the heat capacity of the same air. Further approximations are made in estimating R and C. The resulting formula will obviously be used to check the results of the separation of variables—any gross discrepancy would be evidence of theoretical or computational error. It turns out, however, that the approximate formula can be made accurate enough not only for a "ballpark" estimate, but also for the practical calculation of time constants: by adjusting a single undetermined coefficient in the formula, the time constants calculated from the formula and from the separation of variables can be made to agree to within 2% for all possible filling factors. The more elaborate method, having served its purpose of validating the analytical approximation, can then be put aside.

Consider a segment of heat tube of length l. In cylindrical coordinates, the air occupies the region

$$a \le r \le ma\,;\ 0 \le z \le l \tag{8.4}$$

and the glass occupies the region

$$r \le a\,;\ 0 \le z \le l. \tag{8.5}$$

If thermal resistance is analogous to electrical resistance, then thermal conductivity κ is analogous to electrical conductivity σ, so that the thermal resistance of the cylindrical shell between radius r and radius $r + dr$ is

$$dR = \frac{dr}{\kappa\, 2\pi r\, l}. \tag{8.6}$$

To estimate the total thermal resistance between the fiber and the air, let us consider the heat capacity of the air to be concentrated at the "representative radius"

$$r = \tfrac{m+1}{2}\, a \tag{8.7}$$

i.e. midway between the fiber surface and the heatshed. Then the total thermal resistance is simply

$$R = \int_a^{\frac{m+1}{2}\,a} \frac{dr}{\kappa\, 2\pi r\, l} \;=\; \frac{1}{2\pi l \kappa}\, \ln\left(\tfrac{m+1}{2}\right). \tag{8.8}$$

In this result, the representative radius determines the argument of the "ln" function, which is a weak function for large arguments. So for large m, i.e. for small filling factors, the choice of the representative radius does not greatly affect the accuracy of the result. This is not so, however, if m is close to unity; this case will be considered later.

[3]Both authors cite Luikov [34, p. 148ff] as a procedural guide; the problem considered by Luikov has a zero-excess-temperature condition at both the inner and outer boundaries.

Notice that the expression for R is defined for all $m > 1$. If any step in this derivation were to place unnecessary limits on the range of m, the final approximation for $\tau_{\mathrm{f}p}$ would be expected to behave badly (e.g. become unbounded) as m approached these limits. Hence limits on m would not only restrict the applicability of the formula, but also impair its accuracy over part of the range of applicability. Moreover, unnecessary limits on m would prevent us from exploiting any knowledge of the asymptotic behavior of $\tau_{\mathrm{f}p}$ as m approaches unity or infinity. Therefore care has been taken to ensure that all expressions used in this derivation are defined for all possible values of m.

Concerning the heat capacity of the air in the heat tube, the first question is whether we should use C_v or C_p as the specific heat. It is tempting to say simply that we must use C_p because we want $\tau_{\mathrm{f}p}$, which is defined at constant pressure. But the accurate solution of the heat equation allows different regions of air to be heated or cooled at different rates; therefore, for consistency throughout this chapter, we must seek a condition common to all regions. If we use C_v, we assume that heat is conducted so fast that local regions of air do not have time to expand or contract as they are heated or cooled. This would require the conducted heat to travel faster than sound, which contradicts the well-known fact that acoustic compressions are almost adiabatic (see Subsection 2.2.4). If we use C_p, we assume that heat conduction is so slow that any local variations in pressure with temperature have ample time to dissipate or "equalize"—in other words, that acoustic disturbances propagate much faster than thermal disturbances. This is none other that the familiar "adiabatic compression" assumption. Therefore we can use C_p, but not C_v. Consequently we can use the methods of this chapter to find $\tau_{\mathrm{f}p}$, but not $\tau_{\mathrm{f}v}$. That is why the previous chapter expresses all other time constants in terms of $\tau_{\mathrm{f}p}$.

For constant pressure, the heat capacity of the air is C_p multiplied by the effective mass of air; that is,

$$C = \rho_{\mathrm{o}} C_p A l \tag{8.9}$$

where A is the effective cross-sectional area. We could assume that A is simply the total air area, i.e. the annular area between the fiber and the heatshed. However, to allow for the fact that the temperature variations close to the fiber (modeled as an infinite heatsink) must be less that those further out, it is desirable to exclude an area somewhat greater than that of the cross-section of the fiber. So let us assume

$$A = \pi(ma)^2 - \epsilon\pi a^2 = (m^2 - \epsilon)\,\pi a^2 \tag{8.10}$$

where

$$1 \le \epsilon < m^2. \tag{8.11}$$

Notice that A becomes the total air area if we take $\epsilon = 1$.

Substituting Eq. (8.10) into Eq. (8.9), then multiplying our expressions for R and C, we obtain the time constant

$$\tau_{\mathrm{f}p} = \frac{a^2}{2\alpha}\,(m^2 - \epsilon)\,\ln\left(\tfrac{m+1}{2}\right) \tag{8.12}$$

where α, known as the thermal diffusivity, is defined as [21, p. 4-144]

$$\alpha = \frac{\kappa}{\rho_{\mathrm{o}} C_p}. \tag{8.13}$$

(Note: On pp. *3*-70 and *3*-71 of [21], the thermal diffusivity is defined as $\kappa/(\rho_o C_v)$. But p. *4*-144 of the same reference uses C_p instead of C_v and agrees with Eq. (8.13). The former definition obviously assumes that heating occurs at constant volume, while the latter assumes constant pressure. As explained above, the latter assumption is more appropriate for present purposes.)

The remaining problem is to find ϵ. This is where it is useful to consider the asymptotic behavior for large and small values of m. Because the greatest temperature gradients occur near the fiber, we should exclude only a small fraction of the cross section for large m. Hence we want $\epsilon \ll m^2$ for large m. But if m is close to unity, the temperature gradient will be significant throughout the annular cross-section of the air, so that we need to exclude a substantial fraction of this annular area by making ϵ significantly greater than unity. We can satisfy both the large-m and small-m requirements, as well as the fundamental constraint (8.11), by taking

$$\epsilon = m^\zeta \; ; \; 0 \leq \zeta < 2. \tag{8.14}$$

Substituting this into Eq. (8.12), we obtain

$$\tau_{fp} = \frac{a^2}{2\alpha} \left(m^2 - m^\zeta\right) \ln\left(\tfrac{m+1}{2}\right) \tag{8.15}$$

or, in terms of the fiber diameter d,

$$\tau_{fp} = \frac{\mathsf{d}^2}{8\alpha} \left(m^2 - m^\zeta\right) \ln\left(\tfrac{m+1}{2}\right). \tag{8.16}$$

ζ is as yet unknown, except that $0 \leq \zeta < 2$.

Part of the motivation for Eq. (8.14) was that any value of ζ less than 2 gives an accurate cross section and heat capacity for *large* values of m. We have also noted above that any reasonable representative radius gives an accurate thermal resistance for large m. Hence for large m, Eq. (8.15) is quite accurate for all permissible values of ζ. Therefore we determine ζ by considering *small* values of m.

Because $m > 1$, a "small" value of m is

$$m = 1 + \delta \tag{8.17}$$

where $0 < \delta \ll 1$. Hence we have

$$m^2 \approx 1 + 2\delta \tag{8.18}$$

$$m^\zeta \approx 1 + \zeta\delta \tag{8.19}$$

$$\ln\left(\tfrac{m+1}{2}\right) \approx \delta/2. \tag{8.20}$$

Substituting the small-m approximations into Eq. (8.15) gives

$$\tau_{fp} \approx \frac{a^2}{2\alpha} \, \frac{2-\zeta}{2} \, \delta^2 \tag{8.21}$$

so that $\tau_{fp} \propto \delta^2$ if ζ is constant. Let us check this proportionality. If δ is very small, the air cross-section is a thin annulus whose area is nearly proportional to its width, which in turn is proportional to δ. Hence the heat capacity and thermal resistance of the air are both proportional to δ and their product is proportional to

δ^2. So we can indeed take the index ζ to be a constant, and an appropriate choice of ζ will make Eq. (8.15) agree closely with the full solution of the heat equation for small m. We may then hope that the adjusted analytical formula for $\tau_{\mathrm{f}p}$ makes a smooth transition from large-m to small-m behavior, giving acceptable accuracy for all values of m.

Before the optimal value of ζ is known, we can obtain a rough estimate of $\tau_{\mathrm{f}p}$ (suitable for detecting any gross errors in the subsequent solution of the heat equation) by taking $\epsilon = 1$, i.e. by assuming that the entire cross-section of the air contributes to the heat capacity. By Eq. (8.14), this is equivalent to taking $\zeta = 0$, which satisfies the large-m requirement that $\zeta < 2$. Hence the "rough" estimate will be quite accurate for large m.

N.B.: While Eq. (8.16) may accurately predict the thermal time constant of a *coaxial cylindrical* heat tube for all m, the assumption that the heat tube is coaxial and cylindrical is valid only for sufficiently large m, i.e. for sufficiently small packing factors. With densely-packed fibers we can no longer say that the temperature gradient is small in regions far from the fibers and that such regions make negligible contribution to the overall thermal resistance, because there are no such regions. The purpose of studying small-m behavior was to find a procedure for fixing ζ, in the hope that this would enhance the accuracy of the analytical approximation for more realistic values of m.

8.2 Solving the heat equation

The temperature field in the air is described by the heat equation [21, p. 4-144]

$$\dot{\theta} = \alpha \nabla^2 \theta \tag{8.22}$$

where θ is the "excess temperature" (temperature rise above equilibrium) and α is the thermal diffusivity defined by Eq. (8.13). For our assumed geometry we may use cylindrical coordinates and write $\theta = \theta(r, t)$; by symmetry, θ is independent of the other coordinates ϕ and z. Because the fiber is held at the equilibrium temperature, its excess temperature is zero, giving the boundary condition

$$\theta(a, t) = 0 \tag{8.23}$$

for the inner boundary. The outer boundary is the heatshed; absence of heat flow across the heatshed implies the zero-temperature-gradient boundary condition

$$\frac{\partial \theta}{\partial r}(ma, t) = 0. \tag{8.24}$$

The initial condition is less important because, as we shall see, it determines the coefficients of the modes of the solution and does not affect the time constant of any particular mode. But we shall follow the existing literature by supposing that we have thermal equilibrium for $t < 0$ and that the air is subject to a *step-increase in pressure* at time $t = 0$, causing a uniform step-increase in temperature. If the initial temperature rise is θ_0, we have the initial condition

$$\theta(r, 0) = \theta_0 \quad \text{for} \quad a < r < ma. \tag{8.25}$$

Thus our problem is to solve Eqs. (8.22) to (8.25). The solution will be presented in detail so as to show the points at which the author disagrees with the published solutions by Chase [14] and Leach [30].

8.2.1 Separation of variables

Suppose Eq. (8.22) has a product solution with spatial and temporal factors; that is

$$\theta = S(\mathbf{r})\, T(t) \tag{8.26}$$

where $\mathbf{r}$ is the position vector and t is time. Substituting this solution into Eq. (8.22) and dividing through by ST gives

$$\frac{\dot{T}}{T} = \alpha \frac{\nabla^2 S}{S}. \tag{8.27}$$

This equation is separated; all temporal factors are on the left and all spatial factors on the right, so that both sides are constant. From the left-hand side we see that the separation constant has the dimensions of $(\text{time})^{-1}$; we may therefore let the constant be $-1/\tau$, where τ is a time. Setting both sides of the above equation to this constant gives

$$\dot{T} = -\,T/\tau \tag{8.28}$$

$$\nabla^2 S + \frac{1}{\alpha\tau}\, S = 0. \tag{8.29}$$

Eq. (8.28) has the solution

$$T = A\, e^{-t/\tau} \tag{8.30}$$

where A is a constant. This shows that τ is a time constant in the classical sense, and that τ must be positive if the solution is to be stable. Eq. (8.29) is the ubiquitous Helmholtz equation, with a coefficient depending on the time constant. Thus the product solution must take the form of a solution to the Helmholtz equation with an exponential decay.

In reaching this conclusion we have assumed a spatially-dependent factor but have not assumed a specific coordinate system or exploited the symmetry. For the assumed geometry of the heatshed we may take cylindrical coordinates and write

$$S(\mathbf{r}) = S(r) \tag{8.31}$$

so that the product solution (8.26) becomes

$$\theta = S(r)\, T(t) \tag{8.32}$$

and the Laplacian simplifies to

$$\nabla^2 S = \frac{1}{r}\frac{d}{dr}\left(r\,\frac{dS}{dr}\right) = S''(r) + \frac{1}{r}\, S'(r). \tag{8.33}$$

Substituting Eq. (8.33) into Eq. (8.29) gives the spatial equation

$$S'' + \frac{1}{r}\, S' + \frac{1}{\alpha\tau}\, S = 0 \tag{8.34}$$

and substituting Eq. (8.32) into Eqs. (8.23) and (8.24) gives the boundary conditions

$$S(a) = 0 \tag{8.35}$$

$$S'(ma) = 0. \tag{8.36}$$

Eqs. (8.34) to (8.36) can be normalized by making the substitution

$$S(r) = y(x) \tag{8.37}$$

where

$$x = r/a. \tag{8.38}$$

Differentiating Eq. (8.37) twice using the chain rule gives

$$S'(r) = \frac{1}{a}\, y'(x) \tag{8.39}$$

and

$$S''(r) = \frac{1}{a^2}\, y''(x). \tag{8.40}$$

Substituting the above four equations into the radial equation (8.34) and defining the positive real number μ such that

$$\mu^2 = \frac{a^2}{\tau\alpha}\,, \tag{8.41}$$

we obtain

$$y'' + \frac{1}{x}\, y' + \mu^2 y = 0 \tag{8.42}$$

which may be written in the alternative form

$$(xy')' + \mu^2 xy = 0. \tag{8.43}$$

Substituting Eqs. (8.37) to (8.39) into the boundary conditions (8.35) and (8.36) gives

$$y(1) = 0 \tag{8.44}$$

$$y'(m) = 0. \tag{8.45}$$

For a given m, Eqs. (8.43) to (8.45) constitute a regular Sturm-Liouville problem [39, p. 334]. The problem has the trivial solution $y(x) = 0$. It also has non-trivial solutions for an infinite number of discrete values of μ; these are the eigenvalues. Let the n^{th} eigenvalue (in ascending order) be μ_n and let the corresponding solution, called "the eigenfunction belonging to μ_n", be $y_n(x)$. Each eigenfunction is determined up to an arbitrary scale factor. By the Sturm-Liouville theorem, the eigenfunctions are orthogonal w.r.t. the weight function x on the interval $[1, m]$. (See Kreyszig [26], pp. 218–22, 225–8.)

For the moment, let us put aside the problem of finding the eigenvalues and eigenfunctions and consider how they will be used. From Eq. (8.41),

$$\tau = \frac{a^2}{\mu^2\,\alpha}. \tag{8.46}$$

So each eigenvalue μ_n corresponds to a time constant τ_n. Substituting Eqs. (8.30), (8.37) and (8.38) into Eq. (8.32) and using a subscript n for every quantity depending on the eigenvalue μ_n, we obtain

$$\theta_n = A_n\, y_n(r/a)\, e^{-t/\tau_n} \tag{8.47}$$

where

$$\tau_n = \frac{a^2}{{\mu_n}^2\,\alpha}. \tag{8.48}$$

This is a product solution to the heat equation (8.22) satisfying the boundary conditions (8.23) and (8.24). Because the heat equation is linear and the boundary conditions are homogeneous, the equation and boundary conditions are also satisfied by any linear combination of solutions of the form (8.47). So a general solution of Eqs. (8.22) to (8.24) is

$$\theta = \sum_{n=1}^{\infty} A_n\, y_n(r/a)\, e^{-t/\tau_n}. \tag{8.49}$$

Putting $t = 0$, applying the initial condition (8.25) and using Eq. (8.38), we obtain

$$\sum_{n=1}^{\infty} A_n\, y_n(x) = \theta_0 \quad \text{for} \quad 1 < x < m. \tag{8.50}$$

The coefficients A_n may now be found in the usual manner by exploiting the orthogonality of the eigenfunctions [26, pp. 218–22]. Provided that the eigenfunctions form a complete set [26, pp. 222–4], Eq. (8.49) will then be the exact solution of Eqs. (8.22) to (8.25).

The coefficients will not be investigated further; for present purposes it is more important to note that every term or "mode" in the solution (8.49) has its own time constant which, according to Eq. (8.48), is proportional to the inverse square of the eigenvalue. The longest time constant is τ_1, corresponding to the smallest eigenvalue μ_1, and is given by

$$\tau_1 = \frac{a^2}{{\mu_1}^2\,\alpha}. \tag{8.51}$$

Hence the mode associated with τ_1 (the *fundamental mode*) has the slowest decay and will become dominant as t increases, i.e. *as equilibrium is approached*.

Although we have considered the solution to the heat equation in the case of a *step compression* (see before Eq. (8.25)), this observation concerning near-equilibrium conditions leads to a justification for considering only the fundamental mode when analyzing *sinusoidal* compressions of any frequency. By the principle of causality, the rate of heat transfer at any instant is not affected by subsequent events; in particular, it is not affected by subsequent variations in applied pressure and is the same as it would be if the pressure were subsequently held constant, as it is in the case of a step compression. Thus, for any applied pressure function, the pattern of heat flow at any instant can be reproduced by a step compression with the appropriate initial temperature field at that instant. In the complete solution of the heat equation, the initial temperature field is invoked only in the final step; thus the initial conditions affect the coefficients of the modes but do not affect the eigenfunctions or time constants. Therefore as far as the instantaneous heat flux is concerned, the eigenfunctions and time constants that apply when the air is subject to a step-compression also apply in other cases, including the case of sinusoidal compression. At low frequencies, for which the temperature field has ample time to "equalize" during a single cycle of compression, the departure from thermal equilibrium is small, so that the fundamental mode is dominant. At higher frequencies the higher-order modes become significant; this affects the rate at which the system

approaches adiabatic behavior as frequency increases, but does not alter the fact that the limiting high-frequency behavior is adiabatic. Moreover, it will be seen in Subsection 8.2.6 that the higher-order modes allow only a small fraction of the air volume to exchange heat with the fiber, so that they cannot, by themselves, cause any gross departure from adiabatic behavior. Hence, at all frequencies, only a small error is incurred by assuming that all heat conduction is due to the fundamental mode.

8.2.2 Solution in terms of Bessel functions

The substitution $y(x) = z(\mu x)$ transforms Eq. (8.42) to Bessel's equation of order zero. Hence Eq. (8.42) has the solution

$$y(x) = C\,J_0(\mu x) + D\,Y_0(\mu x) \tag{8.52}$$

where J_0 and Y_0 are the Bessel functions of the first and second kinds, of order zero, and C and D are constants to be determined from the boundary conditions. The boundary condition (8.44) gives

$$\frac{C}{D} = -\frac{Y_0(\mu)}{J_0(\mu)} \tag{8.53}$$

which can be satisfied by taking $C = Y_0(\mu)$ and $D = -J_0(\mu)$, so that the solution (8.52) becomes

$$y(x) = Y_0(\mu)\,J_0(\mu x) - J_0(\mu)\,Y_0(\mu x) \tag{8.54}$$

(the choice of C and D also fixes the scale of $y(x)$). The derivatives of the two Bessel functions are

$$J_0{}'(\xi) = -J_1(\xi) \tag{8.55}$$

and

$$Y_0{}'(\xi) = -Y_1(\xi) \tag{8.56}$$

where ξ is just a dummy argument (these relations may be found by putting $\nu = 0$ in equations 53:10:2 and 54:10:2 in reference [52]). Using these rules we may differentiate Eq. (8.54) and obtain

$$y'(x) = -\mu\,[\,Y_0(\mu)\,J_1(\mu x) - J_0(\mu)\,Y_1(\mu x)\,]\,. \tag{8.57}$$

Hence the second boundary condition (8.45) becomes

$$Y_0(\mu)\,J_1(\mu m) - J_0(\mu)\,Y_1(\mu m) = 0 \tag{8.58}$$

and the values of μ satisfying this relation are the eigenvalues.

8.2.3 Behavior of eigenfunctions; estimates of eigenvalues

Many qualitative properties of the eigenfunctions are more easily deduced from the defining Sturm-Liouville problem (SLP) than from the solutions in terms of Bessel functions. The differences between successive eigenvalues can also be estimated from the SLP. The information gleaned in this way is useful for devising a numerical procedure to find the eigenvalues and for checking the results of that procedure.

The defining SLP comprises Eqs. (8.42), (8.44) and (8.45). Because the eigenfunctions can be arbitrarily scaled, let us normalize them by introducing a fourth equation

$$y'(1) = 1. \tag{8.59}$$

The four equations can then be conveniently regrouped as an initial value problem (IVP)

$$\begin{gathered} y'' + \tfrac{1}{x}\, y' + \mu^2 y = 0 \\ y(1) = 0 \\ y'(1) = 1 \end{gathered} \tag{8.60}$$

with a remote boundary condition

$$y'(m) = 0. \tag{8.61}$$

The IVP expressed by Eqs. (8.60) has a unique solution for each value of μ. The eigenvalues are the values of μ for which the IVP solution satisfies the additional constraint (8.61).

For $\mu = 0$ it is easily shown that the IVP has the exact solution

$$y = \ln x. \tag{8.62}$$

This is the limiting solution of the IVP as $\mu \to 0$. Putting $x = 1$ and combining Eqs. (8.60) gives

$$y''(1) = -1 \tag{8.63}$$

for all μ. Then differentiating the first equation in group (8.60) and inserting all initial values gives

$$y'''(1) = 2 - \mu^2 \tag{8.64}$$

which depends on μ. Therefore all solutions of the IVP, including all eigenfunctions, have second-order contact[4] with the curve $y = \ln x$ at the point $(1, 0)$.

For large x and/or large μ, the "damping coefficient" $1/x$ is small compared with μ^2, so that the first equation in group (8.60) looks like the one-dimensional Helmholtz equation

$$y'' + \mu^2 y = 0 \tag{8.65}$$

whose solutions are sinusoids with wave number μ. In reality the "sinusoids" will be damped somewhat because $1/x$ is positive. So the the eigenfunctions look like damped sinusoids for large x, and oscillate faster as μ increases.

For $\mu = 0$, the IVP solution $y = \ln x$ is monotonic and increasing for all $x \geq 1$ and does not satisfy condition (8.61) for any m. For a small positive μ, as x increases from $x = 1$, the IVP solution will initially look like $y = \ln x$, then oscillate slowly for large x, passing through an infinite sequence of maxima and minima. Because μ is the approximate wave number, all the maxima and minima will move towards the origin as μ increases. For a certain value of μ the first maximum will occur at $x = m$ and satisfy Eq. (8.61); this μ is the first eigenvalue μ_1. For a certain larger value of μ, the first *minimum* will occur at $x = m$; this μ is μ_2. For $\mu = \mu_3$ the second maximum will occur at $x = m$, and so on.

[4]The technical definition of order of contact is given by Struik [55], p. 23. For present purposes it suffices to note that two plane curves have zero-order contact if they intersect but have different slopes at the point of intersection, first-order contact if they are tangential but have different curvatures at the point of tangency, and so on.

Conversely, for any non-zero μ, let the first maximum of the IVP solution occur at $x = s_1$, the first minimum at $x = s_2$, the second maximum at $x = s_3$, and so on, so that s_n is the abscissa of the n^{th} stationary point. Then the same μ is the first eigenvalue for $m = s_1$, the second eigenvalue for $m = s_2$, the third for $m = s_3$, etc. Hence, because all these stationary points move away from the origin as $\mu \to 0$, all eigenvalues approach zero as $m \to \infty$. So the function $y = \ln x$, which is the limiting IVP solution as $\mu \to 0$, is also the limit of all eigenfunctions as $m \to \infty$.

The difference between successive eigenvalues can be estimated by noting that when μ is increased from μ_n to μ_{n+1}, the IVP solution performs an additional half-cycle of oscillation on the interval $[1, m]$. If the solution were sinusoidal with wave number μ, the required increment in μ would be just $\pi/(m-1)$. Now μ can indeed be interpreted as the wave number for large x and/or large μ; hence we can say

$$\mu_{n+1} \approx \mu_n + \frac{\pi}{m-1} \tag{8.66}$$

for reasonably large m or μ. When one eigenvalue is known, this recursive relation yields an initial estimate (suitable for iterative refinement) of the next eigenvalue. Furthermore, because the "wave number" interpretation of μ becomes more accurate as μ increases, we should expect the recursive approximation (8.66) to become more accurate for each successive μ_n. (The error in the wave-number interpretation of μ affects the estimated difference between successive eigenvalues, hence the *absolute* error in the estimate of the next eigenvalue. Thus the absolute error decreases for each successive μ_n. Because the eigenvalues are in an increasing sequence, the percentage error also decreases for each successive μ_n.)

An estimate of the first eigenvalue μ_1 can be found from the analytical approximation to the time constant. Writing τ_1 for $\tau_{\text{f}p}$ in Eq. (8.15) and substituting from Eq. (8.51) gives

$$\mu_1 \approx \left[\tfrac{1}{2}\left(m^2 - m^\zeta\right) \ln\left(\tfrac{m+1}{2}\right)\right]^{-1/2}. \tag{8.67}$$

Because the optimal value of ζ is not yet known, it will be necessary to estimate μ_1 from the "rough" analytical approximation, which is found by setting $\zeta = 0$. Let this first estimate of μ_1 be called μ_a, and let the estimate based on a general value of ζ be called μ_b. Then we have

$$\mu_a = \left[\tfrac{1}{2}\left(m^2 - 1\right) \ln\left(\tfrac{m+1}{2}\right)\right]^{-1/2} \tag{8.68}$$

and

$$\mu_b = \left[\tfrac{1}{2}\left(m^2 - m^\zeta\right) \ln\left(\tfrac{m+1}{2}\right)\right]^{-1/2}. \tag{8.69}$$

Eq. (8.68) will be used to initialize the numerical computation of μ_1, which will then be compared with the result of Eq. (8.69) for trial values of ζ.

8.2.4 Numerical solution of the radial equation

As the introduction to Subsection 8.2.3 suggests, the author prefers to compute the eigenvalues and eigenfunctions directly from the defining SLP rather than from explicit expressions for the solutions; the chosen approach has the advantage of generality and does not require the computation of Bessel functions. To solve the IVP (8.60) for given μ, we may choose a finite step size h and let

$$x_i = 1 + ih \tag{8.70}$$

$$y_i = y(x_i) \tag{8.71}$$

$$y'_i = y'(x_i)\ ,\ \text{etc.} \tag{8.72}$$

Then the initial values are

$$x_0 = 1\ ;\ y_0 = 0\ ;\ y'_0 = 1 \tag{8.73}$$

and we can easily devise a numerical procedure for estimating x_{i+1}, y_{i+1} and y'_{i+1} from x_i, y_i and y'_i. By repeatedly calling this procedure we can construct a function which computes $y'(m)$. Hence one way to find an eigenvalue is to use a root-finder algorithm, e.g. the secant method, to adjust μ until $y'(m)$ is zero (to within some nominated tolerance). Unfortunately this method does not consider the number of maxima and minima on $[1, m]$ and therefore does not guarantee that we will find a *particular* eigenvalue, e.g. μ_1, unless we can be sure that the initial estimates are much closer to the desired eigenvalue than to the adjacent eigenvalue(s). Therefore, instead of computing $y'(m)$, we develop a function called $s(n, \mu)$ which counts the sign reversals of y' and returns the abscissa of the n^{th} stationary point of the IVP solution. Then we use the root-finder algorithm to adjust μ until $s(n, \mu) = m$. The resulting value of μ is the n^{th} eigenvalue μ_n. With this method the initial estimates of the eigenvalue need not be closer to the desired eigenvalue than to the adjacent one(s); we can find μ_{50} as easily as μ_1.

The algorithm for finding the first three eigenvalues is outlined in Table 8.1. The implementation is discussed in detail in Appendix B, which includes the source code for all computer programs used in this thesis. The functions called by the main program are defined by `#include` files so that they can be re-used in other programs. One such file implements the functions Step(μ) and $s(n, \mu)$; a listing of this file, together with further notes on the algorithm and programming, may be found in Section B.1. Another `#include` file, listed in Section B.2, defines the function root(s, n, m). The main program file `efunc.c` is described in Section B.3. It is clear from the listings that Table 8.1 omits many details; for example, the list of parameters passed to the function "root" should also include two estimates of the root and a tolerance.

The graphical output from program `efunc.c` is incorporated in Fig. 8.1. For comparison, the graph also includes the limiting function $y = \ln x$. The assumed value of m is 20, which according to Eq. (8.3) corresponds to the filling factor $f = 0.0025$; this filling factor is cited as typical by Chase [14, p. 299] and Leach [30, p. 592]. The three eigenfunctions are seen to have zero slope at $x = m$, as required. Fig. 8.1 was computed for a step size $h = 0.01$. As a check on accuracy, the computations were repeated for $h = 0.02$. The computed eigenvalues remained the same to five decimal places and most of the computed function values remained the same to three places, with a few changing by one in the third place; these changes are below the resolution of the graph.

The first eigenvalue can now be checked using the "rough" analytical estimate of the time constant. Eq. (8.68) gives $\mu_a = 0.04617$, which is just 0.73% less than the computed value of μ_1 shown in Fig. 8.1. This analytical estimate is independent of, and therefore serves to check, all stages affecting μ_1 in the solution of the heat equation—not only the solution of Eqs. (8.60) and (8.61), but also the derivation of those equations by separation of variables.

Fig. 8.1 is also consistent with the predictions of Subsection 8.2.3. The eigenfunction belonging to the smallest μ is closest (and very close) to the curve $y = \ln x$,

Table 8.1: *Algorithm for finding the first three eigenvalues of the radial Sturm-Liouville problem.*

```
Function Step(μ):
    Perform one step of IVP solution for given μ.
Function s(n, μ): /* abscissa of n^th stationary point */
    Initialize i , x_i , y_i , y'_i;
    For j = 1 to n
        Step(μ) until y'_{i-1} y'_i ≤ 0;
    Find zero of y' by third-order Newton method;
    Return zero of y'.
Function root(s, n, m):
    Using secant method, find μ such that s(n, μ) = m;
    Return μ.
Main program:
    For n = 1 to 3
        μ_n = root(s, n, m).
```

suggesting that the latter curve is the limiting solution as $\mu \to 0$. The four curves become indistinguishable as they approach the point $(1, 0)$, at which they have second-order contact according to Eqs. (8.63) and (8.64). The eigenfunctions are seen to become more oscillatory as μ increases, with each successive eigenfunction having an additional half-cycle on $[1, m]$. If we use Eq. (8.66) to estimate μ_2 and μ_3 from the computed values of μ_1 and μ_2, respectively, the results are $\mu_2 \approx 0.21186$ and $\mu_3 \approx 0.39710$; these values differ from the final computed values by -8.6% and -1.1% (absolute errors -0.0199 and -0.0045) respectively. Notice that the recursive approximation is more accurate for the larger μ, as expected. These observations together with the analytical estimate of μ_1 suggest that the computed solution of Eqs. (8.60) and (8.61) is free from any gross errors such as might be caused by faulty methods or programming bugs.

8.2.5 Results of Chase (1974) and Leach (1989)

After much analysis and computation it is now possible to explain why the results of Chase [14] and Leach [30] differ from those of the present author and from each other.

Both authors have used a solution based on separation of variables and the transformation of the radial equation to Bessel's equation. Both authors give a complete series solution in the form of Eq. (8.49), except that they give explicit expressions for the coefficients A_n and use the notation $V_0(\mu_n x)$ instead of $y_n(x)$; their expressions for V_0 (Eq. (5) in Chase and Eq. (34) in Leach) agree with Eq. (8.54) above (apart from an obvious typographical error in Chase). Their definitions of the eigenvalues (Eq. (6) in Chase and Eq. (35) in Leach) also agree with the above Eq. (8.58).

The most obvious discrepancy, which can be found without computing any eigenvalues, is in Chase's equation (7), which corresponds to the above Eq. (8.51). In place of the inner radius a (which he calls R_1), Chase writes the outer radius ma (which he calls $R_2 = mR_1$). This multiplies the calculated time constant by the factor m^2

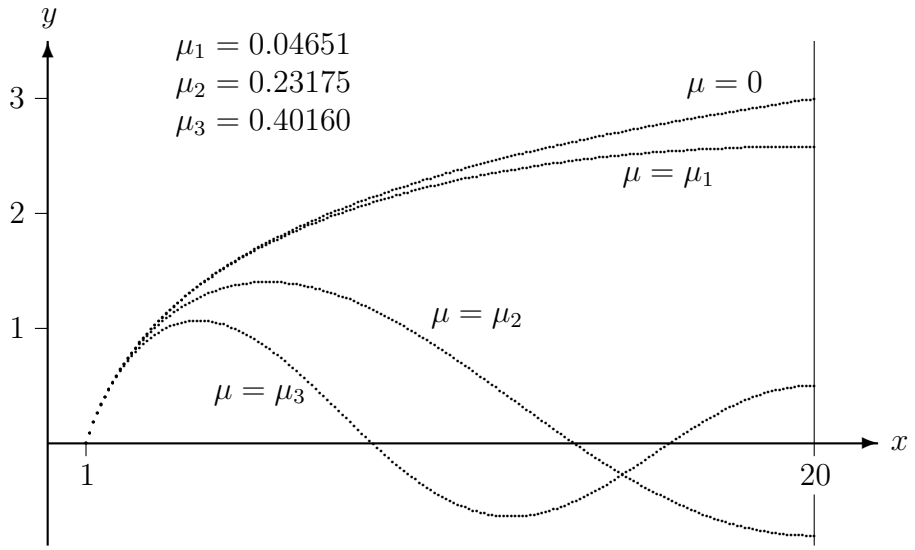

Figure 8.1: *Radial eigenfunctions for $m = 20$, and limiting function.*

($m = 20$ for the "uncompressed" fiber network considered by Chase). Leach's equation (36) corrects Chase's equation (7) and agrees with Eq. (8.51). (N.B.: Both Chase and Leach use a instead of α for the thermal diffusivity.)

For $m = 20$ (the only numerical example that he considers), Leach gives the eigenvalue $\mu_1 = 0.232$, which matches μ_2 in Fig. 8.1 to three decimal places. Thus Leach has found μ_2 instead of μ_1, giving the time constant τ_2 instead of τ_1. Because $\mu_2 \approx 5\mu_1$ (from Fig. 8.1) and because $\tau_n \propto {\mu_n}^{-2}$ (from Eq. (8.48)), τ_2 is about one twenty-fifth of τ_1.

That the dominant time constant must be found from μ_1 (in the notation of Fig. 8.1), and not from one of the other eigenvalues, can be verified by three arguments. The first is merely a review of the solution procedure: by Eq. (8.48), the longest time constant is the one corresponding to the smallest eigenvalue, and μ_1 has been found to be the smallest eigenvalue admitted by the boundary conditions. The second argument appeals to the physical significance of the eigenfunctions: they are the radius-dependent factors in the modes of the excess temperature distribution. A maximum or minimum of an eigenfunction is a *modal heatshed*; for each mode, only the air inside the innermost modal heatshed can exchange heat with the fiber.[5] From Fig. 8.1 we see that the eigenfunction y_1 (belonging to μ_1) is monotonic on the interval $[1, m]$, so that all of the air can exchange heat with the fiber. The eigenfunction for each successive mode has its first maximum at a smaller radius and therefore allows a smaller volume of air to exchange heat with the fiber. A smaller volume of air obviously takes less time to heat or cool, giving a smaller time constant. The third and most convincing argument comes from the analytical approximation; as noted above, this estimates μ_1 with an error of -0.73%.

To see whether the above observations account for the numerical results of Leach and Chase, we first note that both authors use $a = 5\,\mu\text{m}$ and $\alpha = 1.87 \times 10^{-5}\,\text{m}^2\,\text{s}^{-1}$.

[5] If a "heatshed" is a surface across which there is no heat flux, the flow of heat on both sides of the "heatshed" can be away from it (as for a maximum in θ_n) or towards it (as for a minimum in θ_n). This is a slight loosening of the analogy between "heatshed" and "watershed".

Substituting these values into Eq. (8.51) and taking the value of μ_1 from Fig. 8.1, we obtain $\tau_1 = 618\,\mu$s. If we use Leach's value of μ_1 instead, we obtain $\tau_1 = 24.8\,\mu$s; this is about one twenty-fifth of the value obtained from Fig. 8.1 (as expected) and gives a transition frequency of 6.4 kHz, which is the value quoted by Leach. Thus Leach's result is explained.

Chase's case is more complex. Recall that Chase's equation (7) contains an anomalous factor m^2; in the notation of this thesis, it reads

$$\tau_1 = \frac{m^2 a^2}{{\mu_1}^2 \alpha}. \tag{8.74}$$

If we put $m = 20$ and take μ_1 from Fig. 8.1, this equation gives $\tau_1 = 247\,$ms, which of course is 400 times the value obtained from Eq. (8.51). But Chase's Fig. 1 gives $\tau_1 \approx 45.5\,$ms for the "natural density" of the fiber network (for which $m = 20$), so that the discrepancy between Chase and the present author is smaller than expected and further investigation is required.

Chase, unlike Leach, does not report any value of μ_1, but he does provide values for all other quantities in Eq. (8.74), from we me may deduce that he has used the value $\mu_1 = 0.1085$ for the natural density. This is not one of the higher-order eigenvalues in Fig. 8.1, so we must seek another explanation. One possibility is that Chase has found μ_1 using a value of m other than 20. We can quickly investigate this by guessing values of m and estimating the corresponding values of μ_1 from Eq. (8.68). For $m = 10$, i.e. for *half the actual value of* m, Eq. (8.68) gives $\mu_1 \approx 0.1089$, which is remarkably close to Chase's value. The next question is whether Chase has evaluated μ_1 from $m/2$ instead of m for *every* packing density. To see how this might have occurred, consider Eq. (8.74). If a is replaced by $2a$ (the diameter) and m is replaced by $m/2$ (calculated from the diameter instead of the radius?), the changes in a and m will cancel in the numerator, but the different m will give a different μ_1 and hence a different τ_1.

To determine whether m has been halved (for whatever reason), we focus on Chase's Fig. 1 [14, p. 299], which is a log-log plot of the average fiber density $\rho_m = f\rho_\mathrm{f}$ vs. the "crossover frequency" $\omega_\mathrm{c} = 1/\tau_1$. From this graph we may read ordered pairs $(\rho_m, \omega_\mathrm{c})$. For each pair, the filling factor is ρ_m/ρ_f; hence, by Eq. (8.3),

$$m = \sqrt{\rho_\mathrm{f}/\rho_m}. \tag{8.75}$$

This is the actual m, not necessarily the one used by Chase to find μ_1. To find the eigenvalue calculated by Chase, his equation (7) is solved for μ_1, which we shall rename μ_Ch, and the result is rewritten in terms of ω_c instead of τ_1. This gives

$$\mu_\mathrm{Ch} = am\sqrt{\omega_\mathrm{c}/\alpha}. \tag{8.76}$$

For checking purposes the values of ρ_f, a and α in the above two equations must agree with those used by Chase; these are $\rho_\mathrm{f} = 2400\,\mathrm{kg\,m^{-3}}$, $a = 5 \times 10^{-6}\,$m and $\alpha = 1.87 \times 10^{-5}\,\mathrm{m^2\,s^{-1}}$. Similarly we must use Chase's equation (7) *as given*, although Leach and the present author disagree with it. To see whether μ_Ch has been calculated from $m/2$, we find μ_1 by a procedure similar to that of Table 8.1 (with $m/2$ in place of m) and call the result $\mu_{m/2}$; this can then be compared with μ_Ch. The algorithm is outlined in Table 8.2 and implemented by the program `chase.c`, listed in Section B.4. The first three functions in Table 8.2 are the same as those in Table 8.1 and are defined by `#include` files.

Table 8.2: *Algorithm for checking the calculations of L. M. Chase (1974).*

Function Step(μ):
    Perform one step of IVP solution for given μ.
Function $s(n, \mu)$:
    Return abscissa of n^{th} stationary point.
Function root(s, n, m):
    Return μ such that $s(n, \mu) = m$.
Function Check(ρ_m, ω_c): /* Check one point on Chase's graph: */
    $m = \sqrt{\rho_f/\rho_m}$;
    $\mu_{Ch} = am\sqrt{\omega_c/\alpha}$;
    $\mu_{m/2} = \text{root}(s, 1, m/2)$.
Main program:
    For each point (ρ_m, ω_c)
        Check(ρ_m, ω_c).

Table 8.3: *Computer output obtained by the method of Table 8.2. The headings on the columns represent ρ_m, ω_c, m, μ_{Ch} and $\mu_{m/2}$. The rightmost two columns should be compared; μ_{Ch} is the eigenvalue used by Chase, while $\mu_{m/2}$ is the eigenvalue obtained by using $m/2$ in place of m.*

```
CHECK ON EIGENVALUES USED BY CHASE

rom    wc     m     much   muhalfm

 6.0    22  20.00  0.1085  0.1103
 7.1    30  18.39  0.1164  0.1230
10.0    67  15.49  0.1466  0.1541
20.0   430  10.95  0.2626  0.2478
30.0  1100   8.94  0.3430  0.3325
49.0  3000   7.00  0.4432  0.4852
70.0  5400   5.86  0.4975  0.6523
```

The output from program `chase.c` (for a step size $h = 0.01$) is shown in Table 8.3. In the plain text printout, ρ_m, ω_c, m, μ_{Ch} and $\mu_{m/2}$ appear as `rom`, `wc`, `m`, `much` and `muhalfm`, respectively. ρ_m and ω_c are in SI units; m, μ_{Ch} and $\mu_{m/2}$ are dimensionless. For values of ρ_m up to at least $30\,\text{kg}\,\text{m}^{-3}$, the agreement between μ_{Ch} and $\mu_{m/2}$ is as close as could be expected, given the limited accuracy with which ρ_m and ω_c can be read from a log-log graph. The divergence between μ_{Ch} and $\mu_{m/2}$ for larger ρ_m may result from Chase's method of calculating μ_1 from m; Chase says nothing of this method except that it is based on Eq. (8.58), in which case it may involve approximations of Bessel functions that are valid for limited ranges of the argument. In the absence of further information, the conclusion that Chase has calculated μ_1 from $m/2$ cannot be regarded as certain, but seems highly likely.

8.2.6 Why higher-order modes are neglected

Before we determine the optimal value of ζ for the computation of τ_1, we should confirm that the higher-order modes allow only a small fraction of the air volume to exchange heat with the fiber (see the end of Subsection 8.2.1), so that any substantial heat flux is due to the fundamental mode.

For each eigenfunction shown in Fig. 8.1, x is proportional to the radius and y is proportional to the excess temperature of the associated mode, so that every maximum or minimum in an eigenfunction represents a modal heatshed. Thus, for the n^{th} mode, only the air inside the radius corresponding to the first maximum of the eigenfunction y_n can exchange heat with the fiber. For $m = 20$, Fig. 8.1 shows that the radius of the first maximum of y_2 is less than 30% of the outer radius of the heat tube, so that less than 9% of the air volume can exchange heat with the fiber in the second mode. In the third and higher modes, the active volume fraction is even smaller.

Thus the higher-order modes are not important for $m = 20$. To see whether this conclusion holds for all realistic values of m, it suffices to compute the fraction of the air volume that lies within the first maximum of y_2 for a range of values of m. Let us call this fraction f_2. In the notation of Table 8.1, the abscissa of the first maximum of y_2 is $s(1, \mu_2)$, so that the required volume fraction (or cross-sectional area fraction) is

$$f_2 = \frac{[s(1, \mu_2)]^2 - 1}{m^2 - 1}. \tag{8.77}$$

Now it is a simple matter to modify the algorithm of Table 8.1 to find f_2 for various m. For convenience we should also compute the filling factor f and tabulate m, μ_2 and f_2 vs. f. The function definitions of Table 8.1 stay the same, and the main routine becomes

Main program:

For each m
  $\mu_2 = \text{root}(s, 2, m)$;
  $f_2 = \dfrac{[s(1, \mu_2)]^2 - 1}{m^2 - 1}$;
  Print f, m, μ_2, f_2.

The modified algorithm is implemented by the program `f2.c`, listed in Section B.5. Again the program has details not shown in the above algorithm; for example, two sequences of values of m are used and the body of the loop "For each m" is relegated to a function. The printout from the program is shown in Table 8.4, in which the plain-text headings obviously represent f, m, μ_2 and f_2.

The correctness of Table 8.4 is supported by three observations. First, the line for $m = 20$ gives the same μ_2 as Fig. 8.1 and confirms that the active volume fraction f_2 is somewhat less than 9%. Second, as $m \to 1$, Table 8.4 shows that μ_2 is approximately proportional to $(m - 1)^{-1}$. To explain this, we first write $(m - 1)$ for δ and τ_1 for $\tau_{\text{f}p}$ in Eq. (8.21), substitute from Eq. (8.51) and solve for μ_1, obtaining

$$\mu_1 \approx \frac{2(2 - \zeta)^{-1/2}}{m - 1}. \tag{8.78}$$

Then we substitute this result into Eq. (8.66), with $n = 1$, to obtain

$$\mu_2 \approx \frac{2(2 - \zeta)^{-1/2} + \pi}{m - 1} \tag{8.79}$$

Table 8.4: *Fraction of air volume involved in heat exchange for second mode (right column) vs. filling factor (left column).*

f(%)	m	mu2	f2(%)
0.004	160.00	0.02648	4.014
0.008	113.14	0.03779	4.406
0.016	80.00	0.05400	4.874
0.031	56.57	0.07732	5.438
0.062	40.00	0.11103	6.125
0.125	28.28	0.16001	6.970
0.250	20.00	0.23175	8.020
0.500	14.14	0.33799	9.329
1.000	10.00	0.49789	10.967
2.000	7.07	0.74444	13.008
4.000	5.00	1.13919	15.525
8.000	3.54	1.81095	18.568
19.237	2.28	3.61958	23.174
37.180	1.64	7.28635	27.094
57.392	1.32	14.63631	29.813
74.316	1.16	29.35160	31.453
85.734	1.08	58.79364	32.360
92.456	1.04	117.68463	32.838
96.117	1.02	235.47188	33.083
98.030	1.01	471.04913	33.207

which agrees with the observed proportionality. Eq. (8.21) is accurate when m is close to unity and Eq. (8.66) is accurate for large μ_n, so both steps in the approximation of μ_2 are valid. Third, as m approaches unity, f_2 seems to approach $\frac{1}{3}$. Indeed, for large μ, the solution to the IVP (8.60) is nearly sinusoidal, so that the first maximum is about one third of the way from $x = 1$ to the first minimum; that is

$$\frac{s(1,\mu_2) - 1}{m - 1} \approx \frac{1}{3}. \tag{8.80}$$

Hence, if m and $s(1,\mu_2)$ are close to unity, Eq. (8.77) yields

$$f_2 = \frac{[s(1,\mu_2) + 1]\,[s(1,\mu_2) - 1]}{[m + 1]\,[m - 1]} \approx \frac{2\,[s(1,\mu_2) - 1]}{2\,[m - 1]} = \frac{s(1,\mu_2) - 1}{m - 1} \approx \frac{1}{3} \tag{8.81}$$

which agrees with the table.

Having verified Table 8.4 against earlier results and approximations, we can now consider its implications. If we compute $\gamma^\star$ by assuming that all heat conduction between the air and the fiber is due to the fundamental mode, then the worst possible error occurs when all heat conduction is due to the higher-order modes. In this case, neglect of the higher-order modes causes the compression to be modeled as an *adiabatic* process, for which $\gamma^\star = \gamma \approx 1.4$ (see Subsection 7.2.3). Now Table 8.4 indicates that for realistic filling factors, only a small fraction of the air volume can

Table 8.5: *Algorithm for checking a trial value of ζ in Eqs. (8.15) and (8.67).*

Function Step(μ):
    Perform one step of IVP solution for given μ.
Function $s(n, \mu)$:
    Return abscissa of n^{th} stationary point.
Function root(s, n, m):
    Return μ such that $s(n, \mu) = m$.
Function PrintRow(m): /* Process one value of m: */
    $f = m^{-2}$;
    $\mu_1 = \text{root}(s, 1, m)$;
    $\mu_a = \left[\frac{1}{2}(m^2 - 1)\ln\left(\frac{m+1}{2}\right)\right]^{-1/2}$;
    $\mu_b = \left[\frac{1}{2}\left(m^2 - m^\zeta\right)\ln\left(\frac{m+1}{2}\right)\right]^{-1/2}$;
    Print f, m, μ_1, and percentage errors in μ_a & μ_b.
Main program:
    For each m
        PrintRow(m).

exchange heat with the fiber in the second mode, and hence also in the third and higher modes. Thus, in the worst case, most of the air volume cannot exchange heat with the fiber, so that the compression is indeed well approximated as an adiabatic process.

The opposite extreme from an adiabatic process is a *quasi-static* process, which is so slow that the departure from thermal equilibrium is negligible; for such a process, $\gamma^\star$ is real and $1 < \gamma^\star < \gamma$ (see Subsection 7.2.3). Even for the air inside the first heatshed of the second mode, the process is not necessarily quasi-static. Nevertheless, to obtain a conservative estimate of the error caused by neglecting higher-order modes, let us assume that the compression inside the modal heatshed is quasi-static, and let us also exaggerate the contrast with the adiabatic case by assuming that $\gamma^\star = 1$ inside the modal heatshed. Under these assumptions, and in the worst case, the overall $\gamma^\star$ will be the volume-weighted average of the values inside and outside the modal heatshed, which is $f_2 + 1.4\,(1 - f_2)$; hence the true $\gamma^\star$ will differ from the calculated value of 1.4 by the fraction $\frac{2}{7}f_2$. This is an exaggeration even in the worst case. Under near-equilibrium conditions, the heat conduction will be dominated by the fundamental mode and the error in $\gamma^\star$ will be much smaller.

8.2.7 Refining the analytical approximation

To maximize confidence in the numerical computations of μ_1, including those used above to check the results of Chase, μ_1 should be compared with μ_a (Eq. (8.68)) for a wide range of values of m. By computing μ_b (Eq. (8.69)) for the same values of m and comparing the results with μ_1 and μ_a, we can then adjust the parameter ζ in Eqs. (8.15) and (8.69). (Recall that μ_a comes from the "rough" analytical estimate of the time constant, for which $\zeta = 0$, and μ_b from the "refined" estimate with a non-zero ζ.) The necessary comparisons and adjustments will be made easier if we tabulate the percentage errors in the two analytical estimates of μ_1, rather than

Table 8.6: *Computer output obtained by the method of Table 8.5 for $\zeta = 0.37$. The two rightmost columns show the errors in the "rough" and "refined" analytical approximations of μ.*

f(%)	m	mu1	steps	errmu	ermua	ermub
0.016	80.00	0.009224	7901	10.20	-0.38	-0.34
0.031	56.57	0.013698	5557	11.29	-0.42	-0.36
0.062	40.00	0.020448	3901	12.57	-0.48	-0.39
0.125	28.28	0.030717	2729	13.95	-0.58	-0.43
0.250	20.00	0.046509	1900	15.70	-0.73	-0.47
0.500	14.14	0.071135	1315	17.81	-0.95	-0.53
1.000	10.00	0.110270	900	20.07	-1.28	-0.60
2.000	7.07	0.174116	608	22.85	-1.76	-0.68
4.000	5.00	0.282361	401	25.12	-2.46	-0.76
8.000	3.54	0.477237	254	23.92	-3.43	-0.83
19.237	2.28	1.034493	201	0.00	-5.14	-0.84
37.180	1.64	2.216110	200	-12.26	-6.83	-0.74
57.392	1.32	4.636943	200	-15.63	-8.12	-0.59
74.316	1.16	9.524470	201	-15.72	-8.96	-0.46
85.734	1.08	19.329821	201	-15.39	-9.44	-0.38
92.456	1.04	38.958271	200	-17.63	-9.70	-0.33
96.117	1.02	78.224464	201	-12.87	-9.83	-0.30

the estimates themselves. For completeness we should also tabulate f, so that the accuracy of each analytical estimate can be seen as a function of the filling factor. The algorithm for checking a single trial value of ζ is outlined in Table 8.5; again, the first three functions are the same as in Table 8.1.

The algorithm is implemented by the program `mu.c`, listed in Section B.6. The output from the program for $\zeta = 0.37$ (the chosen optimal value) is shown in Table 8.6. The program incorporates some refinements which are not shown in Table 8.5, but which augment the printout. First, the effort expended in making μ_b match μ_1 would be futile if the numerical computation of μ_1 were not accurate. Accordingly, μ_1 is computed using two step sizes, the second being half of the first; the difference between the two results, in parts per million, appears in the printout as `errmu`. The worst discrepancy is seen to be about 25 ppm. Second, the number of steps between $x = 1$ and $x = m$ for the smaller step size is tabulated as `steps`. As can be inferred from the printout, the step size is the lesser of 0.01 and $(m - 1)/200$, so as to guarantee both a maximum step size and a minimum number of steps. The tabulated number of steps may be one more than expected because the function $s(n, \mu)$ must overstep the stationary point for each trial value of μ. Third, there are two sequences of values of m. In the first, m is repeatedly divided by $\sqrt{2}$; in the second, $(m - 1)$ is repeatedly halved. In the plain text printout, f, m and μ_1 appear as `f`, `m` and `mu1`, and the errors in μ_a and μ_b appear as `ermua` and `ermub`.

To facilitate adjustment of ζ, Table 8.6 covers a much wider range of filling factors than would be encountered in practice. Chase's Fig. 1 [14, p. 299] indicates that common fiberglass with a natural density of 6 kg m^{-3} has a "practical maximum

compressed density" of $70\,\mathrm{kg\,m^{-3}}$. The natural and maximum densities correspond to filling factors of 0.25% and 2.9%, respectively. According to Bradbury [13, p. 163], the filling factor is at most 5%. But Table 8.6 includes filling factors approaching 100% in the second sequence; the first sequence approaches 0%.

The "`ermua`" column shows that for the whole range of filling factors, the "rough" estimate μ_a differs from μ_1 by no more than 10%. The error is much smaller for large m, confirming the prediction that the "rough" analytical estimate of the time constant is quite accurate for large m. When m is close to unity, the last few lines of Table 8.6 show that μ_1 is approximately proportional to $1/(m-1)$. This agrees with Eq. (8.78). Moreover, because the proportionality factor depends on ζ, the relative errors in μ_a (for which $\zeta = 0$) and μ_b should approach ζ-dependent constants as $m \to 1$, as is confirmed by the last two columns of Table 8.6. These observations give further reassurance that the numerical computations of μ_1 are free from gross errors.

The "`ermub`" column is calculated for $\zeta = 0.37$. For this value of ζ, which was found by trial and error, the "refined" analytical formula underestimates μ_1 by less than 0.9% for all m. By Eq. (8.51), $\tau_1 \propto {\mu_1}^{-2}$, so that the percentage error in the estimate of τ_1 will be -2 times that in the estimate of μ_1. Hence Eq. (8.15) overestimates τ_1 by no more than 1.8%. Now all the analysis in this chapter has neglected the thermal resistance of the glass. Recalling that the thermal resistivity of the air is about forty times that of the glass, and supposing that most of the air-to-glass thermal resistance is caused by the regions close to the air-glass surface, inclusion of the thermal resistance of the glass would increase the air-to-glass resistance, and hence the thermal time constant, by (very roughly) one part in forty, or 2.5%. Hence overestimating τ_1 tends to compensate for the neglect of the thermal resistance of the glass. For this reason the author has chosen to accept the consistent underestimation of μ_1 shown in the rightmost column of Table 8.6.

(It is possible to estimate ζ by more direct methods than trial and error. If we solve Eq. (8.78) for ζ and use the values of m and μ_1 from the bottom line of Table 8.6, we obtain $\zeta \approx 0.366$. Similarly, solving Eq. (8.79) for ζ and substituting from the bottom line of Table 8.4 gives $\zeta \approx 0.375$. The chosen value of 0.37 is a round figure which gives an acceptable error in the desired direction.)

We are now in a position to estimate the ultimate accuracy of Eqs. (8.15) and (8.16). For $\zeta = 0.37$ and for filling factors up to 8%, Eq. (8.69) underestimates μ_1 by 0.34% to 0.83%; hence Eq. (8.15) overestimates τ_1 by 0.68% to 1.66%. Thus the refined analytical approximation agrees with the numerical computation to within 2% for all possible filling factors. Now suppose that because we have neglected the thermal resistance of the glass, τ_1 underestimates $\tau_{\mathrm{f}p}$ by 2.5%. Then Eq. (8.15) underestimates $\tau_{\mathrm{f}p}$ by 0.84% to 1.82%. We may therefore reasonably expect Eq. (8.15) to be correct to within 2%, provided that the filling factor is small enough to justify the cylindrical-heat-tube assumption.

The neglect of higher-order (i.e. shorter) time constants has a qualitatively similar effect to overestimating a single time constant, and therefore tends to compensate for the underestimation of $\tau_{\mathrm{f}p}$. So the calculated value of $\tau_{\mathrm{f}p}$ will still be within 2% of the effective value provided that the departure from thermal equilibrium is not too great.

8.3 Some numerical results

Table 8.7 shows some values of τ_{fp} computed from Eq. (8.16) with $\zeta = 0.37$, for filling factors from 0.05% to 9% and fiber diameters from 4 μm to 16 μm. The table was produced by the program `tafp.c`, listed in Section B.7. Each row in the table corresponds to one filling factor and each column to one diameter. The assumed temperature and pressure are printed at the top, followed by the computed values of ρ_o, κ and α for the air at the assumed temperature and pressure. For $\mathtt{d} = 10\,\mu$m and $f = 0.25\%$, the table gives $\tau_{fp} \approx 550\,\mu$s, which corresponds to the transition frequency of 289 Hz quoted at the beginning of Section 8.1.

Notice however that the computed value of α differs from that quoted by Chase and Leach; their value of $1.87 \times 10^{-5}\,\mathrm{m^2\,s^{-1}}$ applies to a temperature of 0°C instead of 20°C. In the same paper [30, p. 588], Leach quotes the value $\rho_o = 1.18\,\mathrm{kg\,m^{-3}}$, which is the density at 25°C and 1 atm. The two ambient temperatures clash in Leach's Eqs. (15) and (16), which involve ρ_o and the thermal time constant; the latter depends on α. The inaccuracies caused by unrealistic or inconsistent assumptions concerning ambient temperature and pressure may not always be serious, but in any case are easily avoided by computing all the relevant acoustical properties of air from the specified temperature and pressure, as has been done for Table 8.7. The necessary formulae are given in the next chapter and will be used in the loudspeaker simulations in Chapter 10.

Table 8.7: *Computer printout showing the thermal time constant τ_{fp} at room temperature and pressure, for various filling factors and fiber diameters.*

```
T = 293.15 K;  Po = 101325 Pa.

rho = 1.204; kappa = 0.02572; alpha = 2.121e-05  (SI units).

THERMAL TIME CONSTANT tafp (IN MICROSECONDS)
vs. FILLING FACTOR f AND FIBRE DIAMETER d:

d(um):   4       6       8      10      12      14      16

f(%)
0.05   588.92 1325.06 2355.66 3680.72 5300.24 7214.22 9422.65
0.10   262.29  590.15 1049.15 1639.30 2360.60 3213.03 4196.61
0.15   162.36  365.31  649.45 1014.76 1461.26 1988.94 2597.79
0.20   115.14  259.07  460.56  719.63 1036.27 1410.48 1842.26
0.25    88.01  198.02  352.04  550.06  792.08 1078.11 1408.14
0.30    70.55  158.74  282.21  440.95  634.97  864.27 1128.84
0.35    58.46  131.53  233.83  365.36  526.11  716.10  935.31
0.40    49.62  111.65  198.50  310.15  446.62  607.89  793.98
0.45    42.92   96.56  171.66  268.23  386.24  525.72  686.66
0.50    37.66   84.75  150.66  235.40  338.98  461.39  602.63
0.60    30.01   67.51  120.02  187.54  270.05  367.57  480.10
0.70    24.72   55.62   98.89  154.51  222.49  302.84  395.54
0.80    20.88   46.97   83.51  130.48  187.89  255.74  334.03
0.90    17.97   40.43   71.87  112.29  161.70  220.10  287.47
1.00    15.70   35.32   62.79   98.10  141.27  192.28  251.15
1.20    12.40   27.90   49.60   77.50  111.59  151.89  198.39
1.40    10.14   22.81   40.55   63.35   91.23  124.17  162.19
1.60     8.50   19.12   33.99   53.12   76.49  104.11  135.98
1.80     7.26   16.35   29.06   45.40   65.38   88.99  116.23
2.00     6.31   14.19   25.22   39.41   56.75   77.25  100.89
2.50     4.65   10.47   18.61   29.08   41.88   57.00   74.46
3.00     3.61    8.13   14.46   22.59   32.52   44.27   57.82
3.50     2.91    6.54   11.63   18.17   26.17   35.62   46.53
4.00     2.40    5.40    9.61   15.01   21.62   29.42   38.43
4.50     2.02    4.55    8.10   12.65   18.21   24.79   32.38
5.00     1.73    3.90    6.93   10.83   15.60   21.23   27.73
6.00     1.32    2.96    5.27    8.24   11.86   16.14   21.08
7.00     1.04    2.34    4.16    6.49    9.35   12.73   16.63
8.00     0.84    1.89    3.37    5.26    7.58   10.31   13.47
9.00     0.70    1.57    2.78    4.35    6.27    8.53   11.14
```

Chapter 9

Acoustical properties of air vs. temperature and pressure[1]

Air is a variable medium. Absolute "room temperature" at a single location can vary over a 10% range, or more for inland sites. Geographic variations in temperature are even greater. Atmospheric pressure drops by more than 16% between sea level and 1500 meters [31, p. *14*-14]. The effects of these changes on the acoustical properties of air are *not* negligible; recall, for example, that c is proportional to $T^{1/2}$ and that the adiabatic bulk modulus is proportional to P_0 (Eqs. (2.40) and (2.41)). As these variations obviously affect the characteristics of acoustic devices that work in air, they should be taken into account in computer simulations of such devices—preferably by requiring the user to specify the temperature and pressure, and computing the other properties of air therefrom. This chapter gives simple algebraic formulae for calculating a comprehensive set of acoustical properties of air from the ambient temperature and pressure. For ease of use, the formulae are given in a computational sequence in which later formulae may use the numerical results of earlier ones; consequently the first few formulae are not very interesting.

9.1 The dry-air formulae

9.1.1 Constants

The universal gas constant is fundamental to the kinetic molecular theory of gases. Its value, according to the 1986 least-squares adjustment of the fundamental physical constants [31, p. *1*-1], is

$$\bar{R} = 8.31451\,\mathrm{J\,K^{-1}\,mol^{-1}}. \tag{9.1}$$

The U.S. Standard Atmosphere tables [31, pp. *14*-12, 14] assume that the mean molar mass of dry air is

$$\bar{m} = 0.028964\,\mathrm{kg\,mol^{-1}}. \tag{9.2}$$

The mass-specific heat of dry air at constant pressure will be taken as

$$C_p = 1007\ \mathrm{J\,kg^{-1}\,K^{-1}}. \tag{9.3}$$

[1] A stand-alone version of this chapter has been published as an engineering report in *J. Audio Engineering Soc.* [44]. The report includes two minor corrections to the author's earlier paper [43].

This value is correct at 100 kPa and 300 K, but C_p is quite insensitive to large changes in temperature and pressure [31, pp. *6*-1 to 2].

The ratio of specific heats is

$$\gamma = \frac{C_p}{C_v} = \frac{C_p}{C_p - R} = \frac{C_p}{C_p - \bar{R}/\bar{m}} \tag{9.4}$$

which comes to 1.3987. But to avoid redundant parameters in the simulation programs, C_p will be treated as a given constant and γ will be computed from Eq. (9.4). Note that the constancy of C_p implies the constancy of γ.

9.1.2 Density

Let P_0 be the static pressure, V the overall volume, n the amount of gas (in moles), and T the static absolute temperature. Then at equilibrium, the ideal gas equation gives

$$P_0 V = n\bar{R}T. \tag{9.5}$$

Putting $n = m/\bar{m}$ (where m is the overall mass) and solving for m/V gives the static density:

$$\rho_o = \frac{P_0\,\bar{m}}{\bar{R}T}. \tag{9.6}$$

9.1.3 Speed of sound; characteristic impedance; bulk modulus

Putting $R = \bar{R}/\bar{m}$ in Eq. (2.40) gives

$$c = \sqrt{\gamma \bar{R}T/\bar{m}} \tag{9.7}$$

(cf. [21, p. *3*-73]). Having established that γ is constant, we see that c depends on temperature alone.

Recalling Subsection 3.3.5, the characteristic impedance is $\rho_o c$. This may be computed using the numerical results of Eqs. (9.6) and (9.7). Substituting from these equations is of interest because it gives the proportionality

$$\rho_o c \propto P_0 T^{-1/2} \tag{9.8}$$

(cf. [21], p. *3*-77).

From Eq. (2.42), the adiabatic bulk modulus is $\rho_o c^2$. Substituting from Eqs. (9.6) and (9.7) gives

$$\rho_o c^2 = \gamma P_0 \tag{9.9}$$

in agreement with Eq. (2.41). So, whereas the speed of sound depends on temperature alone, the adiabatic bulk modulus depends on pressure alone.

9.1.4 Viscosity

The *dynamic viscosity*, denoted by η in this thesis, is the ratio of shear stress to shear strain rate. The simple kinetic molecular theory predicts that for a given gas, η is independent of pressure and proportional to the square root of the absolute temperature [9, p. 49]. Kadoya *et al* [27, p. 954] have published a correlation of

numerous earlier measurements of η for dry air. Their figures confirm that η is remarkably insensitive to pressure (e.g. at 300 K, reducing the pressure from 100 kPa to 10 kPa reduces η by 0.054%) but show a different temperature-dependence from that predicted by the simple theory. For realistic room temperatures, the results of Kadoya et al. are well matched by the formula

$$\eta \approx 18.57\,(T/300\,\mathrm{K})^{0.7829}\ \mu\mathrm{Pa\,s}. \tag{9.10}$$

For a pressure of 100 kPa, this formula agrees with Kadoya et al. at 300 K and deviates by +0.25% at 250 K and 350 K, +1.43% at 200 K, and +0.69% at 400 K.

The *kinematic viscosity* ν (which is not used in this thesis) is defined as [21, p. *3*-69]

$$\nu = \eta/\rho_\mathrm{o}. \tag{9.11}$$

The quantities on the right-hand side are already known from Eqs. (9.10) and (9.6); substituting from these equations gives the proportionality

$$\nu \propto T^{1.7829}\,P_0^{-1}. \tag{9.12}$$

9.1.5 Heat conduction

For a particular gas, the value of κ, like that of η, is theoretically a function of temperature alone [21, p. *4*-145]. The above-mentioned paper by Kadoya et al. includes a correlation of numerous measurements of κ for dry air [27, p. 962], and confirms that κ is insensitive to gross variations in pressure (e.g. at 300 K, reducing the pressure from 100 kPa to 10 kPa reduces κ by 0.11%). The temperature-dependence of κ, for realistic room temperatures, is well described by the formula

$$\kappa \approx 0.02623\,(T/300\,\mathrm{K})^{0.851}\ \mathrm{W\,m^{-1}\,K^{-1}}. \tag{9.13}$$

For a pressure of 100 kPa, the formula agrees with Kadoya et al. at 300 K and deviates by +0.22% at 250 K and 350 K, +1.17% at 200 K, and +0.68% at 400 K.

The *thermal diffusivity* α is defined by Eq. (8.13), which is repeated here:

$$\alpha = \frac{\kappa}{\rho_\mathrm{o} C_p}. \tag{9.14}$$

All quantities on the right-hand side of this equation are known from earlier formulae. Substituting from Eqs. (9.13) and (9.6) yields the proportionality

$$\alpha \propto T^{1.851}\,P_0^{-1}. \tag{9.15}$$

Thus α has the strongest temperature-dependence of all the properties mentioned so far.

9.2 Numerical results

Table 9.1 is a computer printout of some acoustical properties of air for selected temperatures and pressures, calculated using Eqs. (9.1), (9.2), (9.3), (9.4), (9.6), (9.7), (9.10), (9.13) and (9.14). The table was computed and printed by the program `air.c`, listed in Section B.8.

Table 9.1: *Some acoustical properties of dry air, computed using the formulae in this chapter. The headings on the columns obviously represent* T, P_0, ρ_o, c, $\rho_o c$, η, κ *and* α.

ACOUSTICAL PROPERTIES OF AIR vs. TEMPERATURE AND PRESSURE

All units are SI.

Rbar = 8.31451 ; mbar = 0.028964 ; Cp = 1007 ; gamma = 1.3987 .

T	Po	rho	c	rhoc	eta	kappa	alpha
200.00	101325	1.76485	283.38	500.13	1.352e-05	0.01858	1.05e-05
250.00	101325	1.41188	316.83	447.33	1.610e-05	0.02246	1.58e-05
300.00	101325	1.17657	347.07	408.35	1.857e-05	0.02623	2.21e-05
350.00	101325	1.00849	374.88	378.06	2.095e-05	0.02991	2.94e-05
400.00	101325	0.88243	400.76	353.64	2.326e-05	0.03351	3.77e-05
273.15	101325	1.29222	331.17	427.95	1.726e-05	0.02422	1.86e-05
278.15	101325	1.26899	334.19	424.09	1.750e-05	0.02460	1.92e-05
283.15	101325	1.24659	337.18	420.33	1.775e-05	0.02497	1.99e-05
288.15	101325	1.22495	340.15	416.66	1.799e-05	0.02535	2.05e-05
293.15	101325	1.20406	343.08	413.10	1.824e-05	0.02572	2.12e-05
298.15	101325	1.18387	346.00	409.62	1.848e-05	0.02609	2.19e-05
303.15	101325	1.16434	348.89	406.22	1.872e-05	0.02646	2.26e-05
307.66	142970	1.61881	351.47	568.97	1.894e-05	0.02680	1.64e-05
297.90	120690	1.41130	345.85	488.10	1.847e-05	0.02607	1.83e-05
288.15	101325	1.22495	340.15	416.66	1.799e-05	0.02535	2.05e-05
278.40	84559	1.05806	334.34	353.75	1.751e-05	0.02461	2.31e-05
268.66	70121	0.90922	328.44	298.62	1.703e-05	0.02388	2.61e-05
258.92	57752	0.77700	322.43	250.53	1.655e-05	0.02314	2.96e-05
249.19	47217	0.66008	316.31	208.79	1.606e-05	0.02240	3.37e-05

Three sequences of temperatures are used in Table 9.1. The first sequence, for which the pressure is held at 1 atm, allows the computed values of η and κ to be compared with those given by Kadoya et al. [27]. The discrepancies have already been noted; see after Eqs. (9.10) and (9.13). The second sequence, for which P_0 is again held at 1 atm, extends from 0°C to 30°C in 5° increments. This covers a realistic range of room temperatures and allows the tabulated values of c to be compared with those in [31, p. *14*-40]; the values of c in Table 9.1 are consistently about 0.084% less than those in the reference. The third sequence uses the standard values of T and P_0 at altitudes from −3000 m to +6000 m in 1500 m increments. These values are taken from the tables of the U.S. Standard Atmosphere, 1976 [31, pp. *14*-12, 14], which also include the corresponding values of ρ_o, c, η, ν and κ. If the U.S. Standard Atmosphere[2] is taken as correct, the errors in the third sequence

[2]The U.S. Standard Atmosphere tables use "μ" for the dynamic viscosity and "η" for the kinematic viscosity. This thesis, following the convention of [21, p. *3*-69], uses "η" for the dynamic viscosity and "ν" for the kinematic viscosity.

of Table 9.1 are within the following limits:

For ρ_o: $-0.0033\,\%$ to $-0.0071\,\%$;
For c: $-0.041\,\%$ to $-0.046\,\%$;
For η: $+0.52\,\%$ to $+0.70\,\%$;
For κ: $-0.08\,\%$ to $-0.74\,\%$.

These results are readily acceptable. One point of concern is that the deviations in η and κ from the values of the U.S. Standard Atmosphere are greater than would be expected from the earlier comparison with Kadoya et al.; the deviations in κ are even in the opposite direction. However, the U.S. Standard Atmosphere figures are within the range of experimental data on which Kadoya et al. base their correlation [27, pp. 956, 964]. In this chapter, the results of Kadoya et al. are preferred over other published figures because they are the most recent and are based on the largest collection of measurements.

From the second sequence of Table 9.1, we see that the value of α used by Chase [14] and Leach [30], namely $1.87 \times 10^{-5}\,\mathrm{m^2\,s^{-1}}$, is correct at about 0°C and 1 atm, whereas Leach's value of ρ_o, namely $1.18\,\mathrm{kg\,m^{-3}}$, is correct to three significant figures for 25°C and 1 atm. Calculating the required properties of air from the temperature and pressure would have removed the risk of unrealistic or inconsistent data, and would have avoided the inconvenience of finding the data in scattered tables or papers.

9.3 Errors due to humidity

Eqs. (9.2) to (9.14) assume dry air. To justify this assumption, we must show that humidity has negligible effect on the properties of interest—or at least that the effects of likely variations in humidity are of a lesser order of magnitude than the effects of likely variations in temperature and pressure, which are included in the equations. This will be done by means of some numerical examples.

First consider $\bar{m}$. At 33°C and 100% humidity (an extreme case), the vapor pressure of water is about 0.05 atm [31, p. *6*-15]. Assuming molar masses (in g/mol) of 29 for dry air and 18 for water (approximate values are sufficient for a sensitivity calculation), the mean molar mass of this saturated air is about $0.95 \times 29 + 0.05 \times 18 = 28.45$, which is 1.9% less than the assumed value for dry air. The effect is reduced at lower relative humidities and lower temperatures; for example, at 20°C and 100% humidity, the mean molar mass is only 0.9% below that of dry air.

Next, consider the acoustical properties calculable from $\bar{m}$. By Eq. (9.6), ρ_o is equally sensitive to $\bar{m}$, T and P_0. But the expected variations in $\bar{m}$ are small compared with those in T and P_0. At 20°C, increasing humidity from 0% to 100% reduces $\bar{m}$ by 0.9% (as noted above) and hence reduces ρ_o by 0.9% (by Eq. (9.6)). This figure may be combined with published data concerning the effect of humidity on the speed of sound: at 20°C, increasing humidity from 0% to 100% increases c by 0.35% [31, pp. *14*-37 to 40]. Hence the impedance $\rho_o c$ decreases by 0.55% and the bulk modulus $\rho_o c^2$ decreases by 0.2%. By Eq. (9.9), this means that γ also decreases by 0.2%. These fractional changes are equal to or less than the corresponding changes in $\bar{m}$, and are small compared with likely variations in c with T and in bulk modulus with P_0.

The figures for viscosity and thermal conductivity given by Kadoya *et al.* are for dry air. The effect of humidity on these quantities can be roughly estimated by comparing the properties of air and water vapor and assuming that the properties of the mixture are an interpolation (not necessarily linear) between the corresponding properties of the constituents.

The dynamic viscosity of water vapor at 25°C is about 53% of that of dry air [9, p. 22]; this is the limiting value of η as the mole fraction of water approaches unity. For the small mole fractions of water in humid air, the deviations in η from the dry-air value may be expected to be correspondingly small. The molar mass of water is about 62% of that of air, and $\rho_o \propto \bar{m}$ by Eq. (9.6). So the effects of humidity on η and ρ_o have opposing effects on ν (Eq. (9.11)). In this thesis, ν is not used at all, and η is used only for the purpose of calculating the pneumatic resistivity λ. Given that λ also depends on the filling factor f (and may even be anisotropic), and that f is likely to be only approximately known (because it changes when the fiber is handled), there seems to be little point in considering such fine details as the effect of humidity on η.

The thermal conductivity of water vapor at 300 K is about 71% of that of dry air [31, p. *6*-199]. Hence humidity reduces κ, but should not effect κ as much as it affects η. Now consider the effect of humidity on $\alpha = \kappa/(\rho_o C_p)$. The molar mass of water is about 62% of that of air, suggesting that the reduction in ρ_o due to humidity will be comparable with the reduction in κ. The C_p of water vapor is about $2000\,\mathrm{J\,kg^{-1}\,K^{-1}}$, or about twice that of air [31, p. *6*-18]. So it seems that the dominant effect of humidity on α will be the increase in C_p, which will reduce α by a fraction comparable to the mole fraction of H_2O. In that case, α has the greatest sensitivity to humidity of all the properties considered so far, but the variation is still small—perhaps 5% under extreme conditions, and usually much less. By Eq. (7.119), a reduction in α will increase the thermal time constant $\tau_{\mathrm{f}p}$. Hence, if the dry-air value of α is used, Eq. (7.119) will underestimate $\tau_{\mathrm{f}p}$ by a somewhat greater margin than that predicted at the end of Subsection 8.2.7. Again the neglect of higher-order time constants tends to compensate for this. More importantly, for the small mole fractions of water in humid air, the effect on C_p, α and $\tau_{\mathrm{f}p}$ will be correspondingly small. When we consider the possible error in $\tau_{\mathrm{f}p}$ caused by the cylindrical-heat-tube assumption, together with the larger uncertainty in λ (which also appears in any simulation involving $\tau_{\mathrm{f}p}$), further investigation of the effect of humidity on α does not seem productive.

In summary, because of the small mole fractions involved, it appears that the influence of humidity on the above properties of air is less significant than that of temperature and pressure, and that the neglect of humidity is not a major source of error when compared with the other approximations involved in the analysis of damping materials.

9.4 Absorption and humidity

The "classical" mechanisms of sound absorption, namely viscosity and heat conduction, can be understood by modeling the medium as a continuum. The plane-wave absorption coefficient due to viscosity is

$$\alpha_\eta = \frac{2\eta\,\omega^2}{3\rho_o c^3} \tag{9.16}$$

while the corresponding coefficient due to heat conduction is

$$\alpha_\kappa = \frac{\kappa(\gamma-1)\,\omega^2}{2\rho_\mathrm{o}C_p c^3}. \tag{9.17}$$

Both coefficients are in Np/m (nepers per meter) for the pressure wave [21, pp. 3-69, 71].

Viscosity and heat conduction are the dominant absorption mechanisms only in monoatomic gases.[3] In diatomic and polyatomic gases, the dominant mechanism is known as *molecular thermal relaxation*. A mathematical treatment of this effect is given by Morse and Ingard [38, pp. 294–300]. Further formulae and supporting data for air are given in ANSI S1.26-1978 [41]. For present purposes a brief overview is sufficient.

Whereas monoatomic gas molecules have only translational kinetic energy, non-monoatomic molecules have translational, rotational and vibrational energy. The translational motion is adequately described by Newtonian physics, but the rotational and vibrational energies assume discrete values permitted by quantum mechanics [9, pp. 73–9, 86–9]. When a non-monoatomic gas is compressed, the work of compression is initially taken up in the translational energy of the molecules, because only the translational motion affects the pressure. But over time, part of the added energy is transferred to the rotational and vibrational degrees of freedom, reducing the change in pressure—hence the term "relaxation". The transfer of energy to each degree of freedom (or "mode") has its own time constant or *relaxation time*.

Now consider a sinusoidal variation in pressure. If the relaxation time of a particular mode is much longer than one cycle, the transfer of energy to and from that mode is very small, so that there is little opportunity for dissipation. If a relaxation time is much shorter than one cycle, the transfer of energy to and from the associated mode is a quasi-equilibrium process, so that the energy transferred to the mode during compression is almost completely returned during decompression, and again there is little dissipation. But if a mode has a relaxation time comparable with one cycle (or, more precisely, one radian-period), a significant fraction of the energy transferred to the mode during compression will not revert to translational energy during decompression, will not contribute to pressure, and will be dissipated as heat rather than recovered as work.

Suppose a mode with a relaxation time τ_i causes an attenuation coefficient $\alpha_{\mathrm{r}i}$ (in Np/m), so that the absorption in one cycle (or one wavelength) due to this mode is $\alpha_{\mathrm{r}i}\lambda$, where λ is the wavelength. Then the $\alpha_{\mathrm{r}i}\lambda$ product is a maximum at the frequency

$$f_{\mathrm{r}i} = \frac{1}{2\pi\tau_i} \tag{9.18}$$

[38, p. 300], and is approximately proportional to f at lower frequencies and to $1/f$ at higher frequencies. Hence the modal absorption coefficient $\alpha_{\mathrm{r}i}$ is an increasing function of frequency, being approximately proportional to f^2 for $f \ll f_{\mathrm{r}i}$ and nearly constant for $f \gg f_{\mathrm{r}i}$ (see Figs. B-1 and B-2 of reference [41]). $f_{\mathrm{r}i}$ is known as the *relaxation frequency*.

[3] On p. 449 of the author's paper [43], it is stated that in the absence of boundary surfaces, "conduction of the heat of compression is largely responsible for the absorption of sound in air." It is fortunate that this remark was made only in passing—in parentheses in an appendix. A correction is included in [44].

Because the relaxation times for the rotational modes are extremely short, rotational relaxation is usually not a major contributor to absorption, except at ultrasonic frequencies. In contrast, the vibrational relaxation times for *dry* air are very long ($f_{ri} \approx 24\,\text{Hz}$ for O_2 and 9 Hz for N_2). But the presence of H_2O raises the vibrational relaxation frequencies of oxygen and nitrogen by catalyzing the vibrational energy transitions. For oxygen, f_{ri} increases remarkably rapidly with humidity and can easily become ultrasonic, while for nitrogen, f_{ri} increases less rapidly and remains in the audio range (see Eqs. (8) and (9) of reference [41]). As a result, humidity has a strong effect on absorption at all audible frequencies, with the dominant mechanism tending to be nitrogen relaxation at lower audio frequencies and oxygen relaxation at higher frequencies.[4]

Pressure and temperature also affect the absorption coefficient. For each mode, f_{ri} is proportional to pressure, while the peak value of $\alpha_{ri}\lambda$ depends on the fraction of the total kinetic energy carried by that mode at thermal equilibrium. For vibration of oxygen or nitrogen, that fraction is very small under ordinary conditions but increases with temperature [38, p. 296]. Hence, for given frequency and absolute humidity, $\alpha_{ri}\lambda$ increases with temperature [41, pp. 8, 16, 17].

Practical formulae for calculating the absorption coefficient of air, in terms of temperature, pressure and humidity (absolute or relative), are given in ANSI S1.26-1978 [41], Section 4.5 and Appendix D.

Thus it is not permissible to assume dry air for calculations in which absorption of sound is significant. For temperatures from 0°C to 40°C and relative humidities from 10% to 100%, the total absorption coefficient is less than 0.01 dB/m at 500 Hz, 0.05 dB/m at 2 kHz, and 0.34 dB/m at 10 kHz [41, pp. 4–8]. These figures suggest that while atmospheric absorption is a major influence on the acoustic characteristics of rooms and halls, it does not greatly affect the internal workings of small acoustic devices such as loudspeakers, especially if the absorption of sound in such devices is dominated by damping components which have been deliberately included in the design.

9.5 Refined formulae for η and κ

By introducing polynomial correction factors into Eqs. (9.10) and (9.13), it is possible to obtain closer agreement with Kadoya et al. [27]. For example, dividing the right-hand side of Eq. (9.10) by

$$1 + 0.0025\left(\frac{T - 300\,\text{K}}{50\,\text{K}}\right)^2 \tag{9.19}$$

gives a formula which matches Kadoya et al. at 250 K, 300 K and 350 K, with errors of +0.41% at 200 K and −0.3% at 400 K. But at temperatures between 0°C and

[4]The author is indebted to an anonymous reviewer of his article "Acoustical Properties of Air versus Temperature and Pressure" [44] for explaining that humidity affects absorption mainly because of catalysis of the vibrational energy transitions in N_2 and O_2, and *not* because of the vibrational transitions of the H_2O molecule itself. On this point it is possible to misunderstand Morse and Ingard [38, pp. 299–300], who refer to the vibrational modes of polyatomic (as opposed to diatomic) molecules just before mentioning the reduction in relaxation times due to water vapor. The same reviewer drew the author's attention to ANSI S1.26-1978 [41], which is cited frequently in the final version of the article and is the principal authority for the present discussion.

50°C, the "refined" value differs from that given by Eq. (9.10) by less than 0.1%. Such a fine adjustment does not seem to be warranted by the accuracy of the raw data [27, pp. 956–7], let alone the accuracy of any model in which the value of η might be used.

Similarly, dividing the right-hand side of Eq. (9.13) by

$$1 + 0.0022 \left(\frac{T - 300\,\mathrm{K}}{50\,\mathrm{K}} \right)^2 \tag{9.20}$$

gives a formula which matches Kadoya et al. at 250 K, 300 K and 350 K, with errors of +0.29% at 200 K and −0.2% at 400 K. Again the adjustment amounts to less than 0.1% at normal temperatures. At elevated operating temperatures, such as exist near a hot voice coil, one might be inclined to use a refined form of Eq. (9.13) in an effort to improve the modeling of heat removal. Even so, one would have a remarkably good system model if one could claim that the improvement were significant.

The above adjustments would have only slight effects on the discrepancies between the U.S. Standard Atmosphere tables and Eqs. (9.10) and (9.13), and the discrepancies in κ would actually increase. This is further evidence that there is little point in refining the equations.

For these reasons, Eqs. (9.10) and (9.13) were used as written in the computation of Table 9.1; no correction factors were introduced.

Finally, it should be noted that the "correlations" of Kadoya *et al* [27] take the form of elaborate equations, with many coefficients, expressing η and κ in terms of temperature and pressure. Hence, to obtain accurate data for a wide range of conditions, the results of [27] may be used in precisely the same way as the results of the present chapter. But Eqs. (9.10) and (9.13) are more convenient for the conditions likely to be encountered in audio engineering.

9.6 Conclusion

Under realistic atmospheric conditions, all the linear acoustical properties of air except the absorption coefficient can be calculated with acceptable accuracy from the temperature and pressure, using simple algebraic formulae which assume dry air. These formulae are sufficient for the analysis of small acoustic devices, in which atmospheric absorption is not a major contributor to damping. The absorption coefficient, which is sensitive to humidity as well as temperature and pressure, can be calculated from the formulae in reference [41].

Chapter 10

Simulation of a fiber-filled bass enclosure

The equations and equivalent circuits developed in Chapters 6 and 7 will be used in this chapter to calculate the half-space frequency response of the system shown in Fig. 10.1. A woofer of overall diameter `D` is assumed to be mounted in a rectangular sealed box with a separate internal enclosure for the midrange and treble drivers. The woofer is as close as possible to the bottom of the box, minimizing the separation between the driver and its acoustic image (reflected in the floor) and ensuring that the interference between the two is constructive. The midrange/treble subenclosure is as close as possible to the woofer, minimizing the separation between the woofer and midrange and avoiding interference fringes in the vertical radiation pattern in the crossover frequency range. The fiberglass filling takes the form of a single rectangular block, which sits behind the subenclosure and completely fills the box apart from the region directly below the subenclosure. This arrangement supports the fiberglass and minimizes the risk of fibers falling or sagging into the woofer frame.

The dimensions shown in Fig. 10.1, along with the `width` of the box, are `#define`d in the model-building program "`box.c`", described below in Section 10.3 and listed in Section B.9. The main purpose of this program is to convert the parameters of the box, driver and fiber into an equivalent circuit specification that can be read by a circuit analysis program (see the introduction to Chapter 6). The chosen circuit simulator is a version of SPICE.[1] The model-builder also accepts command-line switches which cause selected components in the FDEC unit cells to be omitted (opened or shorted). From the resulting changes in frequency response, we can determine which characteristics of the fiber—added moving mass, viscous damping, added heat capacity, or thermal relaxation—are most significant in shaping the overall response of the loudspeaker. The omission of one or more component(s) in every circuit cell gives an approximation which is valid for a certain range of frequencies, and should not noticeably affect the response at those frequencies; this prediction can be checked to ensure that the modified circuit specification is correctly written. One of the command-line options causes the box to be modeled as a lumped compliance, allowing the results of the FDEC model to be compared with those of the classical model.

[1] SPICE3 by Tom Quarles, with the `nutmeg` user interface by Wayne Christopher; the version number for both SPICE and `nutmeg` is ver. 3f3, patchlevel 2.

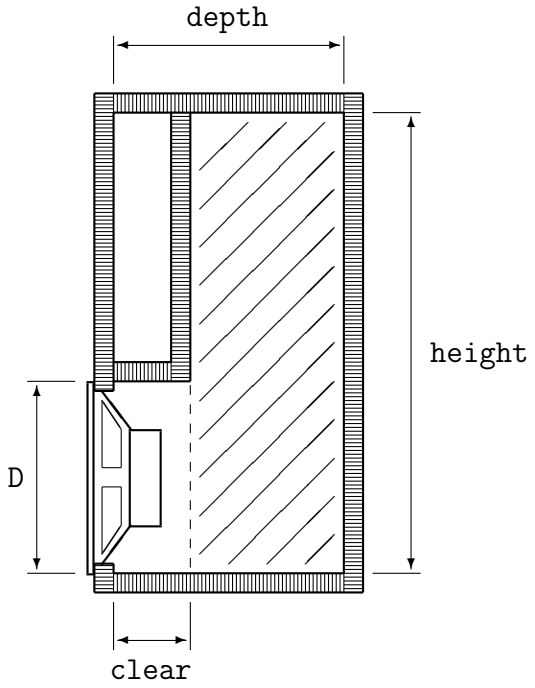

Figure 10.1: *Layout of the loudspeaker box to be simulated. The box features a midrange/tweeter subenclosure (above woofer) and partial fiber-filling (hatched region in woofer enclosure). Higher-frequency drivers are not shown. The indicated dimensions are* `#define`*d in the program* `box.c`.

10.1 The moving-coil driver

Before the model-building program could be written, it was necessary to obtain the equivalent circuit of the moving-coil driver in a form that allows the area of the diaphragm to be shared between several volume elements. While the chosen model allows for diaphragm sharing, it does *not* allow for diaphragm "break-up"; that is, it assumes that the diaphragm behaves as a rigid piston in its working frequency range.

The departure from rigid-piston behavior becomes audibly significant when it causes part of the diaphragm to vibrate in antiphase with the rest; this produces destructive interference and causes the driving impedance of the diaphragm to be influenced by elasticity so that it no longer resembles a simple mass. Such out-of-phase vibration occurs at frequencies comparable with the *first radial resonance frequency* of the diaphragm-coil-former assembly—i.e. the frequency at which the assembly vibrates in bending about a single nodal circle—but not at much lower frequencies. Sakamoto et al. [48] have noted that if the voice-coil former meets the diaphragm at the first nodal circle, the first resonance cannot be excited, so that the rigid piston assumption holds at frequencies well below the *second* resonance of the assembly; thus a suitable choice of voice-coil diameter can extend the "piston range" of the driver. This technique can be combined with modern materials and construction yielding high stiffness and low mass. The example given by Sakamoto et al. is a production 32 cm woofer with a planar radiating surface, whose diaphragm is nodally driven and takes the form of an aluminum honeycomb sandwiched between two sheets of aluminum foil. Its second resonance frequency is over 2 kHz, which is

substantially higher than the likely crossover frequency in a three-way system. Thus it is quite possible to build a system in which the woofer diaphragm behaves for all practical purposes as a rigid piston.[2]

The problem of resonances in the surround remains [56, pp. 101–2], but is less serious than diaphragm break-up; the small area of the surround not only restricts the radiation therefrom but also allows the first resonance frequency to be kept high.

10.1.1 Radiation impedance, radiated power, sound intensity level

As explained in Subsection 2.5.2, the *radiation impedance* seen by the diaphragm is the ratio of the average excess pressure over the surface to the volume flux, with both pressure and flux expressed in phasor form. It is shown in the acoustic circuit as an impedance between the diaphragm and ground, but may also be understood as the acoustic impedance between the radiating surface and an imaginary surface at infinity.

The analysis in this chapter assumes that the radiation impedance is that of a circular rigid piston in an infinite rigid planar baffle, radiating into a solid angle of 2π ("half-space"). One can easily attack this assumption by noting that the diaphragm is not necessarily planar, that the front panel of the box is not infinite, that the nearest approximation to a "half-space" is the space above the floor on which the loudspeaker rests, that the floor is finite and is met by reflecting/absorbing walls, that the diaphragm may effectively radiate into "quarter-space" if it is located in a dihedral angle (against a wall), or "eighth-space" if located in a trihedral angle (in a corner of the room), and so on. Against this, one may argue that the reflections from the floor and walls are legitimate additions to the signal because they would affect the acoustic radiation from an actual musical instrument in the listening room, that there is a certain frequency range over which a speaker effectively radiates into the half space above the floor, that the sensitivity of the driver is easily recalculated for quarter-space or eighth-space, etc. But all such arguments can be avoided if it is understood that the disk-in-infinite-baffle assumption does not purport to be a realistic model of a loudspeaker in a room, but is merely an agreed standard configuration *outside the box*, which is held constant as we compare various configurations and models of the system *inside the box*. The notion of a "basis for comparison" may be extended to include not only the disk-in-infinite-baffle model, but also the further approximations which will be made in reducing that model to a convenient equivalent circuit. Because such approximations give the same error for all simulations of the same system, they do not invalidate comparisons designed to show the effects of particular fiber properties on the frequency response.

Let the radius of the diaphragm be a. For frequencies below $c/2\pi a$, i.e. for wavelengths longer than the circumference of the diaphragm, the half-space radiation

[2]The aluminum honeycomb was one of several forms of sandwich construction suggested by D. A. Barlow as early as 1958. In his first article [5], Barlow noted that the flexural stiffness of the sandwich would make planar diaphragms feasible. He also took the first step towards the concept of nodal drive by suggesting that the driving force should be applied "near the center of the annular area constituting the cone". The original article was followed by numerous experiments using the form of sandwich construction that Barlow regarded as most promising: aluminum skins over a polystyrene foam core. Disks of this construction were found to have *first* radial resonance frequencies between 400 and 900 Hz [6], and a 25 cm cone had its first radial resonance at 1700 Hz [8].

impedance can be modeled as in inertance

$$M_{\mathrm{ar}} = \frac{8\rho_{\mathrm{o}}}{3\pi^2 a} \tag{10.1}$$

in parallel with a resistance

$$R_{\mathrm{ar}} = \frac{128\rho_{\mathrm{o}} c}{9\pi^3 a^2} \tag{10.2}$$

(see Beranek [11], p. 121 and Figs. 5.4 and 5.5(b)). For $a = 10\,\mathrm{cm}$, this model is valid up to about 550 Hz. The model does not predict the correct high-frequency limit of the radiation resistance—which is $\rho_{\mathrm{o}} c/(\pi a^2)$, or about 69% of R_{ar}—and does not predict the high-frequency undulations in the graph of radiation resistance vs. frequency [11, p. 121]. However, the latter error ensures that any ripples in the calculated frequency response are due to internal resonances of the box; this feature may assist the study of damping.

Let the average pressure over the radiating surface of the diaphragm be p_{r}, with r.m.s. phasor form P_{r}. Then, according to the above model of the radiation impedance, the real (time-averaged) radiated power is simply $|P_{\mathrm{r}}|^2/R_{\mathrm{ar}}$. Assuming isotropic radiation (another low-frequency approximation) into half-space, the intensity at distance r is

$$I = \frac{|P_{\mathrm{r}}|^2}{2\pi r^2 R_{\mathrm{ar}}}. \tag{10.3}$$

Now the reference intensity for a *intensity level* (IL) of 0 dB is [11, p. 13]

$$I_0 = 10^{-12}\,\mathrm{W\,m^{-2}}. \tag{10.4}$$

Suppose this reference intensity is produced by an r.m.s. pressure of P_{r0} at the radiating surface. Putting $I = I_0$ and $P_{\mathrm{r}} = P_{\mathrm{r0}}$ in Eq. (10.3) and solving for P_{r0} gives

$$P_{\mathrm{r0}} = \sqrt{2\pi r^2 I_0 R_{\mathrm{ar}}}\,. \tag{10.5}$$

Since $I \propto |P_{\mathrm{r}}|^2$, the IL at distance r is given by

$$\mathrm{IL} = 20 \log |P_{\mathrm{r}}/P_{\mathrm{r0}}|. \tag{10.6}$$

If r is taken as one meter, and if P_{r} is calculated for a nominal electrical input of one watt into 8 ohms, then Eqs. (10.5) and (10.6) yield the sensitivity of the loudspeaker in terms of IL at one watt and one meter. This technique is used in the program "`box.c`".

It must be emphasized that the above calculation of IL assumes isotropic radiation into half-space; no allowance is made for narrowing of the radiation pattern at high frequencies. In the frequency response graphs in this chapter, the ordinate is labeled "SIL" ("sound intensity level") to distinguish it from the usual IL. So SIL represents the radiated power level, calculated for a constant parallel R_{ar}, and normalized so as to coincide with IL in the midband.

10.1.2 Equation of motion

Newton's second law of motion for the driver, in the form

$$\text{mass} \times \text{acceleration} = \text{sum of forces},$$

is

$$m\ddot{x} = Bli + S(p_\mathrm{b} - p_\mathrm{f}) - R_\mathrm{ms}\dot{x} - \frac{x}{C_\mathrm{ms}} \tag{10.7}$$

where

m is the effective moving mass, comprising the diaphragm, voice coil and former, and parts of the spider and cone-surround,

x is the displacement of the diaphragm from its equilibrium position (towards the listener),

B is the magnetic flux density in the pole gap,

l is the effective length of the voice-coil, i.e. the length of wire that interacts with the field B (in an "underhung" coil, l is the entire length of wire in the coil; in an "overhung" coil, it is only part thereof),

i is the voice coil current (whose positive sense is defined by the above equation),

S is the effective area of the diaphragm (including a fraction of the flexible surround), projected on a plane normal to the direction of motion,

p_b is the excess pressure behind the diaphragm, averaged over the diaphragm area ("b" is for "back"),

$p_\mathrm{f} = p_\mathrm{r}$ is the excess pressure in front of the diaphragm, averaged over the diaphragm area ("f" is for "front"; "r" is for "radiated"),

R_ms is the mechanical damping coefficient, accounting for the damping effects of the spider (rear suspension), the surround (front suspension), the air or ferrofluid in the pole gap, and the induced current in the voice-coil former (if the former is made of a conducting material), but *not* the induced component of the voice-coil current (which is included in the Bli term), and

C_ms is the compliance of the suspension, determined by the spider and surround (and assumed to be linear).

Thus the force terms on the right of Eq. (10.7) are, from left to right, the Lorentz force developed by the moving-coil "motor", the force due to the pressure difference, the retarding force due to damping in the suspension, and the restoring force due to the stiffness of the suspension.

Before Eq. (10.7) can be used in deriving an equivalent circuit, it must be rewritten in terms of acoustic quantities instead of linear mechanical quantities. Under the rigid-piston assumption, the volume flux "pumped out" by the diaphragm is

$$u = S\dot{x}. \tag{10.8}$$

Rewriting Eq. (10.7) in terms of u and dividing through by S, we obtain

$$\frac{m}{S^2}\,\dot{u} = \frac{Bl}{S}\,i + p_\mathrm{b} - p_\mathrm{f} - \frac{R_\mathrm{ms}}{S^2}\,u - \frac{1}{S^2 C_\mathrm{ms}}\int u\,dt. \tag{10.9}$$

Noting that every term in this result has the dimensions of pressure, we can easily define subexpressions having the dimensions of acoustic mass, acoustic resistance

and acoustic compliance. By analogy with Eq. (2.26), the acoustic mass of the diaphragm-coil-former assembly is

$$M_{\mathrm{ad}} = m/S^2 \tag{10.10}$$

(M_{ad} is not to be confused with M_{as}, which includes the free-air load; the distinction will be discussed further in Subsection 10.1.4). The acoustic resistance of the suspension is

$$R_{\mathrm{as}} = R_{\mathrm{ms}}/S^2 \tag{10.11}$$

and the acoustic compliance of the suspension is

$$C_{\mathrm{as}} = S^2 C_{\mathrm{ms}}. \tag{10.12}$$

In addition, it is convenient to define the *transfer resistance* of the driver as

$$H = Bl/S \tag{10.13}$$

(in a SPICE circuit definition file, the name of any current-controlled voltage source begins with "`H`"). With these substitutions, the equation of motion can be written in the form

$$p_{\mathrm{f}} - p_{\mathrm{b}} = Hi - M_{\mathrm{ad}}\dot{u} - R_{\mathrm{as}}u - \frac{1}{C_{\mathrm{as}}}\int u\,dt. \tag{10.14}$$

10.1.3 Equivalent circuit

On the electrical side of the transducer, let v_{g} be the terminal voltage ("g" is for "generated) and let V_{g} be its phasor representation. It is convenient to set $V_{\mathrm{g}} = \sqrt{8}$ volts r.m.s., giving a nominal power of one watt into $8\,\Omega$. Let R_{e} be the resistance of the voice coil ("e" for "electrical"). The self-inductance of the voice-coil will be neglected in this analysis, but can easily be added to the finished equivalent circuit if desired. The remaining quantity of interest is the back e.m.f. generated in the voice coil; by Faraday's law, this is given by

$$e = Bl\dot{x} \tag{10.15}$$

or, using the substitutions defined above,

$$e = Hu. \tag{10.16}$$

So the transfer resistance H is *bilateral* and the coupled controlled sources form a *gyrator*.[3] H is the ratio of the effort variable (pressure or e.m.f.) on each side of the gyrator to the flow variable (current or volume flux) on the other side.

[3]The term *gyrator* was coined and applied to electrical networks by Tellegen [58] in 1948. Other methods for constructing electrical analogs of systems involving effort-flow coupling, such as "dual" analogies and ideal transformers with imaginary turns ratios, were discussed by several earlier authors [25, pp. 109–12]. The classical example of effort-flow coupling is the precession or nutation of a gyroscope. If a gyroscope is spinning clockwise about the z axis, a small clockwise moment (the effort) about the x axis causes a proportional clockwise precession (flow) about the y axis, while a small clockwise moment about the y axis produces a proportional *anticlockwise* precession (note the antisymmetry) about the x axis [28, pp. 47–8]. The gyrator is named after the gyroscope.

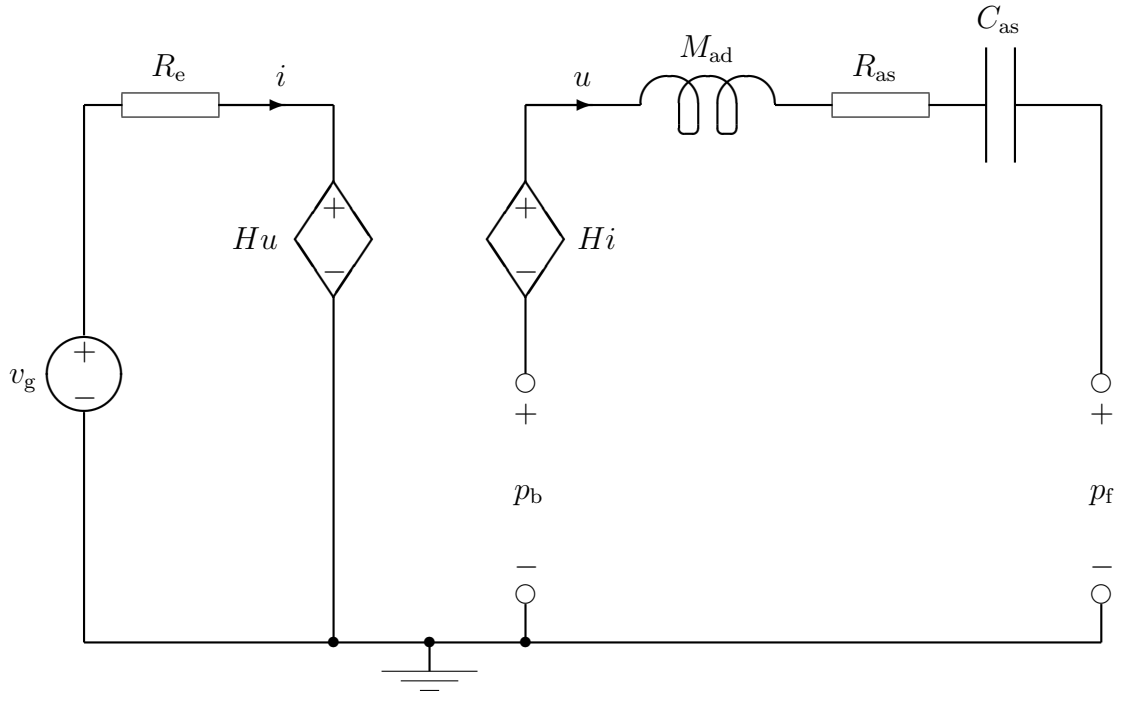

Figure 10.2: *Equivalent circuit of moving-coil driver connected to time-dependent voltage source* v_{g}.

Using Eq. (10.16) for the value of the back e.m.f., the electrical side of the equivalent circuit can be drawn directly. As Eq. (10.14) expresses Kirchhoff's pressure law for a series circuit, the acoustic side is also easily drawn. The complete driver circuit is shown in Fig. 10.2.

Notice that the assumed direction of flow is *against* the controlled effort source on the electrical side, but *with* the controlled effort source on the acoustic side. If the gyrator were represented as a two-port impedance matrix, the assumed direction of u would be reversed and the source Hu would become $-Hu$, so that the matrix would be skewsymmetric. Thus the transfer resistance is bilateral but *antisymmetric*. The antisymmetry is necessary because the gyrator simply transfers power; it cannot create energy, and all dissipation or storage of energy is represented by the surrounding components. The antisymmetry can also be understood by writing the developed force and the back e.m.f. as vector cross products. Each product involves a 90° spatial rotation and the two rotations are additive, so that the induced e.m.f. in the voice coil opposes the current in accordance with Lenz's law [25, 112–14]. In the derivation of the equivalent circuit, Lenz's law was tacitly assumed when the induced e.m.f. was called a "back e.m.f." in the preamble to Eq. (10.15).

Antisymmetry is a problem if one wishes to model a system using *passive* all-electrical networks [25, pp. 109–12]. But in simulation programs such as SPICE, in which the two halves of a gyrator can be defined as separate controlled sources, antisymmetry presents no special difficulty. If the node-numbering conventions for controlled sources are correctly followed, the effect of the antisymmetry is that the terminals on one side of the gyrator are listed in the same order in both sources, whereas the other two terminals appear in one order when they are "controlled" and in the reverse order when they are "controlling".

10.1.4 Calculation of component values from data sheets

Unfortunately one is not likely to find all the component values in Fig. 10.2—or even the mechanical quantities in Eq. (10.7)—in the manufacturer's or retailer's catalog. R_e is easily measured but not generally advertised; when choosing a driver from a catalog, one usually has to assume that R_e is slightly less than the nominal impedance. If an effective piston diameter is not given, S can be estimated from the overall diameter and any available illustration. Instead of C_as, most catalogs specify the equivalent volume V_as, in which case we use the familiar volume-compliance relation

$$C_\mathrm{as} = \frac{V_\mathrm{as}}{\gamma P_0}. \tag{10.17}$$

Occasionally C_ms is given instead of V_as. The Bl product is sometimes stated, in which case it is trivial to calculate H. But usually H must be calculated, along with M_ad, from the *free-air resonance parameters* defined by Thiele [59] and Small [49].

The diaphragm of a driver in free air (i.e. without a box or baffle) may be roughly modeled as a rigid disk vibrating along its axis in free air. Let the radius of the disk be a. Then, for frequencies below $c/(2\pi a)$, i.e. for wavelengths greater than the circumference, the acoustic impedance between the front and back surfaces of the disk is almost a pure inertance [11, p. 127], whose value is very nearly equal to the half-space radiation inertance of the same disk [11, pp. 124, 126]. If we connect the half-space radiation inertance M_ar between the front and back surfaces of the disk in Fig. 10.2, we see that

$$p_\mathrm{f} - p_\mathrm{b} = M_\mathrm{ar}\dot{u}. \tag{10.18}$$

If the terminals of the driver are *short-circuited*—that is, if $v_\mathrm{g} = 0$ in Fig. 10.2—we have

$$i = -e/R_\mathrm{e} \tag{10.19}$$

or, using Eq. (10.16),

$$i = -Hu/R_\mathrm{e}. \tag{10.20}$$

Substituting Eqs. (10.18) and (10.20) into Eq. (10.14) and differentiating w.r.t. time gives

$$M_\mathrm{as}\ddot{u} + (R_\mathrm{as} + H^2/R_\mathrm{e})\dot{u} + u/C_\mathrm{as} = 0 \tag{10.21}$$

where M_as is the acoustic mass of the speaker *including the free-air mass load* and is given by

$$M_\mathrm{as} = M_\mathrm{ad} + M_\mathrm{ar}. \tag{10.22}$$

Eq. (10.21) is the differential equation describing the free vibration of the driver in free air when the terminals are short-circuited. It may be written in the standard form

$$\ddot{u} + \frac{\omega_\mathrm{s}}{Q_\mathrm{ts}}\dot{u} + \omega_\mathrm{s}^2 u = 0 \tag{10.23}$$

where

$$\omega_\mathrm{s} = 2\pi f_\mathrm{s} = \frac{1}{\sqrt{M_\mathrm{as}C_\mathrm{as}}} \tag{10.24}$$

and

$$Q_\mathrm{ts} = \frac{\sqrt{M_\mathrm{as}/C_\mathrm{as}}}{R_\mathrm{as} + H^2/R_\mathrm{e}}. \tag{10.25}$$

The frequency f_s is the "free-air resonance" and Q_{ts} is the "total Q"; both quantities are usually quoted in suppliers' catalogs.

To find the corresponding *open-circuit* parameters, we simply let $R_e \to \infty$. The resonance frequency is unchanged, but Q_{ts} is replaced by

$$Q_{ms} = \frac{\sqrt{M_{as}/C_{as}}}{R_{as}}. \tag{10.26}$$

Q_{ms} is known as the "mechanical Q" because it does not include the damping effect of induced current in the voice coil.

There is also an "electrical Q", called Q_{es}, which includes the damping effect of induced voice-coil current but neglects all other damping. It is found by setting $R_{as} = 0$ in Eq. (10.25):

$$Q_{es} = \frac{R_e \sqrt{M_{as}/C_{as}}}{H^2}. \tag{10.27}$$

From the above three equations one can easily verify that

$$\frac{1}{Q_{ts}} = \frac{1}{Q_{ms}} + \frac{1}{Q_{es}} \tag{10.28}$$

so that any two Q factors determine the third. Some suppliers routinely specify all three Q factors, but unfortunately most specify only Q_{ts}.

We now have sufficient information to calculate M_{as}, H and R_{as} from the most frequently advertised driver parameters. From Eq. (10.24) we have

$$M_{as} = \frac{1}{\omega_s^2 C_{as}}. \tag{10.29}$$

Substituting this into Eqs. (10.26) and (10.27) and solving for R_{as} and H, respectively, we find

$$R_{as} = \frac{1}{Q_{ms}\,\omega_s\,C_{as}} \tag{10.30}$$

and

$$H = \sqrt{\frac{R_e}{Q_{es}\,\omega_s\,C_{as}}}. \tag{10.31}$$

For reasons to be explained in Subsection 10.1.5, it is convenient to define the *transconductance* of the driver as

$$G = \frac{1}{H} = \sqrt{\frac{Q_{es}\,\omega_s\,C_{as}}{R_e}}. \tag{10.32}$$

Program "`box.c`" expects the values of f_s, Q_{ts}, Q_{ms}, V_{as}, R_e and a to be specified using `#define` statements, and calculates ω_s, Q_{es}, C_{as}, R_{as}, M_{as}, G, M_{ar}, R_{ar} and M_{ad}, using Eqs. (10.24), (10.28), (10.17), (10.30), (10.29), (10.32), (10.1), (10.2) and (10.22), respectively.

10.1.5 Sharing the diaphragm area among several volume elements

Modeling the gyrator element as a transfer resistance is natural in that it conforms to common notions of causality: the voice-coil current causes the developed force

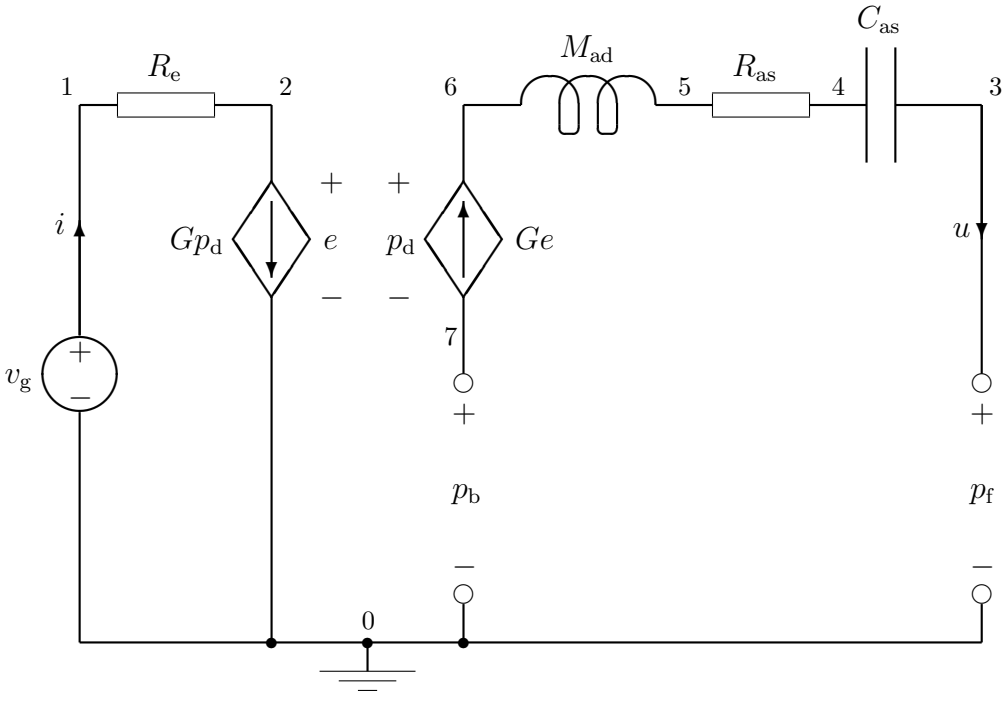

Figure 10.3: *Electroacoustic circuit of Fig. 10.2, with the gyrator remodeled as a bilateral transconductance. Node numbers are also shown.*

according to the Lorentz force law, while the resulting motion causes the back e.m.f. according to Faraday's law. In Fig. 10.2, if the pressure developed by the current-controlled pressure source is p_{d} and the back e.m.f. is e, the equations describing the transduction are

$$p_{\text{d}} = Hi \; ; \; e = Hu. \tag{10.33}$$

If we let $G = 1/H$, these equations are equivalent to

$$i = Gp_{\text{d}} \; ; \; u = Ge. \tag{10.34}$$

Eqs. (10.34) describe a pressure-controlled current source and a voltage-controlled flux source, and imply that G is a bilateral transconductance, i.e. the ratio of the flow variable on each side of the gyrator to the effort variable on the other side. ("G" is a standard symbol for conductance, and the first letter of the name of a voltage-controlled current source in SPICE; both G and H are named after SPICE conventions.) The new sources appear to reverse the direction of physical causation, but the resulting network equations are equivalent to those for the old sources; equations are acausal.

When the new sources replace the ones in Fig. 10.2, the new circuit is as shown in Fig. 10.3. Because of the opposing arrows in the controlled flow sources, the antisymmetry of the gyrator is more apparent here than in Fig. 10.2. Fig. 10.3 also includes the node numbers for the SPICE model. To complete the model of the driver-box system, the radiation impedance (M_{ar} in parallel with R_{ar}) is connected between nodes 3 and 0, and the box impedance (yet to be discussed) is connected between nodes 7 and 0.

Modeling the gyrator as a transconductance is convenient because it allows the equivalent circuit to be easily modified for the case in which the diaphragm area is

shared between several volume elements in the box; in the following discussion it is shown that because G is proportional to S, the transconductance is shared between the volume elements in the same fractions as the diaphragm area.

Using Eq. (10.13), we may write G in terms of the Bl product as

$$G = \frac{1}{H} = \frac{S}{Bl}. \tag{10.35}$$

When the box is modeled as a finite-difference equivalent circuit, each of the volume elements adjacent to the diaphragm covers part of the diaphragm area. Denoting the partial areas by S_j, where $j = 1, 2, \ldots, n$, we have

$$S = \sum_j S_j. \tag{10.36}$$

By analogy with Eq. (10.35), let us define

$$G_j = \frac{S_j}{Bl}. \tag{10.37}$$

Then dividing Eq. (10.36) by Bl gives

$$G = \sum_j G_j. \tag{10.38}$$

The flux pumped out of the j^{th} volume element adjacent to the diaphragm is

$$u_j = S_j \, \dot{x}. \tag{10.39}$$

Hence multiplying Eq. (10.36) by $\dot{x}$ yields

$$u = \sum_j u_j \tag{10.40}$$

as expected.

To model the acoustic side of the gyrator, we substitute Eq. (10.38) into the second Eq. (10.34), obtaining

$$u = \sum_j G_j \, e. \tag{10.41}$$

This indicates that the controlled flux source in Fig. 10.3 must be replaced by n sources, with the j^{th} source feeding a flux $G_j \, e$ into node 6.

Modeling the electrical side is more difficult because the current is no longer controlled by a single pressure drop on the acoustic side. But we know that the *average* excess pressure on the back of the driver is p_{b}. Let us define the area fractions as

$$a_j = \frac{S_j}{S} \; ; \; j = 1, 2, \ldots, n \tag{10.42}$$

so that Eq. (10.37) can be rewritten

$$G_j = a_j \, G. \tag{10.43}$$

If $p_{\text{b}j}$ denotes the average excess pressure on the back of the j^{th} area element (whose area is S_j), the area-weighted average is

$$p_{\text{b}} = \sum_j a_j \, p_{\text{b}j}. \tag{10.44}$$

Applying Kirchhoff's pressure law to the right-hand mesh in Fig. 10.3, we have

$$p_{\mathrm{d}} = p_{\mathrm{f}} + \frac{1}{C_{\mathrm{as}}} \int u \, dt + R_{\mathrm{as}} u + M_{\mathrm{ad}} \dot{u} - p_{\mathrm{b}}. \tag{10.45}$$

Substituting from Eq. (10.44) and multiplying through by G gives

$$G p_{\mathrm{d}} = G \left[p_{\mathrm{f}} + \frac{1}{C_{\mathrm{as}}} \int u \, dt + R_{\mathrm{as}} u + M_{\mathrm{ad}} \dot{u} \right] - G \sum_j a_j \, p_{\mathrm{b}j}. \tag{10.46}$$

The left-hand side is just i (from the circuit or from Eqs. (10.34)). In the first term on the right, we substitute for G from Eq. (10.38) and take the bracketed expression inside the resulting summation. In the last term on the right, we take G inside the summation and substitute from Eq. (10.43). The result may be written

$$i = \sum_j G_j \, p_{\mathrm{d}j} \tag{10.47}$$

where

$$p_{\mathrm{d}j} = p_{\mathrm{f}} + \frac{1}{C_{\mathrm{as}}} \int u \, dt + R_{\mathrm{as}} u + M_{\mathrm{ad}} \dot{u} - p_{\mathrm{b}j}. \tag{10.48}$$

Eqs. (10.47) and (10.48), together with the earlier Eq. (10.41) and the electrical components of the driver, are modeled by the circuit of Fig. 10.4, in which we take $n = 3$ for the purpose of illustration. Because the back e.m.f. e is simply the voltage at node 2 relative to ground, it is written "in the node" to save space in the diagram. The developed pressures $p_{\mathrm{d}1}$ to $p_{\mathrm{d}3}$ cannot be similarly treated and must be shown as separate pressure drops. On the acoustic side of the circuit, grounded terminals are included to facilitate the labeling of pressures. In the equivalent circuit of the interior of the box (see next heading), the number of ground connections will be greater than the number shown in Fig. 10.4.

In summary, if the diaphragm area is shared among several volume elements, the equivalent circuit is modified as follows:

- the transconductance is partitioned in the same proportions as the diaphragm area;
- The ratio of the j^{th} partial flux to the common back e.m.f., and of the j^{th} partial current to the j^{th} developed pressure, is the j^{th} partial transconductance.

These changes are quite intuitive, especially when it is remembered that the total developed pressure is a weighted average of the individual developed pressures: at low frequencies, these developed pressures are nearly equal, so that the partial transconductance may be understood as the ratio of the partial flow on one side of the transducer to the common effort on the other side, for both directions of transduction.

10.2 The interior of the box

To avoid consuming unreasonable amounts of CPU time during experiments, the equivalent circuits constructed in this chapter will model the interior of the box as a two-dimensional network, with volume elements extending across the full `width`

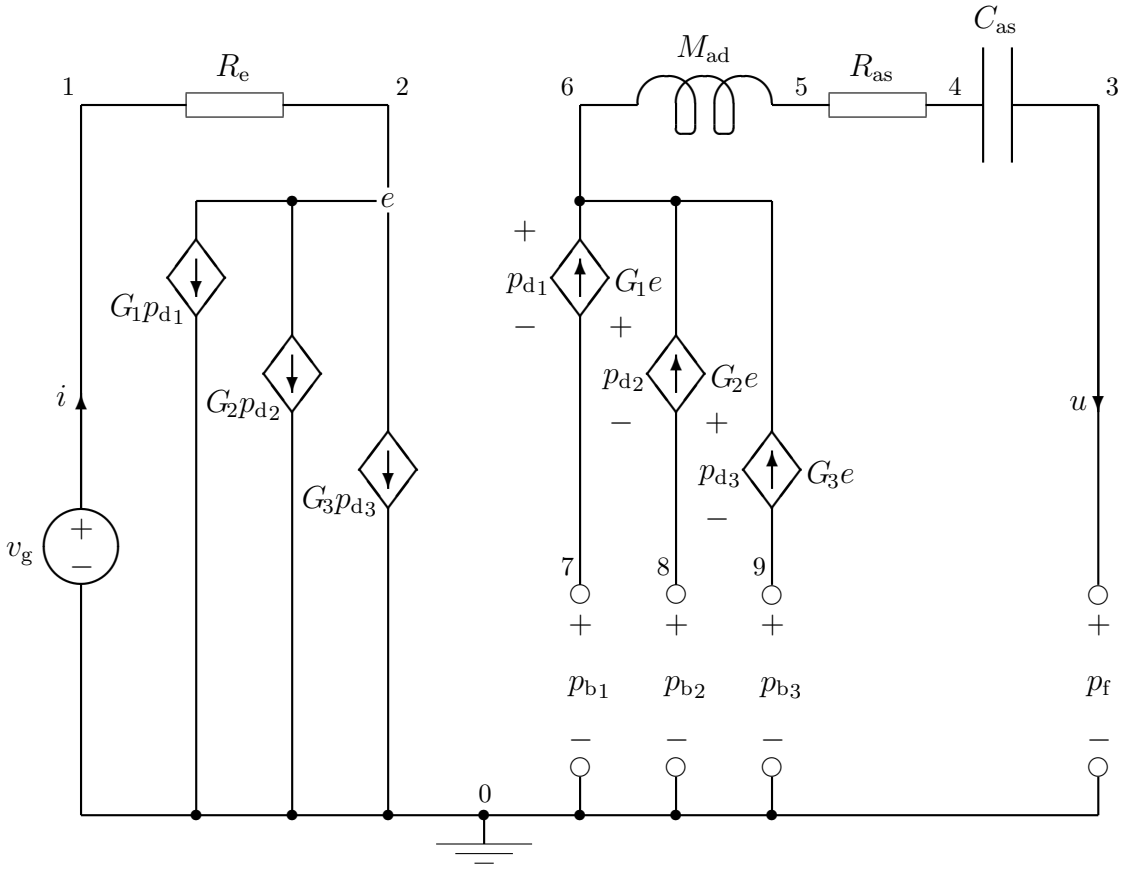

Figure 10.4: *Electroacoustic circuit of a moving-coil driver whose diaphragm area is shared between n volume elements, for n = 3. The back e.m.f. is written "in the node".*

of the box. This is a reasonable approximation not only because the `width` is the smallest overall dimension in the given examples, but also because the driver-box geometry is symmetrical in the `width` direction, so that the fundamental left-right resonance of the box, unlike the fundamental vertical and front-back modes, cannot be excited. Thus the *effective* element size in the left-right direction is half the overall `width`, whereas the element sizes in the other two directions (`delx` and `dely`) can be made arbitrarily small.

The FDEC components may be calculated from the formulae in Chapters 6 and 7, in which $h_u \Delta u$ and $h_v \Delta v$ are replaced by Δx and Δy respectively, and $h_w \Delta w$ is replaced by `width`, which will be abbreviated "w" in the following discussion.

When these substitutions are made in Eq. (6.38), the undamped compliance element is found to be

$$\Delta C = \frac{w \, \Delta x \, \Delta y}{\gamma P_0}. \tag{10.49}$$

The damped compliance element is ΔC_a in parallel with the series combination of ΔR_{th} and ΔC_{th}. From Eqs. (7.82) and (7.85),

$$\Delta C_a = \frac{(1-f) \, w \, \Delta x \, \Delta y}{\gamma P_0} = (1-f) \, \Delta C \, , \tag{10.50}$$

whence Eqs. (7.116) and (7.117) may be used without modification to find ΔR_{th} and

ΔC_{th}. In the circuit diagram, the combination of ΔC_{a}, ΔR_{th} and ΔC_{th} will be given the symbol "X_C" (in SPICE, the name of a subcircuit instance begins with "`X`").

The undamped inertance elements, given in general orthogonal coordinates by Eqs. (6.39) to (6.44), reduce to two cases:

$$\Delta M_x = \frac{\rho_{\mathrm{o}} \Delta x}{w\, \Delta y} \tag{10.51}$$

$$\Delta M_y = \frac{\rho_{\mathrm{o}} \Delta y}{w\, \Delta x}. \tag{10.52}$$

The boundary inertance element between the j^{th} segment of the diaphragm area and the adjacent compliance element has length $\Delta x/2$ and area S_j, so its inertance may be estimated as

$$\Delta M_j = \frac{\rho_{\mathrm{o}} \Delta x/2}{S_j}. \tag{10.53}$$

The damped inertance element in the x direction is $\Delta M_{x\mathrm{a}}$ in series with the parallel combination of ΔR_x and $\Delta M_{x\mathrm{f}}$. From Eqs. (7.28) to (7.30), we obtain the values

$$\Delta M_{x\mathrm{a}} = \frac{\rho_{\mathrm{o}} \Delta x}{(1-f)\, w\, \Delta y} = \frac{\Delta M_x}{1-f} \tag{10.54}$$

$$\Delta R_x = \frac{\lambda\, \Delta x}{(1-f)\, w\, \Delta y} = \frac{\lambda\, \Delta M_{x\mathrm{a}}}{\rho_{\mathrm{o}}} \tag{10.55}$$

$$\Delta M_{x\mathrm{f}} = \frac{f \rho_{\mathrm{f}} \Delta x}{(1-f)^2 w\, \Delta y} = \frac{f \rho_{\mathrm{f}} \Delta M_{x\mathrm{a}}}{(1-f)\, \rho_{\mathrm{o}}}. \tag{10.56}$$

The corresponding components for the y direction are

$$\Delta M_{y\mathrm{a}} = \frac{\rho_{\mathrm{o}} \Delta y}{(1-f)\, w\, \Delta x} = \frac{\Delta M_y}{1-f} \tag{10.57}$$

$$\Delta R_y = \frac{\lambda\, \Delta y}{(1-f)\, w\, \Delta x} = \frac{\lambda\, \Delta M_{y\mathrm{a}}}{\rho_{\mathrm{o}}} \tag{10.58}$$

$$\Delta M_{y\mathrm{f}} = \frac{f \rho_{\mathrm{f}} \Delta y}{(1-f)^2 w\, \Delta x} = \frac{f \rho_{\mathrm{f}} \Delta M_{y\mathrm{a}}}{(1-f)\, \rho_{\mathrm{o}}}. \tag{10.59}$$

The subcircuits representing the damped inertance elements will be called X_{Mx} for the x direction and X_{My} for the y direction. In the x direction there is also a group of elements, denoted by $X_{M\mathrm{b}}$, which straddle the boundary between the undamped and damped regions. Each of these elements comprises an undamped inertance in series with a damped inertance, each inertance being of length $\Delta x/2$ instead of Δx. Hence $X_{M\mathrm{b}}$ comprises an inertance $(\Delta M_x + \Delta M_{x\mathrm{a}})/2$ in series with the parallel combination of $\Delta R_x/2$ and $\Delta M_{x\mathrm{f}}/2$.

With the above definitions of the components and subcircuits, the equivalent circuit of the interior of the box is as shown in Fig. 10.5. For the purpose of illustration it is assumed that the diaphragm area is shared among three volume elements (as in Fig. 10.4), that the clear region behind the driver is two elements deep, and that the fiber-filled region is three elements deep and five elements high; these dimensions differ from those of the models constructed and analyzed later in this chapter. Where a compliance element is to be connected between a node and ground, the

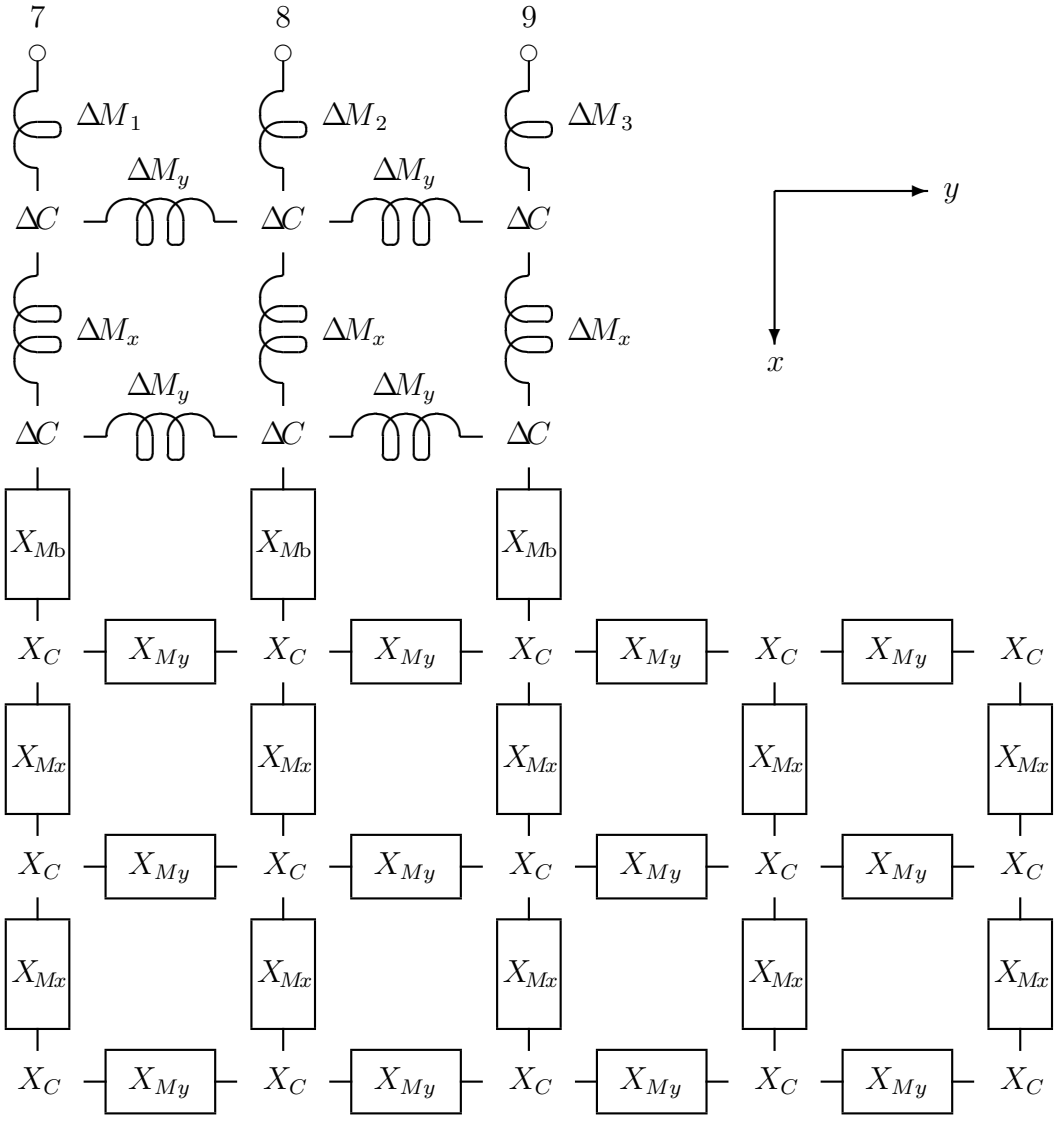

Figure 10.5: *Two-dimensional finite-difference equivalent circuit for the interior of the box in Fig. 10.1, with* `clear` $= 2\,\Delta x$, `depth` $= 5\,\Delta x$, `D` $= 3\,\Delta x$ *and* `height` $= 5\,\Delta x$. *Coordinate directions are indicated by the labeled axes. Rectangular blocks represent lossy mass elements; the "$X_{M\mathrm{b}}$" elements straddle the boundary between the clear and fiber-filled regions. "ΔC" denotes an undamped compliance element and "X_C" a damped compliance element; when either of these symbols appears at a node, the corresponding element is connected between that node and ground. Subcircuit names begin with "X". The node numbers at the top indicate where this circuit should be connected to that of Fig. 10.4. As explained in the text, boundary elements ΔM_1 to ΔM_3 may be combined in parallel and added to M_{ad} in Fig. 10.4, in which case the nodes connected to the top three "ΔC" elements will be renumbered 7, 8 and 9.*

compliance symbol is written "in the node". This convention, when combined with the small number of elements, gives a clear and uncluttered diagram. It also explains why no ground connections are visible.

The equivalent circuit of the driver-box combination can be simplified slightly by comparing the pressure drops across the inertance elements adjacent to the driver. The pressure difference across ΔM_j is

$$\Delta M_j \dot{u}_j = \frac{\rho_o \Delta x/2}{S_j} \frac{S_j \dot{u}}{S} = M_{ab} \dot{u} \tag{10.60}$$

where

$$M_{ab} = \frac{\rho_o \Delta x/2}{S}. \tag{10.61}$$

In words, the pressure drop across each ΔM_j is the same as that which would result from the entire flux u flowing through the inertance M_{ab}. Hence the sums of voltage drops around the acoustic mesh of Fig. 10.4 will be preserved if we omit each ΔM_j and lump M_{ab} in series with M_{ad}. The inertance M_{ab} may be recognized as the parallel combination of all the ΔM_j elements or as an inertance of length $\Delta x/2$ whose cross-sectional area is the diaphragm area. In effect, M_{ab} is an air load behind the driver ("b" for "back" or "behind") and is added to M_{ad} in order to compensate for the omission of the first layer of inertance in the finite-difference equivalent circuit of the box interior.

10.3 Description of modeling programs

The model-building program `box.c` (listed in Section B.9) converts the parameters of the driver and box into an equivalent circuit specification to be processed by SPICE. Hence some familiarity with SPICE is assumed in the following description.

The model-builder uses the `#define` preprocessor command to specify the dimensions of the box, the parameters of the driver and fiberglass filling, the frequency range for the simulation, and the desired volume element size. The actual element dimensions are called `delx` in the x direction (horizontally towards the back of the box) and `dely` in the y direction (vertically), and are computed subject to the restriction that `depth` and `height` must be multiples of `delx` and `dely` respectively. The driver parameters are taken from a locally available catalog [1] and the fiberglass specifications are the same as those used by Leach [30].

From the element sizes and box dimensions, the model-builder must compute the number of volume elements in each coordinate direction and write the circuit definition with the appropriate node numbers. The circuit definition is written to the file "`cct`" and the SPICE command script for analyzing the circuit is written to the file "`go`". When SPICE is invoked, the files `cct` and `go` are sourced either manually or by the `.spiceinit` file. The half-space frequency response of the speaker is graphed on-screen, and the points of the graph are simultaneously written to a file; the name of this output file is given as a command-line argument to the program `box.c`, which copies it into the script `go`.

To facilitate comparison of frequency responses, the program "`sp2tex.c`" (listed in Section B.11) turns the SPICE output files into graphs which can be viewed on-screen or imported into documents. The graph-drawing program accepts one or two input files, allowing two frequency responses to be superimposed on one graph.

10.3.1 Command-line options

In addition to the name of the SPICE output file, the model-building program accepts optional command-line switches indicating that some components are to be omitted from each equivalent-circuit cell (for the command-line syntax, see the listing in Section B.9). With no switches, `box.c` does a "full simulation"; that is, it uses the full equivalent circuits of Figs. 7.1 and 7.2. The following mutually-exclusive switches cause certain components to be omitted from the mass elements (Fig. 7.1) in both the x and y directions:

free (-f) : Resistance to air motion is ignored; ΔM_{ua} and ΔR_u are shorted out (valid at very high frequencies);

stiff (-s) : The fiber does not move; ΔM_{uf} is omitted (valid at sufficiently high frequencies);

unison (-u) : The fiber moves with the air; ΔR_u is omitted (valid at very low frequencies).

Another three mutually-exclusive switches indicate that certain components are to be omitted from the compliance elements (Fig. 7.2):

adiab (-a) : Compression of the air is adiabatic; ΔC_{th} and ΔR_{th} are omitted (valid at very high frequencies);

nearad (-n) : Compression is near-adiabatic; ΔC_{th} is shorted out (valid at sufficiently high frequencies);

equil (-e) : Thermal equilibrium; ΔR_{th} is shorted out (valid at sufficiently low frequencies).

If the following switch is present, it overrides all others:

lumped (-l) : The volume of the box is modeled as a lumped compliance and the fiber is ignored; this gives the classical equivalent-circuit model.

If the **free** and **adiab** switches are used together, they give the so-called **undamped** condition. This condition is equivalent to removing the fiber, except that the volumes and cross-sectional areas of the elements are multiplied by $(1 - f)$. (The use of fiber-reduced areas ensures that the **free**, **adiab** and **undamped** conditions are exact high-frequency limits of the full simulation. If the full areas and volumes are desired, the filling factor should be set to a very small value.) In the following text, the names of most switches will be printed consistently in bold type; the exceptions are "lumped" and "undamped", which are more self-explanatory than the others.

The model-builder makes extensive use of SPICE subcircuits for the inertance and compliance elements, so that the node-numbering code is not affected by the omission of selected components from the FDEC elements. In the subcircuits, every opportunity is taken to lump series or parallel components so as to minimize the numbers of components and nodes.

10.3.2 Circuit modifications required by SPICE

A well-known feature of SPICE, which prevents many errors in the analysis of nonlinear electronic circuits, is that every AC analysis is automatically preceded by a DC operating-point analysis. This has two consequences which are inconvenient for present purposes. First, every node must have a finite-resistance DC path to ground in order to avoid a singular-matrix error. If part of the circuit "floats", every nodal voltage in the floating section contains an arbitrary constant. Thus the solution is not unique, wherefore the system equations must have a singular coefficient matrix. Second, every loop must have a non-zero DC loop resistance; otherwise the loop current is indeterminate and adds an arbitrary constant to every branch current in the loop.

Unless the **nearad** approximation is used, the compliance elements do not provide a DC path to ground, so that nodes 4 to 7 in Fig. 10.3 are left floating. To correct this, $C_{\rm as}$ is bypassed by a large resistance $R_{\rm leak}$, whose value is chosen (somewhat arbitrarily) so that $R_{\rm leak}C_{\rm as} = 1000\,$seconds. The long time constant ensures that the leakage resistor has negligible effect at audio frequencies. The added resistor provides a DC path from ground to every node in the FDEC model of the box interior, via the FDEC inertance elements. It does not increase the node count and therefore does not represent a significant computational penalty.

The requirement of non-zero loop resistances is a more serious problem because the inertance elements form an array of loops and, unless the **stiff** approximation is used, every inertance element is a short circuit for DC. To remove the shorted loops, a small resistance must be connected in series with each of the inertance elements in either the x or the y direction. Program "`box.c`" chooses the x direction; hence, in Fig. 10.5, ΔM_x must be replaced by a subcircuit, and the subcircuit X_{Mx} must be modified. The series resistance is denoted by $\Delta R_{x\rm s}$ and its value is chosen so that $\Delta M_x/\Delta R_{x\rm s} = 1000\,$seconds. Unfortunately the added resistances substantially increase the node count, wasting storage space and CPU time. (For the sake of consistency, and to ensure that the **stiff** approximation is an exact high-frequency limit of the full simulation, $\Delta R_{x\rm s}$ is included in the **stiff** approximation, but it is lumped with ΔR_x so as not to increase the node count.)

10.3.3 Program limitations

The two programs used in the present chapter are research prototypes only. Three limitations of the model-building program should be noted here:

- As explained in Section 10.2, the model of the box interior is two-dimensional. If it were extended to three dimensions, subcircuits would be required for the undamped and damped inertance elements in the z direction, and the `for`-loops for writing out the compliance and inertance elements would be nested three-deep. The avoidance of zero-resistance loops would require small resistances in series with the inertance elements in two of the three coordinate directions.

- The area of the diaphragm is assumed to be divided equally between the volume elements immediately behind the driver. In effect, this assumes that the driver area is uniformly distributed vertically, whereas the two-dimensional approximation assumes that the area is uniformly distributed horizontally.

Hence the errors caused by the two approximations should be of the same order of magnitude.

- No allowance is made for the magnet structure and the basket, which partially obstruct the rear of the diaphragm. Accuracy in calculating the area fractions would be futile unless the obstructions were modeled by means of additional acoustic elements and boundaries.

Production versions of the programs would require numerous other improvements, some of which are mentioned with the listings in Appendix B.

Clearly this is a theoretical thesis and not a software development project, so that some limitations in the software are inevitable. At their present level of development, the programs written for this chapter illustrate the techniques developed in Chapters 6 and 7, show the effect of fiber filling, allow investigation of the influence of various fiber parameters, and—most importantly—are a quantum improvement on any analysis that neglects the spatial variation of the pressure inside the box.

10.4 10-inch woofer in 36-liter box

The listing of `box.c` in Section B.9 has the parameters set for a 10-inch woofer with a polypropylene cone [1]. The box dimensions are

$$\texttt{D} = \texttt{width} = 250\,\text{mm}$$

$$\texttt{depth} = 300\,\text{mm}$$

$$\texttt{height} = 600\,\text{mm}$$

$$\texttt{clear} = 100\,\text{mm}.$$

These are the dimensions which are used for all simulations in this section, and for which Fig. 10.1 is drawn to scale. The resulting internal box volume is 36.25 liters. Unless otherwise noted, all simulations in this section use an element size of 50 mm. The same element size is specified in the version of `box.c` listed in Section B.9. In Section B.10 is a listing of the "`cct`" file produced by that version of `box.c` for the full simulation.

Much of the following discussion compares the results of the full simulation with those of the various approximations, showing how the properties of the fiber affect the frequency response. Because of the large number of graphs to be compared and the numerous features to be explained, the discussion is long and tends to become mired in detail. But four clear points will emerge:

- Viscosity is the dominant mechanism of damping, thermal relaxation being of secondary importance.

- The decision to neglect internal elastic forces in the fibers is vindicated.

- The departure from thermal equilibrium (at frequencies over a few hundred hertz) has very little effect on the response.

- While the addition of fiber increases the output at infrasonic frequencies, it *reduces* the output in the bass rolloff region and does *not* lower the 3 dB rolloff frequency. This conclusion applies not only to the overall effect of the fiber, but also to the thermal capacity alone; the latter finding may be regarded as surprising.

Of course these conclusions apply to the system under study; that they are true for one case does not imply that they are true for all. But neither can they be lightly dismissed as "anecdotal". Concerning the first observation, the influences of viscous and thermal damping are of different orders of magnitude. The second observation is expected for reasons given in Subsection 7.1.1. Physical explanations for the third and fourth observations are offered below, with reference to the relevant graphs. A final point relevant to all observations is that the specifications of the driver-box-fiber system were partly arbitrary and partly determined by the availability of published data—they were not chosen with a view to illustrating or supporting the above conclusions, all of which emerged "after the fact".

10.4.1 Full simulation

The frequency response predicted by the full simulation is shown in Fig. 10.6. At the lowest frequencies, for which the wavelength is much longer than the box dimensions, the curve is smooth. At the highest frequencies, for which the diaphragm acceleration is determined by the moving mass of the driver, the curve is again smooth. At intermediate frequencies, the curve exhibits ripples due to the internal resonances of the box; this feature is not predicted by classical equivalent-circuit models.

For comparison between the full simulation and the various approximations, the curve in Fig. 10.6 will be reproduced in most of the subsequent graphs in this section. Each comparison will be accompanied by some explanation of the similarities and differences. The explanations may be tentative and will certainly not be exhaustive—if it were possible to explain every nuance of the graphs in words, it would hardly have been necessary to develop the numerical techniques for computing the curves—but they will at least mention the frequency range for which the approximation should be valid, and the implications of the comparison concerning the importance of particular fiber properties.

10.4.2 Undamped response and effect of fiber filling

Fig. 10.7 compares the **undamped** approximation with the full simulation. The undamped frequency response is computed and plotted at 100 points per decade, whereas all the other frequency responses in this chapter are computed and plotted at only 50 frequencies per decade. (The "`go`" file for the undamped model was manually edited to increase the resolution of the AC analysis.)

As the **undamped** approximation is a high-frequency approximation, the two curves are indistinguishable at the highest frequencies. At very low frequencies, the presence of fiber increases the heat capacity, and hence the compliance, of the box, so that the full simulation gives more output. But this is not to say that the addition of fiber extends the bass response; on the contrary, the full simulation shows *less* output between 50 Hz and 150 Hz, because the fiber damps the motion

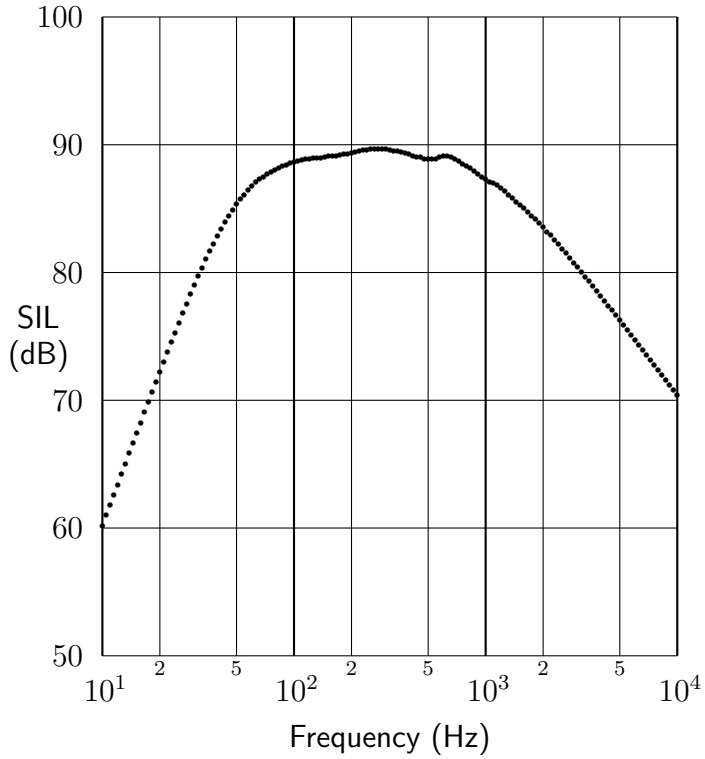

Figure 10.6: *Half-space SIL vs. frequency for a 10-inch woofer in a 36-liter box; full simulation. The SIL (sound intensity level) is the IL at one meter, assuming isotropic radiation into half-space and constant parallel radiation resistance.*

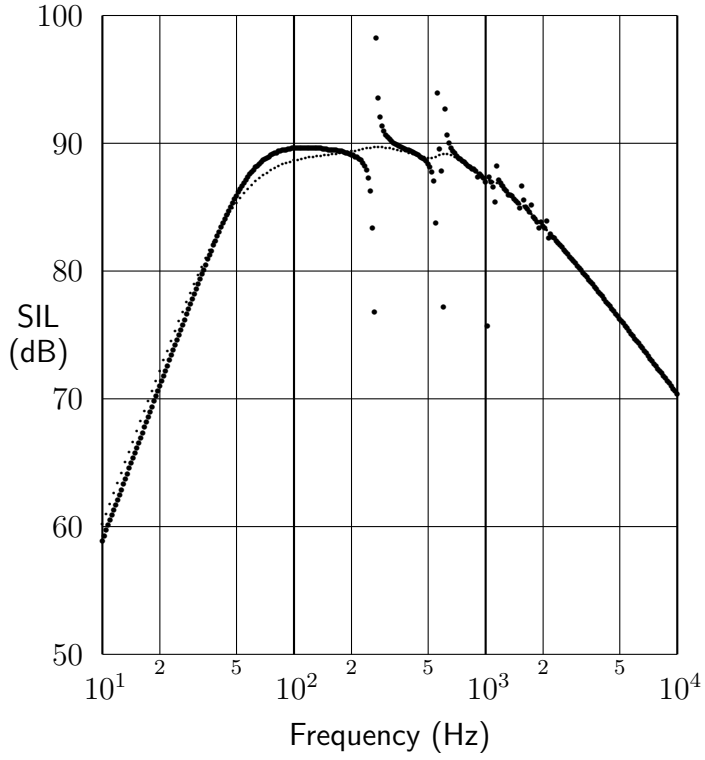

Figure 10.7: *Undamped approximation (large dots) and full simulation (small dots).*

of the diaphragm and/or increases the effective moving mass.[4] In the intermediate frequency range, where the full simulation shows a few ripples, the undamped model has a series of sharp peaks and troughs. The salient features of this series are:

- The maxima and minima alternate as frequency increases;
- Each minimum is followed by a maximum at a marginally higher frequency; then there is a larger frequency gap before the next minimum.

The minima are readily explained in terms of the box impedance, i.e. the acoustic impedance seen by the diaphragm looking into the box. This impedance must be purely imaginary (because the box interior, according to the undamped model, is non-dissipative) and must have poles on the imaginary axis (corresponding to the natural frequencies of the box interior when the diaphragm is held stationary). At the pole frequencies of the box impedance, the diaphragm cannot move, so there is no output. Hence the troughs in Fig. 10.7 theoretically extend to $-\infty$ dB. That they appear to be of finite depth is due mainly to the finite resolution of the graph, and partly to the small resistances which are added to the horizontal inertance elements to avoid singular-matrix errors.

As a matter of interest, the first minimum in the undamped response is at about 263 Hz, corresponding to a wavelength of about 1.3 m, which is slightly more than twice the interior height of the box, and slightly less than twice the centerline-length of the L-shaped cavity behind the driver. So the first minimum can be understood as the half-wave resonance.

The peaks in the undamped frequency response occur *not* at the zeros of the box impedance, but at the frequencies for which the box reactance cancels the net reactance that appears in series with it on the acoustic side of the equivalent circuit. At the frequencies under discussion, the dominant reactance in series with the box is that due to the moving mass of the driver, which is inductive, so that the box reactance at the peak frequencies must be capacitive. Now the box reactance is capacitive at frequencies just above the pole frequencies (because the compliance of every region increases with frequency) and inductive at frequencies just below.[5] This observation alone explains why, as frequency increases, a maximum follows a minimum more closely than it is followed by the next minimum. The effect is exaggerated by the generally low impedance of the box compared with that of the moving mass of the driver; only near the poles does the box reactance become large enough (in absolute value) to cancel that of the moving mass. Hence the minima and maxima in Fig. 10.7 occur in closely-spaced pairs, with each pair corresponding to one resonant mode of the box. (Between 500 Hz and 700 Hz are two resonances which are barely resolved by the graph; the points at 83.5 dB and 94 dB belong to the first resonance, while those at 77 dB and 92.5 dB belong to the second.)

Chapter 1 mentioned the work of Sakai et al. [47], who combined a finite-*element* model of an undamped enclosure with a simple formula expressing the sound pressure

[4] In 1970, Barlow warned that if one uses enough fiber to approach the maximum compliance, "the absorption is excessive and there is no extension of the extreme bass" [6, p. 276].

[5] Of course these properties are shared by the impedance of any lumped passive L-C network, and the box interior is indeed modeled as such a network. However, because of the multiple transconductances used to model the driver, the box impedance does not appear at a single point in the equivalent circuit, so it is not convenient to use general properties of passive L-C networks in the above discussion.

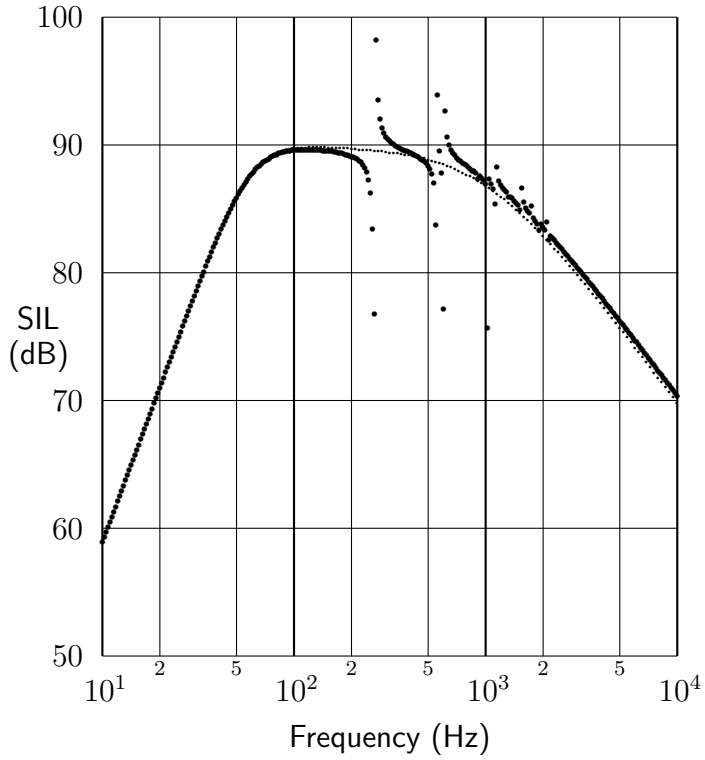

Figure 10.8: *Undamped approximation (large dots) and lumped approximation (small dots).*

level in terms of the enclosure impedance, and thus predicted the frequency response of a moving-coil driver in an undamped enclosure. The frequency responses obtained by Sakai et al. were qualitatively similar to the undamped response in Fig. 10.7, except that the peaks were infinitely high (because *all* damping was neglected, including that in the driver suspension), and the high- and low-frequency rolloffs were not predicted (because the formula for the sound pressure level was accurate only in the midband).

10.4.3 FDEC and lumped-box models

At low frequencies, all the compliance elements in the **undamped** approximation are effectively in parallel (because the inertance elements have low impedances) and their sum is equal to the total box compliance as used in the **lumped** approximation. Hence the lumped model is the low-frequency limit of the undamped model. This is confirmed by Fig. 10.8, which compares the undamped and lumped approximations; the two curves appear to merge at low frequencies.

At high frequencies, according to both the lumped and the undamped approximations, the acceleration of the diaphragm is limited by its effective moving mass. But the two approximations use different estimates of the air load behind the driver; the lumped approximation uses the low-frequency radiation inertance M_{ar}, while the undamped approximation relies on the FDEC components. At the highest frequencies, the FDEC model gives a back air load of M_{ab}, which is less than M_{ar}; therefore the undamped FDEC model predicts a slightly smaller moving mass, and hence slightly more output, at high frequencies.

At intermediate frequencies, the lumped model predicts that the diaphragm mo-

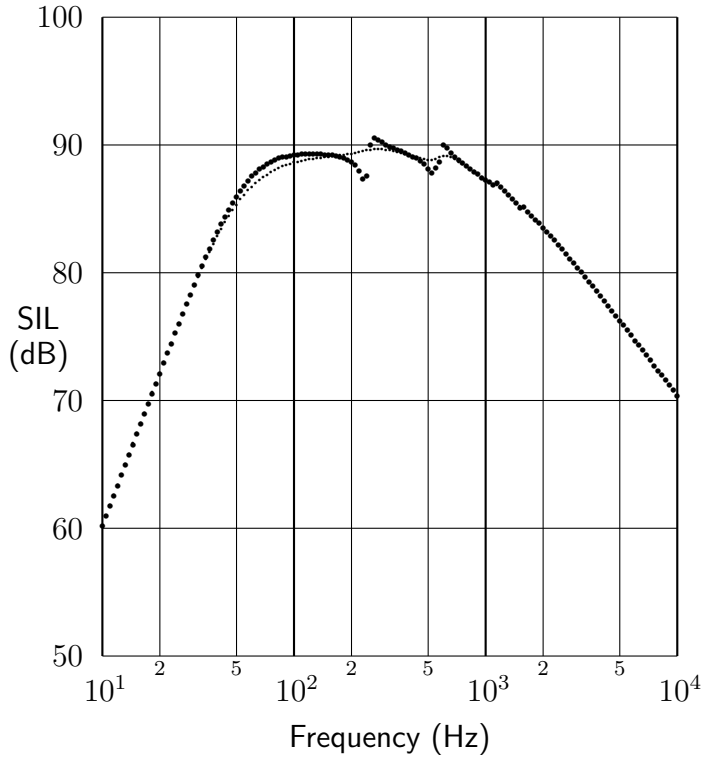

Figure 10.9: *"Free" approximation, for which viscosity is neglected (large dots), and full simulation (small dots).*

tion is determined by the moving mass, giving a smooth curve, while the undamped model is dominated by resonances.

In the lumped model, the number of circuit nodes is fixed; but in the full simulation and all other approximations, the external node count[6] depends only on the element size, while the subcircuits connecting the nodes depend on the approximation in use. Hence the agreement between the lumped and undamped models at low frequencies (for which all the compliance elements in the undamped model contribute to the response) is evidence that the program "`box.c`" calculates the correct compliances and connects them to the correct nodes. If the node-numbering is correct for the undamped model, it is also correct for the other finite-difference models.

10.4.4 Importance of viscous damping

The two approximations that neglect viscous losses but allow for thermal relaxation are the **free** model, which assumes that there is no resistance to air motion through the fiber (zero viscosity), and the **unison** model, which assumes that the fiber moves with the air (infinite viscosity). The resulting frequency responses are compared with that of the full simulation in Figs. 10.9 and 10.10, respectively. In each graph, the substantial difference between the two curves is due to viscous losses and shows that viscosity is an important mechanism of damping.

In the low-frequency limit, both the **free** and **unison** models agree with the full

[6]The "external" node count includes the terminal nodes of SPICE subcircuits, but not their internal nodes.

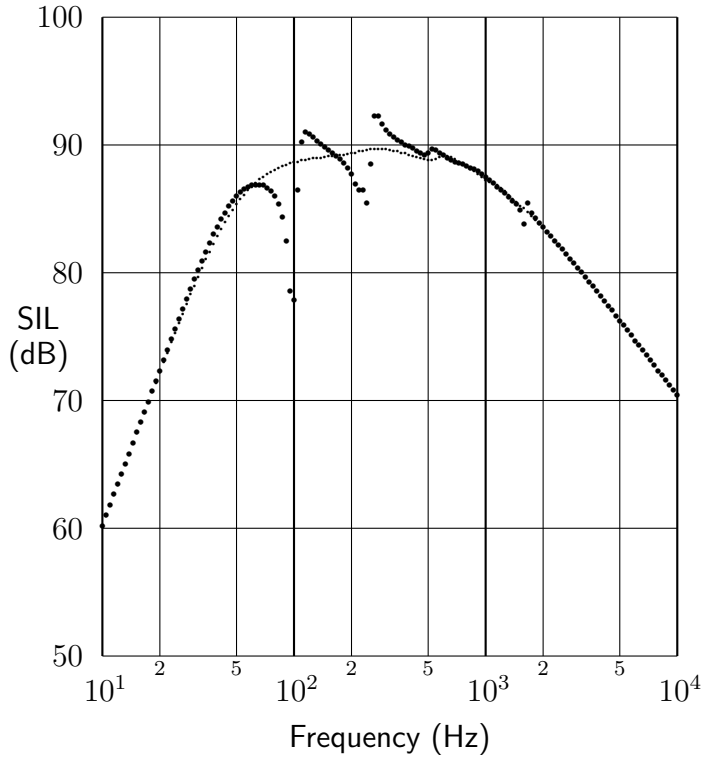

Figure 10.10: *"Unison" approximation, for which the fiber is assumed to move with the air (large dots), and full simulation (small dots).*

simulation because the driver excursion is limited by the box compliance. They also agree in the high-frequency limit because the acceleration is limited by the effective moving mass of the driver, which at high frequencies is not greatly affected by the mass of the fiber, being isolated therefrom by the compliance of the fiber-free region. Compared with the **free** model, the full simulation gives less output between 50 Hz and 150 Hz because the fiber damps the air motion and/or adds to the effective moving mass; at lower frequencies, the fiber still adds to the moving mass, but this effect is swamped by the limited compliance of the box. Compared with the **unison** model, the full simulation gives less output around 50 Hz, probably because it predicts greater damping of the fundamental resonance.

The **unison** response has larger moving masses, hence lower resonance frequencies, than the **free** model. The **unison** model also has a minimum-maximum pair at about 1600 Hz, caused by the horizontal half-wave resonance of the fiber-free region. At the boundary between the clear and fiber-filled regions there is a change in density, hence a change in impedance, hence a reflection. In the full simulation, the acoustic mass elements due to the mass of the fiber are bypassed by resistance elements. According to the "`cct`" file, the pneumatic resistivity of the fiber is 1121 $\mathrm{Pa\,s\,m^{-2}}$, so that it would require a 37 cm depth of fiber to produce a resistance-area product equal to $\rho_o c$. The required depth is much greater than the depth of the fiber-free region behind the driver. So the impedance step is small and the full simulation does not predict a strong reflection at the half-wave resonance of the fiber-free region.

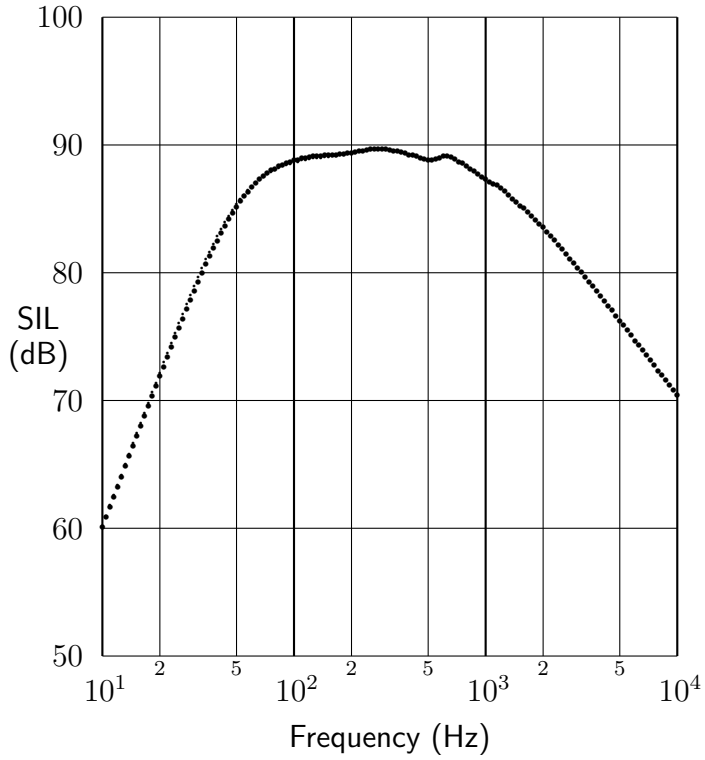

Figure 10.11: *"Stiff" approximation, for which the fiber is assumed stationary (large dots), and full simulation (small dots).*

10.4.5 Unimportance of fiber stiffness

The third approximation affecting the inertance elements is the **stiff** model, which assumes that the fiber remains stationary. In Fig. 10.11, the rigid-fiber model gives almost the same frequency response as the full simulation. *This result supports the decision to neglect restoring forces due to the stiffness of the fibers*; in the example considered, even *infinite* stiffness would have little effect on the result.

Initially the stiffness of the fibers was neglected because it was expected to be small (see Subsection 7.1.1). If even infinite stiffness has little effect, we must conclude that the movement of the fiber is not significant under the operating conditions. In the notation of Fig. 7.1, the **stiff** approximation assumes that most of the flux flows in ΔR_u rather than ΔM_{uf}, which is true at frequencies above $\Delta R_u/(2\pi\Delta M_{uf})$. From the values in the circuit specification file, the transition frequency is about 30 Hz; at frequencies around or below this value, the mobility of the fiber (which is taken into account by the full simulation by not by the **stiff** model) reduces the impedance behind the diaphragm and allows greater output. But at such low frequencies the motion of the diaphragm is limited mainly by the box compliance, whose influence becomes more and more dominant as frequency decreases. Hence, in Fig. 10.11, it can be seen that the full simulation gives slightly more output over a limited frequency range (roughly 20 Hz and 40 Hz), but the difference is barely resolved by the graph (one must look for the vertical displacement between the large and small dots).

The difference between the **unison** and **stiff** models is that ΔM_u in the **unison** model is replaced by ΔR_u in the **stiff** model. As noted above, the resistivity of the fiber (represented by ΔR_u) does not cause a large impedance step at the half-wave

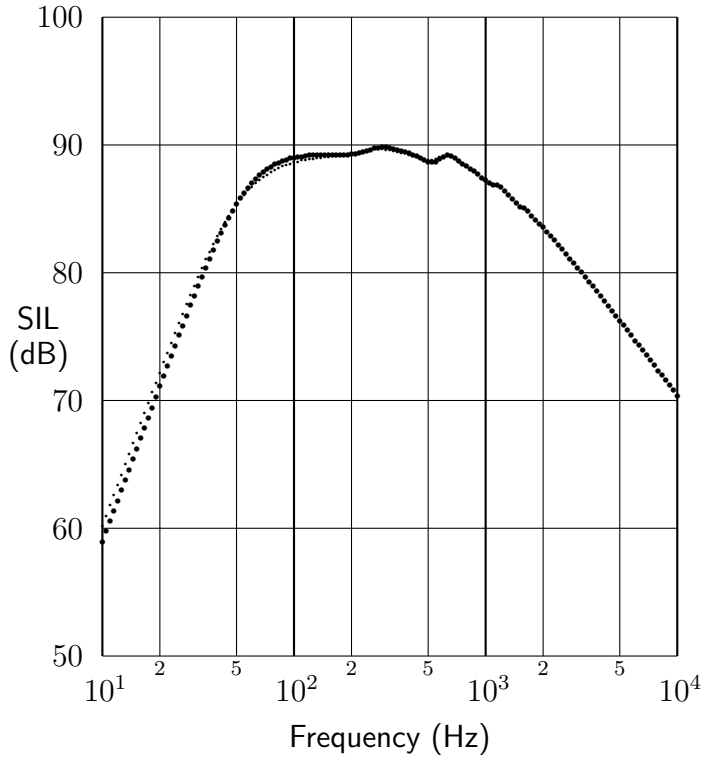

Figure 10.12: *Adiabatic approximation (large dots) and full simulation (small dots).*

resonance frequency of the fiber-free region, so that we should not expect to see such a resonance in the **stiff** frequency response. Fig. 10.11 confirms this.

10.4.6 Secondary importance of thermal relaxation

The two approximations that neglect thermal relaxation but allow for viscous losses are the **adiab** or adiabatic model (infinite thermal resistance) and the **equil** or thermal-equilibrium model (zero thermal resistance), whose frequency responses are compared with that of the full simulation in Figs. 10.12 and 10.13, respectively. In both graphs, the difference between the two curves is due to thermal relaxation. The differences are slight; with the finite resolution of the graphs, the curves for the adiabatic and full simulations are indistinguishable for most of the frequency range, while those for the **equil** and full simulations cannot be distinguished at all. To see that the full simulation gives a slightly smoother frequency response, one must compare these two graphs with Fig. 10.6, in which the response of the full simulation is shown in large dots and not obscured by any other curve.

Thus the neglect of thermal relaxation has little effect on the frequency response, whereas the models that neglect viscous losses while allowing for thermal relaxation (i.e. the **free** and **unison** models, whose results appear in Figs. 10.9 and 10.10) predict very different responses from the full simulation. The contrast between the two classes of models is striking and indicates that *viscosity, not thermal relaxation, is overwhelmingly the dominant mechanism of damping.* Again it should be noted that this conclusion is based on a particular driver-box system.

The close agreement between the **equil** model and the full simulation (Fig. 10.13) is easily explained. The assumption of thermal equilibrium is valid if the reactance of $\Delta C_{\rm th}$ is much greater than $\Delta R_{\rm th}$, which is the case for frequencies well below

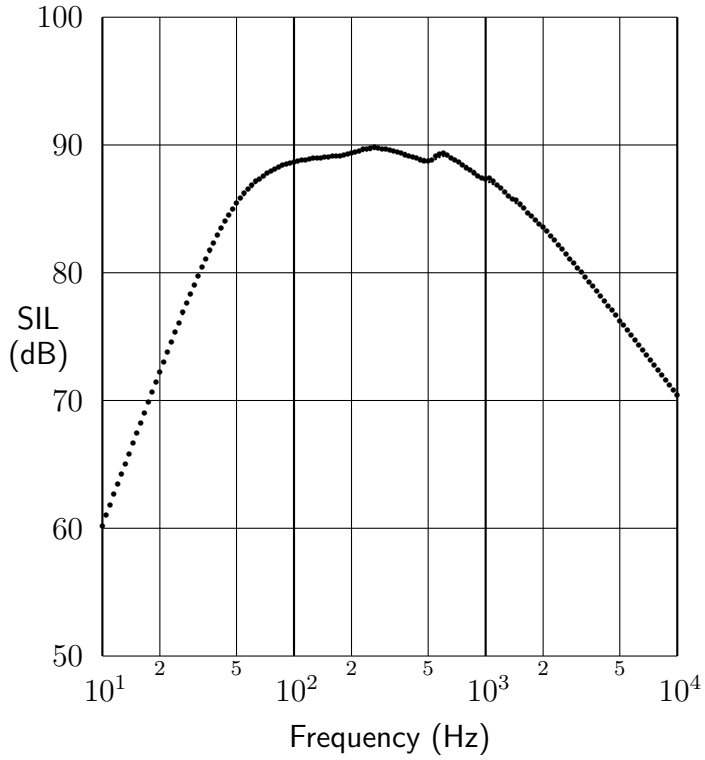

Figure 10.13: *Thermal-equilibrium approximation (large dots) and full simulation (small dots).*

$1/(2\pi\Delta R_{\rm th}\Delta C_{\rm th})$. From the values in the file "`cct`", the transition frequency is 376 Hz, so that the departure from thermal equilibrium is significant for frequencies of a few hundred hertz or more. At these frequencies the acceleration of the diaphragm is controlled mainly by the moving mass, so that *a decrease in compressibility caused by thermal non-equilibrium will have little effect on the acoustic output*. If the travel of the diaphragm were compliance-limited for a range of frequencies extending above the range of thermal equilibrium, the responses predicted by the **equil** and full models would be noticeably different.

The slight difference between the responses predicted by the **adiab** and full simulations (Fig. 10.12) is due to the heat capacity of the fiber. The full simulation gives more output at the lowest frequencies, because the added heat capacity increases the compliance of the box, but gives *less* output between 50 Hz and 150 Hz. One may be tempted to ascribe the latter effect to damping of the driver-box resonance by thermal relaxation. However, as the two curves in Fig. 10.13 are indistinguishable, the **equil** model also gives less output than the adiabatic model in the bass rolloff region, although neither of these models includes damping by thermal relaxation. We can explain this if we note that the **equil** model and the full simulation make the air more compressible in the fiber-filled region than in the fiber-free region and therefore predict greater airflow between the two regions, for a given diaphragm motion, than the adiabatic model. Greater airflow increases the contribution of air load to the effective moving mass, increases viscous losses in the lower reaches of the fiber-filled region, and causes more fiber motion, increasing the contribution of the fiber to the effective moving mass. In short, the difference between the **adiab** and full models in the bass rolloff region is probably due, not to the thermal effects of the fiber alone, but to a cascade effect in which the added heat capacity influences

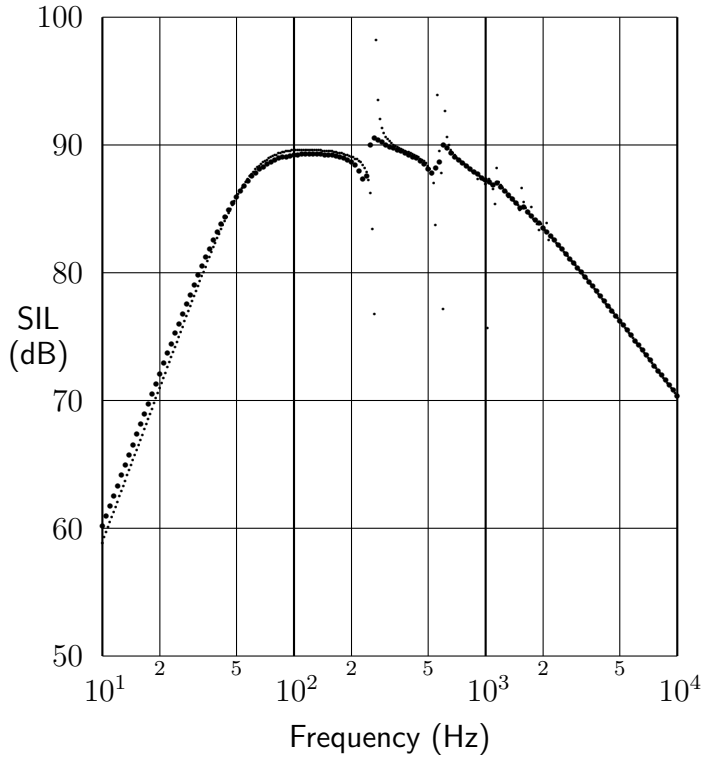

Figure 10.14: *"Free" approximation (large dots) and undamped approximation (small dots).*

the mechanical inertia. Be that as it may, *the example contradicts the theory that the heat capacity of the fiber extends the bass response.*

The adiabatic and full simulations both include viscous damping, but only the latter includes thermal relaxation. There is another pair of models in which only one model includes thermal relaxation while *neither* includes any impediment to the flow of air through the fiber; the two models are the **free** and **undamped** approximations, whose frequency responses are compared in Fig. 10.14. Again we see that the model allowing for thermal relaxation (in this case, the **free** approximation) gives more output at infrasonic frequencies but less output between 50 Hz and 150 Hz. Again the latter effect may be attributed to an increase in the effective moving mass, due to the increased airflow for a given diaphragm motion. We also notice that the resonances in the **free** model, being only lightly damped by thermal relaxation, are easily related to those in the **undamped** model.

The justification of the main findings listed in the introduction to this section is now complete. It remains to discuss one more approximation and investigate the effects of element size, temperature and pressure.

10.4.7 Approximate model of thermal relaxation changes bass rolloff.

The comparison between the **free** and **undamped** models has interrupted the sequence of approximations involving the compliance elements. The third approximation in that sequence is the **nearad** or near-adiabatic model, which approximates the compliance elements as the **stiff** model approximates the inertance elements;

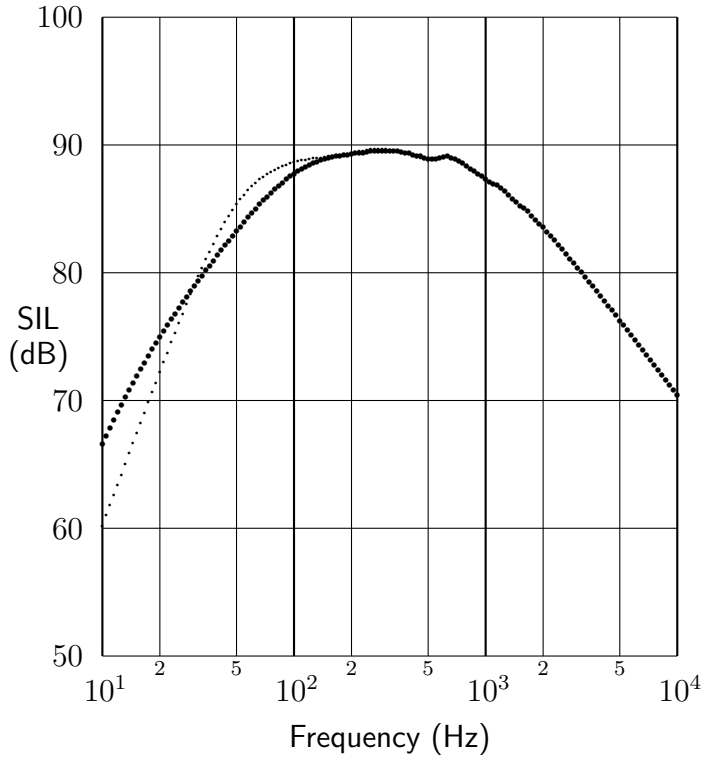

Figure 10.15: *"Near-adiabatic" approximation, for which $\Delta C_{\rm th}$ is shorted (large dots), and full simulation (small dots).*

both models are valid at high frequencies and both represent the damping by means of a single resistance. But because the **nearad** model affects the compliance elements, it gives a much greater error at low frequencies, for which the motion of the diaphragm is compliance-limited. Hence the **nearad** model is unsuitable for calculations involving the bass rolloff. But it is discussed here for the sake of completeness.

The **nearad** approximation includes $\Delta R_{\rm th}$ but neglects the pressure drop across $\Delta C_{\rm th}$, replacing $\Delta C_{\rm th}$ with a short circuit. In physical terms, this means that there is not enough heat conduction to make the added heat capacity significant, which is a valid assumption at sufficiently high frequencies. At low frequencies the **nearad** model becomes an absurdity because it implies that the volume element is a resistance instead of a compliance. If the diaphragm motion is mass-limited in the midband, the bass rolloff is first-order for a resistive box and second-order for a compliant box. Fig. 10.15, which compares the **nearad** and full simulations, confirms this behavior.

It must be emphasized that the near-adiabatic approximation does *not* simply assume that the fiber is an infinite heatsink. The infinite-heatsink approximation saves no computation time because it does not eliminate $\Delta C_{\rm th}$, but causes $\Delta C_{\rm th}$ to assume the finite limiting value of $(\gamma - 1)\Delta C_{\rm a}$ (see Eq. (7.94)). The physical effect of an infinite heatsink is that the compression becomes isothermal as frequency approaches zero. Under isothermal conditions the air in the box is still a compliance, not a resistance as predicted by the **nearad** model.

Because the **nearad** model does not entirely neglect damping due to thermal conduction, it predicts a smoother frequency response, and agrees more closely with the full simulation, than the **adiab** model at frequencies between 200 Hz and 2 kHz. Thus the **nearad** model is valid over a wider frequency range, in spite of its gross

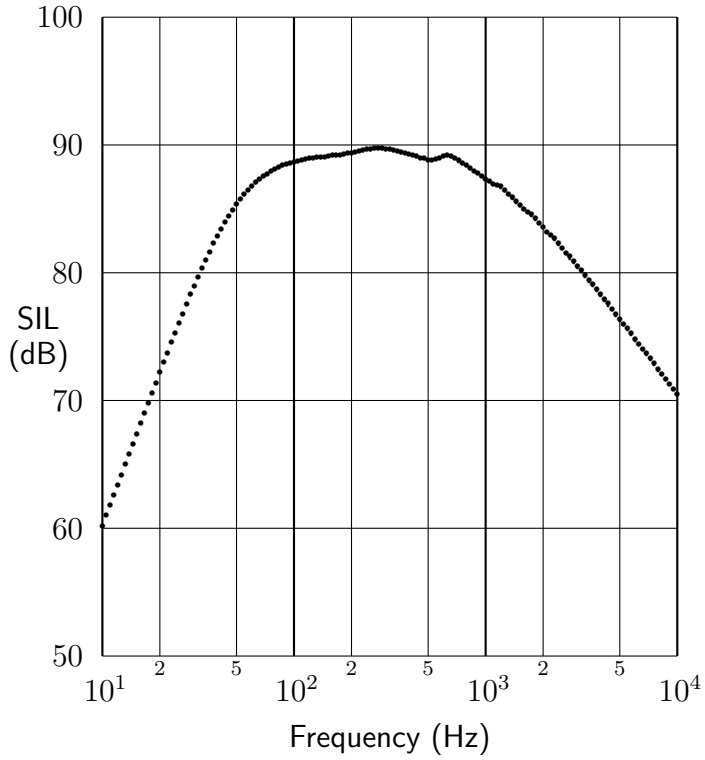

Figure 10.16: *Full simulation with 25 mm elements (large dots) and with 50 mm elements (small dots).*

error outside that range.

10.4.8 Effects of halving the element size

In an acoustic field with sinusoidal time-dependence, a finite-difference approximation to a spatial derivative is accurate if the step size is a small fraction of the wavelength, and therefore becomes less accurate as frequency increases. Hence, if the same field is modeled using two different step sizes, the results should agree closely up to a certain frequency, then diverge at frequencies for which the smaller step size gives a significantly more accurate model. Whether they agree or disagree at frequencies for which *neither* model is accurate depends on whether the output variable of the simulation is sensitive to distributed-field effects at these frequencies. In the driver-box system under study, the influence of the lumped moving mass of the driver becomes more dominant as frequency increases, so that simulations with different step sizes should agree again at the highest frequencies.

If two simulations with different step sizes compare in the predicted manner, the frequency range over which they agree (to some desired accuracy) is an indication of the frequency range for which they are reliable. If they should differ in some other way—e.g. by giving different results at all frequencies or diverging at frequencies that seem too low—one would start looking for bugs in the implementation of the model, especially those parts pertaining to step sizes and step counts.

All previous simulations in this chapter have used a step size of 50 mm. In the present subsection, three of the earlier simulations are repeated for a step size of 25 mm and their results are compared with the corresponding results for 50 mm. In each case the curves are indistinguishable, or nearly so, at frequencies below

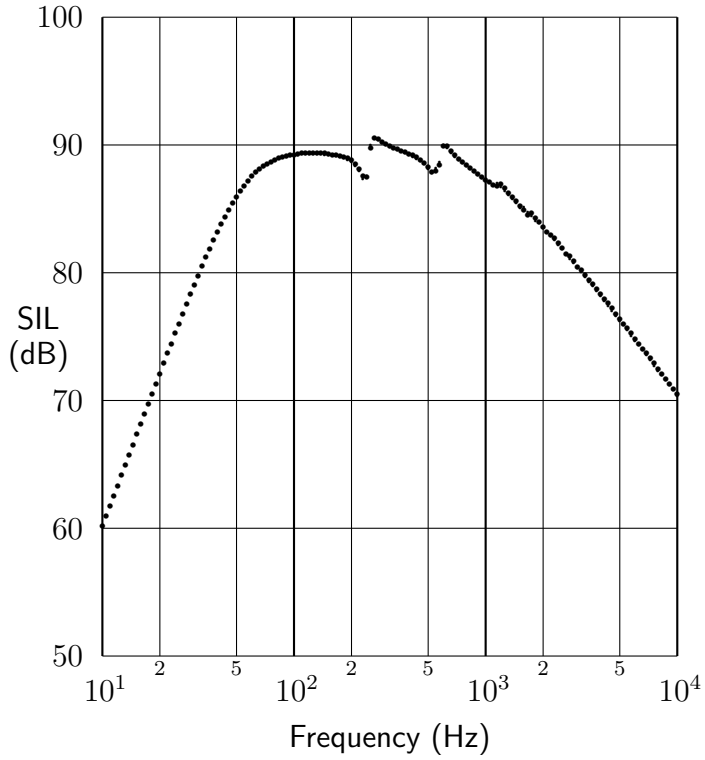

Figure 10.17: *"Free" approximation with 25 mm elements (large dots) and with 50 mm elements (small dots).*

500 Hz and above 5 kHz. This is cause for confidence that the models are correctly implemented. (Actually the smaller step size predicts slightly more output at high frequencies because it gives a smaller value of M_{ab}, but the difference is too small to show on the graphs.)

In Fig. 10.16, which compares the full simulations for the two step sizes, the curves are indistinguishable at all frequencies. If this graph is compared with Fig. 10.6, in which the 50 mm full simulation is shown in large dots, it can be seen that the curve for the 25 mm full simulation is slightly rougher around 1700 Hz, suggesting that the smaller step size detects a damped resonance which is missed by the larger step size.

As an indication of computational complexity, the AC analysis at 50 frequencies per decade for the full simulation with a 25 mm step size required a running time of just over 100 seconds on a MIPS R3000 CPU. The corresponding analysis for the 50 mm step size took just over 10 seconds.

Fig. 10.17 compares the **free** models for the two step sizes. The graph must be inspected closely to find any points of the 50 mm curve which are not obscured by those on the other curve; such deviations occur at about 600 Hz and 1150 Hz, both in the vicinity of resonances. Comparing this graph with Fig. 10.9 shows that the curve for the 25 mm step size is slightly rougher between 2 kHz and 3 kHz.

The greatest sensitivity to step size is shown by the two **undamped** models, whose frequency responses are compared in Fig. 10.18. All the graphs in this thesis show individual data points without any interpolating curves. Fig. 10.18 is one case in which the graph would look much neater if an interpolating function were used. Neatness would be misleading, however, because the sample frequencies would not coincide with the closely-spaced maxima and minima of the response: peaks

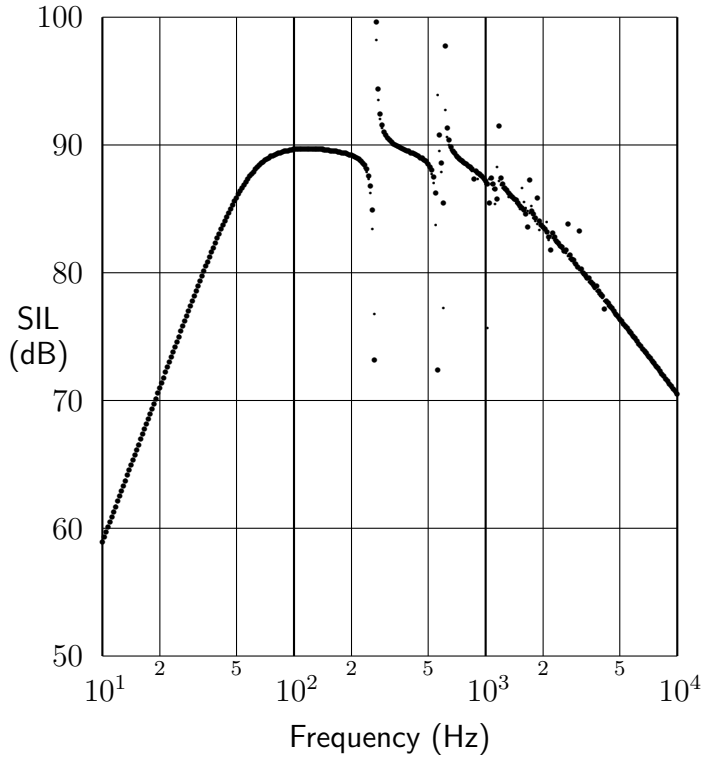

Figure 10.18: *Undamped approximation with 25 mm elements (large dots) and with 50 mm elements (small dots).*

would be too low and troughs too shallow, and some differences between resonance frequencies would not register. It is safer to examine the scattered points.

Both responses in Fig. 10.18 are plotted at 100 frequencies per decade. Most of the resulting 600 points are seen to lie on a single piecewise-smooth curve; the two responses are indistinguishable at most sample frequencies, including all frequencies below 200 Hz or above 5 kHz. Between 2 kHz and 5 kHz, the smaller step size predicts a few resonances which are missed by the larger step size. In the vicinity of the lowest resonance frequency (about 265 Hz), a vertical displacement can be seen between the large and small dots, but the slope of the response is so steep that the vertically-displaced pairs of dots still seem to lie on a common piecewise-smooth curve; hence we may still say that the two responses are "indistinguishable, or nearly so" up to 500 Hz.

The double resonance in the region of 600 Hz can also be interpreted by joining alternate large and small dots with a piecewise-smooth steep curve. The first smooth section ends with the large dot at (562 Hz, 72.3 dB). The second begins with the small dot at (562 Hz, 93.9 dB) and ends with the small dot at (602 Hz, 77.2 dB). The third begins with the large dot at (616 Hz, 97.8 dB) and merges with the next gently-sloping segment. (The numbers quoted in connection with Fig. 10.18 are taken from the text file which was written by the SPICE "`print`" command and read by the plotting program "`sp2tex.c`".) Notice that the frequency of 562 Hz is mentioned twice—the first apparent minimum for the 25 mm step size is at the same frequency as the subsequent apparent maximum for the 50 mm step size. Thus the larger step size predicts a lower resonance frequency.

This observation is consistent with the one-dimensional error analysis carried out by Arai [2, p. 20], in which a length of uniform tube was compared with its

finite-difference equivalent circuit (an L-C ladder network). Arai found that the total phase lag for propagation along the pipe as predicted by the FDEC model was greater than the true value by a fraction

$$\frac{\Delta\theta}{\theta} \approx \frac{(k\Delta x)^2}{24} \tag{10.62}$$

where k is the wave number and Δx is the step size (these notations are different from Arai's). Hence the fractional error in the calculated resonance frequencies (for which the phase lag must assume predetermined values) is

$$\frac{\Delta\nu}{\nu} \approx -\frac{(k\Delta x)^2}{24} \tag{10.63}$$

where ν represents frequency. So the resonance frequencies will be underestimated by a margin which increases with the step size.

If we use at least 2π elements per wavelength, $k\Delta x$ will be not more than unity and the error will be at most one part in 24 or, conservatively, less than 5% (an equivalent result was given by Arai). The condition that $k\Delta x \leq 1$ is satisfied for frequencies up to $c/(2\pi\Delta x)$, which is a little more than 1 kHz for a step size of 50 mm.

To estimate the discrepancy between the resonance frequencies predicted using two step sizes differing by a factor of two, we write $\Delta x/2$ in place of Δx in Eq. (10.63) and subtract the result from that equation. We find that the resonance frequency for the larger step size is lower by a fraction

$$\frac{(k\Delta x)^2}{32} = \left(\frac{\pi\Delta x\,\nu}{\sqrt{8}\,c}\right)^2. \tag{10.64}$$

For $\Delta x = 50$ mm and $c = 343.08\,m/s$, the fraction is $(\nu/6178\,\mathrm{Hz})^2$. This result comes from a one-dimensional plane-wave analysis. Clearly it also applies to the two- and three-dimensional cases in Cartesian coordinates if propagation is restricted to one of the coordinate directions. For propagation in other directions, the discrepancy will be *smaller* because the wavelength in the coordinate directions will be longer than in the direction of propagation. Thus the estimated discrepancy should be an upper bound.

The highest frequency mentioned in connection with the double resonance in Fig. 10.18 is 616 Hz, for which the estimated discrepancy is 1%. All that can be said from the data points is that the difference is less than the frequency resolution of the graph, which is 2.33% (for 100 points per decade). Better estimates of frequency discrepancies can be made by exploiting three cases in which corresponding features of the 50 mm and 25 mm curves occur at consecutive sample frequencies. The 50 mm curve has a deep dip at 1023 Hz and the 25 mm curve a shallower dip at 1047 Hz, suggesting that the resonance frequencies are separated by a little more than 2.33%. Arai's error estimate predicts a maximum discrepancy of 2.9%. The two curves have similar dips at 1122 Hz and 1148 Hz; here the discrepancy is close to 2.33% when Arai's estimate predicts 3.5%. The 50 mm curve has a low peak at 1148 Hz and the 25 mm curve a higher peak at 1174 Hz, suggesting that the resonance frequencies differ by a little more than 2.33%, when Arai's estimate predicts 3.6%. In all three cases, the frequency discrepancy seems to be within the expected range.

In summary, pairs of models with different step sizes produce consistent results which inspire confidence in the FDEC method and in the model-building program.

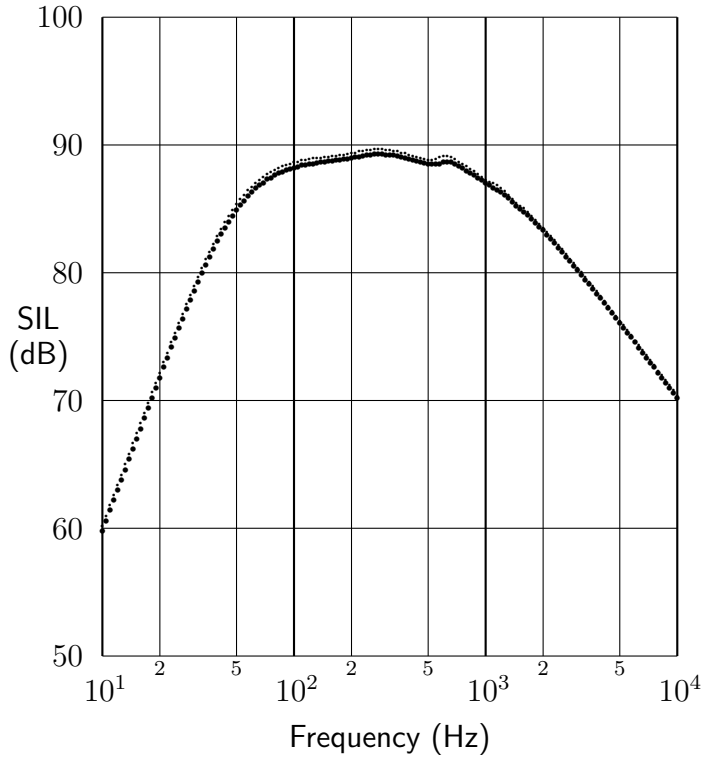

Figure 10.19: *Full simulation at 40°C (large dots) and at 20°C (small dots).*

(But it should be noted that the current version of the program loses accuracy if the dimensions of the box are not all multiples of a common step size. See the preamble to Section B.9.)

10.4.9 Effects of ambient temperature and pressure

All previous simulations in this section assume a temperature of 20°C and a pressure of one standard atmosphere. Figs. 10.19 and 10.20 show the effect of changing the temperature and pressure, respectively, for the full simulation with a 50 mm step size. In the first graph, the temperature is increased to 40°C while the pressure remains at 1 atm. In the second, the pressure is reduced to 84559 Pa, which corresponds to an altitude of 1500 m according to the U.S. Standard Atmosphere tables [31, p. *14*-14], while the temperature remains at 20°C.

It is seen that increasing the temperature gives a slight decrease in SIL at frequencies up to about 1.2 kHz, while decreasing the pressure has no noticeable effect on SIL. More importantly, neither change has a radical effect on the *shape* of the frequency response for this particular system design. Because different designs may have different sensitivities to ambient conditions, it is advisable to check the sensitivities for every design. The model-building program allows this to be done by changing just two parameters in the program.

10.5 6.5-inch woofer in 5-liter box

In an attempt to find a case in which the departure from thermal equilibrium significantly affects the frequency response, the parameters in the model-building program

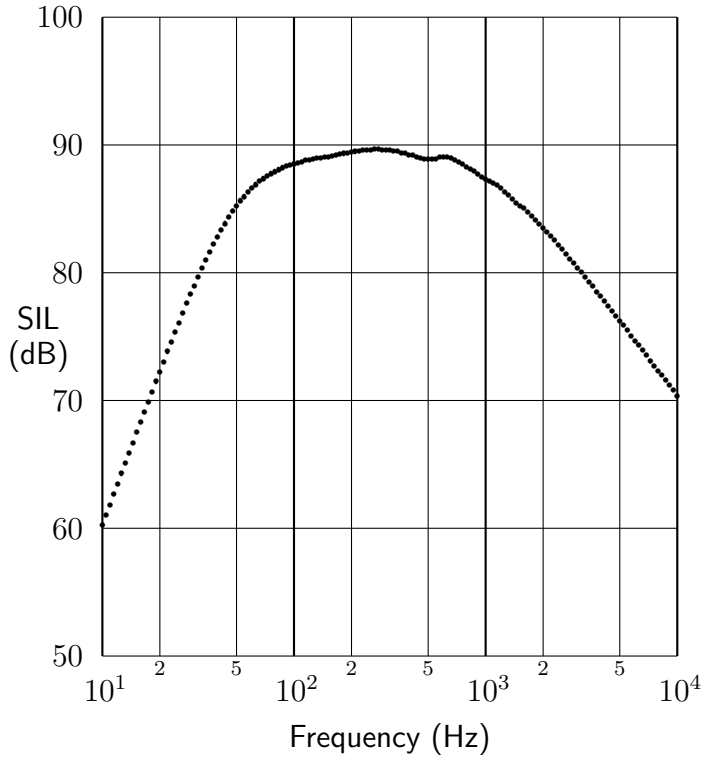

Figure 10.20: *Full simulation at an altitude of 1500 meters (large dots) and at sea level (small dots).*

were reset for a 6.5-inch woofer with a carbon fiber cone [1] in a box with the following dimensions:

$$\texttt{D} = \texttt{width} = \texttt{height} = 160\,\text{mm}$$

$$\texttt{depth} = 200\,\text{mm}$$

$$\texttt{clear} = 80\,\text{mm}.$$

The resulting internal box volume was 5.12 liters. The element size was 20 mm.

The frequency responses for the **adiab** and **equil** models are shown in Figs. 10.21 and 10.22, respectively. Each graph also includes the result of the full simulation. At low frequencies, as expected, the thermal-equilibrium model agrees with the full simulation while the adiabatic model predicts slightly less output. The interesting comparison is in the region of the first resonance (about 800 Hz). Here the **adiab** model is more accurate than the **equil** model, indicating a substantial departure from thermal equilibrium. It can be seen, albeit with some difficulty, that the thermal-equilibrium model predicts a lower resonance frequency than the other two models. This is because the thermal-equilibrium assumption replaces γ with $\gamma_o^\star$, which reduces the speed of sound (cf. Eq. (2.40) and Subsection 7.2.3). The same effect can be seen, with greater difficulty, at the second resonance (about 1500 Hz).

Thus the only apparent effect of the departure from thermal equilibrium is a slight shift in the frequencies of the resonant modes of the box. If this behavior is typical—as seems likely, given that the motion of the diaphragm is mass-limited at high frequencies—the implication is that one is not likely to incur serious errors by assuming thermal equilibrium as recommended by Leach [30], and that the elaborate study of thermal time constants in Chapter 8 will usually have little impact on practical calculations. But of course this conclusion could not have been

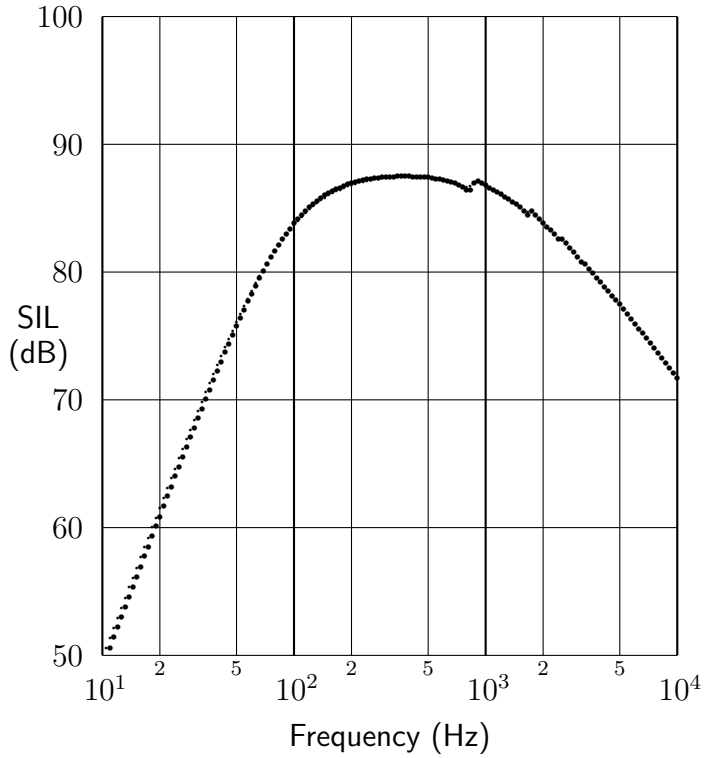

Figure 10.21: *6.5-inch driver in 5-liter box; adiabatic approximation (large dots) and full simulation (small dots).*

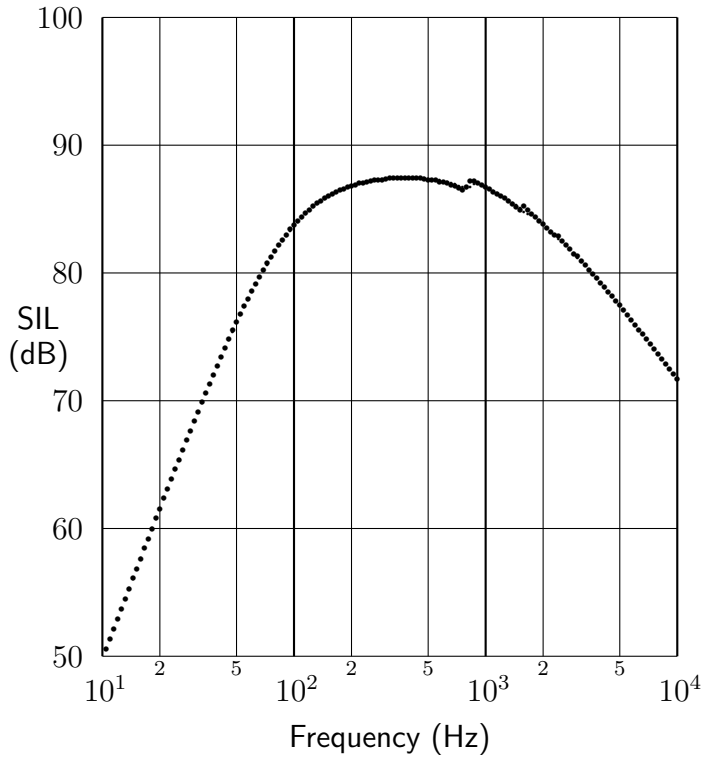

Figure 10.22: *6.5-inch driver in 5-liter box; thermal-equilibrium approximation (large dots) and full simulation (small dots).*

reached without first performing the work in Chapter 8. Moreover, if the characteristics of loudspeakers are not highly sensitive to thermal time constants, then the approximations made in calculating the time constants—such as cylindrical symmetry, perfect conduction in the fibers, and the neglect of higher-order modes—are further justified.

10.6 Simulations vs. experiments

Sometimes computer simulations yield information which would be difficult or impossible to obtain from laboratory measurements. In the simulations of Sections 10.4 and 10.5, the effect of each fiber property has been determined by neglecting that property (by omitting the associated equivalent-circuit element) and comparing the resulting approximate simulation with the "full" simulation. In the laboratory, however, it is not possible to take away the viscosity of air or the heat capacity of fiberglass, or to hold the fibers rigid, or to suspend Fourier's law of heat conduction, while keeping everything else constant. Indeed, given the limitations of real materials, it is probably not even possible to find two types of fiber, or two gases, that differ in only one relevant property.

Furthermore, computer simulations make it possible—or rather obligatory—to idealize all aspects of the system except the one(s) under study. The simulations in this chapter show the effects of the internal air resonances *acting alone*, whereas laboratory measurements might also be affected by cabinet wall vibrations, obstruction by the magnet and basket, diaphragm flexure, cabinet edge diffraction, room reflections, microphone errors, etc. Some of these influences are coupled to the internal acoustic field and consequently would not cancel out in comparisons between damped and undamped responses. Even if the effects of cabinet wall vibrations and diaphragm flexure can be reduced to inaudible levels, as suggested in Chapter 1 and Section 10.1, this does not imply that the effects would be unmeasurable or that they would not mask other phenomena under investigation.

The FDEC simulations indicate that some effects of the fiber filling are insignificant compared with others; for example, it makes little difference if we assume that the fibers are rigid (or, equivalently, have infinite mass), or that the thermal time constant is infinitely long or negligibly short. Hence, in the laboratory, the effects of these parameters would be masked by experimental error. The only parameter whose effect would not be so masked is the pneumatic resistivity λ, which is involved in the dominant mechanism of damping.

Thus the loudspeaker problem considered in this chapter is not a suitable test case for an experimental validation of the FDEC method: measurements on the loudspeaker would not be accurate enough to confirm any aspect of the FDEC model except the treatment of pneumatic resistivity λ. This is especially the case when we recall that the experimental results would be affected by factors not included in the model.

However, for the purpose of understanding the mechanisms by which fiber filling affects the response of a loudspeaker through the damping of internal air resonances, the idealized character of the computer model used in this chapter has been an advantage.

Chapter 11

Radiation from a circular rigid piston

Chapter 10 is primarily concerned with an application, rather than a validation, of the FDEC method. Although the consistency of the results inspires confidence, the results were not known *a priori* and have not been confirmed by any sufficiently accurate independent method. Moreover, Chapter 10 does not use all the features of the FDEC model. While it thoroughly explores the circuit modifications required by fiber filling, it makes no use of curvilinear coordinates (with variable scale factors), and uses a narrow range of boundary conditions (giving a standard treatment of the rigid-wall condition and an *ad hoc* treatment of the coupled fluxes generated by a rigid diaphragm).

Hence, to conclude this study, it seems advisable to use the FDEC method to solve a problem for which an analytical solution is known. To test the range of techniques developed in Chapter 6, the problem should be expressed in curvilinear coordinates and should involve a radiation condition, preferably with a range of angles of incidence at the anechoic boundary.

11.1 Choosing the test problem

Computing the low-frequency radiation impedance on one side of a circular rigid piston in an infinite planar baffle is a well-known problem, and is especially relevant to this thesis because its analytical solution has been used in the loudspeaker simulation (see Subsection 10.1.1). The low-frequency behavior of the impedance is more relevant to the simulation in Chapter 10, and more suitable for computation by the FDEC method, than the high-frequency behavior. The problem involves two kinds boundary conditions, namely a rigid-wall condition at the baffle and an anechoic radiation condition at the free-air boundary of the simulated region.

A third boundary condition can be introduced by studying a second version of the problem: find the low-frequency radiation impedance on one side of an *unbaffled* thin disk vibrating along its axis. The modified problem is also relevant to the loudspeaker model (see Subsection 10.1.4). By symmetry, the excess pressure field on one side of the unbaffled disk is a mirror image of that on the other side, but has the opposite sign or phase. The absence of a baffle imposes continuity of pressure in the plane of the disk, so that the equal and opposite pressures must both be zero in that plane; that is, a *zero-pressure* boundary condition applies in the plane of the

disk.

An unbaffled piston produces a net flux of zero and does not resemble a point-source in the far field (see Subsection 6.5.4). Hence, if the anechoic-boundary terminations used in the baffled case are re-used in the unbaffled case, there will be reflections from the boundary, causing an error in the computed radiation impedance. However, as the distance to the anechoic boundary is increased, the reverberant sound field in the simulated region becomes more diffuse, so that the error caused by reflection decreases. Thus we may still obtain meaningful results from the model. Moreover, because the error due to reflection is ultimately caused by the assumed normal specific acoustic impedance at the boundary, and not by the FDEC representation thereof, it depends on the distance to the outer boundary—not on the step size. Hence, provided that the step size is sufficiently small to make reflection the dominant source of error, the overall error will depend more on the distance to the outer boundary than on the step size. This prediction can be tested. For these reasons, there is some value in proceeding with the unbaffled model even without correcting the anechoic boundary condition.

(The correction would involve finding the specific acoustic impedance in the field of a dipole source, and using that impedance to calculate the FDEC boundary terminations. This in turn would require repetition of much of the working in the present chapter, greatly lengthening the chapter for little additional benefit.)

It remains to choose a coordinate system. The geometry of the problem allows us to use a two-dimensional network if we choose an axisymmetric coordinate system whose axis coincides with that of the disk. For easy representation of the boundary condition on the disk and baffle, the disk should lie in an equicoordinate surface. If we require a range of angles of incidence at the anechoic boundary, the other equicoordinate surfaces must *not* be spheres centered on the disk (which give normal incidence in the far field) or cones with apexes on the disk (which give tangential incidence in the far field and extend into the near field). Using a coordinate system other than those for which Arai formulated his method (Cartesian and cylindrical) might seem to enhance the originality of this chapter, but is also trivial in that it merely requires specifying the scale factors. Hence, for the purpose of testing the method, it is more useful to give a comprehensive illustration of the anechoic radiation condition (which was not considered by Arai) than to use an exotic coordinate system.[1]

In view of these requirements, the present chapter will use cylindrical coordinates (r, ϕ, z), with the disk in the plane $z = 0$ and coaxial with the z axis. The radiating surface is described by

$$z = 0\,;\ 0 \le r \le a \tag{11.1}$$

while the anechoic boundaries are described by

$$r = b\,;\ 0 \le z \le b \tag{11.2}$$

[1]For more practical purposes, however, "exotic" coordinates can be useful. Geddes [18, pp. 558–61] has proposed a variety of acoustic waveguides whose walls are equicoordinate surfaces in separable curvilinear orthogonal coordinate systems. The desire to analyze some of these waveguides (and others derived from non-separable coordinates) motivated the present author to develop the FDEC method in generalized orthogonal coordinates. Both infinite and truncated versions of the waveguides could be modeled in this manner. In the present thesis, the author must be content with just one example in curvilinear coordinates.

and

$$z = b\,;\ 0 \le r \le b. \tag{11.3}$$

Hence the rigid-wall or zero-pressure boundary condition must be applied at the surface

$$z = 0\,;\ a \le r \le b. \tag{11.4}$$

In other words, a is the radius of the source and b is the perpendicular distance from the center of the source to each of the anechoic boundaries. The angle of incidence at the anechoic boundary ranges from zero (i.e. normal) to 45° on both the planar and cylindrical regions of the boundary, and the distance from the source to the boundary also varies, so the FDEC representation of the anechoic condition can be thoroughly tested.

11.1.1 Alternative coordinates—a digression

It should be noted that while the cylindrical coordinate system gives the most wide-ranging test of the FDEC method in solving the chosen problem, it is *not* ideal in terms of computational efficiency or accuracy, for the chosen problem or for more general problems.

Consider a general finite distributed source near the origin of a spherical coordinate system (R, θ, ϕ); here the radial coordinate is called R to distinguish it from the r of cylindrical coordinates. As shown in Subsection 6.5.4, the pressure field can be written in the form

$$P = D(\omega, R, \theta, \phi)\, U_0\, \frac{j\omega\rho_o}{4\pi}\, \frac{e^{-jkR}}{R} \tag{11.5}$$

where the R-dependence of D is negligible for large R. The angular dependence of P is contained in the factor D. Because D approaches a function of frequency and angular position as $R \to \infty$, the angular dependence of P does not become more complex as R increases. This implies that we can maintain nearly uniform accuracy for all R by using *spherical* coordinates to construct the FDEC elements; while the *linear* dimensions of the elements in the tangential directions (θ and ϕ directions) increase with R, there is no loss of accuracy in the tangential finite-difference approximation, because the angular factor of P depends on the *angular coordinates* and not on the associated tangential distances. In other words, there is no point in maintaining a constant linear step size in the tangential direction as the radius increases.

Hence the spherical coordinate system, or any other system which approximates spherical coordinates at large distances from the origin, offers an advantage in computational efficiency: there are two tangential coordinates whose scale factors increase with distance from the origin, so that a finite-difference scheme in these coordinates has a tangential resolution that becomes coarser as radius increases. The cylindrical coordinate system, in contrast, has only one variable-scale coordinate; hence, if a cylindrical FDEC model is to have the same near-field resolution as a spherical model, it will have many more elements in the far field. Cartesian coordinates, which have no variable scale factors, require still more far-field elements for a given near-field resolution. So it seems that spherical coordinates will be more efficient than cylindrical coordinates, which in turn will be more efficient than Cartesian coordinates, for solving a general radiation problem with given accuracy using the FDEC method.

Of course the surface of the source may not be an equicoordinate surface in spherical coordinates, but it may be approximated by a piecewise-equicoordinate surface in spherical (or other) coordinates, and the approximation may be made arbitrarily accurate by taking a sufficiently small step size. The appropriate source boundary condition can then be applied using the techniques of Section 6.5.

For the circular-rigid-piston problem, the most efficient coordinate system is probably the oblate spheroidal system (ξ, θ, ϕ) used by Geddes [19, p. 453], with the origin diameter d set equal to the source diameter. These coordinates not only approximate spherical coordinates at large radii, but also give enhanced resolution around the edges of the disk (see Geddes' Fig. 1), where the air motion is most complex.

For present purposes, however, the choice of coordinates is driven by curiosity rather than efficiency.

11.2 The FDEC components

Following the notation of Chapter 6, let the step sizes be Δr in the radial (r) direction and Δz in the axial (z) direction. As the wavefront will propagate in both directions, we make $\Delta r = \Delta z$. Let the radius of the piston span m elements, so that

$$a = m\Delta r \,, \tag{11.6}$$

and let the radius of the simulated region span n elements, so that

$$b = n\Delta r = n\Delta z = na/m. \tag{11.7}$$

Thus b must be an integral multiple of a/m. Restricting b to discrete values does not reduce the generality of the model; b is not "given", but merely needs to be large enough to place the outer boundary in the far field, so that the normal impedance at the anechoic boundary can be estimated using the point-source assumption (see Subsections 3.3.4 and 6.5.4).

In exploiting the axial symmetry we take $\Delta\theta = 2\pi$, so that the volume elements are coaxial toroids of rectangular cross-section. The coordinates at the "midpoints" (or centroidal circles) of the volume elements are

$$r_i = (i - \tfrac{1}{2})\,\Delta r \,;\; i = 1, 2, \ldots, n \tag{11.8}$$

and

$$z_k = (k - \tfrac{1}{2})\,\Delta z \,;\; k = 1, 2, \ldots, n \tag{11.9}$$

Thus integer values of i and k correspond to the centers of compliance elements, while mass elements have non-integer values; for example, k is half an odd integer for the interior axial mass elements, and $i = n + \frac{1}{4}$ for the "truncated" radial mass elements adjacent to the cylindrical boundary. The scale factor for θ is r, so the linear increment in the θ direction is

$$[h_\theta \Delta\theta]_{ik} = 2\pi r_i. \tag{11.10}$$

N.B.: In this section (Section 11.2), k is the step-counter in the z direction, not the wave number.

11.2.1 Compliance and mass elements

To find the FDEC elements for the simulated region of air, we substitute the coordinate increments and scale factors (in terms of r_i) into Eqs. (6.38) to (6.44), then substitute for r_i from Eq. (11.8). The two steps can be shown on one line. (To preserve clarity of form in the algebraic expressions, the equality of Δr and Δz will not be used until Section 11.3, where we consider *normalizing* the FDEC elements so that the result of the simulation can be scaled for different dimensions and different acoustic media.) Note that because the only variable scale factor depends on r_i only, the values of all the interior elements will be functions of i.

The general compliance element is

$$\Delta C_{ik} = \frac{2\pi r_i \Delta r \Delta z}{\rho_o c^2} = \frac{(2i-1)\pi(\Delta r)^2 \Delta z}{\rho_o c^2}. \tag{11.11}$$

This expression can be used even for elements adjacent to the boundaries; there are no "truncated" volume or compliance elements.

The mass elements in the radial direction are

$$\Delta M_r|_{i+\frac{1}{2},k} = \frac{\rho_o \Delta r}{2\pi r_{i+\frac{1}{2}} \Delta z} = \frac{\rho_o}{2\pi i \Delta z} \tag{11.12}$$

for $i = 1, 2, \ldots, n-1$; $k = 1, 2, \ldots, n$. This expression is valid for all but the outermost elements, which are

$$\tfrac{1}{2}\Delta M_r\Big|_{n+\frac{1}{4},k} = \frac{\rho_o \Delta r}{4\pi r_{n+\frac{1}{4}} \Delta z} = \frac{\rho_o}{(4n-1)\,\pi \Delta z} \tag{11.13}$$

for $k = 1, 2, \ldots, n$.

The interior mass elements in the axial direction are

$$\Delta M_z|_{i,k+\frac{1}{2}} = \frac{\rho_o \Delta z}{2\pi r_i \Delta r} = \frac{\rho_o \Delta z}{(2i-1)\,\pi (\Delta r)^2} \tag{11.14}$$

for $i = 1, 2, \ldots, n$; $k = 1, 2, \ldots, n-1$. The boundary elements are

$$\tfrac{1}{2}\Delta M_z\Big|_{i,\frac{3}{4}} = \tfrac{1}{2}\Delta M_z\Big|_{i,n+\frac{1}{4}} = \frac{\rho_o \Delta z}{4\pi r_i \Delta r} = \frac{\rho_o \Delta z}{(4i-2)\,\pi (\Delta r)^2} \tag{11.15}$$

for $i = 1, 2, \ldots, n$. Because the element values do not depend on k, the boundary elements are simply half the interior elements for the corresponding values of i. In the case of the baffled piston, the truncated axial mass elements adjacent to the baffle carry no flux and may be omitted. For the unbaffled piston, with its "ground-plane" boundary condition, all the truncated mass elements must be included.

11.2.2 Anechoic-boundary elements

Let R be the spherical radial coordinate and r the cylindrical radial coordinate, so that

$$R^2 = r^2 + z^2. \tag{11.16}$$

In this notation, the radial specific acoustic admittance given by Eq. (3.39) becomes

$$y_R = \frac{1}{\rho_o c} + \frac{1}{j\omega\rho_o R}. \tag{11.17}$$

Let the angle of incidence on the anechoic boundary be α, and let the boundary area element be ΔS. Then the normal acoustic admittance of an anechoic surface segment is

$$\Delta Y = y_R \, \Delta S \, \cos\alpha \tag{11.18}$$

(cf. Eqs. (6.86) and (6.90)).

On the cylindrical part of the boundary we have

$$\begin{aligned} r &= b \\ \Delta S &= 2\pi b \Delta z \\ \cos\alpha &= b/R. \end{aligned}$$

Substituting for y_R, ΔS and $\cos\alpha$ in Eq. (11.18), and introducing the subscript r to indicate that the normal to the boundary is in the r direction, we obtain

$$\Delta Y_r = \frac{2\pi b^2 \Delta z}{\rho_o c R} + \frac{2\pi b^2 \Delta z}{j\omega \rho_o R^2}. \tag{11.19}$$

Now we use the discrete values of z, introducing the subscripts b and k to indicate $r = b$ and $z = z_k$. Substituting from Eqs. (11.16) and (11.9), with $r = b = n\Delta z$ in Eq. (11.16), we obtain

$$\Delta Y_r|_{bk} = \frac{1}{\Delta R_r|_{bk}} + \frac{1}{j\omega \, \Delta M_r|_{bk}} \tag{11.20}$$

where

$$\Delta R_r|_{bk} = \frac{\rho_o c}{2\pi b^2} \left[n^2 + \left(k - \tfrac{1}{2}\right)^2 \right]^{\frac{1}{2}} \tag{11.21}$$

$$\Delta M_r|_{bk} = \frac{\rho_o \Delta z}{2\pi b^2} \left[n^2 + \left(k - \tfrac{1}{2}\right)^2 \right]. \tag{11.22}$$

Thus the acoustic admittance of the k^{th} boundary area element is that of a resistance $\Delta R_r|_{bk}$ in parallel with an inertance $\Delta M_r|_{bk}$.

On the planar part of the boundary we have

$$\begin{aligned} z &= b \\ \Delta S &= 2\pi r \Delta r \\ \cos\alpha &= b/R. \end{aligned}$$

Substituting for y_R, ΔS and $\cos\alpha$ in Eq. (11.18), and introducing the subscript z to indicate that the normal to the boundary is in the z direction, we obtain

$$\Delta Y_z = \frac{2\pi r b \, \Delta r}{\rho_o c R} + \frac{2\pi r b \, \Delta r}{j\omega \rho_o R^2}. \tag{11.23}$$

Now we use the discrete values of r, introducing the subscripts i and b to indicate $r = r_i$ and $z = b$. Substituting from Eqs. (11.16) and (11.8), and putting $z = b = n\Delta z$ everywhere, we obtain

$$\Delta Y_z|_{ib} = \frac{1}{\Delta R_z|_{ib}} + \frac{1}{j\omega \, \Delta M_z|_{ib}} \tag{11.24}$$

where

$$\Delta R_z|_{ib} = \frac{\rho_o c}{2\pi(\Delta r)^2}\left[\frac{1}{n^2} + \frac{1}{(i-1/2)^2}\right]^{\frac{1}{2}} \tag{11.25}$$

$$\Delta M_z|_{ib} = \frac{\rho_o}{2\pi\Delta r}\left[\frac{i-\frac{1}{2}}{n} + \frac{n}{i-\frac{1}{2}}\right]. \tag{11.26}$$

Thus the acoustic admittance of the i^{th} boundary area element is that of a resistance $\Delta R_z|_{ib}$ in parallel with an inertance $\Delta M_z|_{ib}$.

11.2.3 Diaphragm interface

The area of the i^{th} annular segment of the disk surface is

$$\Delta S_i = 2\pi r_i \Delta r = 2\pi(i-\tfrac{1}{2})(\Delta r)^2. \tag{11.27}$$

The corresponding fraction of the total diaphragm area is

$$a_i = \frac{\Delta S_i}{\pi a^2} \tag{11.28}$$

or, substituting from Eqs. (11.6) and (11.27),

$$a_i = \frac{2i-1}{m^2}. \tag{11.29}$$

Let the total flux pumped out by the diaphragm (in phasor form) be U, of which the i^{th} annular segment contributes U_i. Then we have

$$U_i = a_i U = \frac{S_i}{\pi a^2} U \tag{11.30}$$

for $i = 1, 2, \ldots, m$. Let P_i be the (phasor) excess pressure over the i^{th} annular segment, F_r the total force (i.e. the integral of excess pressure over the diaphragm area), and P_{r} the radiated pressure (i.e. the average excess pressure over the diaphragm). Then

$$P_{\text{r}} = \frac{1}{\pi a^2} F_r = \frac{1}{\pi a^2}\sum_{i=1}^{m} S_i P_i = \sum_{i=1}^{m} \frac{S_i}{\pi a^2} P_i = \sum_{i=1}^{m} a_i P_i. \tag{11.31}$$

The i^{th} annular segment is part of the boundary of the volume element ΔV_{i1}, in which the central pressure is P_{i1}. Between the center and the boundary of the volume element is the truncated mass element $\frac{1}{2}\Delta M_z\Big|_{i,\frac{3}{4}}$, so that

$$P_i = P_{i1} + j\omega\, \tfrac{1}{2}\Delta M_z\Big|_{i,\frac{3}{4}} U_i. \tag{11.32}$$

Putting

$$\tfrac{1}{2}\Delta M_z\Big|_{i,\frac{3}{4}} = \frac{\rho_o\, \Delta z/2}{S_i} \tag{11.33}$$

and substituting for U_i from Eq. (11.30) gives

$$P_i = P_{i1} + j\omega M_{\text{af}}\, U \tag{11.34}$$

where

$$M_{\mathrm{af}} = \frac{\rho_{\mathrm{o}}\,\Delta z/2}{\pi a^2}. \tag{11.35}$$

M_{af} may be recognized as the acoustic mass of a cylinder of length $\Delta z/2$ and cross-sectional area πa^2, or as the parallel combination of the m truncated axial mass elements in front of the diaphragm (cf. Section 10.2); the subscript "f" stands for "front". Substituting Eq. (11.34) into Eq. (11.31) yields

$$\begin{aligned} P_{\mathrm{r}} &= \sum_{i=1}^{m} a_i \left(P_{i1} + j\omega M_{\mathrm{af}}\, U\right) \\ &= \sum_{i=1}^{m} a_i P_{i1} \;+\; j\omega M_{\mathrm{af}}\, U \sum_{i=1}^{m} a_i \end{aligned}$$

and the area fractions a_i add up to unity, so that

$$P_{\mathrm{r}} = j\omega M_{\mathrm{af}}\, U \;+\; \sum_{i=1}^{m} a_i P_{i1}. \tag{11.36}$$

At this point we have all the equations needed to construct the equivalent circuit. However, the present form of the equations requires us to construct and solve a different equivalent circuit for each set of values of the parameters a, ρ_{o} and c. As will be shown in the next section, this limitation can be overcome by *normalizing* the circuit, solving the circuit once, and *denormalizing* the solution for each set of problem parameters.

11.3 The normalized FDEC model

We begin with a comment on notation. In most parts of this thesis, maximum clarity is achieved by using the most familiar notation in each context. Inevitably this policy causes some symbols to be reused: T can be a temperature or a period, θ can be a temperature rise or an angle, H can be a transfer resistance or a principal curvature, and so on. Usually the different meanings of a symbol occur in disjoint contexts so that there is no risk of confusion. In this section, however, previously-defined notations mean that k usually represents a counter in the z direction, but sometimes means the wave number. So the meaning of k will be clarified at a few points in the text. There are also cases in which the presence of a subscript has an unusually radical effect, changing the type of quantity represented by a symbol. These will be noted in the appropriate places.

11.3.1 General principles; accuracy

Let the radiation impedance of the circular piston be Z_{ar}. Its area is πa^2. If this area were a segment of a planar wavefront, its acoustic impedance would be

$$Z_{\mathrm{a0}} = \frac{\rho_{\mathrm{o}} c}{\pi a^2}. \tag{11.37}$$

We may regard Z_{a0} as the "natural" unit of impedance for this problem, and hence define the *normalized radiation impedance* as

$$z_{\mathrm{ar}} = \frac{Z_{\mathrm{ar}}}{Z_{\mathrm{a0}}}. \tag{11.38}$$

We may also define the *normalized angular frequency* as

$$h = ka = \omega a/c \tag{11.39}$$

(where k is the wave number), so that a larger piston requires a lower ω for a given h. If $h \gg 1$, the piston emits approximately planar wavefronts, so that $z_{\mathrm{ar}} \approx 1$.

(Note that h with a subscript denotes a coordinate scale factor, while an unsubscripted h is the normalized angular frequency; only the latter appears in the remainder of this chapter.)

For plane waves in Cartesian coordinates, the FDEC model gives a phase error of less than 5% for frequencies in the range $|k\Delta x| < 1$ (see the introduction to Chapter 6). In non-Cartesian coordinates, the first derivatives of the wave function are modulated by functions of the scale factors (see Eq. (6.35)), increasing the bandwidth prior to the second differentiation. Thus, for a given linear step size, we may expect the bandwidth over which a given accuracy is achieved (the "accuracy bandwidth") to be less than for Cartesian coordinates. For non-plane waves, the wave function itself is modulated, so that the accuracy bandwidth should be less than for plane waves. Because the accuracy of the FDEC method depends on the wave function, the step size required for a given accuracy cannot generally be predicted, but can be estimated by studying the convergence of the solution as the step size is reduced. As the purpose of the present chapter is to test the method rather than solve a new problem, we can use signals within the accuracy bandwidth applicable to plane waves traveling in the z direction, i.e. within the band $|k\Delta z| < 1$, noting that the test is made more severe by the coordinate system and the nature of the solution. To express this frequency band in terms of h, we put $\Delta z = a/m$ and multiply through by m, obtaining

$$|ka| < m\,, \tag{11.40}$$

i.e.

$$|h| < m. \tag{11.41}$$

Eqs. (11.38) and (11.39) can be applied to individual acoustic elements in the model. A resistance is normalized by dividing by Z_{a0}. For a mass or compliance, we express the normalized impedance in terms of jh in order to obtain the normalized component value. As an example, let us normalize the radiation inertance M_{ar} (cf. Subsection 10.1.1) and find a physical interpretation of the result. The normalized impedance of M_{ar} is

$$\frac{j\omega M_{\mathrm{ar}}}{Z_{\mathrm{a0}}} = j\omega M_{\mathrm{ar}}\,\frac{\pi a^2}{\rho_{\mathrm{o}} c} = jh\, m_{\mathrm{ar}} \tag{11.42}$$

where m_{ar} is the normalized inertance, given by

$$m_{\mathrm{ar}} = \frac{\pi a}{\rho_{\mathrm{o}}}\, M_{\mathrm{ar}}. \tag{11.43}$$

From this we see that the natural unit of acoustic mass, i.e. the value of M_{ar} required to give $m_{\mathrm{ar}} = 1$, is

$$M_{\mathrm{a0}} = \frac{\rho_{\mathrm{o}}}{\pi a} = \frac{\rho_{\mathrm{o}} a}{\pi a^2}\,, \tag{11.44}$$

which is the acoustic mass of a circular cylinder of length a and radius a. Since the above argument could have used any acoustic mass in place of M_{ar}, Eq. (11.43) shows the general procedure for normalizing an inertance element.

Both the normalized radiation impedance and the normalized frequency are dimensionless. So if we solve the radiation impedance problem for particular values of a, ρ_o and c, and then plot the *normalized* radiation impedance vs. h, we may expect that the resulting plot is valid for all a, ρ_o and c, and that we may account for different values of these parameters when *denormalizing* the abscissa and ordinate to obtain ω and Z_{ar}. To turn this intuitive expectation into a proof, we perform the normalization of Z_{ar} by scaling *all* the impedances in the equivalent circuit—i.e. by normalizing the components. The normalized values of all the components will turn out to be independent of a, ρ_o and c, confirming that the normalized overall impedance must also be independent of these quantities.

11.3.2 Components

In the following text, the normalized components are represented by lower-case letters without a leading "Δ". Redundant k-subscripts (for components whose values are independent of the counter k) are dropped. Non-redundant subscripts are rounded to integers because they become array indices in in the model-building program. (If k appears in a subscript or as an array index, it obviously represents a counter rather than the wave number.) The values of the components to be normalized are given by Eqs. (11.11) to (11.26), above.

The normalized admittance of ΔC_{ik} is

$$Z_{a0}\, j\omega \Delta C_{ik} = jh\, c_i \tag{11.45}$$

where c_i is the normalized compliance element and is given by

$$c_i = \frac{2i-1}{m^3}. \tag{11.46}$$

The notation "c_i" becomes "`c[i]`" in the program `disk.c` (listed in Section B.12), which uses a one-dimensional array to store the possible compliance values.

Recalling Eqs. (11.43) and (11.44), we normalize inertance elements by multiplying by $\pi a/\rho_o$. Where necessary, we also use the relations $a = m\Delta r = m\Delta z$ and $b = n\Delta r = n\Delta z$. The interior radial mass element $\Delta M_r|_{i+\frac{1}{2},k}$ normalizes to

$$m_{ri} = \frac{m}{2i} \tag{11.47}$$

which is represented in the model-building program as `mr[i]`. The truncated radial mass element $\frac{1}{2}\Delta M_r\Big|_{n+\frac{1}{4},k}$ becomes

$$m_{rn} = \frac{m}{4n-1} \tag{11.48}$$

which is represented in the model-building program as `mr[n]`. This notation is inconsistent (in the sense that m_{rn} cannot be obtained from m_{ri} by putting $i = n$) but has the advantage that the truncated mass element can be stored in the same array as the interior elements. The interior axial mass element $\Delta M_z|_{i,k+\frac{1}{2}}$ normalizes to

$$m_{zi} = \frac{m}{2i-1} \tag{11.49}$$

which becomes `mz[i]` in the model-building program. Because the truncated axial mass elements are simply half the corresponding interior elements, their normalized valued are not stored in an array like the truncated radial elements, but are computed as they are written to the circuit definition file. Consequently, the truncated axial mass elements in the normalized circuit diagram (Fig. 11.1) have labels beginning with "$\frac{1}{2}$", while the corresponding radial elements do not.

To normalize the anechoic-boundary elements, the mass elements are treated as above while the resistance elements are simply divided by $Z_{\mathrm{a}0}$ (see Eq. (11.37)). On the cylindrical part of the boundary, $\Delta R_r|_{bk}$ becomes

$$r_{rbk} = \frac{m^2}{2n^2}\left[n^2 + \left(k - \tfrac{1}{2}\right)^2\right]^{\frac{1}{2}} \tag{11.50}$$

while $\Delta M_r|_{bk}$ becomes

$$m_{rbk} = \frac{m}{2n^2}\left[n^2 + \left(k - \tfrac{1}{2}\right)^2\right]. \tag{11.51}$$

These are represented in the model-building program as `rrb[k]` and `mrb[k]` respectively. On the planar part of the boundary, $\Delta R_z|_{ib}$ becomes

$$r_{zib} = \frac{m^2}{2}\left[\frac{1}{n^2} + \frac{1}{(i-1/2)^2}\right]^{\frac{1}{2}} \tag{11.52}$$

while $\Delta M_z|_{ib}$ becomes

$$m_{zib} = \frac{m}{2}\left[\frac{i-\frac{1}{2}}{n} + \frac{n}{i-\frac{1}{2}}\right]. \tag{11.53}$$

These are represented in the model-building program as `rzb[i]` and `mzb[i]` respectively.

The normalized value of M_{af} may be found by the usual scaling method (with the substitution $\Delta z = a/m$), or by combining the first m values of $\frac{1}{2}m_{zi}$ in parallel (using the formula for the sum of an arithmetic progression). The result is

$$m_{\mathrm{af}} = \frac{1}{2m} \tag{11.54}$$

which appears in the program as `mf`.

11.3.3 Pressure, flux, diaphragm interface

So far we have defined procedures for normalizing the radiation impedance and frequency, and hence acoustic resistance, compliance and inertance. Because these methods are based on the *ratio* of pressure to flux, the normalized pressure and normalized flux are only determined up to a common scale factor. But it is easy to choose the scale factor so as to make the normalized quantities dimensionless. The radiation impedance is

$$Z_{\mathrm{ar}} = \frac{P_{\mathrm{r}}}{U}. \tag{11.55}$$

Substituting Eqs. (11.55) and (11.37) into Eq. (11.38), we obtain

$$z_{\mathrm{ar}} = \frac{P_{\mathrm{r}}/U}{\rho_{\mathrm{o}}c/(\pi a^2)} = \frac{P_{\mathrm{r}}/(\rho_{\mathrm{o}}c)}{U/(\pi a^2)} = \frac{P_{\mathrm{r}}/(\rho_{\mathrm{o}}c^2)}{U/(\pi a^2 c)} \tag{11.56}$$

where the last step makes the numerator and denominator dimensionless. Thus we may write

$$z_{\rm ar} = \frac{\hat{P}_{\rm r}}{\hat{U}} \tag{11.57}$$

where $\hat{P}_{\rm r}$ and $\hat{U}$ are the normalized pressure and flux, given by

$$\hat{P}_{\rm r} = \frac{P_{\rm r}}{\rho_{\rm o} c^2} \tag{11.58}$$

$$\hat{U} = \frac{U}{\pi a^2 c}. \tag{11.59}$$

These dimensionless quantities have simple physical meanings. Since $\rho_{\rm o} c^2$ is the adiabatic bulk modulus, $\hat{P}_{\rm r}$ is the phasor form of the fractional increase in density. Let $\bar{Q}$ denote the (phasor) average velocity over the diaphragm area, so that

$$\bar{Q} = \frac{U}{\pi a^2}. \tag{11.60}$$

Then the normalized flux can be written

$$\hat{U} = \frac{\bar{Q}}{c} \tag{11.61}$$

showing that $\hat{U}$ is the average velocity expressed as a fraction of the velocity of sound. These physical interpretations indicate that, if the assumptions of small compressions and small oscillations hold, we will have $\hat{P}_{\rm r} \ll 1$ and $\hat{U} \ll 1$.

The normalized pressure and flux are useful in the normalization of the equations describing the diaphragm interface. When the left-hand equality in Eq. (11.30) is divided through by $\pi a^2 c$, it becomes

$$\hat{U}_i = a_i \hat{U} \tag{11.62}$$

confirming the obvious fact that the normalized fluxes, like the unnormalized fluxes, divide in proportion to the area fractions. A more interesting conclusion is obtained by dividing Eq. (11.36) through by $\rho_{\rm o} c^2$. The result can be expressed in the form

$$\frac{P_{\rm r}}{\rho_{\rm o} c^2} = \frac{j\omega M_{\rm af}\, U}{\rho_{\rm o} c/(\pi a^2)} + \sum_{i=1}^{m} \left[a_i \, \frac{P_{i1}}{\rho_{\rm o} c^2} \right] \tag{11.63}$$

and then rewritten term-by-term to obtain

$$\hat{P}_{\rm r} = jhm_{\rm af}\, \hat{U} + \sum_{i=1}^{m} a_i \hat{P}_{i1} \tag{11.64}$$

which has the same form as Eq. (11.36) but involves only normalized quantities.

Recalling the comment made after Eq. (11.36), we now have all the equations needed to draw the *normalized* finite-difference equivalent circuit; this is shown in Fig. 11.1. The coordinate directions (but not the location of the origin) are indicated by the axes at lower right. As in Fig. 10.5 in the previous chapter, a compliance between a node and ground is indicated by writing the compliance "in the node". Eqs. (11.62) and (11.64), which describe the diaphragm interface, are implemented

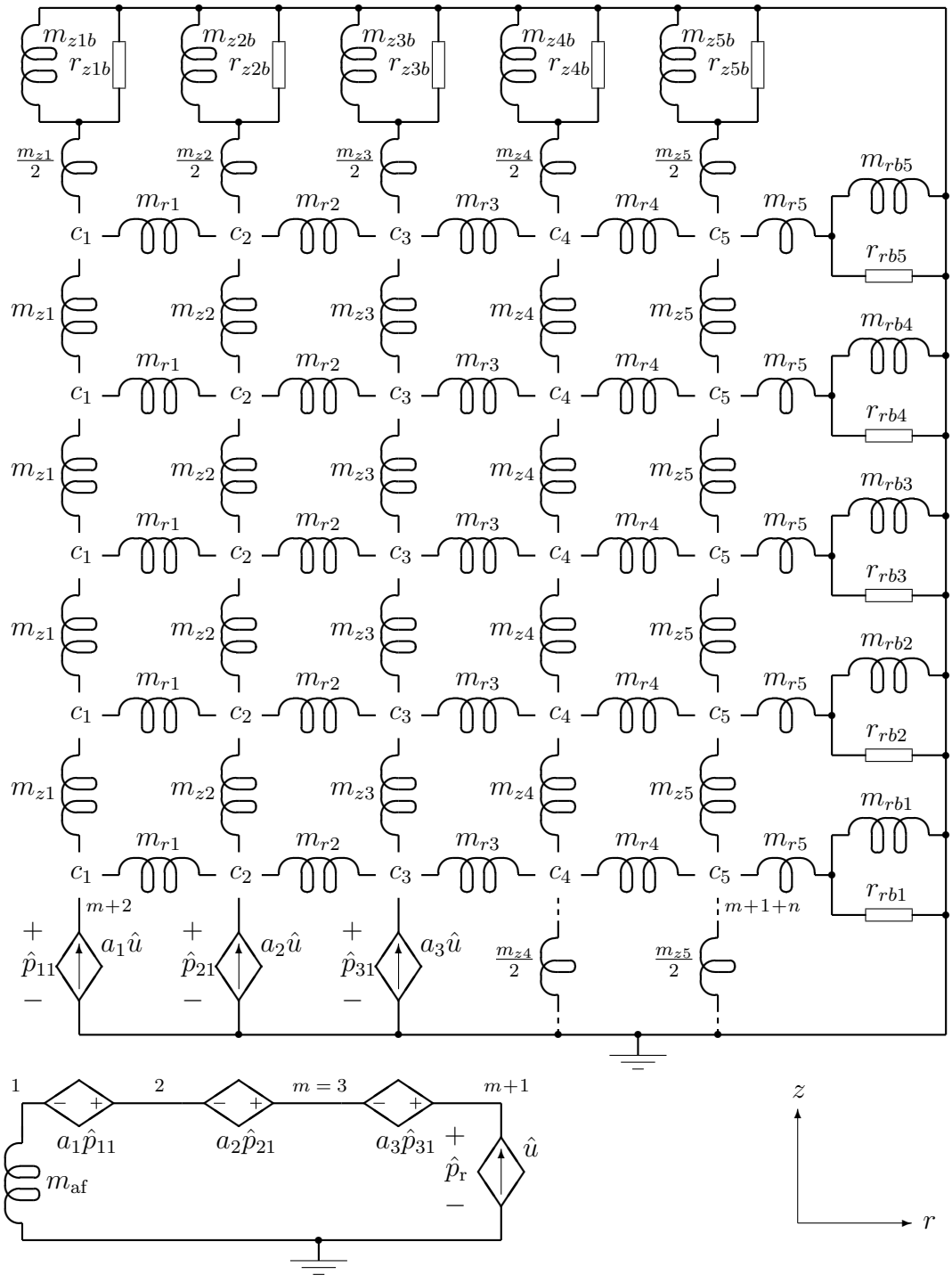

Figure 11.1: *Normalized FDEC model of a circular rigid piston, with or without an infinite planar baffle, in cylindrical coordinates* (r, ϕ, z)*, with* $m = 3$ *and* $n = 5$ *(see text). Selected nodes are numbered in terms of* m *and* n*. The truncated axial mass elements* $\frac{1}{2}m_{zi}$ *are present only in the unbaffled case. The anechoic-boundary admittance elements are strictly valid only in the baffled case.*

by the array of coupled controlled sources at the bottom of the diagram. The flux source $\hat{u}$ is used only for the AC analyses (Section 11.4); it is replaced by a raised-cosine pressure source for the subsequent transient analysis (Section 11.5). The diagram shows both the baffled and unbaffled versions of the problem; dotted lines indicate that the truncated axial mass elements $\frac{1}{2}m_{zi}$ are present only in the unbaffled case. The anechoic-boundary admittance elements (parallel "*R-L*" combinations) are calculated for a point-source and are accurate only in the baffled case. The error caused by the false point-source assumption will be seen in Section 11.4.

A review of the notation used in Fig. 11.1 may help avoid confusion. A subscripted r is an anechoic-boundary resistance element, while r without a subscript (or *in* a subscript) is the radial coordinate. A subscripted m is a mass element (a real number), while an unsubscripted m is the number of elements spanned by the radius of the diaphragm (an integer). A subscripted a is an area fraction, while an unsubscripted a (used in the text but not in the diagram) is the radius of the diaphragm. The values of the truncated axial mass elements are given in terms of the corresponding interior elements (hence the factor $\frac{1}{2}$); the truncated radial elements are labeled independently. Finally, whereas the text discusses phasor quantities (e.g. $\hat{P}_{\mathrm{r}}$ and $\hat{U}$), the diagram shows the corresponding time-dependent quantities ($\hat{p}_r$ and $\hat{u}$) because the mass elements are shown as real inductances rather than imaginary impedances.

A few notes on the node-numbering scheme are also in order. For illustrative purposes Fig. 11.1 is drawn for $m = 3$ and $n = 5$, although actual simulations described in this chapter use larger values of m and n. To facilitate comparison with the model-building program `disk.c`, the diagram shows some selected node numbers in terms of m and n. As always in SPICE, ground is node zero. Numbering of non-grounded nodes begins with the diaphragm interface, and then proceeds to the centers of the volume elements. The node number increases by one for each increment in i (or r_i). The diagram suggests that there are $n + 1$ non-grounded nodes in each row (i.e. in each constant-z plane), so that incrementing k (or z_k) should increases the node number by $n + 1$. However, the SPICE model uses a subcircuit for each combination of a truncated mass element and an anechoic-boundary impedance, so that the outermost non-grounded nodes in Fig. 11.1 (which are not centers of volume elements) become internal nodes in the subcircuits and do not contribute to the global node count. Thus the node number increases by n for each increment in k. Combining these rules, we find that the node number for the center of the i, k^{th} volume element is $m + 1 + (k-1)n + i$.

A listing of the model-building program `disk.c`, together with a discussion of implementation issues specific to SPICE, may be found in Section B.12. Following this, in Section B.13, is a listing of the circuit-definition file for the unbaffled disk with $m = 3$ and $n = 5$; this is the file created by `disk.c` to describe the circuit in Fig. 11.1. The values of m and n are passed to `disk.c` by command-line parameters. A third parameter selects between an AC analysis of a baffled disk, an AC analysis of an unbaffled disk, and a transient analysis of a baffled disk. The fourth and final parameter is the base name of the output files to be written by SPICE.

As in Chapter 10, the model-building program also creates a SPICE command file. The base name of the SPICE output files is obviously copied to this file. Some other features of the command file are explained in the following two sections.

11.4 AC analysis: radiation impedance

As in Subsection 10.1.1, the radiation impedance $Z_{\rm ar}$ will be represented as an acoustic resistance $R_{\rm ar}$ in parallel with an acoustic mass $M_{\rm ar}$. The normalized values of these three quantities are denoted by $z_{\rm ar}$, $r_{\rm ar}$ and $m_{\rm ar}$, respectively. By allowing $r_{\rm ar}$ and $m_{\rm ar}$ to be frequency-dependent, this representation can be extended to arbitrarily high frequencies, although the calculation of the impedance itself is reliable only for normalized frequencies in the range $|h| < m$.

It remains to show how $r_{\rm ar}$ and $m_{\rm ar}$ are calculated using SPICE. Using a notation similar to that of SPICE expressions, let $\hat{P}(\ell)$ denote the (phasor) normalized pressure at node ℓ. Then, with reference to Fig. 11.1, the radiation admittance can be written

$$\frac{\hat{U}}{\hat{P}(m+1)} = \frac{1}{z_{\rm ar}} = \frac{1}{r_{\rm ar}} + \frac{1}{jhm_{\rm ar}}. \tag{11.65}$$

Taking real parts and solving for $r_{\rm ar}$, we obtain

$$r_{\rm ar} = \frac{1}{\mathrm{Re}\left\{\hat{U}/\hat{P}(m+1)\right\}}. \tag{11.66}$$

We could similarly obtain $m_{\rm ar}$ by taking imaginary parts, but the resulting expression would depend on h, which in SPICE would be represented as `2*pi*frequency`. A simpler expression can be obtained by referring again to Fig. 11.1 and noting that

$$\frac{\hat{P}(1)}{\hat{U}} = \frac{1}{jhm_{\rm af}}. \tag{11.67}$$

Multiplying Eqs. (11.65) and (11.67), taking real parts and solving for $m_{\rm ar}$, we obtain

$$m_{\rm ar} = \frac{m_{\rm af}}{\mathrm{Re}\left\{\hat{P}(1)/\hat{P}(m+1)\right\}}. \tag{11.68}$$

Eqs. (11.66) and (11.68) were used in the SPICE command files; the former equation was simplified by choosing $\hat{U} = 1$. In the baffled case, the output generated by the SPICE "`print`" command was processed by the program `taba.c` to produce Table 11.1. In the unbaffled case, the SPICE output was processed by the program `tabu.c` to produce Table 11.2. (The two programs, which are quite similar, are listed in Section B.14.)

The variable `f` in the first column of Table 11.1 is the `frequency` variable used by SPICE, while the second column is the normalized *radian* frequency h; as $h = 2\pi$`f`, we can interpret `f` as the normalized *cycle* frequency. In both the resistance section and the inertance section, the frequency increases as we read down the page; hence the top line of each section should be compared with the low-frequency limit given by Beranek (see Eqs. (10.1) and (10.2)). For the reader's convenience, these limits have been normalized and printed in the headings of the two sections of the table.

The third, fourth and fifth columns use the same n/m ratio (or b/a ratio), but m increases—and the accuracy of the finite-difference approximation consequently improves—as we move to the right. Hence the top resistance or inertance moves closer to the expected LF limit as we move from the third column to the fifth.

The sixth and seventh columns use the same values of m as the third and fifth columns, respectively, but use a slightly higher n/m ratio (3.5 instead of 3.0), so

Table 11.1: *Normalized radiation impedance of a circular rigid piston in an infinite planar baffle, calculated by the FDEC method, and represented as a frequency-dependent resistance in parallel with a frequency-dependent inertance. The low-frequency (*`LF`*) limits of resistance and inertance are quoted from an analytical solution. The simulated region is divided into $n \times n$ volume elements. The radius of the piston spans m elements. The* `frequency` *variable used by SPICE is* `f` $= h/2\pi$*, where h is the normalized angular frequency.*

	m,n:	6,18	7,21	8,24	6,21	8,28
f	h	Resistance (LF limit = 1.4410):				
0.0100	0.0628	1.4960	1.4828	1.4740	1.4960	1.4741
0.0158	0.0996	1.4959	1.4828	1.4739	1.4959	1.4740
0.0251	0.1578	1.4954	1.4823	1.4735	1.4954	1.4736
0.0398	0.2501	1.4940	1.4810	1.4722	1.4940	1.4723
0.0631	0.3964	1.4902	1.4775	1.4689	1.4902	1.4689
0.1000	0.6283	1.4811	1.4689	1.4607	1.4821	1.4613
0.1585	0.9958	1.4628	1.4506	1.4424	1.4626	1.4425
0.2512	1.5783	1.3971	1.3897	1.3847	1.3984	1.3845
0.3981	2.5014	1.2368	1.2346	1.2330	1.2280	1.2265
0.6310	3.9644	0.9327	0.9389	0.9437	0.9292	0.9454
1.0000	6.2832	0.9448	0.9870	1.0033	0.9269	0.9978
1.5849	9.9582	0.8211	0.6576	0.8926	0.8299	0.8894
2.5119	15.7826	33.2095	2.9873	0.3733	33.7279	0.5678
f	h	Inertance (LF limit = 0.8488):				
0.0100	0.0628	0.8652	0.8615	0.8589	0.8652	0.8589
0.0158	0.0996	0.8656	0.8618	0.8593	0.8656	0.8593
0.0251	0.1578	0.8666	0.8628	0.8603	0.8666	0.8603
0.0398	0.2501	0.8690	0.8653	0.8628	0.8690	0.8628
0.0631	0.3964	0.8752	0.8715	0.8691	0.8751	0.8690
0.1000	0.6283	0.8908	0.8875	0.8853	0.8907	0.8852
0.1585	0.9958	0.9335	0.9310	0.9292	0.9348	0.9300
0.2512	1.5783	1.0696	1.0687	1.0682	1.0633	1.0646
0.3981	2.5014	1.6663	1.6744	1.6809	1.6181	1.6504
0.6310	3.9644	1.2516	1.3804	1.4782	1.4667	1.6179
1.0000	6.2832	2.5066	1.8752	1.6959	2.6449	1.7224
1.5849	9.9582	0.6421	0.8185	3.8340	0.3050	0.3843
2.5119	15.7826	0.0507	0.0301	0.0534	0.0510	0.0671

that the "far-field" anechoic boundary is placed further from the source. This might be expected to improve the accuracy further. But we see from the table that for all h less than unity, the calculated resistance and inertance are far more sensitive to m than to n/m, indicating that the FDEC approximations (including non-FDM boundary approximations) are a greater cause of error than the proximity of the "far-field" boundary. This is not surprising when we remember that there is a velocity discontinuity at the edge of the diaphragm—i.e. at the boundary of one of the volume elements whose central pressure contributes to the impedance calculation.

That the impedance is nearly independent of b/a only at low frequencies ($h < 1$) is also to be expected, for two reasons. First, at low frequencies the radius of the piston is a small fraction of a wavelength, so the signals received from different parts of the source vary little in phase and the radiated field resembles that of a point-source even at quite small distances. At higher frequencies the source is acoustically large, so that near-field effects have more influence on the impedance required at the anechoic boundary; to take an extreme example, as the frequency approaches infinity, the field radiated by a planar rigid piston becomes a cylindrical beam of *plane* waves—not spherical waves as assumed in the model of the boundary impedance. Second, all parts of the FDEC model, including the representation of the anechoic boundary, become less accurate as frequency increases. Obviously the position of the boundary has a significant effect if the model of the boundary is not anechoic. This effect explains the erratic behavior of the bottom two lines in each half of the table, in which h is greater than all values of m.

If we take the top right figure in each section of the table, corresponding to the largest m, the larger n/m and the lowest h, we find that the normalized resistance is in error by +2.3% and the normalized inertance by 1.2%. This accuracy is achieved by dividing the diaphragm area into only eight elements, although 784 volume elements are then required to model the simulated region.

Table 11.2 has the same format as Table 11.1 but shows the radiation impedance for *one* side of an unbaffled disk. (In the terminology of Beranek [11, pp. 124, 126], the radiation impedance "for one side" is the impedance between the front face of the piston and the notional surface at infinity, whereas the radiation impedance "for both sides" is the impedance between the front and back faces.) The behavior of the inertance component (lower half of the table) is similar to that of the baffled disk, except that the errors are greater (13.9% in the best case, compared with 1.2% for the baffled disk). Whereas the baffled disk has a velocity discontinuity at the edge, the unbaffled disk has a pressure discontinuity accompanied by a circulating flow of air; hence the velocity singularity is more complex than for the baffled disk, causing a greater finite-difference error. As this error depends on m, the frequency range over which the total error depends mainly on m is greater than in the baffled case. The bottom two lines in each half of Table 11.2 are erratic, as in Table 11.1, because the FDEC model loses accuracy throughout the simulated region. The most salient difference between the two tables, namely the low-frequency behavior of the resistance, requires further discussion.

According to Beranek [11, p. 126], the radiation impedance for *both* sides of an unbaffled circular piston of radius a can be approximated at low frequencies by an inertance of $0.2705\,\rho_o/a$ in series with a frequency-dependent resistance of $0.01901\,a^2\rho_o\omega^4/c^3$. Dividing these values by 2 (to obtain the impedance for one side

Table 11.2: *Normalized radiation impedance on one side of an unbaffled circular rigid piston, calculated by the FDEC method. Symbols have the same meanings as in Table 11.1. The low-frequency limit of inertance is quoted from an analytical solution. The resistance should be proportional to $1/h$ at low frequencies, but the FDEC model predicts a finite limit whose value depends on n/m. The error is caused by the point-source assumption used in the calculation the anechoic-boundary elements; the source would be more accurately modeled as a dipole.*

	m,n:	6,18	7,21	8,24	6,21	8,28
f	h	Resistance:				
0.0100	0.0628	26.4724	26.4795	26.4849	36.0902	36.0947
0.0158	0.0996	26.3748	26.3848	26.3922	35.9020	35.9159
0.0251	0.1578	25.8643	25.8749	25.8827	34.9392	34.9556
0.0398	0.2501	24.5242	24.5339	24.5408	32.4506	32.4653
0.0631	0.3964	21.4239	21.4315	21.4366	26.9069	26.9179
0.1000	0.6283	15.3035	15.3094	15.3128	16.9770	16.9849
0.1585	0.9958	7.1275	7.1292	7.1294	6.6347	6.6329
0.2512	1.5783	2.8915	2.8953	2.8968	2.9581	2.9653
0.3981	2.5014	1.4958	1.4992	1.5005	1.4807	1.4882
0.6310	3.9644	0.9641	0.9628	0.9617	0.9656	0.9664
1.0000	6.2832	0.9901	1.0347	1.0481	0.9646	1.0392
1.5849	9.9582	0.9104	0.6643	0.9741	0.8125	0.9158
2.5119	15.7826	15.1697	3.9446	0.3519	19.3024	0.1776
f	h	Inertance (LF limit approx. 0.425):				
0.0100	0.0628	0.504	0.493	0.484	0.503	0.484
0.0158	0.0996	0.505	0.493	0.485	0.504	0.484
0.0251	0.1578	0.506	0.495	0.486	0.505	0.485
0.0398	0.2501	0.510	0.498	0.489	0.509	0.489
0.0631	0.3964	0.519	0.507	0.498	0.519	0.498
0.1000	0.6283	0.545	0.532	0.522	0.546	0.523
0.1585	0.9958	0.627	0.611	0.599	0.629	0.601
0.2512	1.5783	0.863	0.836	0.816	0.869	0.822
0.3981	2.5014	1.928	1.828	1.760	1.848	1.717
0.6310	3.9644	1.019	1.081	1.125	1.163	1.204
1.0000	6.2832	6.212	2.340	1.842	6.303	1.994
1.5849	9.9582	-1.923	12.718	11.362	0.478	0.392
2.5119	15.7826	0.052	0.032	-0.018	0.051	0.018

only) and normalizing, we obtain an inertance of

$$m = 0.4249 \tag{11.69}$$

in series with a resistance of

$$r_\mathrm{s} = 0.2986\, h^4. \tag{11.70}$$

We require a parallel combination having the same asymptotic behavior at low frequencies. Because $r_\mathrm{s} \propto h^4$ in this case, the inertance is the dominant impedance term at low frequencies, so we require a small-r_s approximation. The admittance of the series combination is

$$\frac{1}{jhm + r_\mathrm{s}} = \frac{1}{jhm\left(1 + \frac{r_\mathrm{s}}{jhm}\right)} \approx \frac{1 - \frac{r_\mathrm{s}}{jhm}}{jhm} = \frac{1}{jhm_\mathrm{ar}} + \frac{1}{r_\mathrm{ar}} \tag{11.71}$$

where

$$m_\mathrm{ar} = m = 0.4249 \tag{11.72}$$

(which is the "LF limit" given in Table 11.2) and

$$r_\mathrm{ar} = h^2 m^2 / r_\mathrm{s} = 6.049/h^2. \tag{11.73}$$

So $r_\mathrm{ar} \to \infty$ as $h \to 0$. But Table 11.2 suggests that r_ar approaches a finite limit which depends on n/m. The limit is insensitive to m, indicating that FDEC approximations are not the main cause of this error. (Indeed the calculated resistance, and hence the error therein, remains comparatively insensitive to m for all $h < 1$.) Since n/m is proportional to the distance from the origin to the simulated boundary, the dependence of the calculated resistance on n/m implies that the model of the boundary is not anechoic. Having absolved the FDEC approximations, we must attribute the non-anechoic behavior to the assumed boundary impedance. As explained in Subsection 6.5.4, the point-source radiation condition is not valid for a source producing a net flux of zero; Table 11.2 is the promised illustration of this effect.

That said, we should also note that the error in r_ar caused by the radiation condition is minor compared with the error in m_ar caused by FDEC effects. The computed low-frequency values of m_ar and r_ar give a normalized time constant of about 0.0134, corresponding to a transition frequency $h \approx 75$, whereas the limit of the computed r_ar is approached for values of h less than about 0.1. The high transition frequency indicates that the computed radiation impedance is almost purely inductive—as it should be—as the computed r_ar approaches its false limit.

11.5 Transient analysis: checking for echoes

In the case of the baffled circular piston, the simulation of the anechoic boundary condition is claimed to be a valid far-field approximation. The most direct way to test this claim is to perform a transient analysis in which we transmit a pulse from the source and verify that there are no significant echoes from the boundary of the simulated region.

11.5.1 Normalized time

Because frequency in the FDEC model has been normalized, the abscissa of the transient response will be a *normalized time*, denoted by $\hat{t}$. Eq. (11.39) indicates that ω is normalized by multiplying by a/c. So any quantity proportional to ω^{-1} is normalized by multiplying by c/a. The period T becomes

$$\hat{T} = \frac{cT}{a} \tag{11.74}$$

and in general,

$$\hat{t} = \frac{ct}{a}. \tag{11.75}$$

Alternatively, we can argue that dimensionless expressions must remain invariant under the normalization; in particular,

$$\omega t = h\hat{t}. \tag{11.76}$$

Substituting from Eq. (11.39) and solving for $\hat{t}$ gives Eq. (11.75). Physically, $\hat{t}$ is the ratio of the distance traveled by sound in time t to the radius of the piston.

11.5.2 The test signal

To ensure that any reflections will not be masked by time-overlap between the direct and reflected signals, the pulse must be of finite duration. Furthermore, to minimize the number of volume elements needed for the simulation, the spatial spread of the pulse and hence the duration of the pulse should be as short as possible. But the pulse cannot be made arbitrarily short; because the FDEC model is accurate only for frequencies in the range $|h| < m$, the pulse must not contain substantial spectral energy outside this range. Thus we require a function which is time-limited and almost band-limited.

It is well known that a raised-cosine pulse of duration $2T$ has almost all of its spectral energy in the band $|\omega| < 2\pi/T$ (see e.g. [40], p. 62). Indeed, it is shown in Section B.12 that only 0.0515% of the energy—corresponding to 2.27% of the r.m.s. amplitude—is outside the band $|\omega| < 2\pi/T$. If this pulse has a peak amplitude of 2 at time $t = 0$, it is described by the equation

$$g(t) = \begin{cases} 1 + \cos\left(\dfrac{\pi t}{T}\right) & \text{if } |t| < T, \\ 0 & \text{otherwise.} \end{cases} \tag{11.77}$$

It remains to choose a suitable T for the pulse. Recalling Eq. (11.41), let us choose $\hat{T}$ so that no more than 0.0515% of the energy is outside the band $|h| < m$. As $g(t)$ has this fraction of its energy outside the band

$$|\omega| < \frac{2\pi}{T}\,, \tag{11.78}$$

our problem is to ensure that $|h| < m$ inside this band. Eq. (11.78) can be normalized (e.g. by multiplying both sides by a/c) to obtain

$$|h| < \frac{2\pi}{\hat{T}} \tag{11.79}$$

so we can be sure that $|h| < m$ if

$$\frac{2\pi}{\hat{T}} < m\,, \tag{11.80}$$

i.e. if

$$\hat{T} > \frac{2\pi}{m}. \tag{11.81}$$

When this condition is met, less than 2.27% of the r.m.s. amplitude is outside the band $|h| < m$.

Condition (11.81) is just met by setting $\hat{T} = 6.5/m$; a short $\hat{T}$ minimizes the number of elements required for the simulation, but severely tests the accuracy bandwidth of the FDEC model.

If the test function is to be implemented in a SPICE transient analysis, it must be time-shifted so that it is zero for $t < 0$. This is accomplished by writing $(t-T)$ for t in Eq. (11.77). We normalize the times by noting that $t/T = \hat{t}/\hat{T}$, and consider g to be a function of $\hat{t}$. Dividing the function by $2\hat{T}$ normalizes the magnitude so that

$$\int_{-\infty}^{\infty} g(\hat{t})\, d\hat{t} = 1 \tag{11.82}$$

giving a pulse of unit area[2] for any value of $\hat{T}$. Finally we put $\hat{T} = 6.5/m$. The result is

$$g(\hat{t}) = \begin{cases} \dfrac{1 - \cos\left(\frac{m\pi\hat{t}}{6.5}\right)}{13/m} & \text{if } 0 < \hat{t} < 13/m, \\ 0 & \text{otherwise.} \end{cases} \tag{11.83}$$

In the model-building program the non-constant segment of $g(\hat{t})$ is implemented by the function "`rc`". For a discussion of the code which produces the transient source specification, illustrated by a listing of the specification used later in this section, see Section B.12.

It remains to decide whether the test function represents a pressure or a flux. In a diverging spherical wave, according to Eqs. (3.17) and (3.35), the pressure falls of as $1/R$ regardless of frequency, while the velocity falls off in a more complex, frequency-dependent manner. If the waveform is a pulse whose spectrum spans a range of frequencies, the shape of the pressure wave (in time, not in space) is independent of radius, whereas the velocity waveshape varies. But at large radii, the velocity wave approaches geometric similarity with the pressure wave (see Subsection 3.3.5). Thus we can fix the pressure waveshape at all radii and the velocity waveshape in the far field by specifying the pressure at a single radius. This conclusion applies exactly to a point source; for a sufficiently small distributed source, it suggests that the source pressure is more similar to its far-field counterpart than the source velocity.

11.5.3 Prediction of reflections by geometrical optics

The total path lengths for reflected signals, and hence their arrival times, can be calculated by geometrical optics. If any reflections are observed in the transient response, the arrival times may identify the path of the reflection or at least reduce

[2]The area normalization was done with a view to experimenting with shorter pulses and observing the finite-difference errors; but this option has not been pursued within the present thesis.

the range of possibilities. Because the geometry of the problem is determined by the ratio n/m, we must first choose reasonable values for these variables.

For a given n/m ratio, a smaller m gives fewer elements in the model. To ensure that the model represents a *distributed* source and tests the claim that a distributed source has the same far-field radiation condition as a point-source, we refrain from choosing $m = 1$. A somewhat arbitrary compromise is $m = 4$. This gives $\hat{T} = 6.5/m = 1.625$. Since T is the shortest period of the significant components of the test pulse (by Eq. (11.78)), the shortest significant wavelength is 1.625 times the radius of the diaphragm; that is, the diameter of the source is slightly greater than a wavelength. Thus the source is not acoustically small at all frequencies of interest. Moreover, because the pressure at every point on the diaphragm is coupled to the velocities at all other points, we do not have a simple specification of the pressure at a single radius (i.e. over a single spherical surface). Hence we may expect the pressure waveform in the far field to be noticeably different from that at the source.

Now consider the constraints on n. To avoid masking of weak reflections by the strong direct signal, there must be no time-overlap between the direct and reflected signals at the test point(s). The spatial spread of the pulse is $2\hat{T}m = 13$ elements, so that a clearance of at least 6.5 elements between the test point and the boundary seems to be sufficient. The clearances should be increased, however, to allow for distortion of the waveforms. As the direct signals have shorter paths than the reflected signals, the suppression of echoes is exaggerated by geometric spreading; to minimize this effect, the test point(s) should *not* be much closer to the source than to the boundaries. These requirements have been met by taking $n = 32$ and using two test points, denoted by A and B, at the centers of compliance elements $\Delta C_{16,7}$ and $\Delta C_{16,17}$, respectively, giving a minimum clearance of 15.5 elements between the test points and the anechoic boundary. (The model-building program calculates these subscripts in terms of n to ensure that they are legal for all n.) Points A and B, together with their coordinates in terms of Δr and Δz, are shown in the upper inset of Fig. 11.2.

Because sound travels through a distance a in a normalized time of unity (see Eq. (11.75)), the coordinates and the overall dimensions of the model can be expressed as equivalent normalized times[3] by dividing by $a = m\Delta r = m\Delta z$, where $m = 4$. Hence we can calculate the normalized propagation times of direct and reflected signals according to geometrical (ray) optics. For the reflected rays there is no need to calculate the coordinates of the points of reflection; as the reflecting surfaces are mutually parallel or perpendicular, it is a simple matter to locate the virtual images of the source (which form a two-dimensional array) and find the straight-line path lengths from the virtual sources to the observation points. (For the purpose of locating images, the z axis can be treated as a perfect reflector because of the rotational symmetry. When the problem is visualized in three dimensions, the virtual images of the origin, other than those on the z axis, are coaxial circles, not points.) The normalized propagation times are converted to normalized peak-arrival times by adding $\hat{T} = 13/8$, i.e. by adding the delay between $\hat{t} = 0$ and the peak of the test pulse.

[3]The author resists the temptation to use the term "normalized distance" because the normalization process began with acoustic impedance, which depends on area, not length. If area is normalized by dividing by πa^2, distance is normalized by dividing by $\sqrt{\pi}\, a$, which is not convenient.

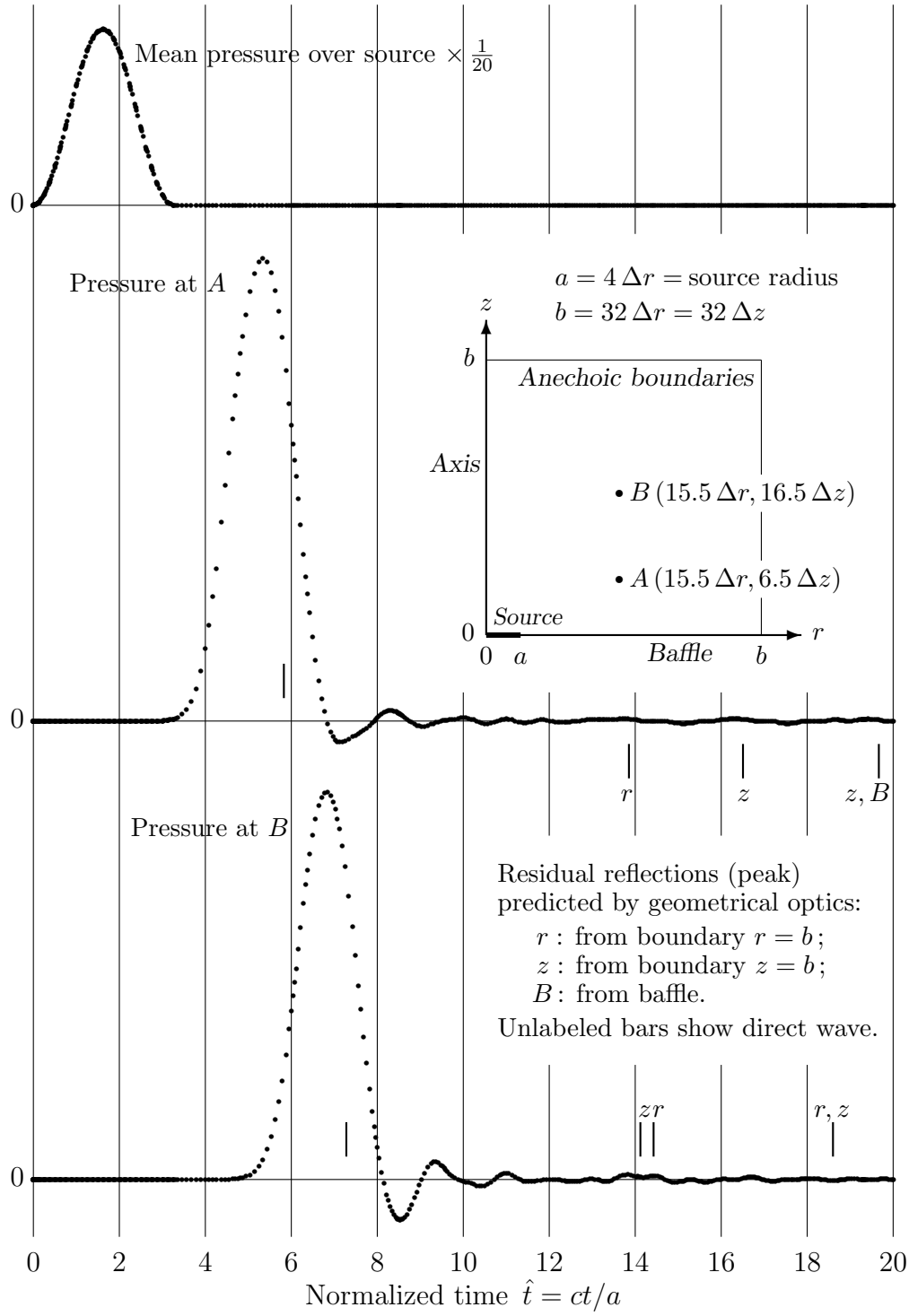

Figure 11.2: *FDEC calculation of the transient response at two points A and B (see upper inset) in the field of a circular rigid piston in an infinite planar baffle, in cylindrical coordinates* (r, ϕ, z)*, with* $m = 4$ *and* $n = 32$*. The vertical scale is arbitrary except that the top trace (showing the initial pressure pulse produced by the piston) is compressed by a factor of 20 relative to the other two. Vertical bars show arrivals of direct and reflected wave crests as predicted by geometrical optics (see lower inset). Reflections from the model boundaries are weak, as intended.*

The resulting arrival times are indicated by the short vertical bars in Fig. 11.2. As an aid to interpreting the time scale, note that it takes 8 units of normalized time for sound to travel a distance b, i.e. from the origin to the closest points on the anechoic boundary. So a time frame of 20 units includes a manageable number of single and double reflections.

11.5.4 Simulation results and discussion

The top trace in Fig. 11.2 is the test pulse. The middle trace is the pressure at point A and the bottom trace the pressure at point B. As in all graphs in this thesis, no interpolation is used. The three pressures are plotted at the discrete times used by SPICE in the transient analysis; the variable increment used by SPICE is manifested as a variable spacing between the plotted points. On each of the lower two traces, an unlabeled bar shows the expected arrival of the direct signal, and bars labeled "r" and "z" show the expected arrivals of the signals reflected from the constant-r and constant-z boundaries, respectively. The bar labeled "r, z" predicts the arrival at B of the signal reflected first by the constant-r boundary and then by the constant-z boundary; both points of reflection are near the top right hand corner of the simulated region (as it is seen in cross-section in the upper inset). Because both boundaries involved are meant to be anechoic, this doubly-reflected signal should be much weaker than the singly-reflected signals. The same cannot be said for the signal which strikes the constant-z boundary and the baffle before arriving at A, because a rigid baffle is totally reflective. The arrival of this signal is predicted by the "z, B" bar on the middle trace. These are all the reflections expected within the time frame of the graph.[4]

The reflections are exceedingly weak and clearly vindicate the FDEC model of the anechoic boundary condition. On the middle trace, we can just discern three ripples whose location and duration may be consistent with weak reflections. The bottom trace has a more obvious double ripple at about the expected time, but the duration seems too short for a reflection of the test pulse. It is just possible that the two singly-reflected signals happen to cancel at B (bottom trace), where their arrival times almost coincide, but no such possibility exists at A (middle trace). At A, the reflected wavefront is expanding in the z direction but *contracting* in the ϕ direction; as this contraction reduces the attenuation due to geometric spreading, the weakness of the reflection from the cylindrical boundary is especially significant.

As predicted above, there is some distortion of the raised-cosine waveform because the pressure is not imposed over a constant-R surface (where R is the spherical radial coordinate). Another possible reason for the distortion is suggested by Eq. (10.63), which indicates that the FDEC method underestimates the resonance frequencies of pipes—and hence the speed of sound—by a fraction which increases with frequency. This conclusion is based on Arai's error analysis [2], which uses plane waves in Cartesian coordinates, but can be generalized in a qualitative way as follows. If P has a spatial average of zero, so does $\nabla^2 P$, so that any finite-difference estimate of $\nabla^2 P$ must approach zero as the step size increases. Hence, for large step

[4]The first reflected signal to arrive outside the time frame strikes the constant-r boundary on the far side of the z axis (i.e. the left side in the upper inset), and crosses the z axis on its way to point A. Of course "point" A is really a circle about the z axis, so we may regard the same signal as striking the constant-r boundary on the right side of the z axis, then crossing the axis and reaching point A on the left side.

sizes and/or high frequencies, the FDEC method will tend to underestimate $|\nabla^2 P|$ for given P. Now the Helmholtz equation can be written

$$-\omega^2 P = c^2 \nabla^2 P. \tag{11.84}$$

An underestimate of $\nabla^2 P$ unbalances this equation in the same direction as an underestimate of c^2 and therefore has a similar effect on the calculated pressure distribution. If the FDEC model underestimates c^2, and hence c, by a margin which increases with frequency, it effectively represents a *dispersive medium* in which high-frequency components of signals are delayed more than low-frequency components. This effect may be partly responsible for the overshoot and ringing in the calculated waveforms at A and B.

Another apparent anomaly in Fig. 11.2 is that, at both observation points, the wave peak arrives sooner than predicted by geometrical optics. There are two reasons for this. First, the prediction assumes that the temporal peak of the waveform coincides with the spatial peak. But in fact, because the wave decays as it propagates, the *envelope* of the wave—i.e. the graph of the (temporal) peak pressure versus radius—is a decreasing function of radius. Hence the temporal peak occurs not at the spatial peak but rather at the point of tangency between the spatial waveform and its envelope, and this point is on the leading slope of the wave. So the temporal peak arrives *before* the spatial peak and hence before the "predicted" time shown in Fig. 11.2. Second, because the source is distributed, and because the amplitude of the signal radiated from each point on the source decays with distance, the signals received from the near side of the source are weighted more than those received from the far side. As the time delay applicable to the near side of the source is shorter, the weighting of the near side reduces the delay of the peak of the total signal. Both of these effects become less pronounced as the propagation distance increases; hence the arrival times of the reflected signals should be more accurately predicted than those of the direct signals.

In summary, the FDEC model of the free-air boundary has been tested in the time domain, at several angles of incidence, using a pulsed signal containing the full range of frequencies over which the FDEC method is claimed to be reliable under the most favorable conditions (plane waves and Cartesian coordinates). Although these conditions did not hold, the simulated boundary was found to be nearly anechoic, as intended.

Chapter 12

Conclusions

From the large volume of theory and computation in this thesis, together with the numerous references to possible extensions or improvements of the models, it can be seen that the linear modeling of loudspeaker components was and remains a fertile area of research. The restriction to linear models does not greatly diminish the usefulness of this work, because the linear distortions of loudspeakers are a continuing problem in analysis and design. Moreover, linearity makes the problem tractable, so that there is no excuse for not attempting a solution. This thesis does not come close to offering a complete solution—for example, it does not (yet) allow for non-local boundary conditions caused by non-rigid walls—but it offers an equivalent-circuit model of a loudspeaker which, unlike older equivalent-circuit models, takes account of the wave-like nature of the acoustic field in the enclosure and the effects of the resulting resonances on the system response. The ability to predict the response of a given system is of course a first step towards designing a system with a prescribed response.

In the presentation of the foundations of linear acoustics, much theoretical economy has been achieved by using the techniques of vector analysis to derive the fundamental equations in a hierarchy of forms. The "one-parameter" or "1P" forms have been expressed with novel generality. These apply to a "1P" pressure field, which is initially defined as a field in which the excess pressure depends on only one spatial coordinate ξ measuring arc length normal to the constant-ξ surfaces (isobaric surfaces).

The equation of motion, which expresses Newton's second law for a non-viscous fluid, has a sequence of forms in which each form inherits the assumptions of its predecessor. The most general integral form applies to a closed surface moving with the fluid. The linearized point form (differential form) assumes irrotational flow, low gravity, and small oscillations and compressions. In a 1P pressure field, this point form can be integrated to obtain the 1P form, which applies to normal oscillations of a uniform thin shell between two isobaric surfaces. The 1P form leads to the concept of distributed acoustic mass, whose electrical analog is distributed inductance. If the fluid is assumed incompressible in some region, the 1P form can be integrated to give a fourth form, which applies to ports or vents and leads to the concept of (lumped) acoustic mass, whose electrical analog is (lumped) inductance.

The equation of continuity expresses conservation of mass and, when combined with a relationship between pressure and density, yields the equation of compression. The integral form of the equation of continuity applies to a stationary closed surface.

If we assume small compressions and barotropic conditions, we obtain the linearized point form (differential form) of the equation of compression, which can be integrated over a fixed volume to obtain the integral form of the equation of compression. This form leads to two others. The first assumes uniform excess pressure throughout the volume, and leads to the concept of (lumped) acoustic compliance, whose electrical analog is (lumped) capacitance. The second is the 1P form, which applies to a uniform thin shell between two isobaric surfaces in a 1P pressure field. The 1P form leads to the concept of distributed acoustic compliance, whose electrical analog is distributed capacitance. Thus the four forms of the equation of compression do not form a linear sequence.

The point forms of the equations of motion and compression lead to the wave equation, while the 1P forms lead to Webster's horn equation. Both equations apply not only to the excess pressure, but also to the velocity potential, whose existence is guaranteed by the linearizing assumptions. Provided that the compressibility of air is explicitly represented by compliance elements, Kirchhoff's laws are applicable to the pressures and fluxes in lumped acoustic masses and compliances, so that these components can legitimately be connected into "acoustic circuits".

The well-known "Webster" horn equation has been placed on a new theoretical foundation which assumes (exact or approximate) 1P waves. This approach removes any *a priori* assumption concerning the wavefront shape, but leads to the conclusion that there are only three wavefront shapes allowing exact 1P propagation.

Webster's equation follows *exactly* from the 1P forms of the equations of motion and compression. The ξ coordinate is the axial coordinate of the horn while $S(\xi)$ is the area of a constant-ξ surface segment bounded by a tube of orthogonal trajectories to all the constant-ξ surfaces; such tubes (and no others) are possible boundary surfaces for a horn satisfying Webster's equation in ξ. As far as the derivation of Webster's equation is concerned, the shape of the wavefront (isobaric surface) is arbitrary—in particular, it is not necessarily planar. Note that $S(\xi)$ must be calculated from the actual wavefront, and not from a tangent plane.

It has also been shown that the Helmholtz equation admits solutions depending on a single spatial coordinate u if and only if $|\nabla u|$ and $\nabla^2 u$ are functions of u alone. The $|\nabla u|$ condition allows u to be transformed to the coordinate ξ which measures arc length normal to the isobaric surfaces; that is, $|\nabla \xi| = 1$. Hence, in the initial definition of a "1P" pressure field, the normal-arc-length condition is redundant, and the definition can be weakened accordingly. The condition that $|\nabla \xi| = 1$ yields an expression for the Laplacian of a 1P pressure field, from which it has been shown the wave equation reduces *exactly* to Webster's horn equation; this is a second derivation making no *a priori* assumption concerning the wavefront shape.

A 1P acoustic field has uniform excess pressure, uniform velocity potential, normal and uniform fluid velocity and uniform intensity over every isoparametric surface (wavefront), and exhibits rectilinear propagation; these conditions apply at all frequencies. The conditions on excess pressure, velocity potential and velocity are equivalent, so there is no ambiguity in the description "1P".

The only coordinates admitting *exact* 1P waves are those whose level surfaces are parallel planes or coaxial cylinders or concentric spheres; consequently, the guiding surface of an exact 1P waveguide must be a cylinder or a cylindrical sector or a cone, respectively. The proof of this fact is complex and depends on most of the theory leading to the general derivation of Webster's equation in a coordinate admitting 1P

waves. Hence, although it is possible to obtain Webster's equation from the wave equation in each of the three permitted coordinates, the general derivation requires less supporting theory. The general derivation also reveals the common feature of all 1P acoustic fields which makes Webster's equation applicable: such fields can be described in terms of a normal-arc-length coordinate.

A true 1P waveguide must be infinite, but if a 1P waveguide is truncated, it will remain approximately 1P at sufficiently high frequencies, and will therefore approach constant directivity as the frequency is increased; the constant directivity is confined to the near field for a cylindrical tube and for a cylindrical sectorial horn, but extends to the far field for a conical horn.

Webster's equation is approximately true for a horn carrying an approximately 1P wave. A tube or horn is approximately 1P if

(a) the cross-section remains small compared with the wavelength and varies gradually (i.e. changes by a small fraction in a distance comparable with the cross-sectional dimensions) and any curvature in the centroidal axis has a radius much larger than the cross-sectional dimensions, *or*

(b) the cross-section is large, but the tube or horn has a shape approximating that of one of the three families of exact 1P waveguides and is uniformly driven over one isoparametric cross-section, and the dimensions of the mouth (for a truncated horn) are much larger than a wavelength, *or*

(c) condition (a) holds for part of the length (possibly including the driving point) and condition (b) holds for the remainder.

A practical 1P horn having nearly constant directivity in the far field must be based on a conical horn. Directivity may be controlled by shaping the cross-section of the cone, and the loading characteristics (predicted by Webster's equation) may be varied by departing from the conical shape in the region of small cross-section. But such adjustments are only evolutionary; the design of practical constant-directivity horns cannot be fundamentally advanced by finding a new geometry for an exact 1P waveguide, because all possible 1P wavefront shapes are already known.

The finite-difference equivalent-circuit (FDEC) method for modeling acoustic fields has been extended to include 1P horns, three-dimensional fields in curvilinear orthogonal coordinates, 3D boundary conditions, and fiber-damped regions. The practical feasibility of the method has been illustrated with two computational examples, the first of which predicts the effects of internal resonances on the frequency response of a loudspeaker.

A finite-difference approximation to Webster's equation yields the nodal equations of an L-C ladder network, while a similar approximation to the wave equation in general curvilinear orthogonal coordinates yields the nodal equations of a three-dimensional L-C network. The same circuits can be obtained from the equations of motion and compression, confirming that "current" in the equivalent circuit is volume flux.

The topology and component values of the undamped 3D model are quite intuitive. The region to be simulated is divided into contiguous quasi-rectangular volumes, which are the compliance elements. The mass elements are also contiguous and quasi-rectangular, but are displaced (relative to the compliance elements)

by a half-element in each of the three coordinate directions. The value of each component is found by assuming that it is a rectangular prism, calculating its dimensions from the scale factors at its center (i.e. for the central values of the coordinates), and using the usual lumped-component formulae. For the truncated elements at the boundaries of the model, the same rules are applied to the reduced ranges of the coordinates. In all cases, pressure is sampled at the centers of two opposite faces of each mass element and at the body-center of each compliance element. For the purpose of calculating the fluxes through the six faces of each compliance element, velocities and scale factors are sampled at the centers of the faces. The scale factors at the centers of boundary surface elements are used to convert velocities to fluxes when applying boundary conditions.

The effects of fibrous filling materials can be represented by modifications to the equivalent circuit. The free-air components are retained in the model, except that their values are slightly changed because the fiber reduces the effective volumes and cross-sectional areas. A parallel mass-resistance combination appears in series with each mass element. The flux through the added mass represents motion of the fibers, while the flux through the added resistance represents motion of the air relative to the fibers. A series compliance-resistance combination appears in parallel with each compliance element. The time constant of the added R-C combination is the thermal time constant of the air-fiber system at constant pressure, while the time constant of the resulting C-R-C loop is the thermal time constant at constant volume. Two more time constants can be defined by fixing the fiber temperature, and one more by fixing the air temperature. All five time constants can be expressed in term of one of them, denoted by $\tau_{\mathrm{f}p}$, which is defined for constant fiber temperature and constant pressure. This can be calculated for practical purposes from the formula

$$\tau_{\mathrm{f}p} \approx \frac{\mathsf{d}^2}{8\alpha} \left(m^2 - m^{0.37}\right) \ln\left(\tfrac{m+1}{2}\right)$$

where d is the fiber diameter, α is the thermal diffusivity of air, f (not in the formula) is the fraction of the overall volume occupied by the fiber, and $m = f^{-1/2}$.

The thermal diffusivity (used in the above formula) is just one of the properties of air that affect the values of the FDEC elements. With the exception of the absorption coefficient (which does not appear in the models), all the linear acoustical properties of air can be calculated with acceptable accuracy from the temperature and pressure, using simple algebraic formulae which assume dry air. These formulae are sufficient for the analysis of small acoustic devices, in which atmospheric absorption is not a major contributor to damping.[1]

When constructing an FDEC model of a moving-coil loudspeaker in an enclosure, one must allow for the sharing of the diaphragm area between several volume elements. This can be accomplished by redrawing the conventional equivalent circuit of the driver so that it includes a transconductance instead of a transfer resistance, and partitioning the transconductance in the same fractions as the diaphragm area. The ratios of the j^{th} partial flux to the common back e.m.f. and of the j^{th} partial current to the j^{th} developed pressure are equal to the j^{th} partial transconductance.

In the FDEC model of a particular driver in a particular fiber-filled box, the

[1]Formulae for the absorption coefficient, which is sensitive to humidity as well as temperature and pressure, may be found in ANSI S1.26-1978 [41].

following observations have been made by neglecting selected components and comparing the response with that of the full simulation:

- Viscosity is the dominant mechanism of damping, thermal relaxation being of secondary importance;
- The neglect of internal elastic forces in the fibers is justified;
- The departure from thermal equilibrium (which occurs at high frequencies) has very little effect on the frequency response;
- While the addition of fiber increases the output at infrasonic frequencies, it *reduces* the output in the bass rolloff region and does *not* lower the 3 dB rolloff frequency; this conclusion applies not only to the overall effect of the fiber, but also to its thermal capacity alone.

All four observations are expected to be almost universally true—the first because it is so pronounced, and the others because they are consistent with qualitative predictions.

The classical problem of the circular rigid-piston radiator has been used to test the FDEC method in cylindrical coordinates with a free-air (anechoic) boundary condition. In the baffled version of the problem, the calculated radiation impedance depends more on the step size than on the distance to the anechoic boundary, indicating that the boundary impedance is accurately modeled. In the unbaffled version, at extremely low frequencies, the calculated parallel resistance depends more on the distance to the boundary, supporting the theoretical prediction that the anechoic boundary condition, which is calculated for a point-source, is not accurate for a dipole source. In the baffled case, the FDEC model of the free-air boundary has been tested in the time domain, at several angles of incidence, using a pulsed signal containing a comprehensive range of frequencies. The small amplitudes of the calculated echoes provide direct confirmation that the "anechoic" boundary is accurately represented.

12.1 Further work

The undamped FDEC method could be used to determine the loading and directional characteristics of a wide variety of infinite and truncated acoustic waveguides, some of which have been proposed by Geddes [18]. Each analysis requires an orthogonal coordinate system with known scale factors, and is greatly facilitated if the guiding surface is an equicoordinate surface, but the coordinate system need not be separable.

While the conditions under which a coordinate system admits one-parameter waves have been rigorously studied in this thesis, the discussion of the existence of *two*-parameter waves has been confined to the issue of what we mean when we say "By symmetry, the pressure is independent of…". A similarly rigorous study of two-parameter waves would be of interest because of the computational savings that follow from a reduction to two dimensions.

The loudspeaker model presented in this thesis does not allow for cabinet-wall vibrations. It may be possible to include these effects in the FDEC model using

finite-difference approximations to the equations describing flexural vibrations of planar sheets. The non-local nature of the boundary impedance presented by the wall would probably be expressed by coupled flux sources. Expected difficulties include edge conditions (coupling of panel motions through the corners of the box) and radiation loading. It may also be possible to model flexure of the diaphragm using the same technique.

The equation used for estimating the pneumatic resistivity of loosely-packed fibrous filling material (Eq. (7.33)) is believed to be much less accurate than that used for calculating the basic air-fiber thermal time constant (Eq. (7.119), quoted above). Unfortunately the pneumatic resistivity has been found to be the more important of the two quantities for the damping of resonances in loudspeaker enclosures, so that further work on the estimation of pneumatic resistivity is warranted. This work would involve the Navier-Stokes equations rather than the heat equation, and would require an averaging over possible orientations of the fibers; hence it would be more difficult than the estimation of the thermal time constant.

Other desirable improvements to the FDEC model-building program for the loudspeaker have been mentioned in the text and appendices, and are briefly reviewed here:

- The model could be extended to three dimensions and modified to take account of the precise diaphragm shape and the presence of the spider and magnet assembly.
- Restrictions on the topology and dimension-ratios of the box should be loosened.
- Elevation of the internal temperature of the box should be modeled.
- Alternative means of specifying the driver parameters should be allowed.
- The range of available graphs should be widened.
- The handling of input should be made more robust, e.g. to remove possible sources of floating-point exceptions.
- Specifications of boxes and drivers should be stored in files.
- The model builder and the circuit simulator should have a common interactive shell. More functions and options should be made interactive.
- The interface to SPICE should be at a lower level than that provided by the standard command cards.

The model-building program used in this thesis was developed to a level sufficient for its primary purpose: to include an approximate model of the spatial variation of pressure throughout the interior of the box and across the back of the diaphragm, and hence predict the effects of internal aeroacoustic resonances on the response of the loudspeaker.

The FDEC model of the loudspeaker-box system was developed with a view to analyzing box designs intended to suppress or control the effects of internal resonances. In this thesis it was possible to include only a simple fiber-filled design. The

author initially intended to include a study of alternative box topologies incorporating internal acoustic filters (combinations of chambers and vents, analogous to capacitors and inductors) designed to ensure that all parts of the enclosure behave approximately as lumped components. The adequacy of that approximation was to be assessed by the FDEC method. However, because of the unexpected expansion of other parts of the thesis, including the work on 1P acoustic fields and the air-fiber thermal time constant, the study of anti-resonant box designs must be reserved for a future project.

Appendix A

Somigliana's letter to *Atti Torino* (1919)

The following is a paraphrase of the letter "Sulle relazioni fra il principio di Huygens e l'ottica geometrica" by Carlo Somigliana, which appeared in *Atti della Reale Accademia delle Scienze di Torino*, vol. 54, no. 14a (1919), pp. 974–9. The Italian text was translated orally by Br. A. Moss, who was then at the Department of Studies in Religion, University of Queensland. In this English version, the author has removed much redundancy and circumlocution, introduced the Gibbs vector notation (which radically changes the appearance of most equations), replaced Somigliana's symbols with the symbols used elsewhere in this thesis, and added some explanatory clauses. The use of italics follows that in the original letter.

The two footnotes referring to the works of Laura and Bianchi are found in Somigliana's letter and are here labeled "(Original)". Other footnotes are explanatory notes added by the present author.

The letter shows that there are only three possible geometries in which a solution to the wave equation depends on only one spatial coordinate and has parallel level surfaces, namely those in which the level surfaces are parallel planes, coaxial cylinders, and concentric spheres.

On the Relations between Huygens' Principle and Geometrical Optics

Note of the resident National Associate CARLO SOMIGLIANA

The triply orthogonal system comprising a series of parallel surfaces and the rows of common perpendiculars along their lines of curvature[1] constitutes a complete and simple model of the propagation of waves in an isotropic medium according to Huygens' principle. The successive parallel surfaces, each of which may be regarded as the envelope of a set of spheres with equal radii and centered on a preceding surface, are the wavefronts. The common perpendiculars may be considered as the rays corresponding to these waves. According to Malus's theorem[2], the laws of rectilinear propagation and of reflection and refraction find a complete representation.

However, if this model, which constitutes the foundation of geometrical optics, is to be reconciled with the theory of mechanical and electromagnetic propagation, one must find solutions of the wave equation

$$\frac{\partial^2 \phi}{\partial t^2} = c^2 \nabla^2 \phi \tag{A.1}$$

(where ϕ is the wave function, t the time, and c the velocity of propagation) for which the constant-ϕ surfaces at any instant are parallel. Three special cases of this are well known: spherical, planar and cylindrical waves. But it can be shown that *these are the only cases*, so that there is a substantial difference between geometrical optics and the optics of mechanical and electromagnetic vibrations. Therefore a justification of Huygens' principle and of rectilinear propagation can be found only in the theory of retarded potentials, and in the hypotheses on extremely short wavelengths developed by Kirchhoff in his classic dissertation *Zur Theorie der Lichtstrahlen* of 1882.

A contrary result to that stated above was recently obtained by Prof. E. Laura in an article[3] included in the volume *Scritti matematici offerti ad Enrico D'Ovidio*, published last year upon his [D'Ovidio's?] retirement from teaching. In this very brief note, I show how one can arrive at the correct result directly and simply, avoiding the extrapolations to the limit which Laura uses but does not exhaustively discuss.

---

[1] This description assumes that the orthogonal trajectories to a family of parallel surfaces are straight lines (see Theorem 5.1) and that a perpendicular moving along the lines of curvature of one surface will trace out orthogonal curves on the other parallel surfaces (see Theorem 5.2 and the surrounding paragraphs in Section 5.4).

[2] This theorem, also known as the Malus-Dupin theorem, concerns the equivalence of the ray-based and wave-based formulations of the laws of reflection and refraction. The assemblage of normal lines to a surface Σ_0 is called a *normal congruence*. Eq. (5.26) in the proof of Theorem 5.2 implies that a normal congruence is cut orthogonally by *infinitely many* parallel surfaces; since $\mathbf{t}_0$ is normal to $\mathbf{n}$, so is $\mathbf{t}$. Now the Malus-Dupin theorem states that a normal congruence of rays remains a normal congruence when subjected to any number of reflections and refractions at smooth surfaces separating homogeneous media. If the normal surfaces to the rays are understood as wavefronts, the truth of the theorem becomes obvious; but the theorem can also be proven by ray-based methods [61, vol. 1, pp. 196–8].

[3] (Original) E. Laura, *Sopra la propagazione di onda in un mezzo indefinito.*

Let $\mathbf{r}_0$ be the position vector of a point of the initial surface (denoted by Σ_0) in a series of parallel surfaces, and let u, v be the parameters of this surface, so that

$$\mathbf{r}_0 = \mathbf{r}_0(u, v). \tag{A.2}$$

We assume that in some 3D region containing a segment of this surface, every point in space may be uniquely specified by its perpendicular distance from Σ_0 (positive on one side of the surface and negative on the other) together with the parameters u and v of the point $\mathbf{r}_0$ at the foot of the perpendicular; that is, we assume that we can use (u, v, r) as coordinates. Letting $\mathbf{r}$ be the position vector of a general point in the 3D region, we will have

$$\mathbf{r}(u, v, r) = \mathbf{r}_0(u, v) + r\,\mathbf{n}(u, v) \tag{A.3}$$

where $\mathbf{n}$ is the unit normal to Σ_0 in the sense of increasing r.[4]

If ds denotes the linear element of the space, we have

$$ds^{\,2} = d\mathbf{r}.d\mathbf{r}. \tag{A.4}$$

Taking differentials of Eq. (A.3) and substituting into Eq. (A.4), and using the relations

$$ds_0{}^2 = d\mathbf{r}_0.d\mathbf{r}_0$$

$$\mathbf{n}.\mathbf{n} = 1\ ; \quad \mathbf{n}.d\mathbf{n} = 0$$

$$\mathbf{n}.d\mathbf{r}_0 = 0\ ,$$

we obtain

$$ds^{\,2} = ds_0{}^2 + r^2\, d\mathbf{n}.d\mathbf{n} + dr^{\,2} + 2r\, d\mathbf{r}_0.d\mathbf{n}. \tag{A.5}$$

In Eq. (A.5), ds_0 represents the linear element of the surface Σ_0. If we now adopt the lines of curvature (which are orthogonal) as the parametric curves on Σ_0, this linear element will satisfy

$$ds_0{}^2 = h_{u0}^2\, du^{\,2} + h_{v0}^2\, dv^{\,2} \tag{A.6}$$

where h_{u0} and h_{v0} are the scale factors of u and v respectively on Σ_0. The last dot product in Eq. (A.5), with a change of sign, is the second fundamental quadratic differential form of the surface Σ_0. So we may write[5]

$$d\mathbf{r}_0.d\mathbf{n} = \frac{h_{u0}^2}{R_0}\, du^{\,2} + \frac{h_{v0}^2}{S_0}\, dv^{\,2} \tag{A.7}$$

where R_0 and S_0 are the normal radii of curvature of the surface Σ_0 in the u and v

[4] Somigliana uses Cartesian coordinates instead of "$\mathbf{r}$" and "$\mathbf{r}_0$", and direction cosines instead of "$\mathbf{n}$".

[5] (Original) V. Bianchi, *Lezioni di Geometria differenziale* (Pisa, 1902), vol. 1, p. 131.

directions, respectively.[6] With these notations, we know that[7]

$$d\mathbf{n} = \frac{1}{R_0}\frac{\partial \mathbf{r}_0}{\partial u}\,du + \frac{1}{S_0}\frac{\partial \mathbf{r}_0}{\partial v}\,dv. \tag{A.8}$$

If we dot-multiply each side of this equation with itself and use the orthogonality of the coordinates, we obtain

$$d\mathbf{n}.d\mathbf{n} = \frac{h_{u0}^2}{R_0^2}\,du^{\,2} + \frac{h_{v0}^2}{S_0^2}\,dv^{\,2}. \tag{A.9}$$

Substituting Eqs. (A.6), (A.7) and (A.9) into Eq. (A.5) yields the useful form

$$ds^{\,2} = \left(1+\frac{r}{R_0}\right)^2 h_{u0}^2\,du^{\,2} + \left(1+\frac{r}{S_0}\right)^2 h_{v0}^2\,dv^{\,2} + dr^{\,2}. \tag{A.10}$$

From Eq. (A.10), the scale factors h_u,h_v,h_r for the triply orthogonal coordinates u, v, r are[8]

$$h_u = h_{u0}\left(1+\frac{r}{R_0}\right)\ ;\quad h_v = h_{v0}\left(1+\frac{r}{S_0}\right)\ ;\quad h_r = 1. \tag{A.11}$$

Knowing the scale factors, we can write the wave equation (A.1) in the coordinates (u, v, r) and simplify it for the case in which ϕ is a function of r and t only.[9] The

[6] Although Somigliana evidently did not obtain Eq. (A.7) from Eq. (A.8), it is permissible to do so because the derivation of Eq. (A.8) need not depend on Eq. (A.7) (see next footnote). By the chain rule,

$$d\mathbf{r}_0 = \frac{\partial \mathbf{r}_0}{\partial u}\,du + \frac{\partial \mathbf{r}_0}{\partial v}\,dv.$$

If we dot-multiply this equation with Eq. (A.8), noting that

$$\frac{\partial \mathbf{r}_0}{\partial u}.\frac{\partial \mathbf{r}_0}{\partial u} = h_{u0}^2\ ;\quad \frac{\partial \mathbf{r}_0}{\partial v}.\frac{\partial \mathbf{r}_0}{\partial v} = h_{v0}^2\ ;\quad \frac{\partial \mathbf{r}_0}{\partial u}.\frac{\partial \mathbf{r}_0}{\partial v} = 0$$

because of the orthogonality of the coordinates, we obtain Eq. (A.7).

[7] On Σ_0, we have by Rodrigues' theorem [60, pp. 59–60]

$$\frac{\partial \mathbf{n}}{\partial u} = -K_{u0}\frac{\partial \mathbf{r}_0}{\partial u} = \frac{1}{R_0}\frac{\partial \mathbf{r}_0}{\partial u}$$

where K_{u0} is the principal curvature in the u direction; the signs indicate that K_{u0} is positive for a surface which is *concave* in the direction of $\mathbf{n}$, while R_0 is positive for a surface which is *convex* in that direction. Similarly,

$$\frac{\partial \mathbf{n}}{\partial v} = -K_{v0}\frac{\partial \mathbf{r}_0}{\partial v} = \frac{1}{S_0}\frac{\partial \mathbf{r}_0}{\partial v}.$$

These two equations may be used with the chain rule

$$d\mathbf{n} = \frac{\partial \mathbf{n}}{\partial u}\,du + \frac{\partial \mathbf{n}}{\partial v}\,dv$$

to obtain Eq. (A.8).

Somigliana describes R_0 and S_0 loosely as the radii of curvature of the parametric curves; but the derivation of Eq. (A.8) using Rodrigues' theorem, which involves the principal (normal) curvatures, suggests that the curvatures are meant to be resolved in the $\mathbf{n}$ direction.

[8] Somigliana gives these results in terms of E and G, where $E = h_u^2$ and $G = h_v^2$.

[9] This is the first use of the one-parameter assumption; the assumptions of parallel wavefronts and rectilinear propagation were introduced in the opening paragraph. Before assuming 1P waves, Somigliana gives expressions for $\Delta_1\phi$ $(= |\nabla\phi|^2)$ and $\Delta_2\phi$ $(= \nabla^2\phi)$, where ϕ is allowed to depend on u, v, r and t; as no further use is made of these expressions, they are not reproduced here.

result is

$$\frac{\partial^2\phi}{\partial t^2} = c^2\left\{\frac{\partial^2\phi}{\partial r^2} + \left(\frac{1}{R_0+r} + \frac{1}{S_0+r}\right)\frac{\partial\phi}{\partial r}\right\}. \tag{A.12}$$

If this equation is to have a solution depending on r and t only, we must have[10]

$$\frac{1}{R_0+r} + \frac{1}{S_0+r} = 2H(r) \tag{A.13}$$

where $H(r)$ is some function of r alone. Now, a simple geometric consideration indicates that the radii of curvature of the surface at distance r from Σ_0 must be[11]

$$R = R_0 + r\ ;\ S = S_0 + r. \tag{A.14}$$

Using these relations, Eq. (A.13) may be written

$$H(r) = \frac{1}{2}\left(\frac{1}{R} + \frac{1}{S}\right) \tag{A.15}$$

showing that $H(r)$ is the mean curvature of the surface at distance r from Σ_0. Since this is a function of r only, *the mean curvature of every parallel surface must be constant over the surface.* As Σ_0 is one such surface, its mean curvature is also constant.

Using a common denominator, Eq. (A.13) can be rewritten

$$\frac{rK_0 + H_0}{r^2K_0 + 2rH_0 + 1} = H(r) \tag{A.16}$$

where

$$H_0 = \frac{1}{2}\left(\frac{1}{R_0} + \frac{1}{S_0}\right) \tag{A.17}$$

$$K_0 = \frac{1}{R_0S_0}. \tag{A.18}$$

Comparing Eqs. (A.13) and (A.17), we see that $H_0 = H(0)$; i.e. H_0 is the mean curvature of Σ_0, which is constant. Eq. (A.18) indicates that K_0 is the Gaussian curvature of Σ_0. Solving Eq. (A.16) for K_0, we obtain

$$K_0 = \frac{(2rH_0 + 1)\,H(r) - H_0}{r - r^2H(r)}. \tag{A.19}$$

Since H_0 is constant, K_0 is a function of r only; but K_0, being a property of one surface Σ_0, is also independent of r, and must therefore be constant like H_0. Hence, by inverting Eqs. (A.17) and (A.18), we can show that the principal curvatures R_0 and S_0 are constant over the initial surface Σ_0; that is, the surface Σ_0 must be planar ($R_0 = S_0 = \infty$), circular-cylindrical ($R_0 =$ constant, $S_0 = \infty$) or spherical ($R_0 = S_0 =$ constant).[12] This conclusion applies to all the parallel surfaces because of the generality of Σ_0.

[10] Here Somigliana reasons that if the solutions of the differential equation are independent of u and v, so are the coefficients. Compare this with Eqs. (4.23) and (4.24), which imply that the coefficients of Eq. (4.15) are functions of u alone.

[11] For a proof, see Subsection 5.4.1. Somigliana states these relations immediately after Eq. (A.11).

[12] For a justification of this logical leap, see Lemma 5.2 and Theorem 5.4 (in Chapter 5).

When the appropriate values of R_0 and S_0 are substituted into Eq. (A.12), with the origin of r chosen to make each "constant" equal to zero, we obtain the familiar forms of the wave equation in the three coordinate systems. For the planar and spherical cases, the admissible solutions are respectively

$$\phi = f(r - ct) + g(r + ct) \tag{A.20}$$

and

$$\phi = \frac{1}{r} f(r - ct) + \frac{1}{r} g(r + ct), \tag{A.21}$$

and the cylindrical case admits solutions given by Poisson integrals:[13]

$$\phi = \int_{-\pi}^{\pi} f(r \sin\alpha - ct)\, d\alpha + \int_{-\pi}^{\pi} g(r \sin\alpha + ct)\, d\alpha. \tag{A.22}$$

If, instead of the wave equation, we consider Laplace's Equation, i.e. if we suppose that ϕ is independent of time, the above results lead to the following conclusion:

The only Newtonian distributions of mass for which the gravitational equipotential surfaces outside the distribution are parallel are those whose equipotentials are planar, circular-cylindrical or spherical.

[13]Somigliana omits the first integral, but the admissibility of the second integral implies that of the first because the wave equation is even in c. Each term in the solution can be verified by direct substitution into the wave equation. The functions f and g are arbitrary except that they must be smooth enough to permit two differentiations under the integral sign; it is sufficient that they are everywhere twice *continuously* differentiable (cf. [53], p. 163).

Appendix B

Program listings and explanatory notes

B.1 IVP solver and modified Newton method

The `#include` file `stepstat.c` implements the functions Step(μ) and $s(n, \mu)$, which are defined in Table 8.1 and used throughout Chapter 8. The file contains copious comments, which will be supplemented rather than repeated in the text.

The long introductory comment explains how the third-order iterative solution scheme of `step(mu)` is derived from the second-order IVP. In the notation of Subsection 8.2.4, the body of the function `step(mu)` would be written

$$
\begin{aligned}
y_{i+1} &= y_i + hy'_i + \tfrac{1}{2}h^2\, y''_i + \tfrac{1}{6}h^3\, y'''_i && \text{(B.1)}\\
y'_{i+1} &= y'_i + hy''_i + \tfrac{1}{2}h^2\, y'''_i && \text{(B.2)}\\
i &:= i + 1 && \text{(B.3)}\\
x_i &= 1 + ih && \text{(B.4)}\\
y''_i &= -\left(\mu^2 y_i + \frac{y'_i}{x_i}\right) && \text{(B.5)}\\
y'''_i &= \left(\frac{1}{{x_i}^2} - \mu^2\right) y'_i - \frac{y''_i}{x_i}. && \text{(B.6)}
\end{aligned}
$$

The order of evaluation is chosen so that, after each iteration, x, y and all three derivatives of y are simultaneously available for the same i. The new values of y and y' are estimated using truncated Taylor expansions, whereas the new values of y'' and y''' are found directly from the differential equation using the newly-incremented i. To maximize the versatility of the function, the old values are not overwritten but are accumulated in externally-declared arrays.

For each step, the dominant error in y'_{i+1} is proportional to h^3. The number of steps taken to reach the n^{th} stationary point is proportional to h^{-1}. Hence the error in $s(n, \mu)$ due to the IVP solver is approximately proportional to h^2. (The truncated Taylor expansion for y_{i+1} has one more term than that for y'_{i+1}, so that the error in y for a particular x is approximately proportional to h^3 rather than h^2. Therefore the iterative scheme is described as "third-order", although it is only second-order for purposes involving y'.)

If y'_{i-1} and y'_i are not strictly of the same sign, `step(mu)` has reached or just passed a zero of y'. The function `s(n,mu)` steps up to or just past the n^{th} zero of

y', then finds the zero using one step of the "modified" or "third-order" Newton method. This method was derived independently by the author and will therefore be described here, although it is likely that the same method is described somewhere in the vast mathematical literature.

The purpose of the third-order Newton method is to find a root x of the equation $y(x) = 0$. If x_k is an estimate of the root, a single step of the method gives an improved estimate x_{k+1}. Let

$$x = x(y) = x(y(x)) \tag{B.7}$$

so that the desired root is $x(0)$. If $x(y)$ is sufficiently differentiable, we may use the Taylor expansion

$$x(y + \epsilon) = x(y) + \epsilon x'(y) + \tfrac{1}{2}\epsilon^2 x''(y) + O(\epsilon^3) \tag{B.8}$$

where the "error term" $O(\epsilon^3)$ is approximately proportional to ϵ^3 for small ϵ. Differentiating Eq. (B.7) w.r.t. x and solving for $x'(y)$ gives

$$x'(y) = \frac{1}{y'(x)}. \tag{B.9}$$

Differentiating again w.r.t. x and solving for $x''(y)$ gives

$$x''(y) = -\frac{y''(x)}{[y'(x)]^3}. \tag{B.10}$$

Because we want Eq. (B.8) to give us $x(0)$, we put $y + \epsilon = 0$, whence

$$\epsilon = -y. \tag{B.11}$$

Substituting Eqs. (B.9) to (B.11) into Eq. (B.8), and putting $x = x_k$ and $y(x_k) = y_k$, we obtain

$$x(0) = x_k - \frac{y_k}{y'_k} - \frac{{y_k}^2 y''_k}{2(y'_k)^3} - O({y_k}^3). \tag{B.12}$$

The well-known Newton-Raphson method uses just the first two terms on the right of Eq. (B.12). The dominant error term is proportional to ${y_k}^2$, which in turn is approximately proportional to $[x_k - x(0)]^2$ if the problem is well-conditioned. Thus the classical Newton-Raphson method is second-order: the error in x_{k+1} is roughly proportional to the square of error in x_k.

As the reader will have anticipated, the "modified" Newton method uses the first *three* terms on the right of Eq. (B.12). The remaining error is approximately proportional to ${y_k}^3$, so the method is third-order.

Both the classical method and the modified method come from the same Taylor expansion of $x(y)$. Whereas the classical method is exact for linear functions, the modified method is exact if x is a *quadratic* function of y (so that Eq. (B.8) is exact without the error term). Thus the modified method is an obvious extension of the classical method.

The function $s(n, \mu)$ finds a zero of y' rather than y, so that every "y" in Eq. (B.12) must be given an extra prime ($'$). Only a single iteration is used. The initial estimate is x_i, where i denotes the i^{th} iteration of the IVP solver Step(μ), not

the i^{th} iteration of the modified Newton method. Thus, using the form of Eq. (B.12), the last statement in the function `s(n,mu)` would be written

$$s(n,\mu) = x_i - \frac{y_i'}{y_i''} - \frac{(y_i')^2\, y_i'''}{2(y_i'')^3}. \tag{B.13}$$

This formula is convenient to use because all the necessary values of y and its derivatives are available from the IVP solver.

The error in $s(n,\mu)$ caused by the modified Newton method is approximately proportional to the cube of the difference between x_i and $s(n,\mu)$, which difference is less than the step size h. Hence the error due to the modified Newton method is at worst third-order w.r.t. h, whereas the error due to the IVP solver, as noted above, is second-order. Therefore, if h is sufficiently small, the overall algorithm for finding $s(n,\mu)$ is second-order, and the modified Newton method does not significantly contribute to the error.

Of course, `step(mu)` can easily be modified to solve a different IVP, while `s(n,mu)` can be modified to handle a boundary condition involving y instead of y'. Thus the two functions can serve as templates for solving other Sturm-Liouville problems which may arise in future work. For this reason, the author has chosen to ignore the fact that the problem of Chapter 8 can be solved in terms of Bessel functions.

A listing of the file `stepstat.c` follows.

```
/*
 *    #include file 'stepstat.c'  (Gavin R. Putland)
 *
 *    DIFFERENTIAL EQUATION SOLVER, STATIONARY POINT FINDER
 *    AND ASSOCIATED GLOBAL VARIABLES (EXCEPT h AND max).
 *
 *    STEP SIZE h AND MAXIMUM NO. OF STEPS max
 *    ARE EXTERNALLY DECLARED OR #defined IN CALLING PROGRAM.
 *
 *    FUNCTION s(n,mu) RETURNS THE ABSCISSA OF THE nth STATIONARY POINT
 *    OF y(x), WHERE y(x) IS THE SOLUTION TO THE INITIAL VALUE PROBLEM
 *
 *          y'' + (1/x) y' + mu^2 y = 0                          (1)
 *                y(1) = 0                                       (2)
 *               y'(1) = 1.                                      (3)
 *
 *    FUNCTION s(n,mu) REPEATEDLY CALLS FUNCTION step(mu),
 *    WHICH PERFORMS ONE STEP OF THE IVP SOLUTION FOR GIVEN mu.
 *
 *    To obtain a third-order method of solving the IVP, we note that
 *    Eqs. (1), (2) and (3) give
 *
 *              y''(1) = -1.                                     (4)
 *
 *    Then we differentiate (1) wrt x to obtain
 *
 *          y''' + (1/x) y'' + (mu^2 - 1/x^2) y' = 0.          (5)
 *
 *    Eqs. (5), (2), (3), (4) constitute a new IVP.  Eq. (5) is solved for
 *    y''', and successive values of y'', y' and y can be found using first-,
```

```
 *    second- and third-order truncated Taylor series.  But it is better to
 *    obtain y'' from (1) and use Taylor series for y' and y only.  For
 *    initializing the loop, Eqs. (5), (2), (3), (4) yield
 *
 *            y'''(1) = 2 - mu^2.
 *
 *    Because we are seeking a zero of y', convergence of the method is
 *    second-order; i.e. the error in s(n,mu) is roughly proportional to h^2.
 */

/* GLOBAL VARIABLES FOR ITERATIVE SOLUTION OF IVP: */
   float    x[max], ydd[max], yddd[max];  /* single precision increments */
   double   y[max], yd[max];              /* double precision accumulation */
   int      i;                            /* step counter */
/* See above comment on h and max. */

void step(float mu)

/*
 *    i, x[i], y[i], yd[i], ydd[i], yddd[i] MUST HAVE BEEN INITIALIZED.
 *    i IS INCREMENTED; x[i], y[i], yd[i], ydd[i], yddd[i] ARE COMPUTED
 *    FOR THE NEW i.
 */

{
   y[i+1]  = y[i] + h*(float)yd[i] + 0.5F*h*h*ydd[i] + (h*h*h/6.F)*yddd[i];
   yd[i+1] = yd[i] + h * ydd[i] + 0.5F*h*h * yddd[i];
   i++;
   x[i]    = 1.F + i * h;
   ydd[i]  = - (mu * mu * (float)y[i] + (float)yd[i]/x[i]);
   yddd[i] = (1.F/(x[i]*x[i]) - mu*mu) * (float)yd[i] - ydd[i]/x[i];
}

float s(int n, float mu)

{
   int j;   /* stationary point counter */

   /* INITIALIZATIONS: */
      i = 0; x[i] = 1.F;
      y[i] = 0.0; yd[i] = 1.0; ydd[i] = -1.F; yddd[i] = 2.F - mu*mu;
   /* FIND nth CHANGE IN SIGN OF yd[i]: */
      for (j = 1; j <= n; j++) /* STEP TO ZERO OR SIGN-CHANGE OF yd[i]: */ {
         step(mu); step(mu); /* get clear of any initial stationary point */
         while (yd[i-1]*yd[i] > 0.0)
            step(mu);
      }
   /* LOCATE ZERO OF y'(x) BY ONE STEP OF THIRD-ORDER NEWTON METHOD: */
      return (float)(x[i] - yd[i]/ydd[i]
                     - 0.5*yd[i]*yd[i]*yddd[i]/(ydd[i]*ydd[i]*ydd[i]));
}
```

B.2 Root-finder `root.c`

The `#include` file `root.c` implements the function root(f, n, b) defined in Table 8.1. A standard root-finder function finds a root t of the equation $f(t) = 0$. The function root(f, n, b) is more general: it finds a root t of $f(n, t) = b$ (where n is an integer), which is equivalent to finding a zero of $e(t) = f(n, t) - b$. The C version of the function, which is called `root(f, n, b, t1, t2, err)`, uses the secant method to find a zero of $e(t)$. It requires trial solutions `t1` and `t2` and terminates when $|e(t)| \leq$ `err`.

Execution of the function can be traced by inserting diagnostic `printf` statements. When the function was used in the algorithm of Table 8.1 to produce the data for Fig. 8.1, it required only three iterations to find μ_1, four for μ_2 and three for μ_3.

A listing of the file follows.

```
/*
 *    #include file 'root.c'  (Gavin R. Putland)
 *
 *    FUNCTION root(f, n, b, t1, t2, err) USES THE SECANT METHOD TO RETURN
 *    A ROOT t OF f(n,t) = b, GIVEN TRIAL VALUES t1, t2, AND TOLERANCE err.
 *    N.B.: err IS THE TOLERANCE IN b, NOT IN t.
 */

float root(float (*f)(int, float), int n, float b,
           float t1, float t2, float err)

{
   float    corr,    /* correction to estimate of root */
            e1, e2;  /* e1 = f(n,t1) - b, etc. */

   e1 = (*f)(n,t1) - b;
   while (fabs(e2 = (*f)(n,t2) - b) > err) {
      corr = e2 * (t2 - t1) / (e2 - e1);
      t1 = t2;
      e1 = e2;
      t2 -= corr;
   }
   return t2;
}
```

B.3 Eigenfunction plotter `efunc.c`

Program `efunc.c` implements the algorithm of Table 8.1. It has numerical and graphical printout options, either of which may be commented out. The graphical option produced the plotting commands for Fig. 8.1. Whereas the eigenfunctions are computed with a step size of 0.01, the numerical and graphical printouts use x-increments of 0.5 and 0.1 respectively; this explains the instructions for incrementing i in the printing loops.

In the `for` loop that finds μ_n for $n = 1$ to 3, the root-finder function requires two estimates of μ_n for each n; these estimates are called `t1` and `t2`. To initialize the loop, the second estimate of μ_1 is found from Eq. (8.68). At the end of the loop, the second estimate of μ_{n+1} is found from the final value of μ_n using Eq. (8.66). For each n, `t1` is arbitrarily set to 99% of `t2`, so that `t2` is the more accurate estimate (see the end of Subsection 8.2.4).

A listing of `efunc.c` follows.

```
/*
 *    Program 'efunc.c'  (Gavin R. Putland)
 *
 *    PROGRAM TO FIND AND PLOT THE FIRST THREE EIGENFUNCTIONS OF THE
 *    STURM-LIOUVILLE PROBLEM
 *
 *          y'' + (1/x) y' + mu^2 y = 0                          (1)
 *                y(1) = 0                                       (2)
 *               y'(m) = 0                                       (3)
 *
 *    where mu is the eigenvalue and m is given.  As a normalizing condition,
 *    we will take
 *
 *               y'(1) = 1.                                      (4)
 *
 *    STRATEGY FOR FINDING THE nth EIGENVALUE mu[n]:  Take two trial
 *    values of mu.  For each trial value, solve the initial value problem
 *    (1), (2), (4) for s(n,mu), the abscissa of the nth stationary point
 *    of y(x).  Use the secant method to find further trial values of mu,
 *    making s(n,mu) converge to m.
 *
 *    CONTENTS OF #include FILE 'stepstat.c':
 *
 *    Function s(n,mu) returns the abscissa of the nth stationary point.
 *    It repeatedly calls function step(mu), which is defined first.
 *    step(mu) performs one step of the IVP solution for given mu.
 *    Global array declarations are included.
 *
 *    CONTENTS OF #include FILE 'root.c':
 *
 *    Function root(f, n, b, t1, t2, err) uses the secant method to return
 *    a root t of f(n,t) = b, given trial values t1, t2, and tolerance err.
 *    N.B.: err is the tolerance in b, NOT in t.
 */


#include <stdio.h>
#include <math.h>
```

```
#define  pi    3.141592654F

#define  m     20.F     /* desired abscissa of stationary point of y(x) */
#define  tol   0.00001F /* tolerance to which s(n,mu) must match m */
#define  max   2500     /* maximum number of steps; must be > (m-1)/h */
#define  h     0.01F    /* step size for IVP solution */

#include "stepstat.c"   /* IVP solver, stationary point finder,
                           array declarations */
#include "root.c"       /* secant-method root finder */

main()

{

float    mu[4],      /* eigenvalues of mu;  mu = mu[n] makes s(n,mu) = m,
                        where s(n,mu) is the abscissa of the
                        nth stationary point of y(x). */
         t1, t2,     /* initial estimates of eigenvalue */
         Y[4][max];  /* eigenfunctions; called y1, y2 and y3 in printout */

int      n,          /* index to eigenvalues and eigenfunctions */
         steps;      /* number of steps from x=1 to x=m */

steps = (int)((m - 1.F)/h + 0.1F);

/* Initialize loop using ‘‘rough’’ analytical estimate of mu[1]: */
   t2 = 1.0 / sqrt(0.5 * (m*m - 1.F) * log(0.5 * (m + 1.F)));
for (n = 1; n <= 3; n++) /* FIND mu[n] AND COPY EIGENFUNCTION Y[n][i]: */ {
   t1 = 0.99F * t2;
   mu[n] = root(s, n, m, t1, t2, tol);
   for (i = 0; i <= steps; i++)
      Y[n][i] = (float)y[i];
   t2 = mu[n] + pi/(m - 1.F); /* add a half-cycle; mu <=> wave number */
}

/*
   NUMERICAL PRINTOUT OPTION:
*/

   printf("\n    mu1 = %7.5f ; mu2 = %7.5f ; mu3 = %7.5f .\n",
                 mu[1], mu[2], mu[3]);

   printf("\n    %4s  %6s  %6s  %6s\n\n", "x  ", "y1  ", "y2  ", "y3  ");

   for (i = 0; i <= steps; i += (int)(0.5F/h + 0.1F))
      printf("    %4.1f  %6.3f  %6.3f  %6.3f\n",
                 x[i], Y[1][i], Y[2][i], Y[3][i]);

   printf("\n");

/*
   GRAPHICAL PRINTOUT OPTION:

   This option produces LaTeX picture commands to plot points in the three
   eigenfunctions and the limiting function y = ln x (for mu = 0).  The output
   should be redirected to a file and inserted in another file containing
   the rest of the picture environment, including the axes and labels.  The
```

```
   output also includes a comment listing the eigenvalues.

   printf("%%    mu1 = %7.5f ; mu2 = %7.5f ; mu3 = %7.5f .\n",
                  mu[1], mu[2], mu[3]);
   for (i = 0; i <= steps; i++)
      Y[0][i] = (float)log(x[i]);
   for (i = 0; i <= steps; i += (int)(0.1F/h + 0.1F)) {
      printf("\\put(%4.0f,%4.0f){\\circle*{1}}  ", 60*x[i], 180*Y[0][i]);
      printf("\\put(%4.0f,%4.0f){\\circle*{1}}\n", 60*x[i], 180*Y[1][i]);
      printf("\\put(%4.0f,%4.0f){\\circle*{1}}  ", 60*x[i], 180*Y[2][i]);
      printf("\\put(%4.0f,%4.0f){\\circle*{1}}\n", 60*x[i], 180*Y[3][i]);
   }

*/

}
```

B.4 Program `chase.c`: Check results of Chase.

Program `chase.c` implements the algorithm of Table 8.2 and prints Table 8.3. When the program `efunc.c` has been understood, the following listing of `chase.c` is self-explanatory.

```
/*
 *    Program 'chase.c'  (Gavin R. Putland)
 *
 *    PROGRAM TO CHECK VALUES OF m USED BY CHASE
 *
 *    Unless otherwise noted, the nomenclature of program 'efunc.c' is used.
 *
 *
 *    CONTENTS OF #include FILE 'stepstat.c':
 *
 *    Function s(n,mu) returns the abscissa of the nth stationary point.
 *    It repeatedly calls function step(mu), which is defined first.
 *    step(mu) performs one step of the IVP solution for given mu.
 *    Global array declarations are included.
 *
 *    CONTENTS OF #include FILE 'root.c':
 *
 *    Function root(f, n, b, t1, t2, err) uses the secant method to return
 *    a root t of f(n,t) = b, given trial values t1, t2, and tolerance err.
 *    N.B.: err is the tolerance in b, NOT in t.
 */

#include <stdio.h>
#include <math.h>

#define  h     0.01F    /* step size */
#define  max   2500     /* maximum number of steps; must be > (m-1)/h */
#define  tol   0.00001F /* tolerance to which s(1,mu) must match m */

#define  rof   2400.F   /* density of glass, kg/m^3 */
#define  a     5e-6F    /* fibre radius, metres */
#define  alpha 1.87e-5F /* Chase's thermal diffusivity of air, m^2/s */

#include "stepstat.c"   /* IVP solver, stationary point finder,
                           array declarations */
#include "root.c"       /* secant-method root finder */

void check(float rom, float wc)

/*
 *    FUNCTION check(rom, wc) REPORTS ON THE POINT (rom, wc)
 *    FROM CHASE'S FIGURE 1.
 */

{
   float m, much, t1, t2, muhalfm;

   m = sqrt(rof/rom);                    /* m according to density */
   much = a * m * sqrt(wc/alpha);        /* eigenvalue used by Chase */

   /* COMPUTE EIGENVALUE FOR VALUE OF m APPARENTLY USED BY CHASE: */
```

```
      m /= 2.F;   /* Chase gets eigenvalue from m/2 instead of m ?? */
      t2 = 1.0 / sqrt(0.5 * (m*m - 1.F) * log(0.5 * (m + 1.F)));
      t1 = 0.99F * t2;
      muhalfm = root(s, 1, m, t1, t2, tol);
      m *= 2.F;   /* restore m */

   printf("   %4.1f  %4.0f  %5.2f  %6.4f  %6.4f\n",
          rom, wc, m, much, muhalfm);

}

main()

{

float    rom,        /* packing density of fibre = f * rof */
         wc;         /* transition angular frequency = 1/tau */

/* PRINT HEADING: */
   printf("\n   CHECK ON EIGENVALUES USED BY CHASE\n");
   printf("\n   %4s  %4s  %5s  %6s  %7s\n\n",
          "rom ", "wc ", "m  ", "much ", "muhalfm");

/* PROCESS VALUES FROM CHASE'S FIGURE 1: */
   check(6.0F,   22.F);
   check(7.1F,   30.F);
   check(10.F,   67.F);
   check(20.F,  430.F);
   check(30.F, 1100.F);
   check(49.F, 3000.F);
   check(70.F, 5400.F);

printf("\n");

}
```

B.5 Program `f2.c`: Locate 2nd-mode heatshed.

The program `f2.c` produces the output shown in Table 8.4. It uses the algorithm described in Subsection 8.2.6, except that the body of the loop headed "For each m" is relegated to the function `printrow(m)`. The values of m are chosen so that m can approach both unity and infinity while assuming "round-figure" values. (Similar sequences also occur in the program `mu.c`, to be described in the next section.)

The root-finder function requires two estimates of μ_2. The more accurate estimate, called `t2`, is obtained from Eqs. (8.68) and (8.66); see the comments in the function `printrow(m)`.

The source file for `f2.c` is listed below.

```
/*
 *    Program 'f2.c'  (Gavin R. Putland)
 *
 *    FOR A RANGE OF VALUES OF m, FIND THE FRACTION OF THE AIR VOLUME
 *    THAT CAN EXCHANGE HEAT WITH THE FIBRE IN THE SECOND MODE,
 *    i.e. THE FRACTION OF THE AIR CROSS-SECTIONAL AREA INSIDE THE FIRST
 *    MAXIMUM OF THE SECOND EIGENFUNCTION.
 *
 *    m AND mu ARE AS DEFINED IN PROGRAM 'efunc.c'.
 *
 *    CONTENTS OF #include FILE 'stepstat.c':
 *
 *    Function s(n,mu) returns the abscissa of the nth stationary point.
 *    It repeatedly calls function step(mu), which is defined first.
 *    step(mu) performs one step of the IVP solution for given mu.
 *    Global arrays and the global array index are declared.
 *
 *    CONTENTS OF #include FILE 'root.c':
 *
 *    Function root(f, n, b, t1, t2, err) uses the secant method to return
 *    a root t of f(n,t) = b, given trial values t1, t2, and tolerance err.
 *    N.B.: err is the tolerance in b, NOT in t.
 */


#include <stdio.h>
#include <math.h>

#define  min(A,B) ((A)<(B)?(A):(B))

#define  pi    3.141592654F

#define  max   9000     /* maximum number of steps; must be > (m-1)/h */

float    h;             /* step size for #included functions */

#include "stepstat.c"   /* IVP solver, stationary point finder,
                           array & array index declarations */
#include "root.c"       /* secant-method root finder */

void printrow(float m)

/*
 *    FUNCTION printrow(m) PROCESSES ONE VALUE OF m
```

```
 *    AND PRINTS A ROW OF OUTPUT.
 */

{
   float

         f,             /* filling factor */
         mu2,           /* second eigenvalue */
         t1, t2,        /* initial estimates of mu2 */
         tol,           /* tolerance to which s(2,mu) must match m */
         f2;            /* volume fraction inside s(1,mu2) */

   /* Find filling factor: */
      f   = 1.F / (m * m);
   /* Initialize root-finder using rough analytical estimate of mu1... */
      t2  = 1.0 / sqrt(0.5 * (m*m - 1.F) * log(0.5 * (m + 1.F)));
   /* ...followed by estimated difference between eigenvalues: */
      t2 += pi / (m - 1.F);
      t1  = 0.99F * t2;
   /* Find mu2 and f2: */
      tol = m * 2e-7F;
      h   = min(0.02F,(m - 1.F)/100.F);
      mu2 = root(s, 2, m, t1, t2, tol);
      f2  = (float)(pow(s(1,mu2),2)-1.0) / (m*m - 1.F);
   printf("%6.3f  %6.2f  %9.5f  %6.3f\n",
          1e2*f, m, mu2, 1e2*f2);
}

main()

{

float    m;             /* normalized variable related to filling factor
                           and appearing in Sturm-Liouville problem */

/* HEADING OF PRINTOUT: */
   printf("\n%6s  %6s  %9s  %6s\n\n",
          "f(%) ", "m   ", "mu2  ", "f2(%)");

for (m = 160.F; m > 3.F; m /= 1.414213562F)
   printrow(m);

printf("\n");

for (m = 2.28F; m > 1.009F; m -= 0.5F * (m - 1.F))
   printrow(m);

printf("\n");

}
```

B.6 Program `mu.c`: Check eigenvalue approximations.

Program `mu.c` implements the algorithm of Table 8.5, with some refinements mentioned in the text of Subsection 8.2.7. When `zeta` is defined as 0.37, the program produces the output shown in Table 8.6.

The listing follows.

```
/*
 *    Program 'mu.c'  (Gavin R. Putland)
 *
 *    FIND THE FIRST EIGENVALUE OF mu IN THE STURM-LIOUVILLE PROBLEM
 *
 *          y'' + (1/x) y' + mu^2 y = 0                          (1)
 *                y(1) = 0                                       (2)
 *               y'(m) = 0                                       (3)
 *
 *    FOR A RANGE OF VALUES OF m, AND COMPARE THE EIGENVALUE WITH TWO
 *    ANALYTICAL ESTIMATES THEREOF.
 *
 *    As a normalizing condition we will take
 *
 *               y'(1) = 1.                                      (4)
 *
 *    STRATEGY FOR FINDING THE 1st EIGENVALUE mu1:  Take two trial
 *    values of mu.  For each trial value, solve the initial value problem
 *    (1), (2), (4) for s(1,mu), the abscissa of the 1st stationary point
 *    of y(x).  Use the secant method to find further trial values of mu,
 *    making s(1,mu) converge to m.
 *
 *    CONTENTS OF #include FILE 'stepstat.c':
 *
 *    Function s(n,mu) returns the abscissa of the nth stationary point.
 *    It repeatedly calls function step(mu), which is defined first.
 *    step(mu) performs one step of the IVP solution for given mu.
 *    Global arrays and the global array index are declared.
 *
 *    CONTENTS OF #include FILE 'root.c':
 *
 *    Function root(f, n, b, t1, t2, err) uses the secant method to return
 *    a root t of f(n,t) = b, given trial values t1, t2, and tolerance err.
 *    N.B.: err is the tolerance in b, NOT in t.
 */


#include <stdio.h>
#include <math.h>

#define  min(A,B) ((A)<(B)?(A):(B))

#define  max   9000     /* maximum number of steps; must be > (m-1)/h */
#define  zeta  0.37     /* parameter in ''refined'' analytical approx. */

float    h;             /* step size for #included functions */

#include "stepstat.c"   /* IVP solver, stationary point finder,
```

```
                           array & array index declarations */
#include "root.c"       /* secant-method root finder */

void printrow(float m)

/*
 *    FUNCTION printrow(m) PROCESSES ONE VALUE OF m
 *    AND PRINTS A ROW OF OUTPUT.
 */

{
   float

         f,             /* filling factor */
         mu1,           /* first eigenvalue (computed from smaller h) */
         mu1d,          /* first eigenvalue (computed from larger h) */
         t1, t2,        /* initial estimates of eigenvalue */
         tol,           /* tolerance to which s(1,mu) must match m */
         errmu,         /* difference between mu1 and mu1d (in ppm) */
         mua, mub,      /* analytical estimates of mu1 (from m) */
         ermua, ermub;  /* percentage errors in mua and mub */

   /* Find filling factor: */
      f   = 1.F / (m * m);
   /* Initialize root-finder using ‘‘rough’’ analytical estimate of mu1: */
      t2 = 1.0 / sqrt(0.5 * (m*m - 1.F) * log(0.5 * (m + 1.F)));
      t1 = 0.99F * t2;
   /* Find eigenvalue using two step sizes and estimate error: */
      tol   = m * 1e-7F;
      h     = min(0.02F,(m - 1.F)/100.F);
      mu1d  = root(s, 1, m, t1, t2, tol);
      h    /= 2.F;
      mu1   = root(s, 1, m, t1, t2, tol);
      errmu = 1e6F * (mu1d - mu1) / mu1;
   /* Find ‘‘rough’’ and ‘‘refined’’ analytical estimates & their errors: */
      mua   = t2;
      mub   = 1.0 / sqrt(0.5 * (m*m - pow(m,zeta)) * log(0.5 * (m + 1.F)));
      ermua = 100.F * (mua - mu1) / mu1;
      ermub = 100.F * (mub - mu1) / mu1;
   printf("%9.3f  %5.2f  %9.6f  %5i  %6.2f  %5.2f  %5.2f\n",
          1e2*f, m, mu1, i, errmu, ermua, ermub);
}

main()

{

float    m;             /* normalized variable related to filling factor
                           and appearing in Sturm-Liouville problem */

/* HEADING OF PRINTOUT: */
   printf("\n%9s  %5s  %9s  %5s  %6s  %5s  %5s\n\n",
          "f(%) ", "m  ", "mu1    ", "steps", "errmu", "ermua", "ermub");

for (m = 80.F; m > 3.F; m /= 1.414213562F)
   printrow(m);

printf("\n");
```

```
for (m = 2.28F; m > 1.019F; m -= 0.5F * (m - 1.F))
   printrow(m);

printf("\n");

}
```

B.7 Program tafp.c: Tabulate thermal time constant τ_{fp}.

Program tafp.c estimates thermal time constants using Eq. (8.16), with $\zeta = 0.37$. It also uses some acoustical properties of air, which are calculated using the formulae of Chapter 9. Its output is shown in Table 8.7.

The listing follows.

```
/*
 *    Program 'tafp.c'  (Gavin R. Putland)
 *
 *    PROGRAM TO COMPUTE THE THERMAL TIME CONSTANT tafp
 *    FOR VARIOUS VALUES OF FILLING FACTOR f AND FIBRE DIAMETER d
 *    USING THE ''REFINED'' ANALYTICAL FORMULA FROM PROGRAM 'tau.c',
 *    WITH zeta = 0.37.
 */

#include <stdio.h>
#include <math.h>

#define pi     3.141592654F
#define Rbar   8.31451F          /* universal gas constant, J/(K.mol) */
#define mbar   0.028964F         /* molecular mass of air, kg/mol */
#define Cp     1007.F            /* Cp of air, J/(kg.K) */
#define Po     101325.F          /* atmospheric pressure, Pa */
#define T      293.15F           /* ambient temperature, K */

float
      d,             /* fibre diameter, metres (um in printout) */
      f,             /* filling factor (percent in printout) */
      m,             /* m = 1/sqrt(f) */
      mfac,          /* m-dependent factor in expression for tafp */
      tafp,          /* time constant, seconds (usec in printout) */
   /* PROPERTIES OF AIR: */
      rho,           /* density, kg/m^3 */
      kappa,         /* thermal conductivity, W/(m.K) */
      alpha;         /* thermal diffusivity, m^2/s */

main()

{

/* COMPUTE PROPERTIES OF AIR: */
   rho   = Po * mbar / (Rbar * T);
   kappa = 0.02623 * pow((T/300.F),0.851);
   alpha = kappa / (rho * Cp);

/* HEADING OF PRINTOUT: */
   printf("\n   T = %6.2f K;  Po = %6.0f Pa.\n", T, Po);
   printf("\n   rho = %5.3f; kappa = %7.5f; alpha = %8.3e  (SI units).\n",
          rho, kappa, alpha);
   printf("\n   THERMAL TIME CONSTANT tafp (IN MICROSECONDS)");
   printf("\n   vs. FILLING FACTOR f AND FIBRE DIAMETER d:\n");
   printf("\n   %6s", "d(um):");
   for (d = 4e-6; d < 17e-6; d += 2e-6)
      printf("  %2.0f    ", 1e6*d);
```

```
   printf("\n\n   %4s\n", "f(%)");

/* COMPUTE AND PRINT VALUES OF tafp: */
   for (f = 0.0005; f < 0.0901; /* f is incremented at end of loop */ ) {
      m    = 1.0 / sqrt(f);
      mfac = (m*m - pow(m,0.37)) * log(0.5 * (m + 1.0));
      printf("   %4.2f ", 1e2*f);
      for (d = 4e-6; d < 17e-6; d += 2e-6) {
         tafp = d * d * mfac / (8.F * alpha);
         printf(" %7.2f", 1e6*tafp);
      }
      printf("\n");
      /* INCREMENT f: */
         if      (f < 0.0049)
            f += 0.0005;
         else if (f < 0.0099)
            f += 0.001;
         else if (f < 0.0199)
            f += 0.002;
         else if (f < 0.0499)
            f += 0.005;
         else
            f += 0.01;
   }

printf("\n");

}
```

B.8 Program air.c: Tabulate acoustical properties of air.

The program air.c, listed below, is a straightforward application of the formulae developed in Chapter 9. It produces the output shown in Table 9.1.

```
/*
 *    Program 'air.c'  (Gavin R. Putland)
 *    ACOUSTICAL PROPERTIES OF AIR vs. TEMPERATURE AND PRESSURE
 */

#include <stdio.h>
#include <math.h>

#define Rbar   8.31451F          /* universal gas constant, J/(K.mol) */
#define mbar   0.028964F         /* molecular mass of air, kg/mol */
#define Cp     1007.F            /* Cp of air, J/(kg.K) */

float    gam, T, Po, rho, c, rhoc, eta, kappa, alpha;

void printline(void)

/* FUNCTION TO COMPUTE & PRINT ONE LINE OF OUTPUT: */

{
   rho   = Po * mbar / (Rbar * T);              /* density, kg/m^3 */
   c     = sqrt(gam * Rbar * T / mbar);         /* speed of sound, m/s */
   rhoc  = rho * c;                             /* impedance, Pa s/m */
   eta   = 1.857e-5 * pow((T/300.F),0.7829);    /* viscosity, Pa s */
   kappa = 0.02623 * pow((T/300.F),0.851);      /* conductivity, W/(m.K) */
   alpha = kappa / (rho * Cp);                  /* diffusivity, m^2/s */
   printf("%6.2f  %6.0f  %7.5f  %6.2f  %6.2f  %9.3e  %7.5f  %8.2e\n",
          T, Po, rho, c, rhoc, eta, kappa, alpha);
}

main()

{

gam = Cp / (Cp - Rbar/mbar);  /* ratio of specific heats */

/* HEADING OF PRINTOUT: */
   printf("\n");
   printf("ACOUSTICAL PROPERTIES OF AIR vs. TEMPERATURE AND PRESSURE\n\n");
   printf("All units are SI.\n\n");
   printf("Rbar = %7.5f ; mbar = %8.6f ; Cp = %4.0f ; gamma = %6.4f .\n\n",
          Rbar, mbar, Cp, gam);
   printf("%6s  %6s  %7s  %6s  %6s  %9s  %7s  %8s\n\n",
          "T   ","Po  ","rho  ","c   ","rhoc ","eta    ","kappa ","alpha  ");

Po  = 101325.F;                       /* atmospheric pressure, Pa */

for (T = 200.F; T < 405.F; T += 50.F)  /* fixed Po */
   printline();
printf("\n");
```

```
for (T = 273.15F; T < 305.F; T += 5.F) /* fixed Po */
   printline();
printf("\n");

/* U.S. Standard Atmosphere sequence (variable Po): */
   T = 307.659F; Po = 142970.F; printline();
   T = 297.902F; Po = 120690.F; printline();
   T = 288.150F; Po = 101325.F; printline();
   T = 278.402F; Po =  84559.F; printline();
   T = 268.659F; Po =  70121.F; printline();
   T = 258.921F; Po =  57752.F; printline();
   T = 249.187F; Po =  47217.F; printline();
printf("\n");

}
```

B.9 Model builder box.c (for loudspeaker)

The model-building program box.c produced the SPICE models for Chapter 10. A functional description of the program is given in Section 10.3. The version given here is for the 10-inch woofer in the 36-liter box with a 50 mm element size. Changing the woofer parameters, element size or atmospheric conditions requires editing of the #define commands (and, if presentation is important, the heading of the "cct" file). Approximations are specified by command-line switches; the command-line syntax is given in the comment at the top of the source file.

A production version of this program would require numerous improvements. Some limitations of the prototype, in addition to those mentioned in Section 10.1 and Subsection 10.3.3, are listed below:

- The component values in fiber-free region are accurate only if D is a multiple of delx and clear is a multiple of dely. To overcome this restriction, different step sizes should be allowed in different regions. The model-builder should also handle a greater variety of box geometries than can be obtained by varying the dimensions in Fig. 10.1.

- The analysis assumes that the speaker is running cold, i.e. that the temperatures inside and outside the box are the same. Ideally the software should not only allow for the internal temperature rise, but be able to calculate it as a function of time.

- The computation of the components in the equivalent circuit of the moving-coil driver should accommodate alternative sets of driver parameters, e.g. one Q factor and the Bl product instead of two Q factors, or C_{ms} instead of V_{as}.

- The production of graphs other than SIL vs. frequency should be automated. As a minimum, the available graphs should include phase response, input impedance, diaphragm excursion and power dissipation. (Of course such graphs can be produced manually by typing plot commands in SPICE.) It should also be possible to plot SPL instead of SIL (this would affect the temperature-dependence and pressure-dependence of the response).

- The "undamped" approximation should be handled separately, using the exact areas and volumes. An "undamped" flag should be set either by a switch or by putting $f = 0$, and should cause the computation of all fiber-related parameters to be omitted (at present, putting $f = 0$ causes a floating-point exception).

- Specifications of drivers and boxes should be stored in files. Editing of specifications should be interactive and should not require recompilation.

- The interface to SPICE should be at a lower level than that provided by the standard command cards. In particular, it is desirable to prevent SPICE from performing a DC operating-point analysis before the AC analysis (see Subsection 10.3.2).

- The choice of approximations and the superposition of the resulting graphs should be interactive.

The source file `box.c` follows.

```
/*************************************************************************
*************************************************************************

   PROGRAM box.c (GAVIN R. PUTLAND)
   CALCULATION OF SOUND INTENSITY LEVEL VS. FREQUENCY AT ONE METRE.
   Box interior is modeled as lumped compliance or 2D network.
   SPICE3 CIRCUIT DEFINITION IS WRITTEN TO FILE 'cct'.
   SPICE3 COMMAND SCRIPT IS WRITTEN TO FILE 'go'.

   USAGE (assuming executable file is called 'box'):

      box outfile
      box -l outfile
      box -[f|s|u][a|n|e] outfile

   where outfile is the name of the file to which the frequency response
   vector is written (in the SPICE3 command script).  With no switches, box
   does a full simulation.  The switches denote the following approximation
   conditions:

      l     lumped   lumped-compliance box model; no fibre
      f     free     no resistance to air motion            (HF)
      s     stiff    fibre matrix is stiff                  (HF)
      u     unison   fibre moves with air                   (LF)
      a     adiab    adiabatic compression                  (HF)
      n     nearad   near-adiabatic, delCth shorted         (HF)
      e     equil    thermal equilibrium                    (LF)

   Actually any combination of the above switches is accepted, but 'l'
   renders all others superfluous.  Among the other switches, the following
   pecking orders apply:  f>s>u  and  a>n>e.

*************************************************************************
*************************************************************************/

#include <stdio.h>
#include <math.h>
#include <string.h>

/*****************
   DEFINITIONS:
*****************/

/* CONSTANTS: */
   #define pi     3.141592654F

/* FIXED PROPERTIES OF AIR: */
   #define  Rbar   8.31451F        /* universal gas constant, J/(K.mol) */
   #define  mbar   0.028964F       /* molecular mass of air, kg/mol */
   #define  Cp     1007.F          /* Cp of air, J/(kg.K) */

/* AMBIENT CONDITIONS: */
   #define  T     293.15F          /* absolute temperature, K */
   #define  Po    101325.F         /* pressure, Pa */

/* GIVEN DRIVER PARAMETERS (ALTRONICS C3065 10-INCH WOOFER): */
```

```
   #define  fs    35.F             /* free air resonance, Hz */
   #define  Qts   0.4224F
   #define  Qms   2.26F
   #define  Vas   0.0774F          /* suspension equiv. volume, m^3 */
   #define  Re    7.F              /* approx. voice coil resistance, ohms */
   #define  D     0.25F            /* overall diameter, metres */
   #define  a     0.1F             /* diaphragm radius, metres */

/* SIMULATION CONDITIONS: */
   #define  Vg    2.828427125F     /* rms voltage for 1W into 8 ohms */
   #define  fbot  10.F             /* bottom frequency of AC plot */
   #define  ftop  10000.F          /*    top frequency of AC plot */
   #define  del   0.05F            /* min. vol. element size, metres */

/* BOX INTERIOR DIMENSIONS, metres: */
   #define  width    0.25F
   #define  depth    0.3F
   #define  height   0.6F
   #define  clear    0.1F          /* fibre-free clearance behind driver */

/* SPECIFICATIONS OF FIBRE FILLING: */
   #define  d     10e-6F           /* diameter, metres */
   #define  f     0.0025F          /* filling factor */
   #define  rof   2400.F           /* intrinsic density, kg/m^3 */
   #define  Cf    670.F            /* specific heat, J/(kg.K) */

/************************
   EXTERNAL VARIABLES:
************************/

/* FILE POINTERS TO SPICE3 CIRCUIT DEFINITION AND COMMAND SCRIPT: */
   FILE  *cct, *go;

/* FILE NAME FOR FREQUENCY RESPONSE VECTOR (SPICE3 OUTPUT): */
   char  outfile[32];

/* COUNTS AND COUNTERS: */
   int   nhor, nvert,   /* network dimensions */
         nclear,        /* no. clear elements behind driver (horizontally) */
         split,         /* no. clear elements behind driver (vertically) */
         i, j, k;       /* horizontal & vertical indices and node number */

/* REAL VARIABLES (commented in main): */
   float    gam, roo, c, eta, kappa, alpha, ws, Qes, Cas, Ras, Mas, G,
            Mar, Rar, Pro, Mad, lambda, beta, m, tafp, delx, dely,
            delMx, delMy, delMxa, delRx, delMxf, delMya, delRy, delMyf,
            delC, delCa, delRth, delCth, Mab, delRxs, Rleak, Vab, Cab;

main(int argc, char *argv[])

{

/* APPROXIMATION CONDITIONS (from command-line switches): */
   int   lumped = 0,    /* lumped-compliance box model; no fibre */
         free   = 0,    /* no resistance to air motion    (HF) */
         stiff  = 0,    /* fibre matrix is stiff          (HF) */
         unison = 0,    /* fibre moves with air           (LF) */
         adiab  = 0,    /* adiabatic compression          (HF) */
```

```
         nearad = 0,    /* near-adiabatic, delCth shorted (HF) */
         equil  = 0;    /* thermal equilibrium            (LF) */

/***********************************
   PROCESS COMMAND LINE ARGUMENTS:
***********************************/

/* CHECK FOR ILLEGAL ARGUMENTS: */

   if (argc < 2) {
      fprintf(stderr, "Too few arguments.\n");
      exit(1);
   }
   if (argc > 3) {
      fprintf(stderr, "Too many arguments.\n");
      exit(1);
   }
   if (argc == 2 && *(argv[1]) == '-') {
      fprintf(stderr, "You can't start filename with minus sign.\n");
      exit(1);
   }
   if (argc == 3 && *(argv[2]) == '-') {
      fprintf(stderr, "You can't start filename with minus sign.\n");
      exit(1);
   }
   if (argc == 3 && *(argv[1]) != '-') {
      fprintf(stderr, "Switch(es) must follow single minus sign.\n");
      exit(1);
   }

/* SET FLAGS AND SPICE3 OUTPUT FILE NAME: */

   if (argc == 2)
      strcpy(outfile, argv[1]);

   if (argc == 3) {
      strcpy(outfile, argv[2]);
      while (i = *++argv[1]) /* while i is not null character */ {
         switch (i) {
            case 'l':
               lumped = 1;
               break;
            case 'f':
               free   = 1;
               break;
            case 's':
               stiff  = 1;
               break;
            case 'u':
               unison = 1;
               break;
            case 'a':
               adiab  = 1;
               break;
            case 'n':
               nearad = 1;
               break;
            case 'e':
```

```
               equil  = 1;
               break;
            default:
               fprintf(stderr, "Illegal switch \'%c\'.\n", i);
               exit(1);
         }
      }
   }


/**********************************
   EQUIVALENT CIRCUIT COMPONENTS:
**********************************/

/* DERIVED ACOUSTICAL PROPERTIES OF AIR: */
   gam   = Cp / (Cp - Rbar/mbar);               /* gamma (constant) */
   roo   = Po * mbar / (Rbar * T);              /* density, kg/m^3 */
   c     = sqrt(gam * Rbar * T / mbar);         /* speed of sound, m/s */
   eta   = 1.857e-5 * pow((T/300.F),0.7829);    /* viscosity, Pa s */
   kappa = 0.02623 * pow((T/300.F),0.851);      /* conductivity, W/(m.K) */
   alpha = kappa / (roo * Cp);                  /* diffusivity, m^2/s */

/* DERIVED DRIVER PARAMETERS: */
   ws  = 2.0 * pi * fs;
   Qes = 1 / (1/Qts - 1/Qms);
   Cas = Vas / (gam * Po);
   Ras = 1/(ws * Cas * Qms);
   Mas = 1/(Cas * ws * ws);
   G   = sqrt(Qes * ws * Cas / Re);    /* driver gyrator ratio  S/Bl */
   Mar = 8 * roo / (3 * pi * pi * a);  /* radiation inertance */
   Rar = 128*roo*c/(9*pi*pi*pi*a*a);   /* radiation resistance, parallel */
   Pro = sqrt(2e-12 * pi * Rar);       /* O/P pressure for 0dB SIL at 1m
                                          radiating into half-space */
/* Driver inertance without free-air mass load,
   assuming two-sided free-air load equals one-sided baffled air load: */
   Mad = Mas - Mar;

/* DERIVED FIBRE PARAMETERS: */
   lambda = 27.F * eta * (float)pow(f,1.4) / (d*d);
   beta   = gam * f * rof * Cf / ((1.F - f) * roo * Cp);
   m      = 1.0 / sqrt(f);
   tafp   = d*d * (m*m - pow(m,0.37)) * log(0.5 * (m + 1.0)) / (8.F * alpha);

/* DERIVED BOX PARAMETERS: */
   nhor   = (int)(depth/del + 0.01F);
   nvert  = (int)(height/del + 0.01F);
   nclear = (int)(nhor*clear/depth + 0.5F);
   split  = (int)(nvert*D/height + 0.5F);    /* elements spanned by driver */
   delx   = depth / nhor;
   dely   = height / nvert;
   delMx  = roo * delx / (width * dely);     /* for undamped region */
   delMy  = roo * dely / (width * delx);     /* for undamped region */
   delMxa = delMx / (1.F - f);
   delRx  = lambda * delMxa / roo;
   delMxf = f * rof * delMxa / ((1.F - f) * roo);
   delMya = delMy / (1.F - f);
   delRy  = lambda * delMya / roo;
   delMyf = f * rof * delMya / ((1.F - f) * roo);
```

```
   delC   = width * delx * dely / (gam * Po);
   delCa  = (1.F - f) * delC;
   delRth = tafp / ((gam - 1.F) * delCa);
   delCth = (gam - 1.F) * beta * delCa / (gam + beta);
   Vab    = width * (clear * D + (depth - clear) * height);
   Cab    = Vab / (gam * Po);
/* Air load on back of driver, not included in FDM network: */
   Mab = roo * 0.5F * delx / (pi * a*a);
/* To prevent zero DC mesh resistances: */
   delRxs = delMx / 1000.F;   /* giving 'L/R' = 1000 seconds */
/* To give every node a DC path to ground: */
   Rleak  = 1000.F / Cas;   /* giving  'RC' = 1000 seconds */

/************************************************
   WRITE SPICE3 CIRCUIT DEFINITION TO FILE 'cct':
************************************************/

   cct = fopen("cct", "w");

/* HEADER: */
   fprintf(cct, "ALTRONICS C3065 10-INCH WOOFER IN SEALED BOX:\n\n");

/* COMMENTS: */
   fprintf(cct, "* Driver parameters:\n");
   fprintf(cct, "  * fs   = %6.1f Hz\n", fs);
   fprintf(cct, "  * Qts  = %6.4f\n", Qts);
   fprintf(cct, "  * Qms  = %6.4f\n", Qms);
   fprintf(cct, "  * Qes  = %6.4f\n", Qes);
   fprintf(cct, "  * Vas  = %6.1f litres\n", 1e3 * Vas);
   fprintf(cct, "  * Re   = %6.1f ohms\n", Re);
   fprintf(cct, "  * D    = %6.0f mm\n", 1e3F * D);
   fprintf(cct, "  * a    = %6.0f mm\n", 1e3F * a);
   fprintf(cct, "* Box dimensions and divisions:\n");
   fprintf(cct, "  * width  = %4.0f mm\n", 1e3F * width);
   fprintf(cct, "  * depth  = %4.0f mm\n", 1e3F * depth);
   fprintf(cct, "  * height = %4.0f mm\n", 1e3F * height);
   fprintf(cct, "  * clear  = %4.0f mm\n", 1e3F * clear);
   fprintf(cct, "  * Vab  = %6.4f m^3\n", Vab);
   fprintf(cct, "  * delx = %6.0f mm\n", 1e3F * delx);
   fprintf(cct, "  * dely = %6.0f mm\n", 1e3F * dely);
   fprintf(cct, "  * nhor   = %2i\n", nhor);
   fprintf(cct, "  * nvert  = %2i\n", nvert);
   fprintf(cct, "  * nclear = %2i\n", nclear);
   fprintf(cct, "  * split  = %2i\n", split);
   fprintf(cct, "* Properties of air:\n");
   fprintf(cct, "  * T    = %6.2f K\n", T);
   fprintf(cct, "  * Po   = %6.0f Pa\n", Po);
   fprintf(cct, "  * gam  = %6.4f\n", gam);
   fprintf(cct, "  * roo  = %6.4f kg/m^3\n", roo);
   fprintf(cct, "  * c    = %6.2f m/s\n", c);
   fprintf(cct, "* Properties of fibre:\n");
   fprintf(cct, "  * d    = %6.0f um\n", 1e6F * d);
   fprintf(cct, "  * f    = %6.3f %%\n", 100.F * f);
   fprintf(cct, "  * rof  = %6.0f kg/m^3\n", rof);
   fprintf(cct, "  * Cf   = %6.0f J/(kg.K)\n", Cf);
   fprintf(cct, "  * lambda = %4.0f Pa s/m^2\n", lambda);
   fprintf(cct, "  * beta = %6.3f\n", beta);
   fprintf(cct, "  * m    = %6.3f\n", m);
```

```
   fprintf(cct, "  * tafp = %6.2f us\n", 1e6F * tafp);
   fprintf(cct, "* FDM component values:\n");
   fprintf(cct, "  * delMx  = %6.3f kg/m^4\n", delMx);
   fprintf(cct, "  * delMxa = %6.3f kg/m^4\n", delMxa);
   fprintf(cct, "  * delRx  = %6.0f Pa s/m^3\n", delRx);
   fprintf(cct, "  * delMxf = %6.3f kg/m^4\n", delMxf);
   fprintf(cct, "  * delMy  = %6.3f kg/m^4\n", delMy);
   fprintf(cct, "  * delMya = %6.3f kg/m^4\n", delMya);
   fprintf(cct, "  * delRy  = %6.0f Pa s/m^3\n", delRy);
   fprintf(cct, "  * delMyf = %6.3f kg/m^4\n", delMyf);
   fprintf(cct, "  * delC   = %6.3f mm^3/Pa\n", 1e9F * delC);
   fprintf(cct, "  * delCa  = %6.3f mm^3/Pa\n", 1e9F * delCa);
   fprintf(cct, "  * delRth = %6.0f Pa s/m^3\n", delRth);
   fprintf(cct, "  * delCth = %6.3f mm^3/Pa\n", 1e9F * delCth);
   fprintf(cct, "* Simulation specifications:\n");
   fprintf(cct, "  * Vg   = %6.3f V rms\n", Vg);
   fprintf(cct, "  * fbot = %6.0f Hz\n", fbot);
   fprintf(cct, "  * ftop = %6.0f Hz\n", ftop);
   fprintf(cct, "  * Pro  = %6.1f uPa\n", 1e6 * Pro);
   fprintf(cct, "\n");

/* DEFINE LUMPED COMPONENTS: */
   fprintf(cct, "* LUMPED COMPONENTS:\n\n");
   fprintf(cct, "Vg  1 0 dc 0 ac %f\n", Vg);
   fprintf(cct, "Re  1 2 %e\n", Re);
   fprintf(cct, "Lar 0 3 %e\n", Mar);
   fprintf(cct, "Rar 0 3 %e\n", Rar);
   fprintf(cct, "Cas 3 4 %e\n", Cas);
   fprintf(cct, "Rlk 3 4 %e\n", Rleak);         /* DC path to ground */
   fprintf(cct, "Ras 4 5 %e\n", Ras);
   if (lumped) {
      fprintf(cct, "Lad 5 6 %e\n", Mas);        /* with back air load */
      fprintf(cct, "Cab 7 0 %e\n", Cab);        /* lumped box compliance */
      fprintf(cct, "Gf  7 6 2 0 %e\n", G);
      fprintf(cct, "Gb  2 0 6 7 %e\n", G);
   } else {
      fprintf(cct, "Lad 5 6 %e\n", Mad + Mab);  /* with FDM back air load */
      /* Box compliance and gyrator elements are not lumped;
         see next heading. */
   }
   fprintf(cct, "\n");

/* IF NOT 'lumped' APPROXIMATION: ************************************/

if (!lumped) {

/* DEFINE SPLIT TRANSCONDUCTANCE: */
   fprintf(cct, "* SPLIT TRANSCONDUCTANCE:\n\n");
   /* SPLIT FORWARD TRANSCONDUCTANCE: */
      for (j=0; j<split; j++)
         fprintf(cct, "Gf%.2i %3i 6 2 0  %e\n", j, 7+j, G/(float)split);
   /* SPLIT BACKWARD TRANSCONDUCTANCE: */
      for (j=0; j<split; j++)
         fprintf(cct, "Gb%.2i 2 0 6 %3i  %e\n", j, 7+j, G/(float)split);
   fprintf(cct, "\n");

/* DEFINE INERTANCE SUBCIRCUITS */
/* No series resistance needed for y element. */
```

```
/* 'Mxb' is on boundary between fibre-filled and fibre-free regions. */
   fprintf(cct, "* MASS ELEMENT SUBCIRCUITS:\n\n");
   /* 'UNDAMPED' HORIZONTAL MASS ELEMENT: */
      fprintf(cct, ".subckt Mxclearsub 1 3\n");
      fprintf(cct, "Lx  1 2 %e\n", delMx);
      fprintf(cct, "Rxs 2 3 %e\n", delRxs);
      fprintf(cct, ".ends Mxclearsub\n\n");
   if (free) {
      fprintf(cct, ".subckt Mxsub 1 3\n");
      fprintf(cct, "Lx  1 2 %e\n", delMxa);
      fprintf(cct, "Rxs 2 3 %e\n", delRxs);
      fprintf(cct, ".ends Mxsub\n\n");
      fprintf(cct, ".subckt Mysub 1 2\n");
      fprintf(cct, "Ly  1 2 %e\n", delMya);
      fprintf(cct, ".ends Mysub\n\n");
      fprintf(cct, ".subckt Mxbsub 1 3\n");
      fprintf(cct, "Lx  1 2 %e\n", 0.5F*(delMx + delMxa));
      fprintf(cct, "Rxs 2 3 %e\n", delRxs);
      fprintf(cct, ".ends Mxbsub\n\n");
   } else if (stiff) {
      fprintf(cct, ".subckt Mxsub 1 3\n");
      fprintf(cct, "Lxa 1 2 %e\n", delMxa);
      fprintf(cct, "Rx  2 3 %e\n", delRx + delRxs);
      fprintf(cct, ".ends Mxsub\n\n");
      fprintf(cct, ".subckt Mysub 1 3\n");
      fprintf(cct, "Lya 1 2 %e\n", delMya);
      fprintf(cct, "Ry  2 3 %e\n", delRy);
      fprintf(cct, ".ends Mysub\n\n");
      fprintf(cct, ".subckt Mxbsub 1 3\n");
      fprintf(cct, "Lxa 1 2 %e\n", 0.5F*(delMx + delMxa));
      fprintf(cct, "Rx  2 3 %e\n", 0.5F*delRx + delRxs);
      fprintf(cct, ".ends Mxbsub\n\n");
   } else if (unison) {
      fprintf(cct, ".subckt Mxsub 1 3\n");
      fprintf(cct, "Lx  1 2 %e\n", delMxa + delMxf);
      fprintf(cct, "Rxs 2 3 %e\n", delRxs);
      fprintf(cct, ".ends Mxsub\n\n");
      fprintf(cct, ".subckt Mysub 1 2\n");
      fprintf(cct, "Ly  1 2 %e\n", delMya + delMyf);
      fprintf(cct, ".ends Mysub\n\n");
      fprintf(cct, ".subckt Mxbsub 1 3\n");
      fprintf(cct, "Lx  1 2 %e\n", 0.5*(delMx + delMxa + delMxf));
      fprintf(cct, "Rxs 2 3 %e\n", delRxs);
      fprintf(cct, ".ends Mxbsub\n\n");
   } else /* if no approximation */ {
      fprintf(cct, ".subckt Mxsub 1 4\n");
      fprintf(cct, "Lxa 1 2 %e\n", delMxa);
      fprintf(cct, "Rx  2 3 %e\n", delRx);
      fprintf(cct, "Lxf 2 3 %e\n", delMxf);
      fprintf(cct, "Rxs 3 4 %e\n", delRxs);
      fprintf(cct, ".ends Mxsub\n\n");
      fprintf(cct, ".subckt Mysub 1 3\n");
      fprintf(cct, "Lya 1 2 %e\n", delMya);
      fprintf(cct, "Ry  2 3 %e\n", delRy);
      fprintf(cct, "Lyf 2 3 %e\n", delMyf);
      fprintf(cct, ".ends Mysub\n\n");
      fprintf(cct, ".subckt Mxbsub 1 4\n");
      fprintf(cct, "Lxa 1 2 %e\n", 0.5*(delMx + delMxa));
```

```
      fprintf(cct, "Rx  2 3 %e\n", 0.5*delRx);
      fprintf(cct, "Lxf 2 3 %e\n", 0.5*delMxf);
      fprintf(cct, "Rxs 3 4 %e\n", delRxs);
      fprintf(cct, ".ends Mxbsub\n\n");
   }

/* DEFINE COMPLIANCE SUBCIRCUIT */
   fprintf(cct, "* COMPLIANCE ELEMENT SUBCIRCUIT:\n\n");
   if (adiab) {
      fprintf(cct, ".subckt Csub 1 2\n");
      fprintf(cct, "Ca 1 2 %e\n", delCa);
      fprintf(cct, ".ends Csub\n\n");
   } else if (nearad) {
      fprintf(cct, ".subckt Csub 1 2\n");
      fprintf(cct, "Ca  1 2 %e\n", delCa);
      fprintf(cct, "Rth 1 2 %e\n", delRth);
      fprintf(cct, ".ends Csub\n\n");
   } else if (equil) {
      fprintf(cct, ".subckt Csub 1 2\n");
      fprintf(cct, "C   1 2 %e\n", delCa + delCth);
      fprintf(cct, ".ends Csub\n\n");
   } else /* if no approximation */ {
      fprintf(cct, ".subckt Csub 1 3\n");
      fprintf(cct, "Ca  1 3 %e\n", delCa);
      fprintf(cct, "Rth 1 2 %e\n", delRth);
      fprintf(cct, "Cth 2 3 %e\n", delCth);
      fprintf(cct, ".ends Csub\n\n");
   }

/* WRITE UNDAMPED (CLEAR) COMPLIANCE ELEMENTS: */
   fprintf(cct, "* UNDAMPED (CLEAR) COMPLIANCE ELEMENTS:\n\n");
   for (i=0; i<nclear; i++)
      for (j=0; j<split; j++) {
         k = 7 + split*i + j;
         fprintf(cct, "C%.2i %2i 0  %e\n", k, k, delC);
      }
   fprintf(cct, "\n");

/* WRITE UNDAMPED (CLEAR) HORIZONTAL INERTANCE ELEMENTS: */
   fprintf(cct, "* UNDAMPED (CLEAR) HORIZONTAL INERTANCE ELEMENTS:\n\n");
   for (i=0; i<nclear-1; i++)
      for (j=0; j<split; j++) {
         k = 7 + split*i + j;
         fprintf(cct, "XLx%.2ito%.2i %2i %2i  Mxclearsub\n",
                       k, k+split, k, k+split);
      }
   fprintf(cct, "\n");

/* WRITE UNDAMPED (CLEAR) VERTICAL INERTANCE ELEMENTS: */
   fprintf(cct, "* UNDAMPED (CLEAR) VERTICAL INERTANCE ELEMENTS:\n\n");
   for (i=0; i<nclear; i++)
      for (j=0; j<split-1; j++) {
         k = 7 + split*i + j;
         fprintf(cct, "Ly%.2ito%.2i %2i %2i  %e\n",
                       k, k+1, k, k+1, delMy);
      }
   fprintf(cct, "\n");
```

```
/* WRITE HALF-DAMPED HORIZONTAL INERTANCE ELEMENTS: */
   fprintf(cct, "* HALF-DAMPED HORIZONTAL INERTANCE ELEMENTS:\n\n");
      i = nclear-1;
      for (j=0; j<split; j++) {
         k = 7 + split*i + j;
         fprintf(cct, "XLxb%.2i %2i %2i  Mxbsub\n", j, k, k+split);
      }
   fprintf(cct, "\n");

/* WRITE DAMPED COMPLIANCE ELEMENTS: */
   fprintf(cct, "* DAMPED COMPLIANCE ELEMENTS:\n\n");
   for (i=nclear; i<nhor; i++)
      for (j=0; j<nvert; j++) {
         k = 7 + nclear*split + nvert*(i-nclear) + j;
         fprintf(cct, "XC%.3i %3i 0  Csub\n", k, k);
      }
   fprintf(cct, "\n");

/* WRITE DAMPED HORIZONTAL INERTANCE ELEMENTS: */
   fprintf(cct, "* DAMPED HORIZONTAL INERTANCE ELEMENTS:\n\n");
   for (i=nclear; i<nhor-1; i++)
      for (j=0; j<nvert; j++) {
         k = 7 + nclear*split + nvert*(i-nclear) + j;
         fprintf(cct, "XLx%.3ito%.3i %3i %3i  Mxsub\n",
                        k, k+nvert, k, k+nvert);
      }
   fprintf(cct, "\n");

/* WRITE DAMPED VERTICAL INERTANCE ELEMENTS: */
   fprintf(cct, "* DAMPED VERTICAL INERTANCE ELEMENTS:\n\n");
   for (i=nclear; i<nhor; i++)
      for (j=0; j<nvert-1; j++) {
         k = 7 + nclear*split + nvert*(i-nclear) + j;
         fprintf(cct, "XLy%.3ito%.3i %3i %3i  Mysub\n", k, k+1, k, k+1);
      }
   fprintf(cct, "\n");

}

/***************************** END ``IF NOT `lumped' APPROXIMATION''. */

   fprintf(cct, ".end\n");

   fclose(cct);

/*******************************************
   WRITE SPICE3 COMMAND SCRIPT TO FILE `go':
*******************************************/

   go = fopen("go", "w");

   fprintf(go, "ANALYSIS AND PLOTTING INSTRUCTIONS:\n");
   fprintf(go, ".control\n");
   fprintf(go, "ac dec 50 %2.0f %5.0f\n", fbot, ftop);
   fprintf(go, "rusage space time\n");
   fprintf(go, "set units = degrees\n");
   fprintf(go, "set plottype = point\n");
   fprintf(go, "set hcopydevtype = postscript\n");
```

```
   fprintf(go, "set nobreak\n");
   fprintf(go, "set width = 76\n");
   fprintf(go, "plot db(v(3)/%6.0fn) xl %2.0f %5.0f xlog\n",
               1e9F * Pro, fbot, ftop);
   fprintf(go, "print col db(v(3)/%6.0fn)>%s\n",
               1e9F * Pro, outfile);
   fprintf(go, ".endc\n");

   fclose(go);

}
```

B.10 Sample circuit file `cct` (for loudspeaker)

The program `box.c`, listed in the previous section, produces a commented circuit definition file in SPICE3 format called "`cct`". The circuit definition obviously depends on the command-line switches used with `box.c` and on any variations to the program itself; every graph in Chapter 10 came from a different "`cct`" file. The version of "`cct`" presented here was produced by the version of `box.c` listed above (10-inch woofer, 36-liter box, 50 mm elements) with no switches (full simulation).

The conventions of SPICE necessitate some departures from the notation of Chapter 7; for example, names of inductive elements start with "`L`" (not "`M`") and names of subcircuit instances start with "`X`". To ensure that all element names are unique, the name of every compliant element, and of each mass element on the boundary between the clear and fiber-filled regions, includes a node number, while the name of every other mass element includes the numbers of the two nodes between which the element is connected.

The circuit file is listed below. Lines beginning with asterisks or blanks are comments.

```
ALTRONICS C3065 10-INCH WOOFER IN SEALED BOX:

* Driver parameters:
  * fs   =   35.0 Hz
  * Qts  = 0.4224
  * Qms  = 2.2600
  * Qes  = 0.5195
  * Vas  =   77.4 litres
  * Re   =    7.0 ohms
  * D    =    250 mm
  * a    =    100 mm
* Box dimensions and divisions:
  * width  =  250 mm
  * depth  =  300 mm
  * height =  600 mm
  * clear  =  100 mm
  * Vab  = 0.0363 m^3
  * delx =     50 mm
  * dely =     50 mm
  * nhor   =  6
  * nvert  = 12
  * nclear =  2
  * split  =  5
* Properties of air:
  * T    = 293.15 K
  * Po   = 101325 Pa
  * gam  = 1.3987
  * roo  = 1.2041 kg/m^3
  * c    = 343.08 m/s
* Properties of fibre:
  * d    =     10 um
  * f    =  0.250 %
  * rof  =   2400 kg/m^3
  * Cf   =    670 J/(kg.K)
  * lambda = 1121 Pa s/m^2
  * beta =  4.649
```

```
  * m    = 20.000
  * tafp = 550.06 us
* FDM component values:
  * delMx  =  4.816 kg/m^4
  * delMxa =  4.828 kg/m^4
  * delRx  =   4494 Pa s/m^3
  * delMxf = 24.120 kg/m^4
  * delMy  =  4.816 kg/m^4
  * delMya =  4.828 kg/m^4
  * delRy  =   4494 Pa s/m^3
  * delMyf = 24.120 kg/m^4
  * delC   =  4.410 mm^3/Pa
  * delCa  =  4.399 mm^3/Pa
  * delRth = 313604 Pa s/m^3
  * delCth =  1.348 mm^3/Pa
* Simulation specifications:
  * Vg   =  2.828 V rms
  * fbot =     10 Hz
  * ftop =  10000 Hz
  * Pro  =  345.0 uPa

* LUMPED COMPONENTS:

Vg  1 0 dc 0 ac 2.828427
Re  1 2 7.000000e+00
Lar 0 3 3.253251e+00
Rar 0 3 1.894821e+04
Cas 3 4 5.461212e-07
Rlk 3 4 1.831096e+09
Ras 4 5 3.684297e+03
Lad 5 6 3.556792e+01

* SPLIT TRANSCONDUCTANCE:

Gf00   7 6 2 0  5.970905e-04
Gf01   8 6 2 0  5.970905e-04
Gf02   9 6 2 0  5.970905e-04
Gf03  10 6 2 0  5.970905e-04
Gf04  11 6 2 0  5.970905e-04
Gb00 2 0 6   7  5.970905e-04
Gb01 2 0 6   8  5.970905e-04
Gb02 2 0 6   9  5.970905e-04
Gb03 2 0 6  10  5.970905e-04
Gb04 2 0 6  11  5.970905e-04

* MASS ELEMENT SUBCIRCUITS:

.subckt Mxclearsub 1 3
Lx  1 2 4.816245e+00
Rxs 2 3 4.816245e-03
.ends Mxclearsub

.subckt Mxsub 1 4
Lxa 1 2 4.828316e+00
Rx  2 3 4.493505e+03
Lxf 2 3 2.412045e+01
Rxs 3 4 4.816245e-03
.ends Mxsub
```

```
.subckt Mysub 1 3
Lya 1 2 4.828316e+00
Ry  2 3 4.493505e+03
Lyf 2 3 2.412045e+01
.ends Mysub

.subckt Mxbsub 1 4
Lxa 1 2 4.822280e+00
Rx  2 3 2.246752e+03
Lxf 2 3 1.206023e+01
Rxs 3 4 4.816245e-03
.ends Mxbsub

* COMPLIANCE ELEMENT SUBCIRCUIT:

.subckt Csub 1 3
Ca  1 3 4.398869e-09
Rth 1 2 3.136040e+05
Cth 2 3 1.348324e-09
.ends Csub

* UNDAMPED (CLEAR) COMPLIANCE ELEMENTS:

C07  7 0  4.409893e-09
C08  8 0  4.409893e-09
C09  9 0  4.409893e-09
C10 10 0  4.409893e-09
C11 11 0  4.409893e-09
C12 12 0  4.409893e-09
C13 13 0  4.409893e-09
C14 14 0  4.409893e-09
C15 15 0  4.409893e-09
C16 16 0  4.409893e-09

* UNDAMPED (CLEAR) HORIZONTAL INERTANCE ELEMENTS:

XLx07to12  7 12  Mxclearsub
XLx08to13  8 13  Mxclearsub
XLx09to14  9 14  Mxclearsub
XLx10to15 10 15  Mxclearsub
XLx11to16 11 16  Mxclearsub

* UNDAMPED (CLEAR) VERTICAL INERTANCE ELEMENTS:

Ly07to08  7  8  4.816245e+00
Ly08to09  8  9  4.816245e+00
Ly09to10  9 10  4.816245e+00
Ly10to11 10 11  4.816245e+00
Ly12to13 12 13  4.816245e+00
Ly13to14 13 14  4.816245e+00
Ly14to15 14 15  4.816245e+00
Ly15to16 15 16  4.816245e+00

* HALF-DAMPED HORIZONTAL INERTANCE ELEMENTS:

XLxb00 12 17  Mxbsub
XLxb01 13 18  Mxbsub
```

```
XLxb02 14 19  Mxbsub
XLxb03 15 20  Mxbsub
XLxb04 16 21  Mxbsub

* DAMPED COMPLIANCE ELEMENTS:

XC017  17 0  Csub
XC018  18 0  Csub
XC019  19 0  Csub
XC020  20 0  Csub
XC021  21 0  Csub
XC022  22 0  Csub
XC023  23 0  Csub
XC024  24 0  Csub
XC025  25 0  Csub
XC026  26 0  Csub
XC027  27 0  Csub
XC028  28 0  Csub
XC029  29 0  Csub
XC030  30 0  Csub
XC031  31 0  Csub
XC032  32 0  Csub
XC033  33 0  Csub
XC034  34 0  Csub
XC035  35 0  Csub
XC036  36 0  Csub
XC037  37 0  Csub
XC038  38 0  Csub
XC039  39 0  Csub
XC040  40 0  Csub
XC041  41 0  Csub
XC042  42 0  Csub
XC043  43 0  Csub
XC044  44 0  Csub
XC045  45 0  Csub
XC046  46 0  Csub
XC047  47 0  Csub
XC048  48 0  Csub
XC049  49 0  Csub
XC050  50 0  Csub
XC051  51 0  Csub
XC052  52 0  Csub
XC053  53 0  Csub
XC054  54 0  Csub
XC055  55 0  Csub
XC056  56 0  Csub
XC057  57 0  Csub
XC058  58 0  Csub
XC059  59 0  Csub
XC060  60 0  Csub
XC061  61 0  Csub
XC062  62 0  Csub
XC063  63 0  Csub
XC064  64 0  Csub

* DAMPED HORIZONTAL INERTANCE ELEMENTS:

XLx017to029  17  29  Mxsub
```

```
XLx018to030  18  30  Mxsub
XLx019to031  19  31  Mxsub
XLx020to032  20  32  Mxsub
XLx021to033  21  33  Mxsub
XLx022to034  22  34  Mxsub
XLx023to035  23  35  Mxsub
XLx024to036  24  36  Mxsub
XLx025to037  25  37  Mxsub
XLx026to038  26  38  Mxsub
XLx027to039  27  39  Mxsub
XLx028to040  28  40  Mxsub
XLx029to041  29  41  Mxsub
XLx030to042  30  42  Mxsub
XLx031to043  31  43  Mxsub
XLx032to044  32  44  Mxsub
XLx033to045  33  45  Mxsub
XLx034to046  34  46  Mxsub
XLx035to047  35  47  Mxsub
XLx036to048  36  48  Mxsub
XLx037to049  37  49  Mxsub
XLx038to050  38  50  Mxsub
XLx039to051  39  51  Mxsub
XLx040to052  40  52  Mxsub
XLx041to053  41  53  Mxsub
XLx042to054  42  54  Mxsub
XLx043to055  43  55  Mxsub
XLx044to056  44  56  Mxsub
XLx045to057  45  57  Mxsub
XLx046to058  46  58  Mxsub
XLx047to059  47  59  Mxsub
XLx048to060  48  60  Mxsub
XLx049to061  49  61  Mxsub
XLx050to062  50  62  Mxsub
XLx051to063  51  63  Mxsub
XLx052to064  52  64  Mxsub

* DAMPED VERTICAL INERTANCE ELEMENTS:

XLy017to018  17  18  Mysub
XLy018to019  18  19  Mysub
XLy019to020  19  20  Mysub
XLy020to021  20  21  Mysub
XLy021to022  21  22  Mysub
XLy022to023  22  23  Mysub
XLy023to024  23  24  Mysub
XLy024to025  24  25  Mysub
XLy025to026  25  26  Mysub
XLy026to027  26  27  Mysub
XLy027to028  27  28  Mysub
XLy029to030  29  30  Mysub
XLy030to031  30  31  Mysub
XLy031to032  31  32  Mysub
XLy032to033  32  33  Mysub
XLy033to034  33  34  Mysub
XLy034to035  34  35  Mysub
XLy035to036  35  36  Mysub
XLy036to037  36  37  Mysub
XLy037to038  37  38  Mysub
```

```
XLy038to039  38  39  Mysub
XLy039to040  39  40  Mysub
XLy041to042  41  42  Mysub
XLy042to043  42  43  Mysub
XLy043to044  43  44  Mysub
XLy044to045  44  45  Mysub
XLy045to046  45  46  Mysub
XLy046to047  46  47  Mysub
XLy047to048  47  48  Mysub
XLy048to049  48  49  Mysub
XLy049to050  49  50  Mysub
XLy050to051  50  51  Mysub
XLy051to052  51  52  Mysub
XLy053to054  53  54  Mysub
XLy054to055  54  55  Mysub
XLy055to056  55  56  Mysub
XLy056to057  56  57  Mysub
XLy057to058  57  58  Mysub
XLy058to059  58  59  Mysub
XLy059to060  59  60  Mysub
XLy060to061  60  61  Mysub
XLy061to062  61  62  Mysub
XLy062to063  62  63  Mysub
XLy063to064  63  64  Mysub

.end
```

B.11 Graphing program `sp2tex.c`

Program `sp2tex.c` processed the SPICE output files to produce the graphs in Chapter 10. The command-line syntax is given in the introductory comment. The present version assumes fixed ranges for the abscissa and ordinate. Obviously a production version would need to be more versatile, more interactive, and better integrated with the model-building program.

The listing follows.

```
/*************************************************************************

   PROGRAM sp2tex.c (GAVIN R. PUTLAND)
   Convert SPICE3 'print' file(s) to a graph
   using LaTeX 'picture' commands.

   USAGE (assuming executable file is called 'sp2tex'):

      sp2tex in1 [in2] out

   where 'in1' and the optional 'in2' are the names of single-vector files
   generated by the SPICE3 'print col' command, and 'out' is the name of the
   output file.  If in2 is given, the points from the files in1 and in2 are
   combined into one graph, but the latter are plotted using smaller dots.
   If out exists, sp2tex absolutely refuses to overwrite it.  The out file
   begins with

      \setlength{\unitlength}{0.0033333in}
      \begin{picture}(1200,1120)(100,900)

   and ends with

      \end{picture}

   The present version draws axes and grids assuming that the frequency
   column in in1 and in2 extends from 10Hz to 10kHz and that the ordinate
   vector elements are between 50 and 100.

*************************************************************************/

#include <stdio.h>
#include <math.h>
#include <string.h>

main(int argc, char *argv[])

{

/* FILE NAMES AND POINTERS: */

   char  in1name[32], in2name[32], outname[32];
   FILE  *in1, *in2, *out;

/* SCRATCH VARIABLES */

   char  line[99];
   int   i;
```

```
   float x, y;

/* CHECK FOR ILLEGAL USAGE: */

   if (argc < 3) {
      fprintf(stderr, "Too few arguments.\n");
      exit(1);
   }
   if (argc > 4) {
      fprintf(stderr, "Too many arguments.\n");
      exit(1);
   }

/* PROCESS COMMAND-LINE ARGUMENTS AND ATTEMPT TO OPEN FILES: */

   strcpy(in1name, argv[1]);
   if (!(in1 = fopen(in1name, "r"))) {
      fprintf(stderr, "Can't find/open file \'%s\'.\n", in1name);
      exit(1);
   }
   if (argc == 4) {
      strcpy(in2name, argv[2]);
      if (!(in2 = fopen(in2name, "r"))) {
         fprintf(stderr, "Can't find/open file \'%s\'.\n", in2name);
         exit(1);
      }
   }
   strcpy(outname, argv[argc-1]);
   if (fopen(outname, "r")) /* if file `outname' already exists */ {
      fprintf(stderr, "File \'%s\' exists.  Rename/remove it.\n", outname);
      exit(1);
   }
   out = fopen(outname, "w");

/* OPEN picture ENVIRONMENT: */

   fprintf(out, "\\setlength{\\unitlength}{0.0033333in}\n");
   fprintf(out, "\\begin{picture}(1200,1120)(100,900)\n");

/* AXES AND GRID, LABELS, SCALES: */

   fprintf(out, "%% AXES AND GRID:\n");
   fprintf(out, "\\thicklines\n");
   fprintf(out, "\\multiput(300,1000)(300,0){4}{\\line(0,1){1000}}\n");
   fprintf(out, "\\thinlines\n");
   fprintf(out, "\\multiput(300,1000)(0,200){6}{\\line(1,0){ 900}}\n");
   fprintf(out, "\\multiput(390,1000)(300,0){3}{\\line(0,1){1000}}\n");
   fprintf(out, "\\multiput(510,1000)(300,0){3}{\\line(0,1){1000}}\n");
   fprintf(out, "%% LABELS:\n");
   fprintf(out, "\\put(750, 870){\\makebox(0,0){\\sf Frequency (Hz)}}\n");
   fprintf(out, "\\put(200,1530){\\makebox(0,0){\\sf SIL}}\n");
   fprintf(out, "\\put(200,1470){\\makebox(0,0){\\sf (dB)}}\n");
   fprintf(out, "%% SCALES:\n");
   fprintf(out, "\\put( 305,930){\\makebox(0,0)[b]{$10^1$}}\n");
   fprintf(out, "\\put( 605,930){\\makebox(0,0)[b]{$10^2$}}\n");
   fprintf(out, "\\put( 905,930){\\makebox(0,0)[b]{$10^3$}}\n");
   fprintf(out, "\\put(1205,930){\\makebox(0,0)[b]{$10^4$}}\n");
   fprintf(out,
```

```
      "\\multiput(390,970)(300,0){3}{\\makebox(0,0)[b]{\\scriptsize 2}}\n");
   fprintf(out,
      "\\multiput(510,970)(300,0){3}{\\makebox(0,0)[b]{\\scriptsize 5}}\n");
   fprintf(out, "\\put(270,1000){\\makebox(0,0)[r]{50}}\n");
   fprintf(out, "\\put(270,1200){\\makebox(0,0)[r]{60}}\n");
   fprintf(out, "\\put(270,1400){\\makebox(0,0)[r]{70}}\n");
   fprintf(out, "\\put(270,1600){\\makebox(0,0)[r]{80}}\n");
   fprintf(out, "\\put(270,1800){\\makebox(0,0)[r]{90}}\n");
   fprintf(out, "\\put(270,2000){\\makebox(0,0)[r]{100}}\n");

/* PROCESS FIRST INPUT FILE: */

      fprintf(out, "%% POINTS FROM FILE %s:\n", in1name);
   /* SKIP FIRST FIVE LINES (PREAMBLE): */
      for (i=0; i<5; i++)
         fgets(line, 99, in1);
   /* READ LINES; EXTRACT COORDINATES, PLOT POINTS: */
      while (fgets(line, 99, in1)) {
         sscanf(line, "%*d %e, %*e %e", &x, &y);
         if (y > 50.F) {
            x = 300.F * (float)log10(x);
            y = 20.F * y;
            fprintf(out, "\\put(%4.0f,%4.0f){\\circle*{8}}\n", x, y);
         }
      }

/* SIMILARLY, PROCESS SECOND INPUT FILE IF IT EXISTS: */

   if (in2) {
      fprintf(out, "%% POINTS FROM FILE %s:\n", in2name);
      for (i=0; i<5; i++)
         fgets(line, 99, in2);
      while (fgets(line, 99, in2)) {
         sscanf(line, "%*d %e, %*e %e", &x, &y);
         if (y > 50.F) {
            x = 300.F * (float)log10(x);
            y = 20.F * y;
            fprintf(out, "\\put(%4.0f,%4.0f){\\circle*{2}}\n", x, y);
         }
      }
   }

/* CLOSE picture ENVIRONMENT AND CLOSE FILES: */

   fprintf(out, "\\end{picture}\n");
   fclose(in1);
   if (in2)
      fclose(in2);
   fclose(out);

}
```

B.12 Model builder `disk.c` (for circular piston)

Program `disk.c` produced the circuit definition files and command files for the FDEC simulations of a circular rigid piston, presented in Chapter 11. Some details of implementation not discussed in that chapter are explained here. Further explanatory notes accompany the sample circuit file (see next section).

If the command file calls for an AC analysis, the circuit must not contain any loops with zero DC resistance. Such loops can be avoided by introducing small resistances in series with the radial mass elements (including the truncated elements) and the truncated axial mass elements adjacent to the plane of the disk. In transient analyses the added resistances are not needed (because SPICE allows the DC analysis to be bypassed using the "`uic`" option) and should be omitted to save memory and CPU time. Accordingly, the added resistances appear in the circuit file only if the third command-line option is "`a`" or "`u`". To add the series resistance, each internal radial mass element is replaced by a series R-L subcircuit, each truncated axial mass element adjacent to the plane of the disk is similarly replaced, and each cylindrical-boundary subcircuit has a series resistance added. The resulting normalized L/R time constants are 10^6 for the internal and truncated radial elements, and 5×10^5 for the affected axial elements.

Note that the equivalent circuit is driven by a pressure (voltage) source if a transient analysis is required, and by a flux (current) source if an AC analysis is required. This situation arose because the need to use a pressure source for the transient analysis was realized after the AC analysis options were fully developed and tested. In retrospect, Eqs. (11.66) and (11.68), by which the AC radiation resistance and radiation mass were computed, could have been used with a pressure source because the currents in voltage sources are available variables in SPICE expressions. This would have simplified the program slightly and produced the same equivalent circuit for both transient and AC analyses. But the program has been left in its original state as a procedural record.

The function $g(t)$ given by Eq. (11.77) was chosen because its energy is mostly within the band $|\omega| < 2\pi/T$. It is a simple exercise to find the precise fraction of the energy within that band. The total energy is

$$E = \int_{-\infty}^{\infty} g^2(t)\,dt = \int_{-T}^{T} \left[1 + \cos\left(\frac{\pi t}{T}\right)\right]^2 dt = 3T. \tag{B.14}$$

The Fourier transform of $g(t)$ is [40, p. 62]

$$G(\omega) = \frac{2\pi^2 \sin \omega T}{\omega(\pi^2 - \omega^2 T^2)} \tag{B.15}$$

(which has removable singularities at $\omega = 0$ and $\omega = \pm\pi/T$, where the numerator and denominator both vanish). Hence the energy in the band $|\omega| < 2\pi/T$ is

$$E_{|\omega|<2\pi/T} = \frac{1}{2\pi} \int_{-2\pi/T}^{2\pi/T} |G(\omega)|^2\,d\omega \tag{B.16}$$

where the factor $1/(2\pi)$ comes from the energy form of Parseval's identity [40, p. 65]. Substituting for $G(\omega)$ and dividing by Eq. (B.14), we obtain

$$\frac{E_{|\omega|<2\pi/T}}{E} = \frac{1}{6\pi T} \int_{-2\pi/T}^{2\pi/T} \left(\frac{2\pi^2 \sin \omega T}{\omega(\pi^2 - \omega^2 T^2)}\right)^2 d\omega$$

$$= \frac{1}{6\pi}\int_{-2\pi}^{2\pi}\left(\frac{2\pi^2\sin\omega T}{\omega T(\pi^2-(\omega T)^2)}\right)^2 d(\omega T)$$
$$= \frac{4\pi^3}{3}\int_{0}^{2\pi}\left(\frac{\sin\theta}{\theta(\pi^2-\theta^2)}\right)^2 d\theta \qquad \text{(B.17)}$$

where $\theta = \omega T$ and the last step exploits the evenness of the integrand. The integral was evaluated with a Hewlett-Packard 15C pocket calculator, yielding the result

$$\frac{E_{|\omega|<2\pi/T}}{E} = 0.999485. \qquad \text{(B.18)}$$

That is, only 0.0515% of the energy is outside the band $|\omega| < 2\pi/T$.

If a transient analysis is required, the pressure source is represented in SPICE by a time-dependent voltage source; the raised-cosine function is approximated by a piecewise-linear function with 26 segments, using the "`pwl`" option. The complete transient source specification, with the "`pwl`" breakpoints written on continuation lines, is written by following segment of code in `disk.c`:

```
fprintf(cct, "Vtran %2d 0 dc 0 pwl ( 0 0\n", m+1);
for (i=1; i<=25; i++)
   fprintf(cct, "+ %.6f %.7f\n", (float)i/(2*m), rc((double)i/(2*m)));
fprintf(cct, "+ %.6f 0 )\n", 13.F/m);
```

If $m = 4$ (as in Fig. 11.2), the resulting source specification is

```
Vtran  5 0 dc 0 pwl ( 0 0
+ 0.125000 0.0089410
+ 0.250000 0.0352443
+ 0.375000 0.0773813
+ 0.500000 0.1329032
+ 0.625000 0.1985831
+ 0.750000 0.2706041
+ 0.875000 0.3447805
+ 1.000000 0.4168015
+ 1.125000 0.4824814
+ 1.250000 0.5380033
+ 1.375000 0.5801404
+ 1.500000 0.6064436
+ 1.625000 0.6153846
+ 1.750000 0.6064436
+ 1.875000 0.5801403
+ 2.000000 0.5380033
+ 2.125000 0.4824814
+ 2.250000 0.4168015
+ 2.375000 0.3447805
+ 2.500000 0.2706040
+ 2.625000 0.1985830
+ 2.750000 0.1329031
+ 2.875000 0.0773813
+ 3.000000 0.0352443
+ 3.125000 0.0089410
+ 3.250000 0 )
```

This is the driving function plotted in Fig. 11.2 (top trace).

The nodes at which the transient pressures are to be computed are specified in the last part of the program, which writes the SPICE command script. The node numbers, denoted by `s` and `s2`, are computed in terms of m and n to ensure that they are legal for all m and n; this allows testing of the program with small values of n.

For clarity, the following listing of `disk.c` has received some nonsubstantive editing (confined to comments and white space).

```
/*************************************************************************
*************************************************************************

   Program 'disk.c' (GAVIN R. PUTLAND)

   FINITE-DIFFERENCE EQUIVALENT-CIRCUIT MODEL OF CIRCULAR RIGID PISTON
   (in infinite planar baffle, unless 'u' option is used).

   SPICE3 circuit definition is written to file 'cct'.
   SPICE3 command script is written to file 'go'.

   USAGE (assuming executable file is called 'disk'):

      disk m n a|t|u outfile

   where

      m is the number of steps in the radius of the disk;

      n is the number of steps from the centre of the disk to the anechoic
      boundary (n is the same in the r and z directions, as is the step
      size);

      a|t|u means ONE of the following options (if a string is entered, only
      the first character is significant):

         'a' for AC analysis,
         't' for transient analysis,
         'u' for unbaffled (AC analysis);

      outfile is the stem of the SPICE output file names.  The numerical
      (text) output is written to outfile.dat.  The hardcopy (graphical)
      output is written to outfile.ps.  Resource usage is written to
      outfile.rus.  These filenames are not used by 'disk' and are simply
      copied to the 'go' script.

*************************************************************************
*************************************************************************/

#include <stdio.h>
#include <math.h>
#include <string.h>

/*****************
   DEFINITIONS:
*****************/
```

```
/* LIMITS: */
   #define nmax   90          /* max value of n */

/* CONSTANTS: */
   #define pi     3.141592654F

/* SIMULATION CONDITIONS: */
   #define  hmin  0.01F       /* minimum normalized freq. of AC analysis */
   #define  hmax  10.0F       /* maximum normalized freq. of AC analysis */

/************************
   EXTERNAL VARIABLES:
************************/

/* FILE POINTERS TO SPICE3 CIRCUIT DEFINITION AND COMMAND SCRIPT: */
   FILE  *cct, *go;

/* SIMULATION TYPE (string "a" or "t" or "u"): */
   char  mode[32];

/* FILE NAME (LESS EXTENSION) FOR OUTPUT OF SPICE: */
   char  outfile[32];

/* COUNTS AND COUNTERS: */
   int      m,             /* no. elements in disk radius */
            n,             /* no. elements to anechoic boundary */
            i, k, s,       /* radial & axial indices and node number */
            s2;            /* auxiliary node number */

/* REAL VARIABLES: */
   float    a[nmax],       /* area fraction (function of i only) */
            mf,            /* 'front' inertance (see comment in main) */
            rrb[nmax],     /* boundary resistors  at r=b */
            mrb[nmax],     /* boundary inertances at r=b */
            rzb[nmax],     /* boundary resistors  at z=b */
            mzb[nmax],     /* boundary inertances at z=b */
            mr[nmax],      /* radial mass element (function of i only) */
            mz[nmax],      /* axial  mass element           (ditto) */
            c[nmax];       /* compliance element            (ditto) */

/* RAISED COSINE FUNCTION OF PERIOD 13/m and unit area: */

   float rc(float t) {
      return (float)((1.0 - cos(pi*m*t/6.5))/(13.0/m));
   }

main(int argc, char *argv[])

{

/***********************************
   PROCESS COMMAND LINE ARGUMENTS:
***********************************/

/* CHECK NO. ARGUMENTS AND READ m, n, mode, outfile: */

   if (argc != 5) {
      fprintf(stderr, "Usage:  %s m n a|t|u outfile\n", argv[0]);
```

```
      exit(1);
   }
   if (sscanf(argv[1], "%d", &m) != 1) {
      fprintf(stderr, "Problem -- possibly non-numeric m.\n");
      exit(1);
   }
   if (sscanf(argv[2], "%d", &n) != 1) {
      fprintf(stderr, "Problem -- possibly non-numeric n.\n");
      exit(1);
   }
   if (0 >= m || m >= n || n > nmax) {
      fprintf(stderr, "You must have 0 < m < n <= %d.\n", nmax);
      exit(1);
   }
   strcpy(mode, argv[3]);
   if (!(*mode == 'a' || *mode == 't' || *mode == 'u')) {
      fprintf(stderr, "Third argument must be `a' or `t' or `u'.\n");
      exit(1);
   }
   strcpy(outfile, argv[4]);

/* IF WE GET THIS FAR, ARGUMENT LIST IS CORRECT!  ECHO ARGUMENTS: */

   fprintf(stderr,
      "\n\tm = %d ; n = %d ; mode = %s ; outfile = %s ; nmax = %d.\n",
      m, n, mode, outfile, nmax);
   if (*mode != 't')
      fprintf(stderr, "\tFrequency range: ka = %6.4f to %.1f\n", hmin, hmax);
   fprintf(stderr, "\n");

/***********************************
   EQUIVALENT CIRCUIT COMPONENTS:
***********************************/

/* Area fractions: */
   for (i=1; i<=m; i++)
      a[i] = (2*i - 1.F) / (m*m);
/* Front inertance element (parallel combination of axial inertances
   adjacent to disk): */
   mf = 1.F / (2*m);
/* Curved-boundary elements: */
   for (k=1; k<=n; k++) {
      rrb[k] = m*m * (float)sqrt(n*n + (k-0.5F)*(k-0.5F)) / (2.F*n*n);
      mrb[k] = m * (n*n + (k-0.5F)*(k-0.5F)) / (2.F*n*n);
   }
for (i=1; i<=n; i++) {
   /* Flat-boundary elements: */
      rzb[i] = 0.5F*m*m * (float)sqrt(1.F/(n*n) + 1/((i-0.5F)*(i-0.5F)));
      mzb[i] = 0.5F*m * (n/(i-0.5F) + (i-0.5F)/n);
   /* Axial inertance elements: */
      mz[i] = m / (2*i - 1.F);
   /* Compliances: */
      c[i] = (2*i - 1.F) / (m*m*m);
}
/* Radial inertance elements: */
   for (i=1; i<n; i++)
      mr[i] = m / (2.F * i);
   mr[n] = m / (4*n - 1.F); /* truncated at curved boundary */
```

```
/*************************************************
   WRITE SPICE3 CIRCUIT DEFINITION TO FILE 'cct':
*************************************************/

   cct = fopen("cct", "w");

/* HEADER: */
   if (*mode == 'u')
      fprintf(cct, "CIRCULAR RIGID PISTON (UNBAFFLED):\n\n");
   else
      fprintf(cct, "CIRCULAR RIGID PISTON IN INFINITE PLANAR BAFFLE:\n\n");

/* COMMENTS: */
   fprintf(cct,
      "* m = %d ; n = %d ; mode = %s ; outfile = %s ; nmax = %d.\n",
      m, n, mode, outfile, nmax);
   if (*mode != 't')
      fprintf(cct, "* Frequency range: ka = %6.4f to %.1f\n\n", hmin, hmax);
   fprintf(cct, "* FDM component values:\n");
   fprintf(cct, "  * m = %d\n", m);
   fprintf(cct, "  * n = %d\n", n);
   fprintf(cct, "  * a[ 1] = %.5f\n", a[1]);
   fprintf(cct, "  * a[%2d] = %.5f\n", m, a[m]);
   fprintf(cct, "  * mf = %.6f\n", mf);
   fprintf(cct, "  * rrb[ 1] = %.5f\n", rrb[1]);
   fprintf(cct, "  * rrb[%2d] = %.5f\n", n, rrb[n]);
   fprintf(cct, "  * mrb[ 1] = %.5f\n", mrb[1]);
   fprintf(cct, "  * mrb[%2d] = %.5f\n", n, mrb[n]);
   fprintf(cct, "  * rzb[ 1] = %.5f\n", rzb[1]);
   fprintf(cct, "  * rzb[%2d] = %.5f\n", n, rzb[n]);
   fprintf(cct, "  * mzb[ 1] = %.5f\n", mzb[1]);
   fprintf(cct, "  * mzb[%2d] = %.5f\n", n, mzb[n]);
   fprintf(cct, "  * mr[ 1] = %.5f\n", mr[1]);
   fprintf(cct, "  * mr[%2d] = %.5f\n", n-1, mr[n-1]);
   fprintf(cct, "  * mr[%2d] = %.5f\n", n, mr[n]);
   fprintf(cct, "  * mz[ 1] = %.5f\n", mz[1]);
   fprintf(cct, "  * mz[%2d] = %.5f\n", n, mz[n]);
   fprintf(cct, "  * c[ 1] = %.7f\n", c[1]);
   fprintf(cct, "  * c[%2d] = %.7f\n", n, c[n]);
   fprintf(cct, "\n");

/* IF UNBAFFLED, DEFINE AXIAL MASS SUBCIRCUITS ADJACENT TO PLANE OF DISK: */
   if (*mode == 'u') {
      fprintf(cct, "* AXIAL INERTANCE SUBCIRCUITS");
      fprintf(cct, " ADJACENT TO PLANE OF DISK:\n\n");
      for (i=m+1; i<=n; i++) {
         fprintf(cct, ".subckt bplane%02d 1 3\n", i);
         fprintf(cct, "lzho%02d 1 2  %e\n", i, 0.5F*mz[i]);
         fprintf(cct, "rzs%02d  2 3  %e\n", i, 1e-6*mz[i]);
         fprintf(cct, ".ends bplane%02d\n", i);
      }
      fprintf(cct, "\n");
   }

/* DEFINE CURVED-BOUNDARY ELEMENT SUBCIRCUITS: */
   fprintf(cct, "* CURVED-BOUNDARY ELEMENT SUBCIRCUITS:\n\n");
   if (*mode == 't') /* if transient */
```

```
      for (k=1; k<=n; k++) {
         fprintf(cct, ".subckt bcurv%02d 1 3\n", k);
         fprintf(cct, "lr%02d  1 2  %e\n", k, mr[n]);
         fprintf(cct, "rrb%02d 2 3  %e\n", k, rrb[k]);
         fprintf(cct, "lrb%02d 2 3  %e\n", k, mrb[k]);
         fprintf(cct, ".ends bcurv%02d\n", k);
      }
   else /* if AC */
      for (k=1; k<=n; k++) {
         fprintf(cct, ".subckt bcurv%02d 1 4\n", k);
         fprintf(cct, "lr%02d  1 2  %e\n", k, mr[n]);
         fprintf(cct, "rrs%02d 2 3  %e\n", k, 1e-6*mr[n]);
         fprintf(cct, "rrb%02d 3 4  %e\n", k, rrb[k]);
         fprintf(cct, "lrb%02d 3 4  %e\n", k, mrb[k]);
         fprintf(cct, ".ends bcurv%02d\n", k);
      }
   fprintf(cct, "\n");

/* DEFINE FLAT-BOUNDARY ELEMENT SUBCIRCUITS: */
   fprintf(cct, "* FLAT-BOUNDARY ELEMENT SUBCIRCUITS:\n\n");
   for (i=1; i<=n; i++) {
      fprintf(cct, ".subckt bflat%02d 1 3\n", i);
      fprintf(cct, "lzh%02d 1 2  %e\n", i, 0.5F*mz[i]);
      fprintf(cct, "rzb%02d 2 3  %e\n", i, rzb[i]);
      fprintf(cct, "lzb%02d 2 3  %e\n", i, mzb[i]);
      fprintf(cct, ".ends bflat%02d\n", i);
   }
   fprintf(cct, "\n");

/* IF AC ANALYSIS REQUIRED, DEFINE RADIAL INERTANCE ELEMENT SUBCIRCUITS: */
   if (*mode != 't') {
      fprintf(cct, "* RADIAL INERTANCE ELEMENT SUBCIRCUITS:\n\n");
      for (i=1; i<=n; i++) {
         fprintf(cct, ".subckt mr%02d 1 3\n", i);
         fprintf(cct, "lr%02d  1 2 %e\n", i, mr[i]);
         fprintf(cct, "rrs%02d 2 3 %e\n", i, 1e-6*mr[i]);
         fprintf(cct, ".ends mr%02d\n", i);
      }
      fprintf(cct, "\n");
   }

/* SOURCE: */
   fprintf(cct, "* SOURCE:\n\n");
   if (*mode == 't') {
      fprintf(cct, "Vtran %2d 0 dc 0 pwl ( 0 0\n", m+1);
      for (i=1; i<=25; i++)
         fprintf(cct, "+ %.6f %.7f\n", (float)i/(2*m), rc((double)i/(2*m)));
      fprintf(cct, "+ %.6f 0 )\n", 13.F/m);
   } else
      fprintf(cct, "Iac 0 %2d dc 0 ac 1\n", m+1);
   fprintf(cct, "\n");

/* SPLIT FLUX AND AVERAGE BACK PRESSURES: */
   fprintf(cct, "* SPLIT FLUX AND AVERAGE BACK PRESSURES:\n\n");
   for (i=1; i<=m; i++)
      fprintf(cct, "F%02d  0 %2d E01  %e\n", i, m+1+i, a[i]);
   for (i=1; i<=m; i++)
      fprintf(cct, "E%02d %2d %2d %2d 0  %e\n", i, i+1, i, m+1+i, a[i]);
```

```
   fprintf(cct, "\n");

/* WRITE FRONT INERTANCE: */
   fprintf(cct, "* FRONT INERTANCE:\n\n");
   fprintf(cct, "lf 1 0  %e\n", mf);
   fprintf(cct, "\n");

/* IF DISK IS UNBAFFLED, WRITE AXIAL MASSES ADJACENT TO PLANE OF DISK: */
   if (*mode == 'u') {
      fprintf(cct, "* AXIAL INERTANCE ELEMENTS");
      fprintf(cct, " ADJACENT TO PLANE OF DISK:\n\n");
      for (i=m+1; i<=n; i++) {
         s = m + 1 + i;
         fprintf(cct, "xbplane%02d %2d 0  bplane%02d\n", i, s, i);
      }
      fprintf(cct, "\n");
   }

/* WRITE CURVED-BOUNDARY ELEMENTS: */
   fprintf(cct, "* CURVED-BOUNDARY ELEMENTS:\n\n");
   for (k=1; k<=n; k++) {
      s = m + 1 + k*n;
      fprintf(cct, "xbcurv%02d %4d 0  bcurv%02d\n", k, s, k);
   }
   fprintf(cct, "\n");

/* WRITE FLAT-BOUNDARY ELEMENTS: */
   fprintf(cct, "* FLAT-BOUNDARY ELEMENTS:\n\n");
   for (i=1; i<=n; i++) {
      s = m + 1 + (n-1)*n + i;
      fprintf(cct, "xbflat%02d %4d 0  bflat%02d\n", i, s, i);
   }
   fprintf(cct, "\n");

/* WRITE RADIAL INERTANCE ELEMENTS: */
   fprintf(cct, "* RADIAL INERTANCE ELEMENTS:\n\n");
   for (k=1; k<=n; k++)
      for (i=1; i<n; i++) /* only n-1 elements in radial direction */ {
         s = m + 1 + (k-1)*n + i;
         if (*mode == 't')
            fprintf(cct, "lr%02d%02d %4d %4d  %e\n", i, k, s, s+1, mr[i]);
         else
            fprintf(cct, "xmr%02d%02d %4d %4d  mr%02d\n", i, k, s, s+1, i);
      }
   fprintf(cct, "\n");

/* WRITE AXIAL INERTANCE ELEMENTS: */
   fprintf(cct, "* AXIAL INERTANCE ELEMENTS:\n\n");
   for (k=1; k<n; k++) /* only n-1 elements in axial direction */
      for (i=1; i<=n; i++) {
         s = m + 1 + (k-1)*n + i;
         fprintf(cct, "lz%02d%02d %4d %4d  %e\n", i, k, s, s+n, mz[i]);
      }
   fprintf(cct, "\n");

/* WRITE COMPLIANCE ELEMENTS: */
   fprintf(cct, "* COMPLIANCE ELEMENTS:\n\n");
   for (k=1; k<=n; k++)
```

```
      for (i=1; i<=n; i++) {
         s = m + 1 + (k-1)*n + i;
         fprintf(cct, "c%02d%02d %4d 0  %e\n", i, k, s, c[i]);
      }
   fprintf(cct, "\n");

fprintf(cct, ".end\n");

fclose(cct);

/*******************************************
   WRITE SPICE3 COMMAND SCRIPT TO FILE 'go':
*******************************************/

go = fopen("go", "w");

fprintf(go, "ANALYSIS AND PLOTTING INSTRUCTIONS:\n");
fprintf(go, ".control\n");
if (*mode == 't')
   fprintf(go, "tran %.7f %.3f  uic\n", 1.F/(10*m), 2.5F*n/m);
else
   fprintf(go, "ac dec 10 %6.4f %d\n", hmin, m);
fprintf(go, "rusage space time >%s.rus\n", outfile);
fprintf(go, "set plottype = point\n");
fprintf(go, "set hcopydevtype = postscript\n");
fprintf(go, "set numdgt = 5\n");
fprintf(go, "set width = 76\n");
fprintf(go, "set nobreak\n");
fprintf(go, "set noaskquit\n");
if (*mode == 't') /* Output pressure at i=n/2; k=(n/5)+1 and (n/2)+1: */ {
   s  =  m + 1 + (n/5)*n + n/2;  /* truncated integer division */
   s2 =  m + 1 + (n/2)*n + n/2;  /* ditto */
   fprintf(go, "hardcopy %s.ps v(%d)/10 v(%d) v(%d) xlabel ct/a\n",
           outfile, m+1, s, s2);
   fprintf(go, "print v(%d)/10 v(%d) v(%d) >%s.dat\n", m+1, s, s2, outfile);
} else /* Output radiation resistance and inertance: */ {
   fprintf(go, "hardcopy %s.ps 1/real(1/v(%d)) %e/real(v(1)/v(%d))\n",
           outfile, m+1, mf, m+1);
      fprintf(go, "+ xl %6.4f %.1f xlog xlabel ka\n", hmin, hmax);
   fprintf(go, "print 1/real(1/v(%d)) %e/real(v(1)/v(%d)) >%s.dat\n",
           m+1, mf, m+1, outfile);
}
fprintf(go, "quit\n");
fprintf(go, ".endc\n");

fclose(go);

}
```

B.13 Sample circuit file `d35u.cir` (for circular piston)

The circuit files produced by the program `disk.c` were initially called "`cct`", but were manually renamed for permanent storage. The name `d35u.cir` is mnemonic, indicating that the file was produced by `disk.c` with $m = 3$ and $n = 5$ for the unbaffled case. The unbaffled version is chosen for illustration because it yields a "fully-optioned" equivalent circuit—all truncated axial mass elements are included, and subcircuits must be defined in order to remove zero-resistance loops.

The letter "`b`" in a subcircuit name stands for "boundary". While the definition of a subcircuit can be named arbitrarily, SPICE requires each instance of a subcircuit to have a name beginning with "x" or "X". Mass elements must have names beginning with "l" or "L" in SPICE, although the text of this thesis prefers "m" or "M". The names of components include row and/or column numbers to ensure uniqueness.

The circuit file is listed below.

```
CIRCULAR RIGID PISTON (UNBAFFLED):

* m = 3 ; n = 5 ; mode = u ; outfile = d35u ; nmax = 90.
* Frequency range: ka = 0.0100 to 10.0

* FDM component values:
  * m = 3
  * n = 5
  * a[ 1] = 0.11111
  * a[ 3] = 0.55556
  * mf = 0.166667
  * rrb[ 1] = 0.90449
  * rrb[ 5] = 1.21083
  * mrb[ 1] = 1.51500
  * mrb[ 5] = 2.71500
  * rzb[ 1] = 9.04489
  * rzb[ 5] = 1.34536
  * mzb[ 1] = 15.15000
  * mzb[ 5] = 3.01667
  * mr[ 1] = 1.50000
  * mr[ 4] = 0.37500
  * mr[ 5] = 0.15789
  * mz[ 1] = 3.00000
  * mz[ 5] = 0.33333
  * c[ 1] = 0.0370370
  * c[ 5] = 0.3333333

* AXIAL INERTANCE SUBCIRCUITS ADJACENT TO PLANE OF DISK:

.subckt bplane04 1 3
lzho04 1 2  2.142857e-01
rzs04  2 3  4.285714e-07
.ends bplane04
.subckt bplane05 1 3
lzho05 1 2  1.666667e-01
rzs05  2 3  3.333333e-07
.ends bplane05
```

```
* CURVED-BOUNDARY ELEMENT SUBCIRCUITS:

.subckt bcurv01 1 4
lr01  1 2  1.578947e-01
rrs01 2 3  1.578947e-07
rrb01 3 4  9.044887e-01
lrb01 3 4  1.515000e+00
.ends bcurv01
.subckt bcurv02 1 4
lr02  1 2  1.578947e-01
rrs02 2 3  1.578947e-07
rrb02 3 4  9.396276e-01
lrb02 3 4  1.635000e+00
.ends bcurv02
.subckt bcurv03 1 4
lr03  1 2  1.578947e-01
rrs03 2 3  1.578947e-07
rrb03 3 4  1.006231e+00
lrb03 3 4  1.875000e+00
.ends bcurv03
.subckt bcurv04 1 4
lr04  1 2  1.578947e-01
rrs04 2 3  1.578947e-07
rrb04 3 4  1.098590e+00
lrb04 3 4  2.235000e+00
.ends bcurv04
.subckt bcurv05 1 4
lr05  1 2  1.578947e-01
rrs05 2 3  1.578947e-07
rrb05 3 4  1.210826e+00
lrb05 3 4  2.715000e+00
.ends bcurv05

* FLAT-BOUNDARY ELEMENT SUBCIRCUITS:

.subckt bflat01 1 3
lzh01 1 2  1.500000e+00
rzb01 2 3  9.044888e+00
lzb01 2 3  1.515000e+01
.ends bflat01
.subckt bflat02 1 3
lzh02 1 2  5.000000e-01
rzb02 2 3  3.132092e+00
lzb02 2 3  5.450000e+00
.ends bflat02
.subckt bflat03 1 3
lzh03 1 2  3.000000e-01
rzb03 2 3  2.012461e+00
lzb03 2 3  3.750000e+00
.ends bflat03
.subckt bflat04 1 3
lzh04 1 2  2.142857e-01
rzb04 2 3  1.569414e+00
lzb04 2 3  3.192857e+00
.ends bflat04
.subckt bflat05 1 3
lzh05 1 2  1.666667e-01
```

```
rzb05 2 3  1.345362e+00
lzb05 2 3  3.016667e+00
.ends bflat05

* RADIAL INERTANCE ELEMENT SUBCIRCUITS:

.subckt mr01 1 3
lr01  1 2 1.500000e+00
rrs01 2 3 1.500000e-06
.ends mr01
.subckt mr02 1 3
lr02  1 2 7.500000e-01
rrs02 2 3 7.500000e-07
.ends mr02
.subckt mr03 1 3
lr03  1 2 5.000000e-01
rrs03 2 3 5.000000e-07
.ends mr03
.subckt mr04 1 3
lr04  1 2 3.750000e-01
rrs04 2 3 3.750000e-07
.ends mr04
.subckt mr05 1 3
lr05  1 2 1.578947e-01
rrs05 2 3 1.578947e-07
.ends mr05

* SOURCE:

Iac 0  4 dc 0 ac 1

* SPLIT FLUX AND AVERAGE BACK PRESSURES:

F01  0  5 E01  1.111111e-01
F02  0  6 E01  3.333333e-01
F03  0  7 E01  5.555556e-01
E01  2  1  5 0  1.111111e-01
E02  3  2  6 0  3.333333e-01
E03  4  3  7 0  5.555556e-01

* FRONT INERTANCE:

lf 1 0  1.666667e-01

* AXIAL INERTANCE ELEMENTS ADJACENT TO PLANE OF DISK:

xbplane04  8 0  bplane04
xbplane05  9 0  bplane05

* CURVED-BOUNDARY ELEMENTS:

xbcurv01    9 0  bcurv01
xbcurv02   14 0  bcurv02
xbcurv03   19 0  bcurv03
xbcurv04   24 0  bcurv04
xbcurv05   29 0  bcurv05

* FLAT-BOUNDARY ELEMENTS:
```

```
xbflat01   25 0  bflat01
xbflat02   26 0  bflat02
xbflat03   27 0  bflat03
xbflat04   28 0  bflat04
xbflat05   29 0  bflat05

* RADIAL INERTANCE ELEMENTS:

xmr0101    5    6  mr01
xmr0201    6    7  mr02
xmr0301    7    8  mr03
xmr0401    8    9  mr04
xmr0102   10   11  mr01
xmr0202   11   12  mr02
xmr0302   12   13  mr03
xmr0402   13   14  mr04
xmr0103   15   16  mr01
xmr0203   16   17  mr02
xmr0303   17   18  mr03
xmr0403   18   19  mr04
xmr0104   20   21  mr01
xmr0204   21   22  mr02
xmr0304   22   23  mr03
xmr0404   23   24  mr04
xmr0105   25   26  mr01
xmr0205   26   27  mr02
xmr0305   27   28  mr03
xmr0405   28   29  mr04

* AXIAL INERTANCE ELEMENTS:

lz0101     5   10  3.000000e+00
lz0201     6   11  1.000000e+00
lz0301     7   12  6.000000e-01
lz0401     8   13  4.285714e-01
lz0501     9   14  3.333333e-01
lz0102    10   15  3.000000e+00
lz0202    11   16  1.000000e+00
lz0302    12   17  6.000000e-01
lz0402    13   18  4.285714e-01
lz0502    14   19  3.333333e-01
lz0103    15   20  3.000000e+00
lz0203    16   21  1.000000e+00
lz0303    17   22  6.000000e-01
lz0403    18   23  4.285714e-01
lz0503    19   24  3.333333e-01
lz0104    20   25  3.000000e+00
lz0204    21   26  1.000000e+00
lz0304    22   27  6.000000e-01
lz0404    23   28  4.285714e-01
lz0504    24   29  3.333333e-01

* COMPLIANCE ELEMENTS:

c0101     5 0  3.703704e-02
c0201     6 0  1.111111e-01
c0301     7 0  1.851852e-01
```

```
c0401    8 0  2.592593e-01
c0501    9 0  3.333333e-01
c0102   10 0  3.703704e-02
c0202   11 0  1.111111e-01
c0302   12 0  1.851852e-01
c0402   13 0  2.592593e-01
c0502   14 0  3.333333e-01
c0103   15 0  3.703704e-02
c0203   16 0  1.111111e-01
c0303   17 0  1.851852e-01
c0403   18 0  2.592593e-01
c0503   19 0  3.333333e-01
c0104   20 0  3.703704e-02
c0204   21 0  1.111111e-01
c0304   22 0  1.851852e-01
c0404   23 0  2.592593e-01
c0504   24 0  3.333333e-01
c0105   25 0  3.703704e-02
c0205   26 0  1.111111e-01
c0305   27 0  1.851852e-01
c0405   28 0  2.592593e-01
c0505   29 0  3.333333e-01

.end
```

B.14 Table-formatting programs

Programs `taba.c` and `tabu.c` produced Tables 11.1 and 11.2, respectively. The programs are quite trivial and are listed only for the sake of completeness. Most of the code (73 lines out of 83, including comments) is common to both. Each program combines five SPICE output files (produced by the "`print`" command) into a single formatted file. The mnemonic names of the SPICE files appear in the opening comments; each SPICE file corresponds to one pair of values of m and n and is named accordingly.

After inspecting the results of the first successful run, the author decided that sufficient data would be obtained by taking every second line of the SPICE files, i.e. every second frequency in the AC analyses. This decision is seen in the function "`extract`", which appears in both programs.

The listings follow.

```
/*****************************************************************************

   PROGRAM 'taba.c' (GAVIN R. PUTLAND)

   Collect files d618a.dat, d721a.dat, d824a.dat, d621a.dat and d828a.dat
   into a single presentable plain-text table, written to standard output.

*****************************************************************************/

#include <stdio.h>
#include <math.h>
#include <string.h>

#define pi 3.141592654F

/* GLOBAL VARIABLES: */

   FILE  *file;

   char  line[99], filename[32];

   int   i;

   float f[13],                                        /* frequency */
         r6[13], r7[13], r8[13], r62[13], r82[13],  /* rad. resistance */
         m6[13], m7[13], m8[13], m62[13], m82[13];  /* rad. inertance */

/* FUNCTION TO EXTRACT DATA FROM ONE FILE: */

   void extract(char *filename, float *r, float *m) {

      file = fopen(filename, "r");
      /* SKIP FIRST FIVE LINES (PREAMBLE): */
         for (i=0; i<5; i++)
            fgets(line, 99, file);
      /* READ ALTERNATE LINES; EXTRACT r, m: */
         for (i=0; i<13; i++) {
            fgets(line, 99, file);
            sscanf(line, "%*d %*e, %*e %e %e", r+i, m+i);
            fgets(line, 99, file);
```

```
         }
      fclose(file);

   }

main()

{

/* HEAD TABLE: */

   printf("\n");
   printf("          m,n:    %7s %7s %7s   %7s  %7s\n\n",
          "6,18  ", "7,21  ", "8,24  ", "6,21  ", "8,28  ");

/* GET NUMBERS: */

   for (i=0; i<13; i++)
      f[i] = 0.01 * pow(10.0, 0.2*i);

   extract("d618a.dat", r6, m6);
   extract("d721a.dat", r7, m7);
   extract("d824a.dat", r8, m8);
   extract("d621a.dat", r62, m62);
   extract("d828a.dat", r82, m82);

/* PRINT RADIATION RESISTANCE: */

   printf("  f       h        Resistance (LF limit = 1.4410):\n\n");
   for (i=0; i<13; i++)
      printf("%6.4f %7.4f    %7.4f %7.4f %7.4f   %7.4f  %7.4f\n",
             f[i], 2*pi*f[i], r6[i], r7[i], r8[i], r62[i], r82[i]);
   printf("\n");

/* PRINT RADIATION INERTANCE: */

   printf("  f       h        Inertance (LF limit = 0.8488):\n\n");
   for (i=0; i<13; i++)
      printf("%6.4f %7.4f    %7.4f %7.4f %7.4f   %7.4f  %7.4f\n",
             f[i], 2*pi*f[i], m6[i], m7[i], m8[i], m62[i], m82[i]);
   printf("\n");

}
```

```
/*****************************************************************************

   PROGRAM 'tabu.c' (GAVIN R. PUTLAND)

   Collect files d618u.dat, d721u.dat, d824u.dat, d621u.dat and d828u.dat
   into a single presentable plain-text table, written to standard output.

*****************************************************************************/

#include <stdio.h>
#include <math.h>
#include <string.h>

#define pi 3.141592654F

/* GLOBAL VARIABLES: */

   FILE  *file;

   char  line[99], filename[32];

   int   i;

   float f[13],                                        /* frequency */
         r6[13], r7[13], r8[13], r62[13], r82[13],  /* rad. resistance */
         m6[13], m7[13], m8[13], m62[13], m82[13];  /* rad. inertance */

/* FUNCTION TO EXTRACT DATA FROM ONE FILE: */

   void extract(char *filename, float *r, float *m) {

      file = fopen(filename, "r");
      /* SKIP FIRST FIVE LINES (PREAMBLE): */
         for (i=0; i<5; i++)
            fgets(line, 99, file);
      /* READ ALTERNATE LINES; EXTRACT r, m: */
         for (i=0; i<13; i++) {
            fgets(line, 99, file);
            sscanf(line, "%*d %*e, %*e %e %e", r+i, m+i);
            fgets(line, 99, file);
         }
      fclose(file);

   }

main()

{

/* HEAD TABLE: */

   printf("\n");
   printf("          m,n:    %7s %7s %7s   %7s  %7s\n\n",
          "6,18  ", "7,21  ", "8,24  ", "6,21  ", "8,28  ");

/* GET NUMBERS: */

   for (i=0; i<13; i++)
```

```
      f[i] = 0.01 * pow(10.0, 0.2*i);

   extract("d618u.dat", r6, m6);
   extract("d721u.dat", r7, m7);
   extract("d824u.dat", r8, m8);
   extract("d621u.dat", r62, m62);
   extract("d828u.dat", r82, m82);

/* PRINT RADIATION RESISTANCE: */

   printf("  f       h        Resistance:\n\n");
   for (i=0; i<13; i++)
      printf("%6.4f %7.4f    %7.4f %7.4f %7.4f   %7.4f  %7.4f\n",
             f[i], 2*pi*f[i], r6[i], r7[i], r8[i], r62[i], r82[i]);
   printf("\n");

/* PRINT RADIATION INERTANCE: */

   printf("  f       h        Inertance (LF limit approx. 0.425):\n\n");
   for (i=0; i<13; i++)
      printf("%6.4f %7.4f    %7.3f %7.3f %7.3f   %7.3f  %7.3f\n",
             f[i], 2*pi*f[i], m6[i], m7[i], m8[i], m62[i], m82[i]);
   printf("\n");

}
```

B.15 Transient response plotter `tr2tex.c`

The procedure for drawing Fig. 11.2 was as follows. First, program `disk.c` was run with $m = 4$, $n = 32$ and `mode = "t"`, to produce a circuit definition file and command script for SPICE. Running SPICE then produced a text file whose columns indicated the transient responses at the three points of interest. Finally, program `tr2tex.c` was run, converting the SPICE output file to a set of LaTeX `picture` commands.

Program `tr2tex.c` is listed below. It makes no pretensions of generality. Only the last part of the program processes the SPICE file and plots the points. The rest of it is concerned with the `picture` objects that form the axes, labels, insets, reflection marks, etc.; the coordinates of these objects were all calculated manually.

```
/*************************************************************************

   PROGRAM 'tr2tex.c' (GAVIN R. PUTLAND)
   Convert a triple transient response in SPICE3 'print col' format
   to a graph using LaTeX 'picture' commands.

   USAGE (assuming executable file is called 'tr2tex'):

      tr2tex in out

   where 'in' is the name of the SPICE file and 'out' is the name of the
   output file.  If out exists, tr2tex absolutely refuses to overwrite it.
   The out file begins with

      \setlength{\unitlength}{0.0033333in}
      \begin{picture}(1600,2300)(-60,-250)

   and ends with

      \end{picture}

   The present version draws axes and grids assuming that the time column
   extends extends from 0 to 20 units and that the ordinates are in the
   ranges 0 to 65, -5 to 85, and -10 to 70.  The first ordinate is assumed
   to be tabulated at one tenth of the scale of the other two, and is
   graphed at one twentieth.

*************************************************************************/

#include <stdio.h>
#include <math.h>
#include <string.h>

main(int argc, char *argv[])

{

/* FILE NAMES AND POINTERS: */

   char  inname[32], outname[32];
   FILE  *in, *out;

/* SCRATCH VARIABLES */
```

```
   char  line[99];
   int   i;
   float t, po, pa, pb;

/* CHECK FOR ILLEGAL USAGE: */

   if (argc != 3) {
      fprintf(stderr, "Usage:  %s in out\n", argv[0]);
      exit(1);
   }

/* PROCESS COMMAND-LINE ARGUMENTS AND ATTEMPT TO OPEN FILES: */

   strcpy(inname, argv[1]);
   if (!(in = fopen(inname, "r"))) {
      fprintf(stderr, "Can't find/open file `%s\'.\n", inname);
      exit(1);
   }
   strcpy(outname, argv[2]);
   if (fopen(outname, "r")) /* if file `outname' already exists */ {
      fprintf(stderr, "File `%s\' exists.  Rename/remove it.\n", outname);
      exit(1);
   }
   out = fopen(outname, "w");

/* OPEN picture ENVIRONMENT: */

   fprintf(out, "\\setlength{\\unitlength}{0.0033333in}\n");
   fprintf(out, "\\begin{picture}(1600,2300)(-60,-250)\n");

/* AXES AND GRID, LABELS, SCALES: */

   fprintf(out, "%% AXES AND GRID:\n");
   fprintf(out, "\\thinlines\n");
   fprintf(out, "\\put(1500,-100){\\line(0,1){2150}}\n");
   fprintf(out, "\\multiput(  0,-100)(150,0){5}{\\line(0,1){2150}}\n");
   fprintf(out, "\\put( 750,-100){\\line(0,1){ 950}}\n");
   fprintf(out, "\\multiput(900,-100)(150,0){4}{\\line(0,1){ 300}}\n");
   fprintf(out, "\\multiput(900, 600)(150,0){4}{\\line(0,1){ 250}}\n");
   fprintf(out, "\\multiput(750,1650)(150,0){5}{\\line(0,1){ 400}}\n");
   fprintf(out, "\\put(0,   0){\\line(1,0){1500}}\n");
   fprintf(out, "\\put(0, 800){\\line(1,0){1500}}\n");
   fprintf(out, "\\put(0,1700){\\line(1,0){1500}}\n");
   fprintf(out, "%% SCALES:\n");
   fprintf(out, "\\put(-40,   5){\\makebox(0,0)[l]{0}}\n");
   fprintf(out, "\\put(-40, 805){\\makebox(0,0)[l]{0}}\n");
   fprintf(out, "\\put(-40,1705){\\makebox(0,0)[l]{0}}\n");
   fprintf(out, "\\put(   0,-160){\\makebox(0,0)[b]{0}}\n");
   fprintf(out, "\\put( 150,-160){\\makebox(0,0)[b]{2}}\n");
   fprintf(out, "\\put( 300,-160){\\makebox(0,0)[b]{4}}\n");
   fprintf(out, "\\put( 450,-160){\\makebox(0,0)[b]{6}}\n");
   fprintf(out, "\\put( 600,-160){\\makebox(0,0)[b]{8}}\n");
   fprintf(out, "\\put( 750,-160){\\makebox(0,0)[b]{10}}\n");
   fprintf(out, "\\put( 900,-160){\\makebox(0,0)[b]{12}}\n");
   fprintf(out, "\\put(1050,-160){\\makebox(0,0)[b]{14}}\n");
   fprintf(out, "\\put(1200,-160){\\makebox(0,0)[b]{16}}\n");
   fprintf(out, "\\put(1350,-160){\\makebox(0,0)[b]{18}}\n");
   fprintf(out, "\\put(1500,-160){\\makebox(0,0)[b]{20}}\n");
```

```
fprintf(out, "%% LABELS:\n");
fprintf(out, "\\put(750,-230){\\makebox(0,0)[b]{Normalized time");
   fprintf(out, " $\\,\\hat{t}=ct/a$}}\n");
fprintf(out, "\\small\n");
fprintf(out, "\\put(177,1950){Mean pressure over source");
   fprintf(out, " $\\times\\,\\frac{1}{20}$}\n");
fprintf(out, "\\put( 63,1550){Pressure at $A$}\n");
fprintf(out, "\\put(170, 600){Pressure at $B$}\n");
fprintf(out, "%% REFLECTION MARKS AND LABELS:\n");
fprintf(out, "\\thicklines\n");
fprintf(out, "\\put( 437,840){\\line(0,1){60}}\n");
fprintf(out, "\\put( 546, 40){\\line(0,1){60}}\n");
fprintf(out, "\\put(1039,700){\\line(0,1){60}}\n");
fprintf(out, "\\put(1238,700){\\line(0,1){60}}\n");
fprintf(out, "\\put(1475,700){\\line(0,1){60}}\n");
fprintf(out, "\\put(1082, 40){\\line(0,1){60}}\n");
fprintf(out, "\\put(1059, 40){\\line(0,1){60}}\n");
fprintf(out, "\\put(1395, 40){\\line(0,1){60}}\n");
fprintf(out, "\\put(1025,660){$r$}\n");
fprintf(out, "\\put(1228,660){$z$}\n");
fprintf(out, "\\put(1415,660){$z,B$}\n");
fprintf(out, "\\put(1080,110){$r$}\n");
fprintf(out, "\\put(1055,110){$z$}\n");
fprintf(out, "\\put(1362,110){$r,z$}\n");
fprintf(out, "%% DRAW LOWER INSET:\n");
fprintf(out, "\\put( 810, 520){Residual reflections (peak)}\n");
fprintf(out, "\\put( 810, 470){predicted by geometrical optics:}\n");
fprintf(out, "\\put( 870, 410){$\\,r\\;$: from boundary $r=b$\\,;}\n");
fprintf(out, "\\put( 870, 360){$\\,z\\;$: from boundary $z=b$\\,;}\n");
fprintf(out, "\\put( 870, 310){$B$\\,: from baffle.}\n");
fprintf(out, "\\put( 810, 250){Unlabeled bars show direct wave.}\n");
fprintf(out, "%% DRAW UPPER INSET:\n");
fprintf(out, "\\put( 790, 950){\\vector(1,0){550}}\n");
fprintf(out, "\\put( 790, 950){\\vector(0,1){550}}\n");
fprintf(out, "\\put( 790, 953){\\line(1,0){60}}\n");
fprintf(out, "\\put( 790, 947){\\line(1,0){60}}\n");
fprintf(out, "\\thinlines\n");
fprintf(out, "\\put( 790,1430){\\line(1,0){480}}\n");
fprintf(out, "\\put(1270, 950){\\line(0,1){ 65}}\n");
fprintf(out, "\\put(1270,1080){\\line(0,1){ 85}}\n");
fprintf(out, "\\put(1270,1230){\\line(0,1){200}}\n");
fprintf(out, "\\put( 790, 900){\\makebox(0,0)[b]{0}}\n");
fprintf(out, "\\put( 850, 900){\\makebox(0,0)[b]{$a$}}\n");
fprintf(out, "\\put(1270, 900){\\makebox(0,0)[b]{$b$}}\n");
fprintf(out, "\\put( 770, 955){\\makebox(0,0)[r]{0}}\n");
fprintf(out, "\\put( 770,1435){\\makebox(0,0)[r]{$b$}}\n");
fprintf(out, "\\put(1370, 961){\\makebox(0,0)[t]{$r$}}\n");
fprintf(out, "\\put( 790,1536){\\makebox(0,0)[t]{$z$}}\n");
fprintf(out, "\\put(1022,1047){\\circle*{12}}\n");
fprintf(out, "\\put(1022,1197){\\circle*{12}}\n");
fprintf(out,
   "\\put(1040,1035){$A\\,(15.5\\,\\Delta r,6.5\\,\\Delta z)$}\n");
fprintf(out,
   "\\put(1040,1185){$B\\,(15.5\\,\\Delta r,16.5\\,\\Delta z)$}\n");
fprintf(out, "\\put( 802, 968){\\footnotesize\\sl Source}\n");
fprintf(out, "\\put(1070, 905){\\sl Baffle}\n");
fprintf(out, "\\put( 845,1385){\\sl Anechoic boundaries}\n");
fprintf(out, "\\put( 690,1235){\\sl Axis}\n");
```

```
   fprintf(out, "\\put( 910,1560){$a=4\\,\\Delta r=\\:$source radius}\n");
   fprintf(out, "\\put( 910,1500){$b=32\\,\\Delta r=32\\,\\Delta z$}\n");

/* PROCESS SPICE FILE: */

      fprintf(out, "%% POINTS FROM FILE `%s\':\n", inname);
   /* SKIP FIRST FIVE LINES (PREAMBLE): */
      for (i=0; i<5; i++)
         fgets(line, 99, in);
   /* READ LINES; EXTRACT COORDINATES, PLOT POINTS: */
      while (fgets(line, 99, in)) {
         sscanf(line, "%*d %e %e %e %e", &t, &po, &pa, &pb);
         t  = 75.F * t;
         po =  5000.F * po + 1700.F;
 pa = 10000.F * pa +  800.F;
 pb = 10000.F * pb;
 fprintf(out, "\\put(%5.0f,%5.0f){\\circle*{8}}\n", t, po);
         fprintf(out, "\\put(%5.0f,%5.0f){\\circle*{8}}\t", t, pa);
         fprintf(out, "\\put(%5.0f,%5.0f){\\circle*{8}}\n", t, pb);
      }

/* CLOSE picture ENVIRONMENT AND CLOSE FILES: */

   fprintf(out, "\\end{picture}\n");
   fclose(in);
   fclose(out);

}
```

Bibliography

[1] Altronics Electronic Components Catalogue, 12th Ed. (Perth, 1993), pp. 34–5, cat. nos. C 3065, C 3034.

[2] M. Arai: "Study on Acoustic Filters by an Electric Simulator", *J. Acoustical Soc. of Japan*, vol. 16 (1960), pp. 16–28. In Japanese, with English abstract.

[3] G. L. Augspurger: "Theory, ingenuity, and wishful wizardry in loudspeaker design—A half-century of progress?", *J. Acoustical Soc. of America*, vol. 77, pp. 1303–8 (1985 April). Comments by E. Villchur: vol. 79, pp. 177–9 (1986 January).

[4] S. Ballantine: "On the Propagation of Sound in the General Bessel Horn of Infinite Length", *J. Franklin Inst.*, vol. 203, pp. 85–102 (1927 January). Comments by C. R. Hanna, and reply: vol. 203, pp. 849–53 (1927 June).

[5] D. A. Barlow: "Rigidity of Loudspeaker Diaphragms", *Wireless World*, vol. 64, pp. 564–9 (1958 December).

[6] D. A. Barlow: "The Development of a Sandwich-Construction Loudspeaker System", *J. Audio Engineering Soc.*, vol. 18, pp. 269–81 (1970 June). Reprinted in *Loudspeakers: An Anthology*, 2nd Ed. (New York, Audio Eng. Soc., 1980), pp. 159–71.

[7] D. A. Barlow: "Loudspeaker Coloration", *Wireless World*, vol. 84, no. 1507, pp. 34–7 (1978 March).

[8] D. A. Barlow, G. D. Galletly & J. Mistry: "The Resonances of Loudspeaker Diaphragms", *J. Audio Engineering Soc.*, vol. 29, pp. 699–704 (1981 October). Reprinted in *Loudspeakers Vol. 2: An Anthology* (New York, Audio Eng. Soc., 1984), pp. 251–6.

[9] G. M. Barrow: *Physical Chemistry*, 4th ed. (New York: McGraw-Hill, 1979).

[10] A. H. Benade & E. V. Jansson: "On Plane and Spherical Waves in Horns with Nonuniform Flare: I. Theory of Radiation, Resonance Frequencies, and Mode Conversion", *Acustica*, vol. 31, no. 2, pp. 79–98 (1974 August).

[11] L. L. Beranek: *Acoustics* (New York: McGraw-Hill, 1954).

[12] L. Bianchi: *Lezioni di geometria differenziale* (Pisa: Spoerri, 1894). In Italian. Third edition: vol. 1, 1922; vol. 2, 1923. German translation by M. Lukat: *Vorlesungen über Differentialgeometrie*, 2^{e} Aufl. (Leipzig: Teubner, 1910). Cited by Struik [55].

[13] L. J. S. Bradbury: "The Use of Fibrous Materials in Loudspeaker Enclosures", *J. Audio Engineering Soc.*, vol. 24, pp. 162–70 (1976 April). Reprinted in *Loudspeakers: An Anthology*, 2nd Ed. (New York, Audio Eng. Soc., 1980), pp. 404–12.

[14] L. M. Chase: "The Thermo-Acoustic Properties of Fibrous Material", *IEEE Trans. on Acoustics, Speech, and Signal Processing*, vol. ASSP-22, pp. 297–300 (1974 August).

[15] G. Darboux: *Leçons sur la théorie générale des surfaces* (Paris: Gauthier-Villars). In French. First edition: vol. 1, 1887; vol. 2, 1889; vol. 3, 1894; vol. 4, 1896. Second edition: four volumes, 1914. Cited by Struik [55].

[16] E. Eisner: "Complete Solutions of the 'Webster' Horn Equation", *J. Acoustical Soc. of America*, vol. 41, pp. 1126–46 (1967 April).

[17] J. E. Freehafer: "The Acoustical Impedance of an Infinite Hyperbolic Horn", *J. Acoustical Soc. of America*, vol. 11, pp. 467–476 (1940 April).

[18] E. R. Geddes: "Acoustic Waveguide Theory", *J. Audio Engineering Soc.*, vol. 37, pp. 554–69 (1989 July/Aug.).

[19] E. R. Geddes: "Acoustic Waveguide Theory Revisited", *J. Audio Engineering Soc.*, vol. 41, pp. 452–61 (1993 June).

[20] E. R. Geddes: "Sound Radiation from Acoustic Apertures", *J. Audio Engineering Soc.*, vol. 41, pp. 214–30 (1993 April).

[21] D. E. Gray (ed.): *American Institute of Physics Handbook*, 3rd ed. (New York: McGraw-Hill, 1972).

[22] C. R. Hanna & J. Slepian: "The Function and Design of Horns for Loud Speakers", *Trans. American Institute of Electrical Engineers*, vol. 43, pp. 393–404 (1924 February). Discussion: pp. 405–11. Paper reprinted in *J. Audio Engineering Soc.*, vol. 25, pp. 573–85 (1977 September). Discussion reprinted in *J. Audio Engineering Soc.*, vol. 26, pp. 130–38 (1978 March).

[23] D. J. Henwood: "The Boundary-Element Method and Horn Design", *J. Audio Engineering Soc.*, vol. 41, pp. 485–96 (1993 June).

[24] H. P. Hsu: *Applied Vector Analysis* (San Diego: Harcourt Brace Jovanovich, 1984).

[25] F. V. Hunt: *Electroacoustics—the Analysis of Transduction and its Historical Background* (New York: Acoustical Soc. of America, 1954; reprinted 1982).

[26] E. Kreyszig: *Advanced Engineering Mathematics*, 6th ed. (New York: Wiley, 1988).

[27] K. Kadoya, N. Matsunaga & A. Nagashima: "Viscosity and Thermal Conductivity of Dry Air in the Gaseous Phase", *J. Physical and Chemical Reference Data*, vol. 14, pp. 947–70 (1985).

[28] D. C. Karnopp & R. C. Rosenberg: *System Dynamics: a Unified Approach* (New York: Wiley, 1975).

[29] D. B. Keele, Jr.: "Anechoic Chamber Walls: Should They Be Resistive or Reactive at Low Frequencies?", *J. Audio Engineering Soc.*, vol. 42, pp. 454–66 (1994 June).

[30] W. Marshall Leach, Jr.: "Electroacoustic-Analogous Circuit Models for Filled Enclosures", *J. Audio Engineering Soc.*, vol. 37, pp. 586–92 (1989 July/Aug.).

[31] D. R. Lide (ed.): *CRC Handbook of Chemistry and Physics*, 74th ed. (Boca Raton, Florida: CRC Press, 1993).

[32] S. P. Lipschitz, K. M. Heal & J. Vanderkooy: "An Investigation of Sound Radiation by Loudspeaker Cabinets", 90th Convention of the Audio Engineering Soc., (Paris, February 19–22, 1991), Preprint 3074.

[33] B. N. Locanthi: "Application of Electric Circuit Analogies to Loudspeaker Design Problems", *IRE Trans. on Audio*, vol. PGA-6 (1952 March). Reprinted (with SI units) in *J. Audio Engineering Soc.*, vol. 19, pp. 778–85 (1971 October). SI version reprinted in *Loudspeakers: An Anthology*, 2nd Ed. (New York, Audio Eng. Soc., 1980), pp. 217–24.

[34] A. V. Luikov: *Analytical Heat Diffusion Theory* (New York: Academic Press, 1968).

[35] W. F. Meeker, F. H. Slaymaker & L. L. Merrill: "The Acoustical Impedance of Closed Rectangular Loudspeaker Housings", *J. Acoustical Soc. of America*, vol. 22, pp. 206–10 (1949 March).

[36] P. M. Morse: *Vibration and Sound*, 2nd ed. (New York: McGraw-Hill, 1948; reprinted New York: American Inst. of Physics, 1981).

[37] P. M. Morse & H. Feshbach: *Methods of Theoretical Physics*, pt. 1 (New York: McGraw-Hill, 1953).

[38] P. M. Morse & K. U. Ingard, *Theoretical Acoustics* (New York: McGraw-Hill, 1968).

[39] P. V. O'Neil: *Advanced Engineering Mathematics* (Belmont, CA: Wadsworth, 1983).

[40] A. Papoulis: *Signal Analysis* (New York: McGraw-Hill, 1977).

[41] J. E. Piercy (chairman): *American National Standard Method for the Calculation of the Absorption of Sound by the Atmosphere*, ANSI S1.26-1978 (New York: American Institute of Physics [for Acoustical Soc. of America], 1978).

[42] G. R. Putland: "Comments on 'Acoustic Waveguide Theory' ", *J. Audio Engineering Soc.*, vol. 39, pp. 469–71 (1991 June). Reply by E. R. Geddes: pp. 471–2.

[43] G. R. Putland: "Every One-Parameter Acoustic Field Obeys Webster's Horn Equation", *J. Audio Engineering Soc.*, vol. 41, pp. 435–51 (1993 June).

[44] G. R. Putland: "Acoustical Properties of Air versus Temperature and Pressure", *J. Audio Engineering Soc.*, vol. 42, pp. 927–33 (1994 November).

[45] J. W. Strutt (Lord Rayleigh): "On the Propagation of Sound in Narrow Tubes of Variable Section", *Philosophical Magazine and Journal of Science*, Ser. 6, vol. 31, no. 182, pp. 89–96 (1916 February).

[46] C. W. Rice & E. W. Kellogg: "Notes on the Development of a New Type of Hornless Loudspeaker", *Trans. American Institute of Electrical Engineers*, vol. 44, pp. 461–75 (1925 April). Discussion: pp. 475–80. Abridged version: *J. American Institute of Electrical Engineers*, vol. 44, pp. 982–91 (1925 September). Abridged version reprinted in *J. Audio Engineering Soc.*, vol. 30, pp. 512–21 (1982 July/Aug.).

[47] S. Sakai, Y. Kagawa & T. Yamabuchi: "Acoustic Field in an Enclosure and Its Effect on Sound-Pressure Responses of a Loudspeaker", *J. Audio Engineering Soc.*, vol. 32, pp. 218–27 (1984 April).

[48] N. Sakamoto, Katsuaki Satoh, Kazue Satoh & N. Atoji: "Loudspeaker with Honeycomb Disk Diaphragm", *J. Audio Engineering Soc.*, vol. 29, pp. 711–19 (1981 October). Reprinted in *Loudspeakers Vol. 2: An Anthology* (New York, Audio Eng. Soc., 1984), pp. 263–71.

[49] R. H. Small: "Closed-Box Loudspeaker Systems—Part I: Analysis", *J. Audio Engineering Soc.*, vol. 20, pp. 798–808 (1972 December). Reprinted in *Loudspeakers: An Anthology*, 2nd Ed. (New York, Audio Eng. Soc., 1980), pp. 285–95.

[50] R. H. Small: "Vented-Box Loudspeaker Systems—Part I: Small-Signal Analysis", *J. Audio Engineering Soc.*, vol. 21, pp. 363–72 (1973 June). Reprinted in *Loudspeakers: An Anthology*, 2nd Ed. (New York, Audio Eng. Soc., 1980), pp. 316–25.

[51] C. Somigliana: "Sulle relazioni fra il principio di Huygens e l'ottica geometrica", *Atti della Reale Accademia delle Scienze di Torino*, vol. 54, pp. 974–9 (1919). In Italian.

[52] J. Spanier & J. B. Oldham: *An Atlas of Functions* (Washington: Hemisphere, 1987).

[53] M. R. Spiegel: *Advanced Calculus*, SI edition (Singapore: McGraw-Hill [Schaum Outline Series], 1981).

[54] G. W. Stewart & R. B. Lindsay: *Acoustics* (London: Chapman & Hall, 1931).

[55] D. J. Struik: *Lectures on Classical Differential Geometry*, 2nd edition (Reading, Mass.: Addison-Wesley, 1961; reprinted New York: Dover, 1988).

[56] K. Suzuki & I. Nomoto: "Computerized Analysis and Observation of the Vibration Modes of a Loudspeaker Cone", *J. Audio Engineering Soc.*, vol. 30, pp. 98–106 (1982 March). Reprinted in *Loudspeakers Vol. 2: An Anthology* (New York, Audio Eng. Soc., 1984), pp. 301–9.

[57] P. W. Tappan: "Loudspeaker Enclosure Walls", *J. Audio Engineering Soc.*, vol. 10, pp. 224–31 (1962 July). Reprinted in *Loudspeakers: An Anthology*, 2nd Ed. (New York, Audio Eng. Soc., 1980), pp. 88–95.

[58] B. D. H. Tellegen: "The Gyrator, a New Electric Network Element", *Philips Research Reports*, vol. 3, pp. 81–101 (1948 April).

[59] A. N. Thiele: "Loudspeakers in Vented Boxes", *Proc. IRE Australia*, vol. 22, pp. 487–508 (1961 August). Reprinted in *J. Audio Engineering Soc.*, vol. 19, pp. 382–92 (1971 May), vol. 19, pp. 471–83 (1971 June). Reprinted in *Loudspeakers: An Anthology*, 2nd Ed. (New York, Audio Eng. Soc., 1980), pp. 181–204.

[60] K. L. Wardle: *Differential Geometry* (London: Routledge and Kegan Paul, 1965).

[61] C. E. Weatherburn: *Differential Geometry of Three Dimensions*, 2 volumes (Cambridge, 1955).

[62] A. G. Webster: "Acoustical Impedance, and the Theory of Horns and of the Phonograph", *Proc. Nat. Acad. Sciences U.S.A.*, vol. 5, pp. 275–82 (1919). Errata in vol. 6, p. 320 (1920). Reprinted (without Webster's corrections) in *J. Audio Engineering Soc.*, vol. 25, pp. 24–8 (1977 Jan./Feb.).

[63] A. G. Webster: "On a Condition for Helmholtz's Equation Similar to Lame's", *Proc. Nat. Acad. Sciences U.S.A.*, vol. 6, pp. 605–7 (1920).

[64] C. R. Wylie: *Differential Equations* (New York: McGraw-Hill, 1979).